

PHYSICAL ACOUSTICS SUMMER SCHOOL



19970421 002

ASTILOMAR CONFERENCE CENTER

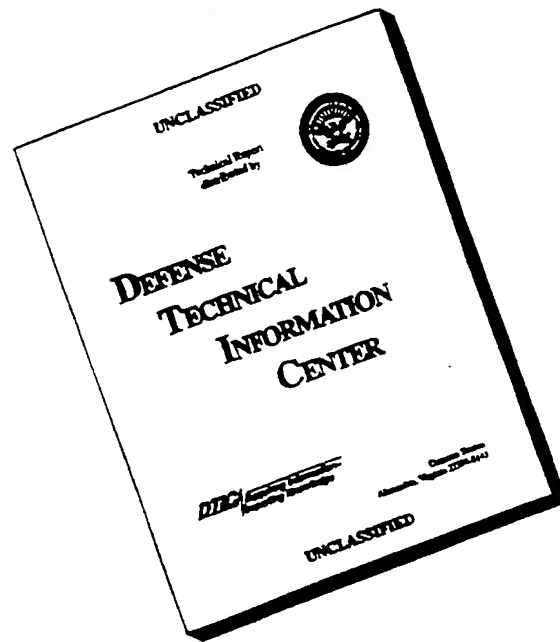
VOLUME II: TRANSPARENCIES

DISTRIBUTION STATEMENT A

Approved for public release;
Distribution Unlimited

DTIC QUALITY INSPECTED 5

DISCLAIMER NOTICE



**THIS DOCUMENT IS BEST
QUALITY AVAILABLE. THE
COPY FURNISHED TO DTIC
CONTAINED A SIGNIFICANT
NUMBER OF PAGES WHICH DO
NOT REPRODUCE LEGIBLY.**

1996 PHYSICAL ACOUSTICS SUMMER SCHOOL

VOLUME II: TRANSPARENCIES

This work relates to Department of Navy Grant N00014-96-1-0033 issued by the Office of Naval Research. The United States Government has a royalty-free license throughout the world in all copyrightable material contained herein.

DTIC QUALITY INSPECTED 3

Copies of this three-volume proceedings can be obtained by contacting: Libby Cauthen, NCPA, University of Mississippi, University, MS 38677; voice: 601-232-5808; fax: 601-232-7494; e-mail: eacauthe@olemiss.edu.

TABLE OF CONTENTS

GENERAL BACKGROUND.....	1
MOLECULAR ACOUSTICS.....	22
RUS AND MATERIALS PHYSICS	62
PERIODIC, RANDOM AND QUASIPERIODIC MEDIA	149
SONOLUMINESCENCE.....	203
FUNDAMENTALS AND APPLICATIONS OF NONLINEAR ACOUSTICS.....	270
ATMOSPHERIC ACOUSTICS	371
SENSOR PHYSICS: SIGNALS AND NOISE.....	445
THERMOACOUSTIC ENGINES AND REFRIGERATORS.....	511
REPORT DOCUMENTATION PAGE.....	545

Physical Acoustics

Summer School

Lecture #1 - 22 June 1996

General Background

Steven L. Garrett
Penn State University

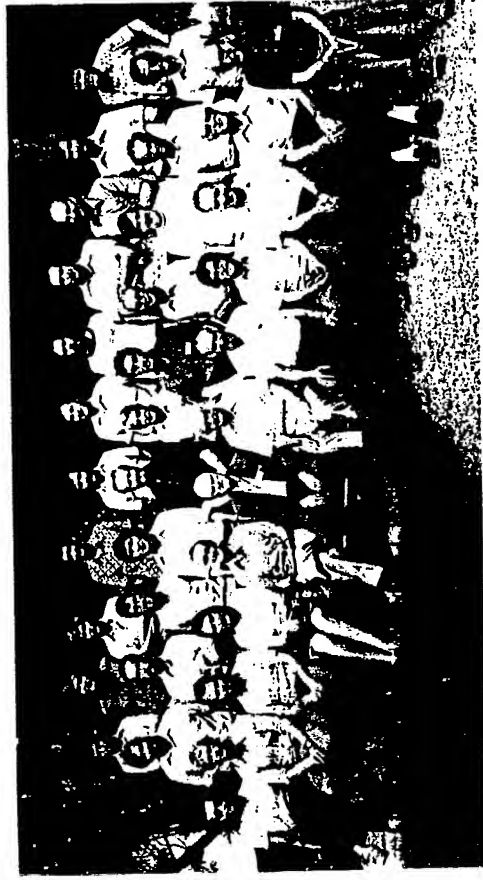
Motivation

- Support the “real” lectures
 - This is an experiment.
- Starting point
 - There is no sound in a vacuum.
 - Let’s start with materials.
- Outline
 - Phenomenology and microscopics
 - Ideal gas thermodynamics
 - Sonic gas analysis
 - Irreversible processes
 - Thermoviscous boundary layer attenuation
 - Resonator quality factor (Q)
 - Isotropic elasticity
 - Modes of a bar

History

Enrico Fermi Summer Schools

Società Italiana di Fisica
Villa Monastero - August 1974
Varenna sul Lago di Como



- The “Old Guys”

- Front row center:
Hunter, Lindsey, Mason, Sette, Rudnick,
Dransfield (?), Cook, Carome
- Who are the “old guys” now?

Phenomenological and Microscopic Models

- Phenomenology

“An acoustician is merely a timid hydrodynamicist.” *A. Larraza*

- Microscopic Models

“If, in some cataclysm, all of the scientific knowledge were to be destroyed, and only one sentence passed on to the next generations of creatures, what statement would contain the most information in the fewest words? I believe it is the atomic hypothesis that all things are made of atoms.” *R. P. Feynman*

Phenomenology

Macroscopic variables

- How many are required to provide a complete description?
- Static homogeneous, isotropic fluid requires two
 - One mechanical (p , ρ , or V)
 - One thermal (T or S)
- With flow, five are required
 - 3-dim velocity field, $\mathbf{v} = (v_x, v_y, v_z)$
- Complex fluids require more variables
 - Superfluids require eight: p , T , \mathbf{v} , and \mathbf{v}_n
 - Plasmas require eleven

Closed description

- Number of equations equal number of variables
 - Conservation Laws
 - Equation of State
- Does the description agrees with experiment?
 - If not, try a different number of variables.

Strength of phenomenological approach

“Thermodynamics is the true testing ground of physical theory since it is model independent.”

A. Einstein

Ideal Gases

- Equation of State
Extensive form:

$$pV = nRT \quad (1)$$

n = Number of moles = m/M

M = Atomic or molecular weight [$M_{\text{mix}} = xM_1 + (1-x)M_2$]

R = Universal Gas Constant (8.3143 J/mole °K)

Intensive form:

$$p = \frac{m}{V} \frac{RT}{M} = \rho \frac{RT}{M} \quad (2)$$

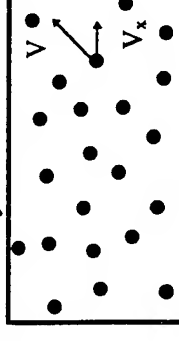
Specify two (e.g., p and T) get the third @

- Microscopic Model

Assume knowledge of constituent “particles”

Tiny hard spheres with lots of space in between

Interactions governed by Newton’s Laws of Motion



Pressure

Momentum change, $\Delta p_x = 2mv_x$, after collision with wall

Right wall elastic collision rate is $v_x/2L$ per particle

Newton’s 2nd Law: $F_x = \Delta p_x/\Delta t = mv_x^2/L$ per particle

$P_x = F_x/A = F_x/L_y L_z = mv_x^2/\text{Volume}$, per particle

Ideal Gases and the Kinetic Model

- Equipartition Theorem

Each quadratic degree of freedom gets $k_B T/2$

Communism is not dead!

Temperature is related to kinetic energy

$$\text{Pythagorean sum: } \langle v_x^2 \rangle + \langle v_y^2 \rangle + \langle v_z^2 \rangle$$

$$\text{Symmetry: } \langle v_x^2 \rangle = \langle v_y^2 \rangle = \langle v_z^2 \rangle = (1/2)k_B T$$

- Ideal Gas Law

Assume N particles in Volume $= L_x L_y L_z$

$$p = \frac{N m \langle v^2 \rangle}{3V} = \frac{2N}{3V} \frac{1}{2} m \langle v^2 \rangle = \frac{N k_B T}{V} \quad (1)$$

If $n = N/N_A$ moles, we recover $pV = nRT$

- The First Law of Thermodynamics

Energy conservation (R. J. Meyer-1842, Joule-1843 to 49)

$$dQ = T dS = dU + dW = dU + p dV \quad (3)$$

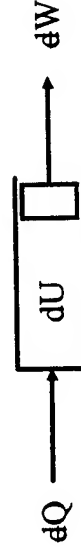
dQ = Change in heat ADDED to the system

dW = Work done BY the system

dU = Change in the internal energy of the system

T = Absolute (Kelvin) temperature

dS = Change in entropy (?) of the system



Heat Capacities

- Heat Capacity at constant volume, $dV = 0$

How much heat does it take to raise T by one degree?

How much is the internal energy changed?

$$C_V = \left(\frac{\partial U}{\partial T} \right)_V = T \left(\frac{\partial S}{\partial T} \right)_V \quad (4)$$

- Heat Capacity at constant pressure, $dV \neq 0$

How much heat does it take to raise T by one degree?

There is additional work against pressure $= p dV$

Assume one mole of ideal gas, from (1)

$$d(pV) = p dV + V dp = R dT \quad (5)$$

Substitute (5), $p dV = R dT - V dp$, into the 1st Law (3),

$$dQ = C_V dT + R dT - V dp \quad (6)$$

Since $dp = 0$

$$C_p = \left(\frac{dQ}{dT} \right)_p = T \left(\frac{\partial S}{\partial T} \right)_p = C_V + R \quad (7)$$

What does this tell us?

This result is true for any ideal gas.

Phenomenology does not give the value of C_V !

A microscopic model of the gas is required.

Adiabatic Equation of State

[α =not, dia =through, $baine$ =to go]

- Polytropic \Leftrightarrow Heat Capacity is independent of T

Assume some "generic" heat capacity, C

Apply the 1st Law,

$$dQ = C dT = C_v dT + p dV \quad (8)$$

$$dQ = C dT = C_p dT - V dp \quad (9)$$

Take the ratio, (9)/(8), set equal to a constant, γ'

$$\frac{V dp}{p dV} = \frac{C_p - C}{C_v - C} = \gamma' \quad (10)$$

Integrate to obtain the "generic" equation of state,

$$pV^{\gamma'} = \text{constant} \quad (11)$$

- Adiabatic Equation of State

In an adiabatic process, no heat enters or leaves.

In an adiabatic process, entropy remains unchanged.

$$dQ = dS = 0$$

Since $dT \neq 0$, $C = 0$ in (8), (9) and (10),

$$\gamma' = \frac{C_p}{C_v} = \gamma, \quad \text{so} \quad pV^{\gamma} = \text{const.} \quad (12)$$

γ is called the **Polytropic Coefficient**

Boyle's Law (isothermal), $dT = 0$, so $C = \infty$ and $\gamma' = 1$

$$pV = \text{const.} \quad (1)$$

The Phenomenological Equations

- Five variables form a complete set

Let's choose p, S and v.

We require five equations.

Assume adiabatic propagation, $dQ = dS = 0$

We now require only four equations.

- Conservation of Mass

$$\frac{\partial \rho}{\partial t} + \vec{\nabla} \cdot (\rho \vec{v}) = 0 \quad (13)$$

Note the form of the conservation law:

Time-rate-of-change of (mass) density, $\partial \rho / \partial t$

Divergence of (mass) flux density, $\mathbf{J} = \rho \mathbf{v}$

- Momentum Conservation

Momentum density, $\mathbf{J} = \rho \mathbf{v}$

$$\frac{\partial}{\partial t}(\rho v_i) + \frac{\partial \Pi_{ik}}{\partial x_k} = 0 \quad (14)$$

Momentum flux density tensor

$$\Pi_{ik} = p \delta_{ik} + \rho v_i v_k \quad (15)$$

For our purposes, we stay with vectors

Equivalent expression with convection

Newton's 2nd Law

$$\rho \left(\frac{\partial \vec{v}}{\partial t} + (\vec{v} \cdot \vec{\nabla}) \vec{v} \right) = -\vec{\nabla} p \quad (16)$$

Phenomenological Equations (Cont.)

- Closure

We now have four equations

- 1 Mass conservation
- 2-4 Momentum conservation (Euler)

We are also back to five variables

p , ρ and \mathbf{v}

Static fluid is completely described by two variables

- Equation of State

Taylor series expansion about equilibrium

$$\rho = \rho_o + \left(\frac{\partial \rho}{\partial p} \right)_s dp + \left(\frac{\partial \rho}{\partial S} \right)_p dS + \frac{1}{2!} \left(\frac{\partial^2 \rho}{\partial p^2} \right)_s (dp)^2 + \frac{1}{2!} \left(\frac{\partial^2 \rho}{\partial S^2} \right)_p (dS)^2 + \left(\frac{\partial^2 \rho}{\partial S \partial p} \right)_p dp dS + \dots \quad (17)$$

Simplifying assumptions

Adiabatic $\Rightarrow dS = 0$

Linearity $\Rightarrow (dp)^2 = 0$

$$d\rho = \rho - \rho_o = \left(\frac{\partial \rho}{\partial p} \right)_s dp \quad (18)$$

Linear Acoustic Phase Speed

- Perturbation expansion (Timid hydrodynamics)

Expand acoustic disturbance around equilibrium

$$p = p_o + p_1 + p_2 + \dots; \quad p_o \ll p_1 \ll p_2 \propto p_1^2$$

$$\mathbf{v} = \mathbf{v}_o + \mathbf{v}_1 + \mathbf{v}_2 + \dots; \quad \mathbf{v}_o = 0$$

- Linearize the phenomenological equations

Retain only first-order terms

Assume complex progressive “wave-like” solutions

$$p_1 = \Re e [p e^{j(\omega t - kx)}]$$

$$\mathbf{v}_1 = \Re e [\mathbf{v} e^{j(\omega t - kx)}]; \quad \mathbf{v} \text{ is a complex amplitude}$$

$$c_{\text{phase}} = \omega/k = f \lambda$$

Assume adiabatic propagation, $s_1 = s_2 = 0$

$$\rho_1 = \left(\frac{\partial \rho}{\partial p} \right)_s p_1 = \frac{p_1}{a^2} \quad (19)$$

- Coupled linear algebraic equations

Conservation of Mass - from (13)

$$j\omega \frac{p_1}{a^2} - j\rho_o \vec{k} \bullet \vec{\mathbf{v}} = 0 \quad (20)$$

Euler's Equation - from (16)

$$-j\vec{k} p_1 + j\omega \rho_o \vec{\mathbf{v}} = 0 \quad (21)$$

The determinant of the co-efficients must vanish,

$$c_{\text{phase}} = \frac{\omega}{|\vec{k}|} = \left(\frac{\partial p}{\partial \rho} \right)_s^{1/2} = a. \quad (22)$$

Energy and Intensity

- Linear combination of Euler and Continuity

Multiply the linearized Mass Conservation (13) by p_1

$$p_1 \vec{\nabla} \bullet \vec{v}_1 = - \frac{p_1}{\rho_o a^2} \frac{\partial p_1}{\partial t} \quad (23)$$

Dot multiply v_1 into the Euler Equation (14)

$$\vec{v}_1 \bullet \vec{\nabla} p_1 = - \rho_o \vec{v}_1 \bullet \frac{\partial \vec{v}_1}{\partial t} \quad (24)$$

Remember the chain rule, $\vec{\nabla} \bullet (p\vec{v}) = \vec{v} \bullet \vec{\nabla} p + p \vec{\nabla} \bullet \vec{v}$

- Conservation of Energy

It is not an "additional" conservation law

$$\frac{\partial}{\partial t} \left[\frac{1}{2} \rho_o v_1^2 + \frac{1}{2} \frac{p_1^2}{\rho_o a^2} \right] + \vec{\nabla} \bullet (p_1 \vec{v}_1) = 0 \quad (25)$$

Rate-of-change of a density (kinetic and potential)

Divergence of a flux (intensity)

This is a non-dissipative result

Sources could include viscosity and thermal conduction
Energies are quadratic in the linear acoustic fields

Sound Speed in an Ideal Gas

- Isothermal Sound Speed

Ideal gas law

$$p = \frac{m}{V} \frac{RT}{M} = \rho \frac{RT}{M} \quad (2)$$

Phase speed

$$c_{phase} = \frac{\omega}{|\vec{k}|} = \left(\frac{\partial p}{\partial \rho} \right)^{1/2}_s = a = \left(\frac{RT}{M} \right)^{1/2} \quad (22a)$$

Newtonian Sound Speed

$$a_N^2 = \frac{RT}{M} \quad (26)$$

Principia, 2nd ed. (1713), $a_N = 979$ ft/sec

Experimental value $\approx 1,130$ ft/sec

- Adiabatic Sound Speed

Define specific volume (per unit mass), $\rho = V^{-1}$

$$p \rho^{-\gamma} = \text{const.} \quad (12a)$$

Take natural log and differentiate ($\int dx/x = \ln(x) + C$)

$$\frac{dp}{p_o} = \gamma \frac{d\rho}{\rho_o} \Rightarrow a^2 = \left(\frac{\partial p}{\partial \rho} \right)_s = \gamma \frac{p_o}{\rho_o} \quad (27)$$

From the Ideal Gas Law (2)

$$a^2 = \gamma \frac{RT}{M} \quad (28)$$

Adiabatic Temperature Change

- Adiabatic compression

Cannot have adiabatic and isothermal compression

$$5/3 \geq \gamma > 1$$

Adiabatic Equation of State

$$p \rho^{-\gamma} = \text{const.} \quad (12a)$$

Use the ideal gas law to substitute for $\rho^{-\gamma}$

$$p \rho^{-\gamma} = p' T^{-\gamma} (R/M) \quad (29)$$

Explicit temperature dependence

$$p \rho^{-\gamma} = p p^{-\gamma} T^{\gamma} = p^{1-\gamma} T^{\gamma} = \text{const.} \quad (30)$$

Take natural log and differentiate (again)

$$(1-\gamma) \frac{p_1}{p_o} = -\gamma \frac{T_1}{T_o} \quad (31)$$

Adiabatic temperature change, T_1

$$T_1 = \frac{(\gamma-1)}{\gamma} \frac{p_1}{p_o} T_o \quad (32)$$

- Typical values

Normal speech in air (74 dB_{SPL} = 0.1 Pa_{rms})

$$p_o = 101,325 \text{ Pa}, \gamma = 1.4027, T = 293 \text{ °K (20 °C)}$$

$$T_1 = 83 \text{ } \mu\text{K}_{\text{rms}}$$

Thermoacoustic refrigerator (SETAC = 65 kPa_{rms})

$$p_o = 2.1 \text{ MPa}, \gamma = 5/3, T = 293 \text{ °K (20 °C)}$$

$$T_1 = 3.6 \text{ °K}_{\text{rms}} = 18.5 \text{ °F}_{\text{p-p}}$$

First Summary

- The Phenomenological Approach

How many variables form a complete description

Closed description

Conservation laws

Equation of State

- Ideal Gas Results

Adiabatic Equation of State

Difference of Specific Heats

$$C_p - C_v = R$$

Ratio of Specific Heats (Polytropic Coefficient)

$$\gamma = C_p/C_v \quad (7)$$

Adiabatic gas law

$$p V^{\gamma} = \text{constant} \quad (12)$$

Adiabatic Sound Speed

$$a^2 = \gamma \frac{R T}{M} \quad (28)$$

Adiabatic Temperature Lapse

$$T_1 = \frac{(\gamma-1)}{\gamma} \frac{p_1}{p_o} T_o \quad (32)$$

- Problems

Specific heats are undetermined

What is the value of γ ?

We must invoke a microscopic (quantum) model!

Why is Adiabatic correct and Isothermal wrong?

Applications (Thermometry)

- Fundamental Measurements

Ideal gas sound speed

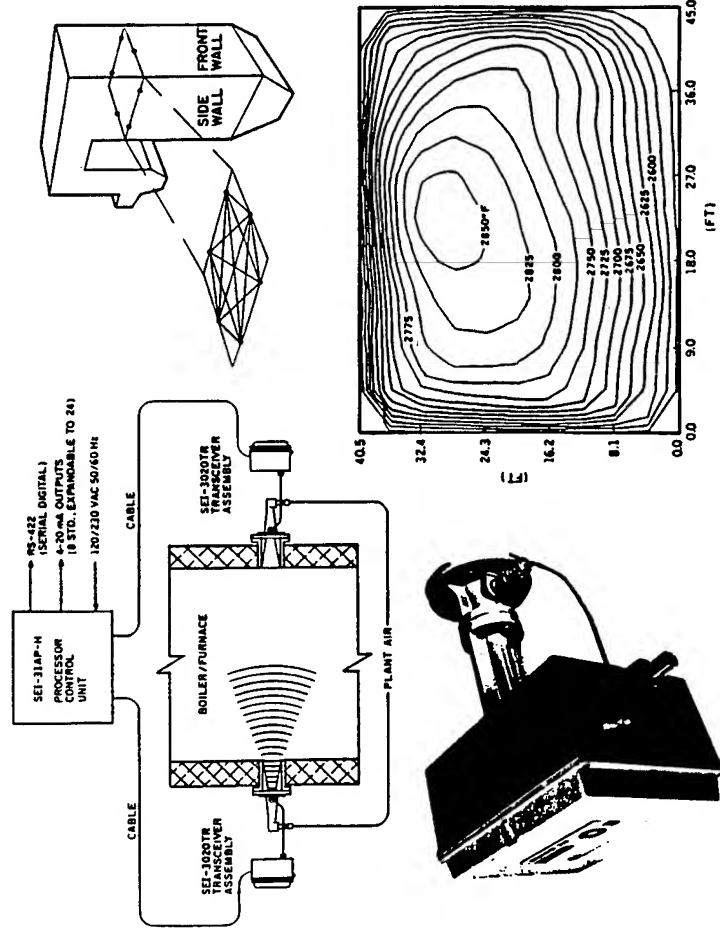
$$a^2 = \gamma \frac{RT}{M} \quad (28)$$

Measure T and a, get Boltzmann's Constant = R/N_A

Know gas (M and γ), measure a, get absolute (Kelvin) T

- Acoustic Pyrometry

J. L. Keppe, *Sensors*, Jan. 1996



Doppler gives mean flow [J. L. Keppe, *Sensors*, May 1995]

Applications (Gas Analysis)

- Mixtures

Mean molecular mass

$$M_{\text{mix}} = x M_1 + (1-x) M_2 \quad (33)$$

Mean polytropic coefficient

$$\gamma_{\text{mix}} = \frac{x C_{p,1} + (1-x) C_{p,2}}{x C_{v,1} + (1-x) C_{v,2}} \neq x \gamma_1 + (1-x) \gamma_2 \quad (34)$$

- Sound Speed in Gas Mixtures

Approximate sound speed ratio

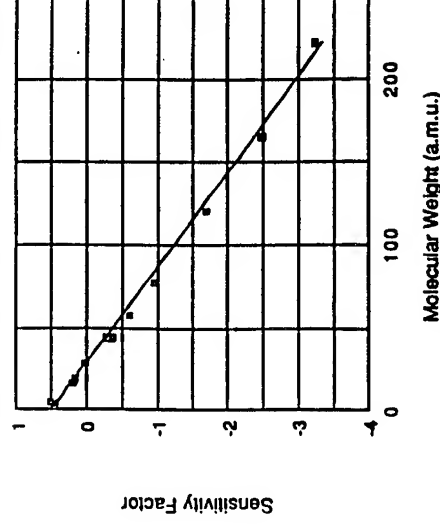
$$\frac{a_{\text{mix}}^2}{a_1^2} \approx \frac{1 + [(\gamma_2 - \gamma_1) / \gamma_1] x}{1 + [(M_2 - M_1) / M_1] x} \quad (35)$$

Sensitivity analysis for resonance freq. shift, δx

$$\frac{\delta f}{f_1} = \frac{\delta a_{\text{mix}}}{a_1} \approx \left[\frac{(\gamma_2 - \gamma_1)}{\gamma_1} \frac{(M_2 - M_1)}{M_1} \right] \frac{\delta x}{2} \equiv \beta \delta x \quad (36)$$

Sensitivity factor for air contaminants

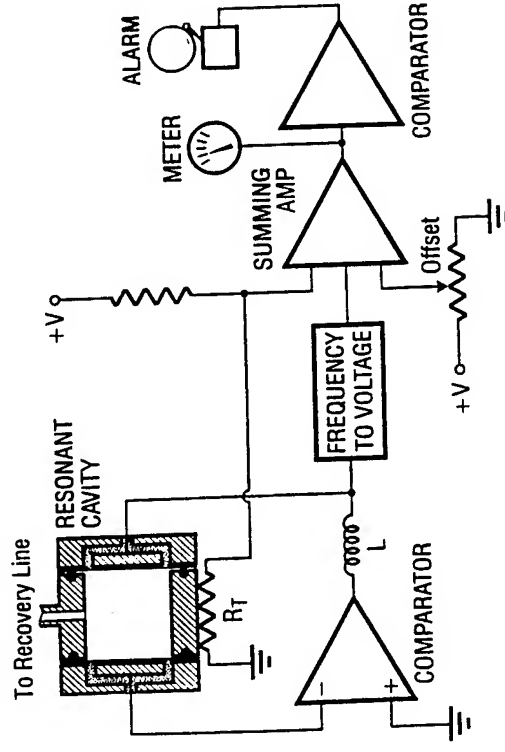
Straight line [$\beta = (M_1 - M_2) / 2M_1$] ignores γ_{mix} effects



Sonic Gas Analyzers

- Schlagwetter-pfeife (1884)
Mine gas exhaust pumped through an organ pipe
Two pipes gives beats and saves the tone deaf
- Isotopic ratios in $^3\text{He}/^4\text{He}$ gas mixtures
Kagiwada and Rudnick, J. Low Temp. Phys. **3** (1970)
Fraser, Rev. Sci. Inst. **11**, 1692 (1972)
Keolian, *et al.*, JASA **64**, S61 (1978)
Differential analyzer with spherical resonators
- "Practical Instrument"

Cost/Precision ratio for frequency (10 ppm \approx \$20)
Garrett, Swift and Packard, Physica **107B**, 601 (1981)



- Limitations

Pressure: $(\partial \ln f / \partial p)_{T,x} = B/RT = 38 \text{ ppm/psi}$

Humidity: $\pm 20\% \text{ RH} \Rightarrow \pm 800 \text{ ppm}$

Irreversibility

- Goals

Understand why sound in gases is (nearly) adiabatic
Develop the dissipative phenomenology
Calculate thermoviscous resonator losses

- Time reversal invariance

The dynamical equation was reversible

No dissipation included in Euler's Equation (14).

Dissipative processes generates entropy

Ordered energy (sound) is converted to heat.

Time reversal symmetry is broken.

Thermal Conduction and Viscosity

- Newton's Law of Cooling

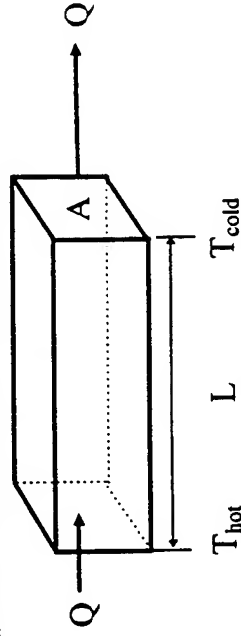
Ohm's law for heat flow ($I = \Delta V/R$)

$$\vec{q} = -\kappa \vec{\nabla} T \quad (40)$$

\vec{q} = Heat flux [Watts/m²]

κ = Thermal conductivity [W/m²K]

One-dimensional thermal conductance



$$\dot{Q} = -\kappa A \frac{(T_{\text{hot}} - T_{\text{cold}})}{L} = \frac{\kappa A}{L} \Delta T \quad (41)$$

Ohm's Law: $I = G \Delta V$ or $\Delta V = R I$

Electrical resistance: $R = L/\sigma A$

- Viscous shear stress

Ohm's Law for one component of shear stress, P_{xy}

$$P_{xy} = \mu \frac{\partial v_x}{\partial y} \quad (42)$$

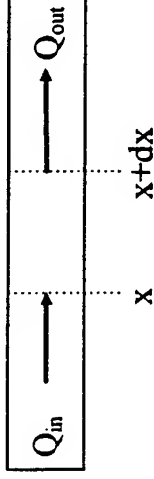
P_{xy} = Force per unit area in x-direction on a surface with its normal in the y-direction [Pa]

μ = Shear viscosity [kg/m-sec]

Thermal (Fourier) Diffusion Equation

- Differential analysis

Heat flow through a differential "slab"



Net heat is deposited in the slab of unit cross-section

$$Q_{\text{net}} = Q_{\text{in}} - Q_{\text{out}} \quad (43)$$

Temperature change rate depends on heat capacity

$$\rho c_p \frac{\partial T}{\partial t} = \dot{Q}_{\text{net}} = -\kappa \left(\frac{\partial T}{\partial x} \right)_x + \kappa \left(\frac{\partial T}{\partial x} \right)_{x+dx} \quad (44)$$

c_p = Specific heat at constant pressure [Joules/kg^oK]

Expand $(\partial T/\partial x)_{x+dx}$ about x in a Taylor series

$$\left(\frac{\partial T}{\partial x} \right)_{x+dx} = \left(\frac{\partial T}{\partial x} \right)_x + \frac{\partial}{\partial x} \left(\frac{\partial T}{\partial x} \right)_x dx + \dots \quad (45)$$

Combine (44) and (45)

$$\frac{\partial T}{\partial t} = \frac{\kappa}{\rho c_p} \nabla^2 T = \chi \nabla^2 T \quad (46)$$

χ = Thermal diffusivity [m²/sec]

Diffusion Equations

- Navier-Stokes Equation

Diffusion of viscous shear stress (vorticity)

$$\frac{\partial \vec{v}}{\partial t} = \frac{\mu}{\rho} \nabla^2 \vec{v} - \frac{\vec{\nabla} p}{\rho} = \nu \nabla^2 \vec{v} - \frac{\vec{\nabla} p}{\rho} \quad (47)$$

ν = Kinematic viscosity [m²/sec]

- Fick's Second Law of Diffusion

Mass diffusion (random walk)

$$\frac{\partial C}{\partial t} = D \nabla^2 C \quad (48)$$

C = Concentration [moles/m³]

D = Mass diffusion constant [m²/sec]

- Maxwell's Equation in a Good Conductor

Electromagnetic energy diffusion

$$\frac{\partial \vec{E}}{\partial t} = \frac{1}{\sigma \mu} \nabla^2 \vec{E} \quad (48)$$

σ = Electrical conductivity [Siemens/m]

μ = Magnetic permeability [N/Amp²]

$(\sigma \mu)^{-1}$ = ??? [m²/sec]

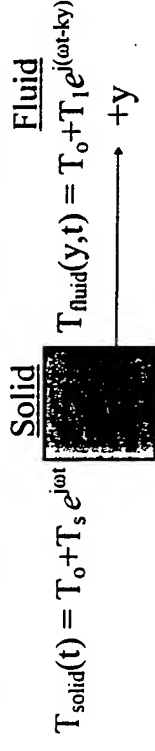
Evanescent Wave

- Wavelike solutions to the diffusion equations

We could choose any of the diffusion equations

Solve Fourier Heat Equation since it is scalar.

Assume a plate with an oscillating temperature



$$T_{\text{solid}}(t) = T_o + T_s e^{j\omega t} \quad \text{Solid}$$

$$T_{\text{fluid}}(y,t) = T_o + T_1 e^{j(\omega t - ky)} \quad \text{Fluid}$$

ω = "Driving" frequency [rad/sec]

k = Complex wave number

Substitute into the Fourier Equation

$$j\omega T_1 = -\chi k^2 T_1 \quad (49)$$

Solve for jk

$$jk = \left(\frac{j\omega}{\chi} \right)^{1/2} = \left(e^{j\frac{\pi}{2}} \right)^{1/2} \left(\frac{\omega}{\chi} \right)^{1/2} = \frac{1+j}{\sqrt{2}} \left(\frac{\rho c_p \omega}{\chi} \right)^{1/2} \quad (50)$$

Wavenumber has equal real and imaginary parts

- Thermal Penetration Depth

Define a real length $\delta_\kappa = \Re[k^{-1}]$

$$\delta_\kappa = \sqrt{\frac{2\chi}{\omega}} = \sqrt{\frac{2\kappa}{\rho c_p \omega}} \quad (51)$$

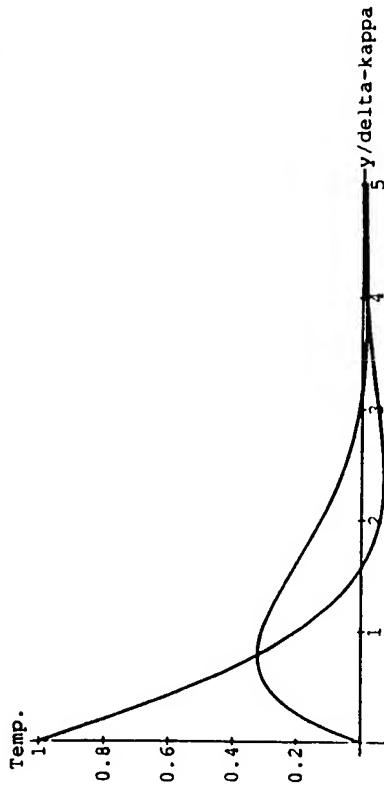
Substitute into wavelike assumption

$$T_1(y,t) = T_1 e^{-y/\delta_\kappa} [\cos(y/\delta_\kappa) + j \sin(y/\delta_\kappa)] e^{j\omega t} \quad (52)$$

Thermal Boundary Layer

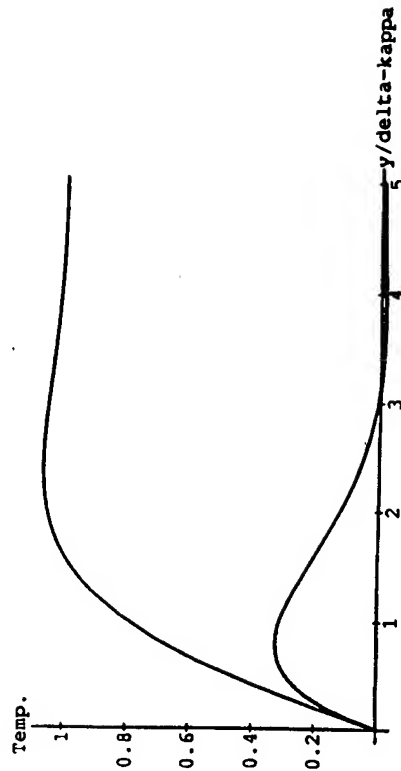
Fluid over a plate with oscillating temperature

$$T_1(y, t) = T_i e^{-\frac{(1+i)y}{\delta_\kappa}} e^{j\omega t} \quad (53)$$



Oscillating fluid temp. over an isothermal plate

$$T_1(y, t) = T_i \left[1 - e^{-\frac{(1+i)y}{\delta_\kappa}} \right] e^{j\omega t} \quad (54)$$



Analogous Boundary Layers

- Viscous boundary layer, δ_μ
Exploit isomorphism with the Navier-Stokes equation

$$\delta_\mu = \sqrt{\frac{2\nu}{\omega}} = \sqrt{\frac{2\mu}{\rho\omega}} \quad (55)$$

In air, $\delta_\mu = 0.21 \text{ cm}/(\text{f})^{1/2}$ or $100 \text{ } \mu\text{m}$ @ 440 Hz

The quantification of the saying "still waters run deep"

- Electromagnetic skin depth

$$\delta = \sqrt{\frac{2}{\omega \sigma \mu}} \quad (56)$$

In sea water $\delta = 30 \text{ m}$ @ 60 Hz and 2 cm @ 1 Mhz

In copper $\delta = 2.2 \text{ mm}$ @ 1 kHz and $66 \text{ } \mu\text{m}$ @ 1 Mhz

- Mass diffusion length

$$\ell = \sqrt{\frac{2D}{\omega}} = \sqrt{2D\tau} \quad (57)$$

τ = Diffusion time

For Argon in Helium, $\ell = 1.2 \text{ cm}$ (τ)^{1/2}

Adiabatic Propagation

Thermal diffusion

What is the "speed of heat"?

We could have solved for the thermal phase speed.

Again, from the Fourier Eq'n: $j\omega = -\chi k^2$ (49a)

$$c_{\text{phase}}^{\text{THERMAL}} = \left| \frac{\omega}{k} \right| = \left| \sqrt{j\chi\omega} \right| = \sqrt{\frac{\omega\chi}{\rho c_p}} \quad (50)$$

Same result is obtained if we set $\delta_\kappa = \lambda = \lambda/2\pi = k^{-1}$

Sound speed is non-dispersive (frequency independent).

The thermal "wave" is dispersive, $c^{\text{THERMAL}} \propto \sqrt{\omega}$

Critical frequency, ω_{crit} , when $c_{\text{phase}} = c^{\text{THERMAL}}$

$$\omega_{\text{crit}} = \frac{\rho c_{\text{phase}}^2}{\gamma p_o} = \frac{\gamma p_o c_p}{\kappa} \quad (51)$$

In air, $f_{\text{crit}} = \omega_{\text{crit}}/2\pi \approx 860 \text{ MHz} \Rightarrow \lambda/2\pi = \lambda \approx 0.065 \text{ } \mu\text{m}$.

Adiabatic at $f < f_{\text{crit}}$ (heat moves too slow)

Isothermal at $f > f_{\text{crit}}$ ($\Delta T = T(t) - T_o$ can't develop)

Mean-free-path

Phenomenology assumes the continuum hypothesis

Many collisions are required in any "fluid volume" $\ll \lambda^3$

$$\langle \ell \rangle = \frac{1}{\sqrt{2}} \pi d^2 n \quad (52)$$

Ballistic propagation for $\lambda < \langle \ell \rangle$

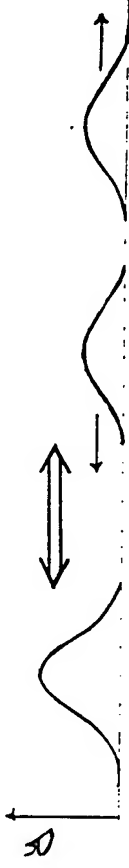
In air, $\langle \ell \rangle \approx 0.10 \text{ } \mu\text{m}$ - ITS NEVER ISOTHERMAL!

Propagation and Diffusion

Sound waves propagate

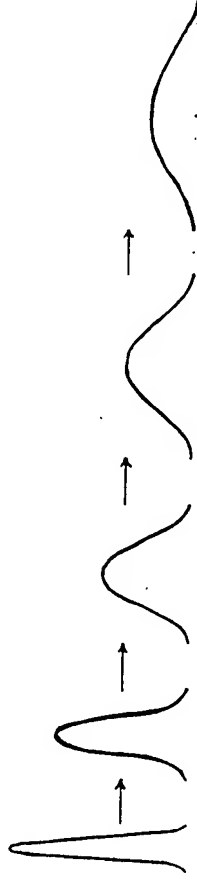
The speed of sound is frequency independent.

Time reversal invariance without dissipation.

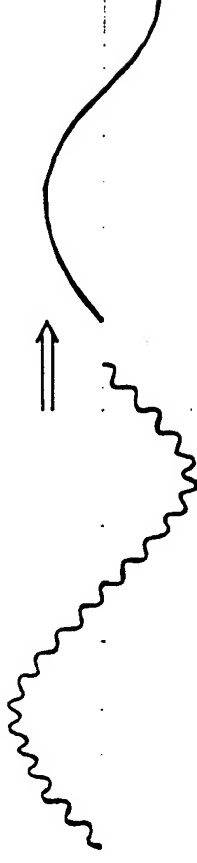


Temperature disturbances diffuse

Thermal diffusion is irreversible and dispersive.



Short wavelengths attenuate more rapidly.



Power Dissipation

- Electrical dissipation

Time-averaged power

Assume sinusoidal current and voltage

$$I_A \cos(\omega t + \phi_I) \text{ and } V_A \cos(\omega t + \phi_V)$$

Time average the product over a cycle, $\tau = 2\pi/\omega$.

$$\langle I(t)V(t) \rangle = \frac{1}{\tau} \int_0^\tau I_A \cos(\omega t + \phi_I) \bullet V_A \cos(\omega t + \phi_V) dt \quad (53)$$

$$\text{Average power} = \langle \Pi_{\text{elect}} \rangle = (1/2) I_A V_A \cos(\phi_I - \phi_V) \quad (54)$$

Complex representation

$$\langle I(t)V(t) \rangle = \frac{1}{2} \Re [I \tilde{V}] = \frac{1}{2} [I_A e^{j\phi_I} V_A e^{j\phi_V}] \quad (55)$$

\tilde{V} is the complex conjugate of V

- Viscous dissipation at a surface

$$\text{Average power} = \Pi = \langle \mathbf{F} \bullet \mathbf{v} \rangle$$

$$\text{Average power/unit area} = \Pi/A = \dot{e}$$

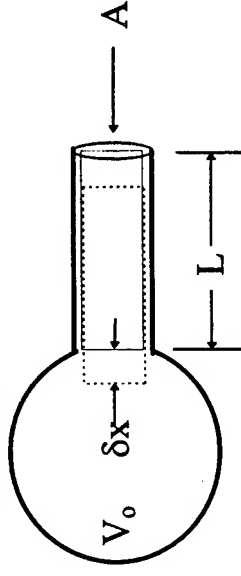
$$\dot{e}_\mu = \frac{\Pi_\mu}{A} = \frac{\langle \vec{F}_\mu \bullet \vec{v} \rangle}{A} = \langle p_{xy} v_x \rangle = \mu \left\langle \frac{\partial v_x}{\partial y} v_x \right\rangle \quad (57)$$

Using the formalism of (55) and integrating to $y = \infty$

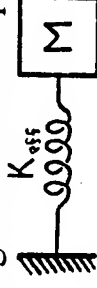
$$\dot{e}_\mu = \mu \frac{v_x^2}{2 \delta_\mu} \quad (58)$$

Helmholtz Resonator

- All dimensions are small compared to λ



- Analogous to a mass-spring system



Mass of "slug", $m = \rho A L$

Stiffness of gas spring

Adiabatic compression

$$\frac{\delta p}{p_0} = \gamma \frac{\delta V}{V_0} = \gamma \frac{A \delta x}{V_0} \quad (60)$$

$$\text{Hooke's Law: } F = A \delta p = -k_{\text{eff}} \delta x \quad (61)$$

Solve for k_{eff} and use $a^2 = \gamma p_0 / \rho_0$

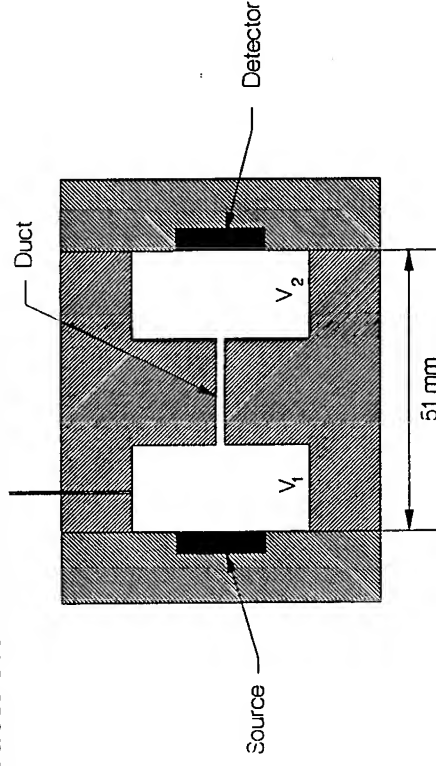
$$k_{\text{eff}} = \frac{A \delta p}{\delta x} = \frac{\gamma p_0}{V_0} A^2 = \rho_0 a^2 \frac{A^2}{V_0} \quad (62)$$

$$\text{Resonance frequency, } \omega_0^2 = k_{\text{eff}}/m \quad (63)$$

$$\omega_0 = a \sqrt{\frac{A}{LV_0}} \quad (64)$$

Greenspan Viscometer

- Double Helmholtz resonator



Advantages over an open Helmholtz resonator

- Sealed for sample purity
- No radiation losses
- Simplified transducer placement
- Emphasis on viscous rather than thermal losses

- Resonance frequency

One mass and two springs, $k_{\text{eff}} = k_1 + k_2$ (65)

$$\omega_o = a \sqrt{\frac{A}{L} \left(\frac{1}{V_1} + \frac{1}{V_2} \right)} \quad (66)$$

Why is it called a “viscometer”?

Helmholtz Resonator Quality Factor

- Quality Factor (Q)

A very useful way to specify dissipation

Dimensionless! (System size does not matter)

Many equivalent definitions

$$\text{Energy: } Q = 2\pi E_{\text{Stored}}/E_{\text{lost-per-cycle}} \quad (67a)$$

$$\text{Lumped parameter: } Q = \omega_o L/R = \omega_o m/R_m \quad (67b)$$

$$\text{Decay time: } Q = \omega_o \tau/2 \quad (67c)$$

$$\text{Phase shift: } Q = (f_o/2)(\partial\phi/\partial f)_{f_o} \quad (67d)$$

$$\text{Complex pole-zero (a±jb): } Q = -(a^2+b^2)/2a \quad (67e)$$

$$\text{Half-power bandwidth: } Q = f_o/\Delta f \quad (67f)$$

$$\text{Complex elastic modulus: } Q = (\tan \delta)^{-1} = E'/E'' \quad (67g)$$

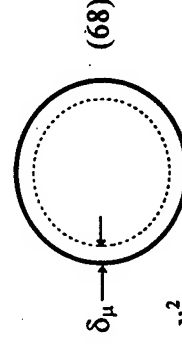
$$\text{Critical damping ratio: } Q = 1/2\zeta \quad (67h)$$

- Viscous losses in the neck

Power dissipation in neck

Neck surface area = $2\pi rL$

Assume $\delta_\mu < r$ and use (58)



$$\Pi_\mu = 2\pi rL \dot{e}_\mu = 2\pi rL \mu \frac{v_x^2}{2\delta_\mu} \quad (69)$$

Helmholtz Quality Factor (Cont.)

- Stored kinetic energy

$$\text{Total Energy, } E_{\text{tot}} = KE + PE = PE_{\text{max}} = KE_{\text{max}}$$

Integrate KE density (25) over the neck volume

$$KE_{\text{max}} = (1/2) m \dot{v}^2 = (1/2) \rho \pi r^2 L v^2 \quad (70)$$

- Quality factor due to viscous loss (Q_μ)

Ratio of energy stored to energy lost per cycle

$$Q_\mu = \frac{2\pi KE_{\text{max}}}{\Pi_\mu / f} = r \delta_\mu \frac{\pi \rho f}{\mu} = \frac{r}{\delta_\mu} \quad (71)$$

Simple dimensionless result.

Boundary layer thinness assumption ($r \gg \delta_\mu$)

For low Q_μ (r not much larger than δ_μ) use Bessel sol'n.

$$Q_\mu = \frac{r}{\delta_\mu} - 0.75 + \frac{0.2}{r/\delta_\mu} \text{ for } Q_\mu \geq 3 \quad (72)$$

- Example

Single Helmholtz resonator

$V_1 = 4.0$ liters, ($V_2 = \infty$) $L = 10$ cm, $2r = 3.0$ cm

$$Q_\mu = 58$$

Radiation loss (KFCFS)

$$Q_{\text{rad}} = \frac{L\lambda}{\pi r^2} = 670 \quad (73)$$

Irreversible Thermal Conduction

- Viscosity measurement

From (71) it is possible to determine viscosity.

Geometry plus resonance frequency and gas density

BUT the gas spring is adiabatic, so $T_1 \neq 0$.

V_1 and V_2 have a lot more surface area than the neck!

- Thermal boundary layer losses

Irreversible conduction to/from gas and wall

From p dV work and the expansion coefficient

$$\dot{e}_\kappa = (\gamma - 1) \frac{\pi f \delta_\kappa}{2 \gamma p_o} p_1^2 \quad (74)$$

Note that (72) vanishes for $\gamma = 1$ (isothermal)

Potential energy density, $p_1^2/2\rho a^2$ (25)

Following the same procedure (68) through (71)

For a spherical volume, $V_o = (4\pi/3) R_o^3$

$$Q_\kappa = \frac{2 R_o}{3(\gamma - 1) \delta_\kappa} \quad (75)$$

This has exactly the same form as $Q_\mu = r/\delta_\mu$ (71)

Same example [$V_1 = 4.0$ liters, $L = 10$ cm, $2r = 3.0$ cm]

$$\frac{1}{Q_{\text{total}}} = \frac{1}{Q_\mu} + \frac{1}{Q_\kappa} + \frac{1}{Q_{\text{rad}}} \quad (76)$$

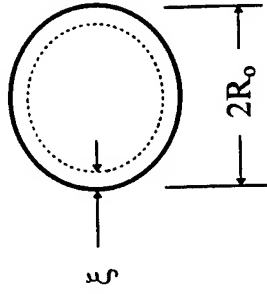
$$Q_\mu = 58; Q_\kappa = 540; Q_{\text{rad}} = 670; Q_{\text{total}} = 49$$

Why is the thermal loss so much smaller?

Damped Bubble Oscillations

- Bubble stiffness

Gas provides the adiabatic stiffness



$$\frac{\delta p}{p_o} = \gamma \frac{\delta V}{V_o} = \gamma \frac{4\pi R_o^2 \xi}{(4\pi/3) R_o^3} \quad (77)$$

Hooke's law give $F = \delta p A = -k_{\text{eff}} \xi$

$$k_{\text{eff}} = 12\pi \gamma p_o R_o \quad (78)$$

- Where's the mass?

Radiation mass

The fluid surrounding the bubble has inertia.

$$m_{\text{rad}} = 4\pi \rho R_o^3 \quad (79)$$

Bubble resonance frequency

$$\omega_{\text{bubble}} = \frac{1}{R_o} \sqrt{\frac{3\gamma p_o}{\rho_{H_2O}}} \quad (80)$$

Bubble Damping

- Radiation loss

The bubble is a monopole radiator

Calculate Q_{rad} the same way

Energy stored

$$KE_{\text{max}} = \frac{1}{2} m v^2 = \frac{1}{2} (4\pi \rho_{H_2O} R_o^3) \dot{\xi}^2 \quad (81)$$

Radiated power, $\langle \Pi_{\text{rad}} \rangle = (1/2) R_{\text{rad}} (\omega V)^2$

Analogous to Joule heating in electricity, $\langle \Pi_{\text{rad}} \rangle = RI^2/2$

$$\langle \Pi_{\text{rad}} \rangle = \frac{\pi}{2} (\rho \alpha)_{H_2O} \frac{\dot{V}^2}{\lambda^2} \quad (82)$$

Volumetric velocity, $\dot{V} = \omega V = 4\pi R_o^2 (d\xi/dt)$

$$Q_{\text{rad}} = \frac{\lambda}{2\pi R_o} = \frac{1}{k R_o} \quad (83)$$

- Thermal conduction losses

Exactly like the Helmholtz resonator

Motion is radial: No shear - no viscous losses

- Example

Single bubble 10 m below the surface, $R_o = 1.0$ mm

Resonance frequency, $f_o = 4.6$ kHz

Radiation loss, $Q_{\text{rad}} = 52$

Thermal loss, $Q_k = 61$

Second Summary

- Irreversibility leads to diffusive processes
 - Thermal Diffusion - Fourier Heat Equation
 - Viscous Diffusion - Navier-Stokes Equation
 - Mass Diffusion - Fick's Second Law
 - Electron Diffusion - Ohm's Law
- Diffusive processes have a characteristic length
 - Penetration depth $\delta \propto \omega^{-1/2}$
- Adiabatic propagation
 - The hot parts of the wave are too far from the cold
 - Thermal diffusion not effective in the available time
 - "Adiabatic" is only a limit
 - Thermal conduction leads to dissipation
- Thermoviscous boundary losses
 - Dissipation occurs within boundary layer thickness δ
 - Quality factor (Q) is a dimensionless measure of loss
 - Energy ratios simplify Q calculations

Sound in Solids

- Tensor elasticity

A (crystalline) solid is not necessarily isotropic
Hooke's law becomes a tensor relation

Three compressive components, u_{11}, u_{22}, u_{33}

Three shear components, u_{12}, u_{23}, u_{31}

Stiffness tensor has 36 elements

Symmetry (e.g., $u_{12} = u_{21}$) reduces number to 21

$$\sigma_{ik} = \frac{\partial F}{\partial u_{ik}} = \lambda_{iklm} u_{lm} \quad (84)$$

Proper alignment of coordinate system reduces to 18

Elastic energy

$$F = \frac{1}{2} \lambda_{iklm} u_{ik} u_{lm} \quad (85)$$

Analogous to PE = $kx^2/2$ in a one-dimensional spring

- Isotropic elasticity

Two moduli form a complete set, for isotropic solid

Young's (E) and Shear (G)

Bulk (B) and Poisson's ratio (ν)

Any one can be expressed in terms of two others

Deformations can be decomposed into two types

Hydrostatic compression: constant shape

Shear: constant volume

Modes of a Thin Bar

- Modes of a long thin bar

If $d \ll \lambda$, the modes are independent

Individual modes can be selectively excited and detected

Bar resonances determine elastic moduli directly

“Free-Free” boundaries are the most reproducible

- Non-Dispersive Modes

Wave speeds are independent of frequency if $d \ll \lambda$

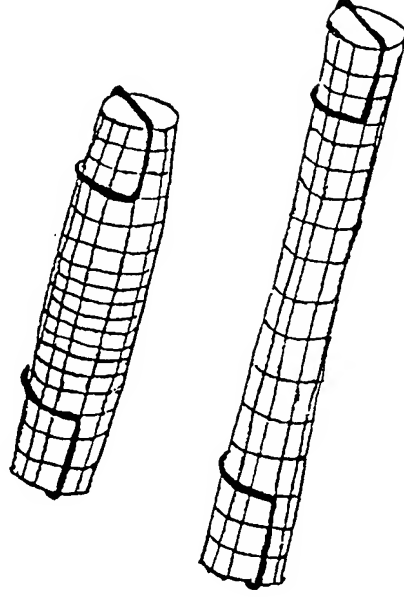
Modes are harmonic, $f_n = nf_1$

Longitudinal wave resonances

Wave equation:

$$\frac{\partial^2 \xi}{\partial t^2} - c_L^2 \frac{\partial^2 \xi}{\partial x^2} = 0; \quad c_L^2 = \frac{E}{\rho} \quad (86)$$

Mode shape (courtesy of R. M. Keolian)



Sound in Solids

- Tensor elasticity

A (crystalline) solid is not necessarily isotropic

Hooke's law becomes a tensor relation

Three compressive components, u_{11}, u_{22}, u_{33}

Three shear components, u_{12}, u_{23}, u_{31}

Stiffness tensor has 36 elements

Symmetry (e.g., $u_{12} = u_{21}$) reduces number to 21

$$\sigma_{ik} = \frac{\partial F}{\partial u_{ik}} = \lambda_{iklm} u_{lm} \quad (84)$$

Proper alignment of coordinate system reduces to 18

Elastic energy

$$F = \frac{1}{2} \lambda_{iklm} u_{ik} u_{lm} \quad (85)$$

Analogous to PE = $kx^2/2$ in a one-dimensional spring

- Isotropic elasticity

Two moduli form a complete set, for isotropic solid

Young's (E) and Shear (G)

Bulk (B) and Poisson's ratio (ν)

Any one can be expressed in terms of two others

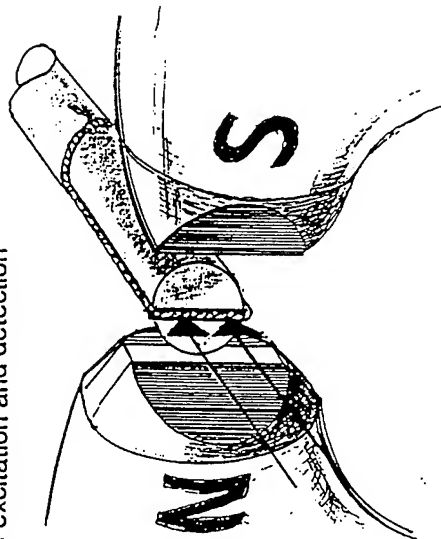
Deformations can be decomposed into two types

Hydrostatic compression: constant shape

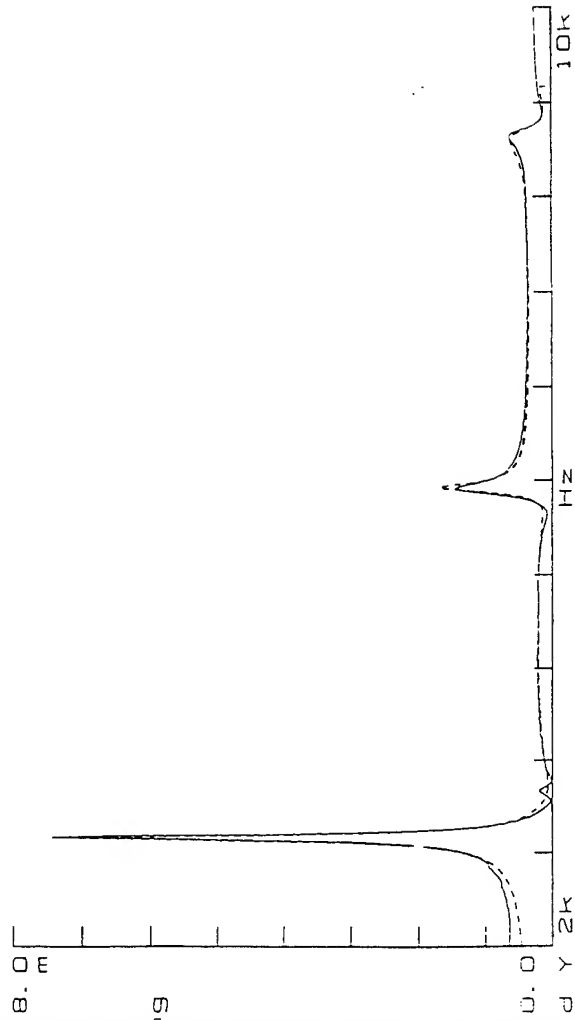
Shear: constant volume

Longitudinal Mode

Selective excitation and detection



Data

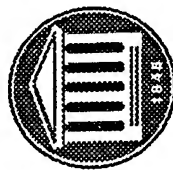


Data Summary

<u>Mode number</u> [n]	<u>Frequency (Hz)</u> [f _n]	<u>Normalized Freq. (Hz)</u> [f _n /n]
TORSIONAL		
1	1644	1644
2	3341	1670
3	5080	1693
4	6750	1688
5	8446	1689
Average		1677 ± 20 (± 0.6%)
FLEXURAL		
(3.0112) ²	203.1	22.40
(4.9994) ²	560.4	22.42
(7.0000) ²	1104	22.53
Average		22.45 ± 0.07 (± 0.2%)
LONGITUDINAL		
1	2941	2941
2	5936	2968
3	8896	2965
Average		2958 ± 15 (± 0.4%)

MOLECULAR ACOUSTICS

- Absorption and Dispersion in Gases
Break ~40 min
- Relaxation Absorption
Break ~60 min
- Diffusion & Absorption at Low Pressure
Break ~20 min
- Discussion of Current Topics ~30 min



The University of Mississippi

Wave Equation - No Dispersion

$$-\frac{\partial u}{\partial x} = \frac{\partial s}{\partial t} \quad \text{From Conservation of Mass} \quad (7a)$$

$$\frac{\partial u}{\partial t} = -\frac{1}{\rho_0} \frac{\partial p_e}{\partial x} \quad \text{Conservation of Momentum}$$

$$c_v \Theta = \frac{m \rho_0}{\rho_0} s \quad \text{First Law - Conservation of Energy}$$

$$p_e = \left(\frac{\partial p}{\partial \rho} \right) \rho_0 s + \left(\frac{\partial p}{\partial T} \right) \rho \Theta \quad \text{Eq. of State}$$

Assume

$$p_e = p_{e0} e^{i(\omega t - kx)}, \text{ etc}$$

Solution gives

$$c_0^2 = \omega^2 / k^2 = (\partial p / \partial \rho)_s = \gamma (p_0 / \rho_0) \quad (11)$$

**Pure Real
Classical Absorption**

Wave Equation - No Dispersion

$$-\frac{\partial u}{\partial x} = \frac{\partial s}{\partial t}$$

From Conservation of Mass (7a)

$$\frac{\partial u}{\partial t} = -\frac{1}{\rho_0} \frac{\partial p_e}{\partial x}$$

Conservation of Momentum

$$c_v \Theta = \frac{m \rho_0}{\rho_0} s$$

First Law - Conservation of Energy

$$p_e = \left(\frac{\partial p}{\partial \rho} \right) \rho_0 s + \left(\frac{\partial p}{\partial T} \right) \rho \Theta \quad \text{g. of State}$$

Assume

$$p_e = p_{e0} e^{i(\omega t - kx)}, \text{ etc}$$

Solution gives

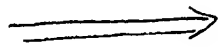
$$c_0^2 = \omega^2/k^2 = (\partial p / \partial \rho)_s = \gamma(\rho_0 / \rho) \quad (11)$$

Pure Real
Classical Absorption

Classical Absorption

$$\rho_0 \ddot{\xi} = -\partial p / \partial x \Rightarrow \frac{\partial(\rho \dot{\xi})}{\partial t} = -\frac{\partial p}{\partial x} + \left(\frac{4}{3}\eta + \dot{\eta}\right) \frac{\partial^2 \xi}{\partial x^2}$$

Eq. 2



Eq. 12

Fig. 1

Assume $\rho \approx \rho_0$, $\eta' = 0$

$$\frac{\partial u}{\partial t} = -\rho_0^{-1} \frac{\partial p_0}{\partial x} + \frac{4}{3} (\eta / \rho_0) \frac{\partial^2 u}{\partial x^2} \quad (15)$$

which gives

$$u = u_0 e^{-\alpha x} e^{i(\omega t - k_r x)}$$

where

$$k_r \approx \omega / c_0 \quad \alpha \approx 2/3 (\eta \omega^2 / \rho_0 c_0^3) \quad (22)$$

For O_2 , $\alpha / k_r \approx 0.88 \times 10^{-8}$ ✓

For water, $\alpha / k_r \approx 1.9 \times 10^{-12}$ ✓

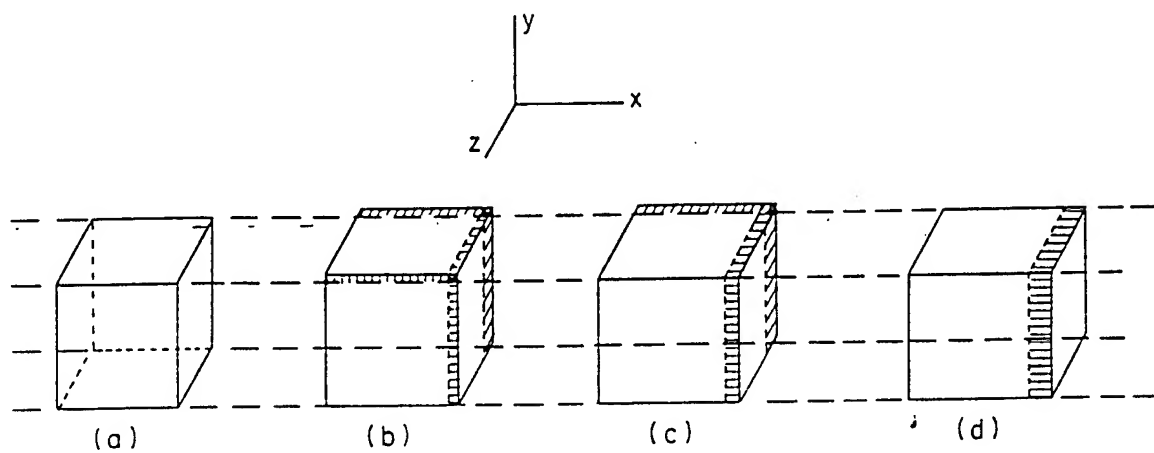


Fig. 1. Steps showing that a longitudinal dilation involves both compressional and shear moduli. See text for description.

Classical Absorption Continued Heat Conduction

Fourier's Law

$$\frac{\partial Q}{\partial t} = (m\kappa/\rho_0) \frac{\partial^2 \theta}{\partial x^2}$$

Some approximations give

$$k_r^2 \approx \omega^2/c_0^2$$

$$\alpha \approx \frac{\omega^2 \kappa}{2c_p \rho_0 c_0^3} (\gamma - 1)$$

(33)

Note reappearance of ω^2 term !

Relaxation Absorption/Dispersion Modes

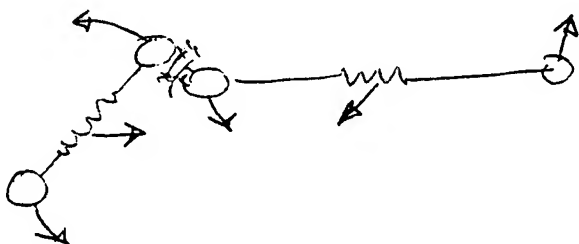
Energy Modes

Translation, Rotation, Vibration

Collision Frequency $\sim 10^{11}$ /second in gas at STP

Translational Relaxation $\gamma_{tr} = 1.25 \gamma_c$

Rotational Relaxation



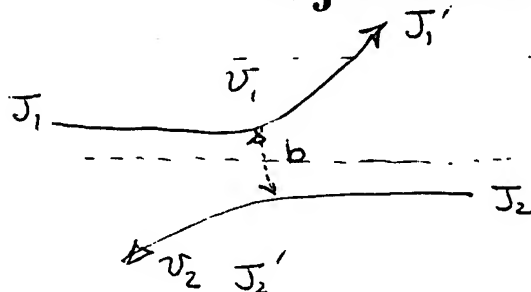
$$Z_{rot}(H_2) \sim 350$$

$$Z_{rot}(N_2) \sim 3 \text{ or } 4$$

\mathcal{P}

$$P_{rot}(1 \rightarrow 2) > P_{rot}(2 \rightarrow 3)$$

Semi-Classical Trajectories



Due to energy spacing



Vibrational Relaxation

$$\left. \begin{array}{l} V-T \\ V-R \\ V-V \end{array} \right\} 10^{12} > z_{vib} > 10$$

Single Relaxation

$$-\frac{dE_v}{dt} = 1/\tau [E_v - E_v(T_r)] \quad (34)$$

$$k_{10} x_1 - k_{01} x_0 = 0 \quad (35)$$

$$(C_v)_{eff} = C_v^\infty + \frac{C'}{1 + i\omega\tau} \quad (39)$$

$$\tau = \frac{1}{k_{10} (1 - e^{-h\nu/kT})} \quad (37)$$

$$\alpha\lambda = \pi (C/C_0)^2 \varepsilon \frac{\omega\tau_s}{1 + (\omega\tau_s)^2} \quad (42)$$

$$(C_0/C)^2 = 1 - \frac{\varepsilon\omega^2\tau_s^2}{1 + \omega^2\tau_s^2} \quad (43)$$

$$\varepsilon = \frac{C_\infty^2 - C_0^2}{C_0^2} \quad \tau_s = [(C_1 + R) / (C_v^\infty + R)] \tau \quad (44)$$

$$f_r = \frac{C_\infty}{C_0} \frac{1}{2\pi\tau_s}$$

Multiple Relaxation

Summary of Absorption Mechanisms

Viscosity

Momentum

Thermal Conduction

Energy

Internal Relaxation

Internal Energy

Relaxation Absorption

The Fun Part!

- - -

Experimental Techniques

Experimental Considerations

Viscous and Thermal Losses in Gas $\propto f^2$

Viscous and Thermal Losses at Walls $\propto f^{1/2}$

Radiation or Leakage - Greater at Low Frequencies

Spreading Losses - 6dB/doubling

Rotational Relaxation $\propto f^2$

= Tough to measure especially in liquids

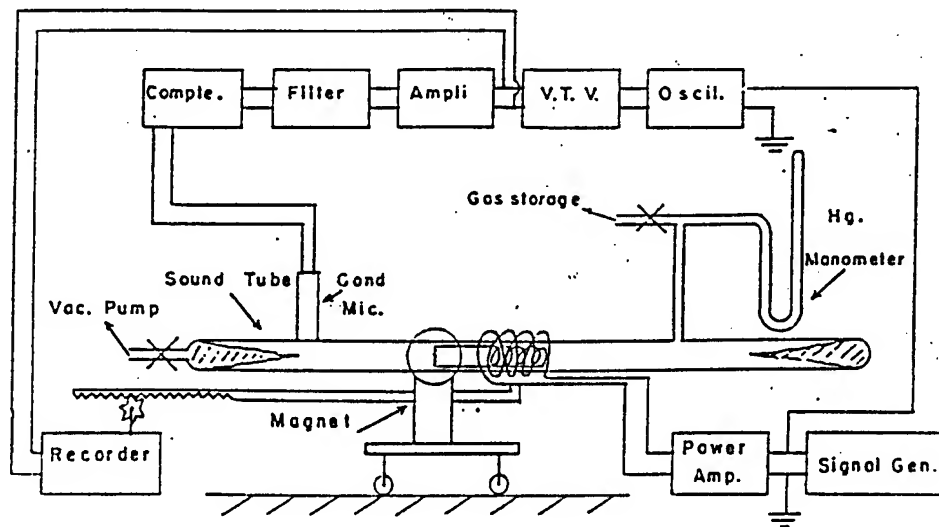


Figure 3. Schematic diagram of the apparatus for measuring the attenuation of sound.

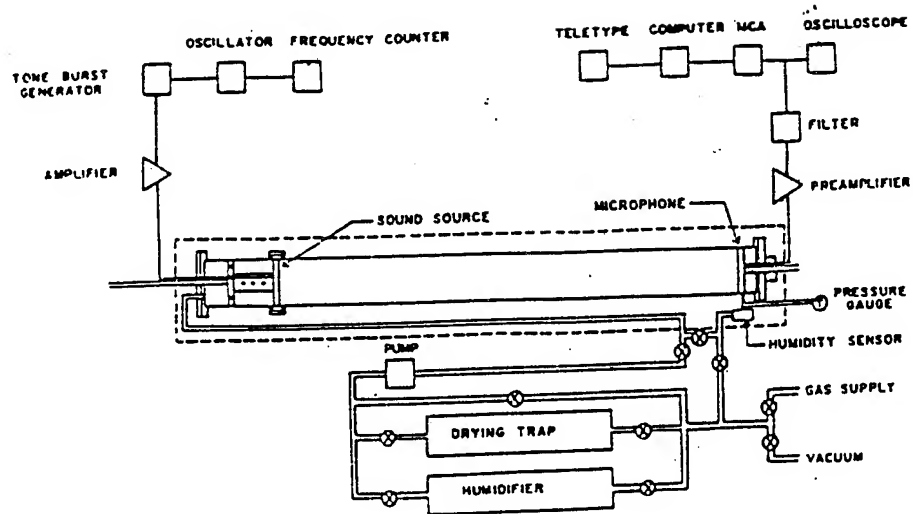
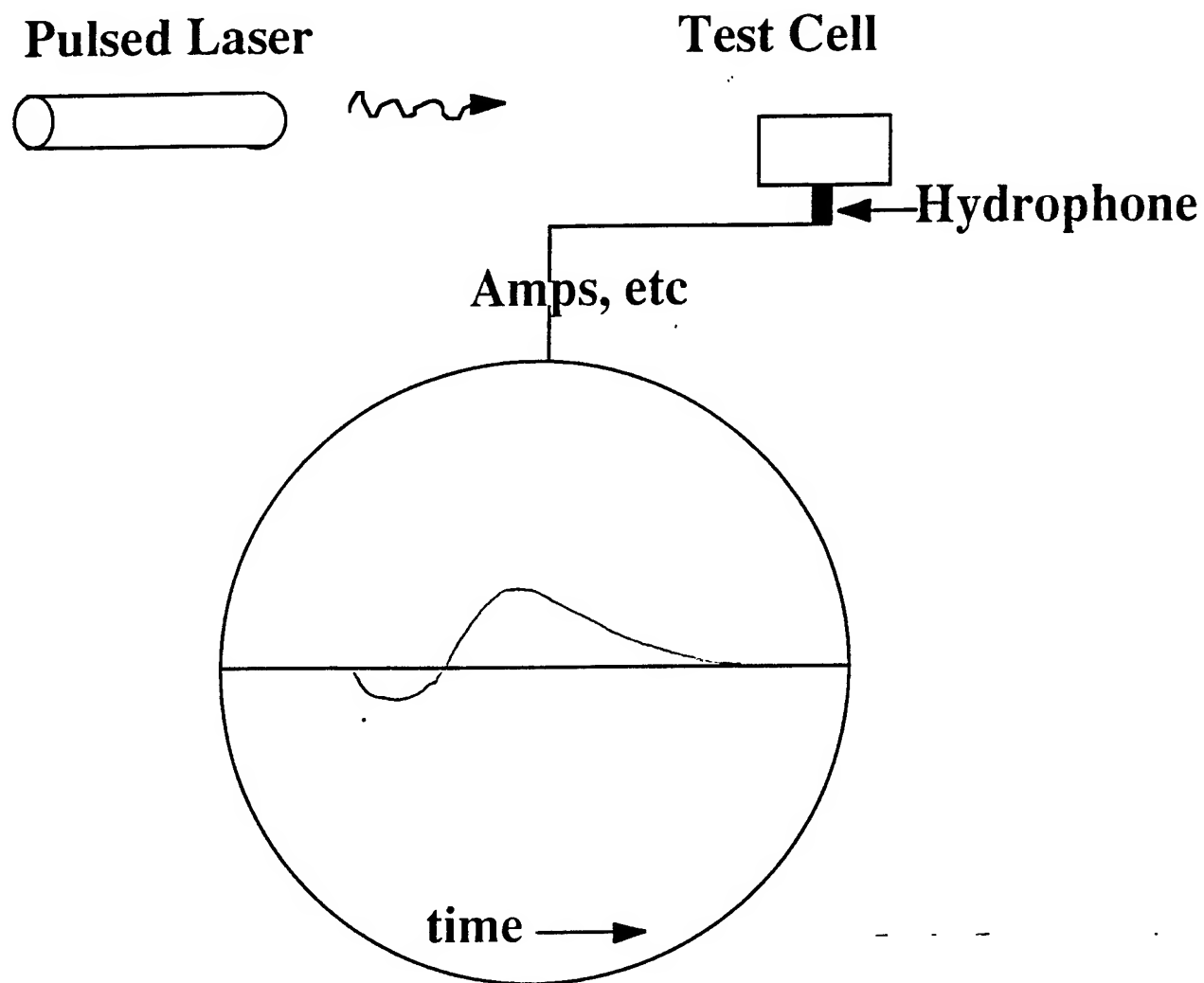


Fig. 4. Diagram of the experimental system for measuring sound absorption.

Spectrophone



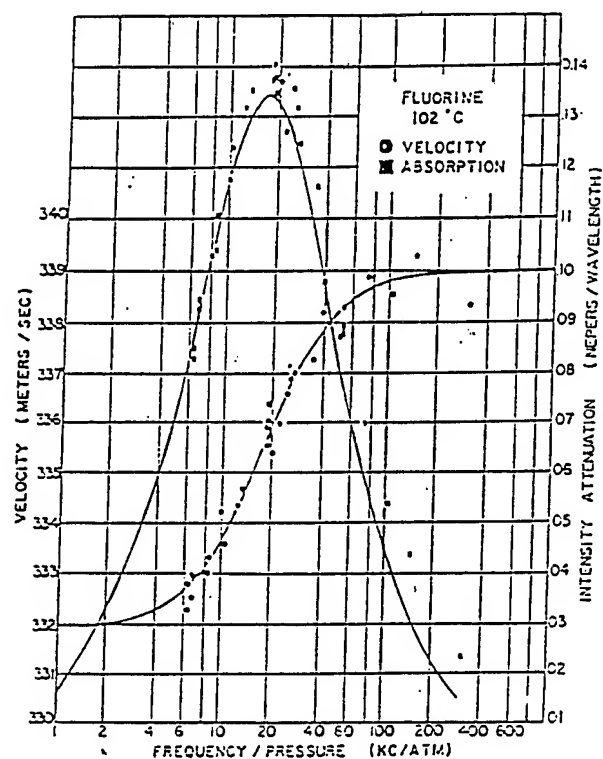


Figure 2 shows typical curves for absorption per wavelength and velocity dispersion to a single relaxation process. The example here is Fl_2 at 102°C. The figure compares curves representing the above theory with measured values.¹¹

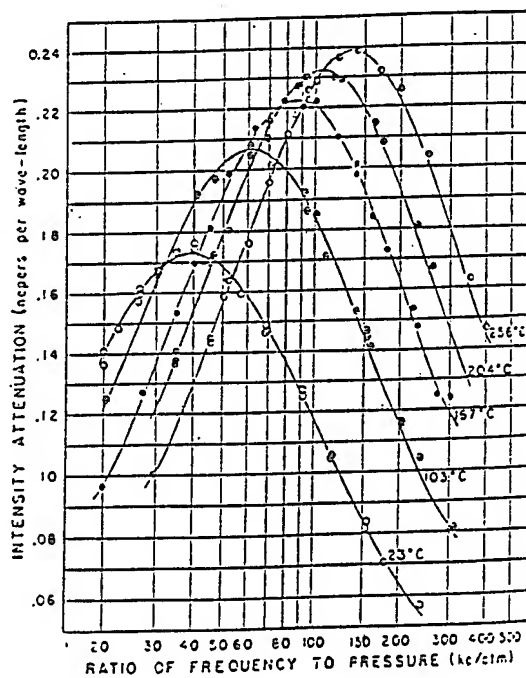


Fig. 5. Relaxation absorption coefficient per wavelength vs log (frequency/pressure) for chlorine. The solid curves are theoretical absorption with values of A_m and f_m adjusted to give the best fit of the experimental points.

SOUND ABSORPTION IN THE HALOGEN GASES

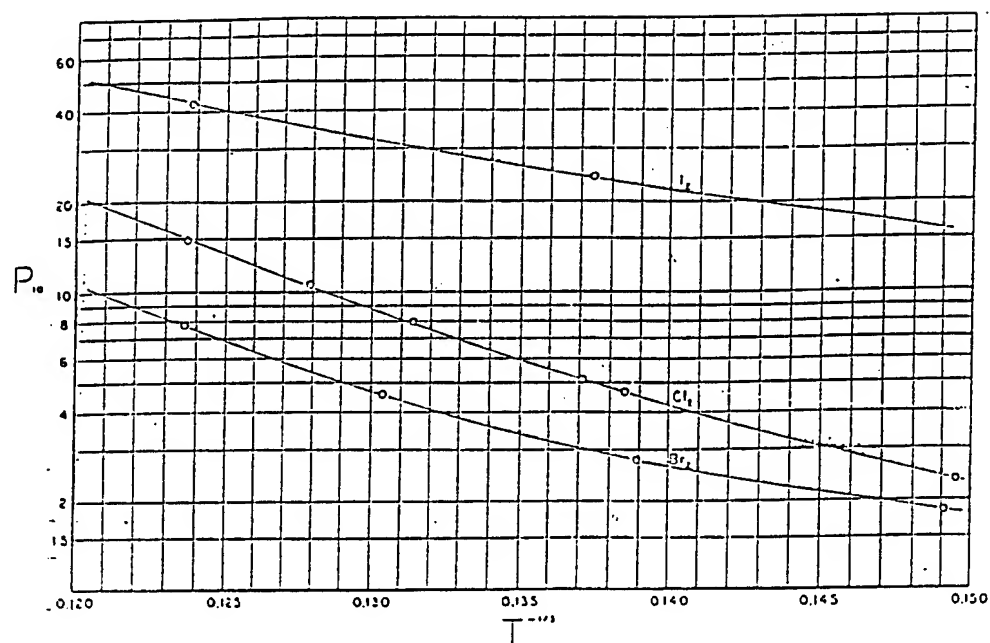


Fig. 6. Log of collision efficiency vs absolute temperature to the minus one-third power. The values of the ordinate should be multiplied by 10^{-5} for Cl_2 and by 10^{-4} for Br_2 and I_2 .

Conclusions from Experiments

$$\log P_{10} \propto T^{-1/3}$$

P_{10} very sensitive to ΔE

P_{10} very sensitive to Δt

P_{10} depends upon geometry of the mode

P_{10} depends upon interaction potential

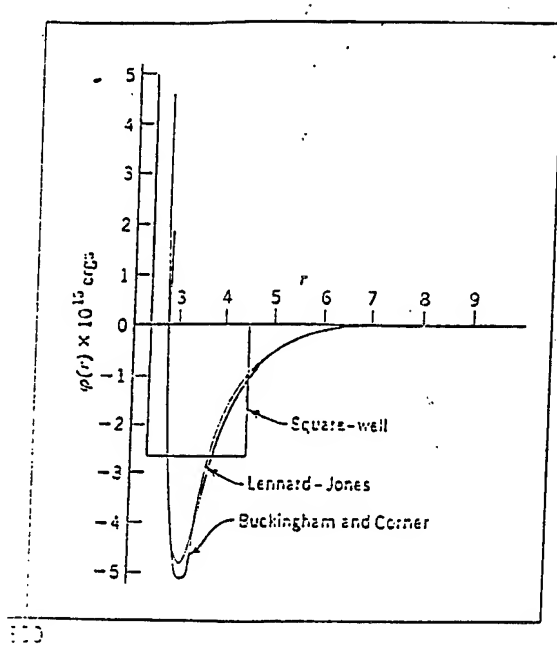


Fig. 7. Potential energy of interaction.

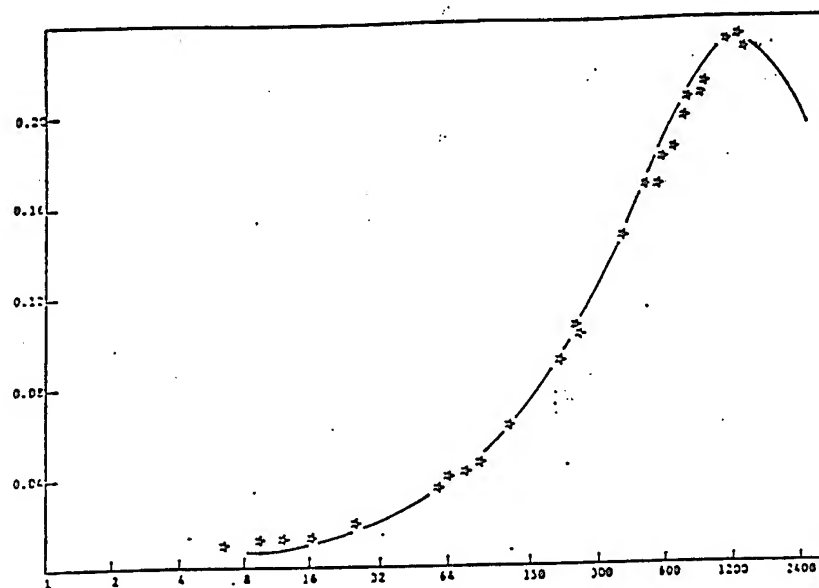


Fig. 8a Relaxation absorption in 75% SO_2 /25% O_2 at 500°K. The solid curve is the theoretical curve for the series relaxation process and was obtained from the transition probabilities in Table II.

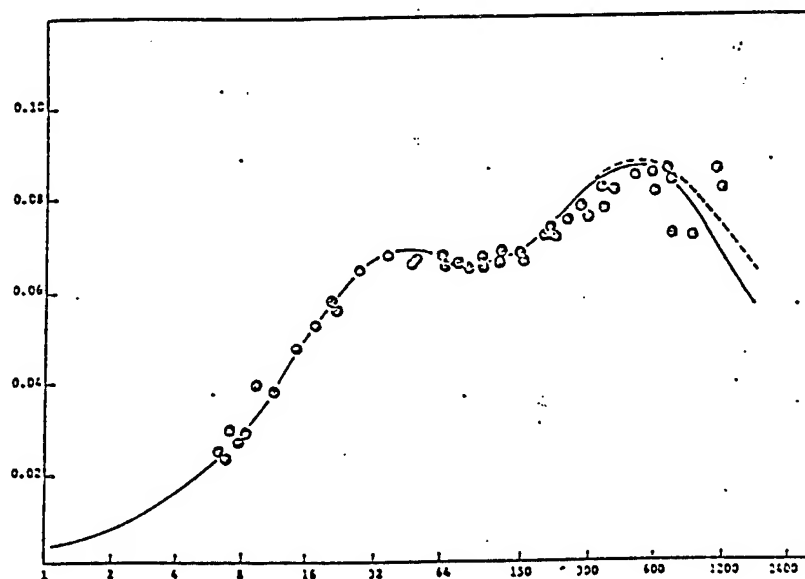


Fig. 8b. Relaxation absorption in 20% SO_2 80% O_2 at 500°K.

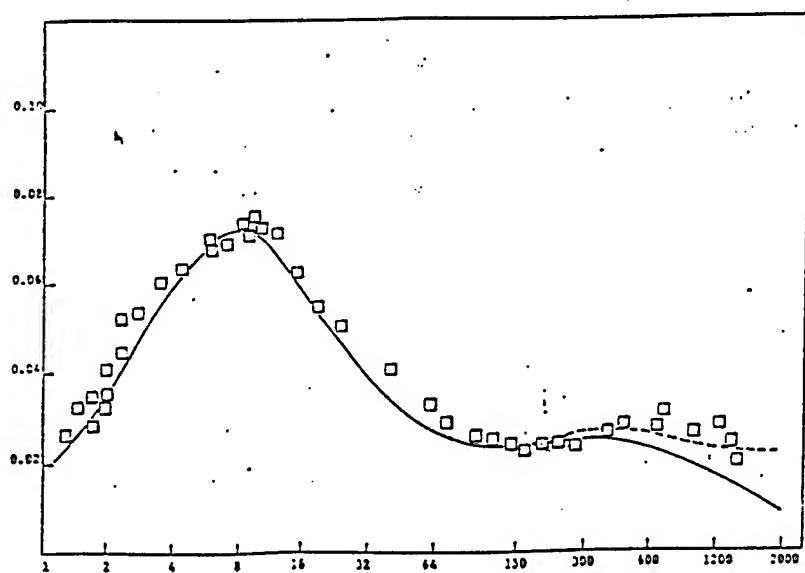
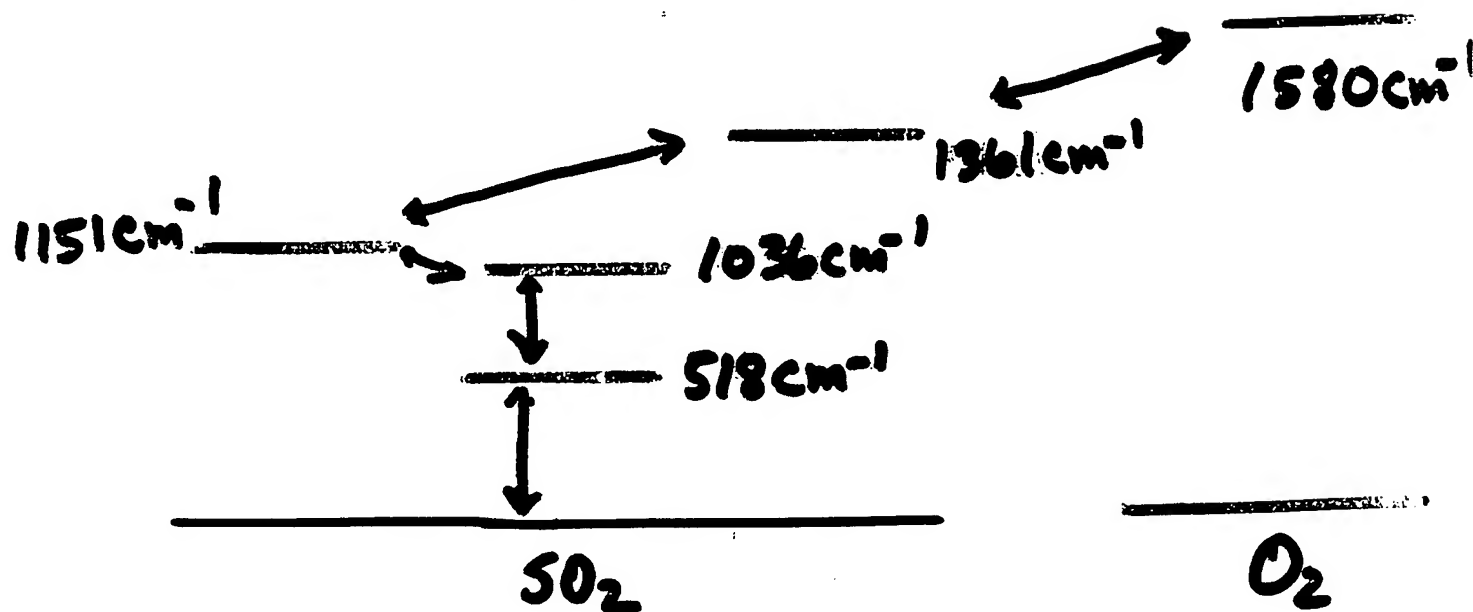


Fig. 8c. Relaxation absorption in 5% SO₂/95% O₂ at 500°K.

Relaxation Studies in SO_2 Energy Level Diagram



Conclusions

Argon 1/10 & O_2 1/4 as effective as SO_2 bend

v-v Coupling with 1361cm^{-1} between SO_2 and O_2

v-t Transfer increases most rapidly with temperature

Relaxation in CS₂

Gas $f_{\max} \sim 370 - 560 \text{ KHz/Atm}$

Liquid $f_c \sim 10^{13}/\text{sec}$

$f_{\max} \sim 10^8/\text{sec}$

$\tau_1 = 22\text{ns}$

$\tau_2 = 30\text{ns}$

Absorption of Sound in Air

$$\alpha_{cl} \approx 5.58 \times 10^{-9} \frac{T/T_0}{T+110.4} f^2 / (P/P_0) \quad (58)$$

$$\alpha_{rot} / \alpha_{cl} = 0.0681 Z_{rot} \quad (65)$$

$$\alpha_{cr} = 1.93 \times 10^{-11} \frac{(T/T_0)^{1/2} f^2}{P/P_0} \quad (69)$$

$$\alpha_{vib,j} = \frac{\pi s_j}{c} \frac{f^2 / f_{r,j}}{1 + (f / f_{r,j})^2} = \frac{4\pi x_j}{35c} \frac{(\theta_j^* / \tau)^2}{(1 - e^{-\theta_j^* / \tau})^2} \cdot \frac{f^2 / f_{r,j}}{1 + (f / f_{r,j})^2} \quad (70)$$

$$f_{r,0} = (P/P_0) \{ 24 + 4.41 \times 10^9 h [(0.05 + h) / 0.391 + h] \} \quad (74)$$

O₂/N₂ V-V

O₂/H₂O V-V

O₂/O₂ or N₂ V-T

CO₂/O₂ V-V

$$f_{r,N} = P/P_0 (9 + 200h) \quad (75)$$

N₂/H₂O V-R or V-V

N₂/N₂ or O₂ V-T

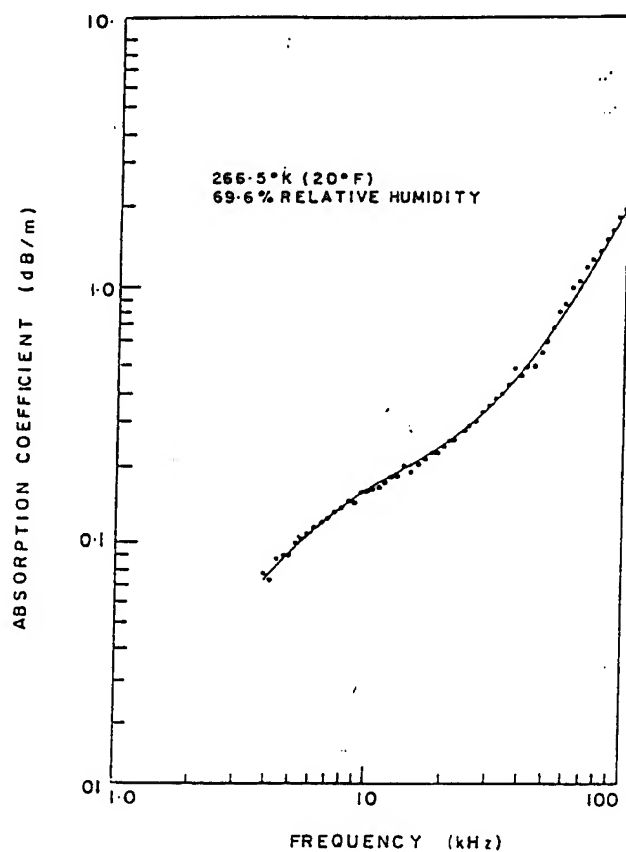


Figure 9. Total free-field sound absorption in air at 266.5° K and 69.9% relative humidity; points represent experimental data; solid line calculated using the computational technique of Ref. 12.

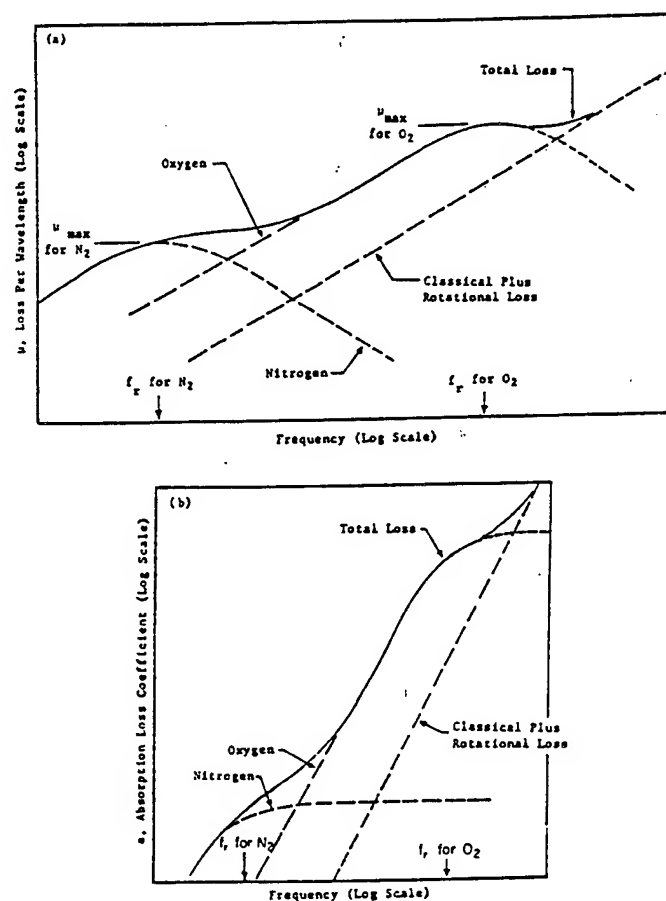
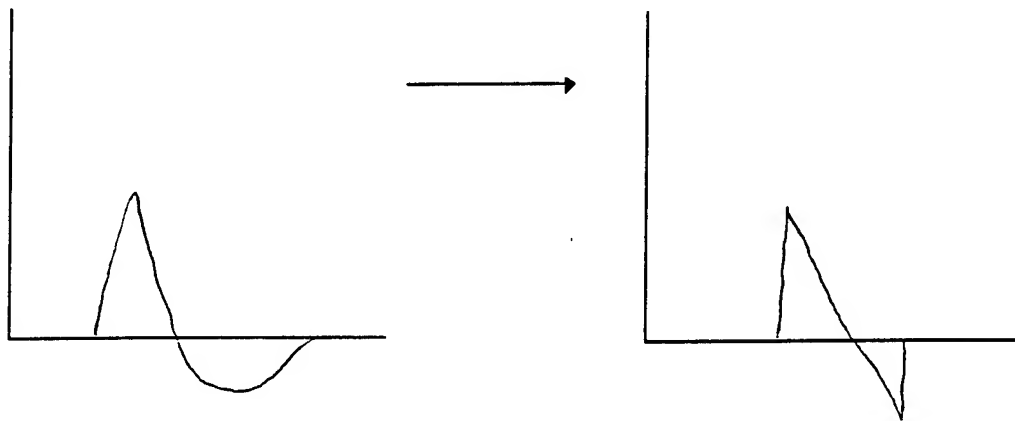


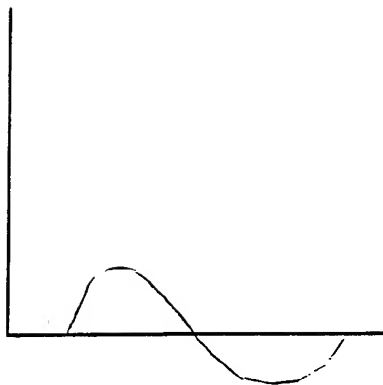
Fig. 8. Components and general behavior of total air absorption in air in terms of (a) loss per wavelength and (b) loss per unit distance:

$$(a) \mu \sim \frac{2(f/f_r)}{1 + (f/f_r)^2}, \quad (b) a \sim \frac{(f/f_r)^2}{1 + (f/f_r)^2}$$

Shock Waves (Sonic Booms)



OR



DIFFUSION ABSORPTION

“ON THE WAVING OF HANDS”

- - -

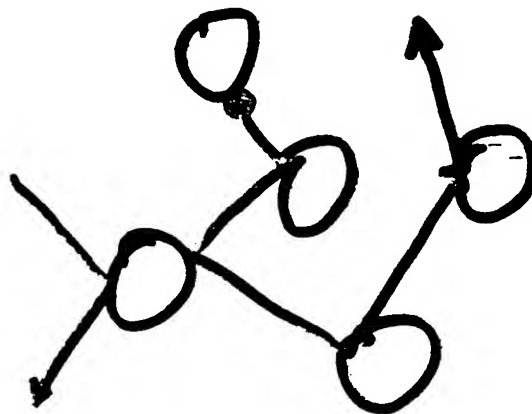
Diffusion

$$\alpha = \frac{2\pi^2 f^2 \gamma X_1 X_2}{\rho C^3} \rho D_{12} \left[\frac{m_2 - m_1}{m} + \frac{(\gamma - 1) kT}{\gamma D_{12} X_1 X_2} \right]^2$$

Let $M_2 - M_1$ get large

Dusty Gas

Biot Solid



Boltzmann's Transport Eq.

Transport described by distribution function $f(c,r,t)$ and its time derivative

$$\frac{\partial f}{\partial t} = -c \text{ grad } f + \underbrace{\frac{\partial f}{\partial t}}_{\text{Collisions}}$$

Collisions

Collisions take f from f to f'

$$\frac{\partial f}{\partial t} + c \text{ grad } f = \int g \sigma (f' f'_i - f f_i) d\Omega dc'$$

Where	1	signifies collision partners
	σ	is the reversible probability
	g	a constant ↑ <i>physics enters here</i>

Solutions are numerous but not exact

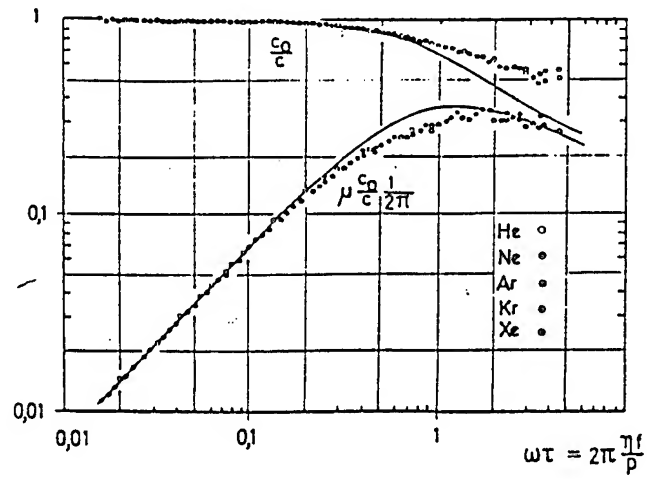


Fig. 10 Sound propagation in monatomic gases (Greenspan).—Kirchhoff–Stokes theory. By courtesy of the author and Academic Press, Inc., New York.

Free Molecule Propagation

$$\frac{\partial f}{\partial t} + c_x \frac{\partial f}{\partial x} = 0$$

Assume vibrating surface

$$\omega = \hat{\omega} \sin \omega t$$

$$f_+(x=0) \neq f_-(x=0)$$

$$k(x) = \frac{\omega}{c_m} \left[1 - j \left(\frac{4}{\pi} - 1 \right) \frac{\omega x}{c_m} - \left(1 - \frac{2\pi}{H} \right) \frac{\omega^2 x^2}{c_m^2} + \dots \right]$$

mean velocity
of molecules

absorption
proportional
to distance

phase velocity
increases with
distance

At large distances,
only fast molecules support propagation

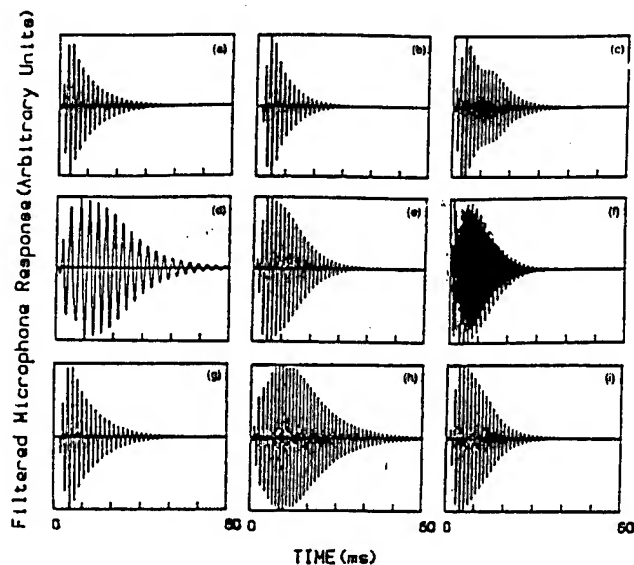


Fig. 11. Filtered microphone response. In moving from the central graph (e), only one of the four variables changes. For (c), (e), and (f) the sound frequency increases; (d) is the fundamental of the 60-cm tube; (e) is the fundamental for the 30-cm tube. Corresponding frequencies are approximately 340, 680, and 1360 Hz. For (b), (e), and (h) the pressure increases from 20 to 40 to 80 Torr. For (a), (e), and (i) and H₂ concentration increases from 0 to 10% to 20%. For (g), (e), and (c) the energy per mole deposited by the discharge in the gas increases from 3700 to 7000 to 9000 J/mol. If all of this energy were to go into vibrations, the corresponding initial vibrational temperatures would be 1600, 2100, and 2400 K.

Energy Conservation

$$\frac{\partial \epsilon}{\partial t} = -(p+q) \frac{\partial 1}{\partial t} + \frac{\partial Q}{\partial t}$$

q = pseudoviscous term

$\frac{\partial Q}{\partial t}$ = rate at which energy is added to or taken from element

Conductivity of plasma

$$\sigma = e^2 n_e \lambda_e (3m_e h T)^{-1/2}$$

λ_e = electron mean free path

$$\sigma = \frac{4.173 \times 10^{-10} (A_1 + A_2) T^{-1/2}}{2 \times 10^{-15} (1 - A_1) + A_1 \langle a \rangle_{av}}$$

A_1 = fraction of atoms which have been ionized

A_2 = fraction of atoms which have lost second electron

$\langle a \rangle_{av}$ = average electron-ion cross section

$$= 2.8 \times 10^{-16} T^{-2} [(A_1 + A_2) / (A_1 + A_2)]^2 \\ \times \log \{ 1.727 \times 10^{-5} [(A_1 + A_2) / (A_1 + 3A_2)] \Gamma(A_1 \rho)^{-1/2} \}$$

Fig. 12. A few equations.

Input

$$I = I_0 (e^{-\alpha t} - e^{-\beta t})$$

$$I_0 = 4 \times 10^4 \text{ A}$$

$$\alpha = 4 \times 10^4 \text{ sec}^{-1}$$

$$\beta = 4 \times 10^5 \text{ sec}^{-1}$$

$$\left(\frac{\partial Q_j}{\partial t} \right) = \frac{E^2 \sigma_j}{\rho_j} \text{ where } j \text{ is a zone outward from center of discharge}$$

Losses

Thermal conduction

Radiative Energy Transport

Bremsstrahlung - Increases as $T^{1/2}$ Black-body type radiation - Increases as T^4

Fig. 13. Energy balance.

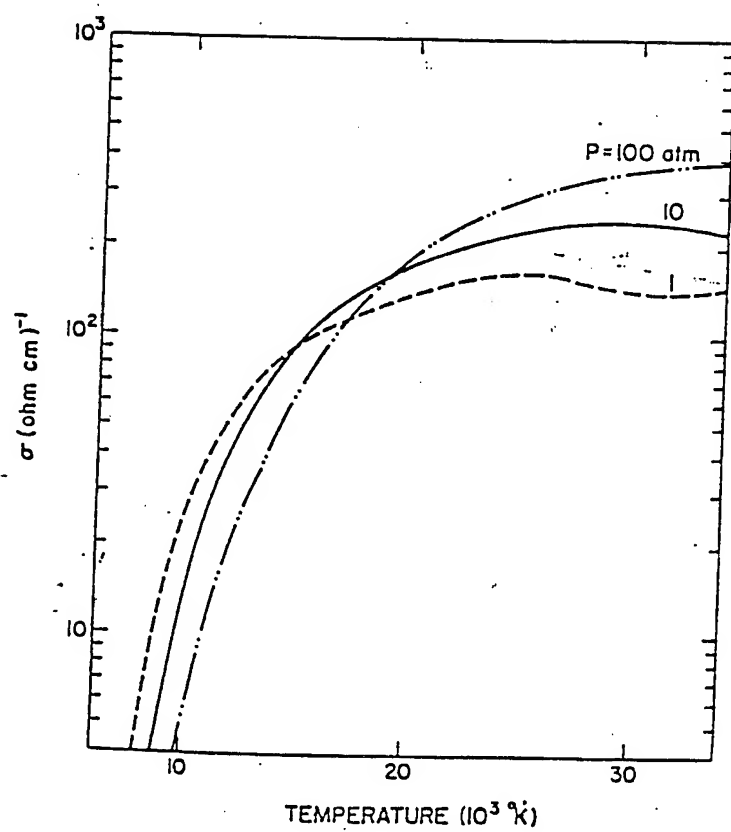


Fig. 14. Computed conductivity.

Typical Lightning Energy $\sim 27 \text{ J/cm} = 2.7 \text{ kJ/m}$

$$E_0 \sim I_0^{1.2}$$

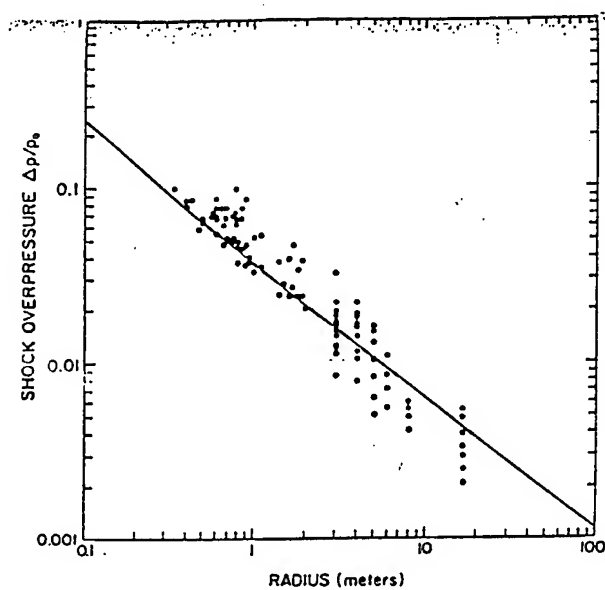


Fig. 15. Sampling of results.

2670

MYRON N. FLOOSTER

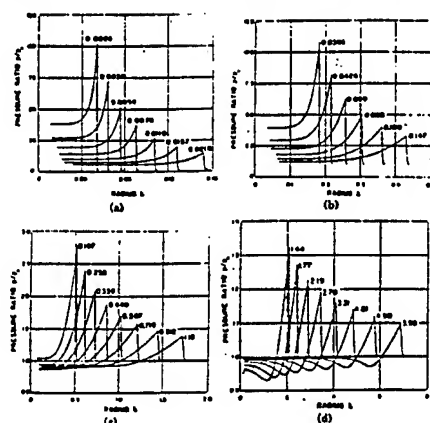


Fig. 2. Pressure ratio, p/p_0 , vs radius r , for a line source of energy in an ideal gas, at indicated times after energy release.

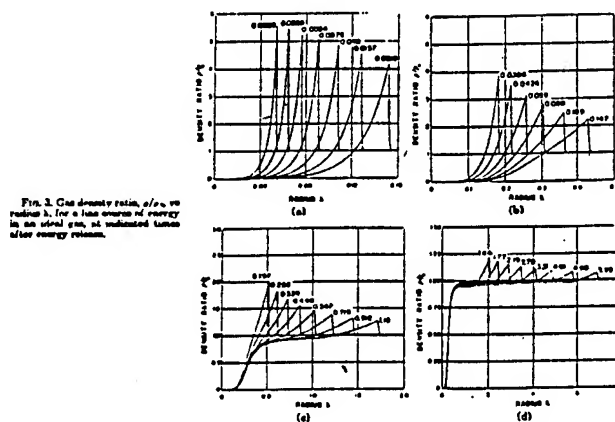


Fig. 3. Gas density ratio, ρ/ρ_0 , vs radius r , for a line source of energy in an ideal gas, at indicated times after energy release.

Fig. 16.

Resonant Ultrasound Spectroscopy

Los Alamos

Los Alamos National Laboratory
Los Alamos, New Mexico 87545

Albert Migliori

Timothy W. Darling

John Sarrao

(Now at Florida State University/NHMFL)

William M. Visscher

J.D. Thompson

Ray Dixon

U.F. Kocks

R.B. Schwartz

Stuart Trugman

David Mandrus

(Now at Oak Ridge National Laboratory)

Paul Johnson

Bob Leisure

Colorado State University

Z. Fisk

Florida State University/NHMFL

Annette Bussman-Holder

Max-Planck

George W. Rhodes

Quatro Corp.

Ming Lei

Quatro Corp.

Hundreds of administrators, the IPC, the STC, Domenici, Bingamen, KOB, dozens of lawyers, the DOE, the New Mexico Highway and Transportation Dept., Quatrosonics Corp., George Rhodes, and many others but I ran out of space!

1. How to do it

2. What it does

3. Non-destructive testing

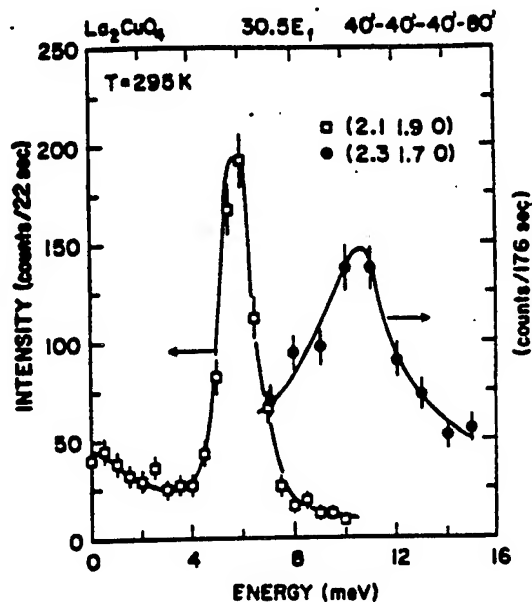


FIG. 4. Spectra of transverse TA_2 phonons measured along $[110]$. The polarization vector is along $[1\bar{1}0]$, i.e., the scattering plane is $(hk0)$ (sample MIT-1).

soft but sharpens significantly. We confirmed by means of additional measurements in other Brillouin zones that this mode has Σ_4 symmetry (in Weber's notation).

Although we expect that the $n=2$ degeneracy is lifted below T_c , we did not observe the expected splitting of the modes, either because the energy resolution of the spectrometer was too coarse or one of the modes renormalizes only weakly and remains buried under the superlattice peak. Further neutron scattering studies are necessary to elucidate this point further.

After identifying the lattice dynamics, which leads to the tetragonal-orthorhombic phase transition, we performed a detailed study of the low-lying phonon branches in order to find evidence for the predicted breathing-mode instability⁴ of the LA mode near the zone boundary. The LA phonons were measured in crystals MIT-1 and MIT-2 using very fine steps in momentum in order to find the instability (see Fig. 3 for some representative scans). The phonons remain sharp and the dispersion has a conventional form, i.e., the LA phonon energy increases monotonically with increasing q . This result is in contrast to an observation in isostructural La_2NiO_4 where the phonon energy decreases near the zone boundary. Moreover,

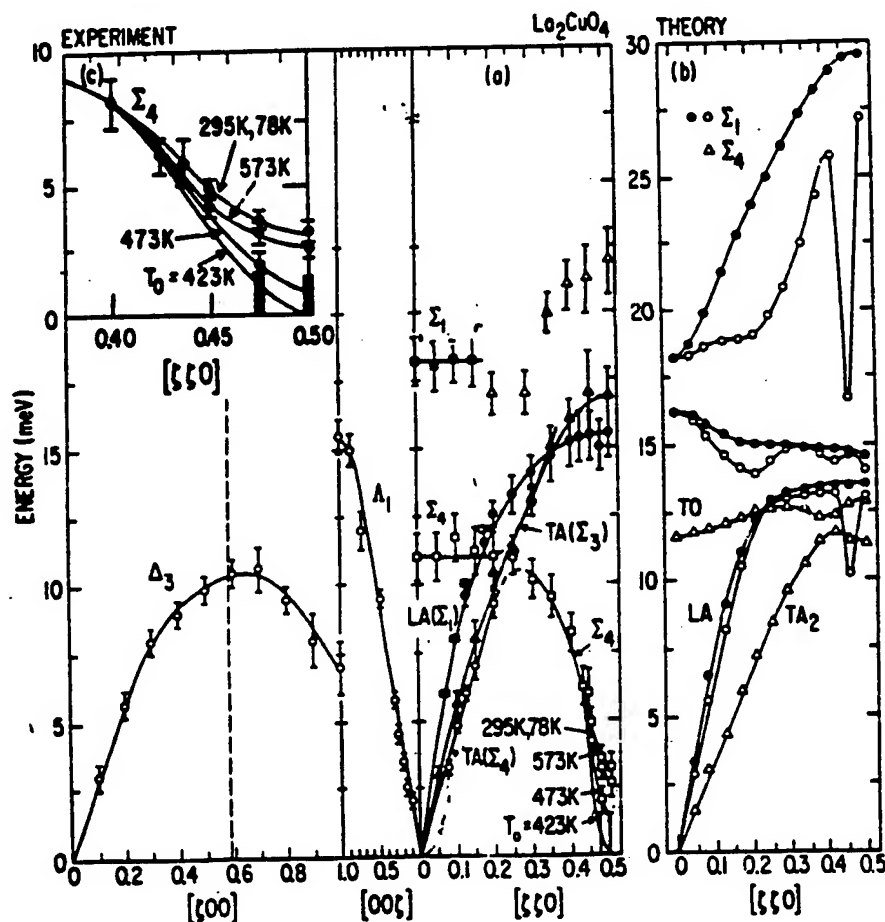


FIG. 5. (a) Summary of the low-lying phonon branches in $La_{2-x}Sr_xCuO_4$ (samples MIT-1 and MIT-2). The lines are guides to the eye. The modes have been labeled according to Ref. 4. The dispersion curves are only weakly temperature dependent, with the exception of the TO phonon near the X point [see inset (c)]. (b) Calculated dispersion curves. Filled symbols show the nonrenormalized energies (bare phonons) and the open circles indicate the phonons with Σ_1 symmetry, which are renormalized by interactions with the conduction electrons. The phonons with Σ_4 symmetry do not renormalize [after Weber (Ref. 4)].

RUS has....

Made significant advances in our understand of the structural phase transition in High Tc materials

Advanced our understanding of the electronic states in new narrow-gap insulators

Provided extensive data on the elastic constants of many new materials for structural and high temperature applications

Generated a new area of measurement science with its own annual conference

Hosted PhD thesis students and postdocs

Generated many patents on the use of resonances for non-destructive testing

Assisted in LANL programmatic efforts involving intelligence and stockpile stewardship

Transferred technology to a private company that now manufactures RUS NDT systems in use on, for example, GM assembly lines.

ELASTIC WAVES

HOOKE'S LAW FOR SMALL DISPLACEMENTS (ISOTROPIC)

$$u_{ik} \cong \frac{1}{2} \left(\frac{\partial u_i}{\partial x_k} + \frac{\partial u_k}{\partial x_i} \right) \quad \text{STRAIN TENSOR}$$

$$W = \frac{1}{2} \lambda u_{ii}^2 + \mu u_{ik}^2 \quad \text{WORK OR FREE ENERGY etc.}$$

REWRITE

$$W = \frac{1}{2} K u_{ii}^2 + \mu \left(u_{ik} - \frac{1}{3} \delta_{ik} u_{ll} \right)^2$$

$$K = \text{BULK MODULUS} = \lambda + \frac{2}{3} \mu$$

$$\mu = \text{SHEAR MODULUS}$$

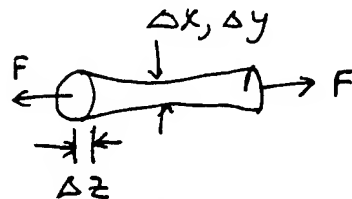
STRESS / STRAIN $\sigma_{ik} = \frac{\partial W}{\partial u_{ik}} \Big|_T$ ↓ DEPENDS ON WHAT YOU WANT

$$W = \frac{1}{2} \sigma_{ik} u_{ik} \quad \begin{array}{l} \text{DEFINES A} \\ \text{STRESS TENSOR} \\ \sigma_{ik} \end{array}$$

ROD



APPLY FORCE F



$$W = \frac{1}{2} \frac{F^2}{E} \quad \boxed{E = \frac{F}{u_{zz}} = \text{YOUNG'S MODULUS}}$$

$$\boxed{u_{xx} = -\sigma u_{zz} \quad \sigma = \text{POISSON'S RATIO}}$$

$$\mu = \frac{E}{2(1+\sigma)} \quad K = \frac{E}{2(1-2\sigma)} \quad \sigma \sim \frac{1}{3} \Rightarrow K \sim E$$

Why study ultrasound?

$$\Delta G = G_{hot} - G_{cold}$$

ΔG is the Gibbs free energy change across a phase boundary

$$\Delta V = \frac{\partial}{\partial P} \Delta G$$

ΔV is the volume change across the boundary, and is zero for second order phase transitions

$$\frac{1}{K_{hot}} - \frac{1}{K_{cold}} = -\frac{1}{V} \frac{\partial \Delta V}{\partial P} = -\frac{1}{V} \frac{\partial^2 \Delta G}{\partial P^2}$$

ΔK is the discontinuity in bulk modulus across the boundary, which ties directly to the speed of sound, and which is not zero for a second order transition

A LITTLE THERMO - SLIGHTLY WRONG

$$\Delta G(H_c, T) = G_n - G_s = \frac{V_s H_c^2}{8\pi} \quad H_c = H_c(T_c)$$

● IF TRANSITION IS SECOND ORDER, $H_c(T_c) = 0!$

ENTROPY, SPECIFIC HEAT

$$\Delta S = -\frac{\partial \Delta G}{\partial T} \Big|_{P,H} = -\frac{V_s H_c}{4\pi} \frac{\partial H_c}{\partial T} \Big|_{P,H}$$

$$T \frac{\partial \Delta S}{\partial T} \Big|_{P,H} = \Delta C_p$$

SPECIFIC HEAT

VOLUME, BULK MODULUS

$$\Delta V = \frac{\partial \Delta G}{\partial P} \Big|_{T,H} = \frac{V_s H_c}{4\pi} \frac{\partial H_c}{\partial P} \Big|_{T,H}$$

$$-V \frac{\partial P}{\partial V} \Big|_{T,H} = \Delta K$$

BULK MODULUS

$$\Delta C_p = -\frac{V_s T}{4\pi} \left[H_c \frac{\partial^2 H_c}{\partial T^2} + \left(\frac{\partial H_c}{\partial T} \right)^2 \right]$$

SPECIFIC HEAT DISCONTINUITY

$$\Delta K = \frac{K_n^2 V_s}{4\pi} \left[H_c \frac{\partial^2 H_c}{\partial P^2} + \left(\frac{\partial H_c}{\partial P} \right)^2 \right]$$

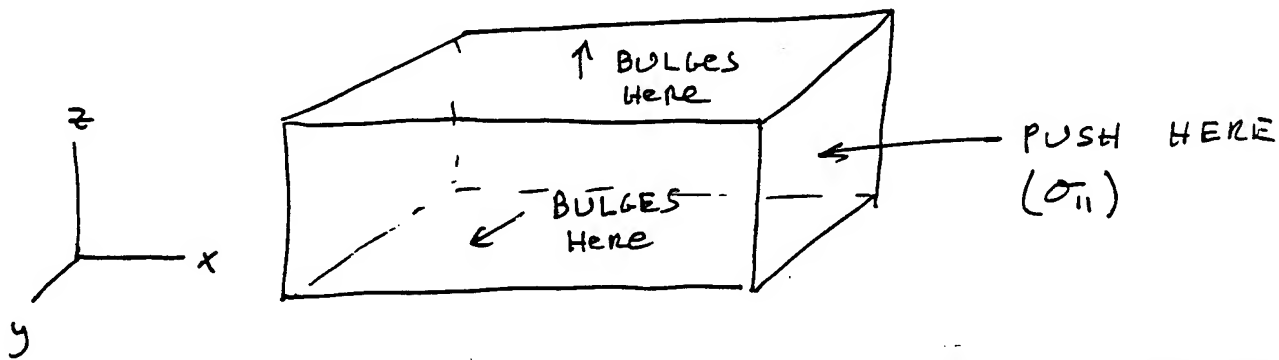
BULK MODULUS DISCONTINUITY

$$\text{ALSO: } \alpha = \text{EXP. COEF.} = \frac{1}{V} \frac{\partial V}{\partial T} \Big|_{P,H} \Rightarrow \Delta \alpha = \frac{1}{4\pi} \left(H_c \frac{\partial^2 H_c}{\partial T \partial P} + \frac{\partial H_c}{\partial T} \frac{\partial H_c}{\partial P} \right)$$

WHATS WRONG?

- USED PRESSURE, VOLUME - NOT STRESS, STRAIN
- IGNORED VOLUME AND STRUCTURAL CHANGES
- WHAT IF $\Delta G = \frac{V_s H_c^2}{8\pi} +$ STRUCTURAL, OTHER MAGNETIC EFFECT?

WHY DO ELASTIC CONSTANTS STRIKE
TERROR INTO THE HEARTS OF PHYSICISTS,
OR WHY IS THIS STUFF SO COMPLICATED?
(CONSIDER ORTHORHOMBIC OR BETTER)



THUS A SIMPLE NORMAL STRESS PRODUCES
THREE STRAINS:

$$1) \frac{\partial u_x}{\partial x}$$

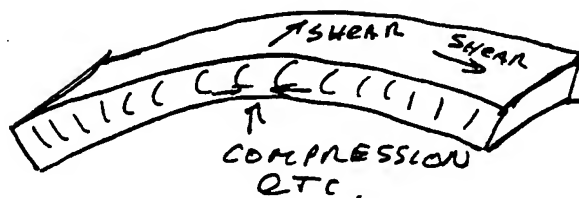
$$2) \frac{\partial u_y}{\partial y}$$

$$3) \frac{\partial u_z}{\partial z}$$

FOR AN ISOTROPIC
BODY,

$$\sigma = - \frac{\text{BULGE}}{\text{SQUISH}} = \text{POISSON'S RATIO}$$

ALSO, A SIMPLE BEND PRODUCES SHEAR



ETC. /

WHY STUDY ELASTIC CONSTANTS?

- $$dF = -SdT + \sigma_{ik} du_{ik}$$

\uparrow
 FREE ENERGY

\uparrow
 STRESS (LIKE PRESSURE)

\nwarrow
 STRAIN (LIKE VOLUME)

- + HOOKE'S LAW : STRESS "PROPORTIONAL" TO STRAIN
- + SYMMETRIES OF REAL OBJECTS
- + WEIRD COLLAPSE OF INDICES

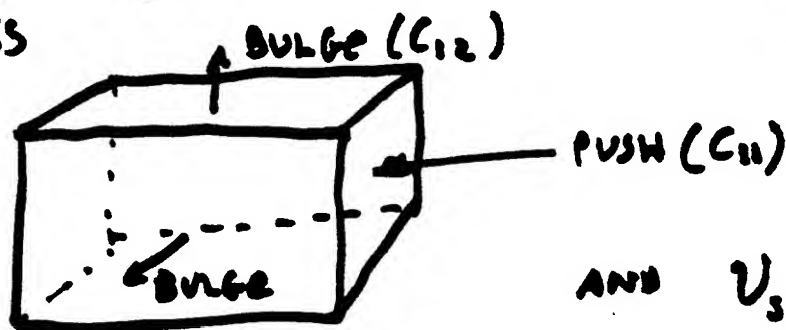
FOR ORTHORHOMBIC SYMMETRY

$$\begin{pmatrix} T_1 \\ T_2 \\ T_3 \\ T_4 \\ T_5 \\ T_6 \end{pmatrix} = \begin{pmatrix} C_{11} & C_{12} & C_{13} & 0 & 0 & 0 \\ C_{12} & C_{22} & C_{23} & 0 & 0 & 0 \\ C_{13} & C_{23} & C_{33} & 0 & 0 & 0 \\ 0 & 0 & 0 & C_{44} & 0 & 0 \\ 0 & 0 & 0 & 0 & C_{55} & 0 \\ 0 & 0 & 0 & 0 & 0 & C_{66} \end{pmatrix} \begin{pmatrix} e_1 \\ e_2 \\ e_3 \\ e_4 \\ e_5 \\ e_6 \end{pmatrix}$$

$\left. \begin{matrix} T_1 \\ T_2 \\ T_3 \\ T_4 \\ T_5 \\ T_6 \end{matrix} \right\}$
 STRESS

$\left. \begin{matrix} e_1 \\ e_2 \\ e_3 \\ e_4 \\ e_5 \\ e_6 \end{matrix} \right\}$
 STRAIN

$\left. \begin{matrix} \text{COMPRESSION} \\ \text{SHEAR} \end{matrix} \right\}$



AND $v_{sound} = \sqrt{\frac{C_{11}}{\rho}}$ etc.

HOW TO USE THIS MESS

ONLY e_1, e_2, e_3 CHANGE VOLUME, THUS
IF WE APPLY A HYDROSTATIC PRESSURE P
WE CAN FIND THE VOLUME CHANGE
AS FOLLOWS

$$\begin{pmatrix} -P \\ -P \\ -P \\ 0 \\ 0 \\ 0 \end{pmatrix} = \begin{pmatrix} C_{11} & C_{12} & C_{13} & & & \\ C_{12} & C_{22} & C_{23} & & & \\ C_{13} & C_{23} & C_{33} & & & \\ & & & C_{44} & & \\ & & & & C_{55} & \\ & & & & & C_{66} \end{pmatrix} \begin{pmatrix} e_1 \\ e_2 \\ e_3 \\ 0 \\ 0 \\ 0 \end{pmatrix} \quad \left. \vphantom{\begin{pmatrix} e_1 \\ e_2 \\ e_3 \\ 0 \\ 0 \\ 0 \end{pmatrix}} \right\} \text{IGNORE}$$

WHERE $\frac{\Delta V}{V} = e_1 + e_2 + e_3$

FOR AN ISOTROPIC BODY

$$C_{12} = C_{13} = C_{23} = \lambda$$

$$C_{44} = C_{55} = C_{66} = \mu$$

$$C_{11} = C_{22} = C_{33} = \lambda + 2\mu$$

$$B = V \frac{\Delta P}{\Delta V} = \lambda + \frac{2}{3}\mu \quad \text{i.e. SHEAR IS INCLUDED}$$

SOUND VELOCITIES

ISOTROPIC

$$v_L = \sqrt{\frac{\lambda + 2\mu}{\rho}} \quad \leftarrow \text{SHEAR AGAIN!}$$

$$v_T = \sqrt{\frac{\mu}{\rho}}$$

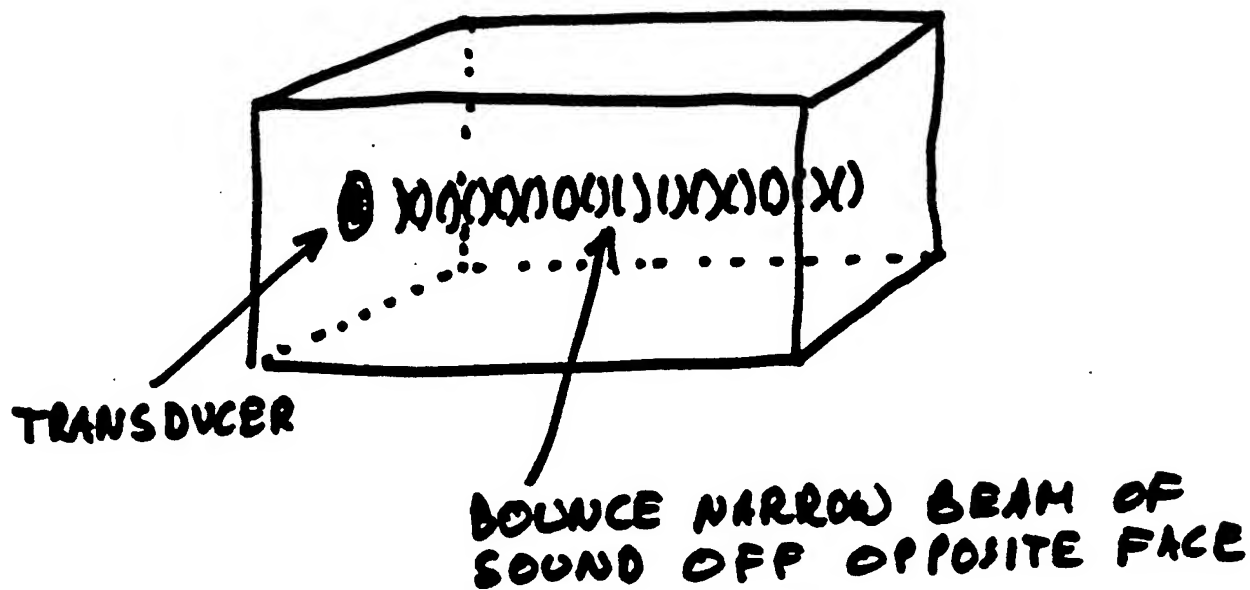
ORTHORHOMBIC

$$v_{L1} = \sqrt{\frac{C_{11}}{\rho}} \quad v_{L2} = \sqrt{\frac{C_{22}}{\rho}} \quad \dots$$

$$v_{L3} = \sqrt{\frac{C_{33}}{\rho}} \quad \text{etc.}$$

WHY RESONANT ULTRASOUND ?

THE USUAL WAY IS PULSE-ECHO



TIME OF FLIGHT, PLANE WAVE SOUND BEAM YIELD, FOR EXAMPLE, $v_s = \sqrt{\frac{E_{II}}{\rho}}$

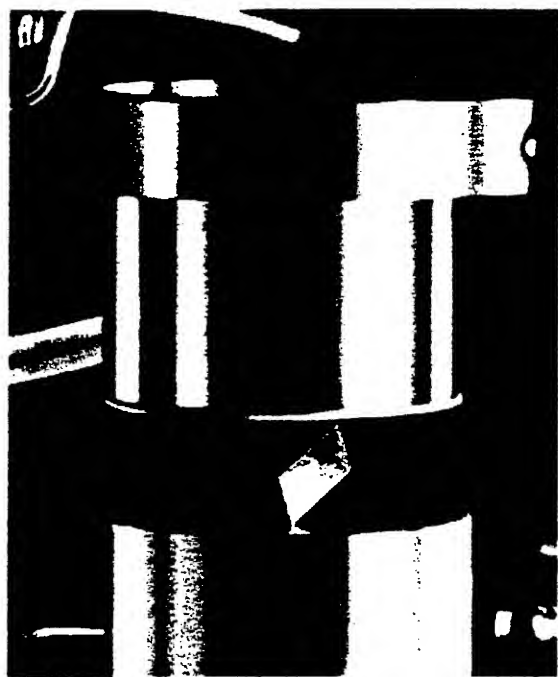
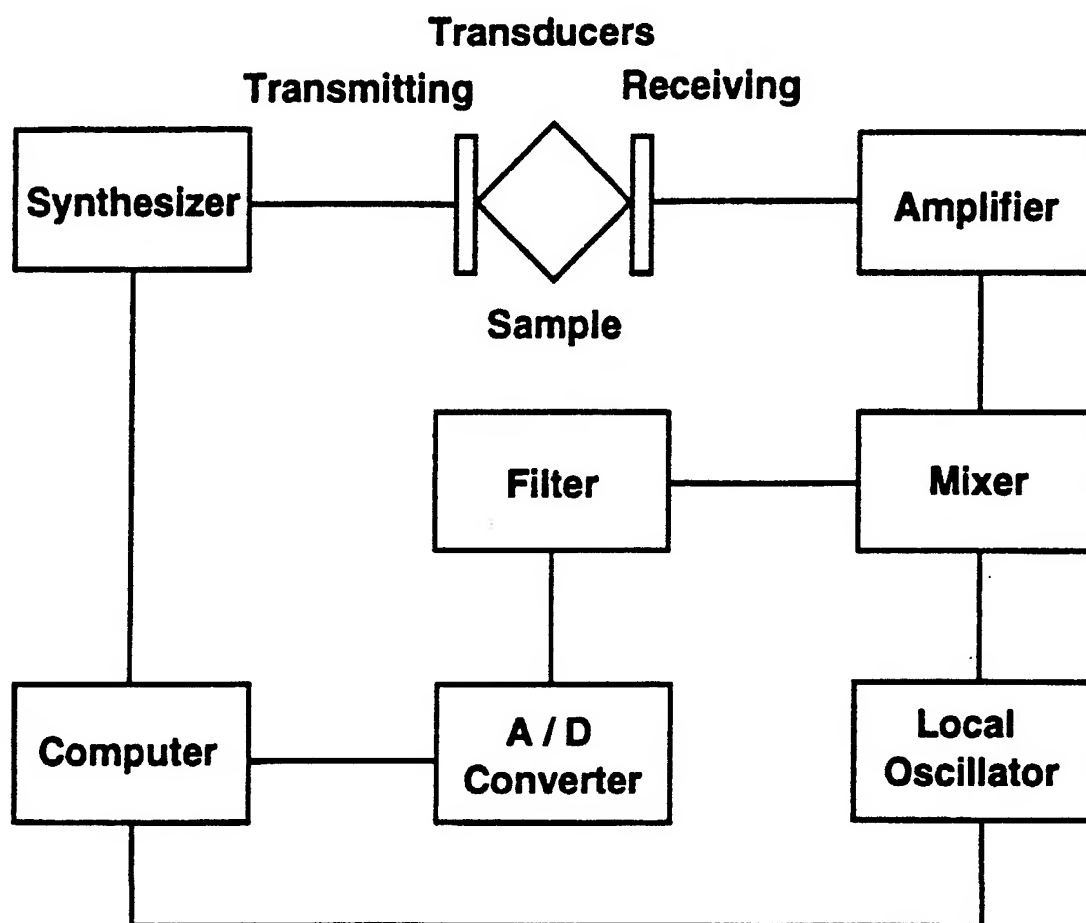
FOR THIS TO WORK, TRANSDUCER AND SAMPLE MUST BE $\gg \lambda_{\text{sound}}$ OR THE SAMPLE BULGES FROM POISSONS RATIO

Signal/noise comparison of pulsed and resonant measurements

parameter	Impulse	Swept Sine
drive power per unit bandwidth	peak power/full bandwidth $10^6/10^9=.001$	peak power/sweep rate $1/100=0.01$
noise bandwidth for complete measurement using optimum receiver	10^9	number of modes x width of each mode x 10= 10^4 Hz
drive duty cycle (typical)	10^{-3}	1
detect duty cycle	1	1
square root of all factors, which is a measure of S/N	3×10^{-7}	10^{-3}

Table I. Signal-to-noise comparison between impulse (pulse-echo) and swept-sine (RUS) resonance measurement methods for a measurement of a 1 cm sample with resonances having a $Q=10^4$, using 10 modes over 0.5 MHz-1.5MHz= 10^6 Hz bandwidth to obtain an elastic modulus. Note that the pulse-echo measurement provides about 0.1% absolute accuracy at best, compared with about 0.01% for the best RUS measurements.

Instrumentation Block Diagram



Low temperature RUS cell with a 2mm rectangular parallelepiped sample set between 2 diamond/LiNbO₃ transducers using no coupling fluids. The force on the sample is equivalent to 1 gm weight. This cell operates between 1K and 400K.

0.0

C:\data\0629.009

T=263.7K PEAK AT .896150MHz F=.896153MHz FWHM=.000030MHz

Amplitude(V)

0.008

0.893

0.894

0.895

0.896

0.897

0.898

Frequency(MHz)

Ultimate accuracy determined by geometry-for a Si_3N_4 ball bearing, geometry errors are less than 1 part in 10^5 . So are the modulus errors!

Table 1

Resonant ultrasound measurement of a 0.63500 cm diameter Si_3N_4 ceramic sphere with a density of 3.2325 g/cm^3 . f_m are measured frequencies, f_r are fitted. n is the mode number. k is our designator (to be discussed below) for the symmetry of the mode and i is in essence the harmonic number of each symmetry type. Multiple entries indicate the mode degeneracy. The fit for $\mu = 1.2374 \times 10^{12} \text{ dyne/cm}^2$ and $\sigma = 0.2703$ has a $\chi^2 (\%) = 0.0124$. This is sufficient to determine μ to about 0.01% and σ to about 0.05%. There are no corrections so these values are absolute.

n	f_r (MHz)	f_m (MHz)	% error	(k, i)
1	0.775706	0.775707	-0.000138	(6, 1), (1, 1), (4, 1), (4, 2), (7, 1)
6	0.819567	0.819983	-0.050778	(5, 1), (3, 1), (5, 2), (8, 1), (2, 1)
11	1.075664	1.075399	0.024614	(1, 2), (7, 2), (6, 2)
14	1.198616	1.198505	0.009239	(5, 3), (2, 2), (3, 2), (8, 2), (3, 3), (8, 3), (2, 3)
21	1.217375	1.217850	-0.039042	(1, 3), (6, 3), (7, 3), (1, 4), (6, 4), (7, 4), (4, 3)
28	1.440760	1.440750	0.000712	(5, 4)
29	1.527080	1.526474	0.039695	(5, 5), (8, 4), (3, 4), (5, 6), (2, 4)
34	1.558358	1.558848	-0.031448	(5, 7), (5, 8), (5, 9), (3, 5), (8, 5), (2, 5), (3, 6), (8, 6), (2, 6)
43	1.580067	1.579871	0.012426	(6, 5), (7, 5), (7, 6), (1, 5), (4, 4), (1, 6), (6, 6), (4, 5), (4, 6)

Determination of high temperature moduli to support the broad DOE initiative in heat treatment distortion

5120 steel - ground parallelepiped

free dimensions are d1, d2, d3 (initial= 0.41205, 0.33973, 0.26380) cm

using 10 order polynomials mass= .2875 gm; density= 7.785 gm/cc

n	f-expt	f-calc	%err	C11 df/d(moduli)	C44
1	.340010	.339607	-.12	.00	1.00
2	.447200	.447109	-.02	.13	.87
3	.490240	.490366	.03	.16	.84
4	.541860	.541482	-.07	.02	.98
5	.557460	.556663	-.14	.00	1.00
6	.591740	.592306	.10	.05	.95
7	.608670	.608417	-.04	.31	.69
8	.615590	.615290	-.05	.02	.98
9	.623100	.622662	-.07	.07	.93
10	.642700	.642897	.03	.12	.88
11	.675510	.676384	.13	.10	.90
12	.683560	.683316	-.04	.05	.95
13	.690650	.690436	-.03	.16	.84
14	.746720	.747335	.08	.10	.90
15	.753860	.754125	.04	.05	.95
16	.827430	.827569	.02	.06	.94
17	.848300	.849153	.10	.03	.97
18	.855320	.854953	-.04	.08	.92
19	.870540	.870865	.04	.12	.88
20	.878390	.878891	.06	.11	.89
21	.882080	.881734	-.04	.33	.67
22	.884870	.884342	-.06	.21	.79
23	.887380	.887639	.03	.20	.80
24	.891190	.891892	.08	.04	.96
25	.916680	.916689	.00	.31	.69

rms error= .0680 %,

Fitted values for elastic constants and dimensions:

Young's Modulus = 30.39×10^6 psi (209.55 GPa)

Shear Modulus = 11.82×10^6 psi (81.50 GPa) Poisson's ratio= 0.285

d1 = 0.4121 cm d2 = 0.3395 cm d3 = 0.2639 cm

Perturbation analysis of error sensitivity : (goodness of fit)

χ^2 increased 2% by the following % changes in independent parameters

C11	C44	d1	d2	d3	
.48	.41	-.42	-.42	-.4	=> errors on fitted values ~ 0.5%

lasrr3.p

La_{1.86}Sr_{0.14}CuO₄ 8/21/91
S.C.

nn, np, it, rho= 6, 10, 1, 6.946	i	fex	fr	%err	wt	k	i	11	33	23	12	44	66
1 0.550101 0.548752 -0.25 0.0 4 1 0.01 0.01 0.00 0.00 0.17 0.33	1	0.550101	0.548752	-0.25	0.0	4	1	0.01	0.01	0.00	0.00	0.17	0.33
2 0.655544 0.653127 -0.37 0.0 4 2 0.01 0.00 0.00 0.00 0.47 0.02	2	0.655544	0.653127	-0.37	0.0	4	2	0.01	0.00	0.00	0.00	0.47	0.02
3 0.767276 0.767542 0.03 1.0 3 1 0.02 0.01 -0.01 0.00 0.00 0.48	3	0.767276	0.767542	0.03	1.0	3	1	0.02	0.01	-0.01	0.00	0.00	0.48
4 0.840904 0.840137 -0.09 1.0 1 1 0.35 0.17 -0.18 0.01 0.01 0.15	4	0.840904	0.840137	-0.09	1.0	1	1	0.35	0.17	-0.18	0.01	0.01	0.15
5 0.842859 0.840724 -0.25 1.0 8 1 0.02 0.01 0.00 0.00 0.48 0.00	5	0.842859	0.840724	-0.25	1.0	8	1	0.02	0.01	0.00	0.00	0.48	0.00
6 0.870588 0.872288 0.20 1.0 2 1 0.02 0.01 -0.01 0.00 0.48 0.00	6	0.870588	0.872288	0.20	1.0	2	1	0.02	0.01	-0.01	0.00	0.48	0.00
7 0.882324 0.882338 0.00 1.0 6 1 0.41 0.03 -0.05 -0.06 0.17 0.00	7	0.882324	0.882338	0.00	1.0	6	1	0.41	0.03	-0.05	-0.06	0.17	0.00
8 0.914348 0.916268 0.21 1.0 7 1 0.31 0.27 -0.24 0.02 0.04 0.10	8	0.914348	0.916268	0.21	1.0	7	1	0.31	0.27	-0.24	0.02	0.04	0.10
9 0.962734 0.985844 0.32 1.0 6 2 0.35 0.06 -0.11 0.01 0.19 0.00	9	0.962734	0.985844	0.32	1.0	6	2	0.35	0.06	-0.11	0.01	0.19	0.00
10 1.017951 1.018350 0.04 1.0 5 1 0.40 0.45 -0.41 0.06 0.00 0.00	10	1.017951	1.018350	0.04	1.0	5	1	0.40	0.45	-0.41	0.06	0.00	0.00
11 1.031479 1.028883 -0.25 1.0 1 2 0.07 0.30 -0.09 0.00 0.14 0.09	11	1.031479	1.028883	-0.25	1.0	1	2	0.07	0.30	-0.09	0.00	0.14	0.09
12 1.064057 1.062296 -0.17 1.0 2 2 0.36 0.04 -0.09 -0.01 0.19 0.01	12	1.064057	1.062296	-0.17	1.0	2	2	0.36	0.04	-0.09	-0.01	0.19	0.01
13 1.070964 1.071351 0.04 1.0 7 2 0.10 0.19 -0.04 -0.01 0.12 0.14	13	1.070964	1.071351	0.04	1.0	7	2	0.10	0.19	-0.04	-0.01	0.12	0.14
14 1.071533 1.072243 0.07 1.0 5 2 0.47 0.31 -0.27 -0.01 0.00 0.00	14	1.071533	1.072243	0.07	1.0	5	2	0.47	0.31	-0.27	-0.01	0.00	0.00
15 1.091915 1.091434 -0.04 1.0 3 2 0.09 0.45 -0.21 0.02 0.04 0.12	15	1.091915	1.091434	-0.04	1.0	3	2	0.09	0.45	-0.21	0.02	0.04	0.12
16 1.101242 1.101298 0.01 1.0 2 3 0.05 0.02 -0.02 0.00 0.21 0.24	16	1.101242	1.101298	0.01	1.0	2	3	0.05	0.02	-0.02	0.00	0.21	0.24
17 1.119834 1.116659 -0.28 1.0 8 2 0.37 0.05 -0.08 -0.02 0.18 0.01	17	1.119834	1.116659	-0.28	1.0	8	2	0.37	0.05	-0.08	-0.02	0.18	0.01
18 0.000000 1.135942 0.00 0.0 5 3 0.63 0.04 -0.02 -0.14 0.00 0.00	18	0.000000	1.135942	0.00	0.0	5	3	0.63	0.04	-0.02	-0.14	0.00	0.00
19 1.163975 1.164571 0.05 1.0 4 3 0.02 0.01 0.00 0.00 0.34 0.13	19	1.163975	1.164571	0.05	1.0	4	3	0.02	0.01	0.00	0.00	0.34	0.13
20 1.186826 1.188038 0.10 1.0 8 3 0.08 0.03 -0.04 0.00 0.19 0.23	20	1.186826	1.188038	0.10	1.0	8	3	0.08	0.03	-0.04	0.00	0.19	0.23
21 1.237561 1.235048 -0.20 1.0 5 4 0.32 0.38 -0.26 0.05 0.00 0.01	21	1.237561	1.235048	-0.20	1.0	5	4	0.32	0.38	-0.26	0.05	0.00	0.01
22 1.264551 1.261810 -0.22 1.0 3 3 0.07 0.06 -0.04 -0.01 0.40 0.01	22	1.264551	1.261810	-0.22	1.0	3	3	0.07	0.06	-0.04	-0.01	0.40	0.01
23 1.296307 1.294200 -0.16 1.0 1 3 0.26 0.33 -0.20 0.01 0.03 0.08	23	1.296307	1.294200	-0.16	1.0	1	3	0.26	0.33	-0.20	0.01	0.03	0.08
24 1.317507 1.316531 -0.07 1.0 7 3 0.30 0.31 -0.20 0.00 0.03 0.06	24	1.317507	1.316531	-0.07	1.0	7	3	0.30	0.31	-0.20	0.00	0.03	0.06
25 1.321605 1.320288 -0.10 1.0 5 5 0.46 0.11 -0.02 -0.07 0.02 0.00	25	1.321605	1.320288	-0.10	1.0	5	5	0.46	0.11	-0.02	-0.07	0.02	0.00
26 1.329940 1.326090 -0.29 1.0 6 3 0.45 0.11 -0.15 -0.02 0.11 0.00	26	1.329940	1.326090	-0.29	1.0	6	3	0.45	0.11	-0.15	-0.02	0.11	0.00
27 1.354530 1.354440 -0.01 1.0 1 4 0.26 0.07 -0.08 -0.02 0.11 0.16	27	1.354530	1.354440	-0.01	1.0	1	4	0.26	0.07	-0.08	-0.02	0.11	0.16
28 1.357242 1.358113 0.06 1.0 7 4 0.24 0.16 -0.15 0.01 0.15 0.09	28	1.357242	1.358113	0.06	1.0	7	4	0.24	0.16	-0.15	0.01	0.15	0.09
29 1.410719 1.410488 -0.02 1.0 6 4 0.27 0.09 -0.09 -0.02 0.24 0.00	29	1.410719	1.410488	-0.02	1.0	6	4	0.27	0.09	-0.09	-0.02	0.24	0.00
30 1.471757 1.474156 0.16 1.0 6 5 0.27 0.15 -0.15 0.01 0.21 0.01	30	1.471757	1.474156	0.16	1.0	6	5	0.27	0.15	-0.15	0.01	0.21	0.01
31 1.510419 1.508057 -0.16 1.0 3 4 0.16 0.02 -0.03 -0.01 0.03 0.34	31	1.510419	1.508057	-0.16	1.0	3	4	0.16	0.02	-0.03	-0.01	0.03	0.34
32 1.511018 1.515919 0.32 1.0 7 5 0.35 0.14 -0.04 -0.06 0.04 0.07	32	1.511018	1.515919	0.32	1.0	7	5	0.35	0.14	-0.04	-0.06	0.04	0.07
33 1.512835 1.516014 0.21 1.0 6 6 0.13 0.04 -0.03 -0.01 0.27 0.11	33	1.512835	1.516014	0.21	1.0	6	6	0.13	0.04	-0.03	-0.01	0.27	0.11
34 1.516509 1.518927 0.16 1.0 1 5 0.23 0.20 -0.09 -0.02 0.14 0.05	34	1.516509	1.518927	0.16	1.0	1	5	0.23	0.20	-0.09	-0.02	0.14	0.05
35 1.564802 1.560320 -0.29 1.0 1 6 0.11 0.06 -0.03 -0.01 0.27 0.10	35	1.564802	1.560320	-0.29	1.0	1	6	0.11	0.06	-0.03	-0.01	0.27	0.10
36 1.566096 1.567781 0.11 1.0 5 6 0.23 0.21 0.01 0.02 0.03 0.00	36	1.566096	1.567781	0.11	1.0	5	6	0.23	0.21	0.01	0.02	0.03	0.00
37 1.586001 1.585657 -0.02 1.0 8 4 0.15 0.09 -0.06 -0.01 0.31 0.01	37	1.586001	1.585657	-0.02	1.0	8	4	0.15	0.09	-0.06	-0.01	0.31	0.01
38 1.592957 1.590255 -0.17 1.0 4 4 0.14 0.06 -0.06 0.00 0.15 0.22	38	1.592957	1.590255	-0.17	1.0	4	4	0.14	0.06	-0.06	0.00	0.15	0.22
39 1.599764 1.600863 0.07 1.0 2 4 0.16 0.10 -0.07 -0.01 0.19 0.13	39	1.599764	1.600863	0.07	1.0	2	4	0.16	0.10	-0.07	-0.01	0.19	0.13
40 1.607484 1.610029 0.16 1.0 3 5 0.17 0.19 -0.16 0.03 0.22 0.06	40	1.607484	1.610029	0.16	1.0	3	5	0.17	0.19	-0.16	0.03	0.22	0.06
41 1.608641 1.611600 0.18 1.0 5 7 0.17 0.24 -0.14 0.01 0.07 0.16	41	1.608641	1.611600	0.18	1.0	5	7	0.17	0.24	-0.14	0.01	0.07	0.16
42 1.628330 1.628521 0.01 1.0 7 6 0.09 0.05 -0.03 0.00 0.27 0.12	42	1.628330	1.628521	0.01	1.0	7	6	0.09	0.05	-0.03	0.00	0.27	0.12
43 1.635094 1.639071 0.24 1.0 8 5 0.20 0.11 -0.08 -0.01 0.18 0.11	43	1.635094	1.639071	0.24	1.0	8	5	0.20	0.11	-0.08	-0.01	0.18	0.11
44 1.672216 1.674642 0.15 1.0 2 5 0.15 0.11 -0.06 -0.01 0.30 0.01	44	1.672216	1.674642	0.15	1.0	2	5	0.15	0.11	-0.06	-0.01	0.30	0.01
45 1.738091 1.735809 -0.13 1.0 4 5 0.13 0.08 -0.06 0.00 0.26 0.07	45	1.738091	1.735809	-0.13	1.0	4	5	0.13	0.08	-0.06	0.00	0.26	0.07
46 1.740325 1.743251 0.17 1.0 5 8 0.28 0.04 -0.05 -0.02 0.25 0.01	46	1.740325	1.743251	0.17	1.0	5	8	0.28	0.04	-0.05	-0.02	0.25	0.01
47 1.775364 1.775280 0.00 1.0 4 6 0.12 0.07 -0.03 -0.01 0.27 0.08	47	1.775364	1.775280	0.00	1.0	4	6	0.12	0.07	-0.03	-0.01	0.27	0.08
48 1.782064 1.779391 -0.15 1.0 7 7 0.26 0.10 -0.10 -0.01 0.12 0.13	48	1.782064	1.779391	-0.15	1.0	7	7	0.26	0.10	-0.10	-0.01	0.12	0.13
49 0.000000 1.818747 0.00 0.0 3 6 0.07 0.02 -0.02 0.00 0.02 0.41	49	0.000000	1.818747	0.00	0.0	3	6	0.07	0.02	-0.02	0.00	0.02	0.41
50 0.000000 1.822177 0.00 0.0 5 9 0.28 0.06 -0.07 -0.01 0.07 0.17	50	0.000000	1.822177	0.00	0.0	5	9	0.28	0.06	-0.07	-0.01	0.07	0.17
51 0.000000 1.826381 0.00 0.0 1 7 0.28 0.07 -0.08 -0.02 0.07 0.18	51	0.000000	1.826381	0.00	0.0	1	7	0.28	0.07	-0.08	-0.02	0.07	0.18

orthorhombic elastic constants (c11,c22,c33,c23,c13,c12,c44,c55,c66):

2.65932 2.65932 2.58209 0.99080 0.99080 0.63820
0.67740 0.67740 0.58697

dimensions

0.11436 0.12371 0.10992

mass error = 0.00000e+00 %

rms= 0.16522 percent

chisquare increased 2% by % change in x's of

-0.25 -0.14 -0.66 -1.70 0.01 -0.01 0.00 0.00 0.00

chisquare increased 2% by % change in x's of

0.06 -0.31 -0.28 0.53 0.00 0.02 0.00 0.00 0.00

chisquare increased 2% by % change in x's of

-0.12 0.03 -0.13 0.39 0.05 0.00 0.00 0.00 0.00

xohmrq61 ctss time 82.350 seconds

cpu= 66.355 i/o= 7.158 mem= 8.837

all done

Elastic constants of copper. B represents bulk modulus.

	Single crystal		Polycrystal (wire-drawn)	
c_{ij} (GPa)	Literature average	Measured ^a	RP	Cylinder
c_{11}	168.75	170.88	193.61	194.25
c_{33}			205.88	203.98
c_{12}	122.14	124.63	105.65	106.84
c_{13}			95.00	95.93
c_{44}	75.48	74.01	39.35	39.46
c_{66}			43.98	43.71
B	137.68	140.05	131.65	132.84

^aCrystal rotated 45.4° about [100].

Elastic constants of tantalum at room temperature.

T (K)	ρ (g/cm ³)	c_{11} (GPa)	c_{12} (GPa)	c_{44} (GPa)
300 ¹	16.678	266.7	160.8	82.5
300 ¹	16.678	266.8	161.4	82.5
300 ²	16.633	260.9	157.4	81.8
298 ³	16.626	260.2	154.5	82.6
295 ⁴	16.641	266.3	160.5	82.8

¹D.I. Bolef, J. Appl. Phys. **33**, 2311 (1962).

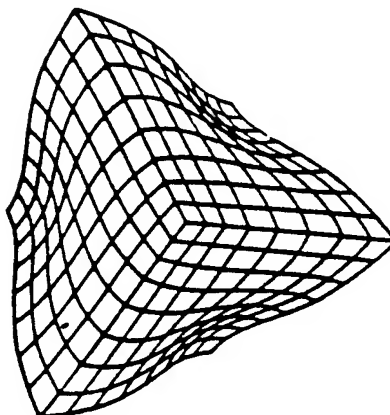
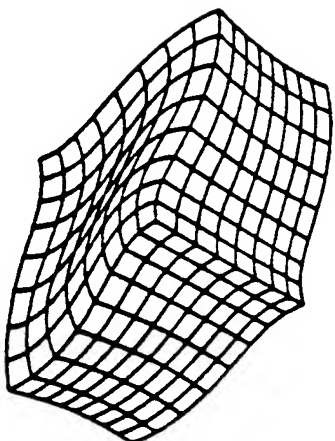
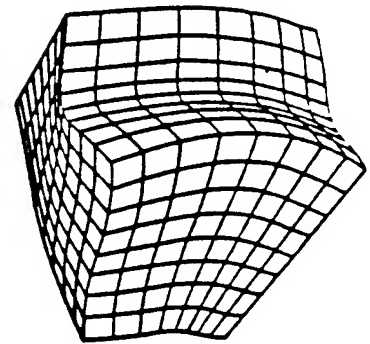
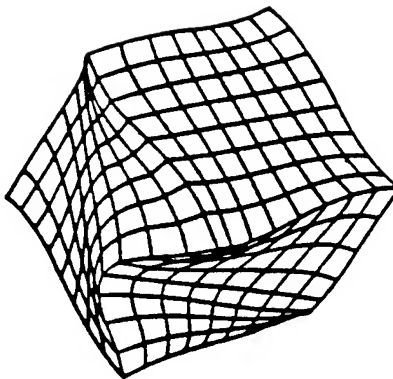
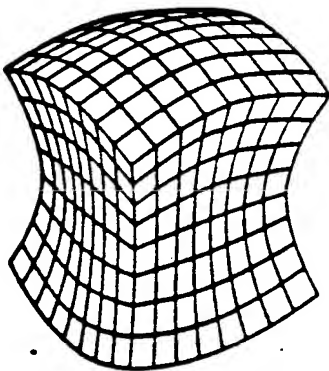
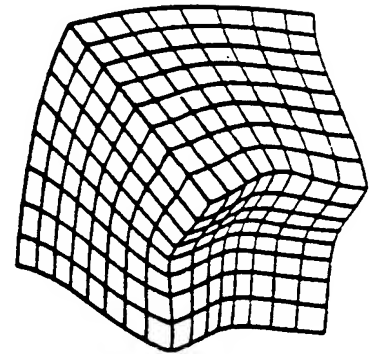
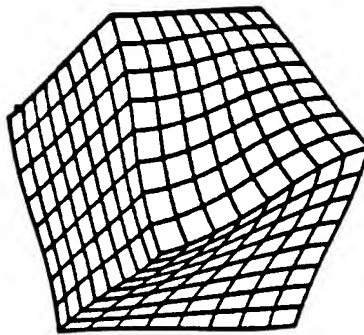
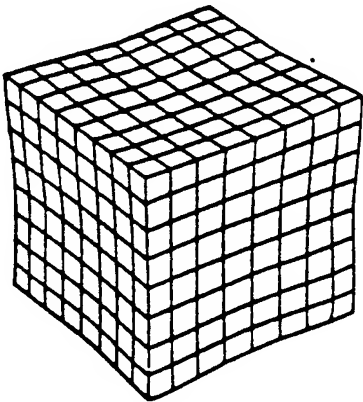
²F.H. Featherstone and J.R. Neighbours, Phys. Rev. **130**, 1324 (1963).

³N. Soga, J. Appl. Phys. **37**, 3416 (1966).

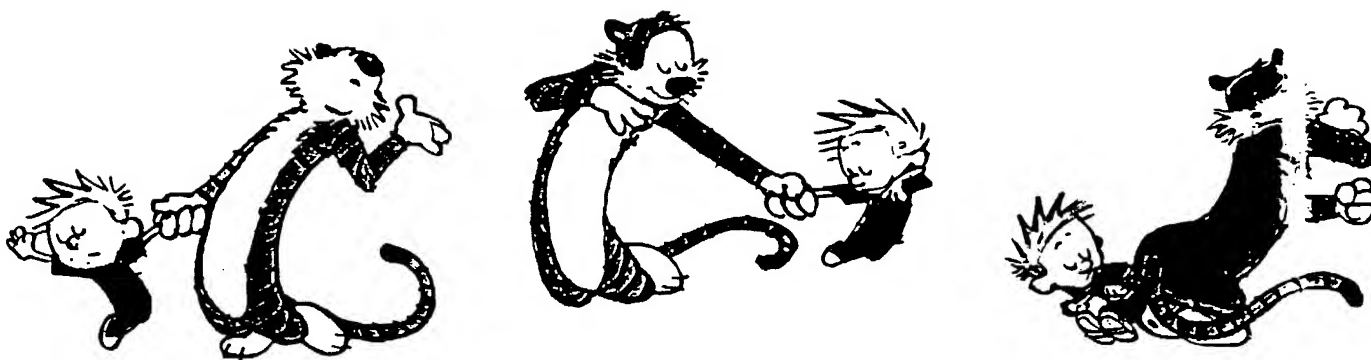
⁴Euler angles (defined in Roe's convention) were determined to be $\alpha = 138.3^\circ$, $\beta = 29.7^\circ$, and $\gamma = 155.1^\circ$ by RUS and $\alpha = 135^\circ$, $\beta = 33^\circ$, and $\gamma = 158^\circ$ by X-ray.

Vibrations of a Rectangular Parallelepiped

- *Not a plane wave among them
- *Sufficiently complex to provide all the elastic moduli
- *Completely understood mechanics problem



The "Calvin and Hobbes" model of the vibrations of a rectangular parallelepiped



John William Strutt, the Baron Rayleigh tried to do this computation. Without a 90MHz Pentium, he found that

In the case of a short rod and of a particle situated near the cylindrical boundary, this lateral motion would be comparable in magnitude with the longitudinal motion, and could not be overlooked without risk of considerable error.

226. The problem of a rectangular plate, whose edges are free, is one of great difficulty, and has for the most part resisted attack¹.

Even with a Pentium, if you try this using finite element methods, the computation time goes like the cube of the numerical accuracy and you can't compute as well as you can measure in a reasonable time on a reasonable computer. However, if you are careful, and smart, as were Orson Anderson and his postdoc Harold Demarest at Bell labs 30 years ago, then.....

Computation of resonances

from Migliori et.al. Physica B **183**,1,1993

The procedure for solving the direct problem for an arbitrarily shaped elastic solid with volume V , elastic tensor c_{ijkl} , density ρ , and with a free surface S begins with the Lagrangian

$$L = \int_V (\text{KE} - \text{PE}) dV \quad (4)$$

where the kinetic energy, KE, is given by

$$\text{KE} = \frac{1}{2} \rho \omega^2 u_i^2, \quad (5)$$

and the potential energy, PE, by

$$\text{PE} = \frac{1}{2} c_{ijkl} u_{i,j} u_{k,l}. \quad (6)$$

Following Hamilton, we allow u_i to vary arbitrarily in the volume V and on the surface S ($u_i \rightarrow u_i + \delta u_i$) and calculate the variation δL in L . The result is

$$\begin{aligned} \delta L = & \int_V (\text{left side of eq. (8)})_i \delta u_i dV \\ & + \int_S (\text{left side of eq. (9)})_i \delta u_i dS \end{aligned} \quad (7)$$

The immediate results are two equations, the elastic wave equation and the vanishing of surface traction

$$\rho \omega^2 u_i + c_{ijkl} u_{k,lj} = 0, \quad (8)$$

$$n_j c_{ijkl} u_{k,l} = 0 \quad (9)$$

where $\{n_i\}$ is the unit outer normal to S .

Because of the arbitrariness of δu_i in V and on S , the u_i 's which correspond to stationary points of L (i.e. $\delta L = 0$) must satisfy eq. (8) in V and eq. (9) on S . There are no such u_i 's, of course, unless ω^2 is one of a discrete set of eigenvalues, the normal mode frequencies of free vibration of the system.

Following the Rayleigh–Ritz prescription, we expand the displacement vector in a complete set of functions $\{\Phi_\lambda\}$,

$$u_i = a_{\lambda i} \Phi_\lambda, \quad (10)$$

and choose as our basis functions powers of cartesian coordinates:

$$\Phi_\lambda = x^l y^m z^n, \quad (11)$$

where $\lambda = (l, m, n)$ is the function label, a set of three nonnegative integers. After substituting eq. (10) into eq. (4), we obtain (\mathbf{a} becomes a column vector)

$$L = \frac{1}{2} \omega^2 \mathbf{a}^T \mathbf{E} \mathbf{a} - \frac{1}{2} \mathbf{a}^T \mathbf{\Gamma} \mathbf{a} \quad (12)$$

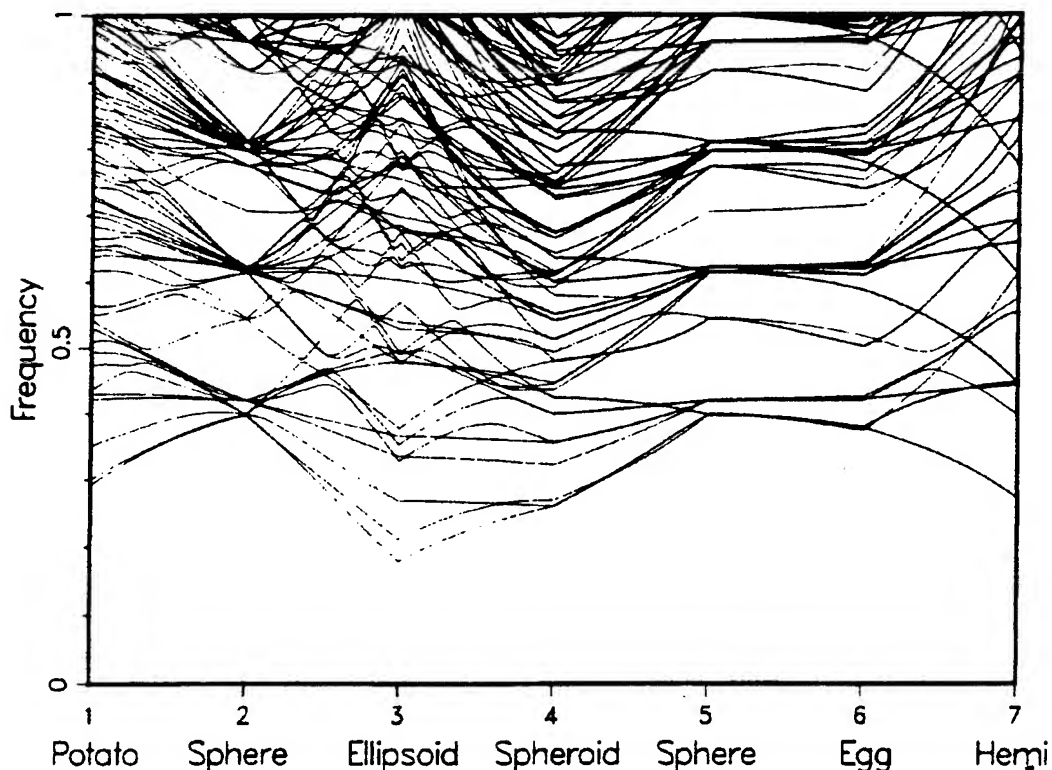


FIG. 8. Frequency spectra of a number of objects in the potato family. The seven stations correspond to shapes as labeled, with semiaxes as given in Table II. The sphere frequencies agree well with those in the literature for these material parameters (Poisson's ratio = $1/4$).²⁰ The dimensional parameters $d_{1+}, d_{1-}, \dots, d_{3-}$ are interpolated linearly between the seven stations here. Several interesting features invite comment. First, the potato has no degenerate lines, because of its low symmetry, and the sphere, conversely, has few lines that are nondegenerate. The ellipsoid has no degeneracies, and the spheroid, the egg, and the hemisphere (all being rotationally symmetric) do, but never more than doubly degenerate lines. Small deviations from the sphere in the egg direction do not change any of the frequencies to first order, because d_{3+} increases as much as d_{3-} decreases, compensating one another as far as affecting resonant frequencies is concerned. As in several other figures, apparent avoided crossings on this plot should be viewed with suspicion because the plotting program does not interchange line identities when physically the modes do, in fact, cross. Spectra are computed for 241 abscissa values here and elsewhere, which sets the scale on which avoided crossings may be spurious.

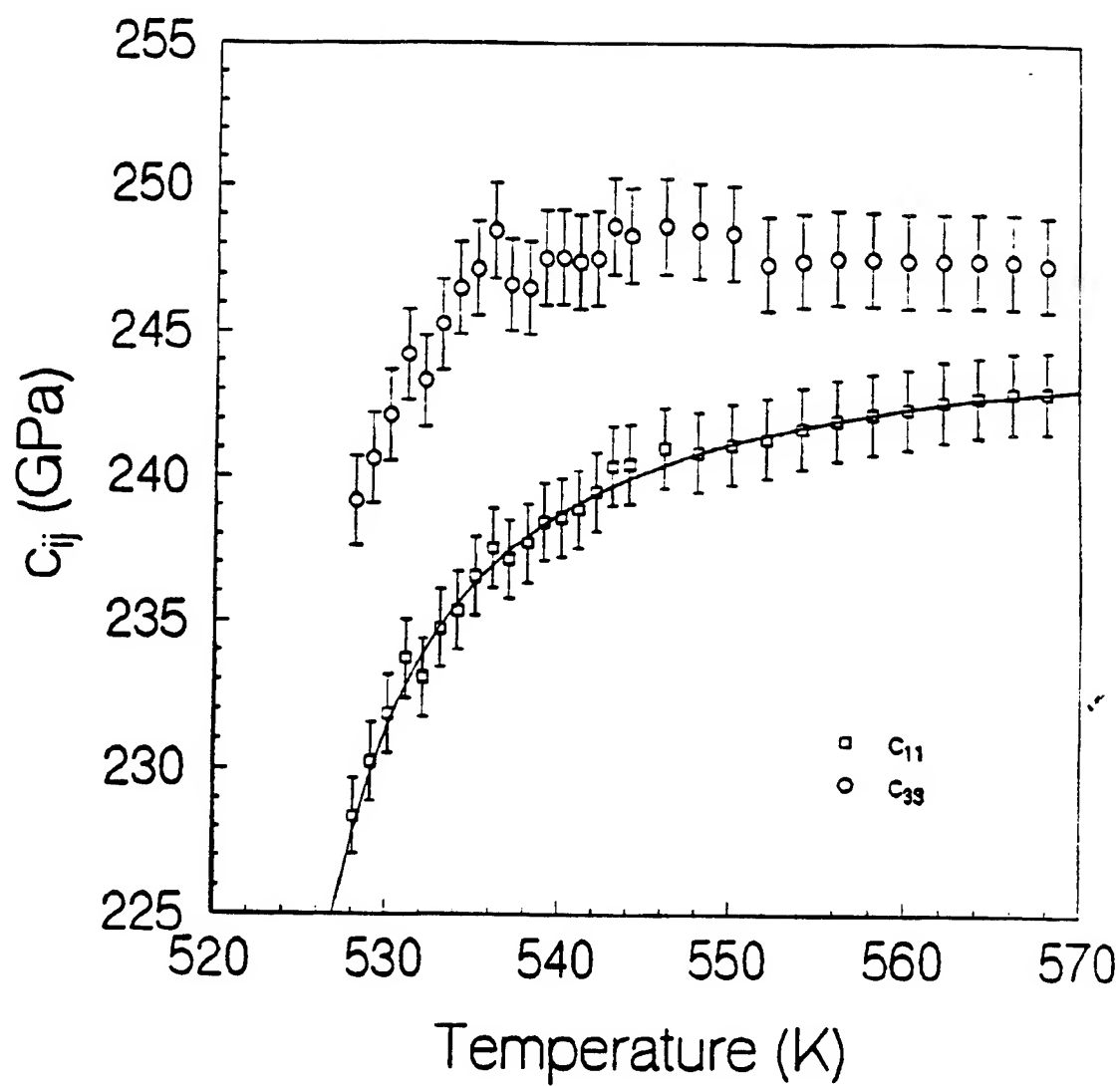


Figure 8
Sarras et al.

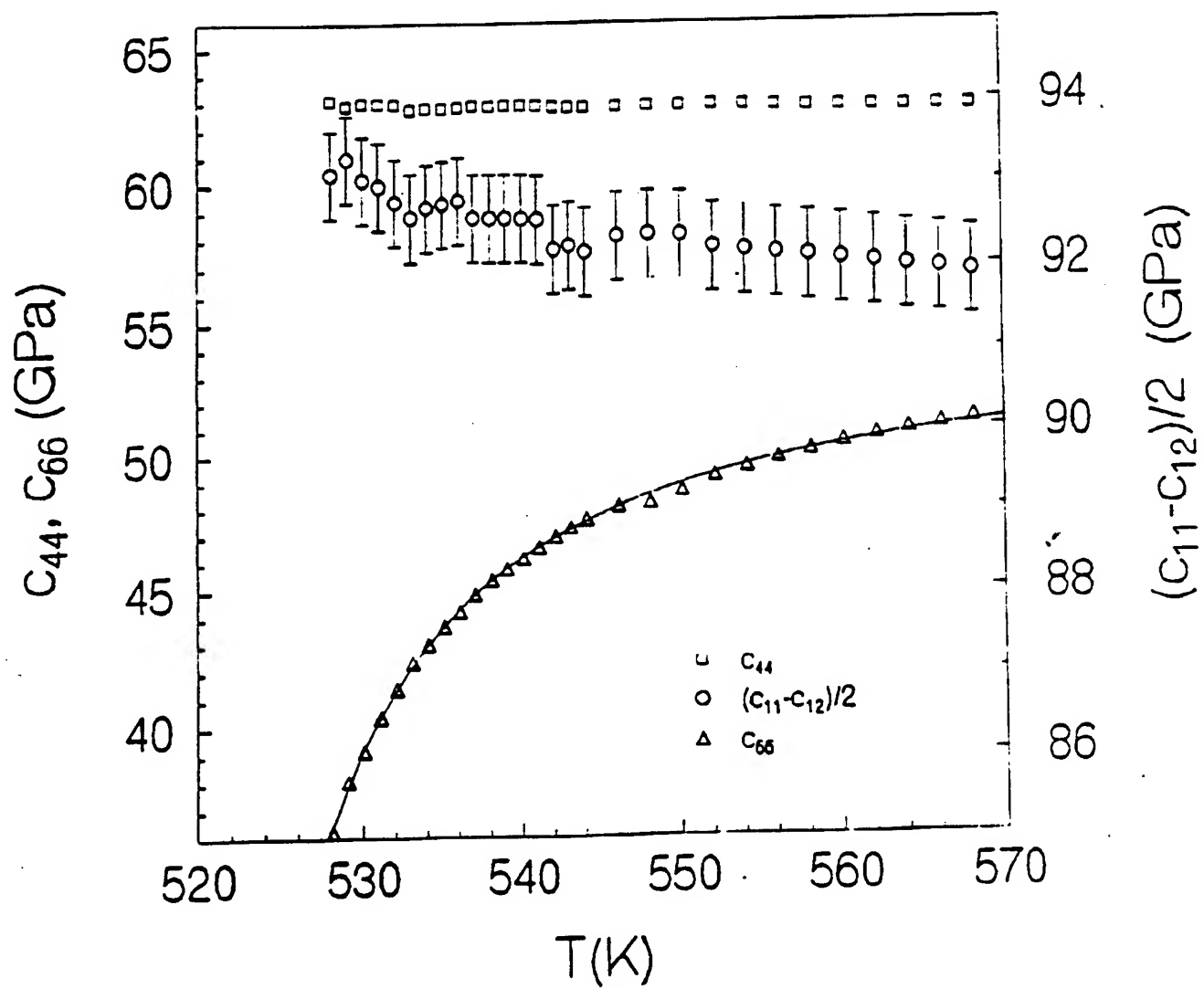


Figure 7
REVISED
Sarma et al.

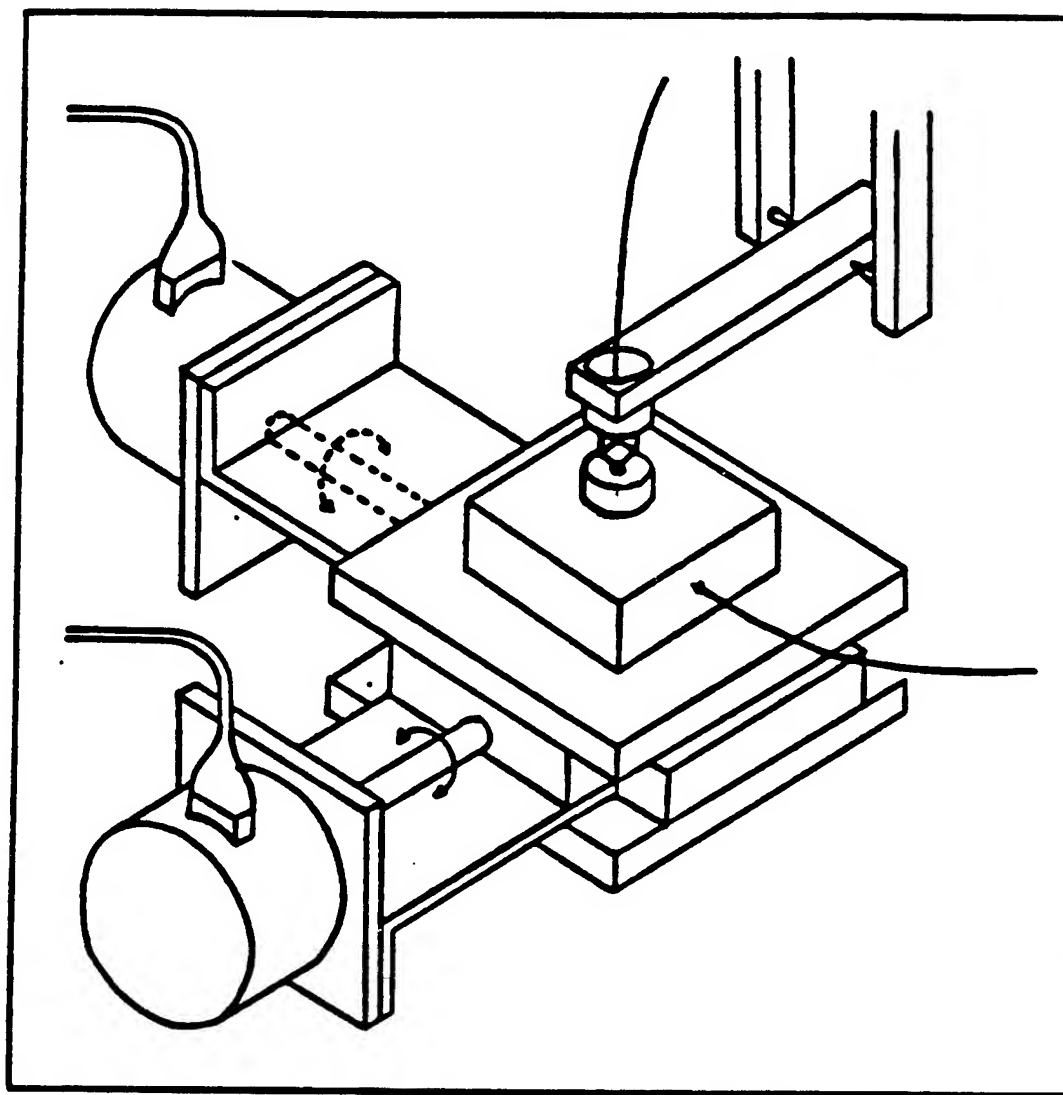


Fig.3 Outline sketch of the stepping-motor driven system used to rock the sample to enable detection of all the modes.

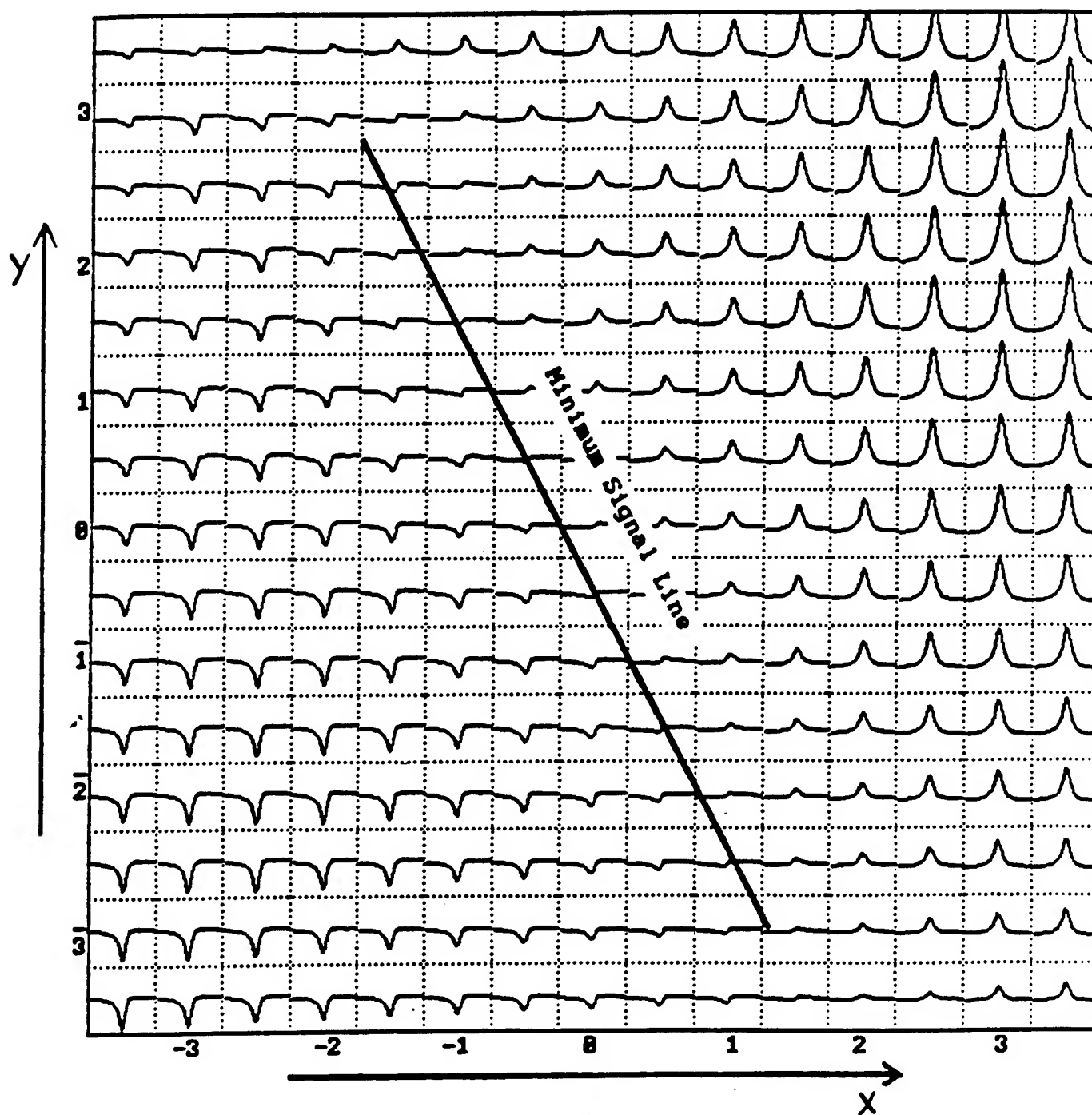


Fig. 6 (a)

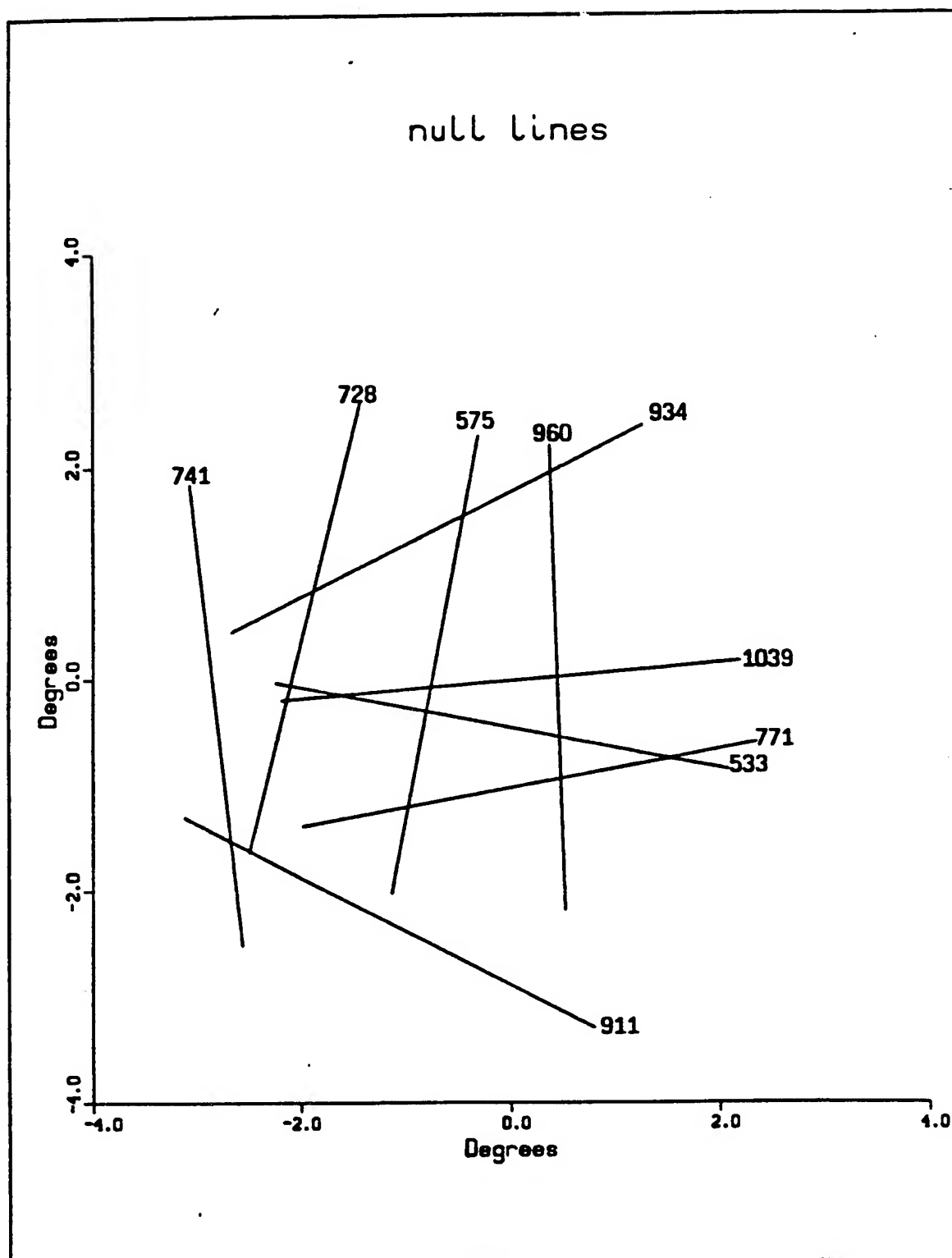


Fig. 5

Transducer construction

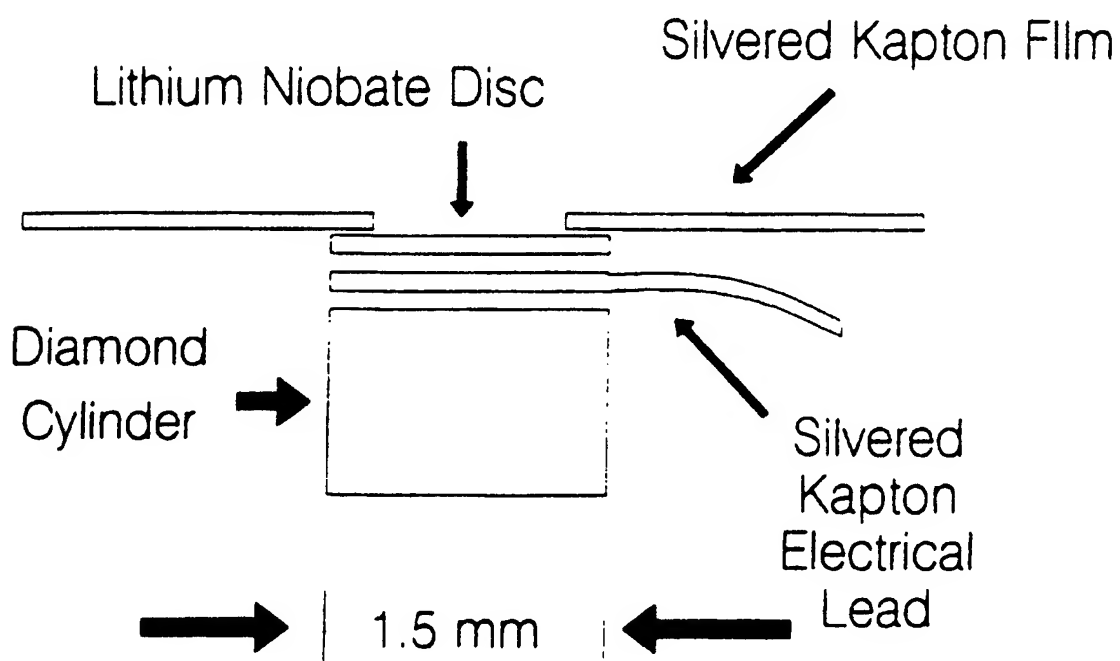


Fig. 3. Shown is a schematic of the diamond/polyimide/ LiNbO_3 composite transducer used for all the measurements.

The "Real" Figures

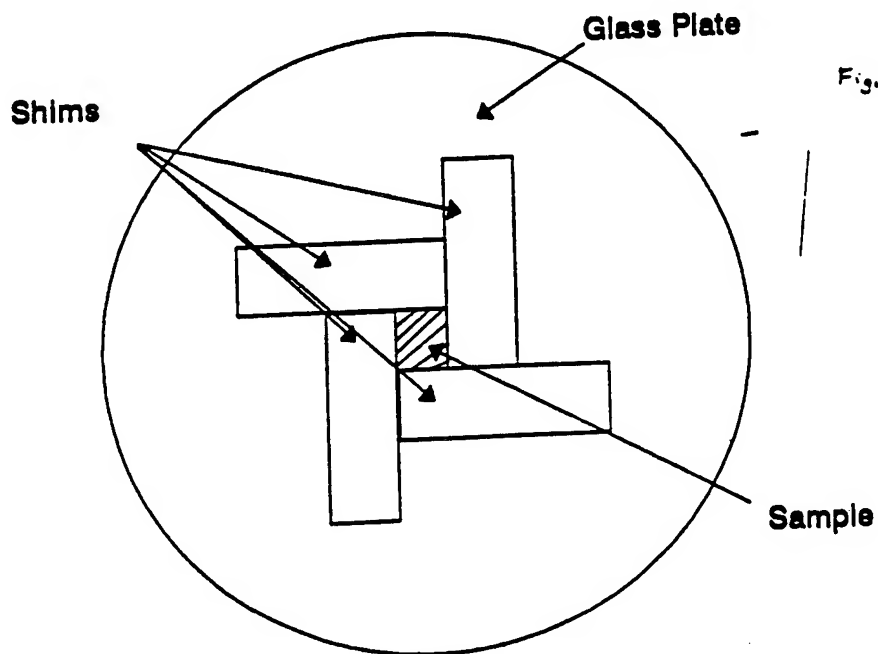
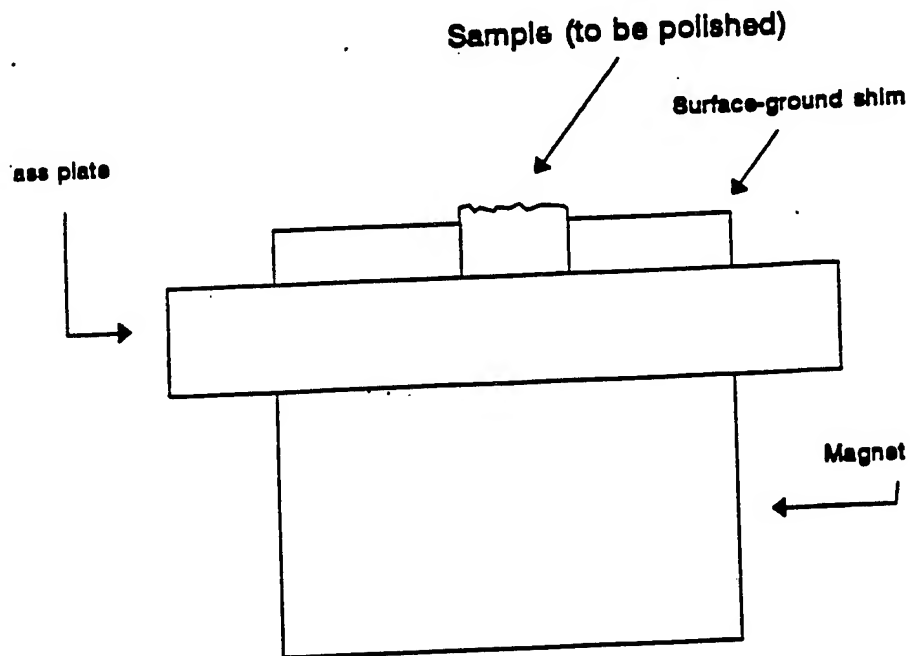


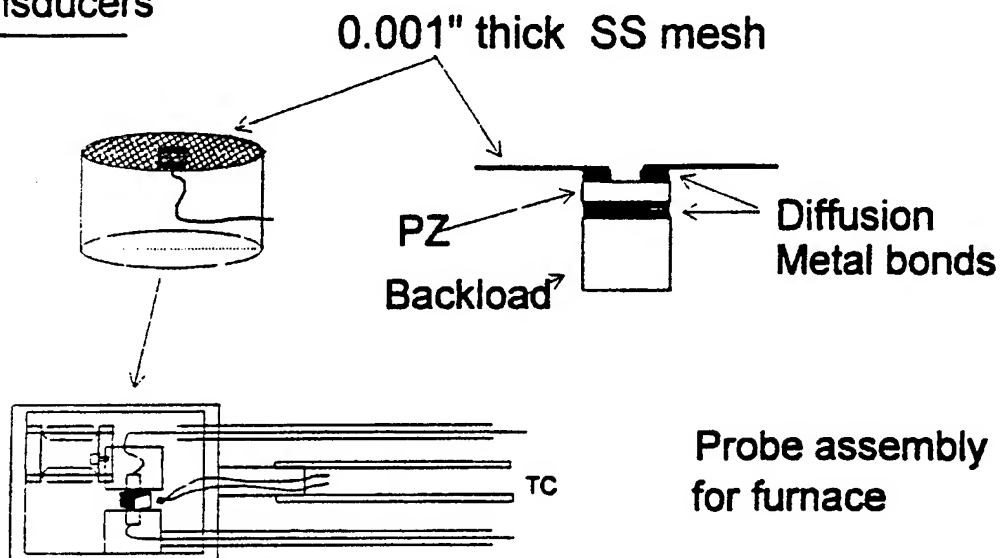
Figure 1 (polish. ch 3)

RUS can be used at temperatures as high as 1800 C (O. Anderson et. al.). For more moderate temperatures (700 C), both frequency and attenuation data can be acquired using all-metal diffusion bonded LiNbO_3 /diamond transducers

High Temperature RUS System

Piezoelectric material : LiNbO_3 : $T_c \sim 1197$, $T_m \sim 1260$

Transducers



Parallelepiped sample held
lightly between transducers

Probe assembly
for furnace

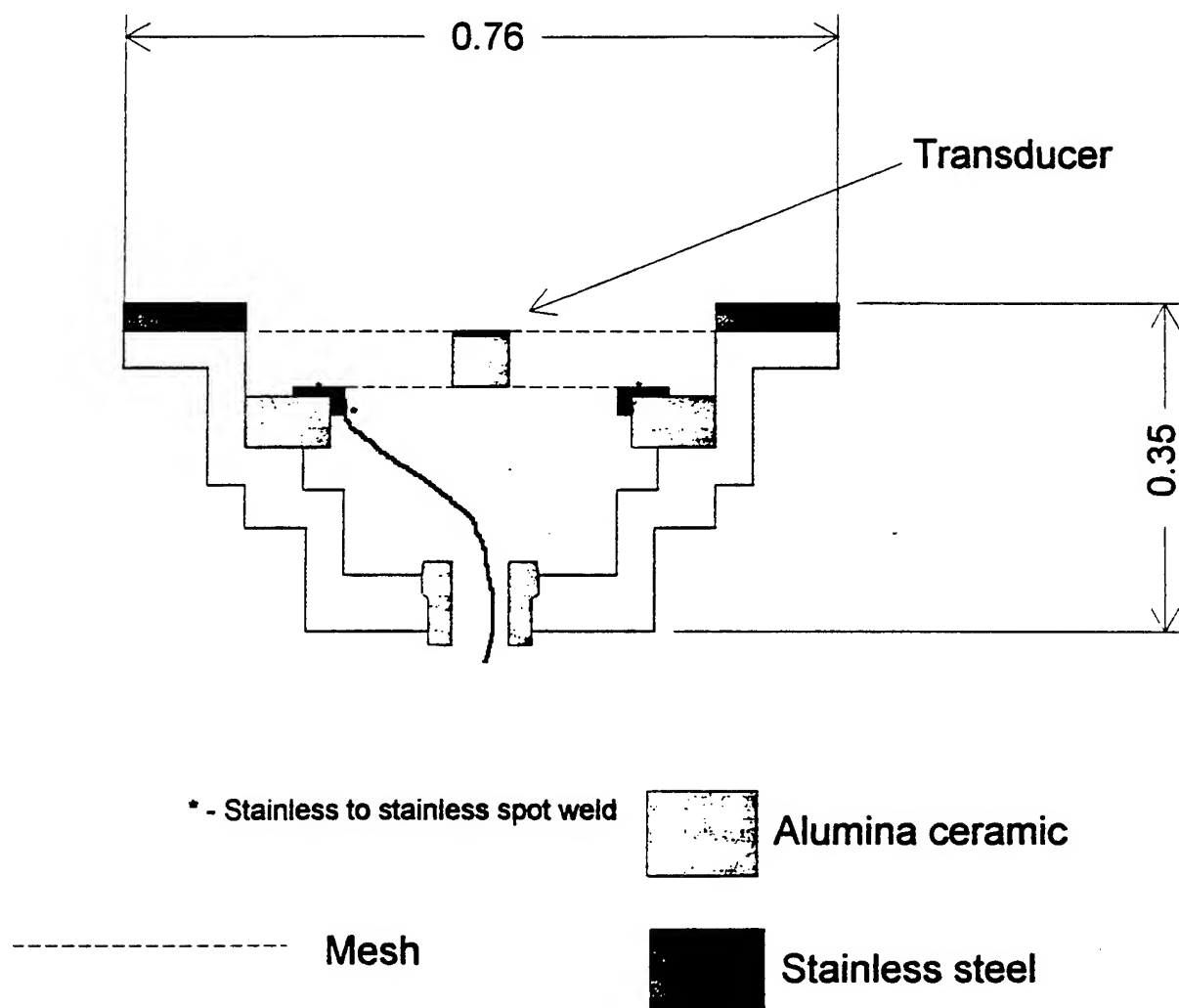
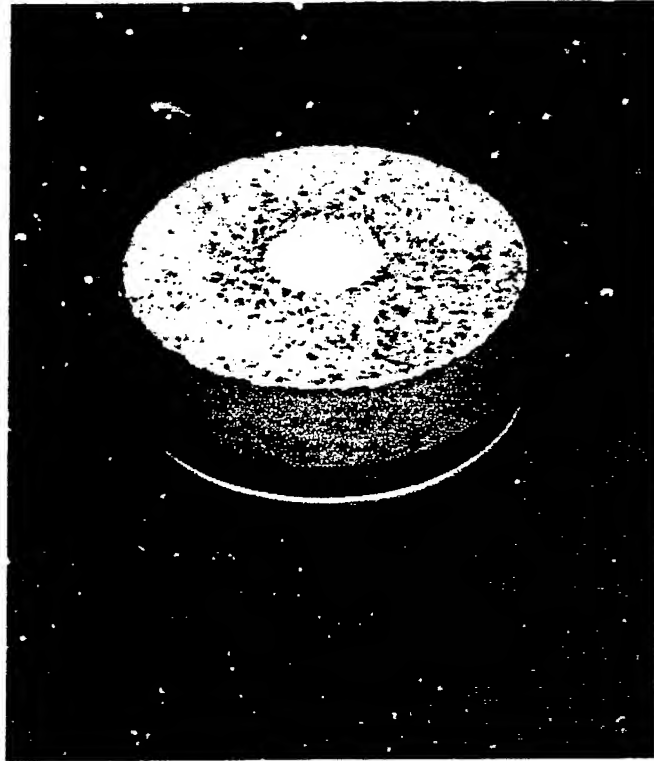
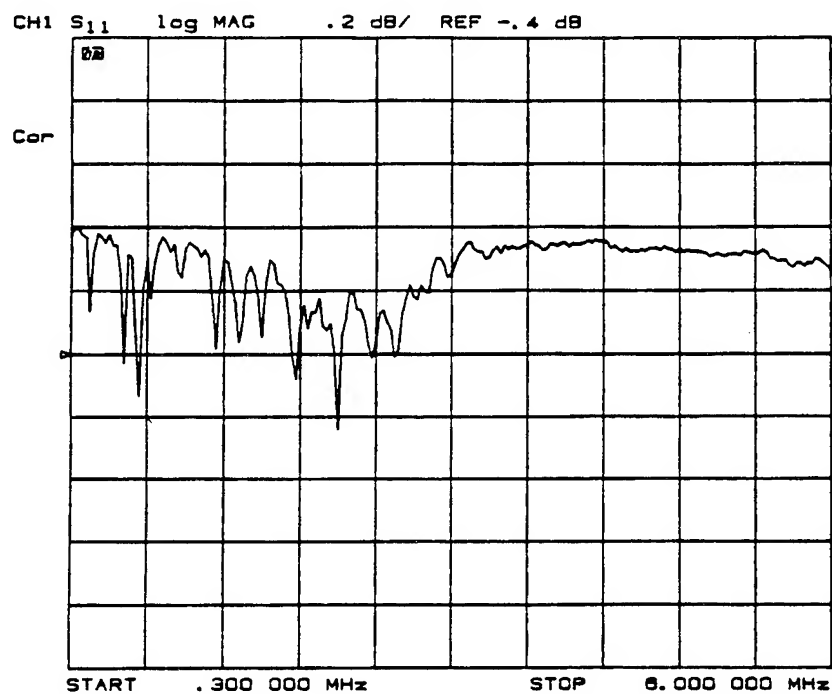


Figure 7

Silver diffusion bonded 0.375" ϕ PZT-5A
Transducer with Alumina wear plate and
alumina backload

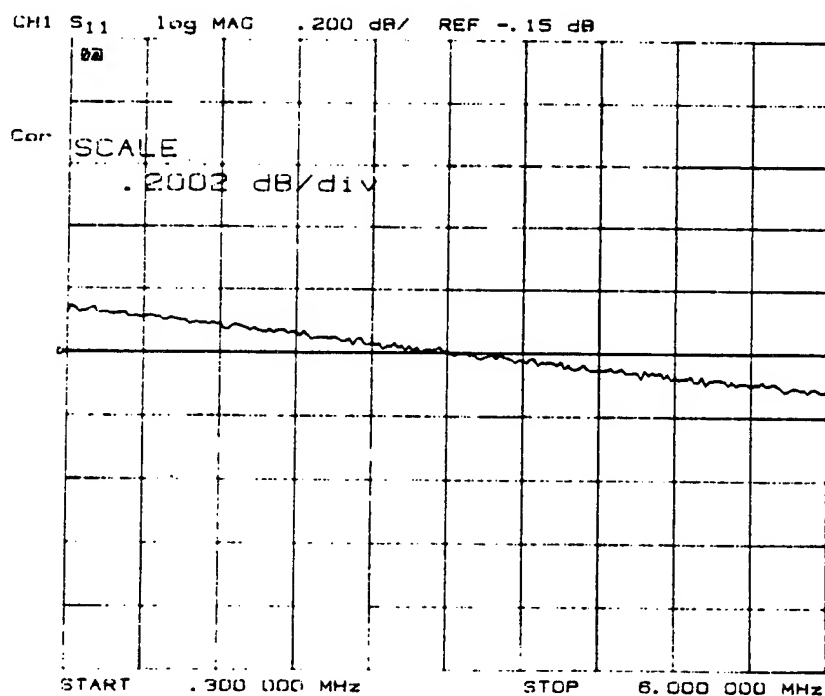


The bare transducer has a 2MHz
fundamental compressional mode
This technology won a 1993 RD100 award



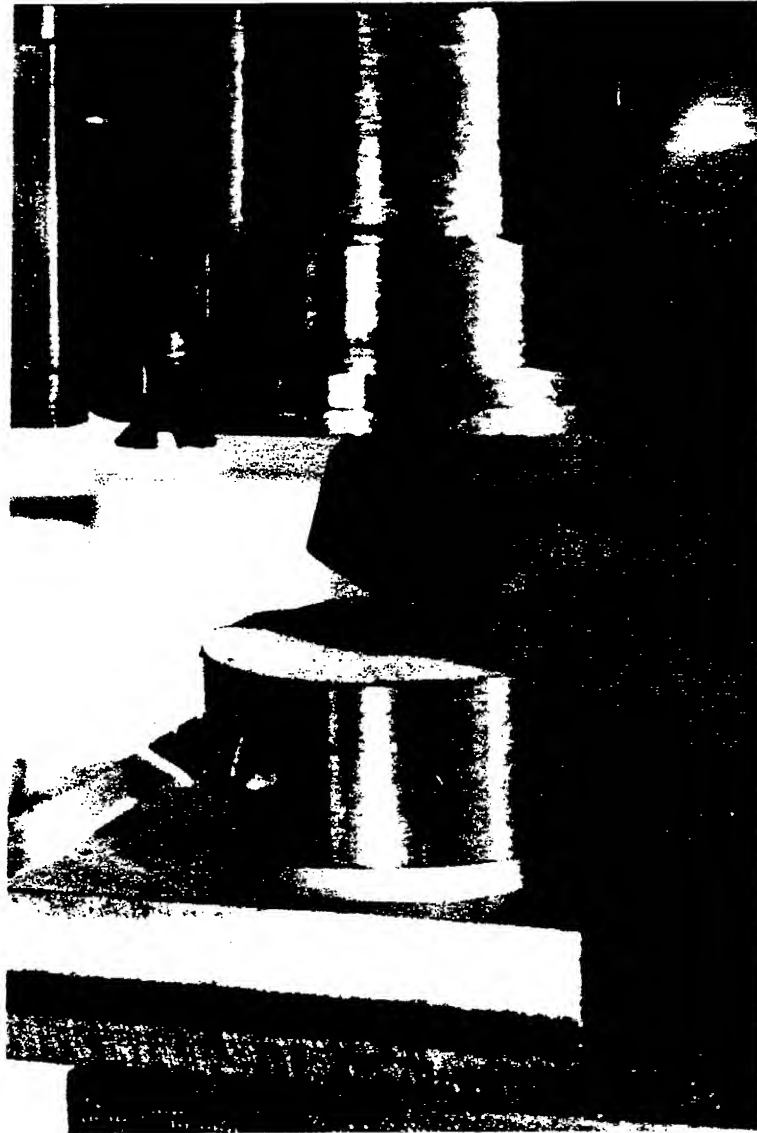
Electrical
response of

Commercial RUS
transducer



All metal
bonded
PZT/Alumina

RUS Cell with Silver diffusion bonded transducers, using LiNbO_3 and an alumina cylinder backload. This cell can reach 500C



The transducers are mounted beneath the 0.500" ϕ 304SS screens that the sample touches. Only the bottom one is visible.

Resonances of a 5120 steel RPR at 38C and 378C
measure using metal diffusion bonded LiNbO_3 /Alumina
transducers

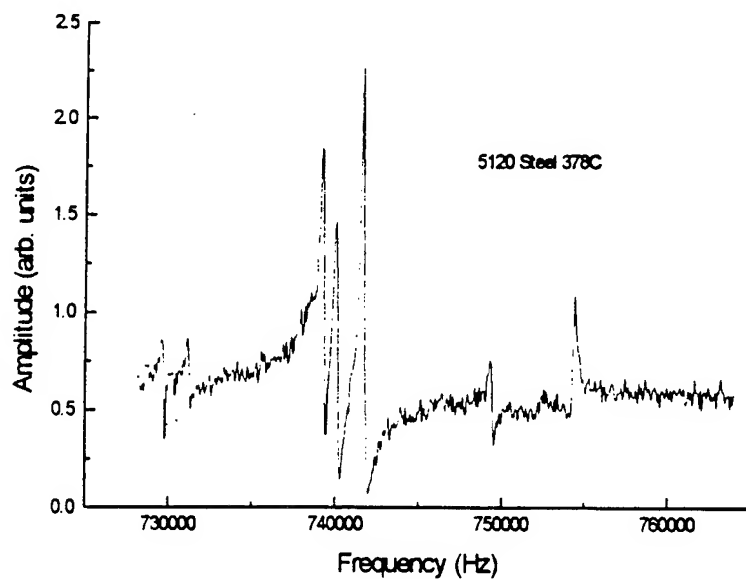
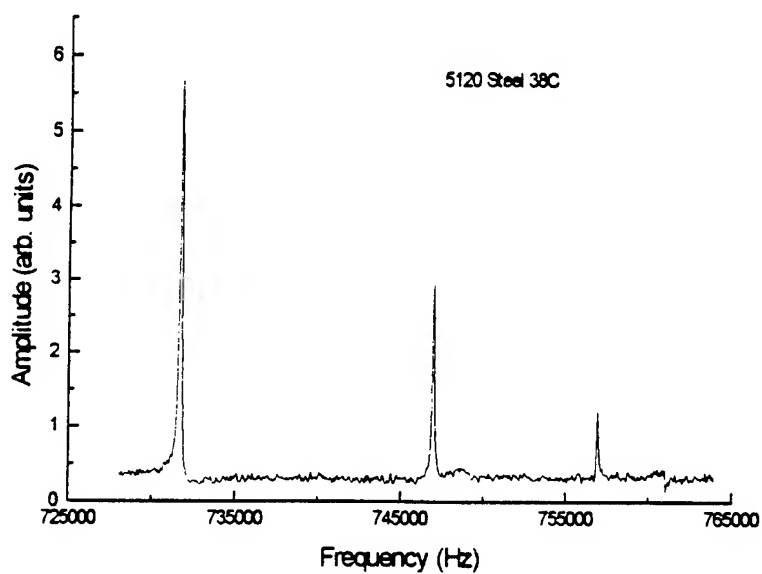
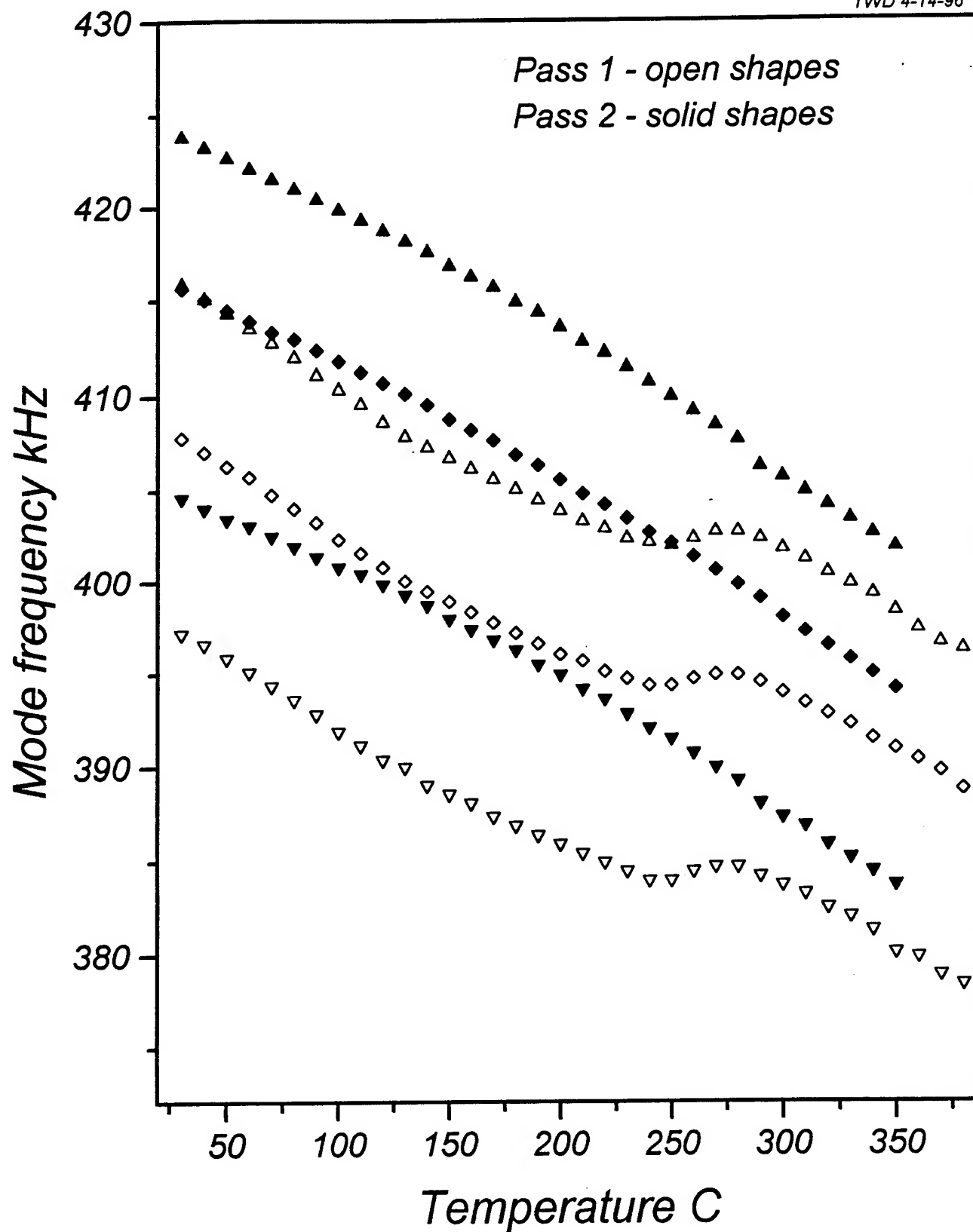
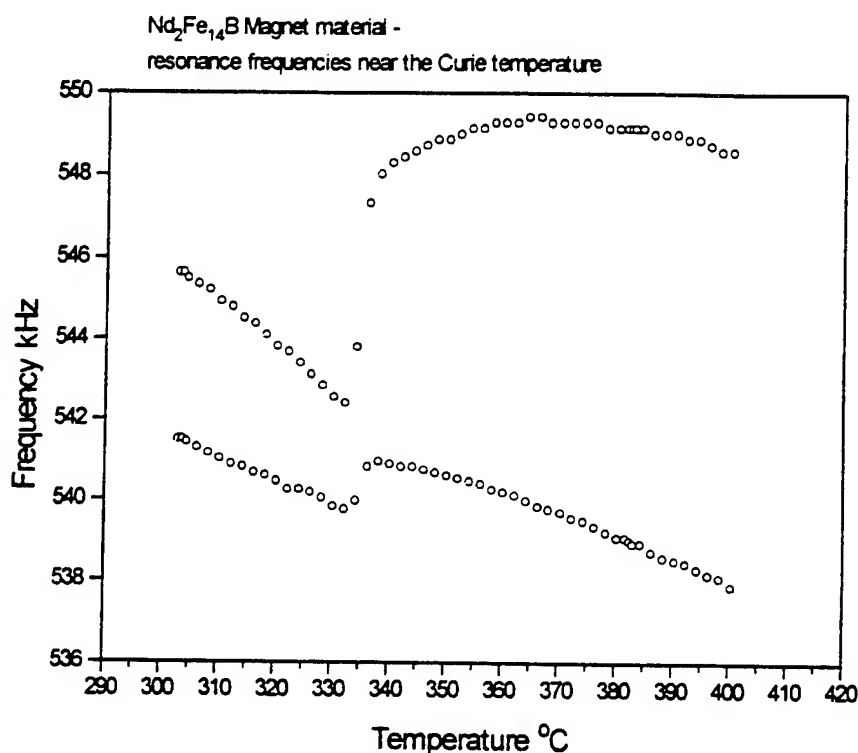


*Figure 2**5180 steel sample A9 - resonance frequencies*

TWD 4-14-96



The mechanical resonances of a solid are determined by the bulk thermodynamic properties as well as the morphology.



Hard magnets are hard because impurities and grain boundaries in very high permeability ferromagnets affect the ability of magnetic domains to track an applied field. If the domains can't move, the magnet is hard. The entire trick with Nd₂Fe₁₄B was to determine the changes to the intergranular region that stopped the domains from moving.

RUS can extract useful information relating to the effect of the intergranular composition on the overall magnetic properties of Nd₂Fe₁₄B.

Use of RUS to determine the spin reorientation temperature of $\text{Nd}_2\text{Fe}_{14}\text{B}$ obtained from GM Research Laboratories

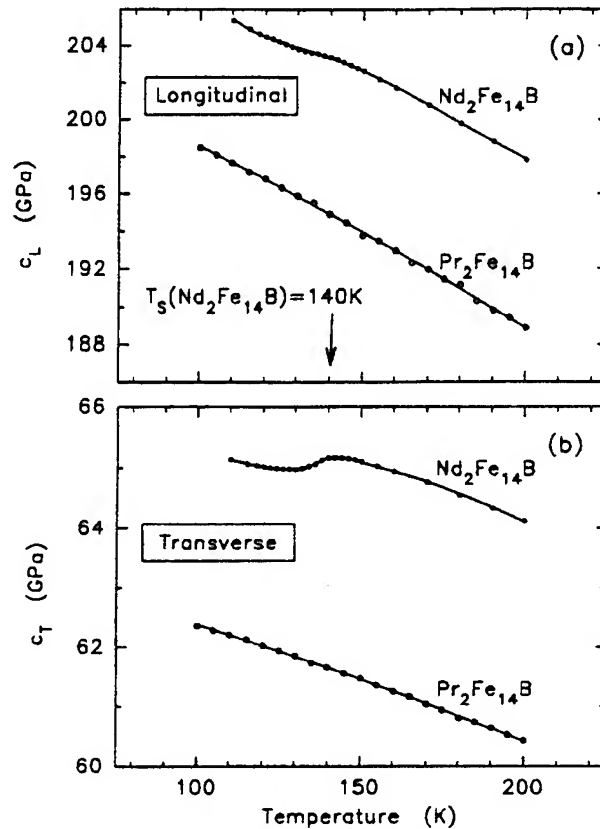
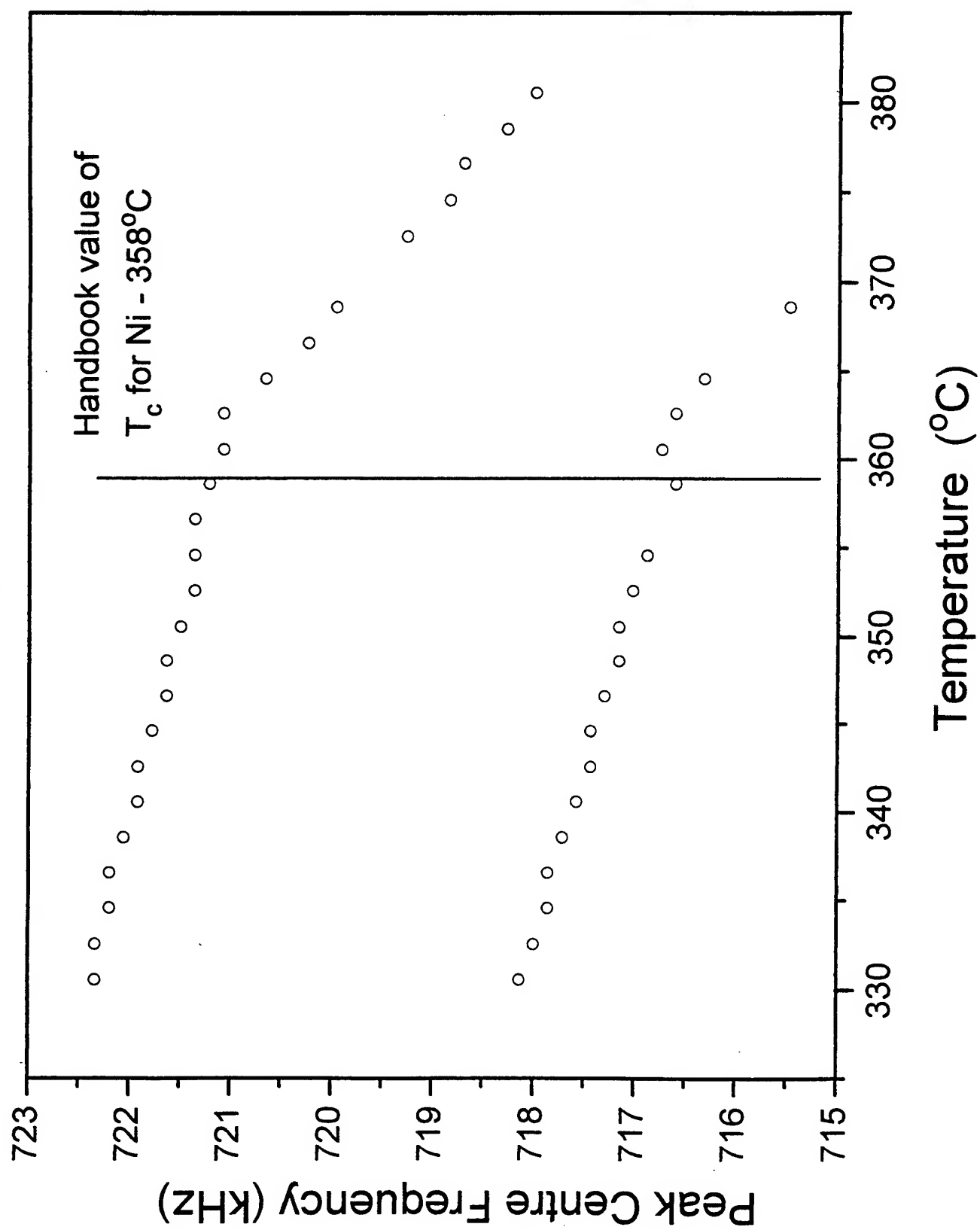


FIG. 1. (a) Longitudinal and (b) transverse elastic constants of $\text{Pr}_2\text{Fe}_{14}\text{B}$ and $\text{Nd}_2\text{Fe}_{14}\text{B}$ in the 100–200 K temperature range.

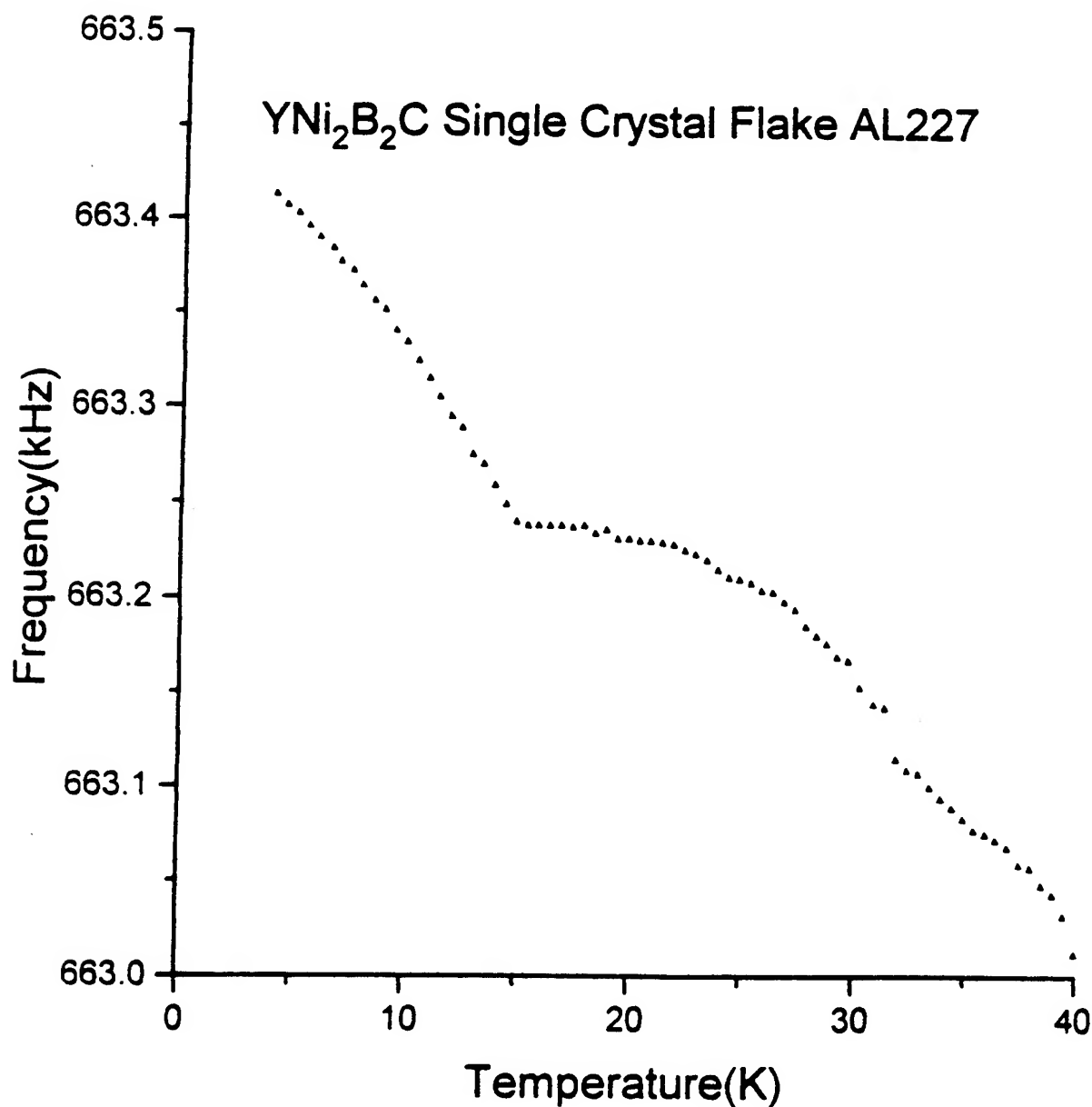
The phenomenon of spin reorientation, depicted above, can occur at technologically inconvenient temperatures, changing the important properties of a permanent magnet used under extreme condition (such as under the hood of an automobile). RUS provides a convenient probe for such effects that is sensitive to the average concentration.

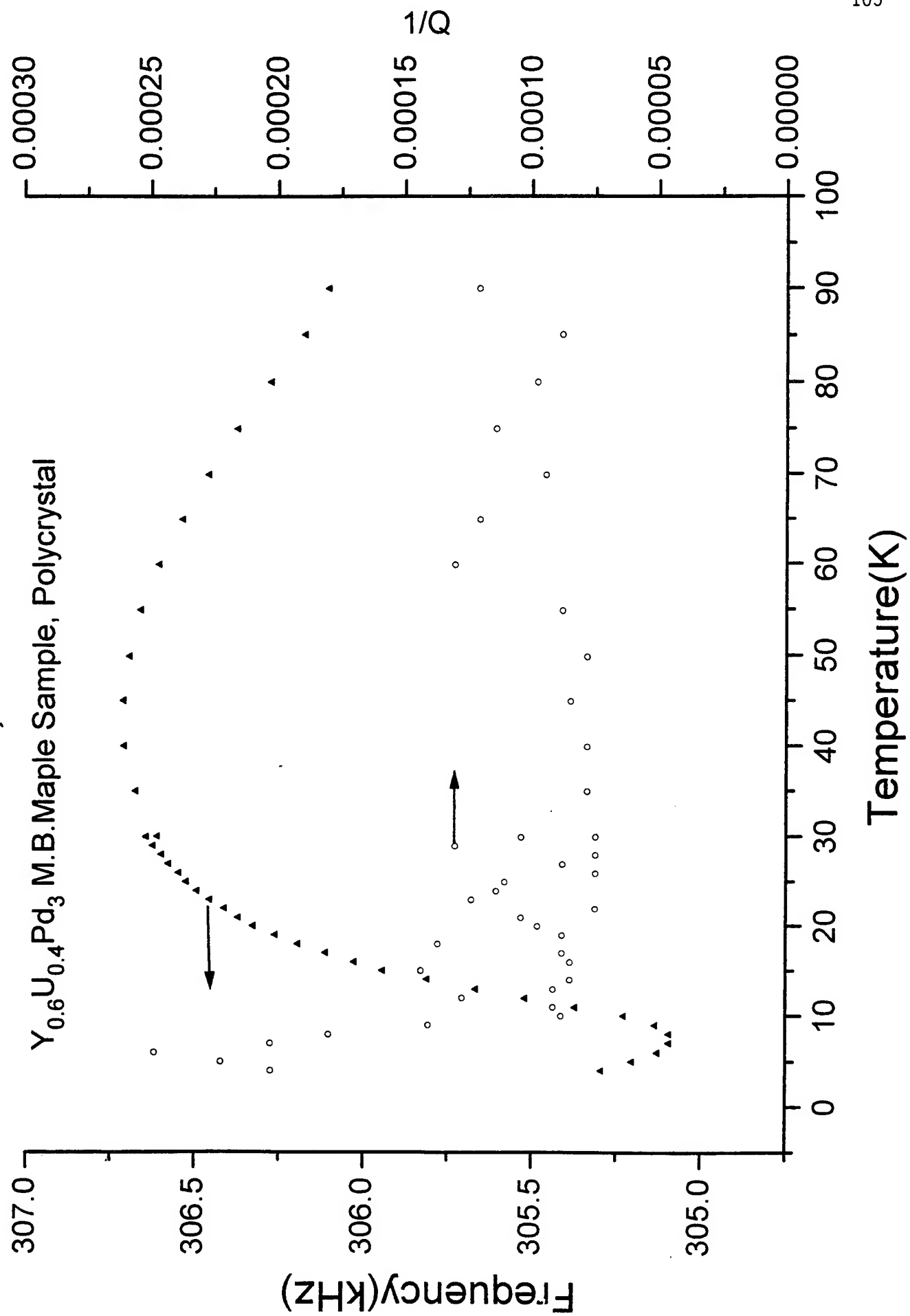
Figure 9



Resonant ultrasound studies -superconductivity

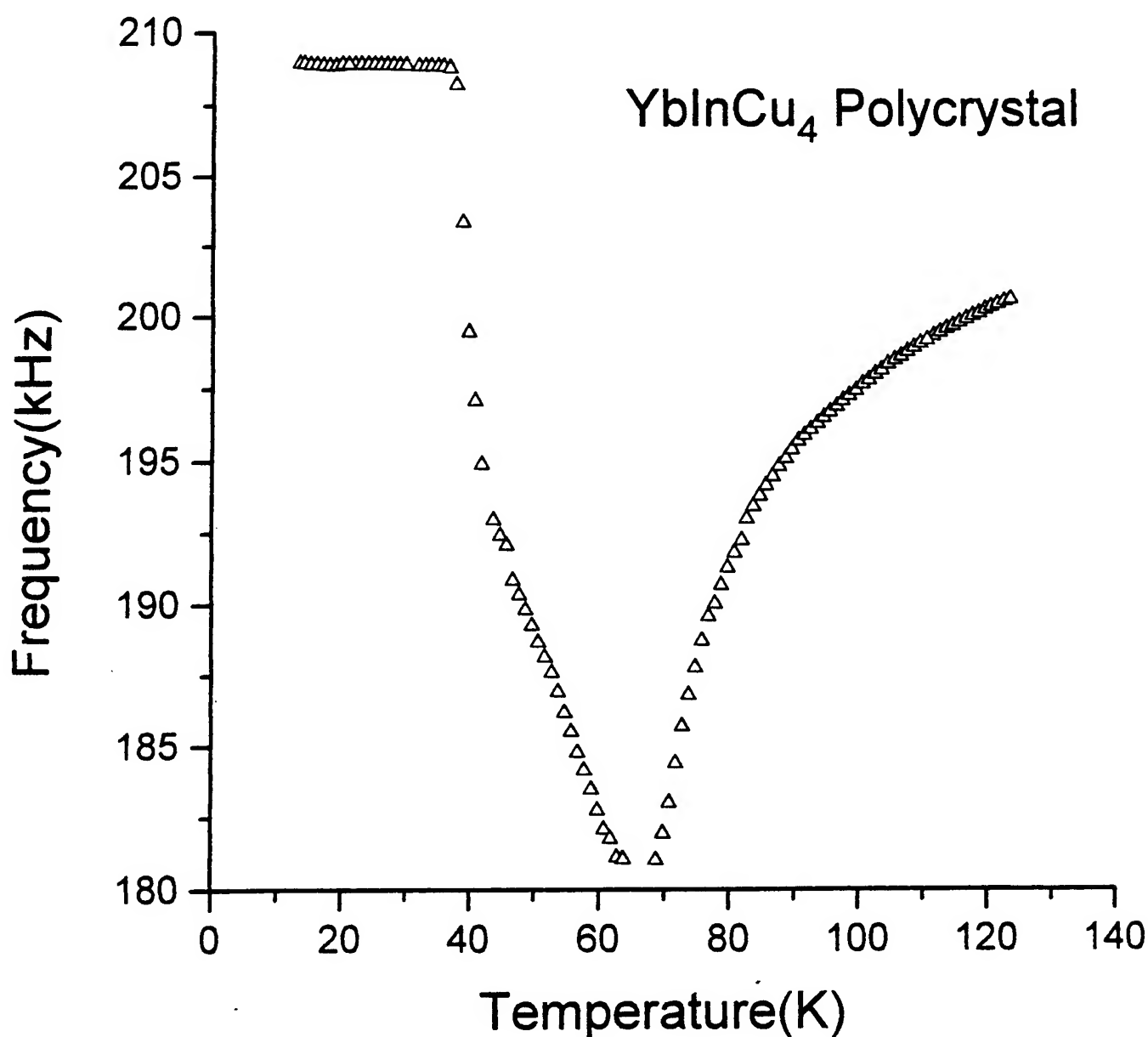
One of the clearest examples ever
of the discontinuity in elastic properties
at a superconducting phase transition





Resonant ultrasound studies -valence transition

Valence transition at 40K and
phase transition of unknown
origin at 66K



U_2Zn_{17}

Rhombohedral, macroscopic
hexagonal symmetry

Mirror twins, stacking faults

Kondo system with enhanced
specific heat and T^3 term

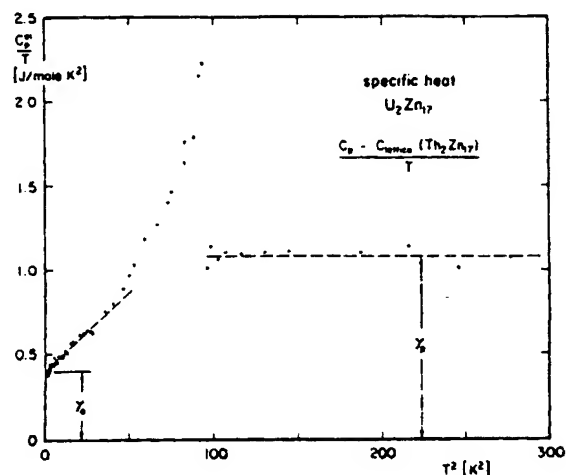


Fig. 11. Specific heat minus the lattice contribution of U_2Zn_{17} , plotted as $C_p - C_{lattice} / T$ versus T^2 . Data are from Ott et al. (1984b). The broken lines indicate the temperature dependences above and below the phase transition.

HEAVY-ELECTRON ACTINIDE MATERIALS

Commensurate Antiferromagnet
Nuclear and magnetic unit cells
the same

Easy axis in hexagonal plane

$T_n = 9.8K$

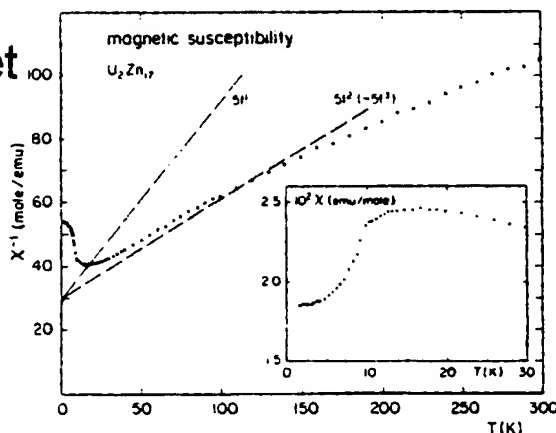


Fig. 25. Temperature dependence of the inverse magnetic susceptibility χ^{-1} of U_2Zn_{17} between 1.5 and 300 K. The inset shows χ^{-1} on an extended temperature scale below 30 K. (Data are taken from Ott et al. (1984b).)

Coherence effects begin at 18K

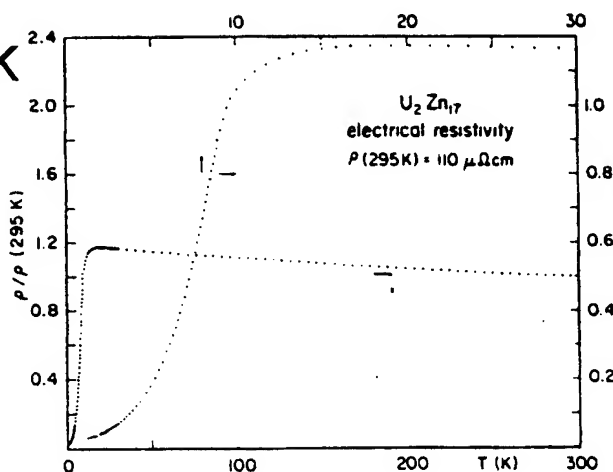


Fig. 51. Temperature dependence of the electrical resistivity of U_2Zn_{17} between 1.2 and 300 K. Note the different scales for different temperature intervals. (Data are from Ott et al. 1984b.)

Antiferromagnetic Ordering of U

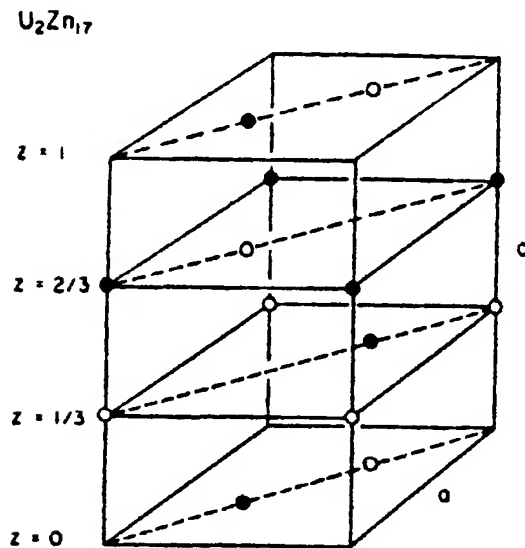


Fig. 113. Proposed magnetically-ordered structure of U_2Zn_{17} , on the basis of neutron-diffraction results by Cox et al. (1986). Open and closed circles denote atoms with oppositely oriented moments. The moment directions are within the basal plane.

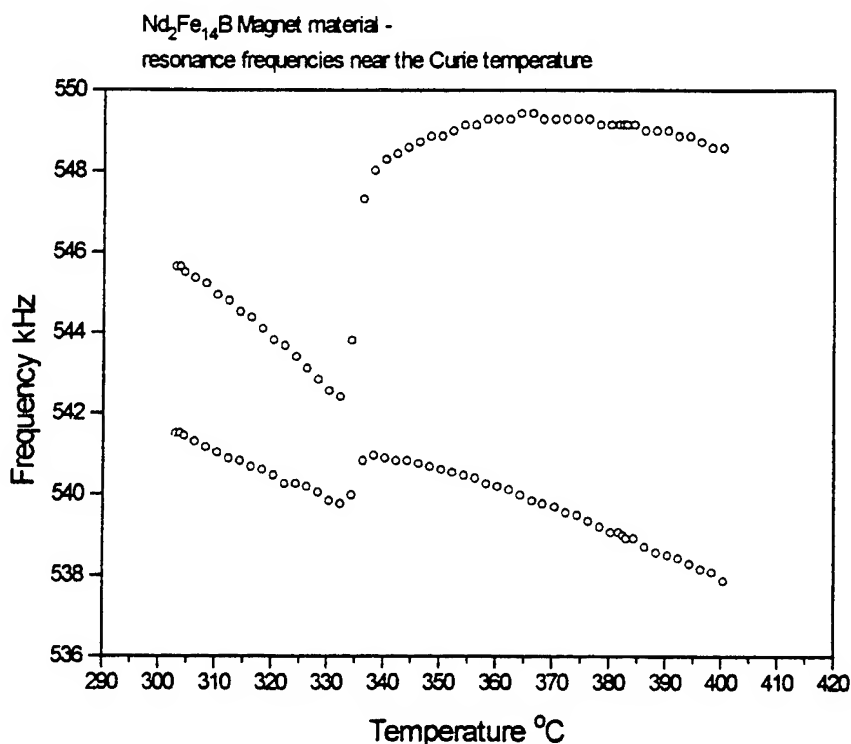
Stacking Faults

Twins

Remnants of high T hexagonal structure in low T rhombohedral phase

The above can lead to weak ferromagnetism and structural effects

The mechanical resonances of a solid are determined by the bulk thermodynamic properties as well as the morphology.



Hard magnets are hard because impurities and grain boundaries in very high permeability ferromagnets affect the ability of magnetic domains to track an applied field. If the domains can't move, the magnet is hard. The entire trick with Nd₂Fe₁₄B was to determine the changes to the intergranular region that stopped the domains from moving.

RUS can extract useful information relating to the effect of the intergranular composition on the overall magnetic properties of Nd₂Fe₁₄B.

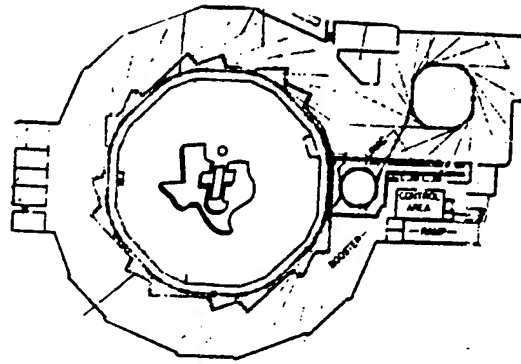
Basic Research in High-Temperature Superconductors Leads to a Unique and Effective Technology



Resonant ultrasound nondestructive inspection is a simple, low-cost technology that applies to objects that weigh a few grams or several tons.



Los Alamos



Particle Accelerators

*An insoluble problem:

*Reason: it is just like chess but without the little men

*Proof: No two particle accelerators are alike

No minimalist approach is possible because the problem is too ill-defined and complex. But nevertheless, great physics comes of it, at, of course, great expense. One cannot give up the physics, one can only lament the expense

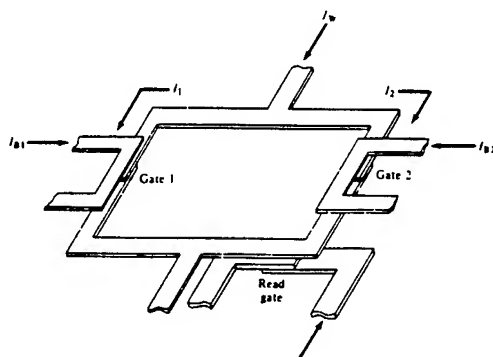
The Josephson Voltmeter

*Benchtop physics with a few basic variants

*Fantastic macroscopic manifestation of quantum mechanics, as wonderful and important as any bit of physics

*Cheap (costs less than a car, is smaller than a Kitchen)

*Redefines the standard for Voltage (i.e. it is very useful)

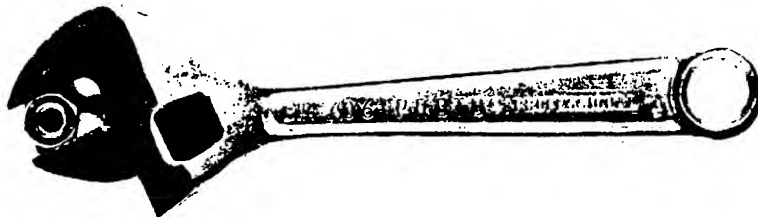


The Crescent Wrench:

*A problem that can be solved:

*Reason: The problem is simple, as are the approaches for solution

*Proof: There is only one basic design left at the hardware store



Chess:

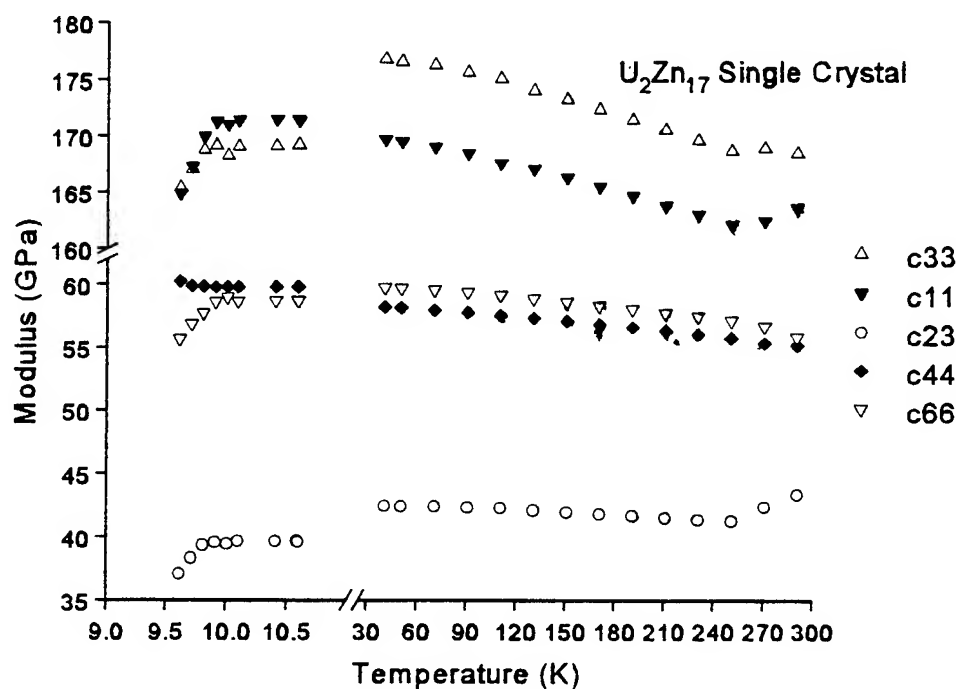
*An insoluble problem:

*Reason: it is too complicated and messy, with too many possibilities

*Proof: People still play chess

Elastic moduli of U_2Zn_{17}

Rectangular parallelepiped, crystal axes not parallel to faces but determined by RUS



Data taken in two separate runs. Failure to get perfect match is typical if morphological flaws exist.

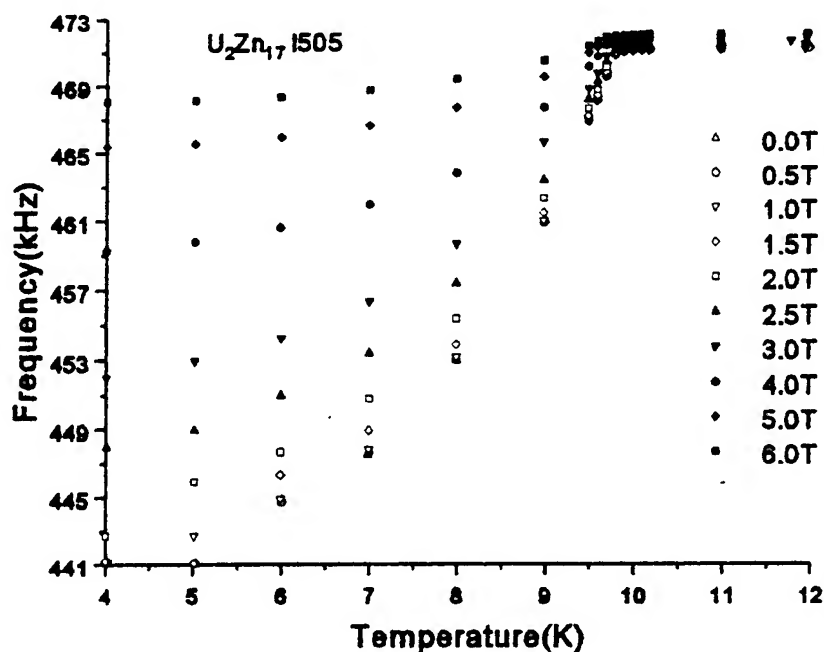
Shear moduli $\pm 0.5\%$, diagonal moduli $\pm 2\%$, off diagonal moduli $\pm 4\%$

c_{44} is unaffected by Neel transition, all other moduli soften

Resonant frequency of single-crystal fragment

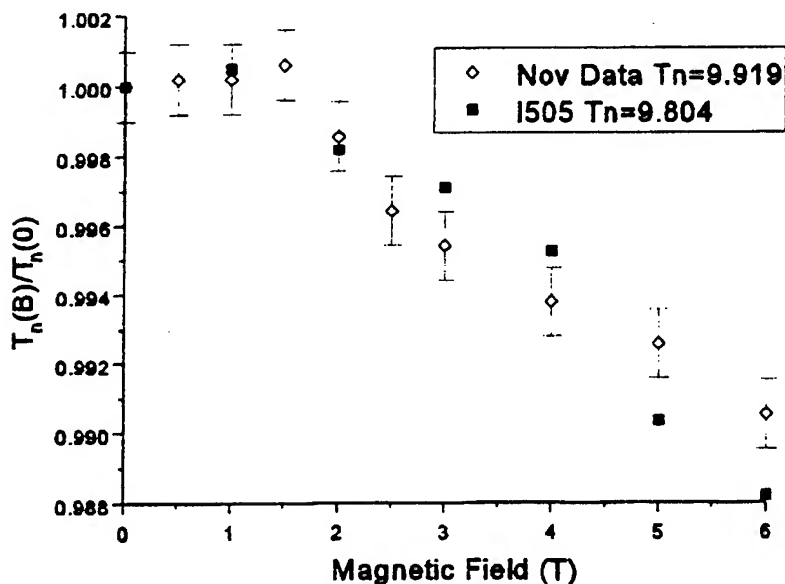
Undetermined mix of c_{44} and c_{66}

Undetermined orientation of field with crystal axes

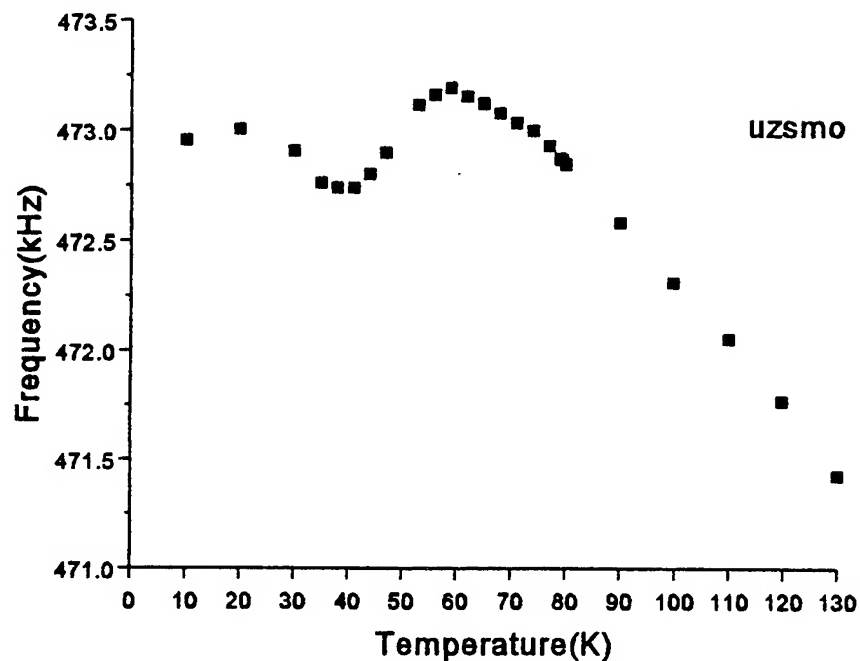


Variation of Neel temperature and softening with field and with c_{44}/c_{66} ratio (undetermined) on several samples with different mixes

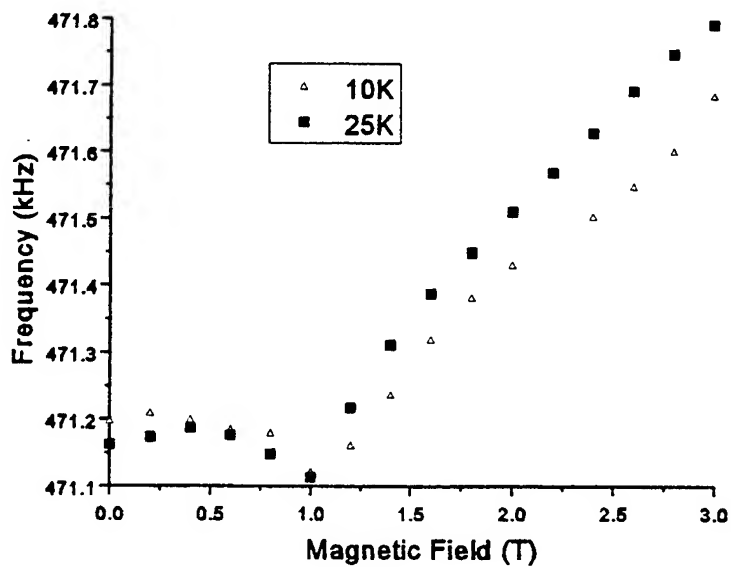
T_n essentially independent of field direction, suggesting free energy couples as M^2H^2



Effects above the Neel transition in applied field

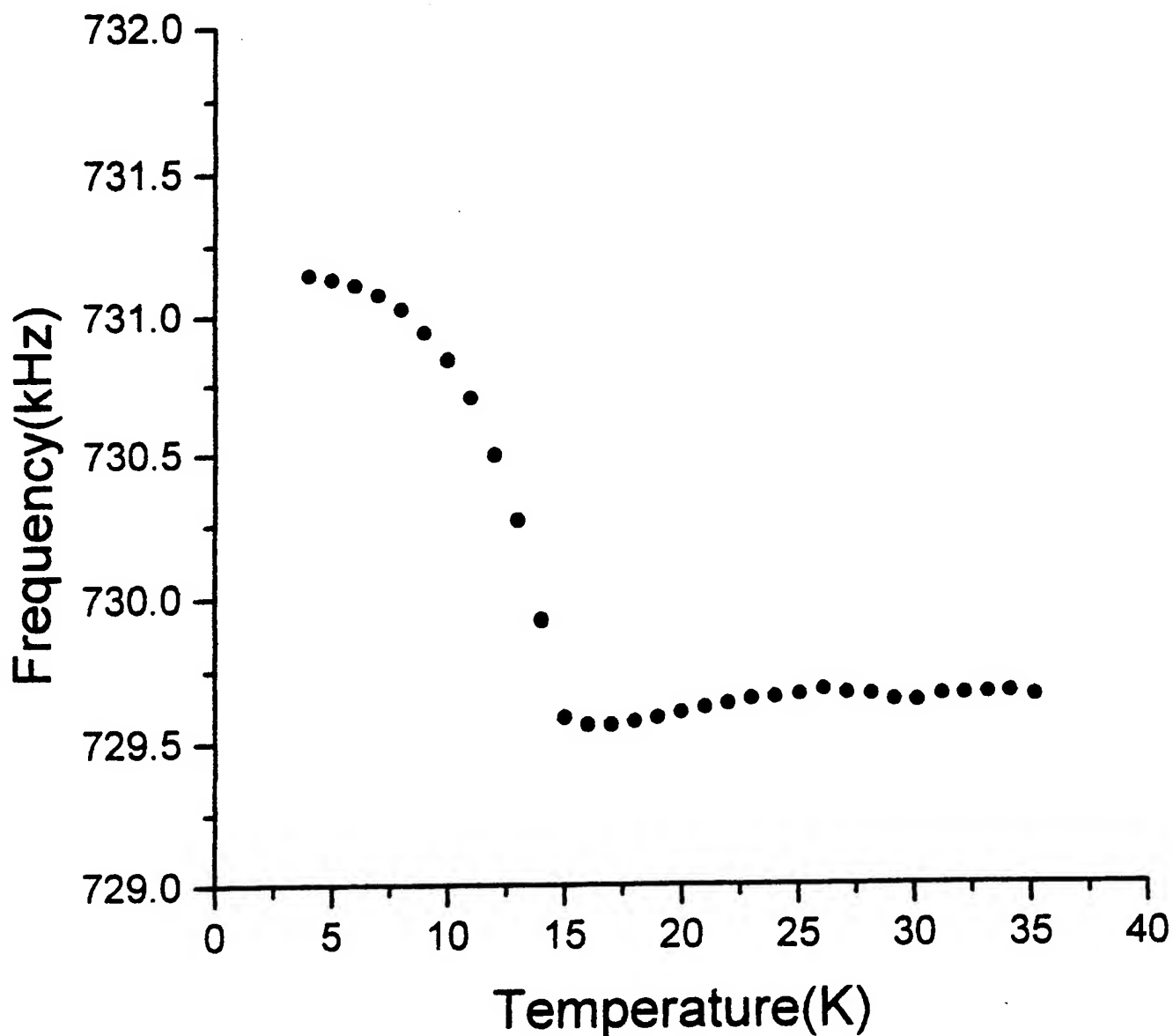


The above is indicative of a weak phase transition of unknown origin



This effect disappears above about 70 K

UCu_{5.05} annealed polycrystal showing
the clear slope break in the shear modulus
at the antiferromagnetic transition



Simple model for the unusual band-edge density of electronic states in FeSi

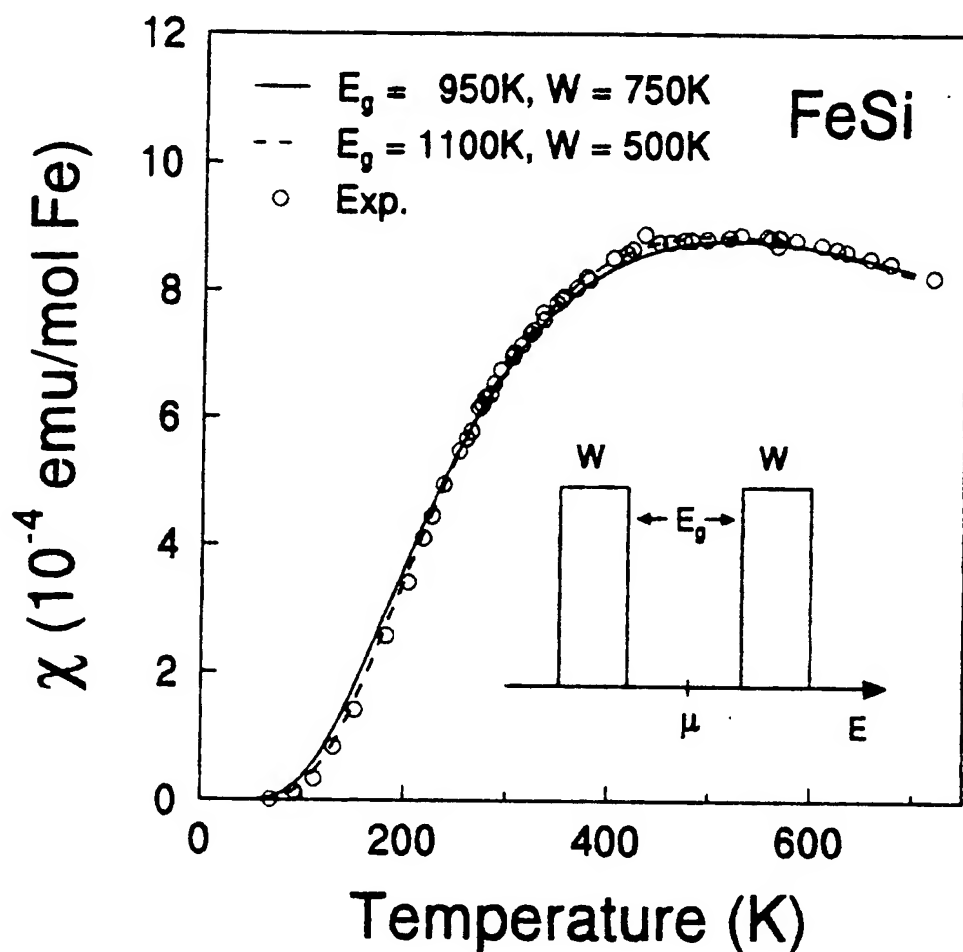


FIG. 1. Magnetic susceptibility of FeSi. Open circles: experimental points after Jaccarino *et al.* (Ref. 5). A low-temperature Curie tail was subtracted from the data as described in Ref. 5. Solid line: calculation using the model density of states shown in the inset with parameters $E_g = 950$ K, $W = 750$ K, and $g = 4.40$ states/cell. Dashed line: calculation using parameters $E_g = 1100$ K, $W = 500$ K, and $g = 4.20$ states/cell.

Electronic Structure of the Narrow-Gap Semiconductor FeSi using RUS

In order to fit the data better, we consider a deformation potential coupling which explicitly includes the contribution of conduction electrons to the elastic moduli through a rigid two-band model ($E(\mathbf{k}) = E^0(\mathbf{k}) + d_r(\mathbf{k})\varepsilon_r$, where $d_r(\mathbf{k})$ is defined as $\partial E(\mathbf{k})/\partial \varepsilon_r$, and ε_r is a symmetry strain)

Consider the free energy for conduction electrons with band index i and energy $E^i(\mathbf{k})$:

$$F_{el} = -k_B T \sum_{i, \mathbf{k}} \ln \left[1 + \exp \left(\frac{\mu - E^i(\mathbf{k})}{k_B T} \right) \right], \quad (2)$$

where μ is the chemical potential. Explicitly calculating the symmetry elastic moduli, $c_r = \partial^2 F / \partial \varepsilon_r^2$, and assuming conservation of the total number of quasiparticles [5] yields

$$c_r = c_r^0 - \frac{1}{k_B T} \sum_{\mathbf{k}} d_r^2(\mathbf{k}) f_{\mathbf{k}} (1 - f_{\mathbf{k}}) + \frac{1}{k_B T} \frac{(\sum_{\mathbf{k}} d_r(\mathbf{k}) f_{\mathbf{k}} (1 - f_{\mathbf{k}}))^2}{\sum_{\mathbf{k}} f_{\mathbf{k}} (1 - f_{\mathbf{k}})}, \quad (3)$$

Thermal expansion of the semi-metal CoSi
provides background thermodynamic
information to enable extraction of the
electronic effects in FeSi

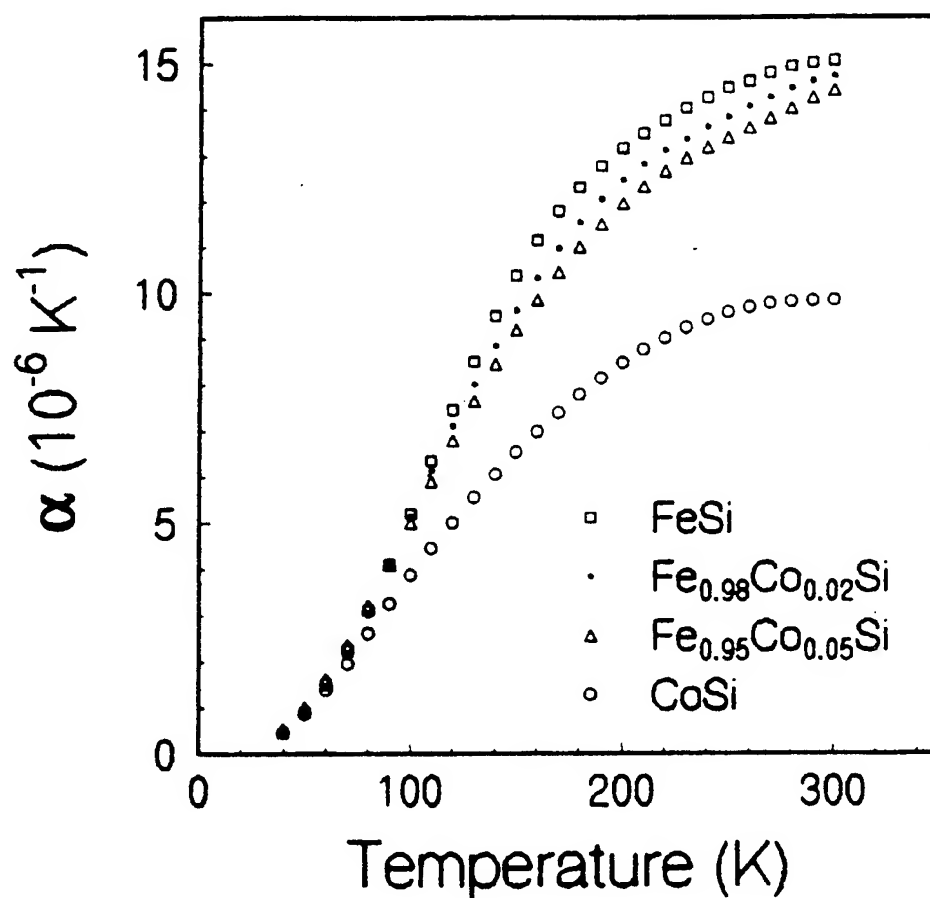


Fig. 1. Linear expansion coefficient, α , versus temperature for $\text{Fe}_{1-x}\text{Co}_x\text{Si}$ with $x = 0, 0.02, 0.05$, and 1.

Elastic Constants of FeSi

Physica B **478**,199 (1994)

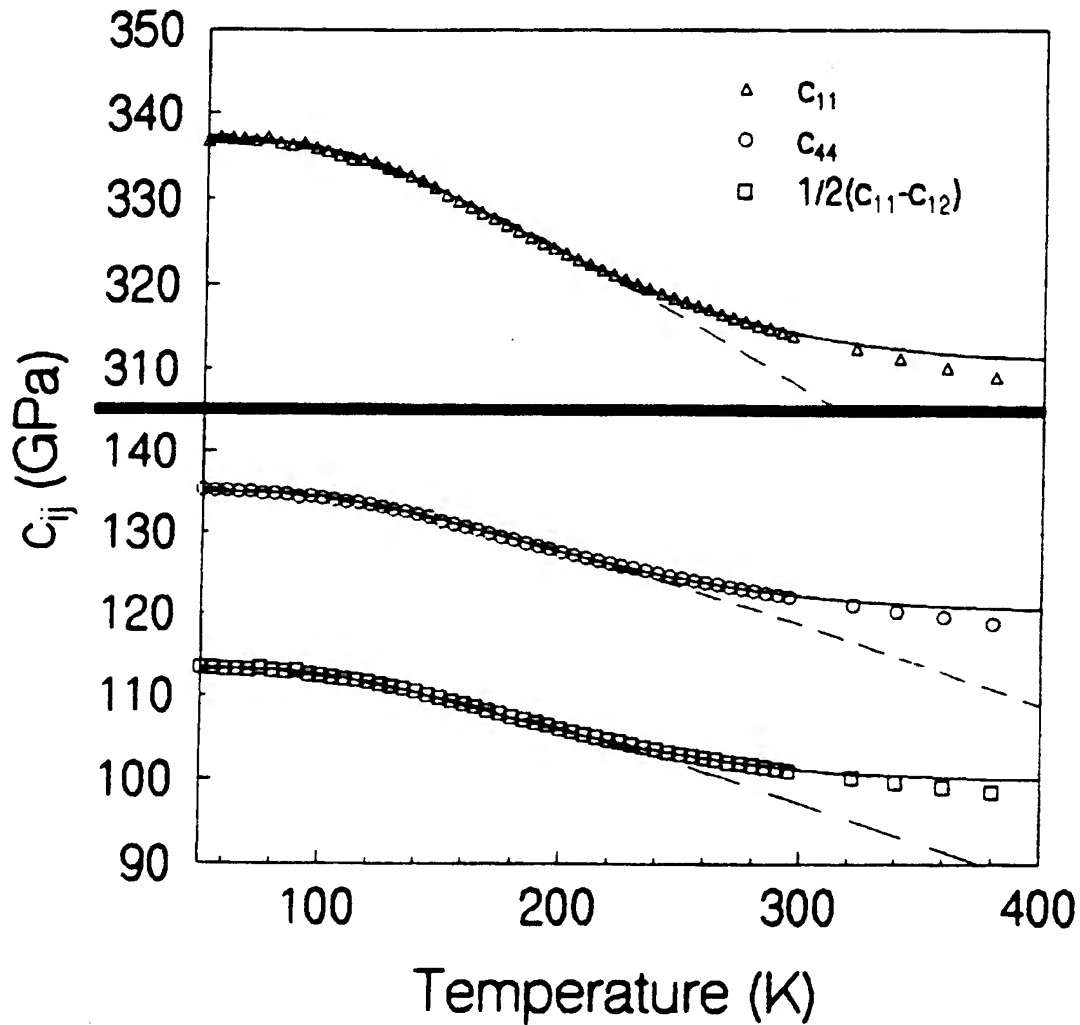


Fig. 1. Elastic moduli of FeSi as a function of temperature. The dashed curves are fits to the Varshni function (Eq. (1); for c_{11} , $s = 70.7$ GPa, $\tau = 365$ K; c_{44} , $s = 39.5$ GPa, $\tau = 366$ K; and for $1/2(c_{11} - c_{12})$, $s = 40.0$ GPa, $\tau = 374$ K). The solid curves are fits using a deformation potential coupling model. The parameters for these fits are given in Table 1.

Ultrasonic Attenuation of FeSi

Physica B **478**,199 (1994)

Modulus	Δ (K)	W (K)	$(d_T^1 - d_T^u)^2 D$ (GPa)
c_{11}	1295	12	13072
c_{44}	1296	17	4951
$\frac{1}{2}(c_{11} - c_{12})$	1250	7	10600

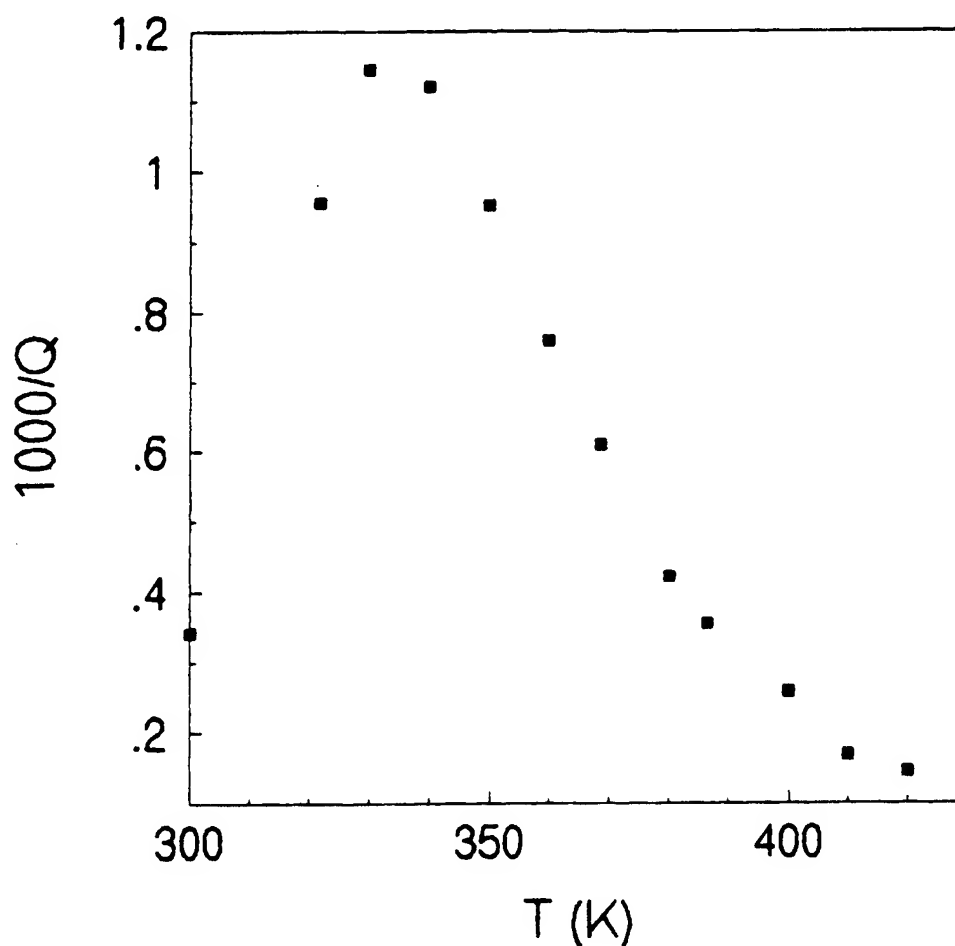


Fig. 2. $1/Q$, which is proportional to attenuation, is plotted for one of the measured resonance frequencies. The peak in attenuation occurs at the activation energy ($\Delta/2$).

Structural phase transition in $\text{La}_{2-x}\text{Sr}_x\text{CuO}_4$

RUS simultaneously sees collapse of c_{66} and no effect on c_{44} in a 2mm single crystal

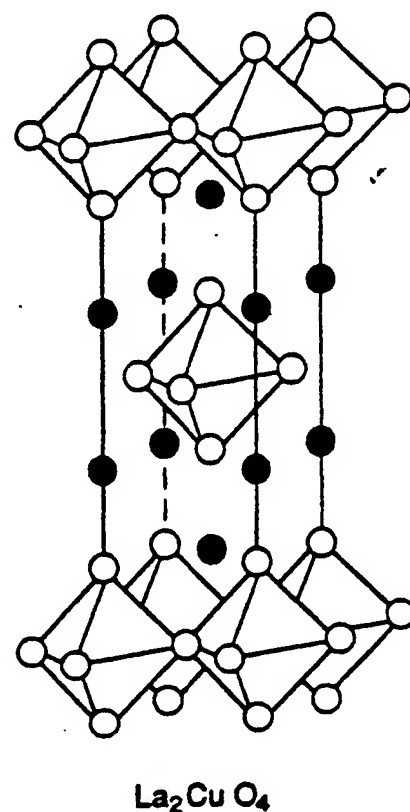
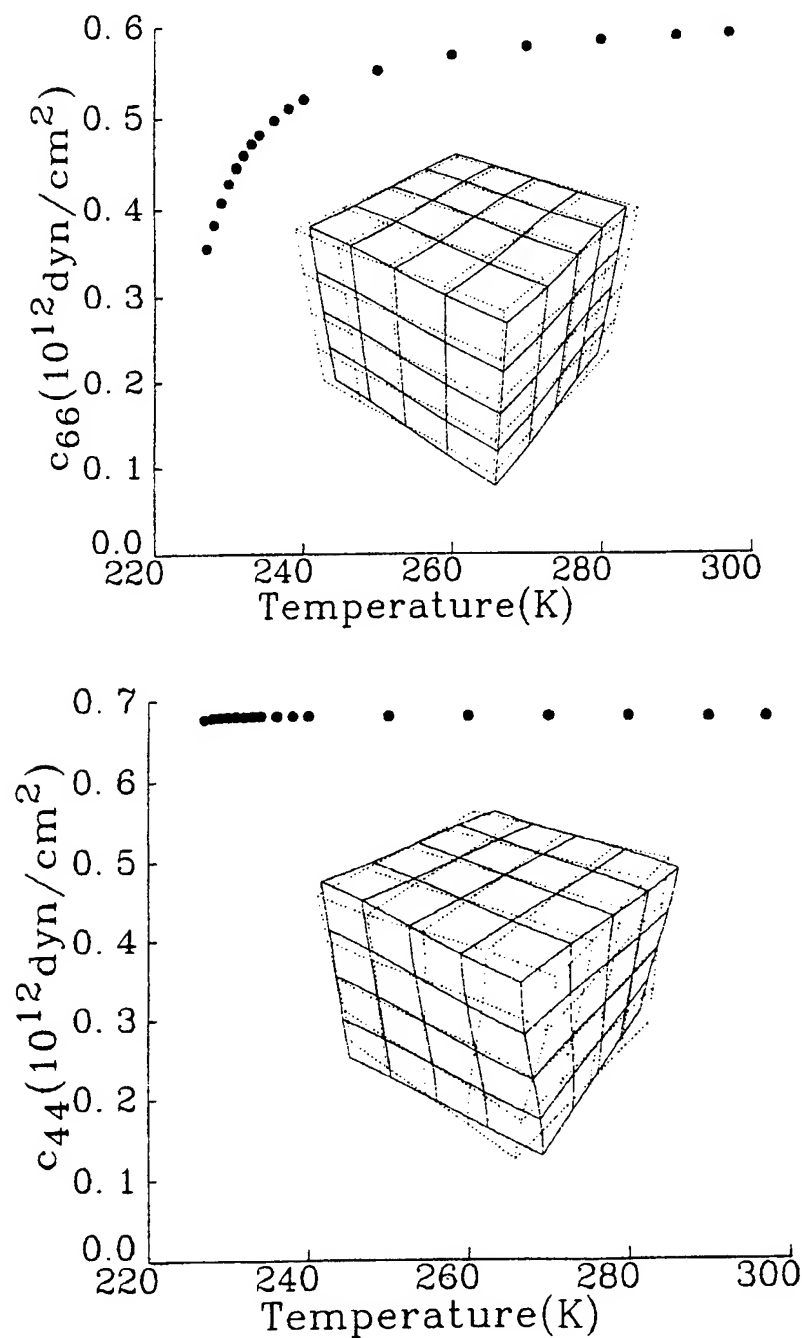
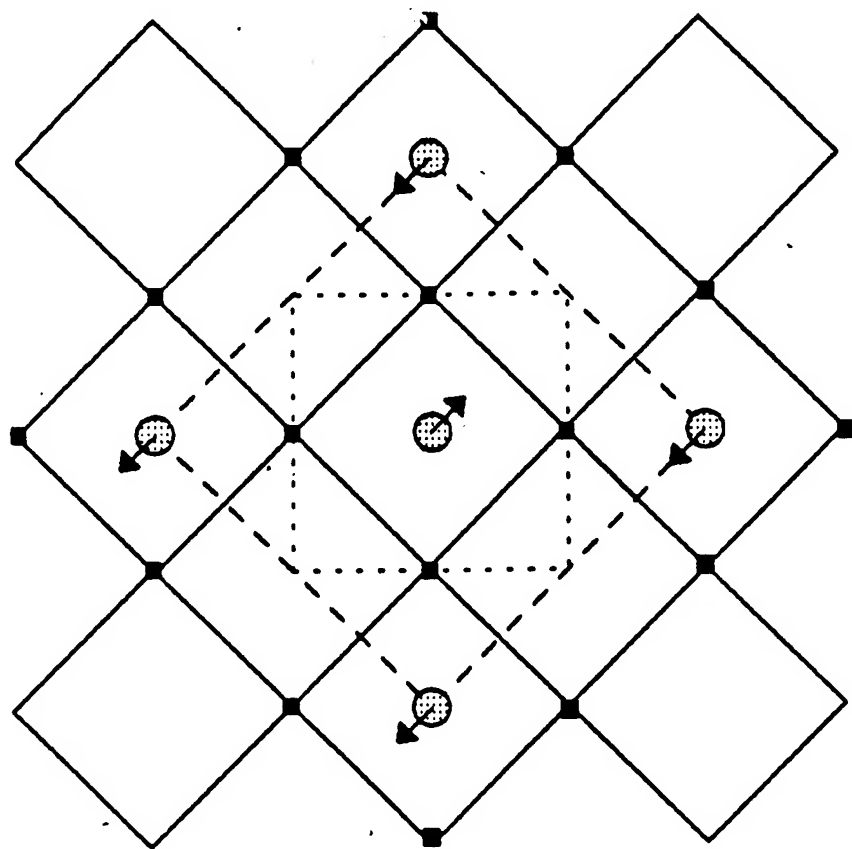


Fig 12 (in planes)



Numerical analysis of the motion (6) establishes that the eigenmode shown in Fig. 1 depends almost purely on c_{66} . Absent dynamical effects, we can treat the temperature dependence of c_{66} with a conventional Ginsburg-Landau (G-L) Hamiltonian. A simplified version of such a Hamiltonian, containing all the essential physics is

$$F = \frac{1}{2} \alpha (T - T_c) q^2 + \frac{1}{4} \beta q^4 + \frac{1}{2} c_{66} e_6^2 + \delta e_6 q^2 \quad (1)$$

where e_6 is the shear strain, q is one component of the order parameter, and α , β , and δ are parameters. The last term in Eq. 1 is the quadratic coupling between strain and order parameter. Minimization of this expression with respect to q determines $q(T)$. Using $q(T)$ we can then calculate $c_{66}(T)$ by taking the second derivative of F with respect to strain to obtain

$$\begin{aligned} c_{66}(T) &= c_{66} & \text{for } T > T_c \\ c_{66}(T) &= c_{66} - 2\delta^2 / \beta & \text{for } T < T_c, \end{aligned} \quad (2)$$

where q is zero above T_c and non-zero below. Eqs. 2 are the usual G-L result, discussed more completely by Rehwald (7). We see, therefore, that simple quadratic coupling and no dynamics produces only a step discontinuity in c_{66} at the structural phase transition. This is not what the data show. The data fit a Curie-Weiss (C-W) softening of the form

$$c_{66}(T) = c_{66} (1 - g/(T - T_c)) \quad (3)$$

where T_c is 223K and the fit, shown as the solid line in Fig. 1, is accurate to 0.2% over more than a decade in $g/(T - T_c)$.

Gaussian fluctuations of the order parameter (8), self-consistent phonons (9), and linear coupling between strain and order parameter (7) all yield a C-W dependence for c_{66} . For Gaussian fluctuations, the critical exponent for the specific heat and for the elastic moduli is $\lambda = 2 - d/2$, where d is the dimension of the order parameter. In our system, the order parameter is two dimensional, thus the critical exponent (the exponent of $1/(T - T_c)$) is unity, in agreement with the data. However, our C-W fit is over a temperature range of about 80K ($g=1.47$ K). This is a very large range for fluctuations to be important. We can make an upper-bound estimate for the fluctuation regime (8) by using a few lattice spacings for the coherence length, and by using a 1% (SrTiO_3 has about a 10% modulus discontinuity at its phase transition temperature) modulus discontinuity to obtain a fluctuation range of about 1K, comparable to the region in Fig. 2 where the ultrasonic attenuation increases sharply. Thus it appears very unlikely that 2-D Gaussian fluctuations can explain what we observe.

A self-consistent phonon treatment of the anharmonic potential associated with the zone-edge soft mode of the O octahedra can also produce C-W modulus softening (9). For this sort of treatment to be successful, the zone-edge soft mode must be linearly coupled to the zone-center acoustic mode. The 1-D treatment in ref. (9) deals with this by inserting an anharmonic spring, used in the shell-model to develop the self-consistent phonon dispersion curve, in series with the ion cores. Thus this spring contributes to the potential energy for any value of k , the phonon wave vector.

Neutron scattering measurements (3) show that the soft mode is part of the phonon branch corresponding to c_{44} , not c_{66} . Without some linear coupling term to the c_{66} dispersion curve, it is not easy to see the applicability of self-consistent phonons to the particular modulus softening of concern here. Were such a term to be added, the model would be forced to become explicitly 3-D, and because both the coupling and the energies would depend on the anharmonicity, the C-W exponent would likely be lost.

The third possibility we consider here is the replacement of quadratic coupling with linear coupling (for $T > T_c$, the inclusion of the quadratic term has no effect with or without the linear term present) between order parameter and strain in Eq. 1. This yields

$$F = \frac{1}{2} \alpha (T - T_c) q^2 + \frac{1}{4} \beta q^4 + \frac{1}{2} c_{66} e_6^2 + \gamma e_6 q \quad (4)$$

and

$$\begin{aligned} c_{66}(T) &= c_{66} - \gamma^2 / (\alpha (T - T_c)) & \text{for } T > T_c \\ c_{66}(T) &= c_{66} - \gamma^2 / (2\alpha (T - T_c)) & \text{for } T < T_c \end{aligned} \quad (5)$$

as required to fit the data of Fig. 1. To justify a linear coupling term, the $\text{La}_{1.86}\text{Sr}_{.14}\text{CuO}_4$ crystal must be either non-linear or not tetragonal.

In Fig. 4 we plot some of the lowest eigenfrequencies of the $\text{La}_{1.86}\text{Sr}_{.14}\text{CuO}_4$ crystal vs. T , and in Fig. 5 are plotted the lowest two eigenmodes on an expanded scale, showing avoided crossings of several percent. Note that in Fig. 4, many avoided crossings are apparent. The mechanical Lagrangian for analysis of the resonances of this material is based on a linear tetragonal solid (1,6). This model produces eight orthogonal symmetry classes for the modes. The dimensions of the crystal are such that the modes that do cross as temperature is varied are all orthogonal so that none of the avoided crossings should occur. Their existence can be explained only if the crystal is non-linear, not tetragonal, or has excessive preparation errors.

Macroscopic Ginsburg-Landau picture

Free energy expansion

$$F = F_{\text{op}} + F_e + F_{\text{op-e}} \quad a = \alpha (T - T_c)$$

$$F_{\text{op}} = a(Q_1^2 + Q_2^2) + u(Q_1^2 + Q_2^2)^2 + v(Q_1^4 + Q_2^4),$$

where Q_1 and Q_2 are the order parameters corresponding to the two directions of octahedral tilt.

$$F_e = 1/2 c_{11}(e_1^2 + e_2^2) + c_{12}e_1e_2 + c_{13}(e_1 + e_2)e_3 \\ + 1/2 c_{33}e_3^2 + 1/2 c_{44}(e_4^2 + e_5^2) + 1/2 c_{66}e_6^2$$

where c_{ij} are the elastic constants and e_i the macroscopic strains.

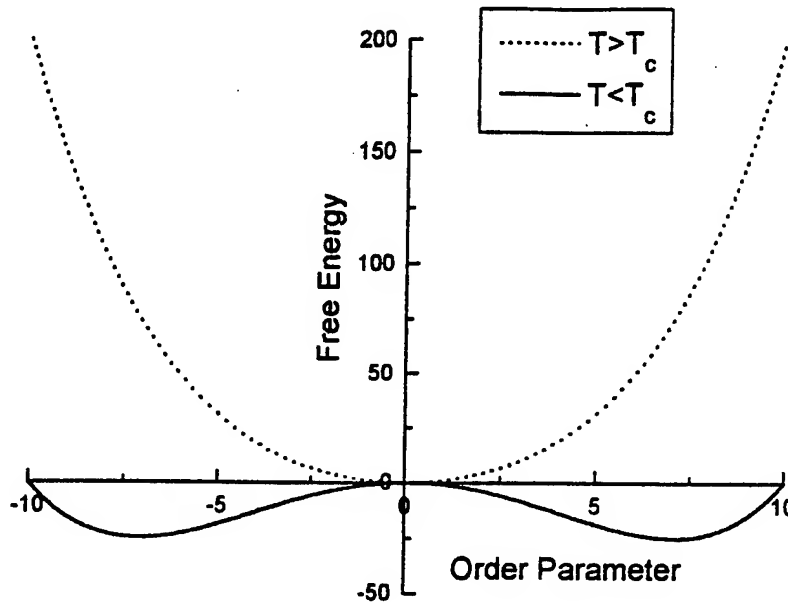
$$F_{\text{op-e}} = [k_{xx}(e_1 + e_2) + k_{zz}e_3](Q_1^2 + Q_2^2) \\ + k_{xy}e_6(Q_1^2 - Q_2^2),$$

where k_{ab} are the symmetry-allowed coefficients from the general expansion

$$F = \sum_{a,b,i} k_{ab}e_{ab}Q_i^2.$$

Ginzburg-Landau description of second order phase transitions

Linear coupling between strain e_4 and order parameter q



$$F = \frac{1}{2}\alpha(T - T_c)q^2 + \frac{1}{4}\beta q^4 + \frac{1}{2}c_{44}e_4^2 + \gamma e_4 q$$

1. Minimize F with respect to q .

$$\frac{\partial F}{\partial q} = \alpha(T - T_c)q + \beta q^3 + \gamma e_4 = 0.$$

Note that at zero strain, $T > T_c$, $q=0$, while for $T < T_c$, $q \neq 0$.

This is the constraint that we use when computing the elastic response.

2. Compute the elastic response under the constraint.

$$c_{44}(T) = \left. \frac{d^2 F}{de_4^2} \right|_{e_4=0}$$

Here's how! Use the constraint that F be a minimum and compute:

$$\frac{\partial}{\partial e_4} [\alpha(T - T_c)q + \beta q^3 + \gamma e_4] = 0$$

$$\frac{\partial q}{\partial e_4} = \frac{-\gamma}{\alpha(T - T_c) + 3\beta q^2}$$

$$\frac{\partial^2 q}{\partial e_4^2} = \frac{3\beta\gamma q}{(\alpha(T - T_c) + 3\beta q^2)^2} \frac{\partial q}{\partial e_4} = \frac{-3\beta\gamma}{\gamma} \left(\frac{\partial q}{\partial e_4} \right)^3$$

Now compute $c_{44}(T)$

$$\frac{\partial^2 F}{\partial e_4^2} = (\alpha(T - T_c) + 3\beta q^2) \left(\frac{\partial q}{\partial e_4} \right)^2 + (\alpha(T - T_c)q + \beta q^3) \frac{\partial^2 q}{\partial e_4^2} + c_{44} + 2\gamma \frac{\partial q}{\partial e_4} + \gamma e_4 \frac{\partial^2 q}{\partial e_4^2}$$

Noting that if $T > T_c$ then $q=0$ and that we are evaluating at $e_4=0$ we get:

$$\frac{\partial q}{\partial e_4} = \frac{-\gamma}{\alpha(T - T_c)}$$

giving

$$c_{44}(T) = c_{44} - \frac{\gamma^2}{\alpha(T - T_c)} \text{ if } T > T_c$$

while for $T < T_c$ we find that

$$c_{44}(T) = c_{44} + \frac{\gamma^2}{2\alpha(T - T_c)} \text{ and } q^2 = \frac{-\alpha(T - T_c)}{\beta}, \text{ producing a so-called}$$

Curie-Weiss behavior on either side of the transition.

Let's now look at quadratic coupling between strain and order parameter

$$F = \frac{1}{2}\alpha(T - T_c)q^2 + \frac{1}{4}\beta q^4 + \frac{1}{2}c_{44}e_4^2 + \gamma e_4 q^2$$

Minimizing F with respect to the order parameter q yields

$$\frac{dF}{dq} = (\alpha(T - T_c) + 2\gamma e_4)q + \beta q^3 = 0$$

which has as solutions

$q=0$ above T_c , *independent* of e_4

and

$$q^2 = -\frac{\alpha(T - T_c) + 2\gamma e_4}{\beta} \quad \text{for } T < T_c \text{ as long as the strain is small.}$$

The effect of this is that for

$$T > T_c \quad c_{44}(T) = c_{44}$$

and for

$$T < T_c \quad c_{44}(T) = c_{44} - \frac{\gamma^2}{2\beta}.$$

Thus a step discontinuity occurs!

What happens when coupling is turned on;

$$F = \frac{1}{2}\alpha(T - T_c)q^2 + \frac{1}{4}\beta q^4 + \frac{1}{2}c_{44}e_4^2 + \gamma e_4 q^n$$

$$\frac{\partial F}{\partial e_4} = 0 = c_{44}e_4 + \gamma q^n$$

$$e_4 = -\frac{\gamma q^n}{c_{44}}$$

$$T'_c = T_c + \frac{\gamma^2}{\alpha c_{44}} \quad \text{if } n = 1$$

$$\beta' = \beta - \frac{2\gamma^2}{c_{44}} \quad \text{if } n = 2$$

Thus the effect is to either renormalize T_c if $n=1$, or if $n=2$, the transition can become first order. Thus elastic coupling can have either weak or strong effects on the underlying physics. Note that a really careful treatment will always produce a first order transition, albeit weak, if $n=2$.

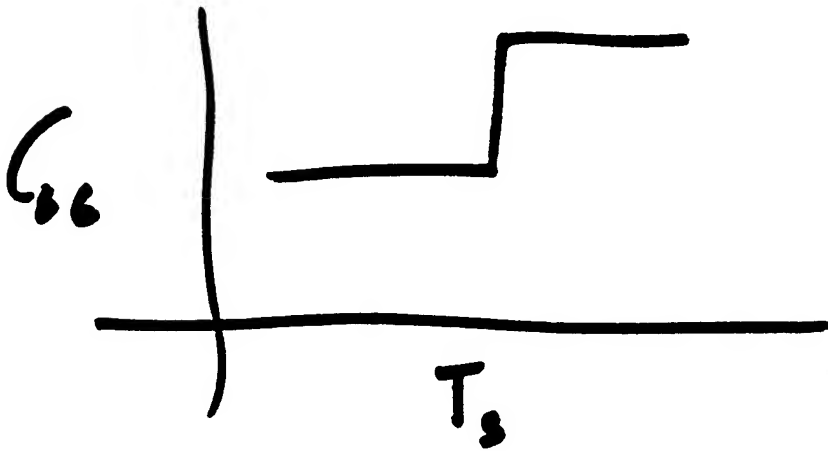
Now to make predictions,

minimize free energy with respect to strain (the e_i 's) and the order parameters (the Q_i 's).

This minimization predicts:

1. $\Delta c_{44} = 0$
2. $\Delta c_{11} = \Delta c_{12}$, so $\Delta (c_{11} - c_{12}) = 0$
3. $\Delta c_{66} \gg \Delta c_{33} > \Delta c_{13} > \Delta c_{11}$.

QUADRATIC COUPLING :



WE OBSERVE CURIE-WEISS

- MICROSCOPIC SHELL MODEL
- GINSBURG-LANDAU + FLUCTUATIONS

BOTH ARE OK

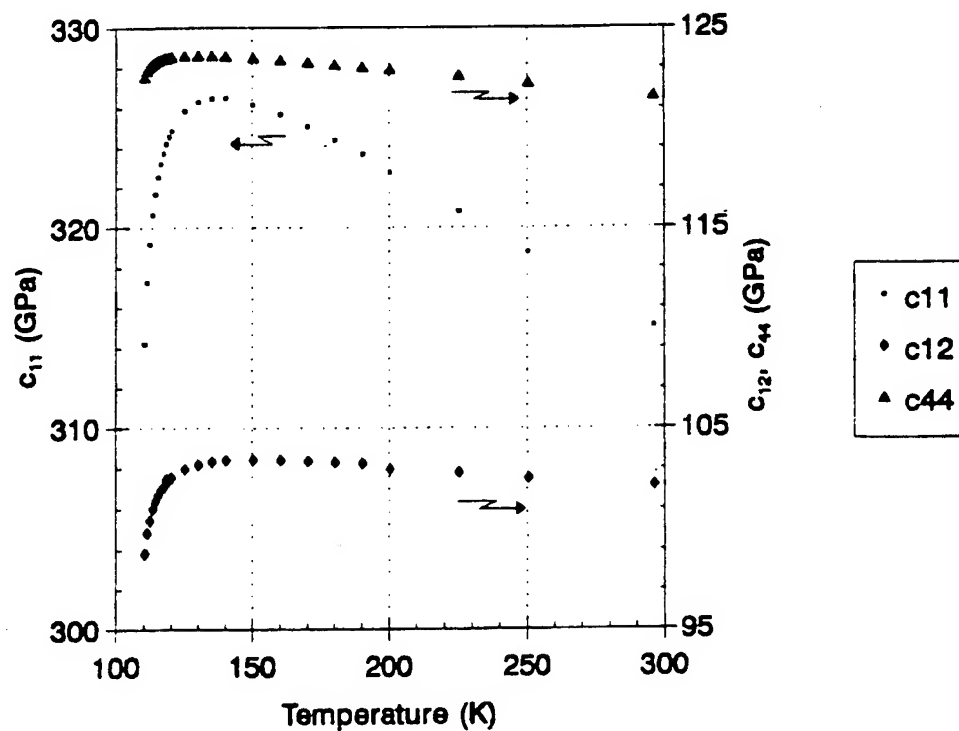
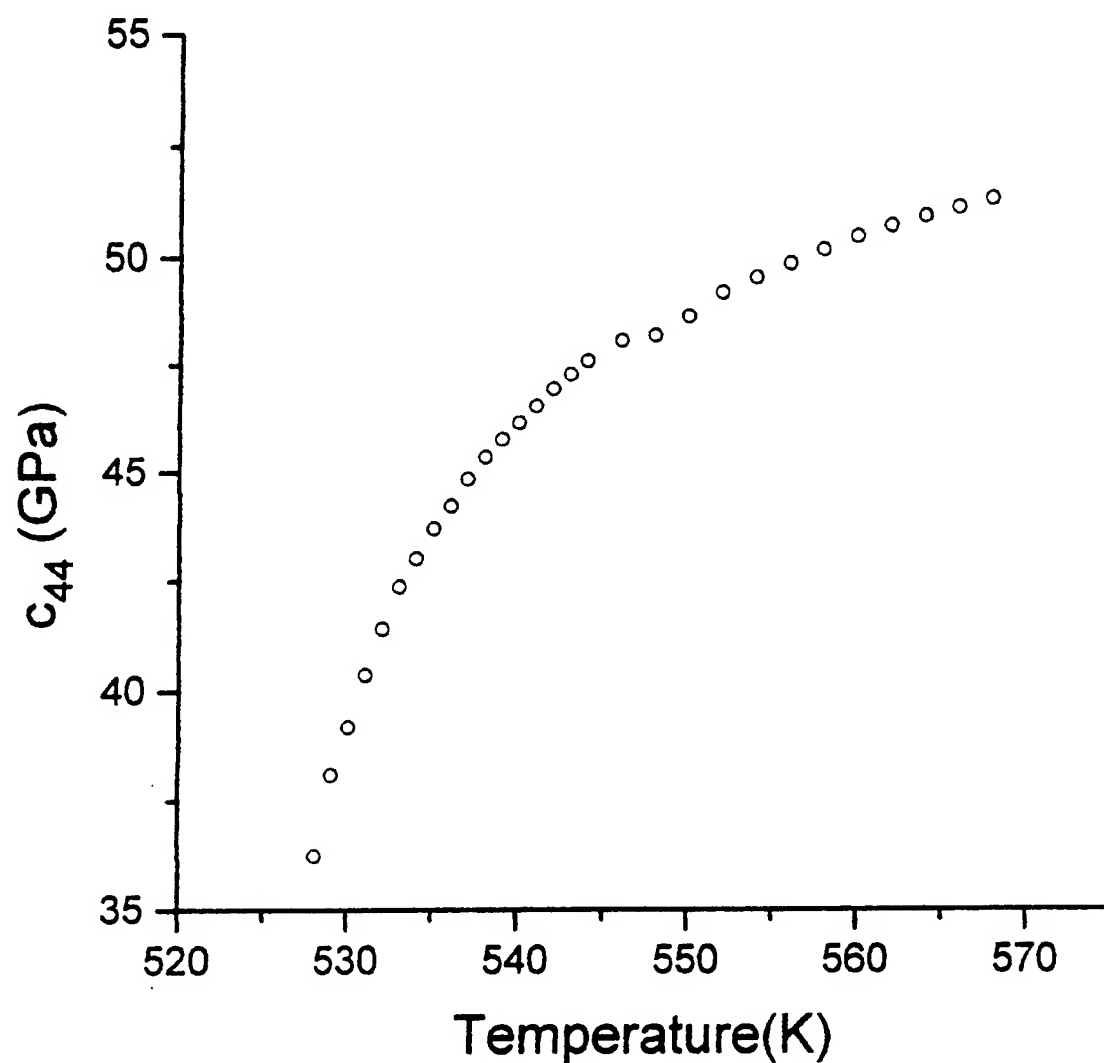


Fig. 10. The three elastic moduli of a single crystal of SrTiO_3 near the structural phase transition are shown as a function of temperature. These data were obtained using RUS.

Structural phase transition in a 1.5mm single crystal of pure La_2CuO_4 at 527K



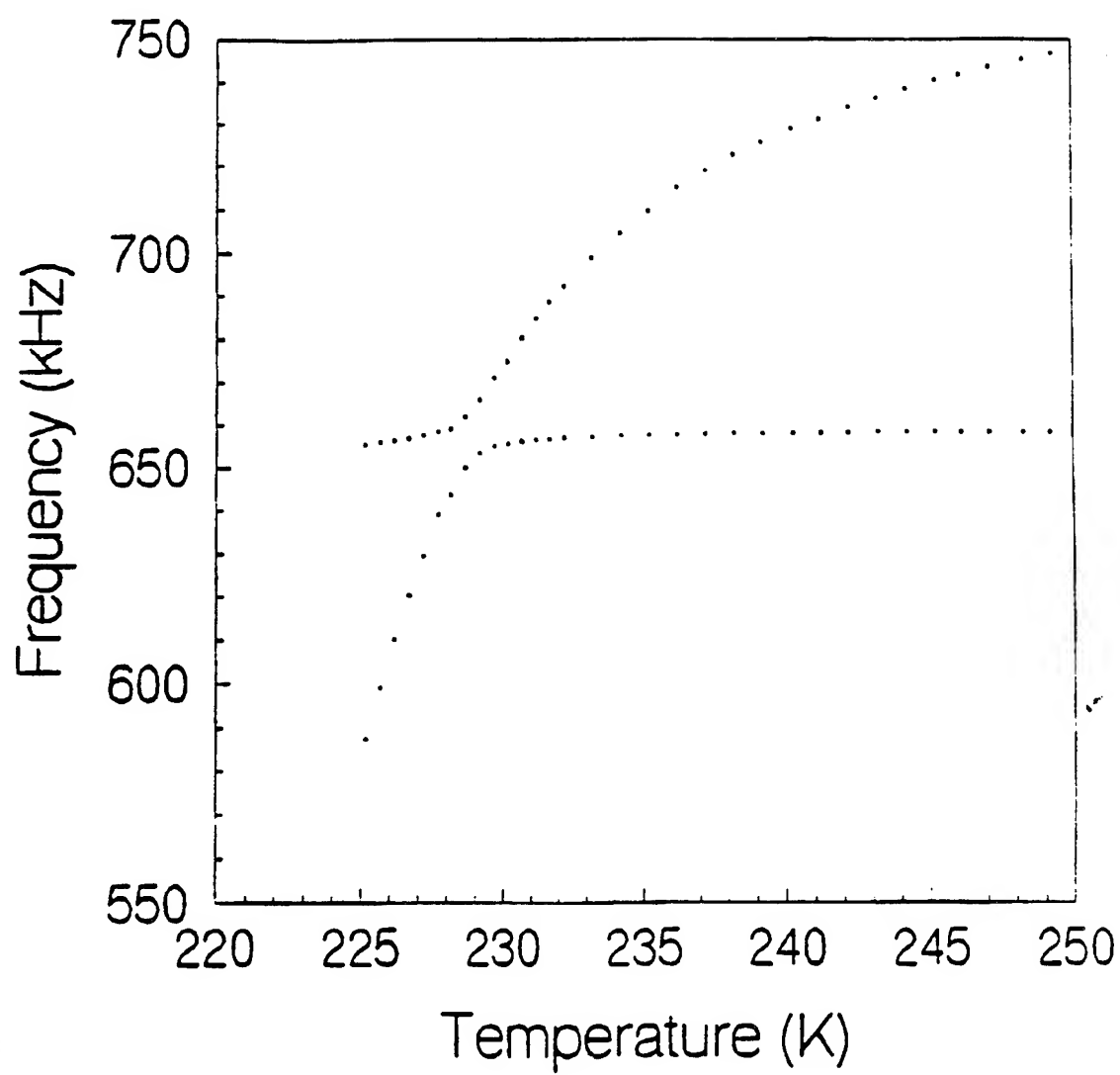
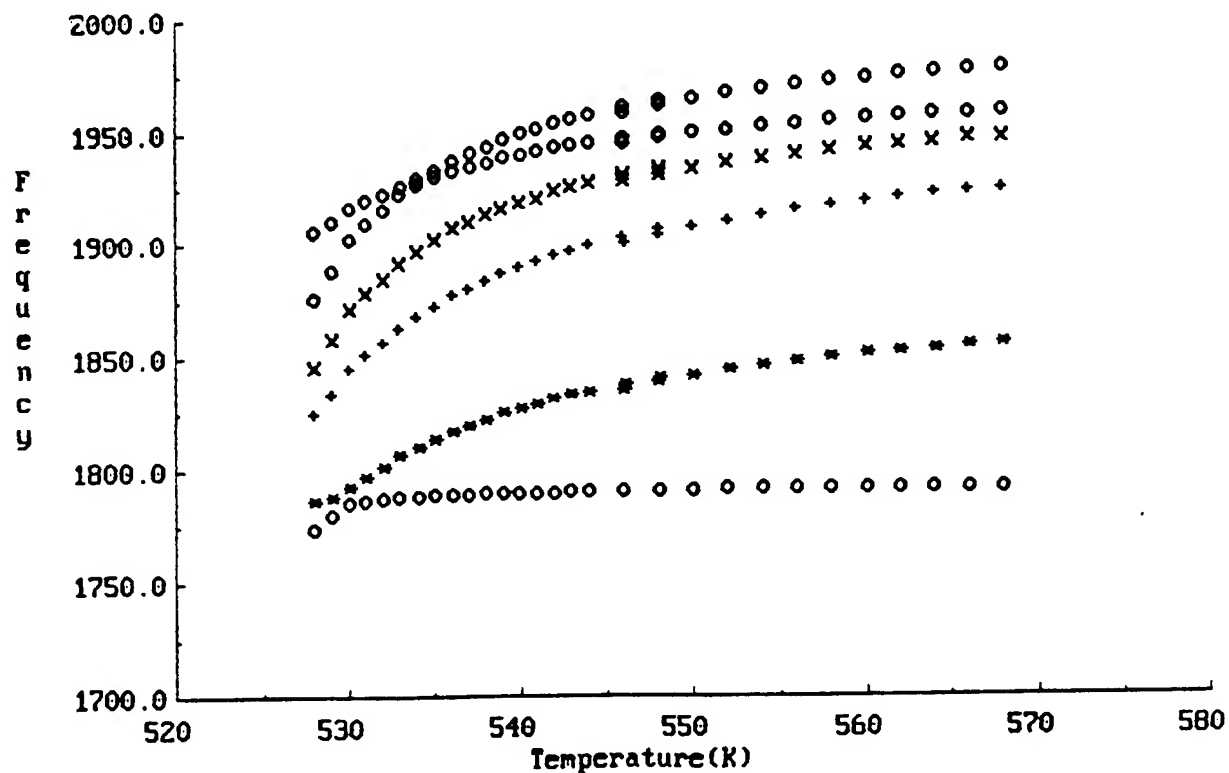
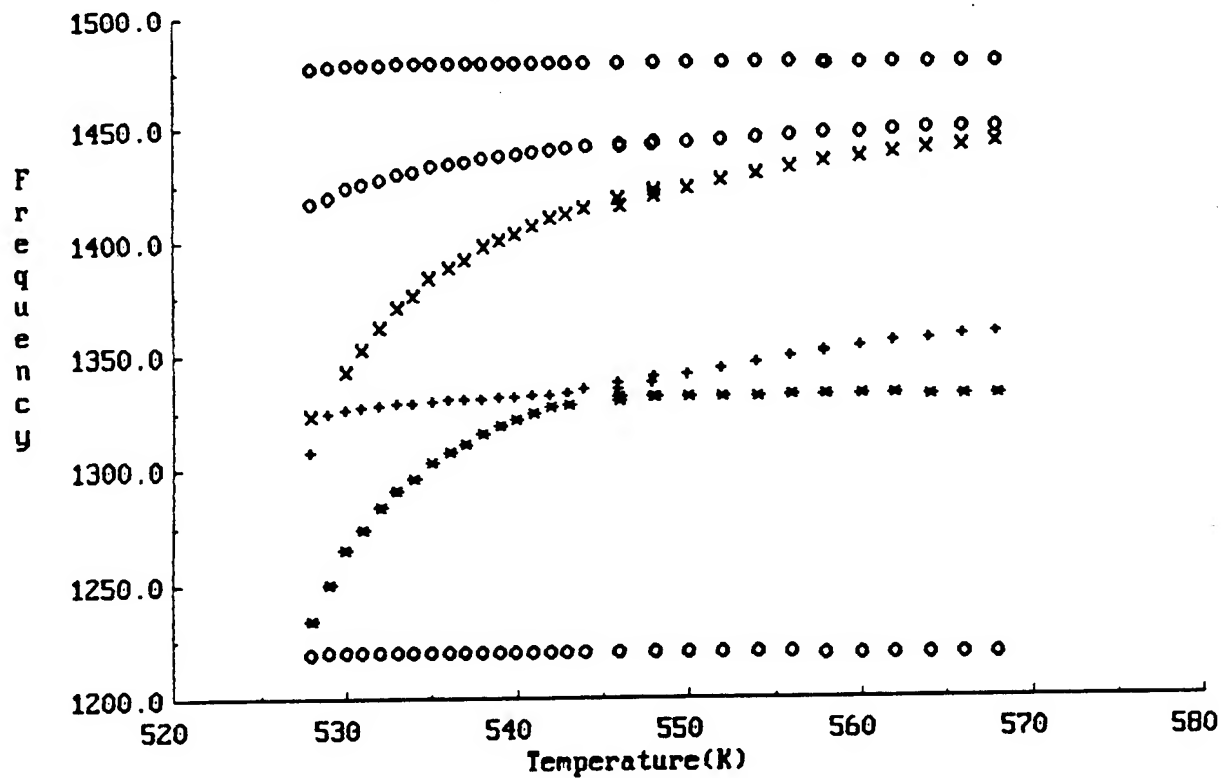
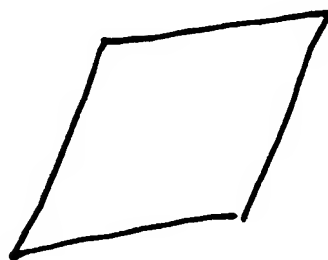
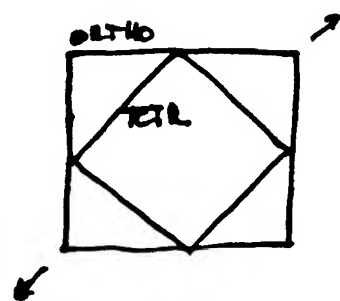


Figure 6

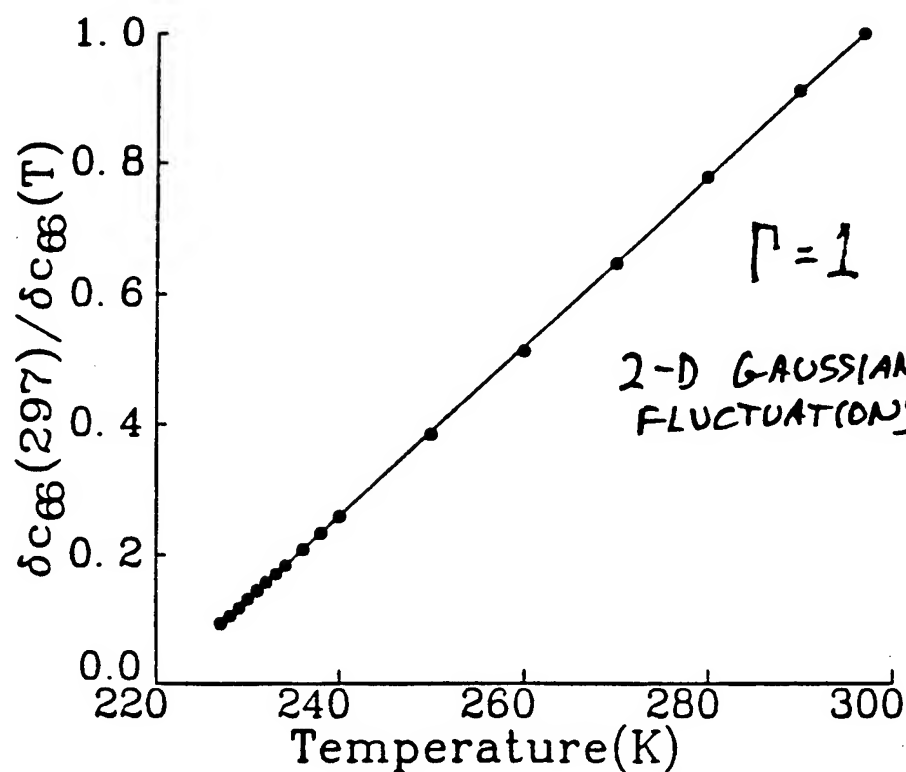


OCTAHEDRA TILT \Rightarrow TETRAGONAL TO ORTHORHOMBIC



LOOKS JUST
LIKE C_{66} SHEAR

QUADRATIC COUPLING OF ORDER PARAM.
TO SHEAR (C_{66}) $\Rightarrow \Gamma = .5$ BUT!



terials. Deuterium was loaded from the gas phase in the usual way.^{8,16} Rectangular parallelepipeds, ≈ 2 mm on an edge, were cut from larger samples using an electric discharge machine. Vacuum fusion analysis of one of the YD_x crystals showed $x = 0.10$, and 260 ppm of N and 2890 ppm of O impurities. Whereas qualitative results were obtained on two different samples, the data reported below were obtained on a single, rectangular-parallelepiped sample of room-temperature dimensions $1.82 \times 1.92 \text{ mm} \times 2.06 \text{ mm}$. The long axis of the parallelepiped was parallel to the c axis to within 0.5° , as determined by x-ray diffraction. Since a crystal of hexagonal symmetry is elastically isotropic in the basal plane, the orientations of the other crystalline axis were not determined relative to the parallelepiped axes.

Resonant ultrasound spectroscopy¹⁷ was used to measure the ultrasonic-attenuation and elastic constants. With this technique a single-crystal, rectangular-parallelepiped sample is placed corner-to-corner between two piezoelectric transducers, one transducer being used for generation and the other for detection of ultrasonic vibrations. By sweeping the excitation frequency, a large number of the lowest vibrational eigenfrequencies can be investigated. The eigenfrequencies are related to the elastic constants, while the inverse of the Q of the resonances is related to the vibrational energy loss in the sample. Using the method of Visscher *et al.*,¹⁸ we have identified the lowest 31 eigenfrequencies of one sample by fitting the measured frequencies to a set of elastic constants. This identification is needed for a microscopic interpretation of the results as discussed below.

III. RESULTS AND DISCUSSION

Figure 1(a) gives results for $1/Q$, for a single-crystal $YD_{0.10}$ sample, obtained at a frequency of 0.81 MHz, over the temperature range of 15–325 K. Three general features are apparent. The loss increases at the highest temperatures; this increase may be associated with the long-range diffusion process, or other processes discussed below. There is a small attenuation effect near 160 K, in the temperature range where resistance anomalies have been observed and associated with hydrogen ordering.¹⁹ The attenuation anomalies in this temperature range were found to depend on the rate and direction of temperature change and have not been well characterized. The main effect, of course, is the large, broad, asymmetric attenuation peak with the maximum near 87 K. The solid line is a theoretical fit to the data to be described below. Figure 1(b) gives data similar to that of Fig. 1(a), but for a different vibrational eigenmode, the difference to be discussed below. The major difference between the data sets for the two eigenmodes is in the magnitude of the low-temperature peak. Figure 2 gives additional data at other frequencies for the low-temperature peak. A temperature-independent background $(1/Q)_{bg}$ was subtracted from the two highest-frequency curves before plotting the data in Fig. 2. $(1/Q)_{bg} = 0.00007$ and 0.0001 for the 1.4- and 2.7-MHz curves, respectively. Since the peak for the lowest frequency was much higher relative to the background, no

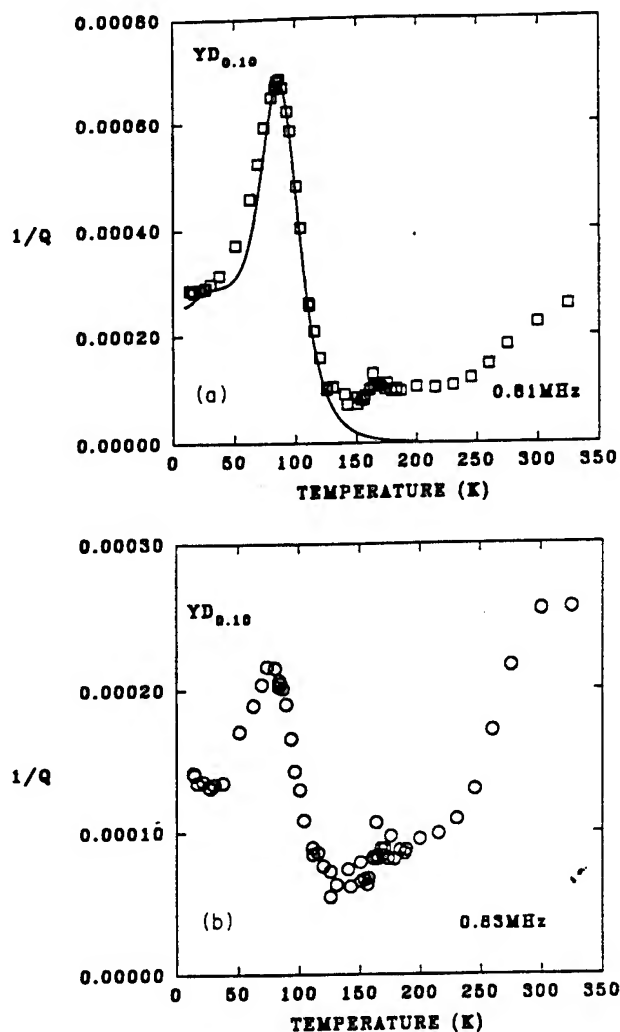


FIG. 1. (a) Ultrasonic loss, $1/Q$ vs temperature for $YD_{0.10}$ at a frequency of 0.81 MHz. The solid line represents a theoretical fit to the data described in the text. This vibrational eigenmode depends almost purely on C_{44} . (b) Ultrasonic loss, $1/Q$, vs temperature for $YD_{0.10}$ at a frequency of 0.83 MHz. This vibrational eigenmode depends almost purely on C_{66} .

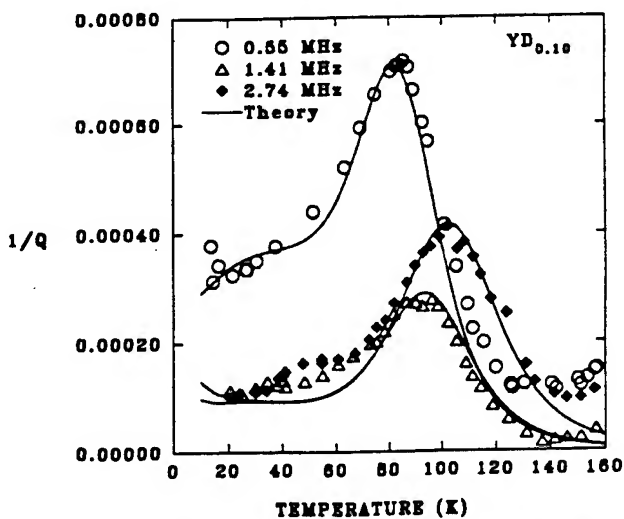


FIG. 2. Ultrasonic loss, $1/Q$, vs temperature at three different frequencies. The solid lines represent theoretical fits to the data described in the text.

HYDROGEN-ISOTOPE MOTION IN SCANDIUM STUDIED BY ...

modes by fitting our measured frequencies to a set of elastic constants using the method described by Visscher *et al.*²⁴ In general, each of the vibrational eigenmodes depends on a combination of elastic constants. However, the lowest eigenfrequency and a few of the higher eigenfrequencies depend on only one or two elastic constants. This fact enables us to obtain a rather accurate description of the temperature dependence of some of the elastic constants by simply measuring the temperature dependence of a selected number of eigenfrequencies. In addition, the ultrasonic attenuation associated with such eigenfrequencies is obtained from these measurements. In the present study the emphasis is on the temperature dependence of the ultrasonic loss, which is obtained from the inverse of the Q of the eigenmodes. Those modes which depend on only one or two elastic constants are particularly useful for making a microscopic interpretation of the phenomena responsible for the ultrasonic loss.

III. RESULTS

Figure 3 shows results for the ultrasonic loss $1/Q$ for two different vibrational eigenmodes in $\text{ScD}_{0.18}$. Our analysis shows that the two modes of Fig. 3 depend only on the shear elastic constants C_{44} and C_{66} ; that is, the derivative of the computed eigenfrequency with respect to the elastic constants is zero for the other three elastic constants. Further, the lower-frequency mode, at 0.73 MHz, is almost pure C_{44} ; the dependence of the higher-frequency mode, at 1.01 MHz, on elastic constants is weighted about 40% C_{44} and 60% C_{66} . There are three main features shown in Fig. 3. First, there is some evidence of an ultrasonic-attenuation anomaly near 170 K, in the temperature range where resistance anomalies have been observed and associated with hydrogen ordering.²⁵ The attenuation anomalies in this temperature range were found to depend on the rate and direction of temperature change and have not been well characterized.

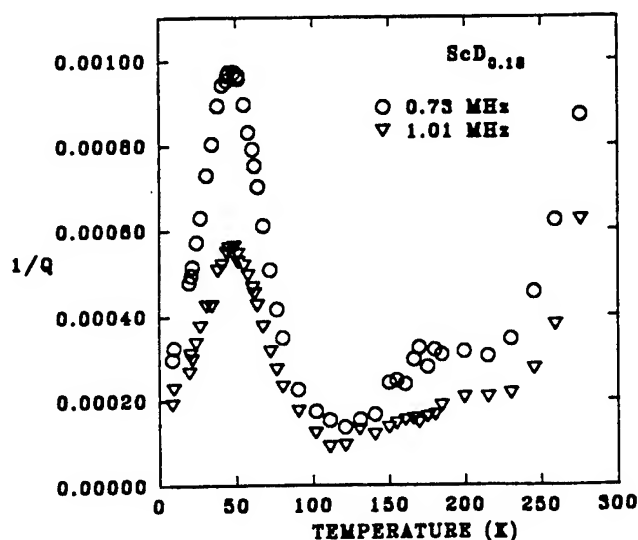


FIG. 3. Ultrasonic loss $1/Q$ for two different vibrational eigenmodes in $\text{ScD}_{0.18}$. The mode at 0.73 MHz is almost pure C_{44} , whereas the mode at 1.01 MHz is about 40% C_{44} and 60% C_{66} .

Second, the loss increases as the temperature approaches room temperature; this increase is probably associated with the long-range diffusion process. Finally, the dominant effect is the broad loss peak with the maximum near 50 K. These results will be discussed in more detail below.

Figure 4 shows data for $\text{ScH}_{0.25}$ at three different frequencies. The solid lines are theoretical fits to the data to be described below. Figure 5 shows similar data for $\text{ScD}_{0.18}$. The different frequencies correspond to different vibrational eigenmodes. It is seen that the attenuation-peak position shifts little, if any, with a change in measuring frequency. The attenuation peak for $\text{ScD}_{0.18}$ occurs at a considerably higher temperature than is the case for $\text{ScH}_{0.25}$.

Measurements were also made on an undoped Sc crystal. There is no low-temperature peak in this case, only a small, almost temperature-independent, attenuation.

IV. DISCUSSION

We describe our results in terms of the theory of two-level systems (TLS's). An interstitial such as hydrogen, which may occupy either of two nearby interstitial sites, can be described as a two-level system with an energy splitting $E = (E_T^2 + A^2)^{1/2}$, where E_T is the tunnel splitting and A is the difference in energy of the two wells (asymmetry). This formalism may be used even in cases where tunneling is not a factor, in which case we simply have $E_T = 0$. The ultrasonic loss due to relaxation is given by²⁶

$$\frac{1}{Q} = \frac{n_0 D^2}{4Ck_B T} \text{sech}^2 \left[\frac{E}{2k_B T} \right] \frac{\omega \tau}{1 + \omega^2 \tau^2}, \quad (1)$$

where n_0 is the concentration of TLS's, $D = \delta E / \delta \epsilon$ is the variation of the energy-level splitting with respect to the ultrasonic strain ϵ , C is an elastic constant, $\omega/2\pi$ is the ultrasonic frequency, and τ is the relaxation time. It is usually the case²⁷ that $\delta A / \delta \epsilon \gg \delta E_T / \delta \epsilon$, so that

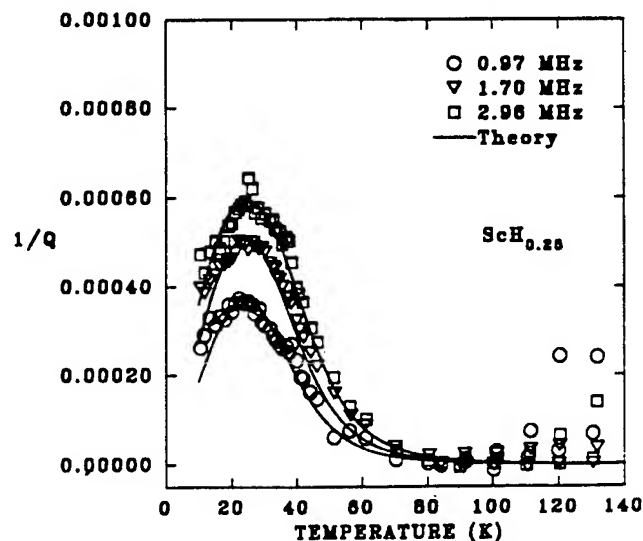


FIG. 4. Ultrasonic loss $1/Q$ for three different frequencies in $\text{ScH}_{0.25}$. The solid lines are fits to the data described in the text.

RUS and non-destructive testing-or how to make everyone happy with good physics!

Quality control and the means to test for it have become of increasingly greater concern to American industry, and therefore, to government and other funding sources.

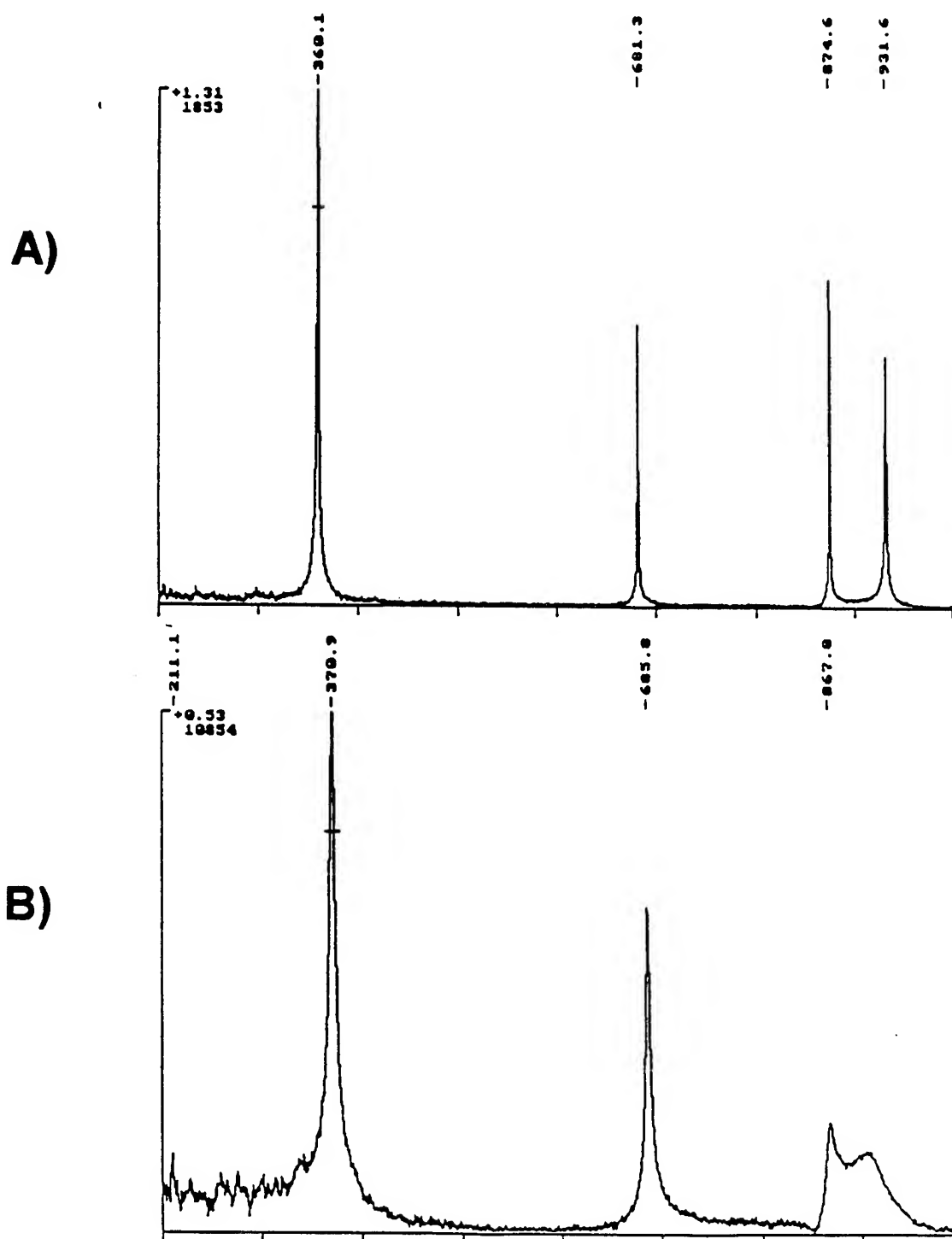


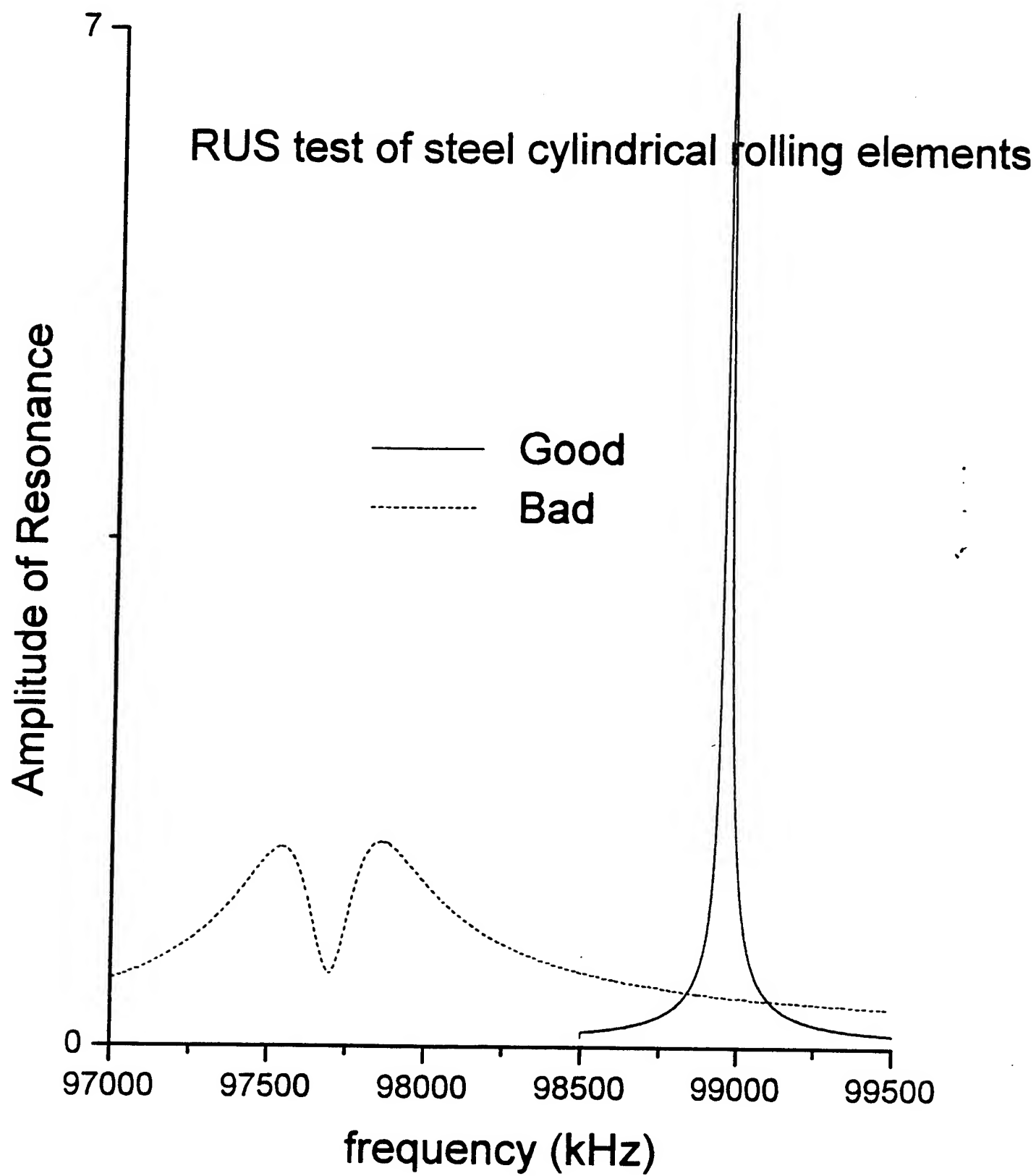
Not like this

Detection of microcracking in a single crystal sample of EuB_6

A) Resonances of the pristine sample

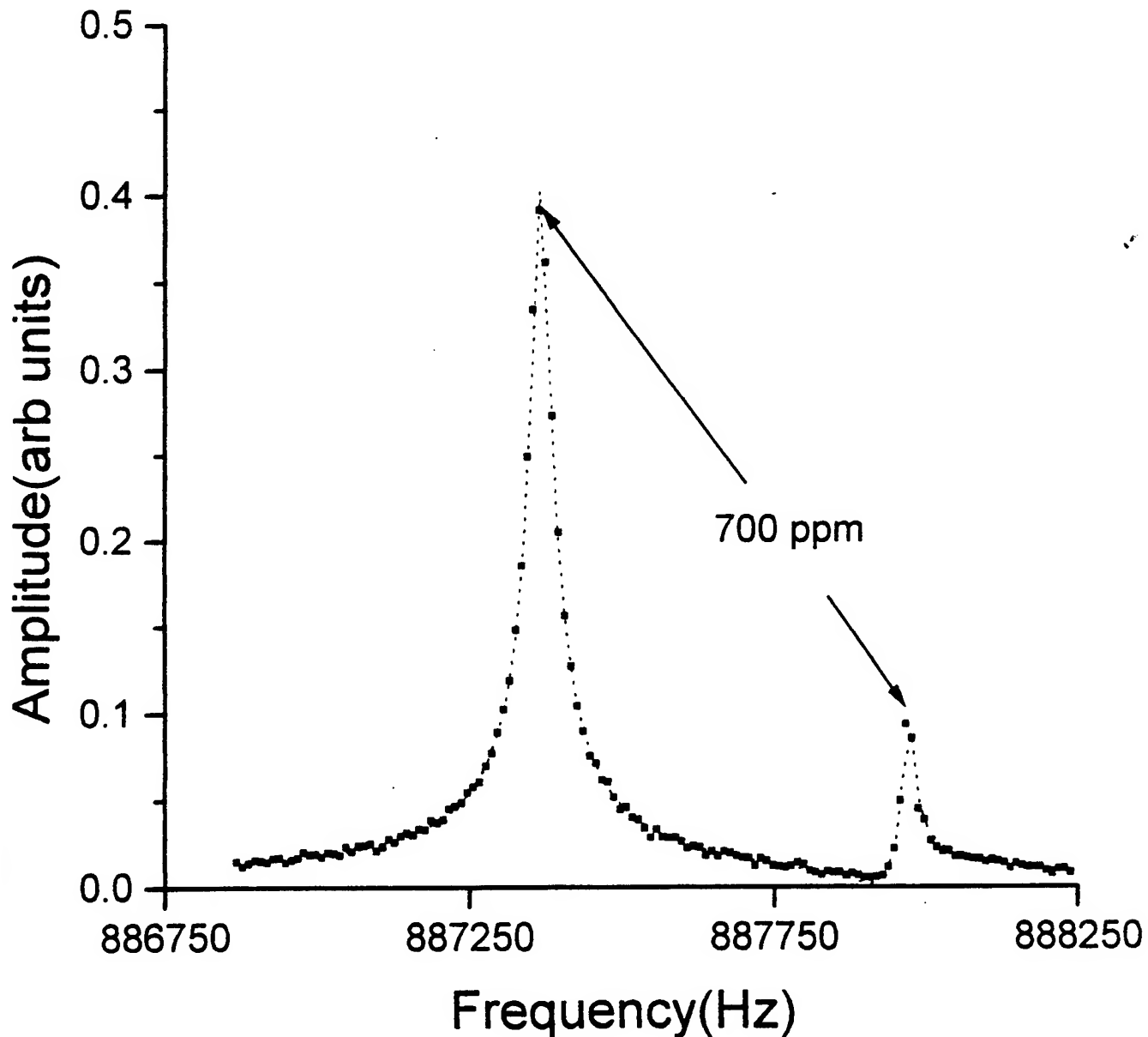
B) Resonances after a small stress has induced microcracking



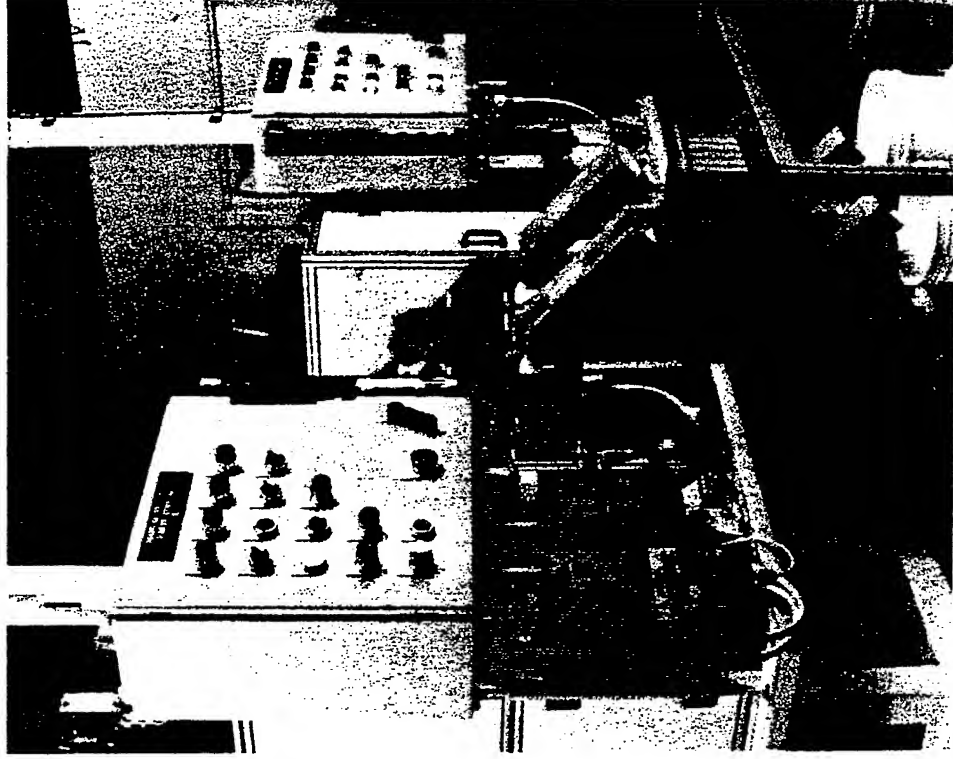
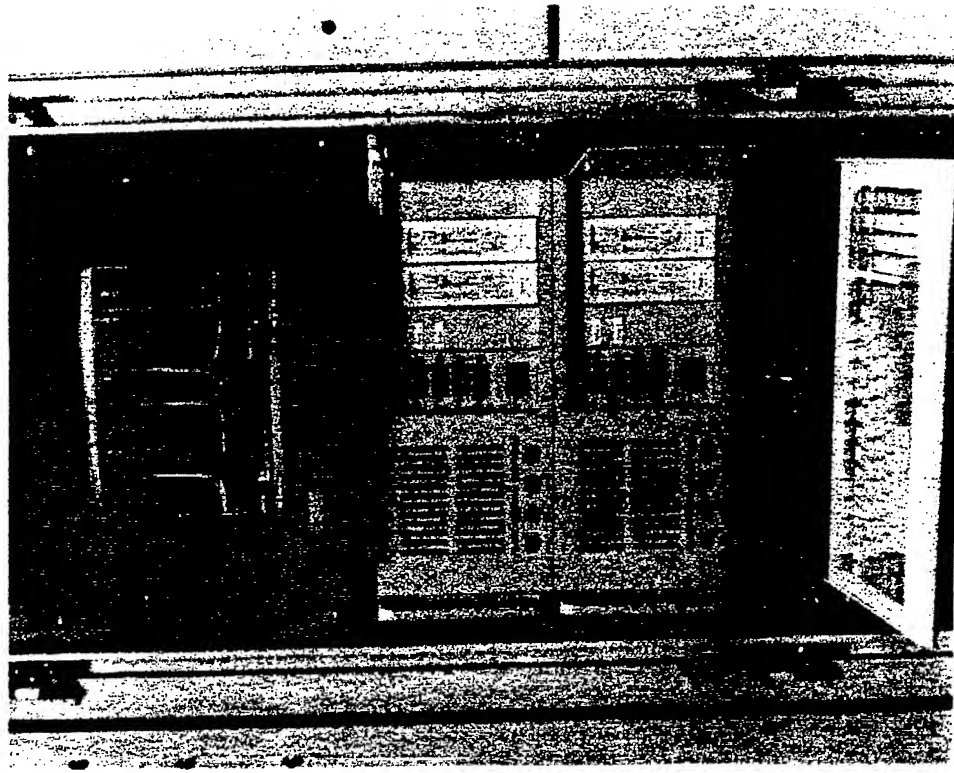


Resonant Ultrasound Spectroscopy -nondestructive testing

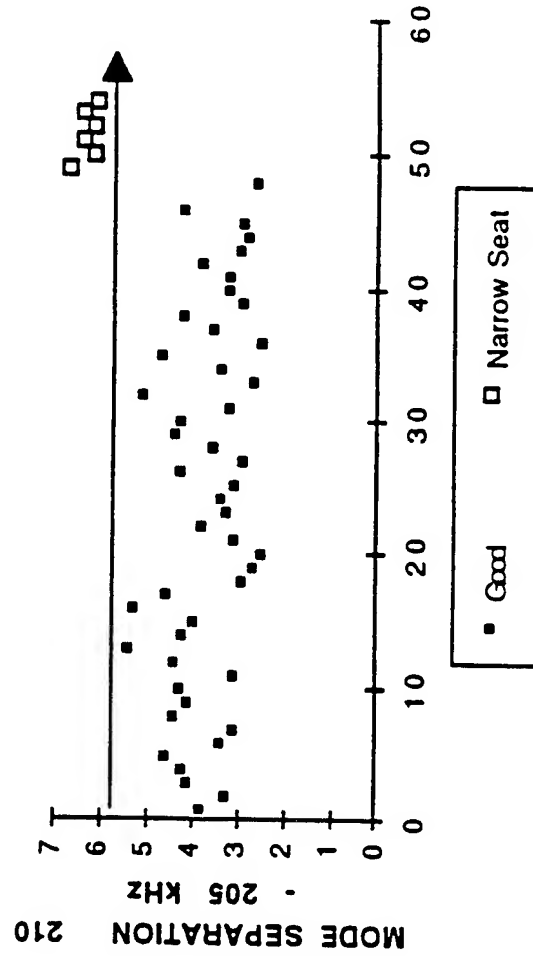
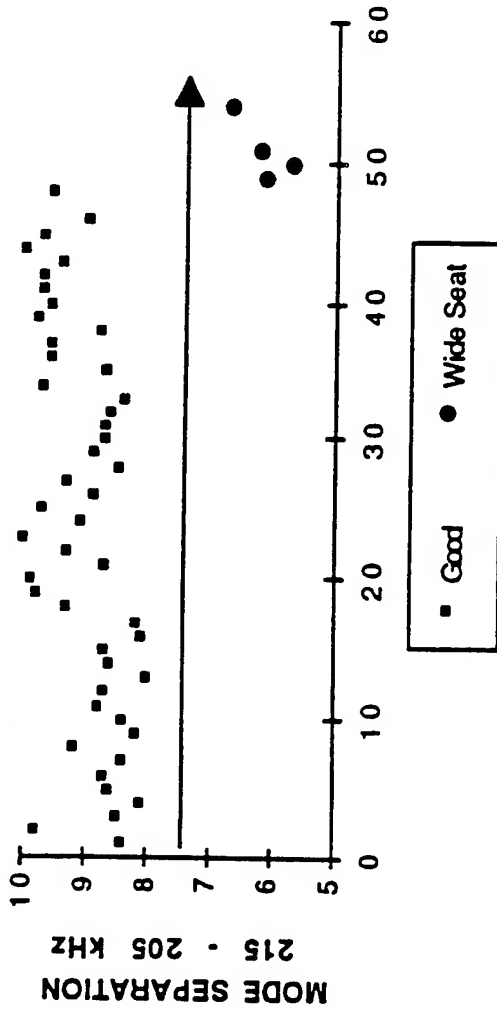
Sphericity error shown by splitting
of degenerate spherical resonance
in a Si_3N_4 ball bearing from NASA



Commercial RUS system for production testing of automotive oxygen sensors.
This system, as well as other RUS systems, is built and marketed by
Quatrosionics Corp. Of Albuquerque, NM



Oxygen sensor testing-flaw selection sensitivity



Production testing of zirconia automotive oxygen sensors using high-speed automated resonant ultrasound spectroscopy (RUS)

- Lab tests show that 10% to 40% of parts are flawed
- Cost of fired oxygen sensor \$ 0.25
- Cost to replace sensor after car has left showroom \$150.00
- NO OTHER PRODUCTION NDT AVAILABLE

Statistical test of RUS system:

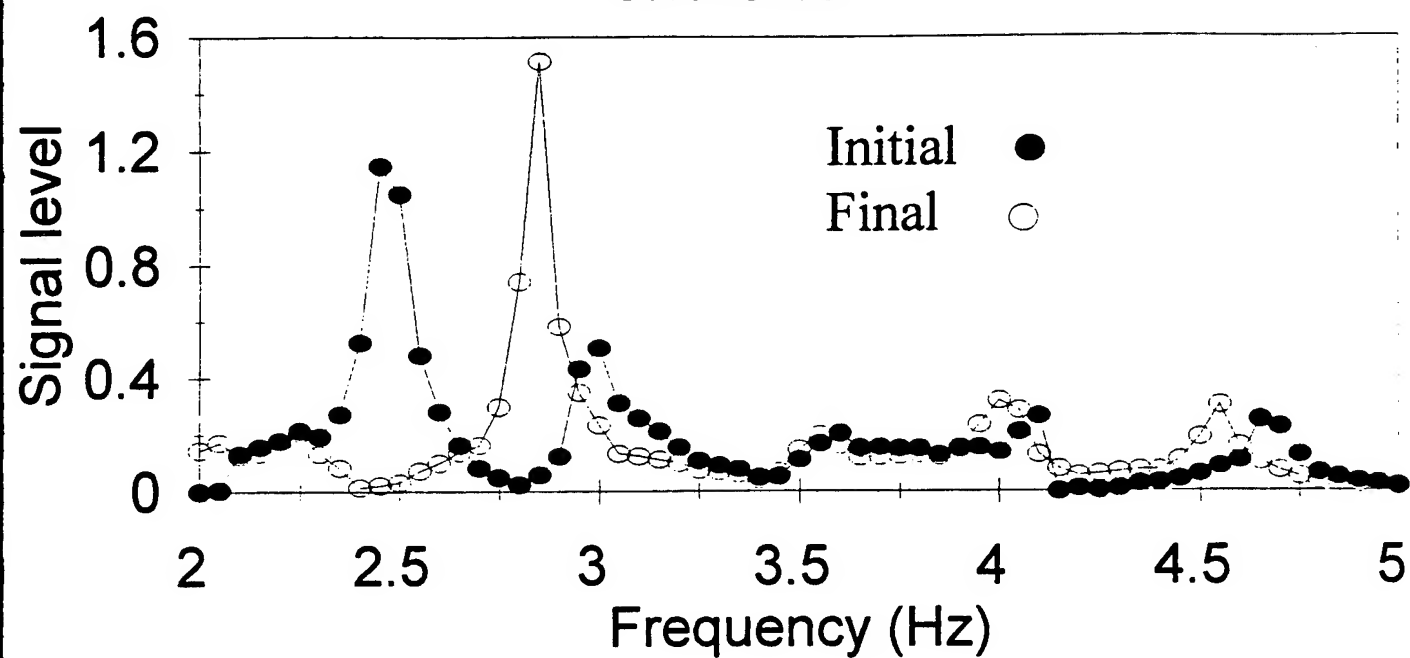
- 8000 parts were run through seven times in 24 hours for a total of 56,000 tests
- 200 known flawed parts and 200 known good parts were marked
- The parts were split equally among four separate test heads
- No stoppages that required operator intervention occurred

Results:

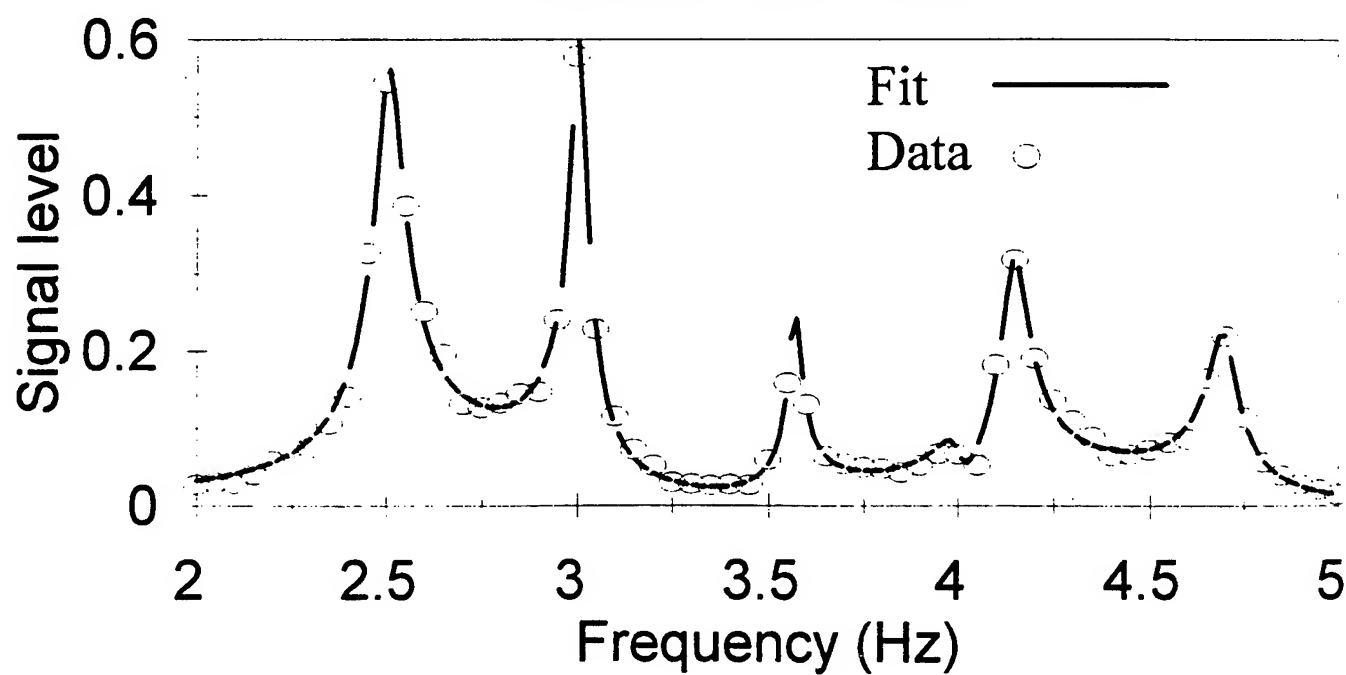
- 98.7% of the bad parts were successfully rejected
- 99.0% of the good parts were accepted

Conclusion: RUS can provide stunning improvements in selected areas of production NDT

Initial and Final measurements
South Girder

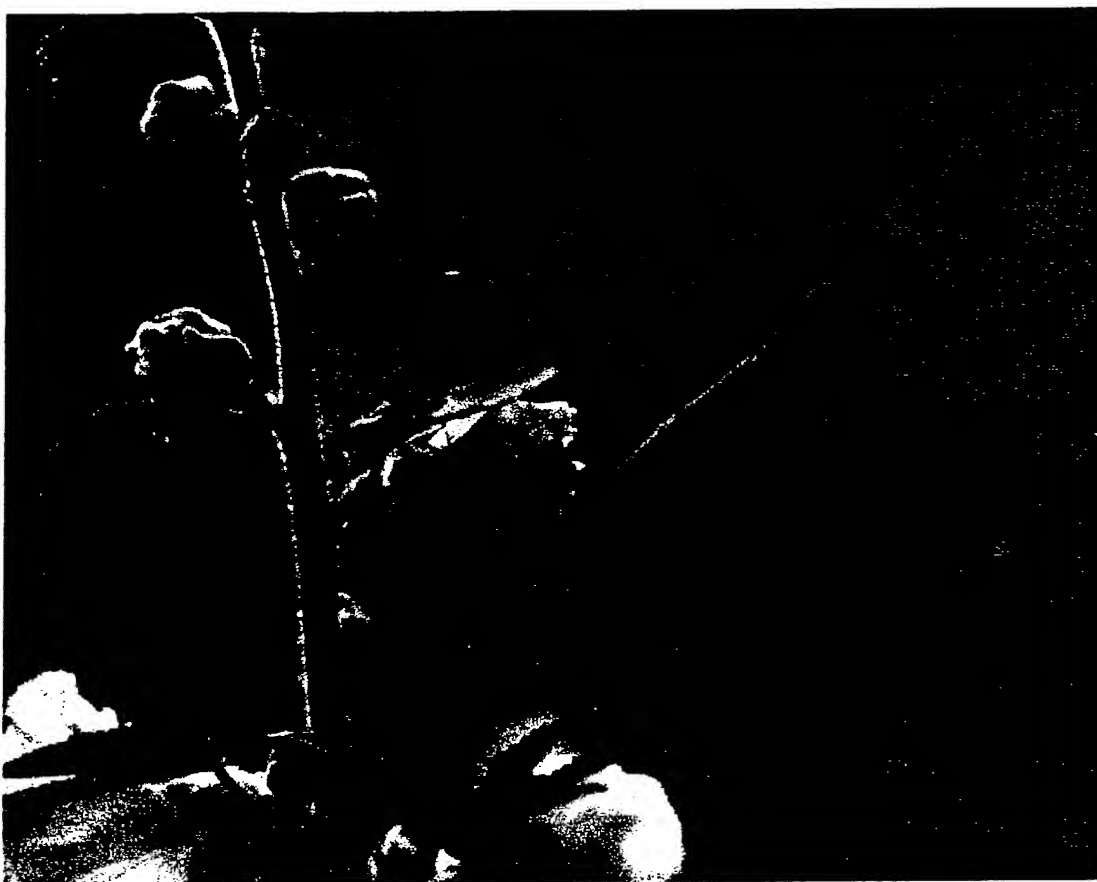


I-40 Bridge - after 2nd cut
D0903362 - North I-beam



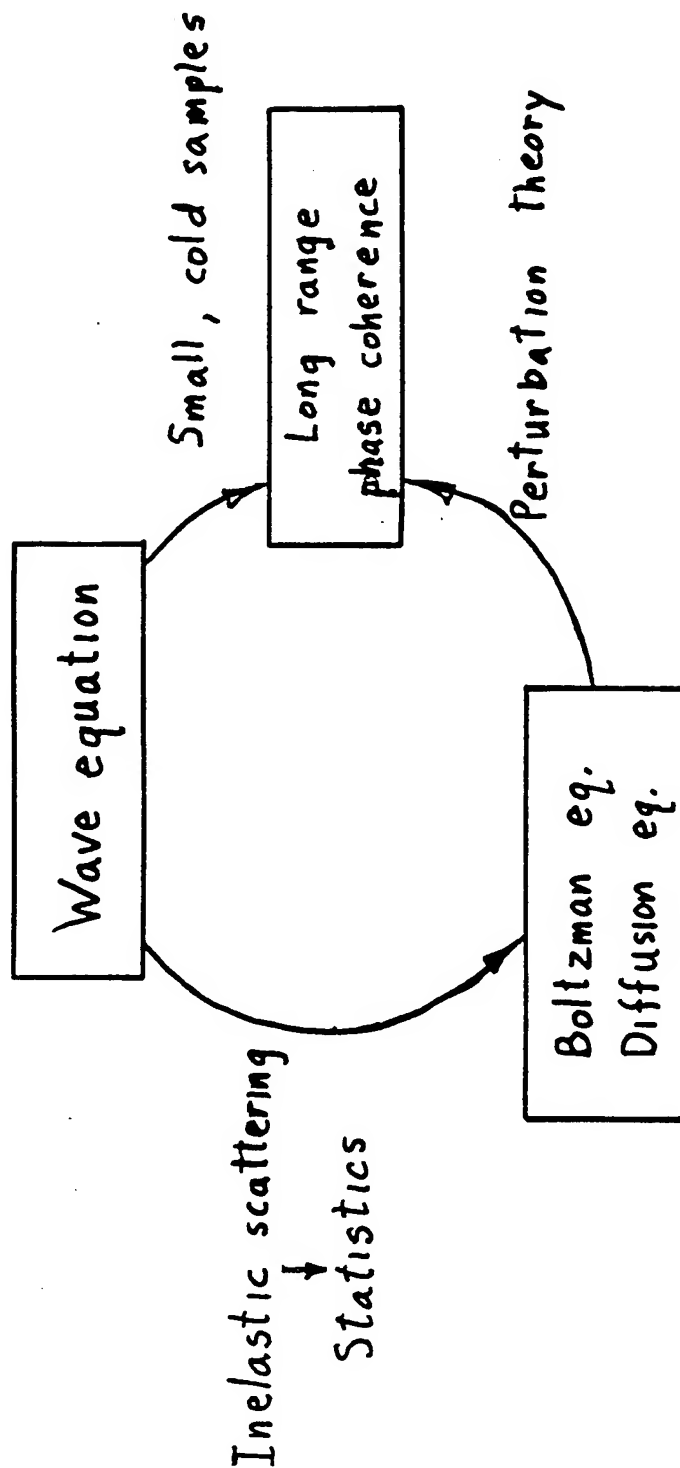
We have not succeeded in answering all of our questions. Indeed, we sometimes feel that we have not completely answered any of them. The answers we have found only served to raise a whole new set of questions. In some ways we feel that we are as confused as ever, but we think we are now confused on a higher level, and about more important things.

-Author unknown



Tuning-up a Quasicrystal

Problem: Solve Schrodinger Eq. for electron scattering from 10^{23} ions



- Anderson localization
- Ahronov-Bohm effect
- Universal conductance fluctuations
- Normal electron persistent currents

Mesoscopic - Phase coherence on the scale of microns

Megascope Phase coherence on the scale of millions of microns

- Experiments:
- Phase coherence in a 1-D wire 10 m long
 - Density of states in a quasicrystal $> 1\text{m}$ in diameter

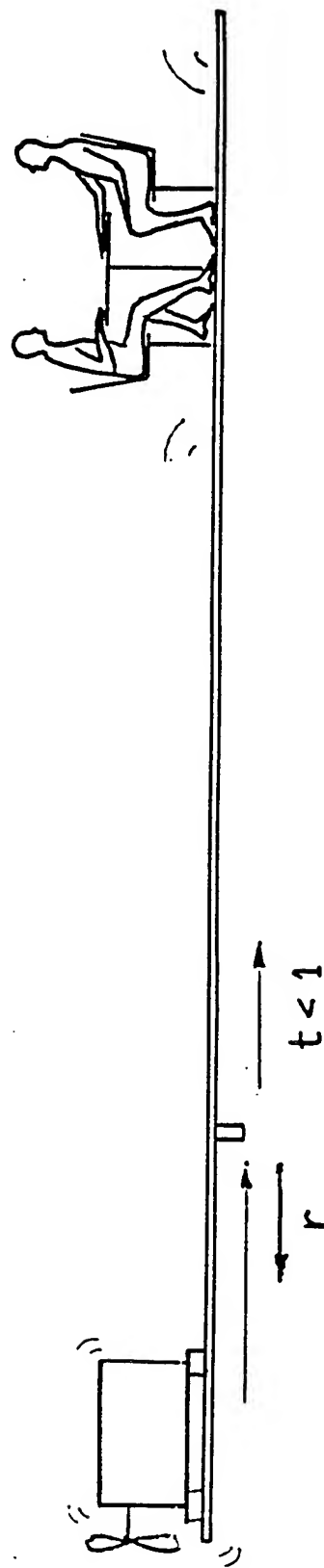
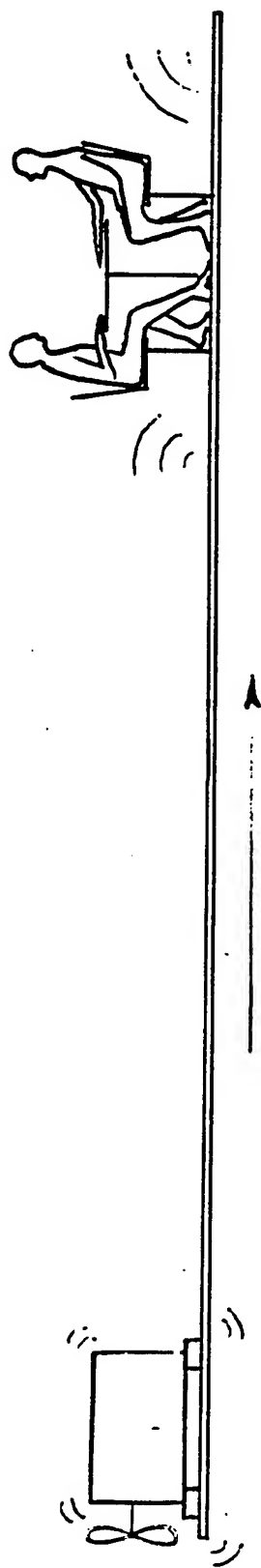
Classical (acoustic) analog systems ("analog computers")

Advantages • Precise analogs; $\nabla^2\psi + [q^2 - V(r)]\psi = 0$

- All conditions and parameters may be precisely controlled or measured
- Precise measurement of eigenvalues, eigenfunctions, density of states, etc.
- May study time-dependent or non-linear effects exactly

CONTROLLING PLATE RADIATION WITH ANDERSON LOCALIZATION

HYPOTHETICAL PROBLEM IN NOISE REDUCTION



Mathematics — FLOQUET'S THEOREM
Solid state — BLOCH'S THEOREM

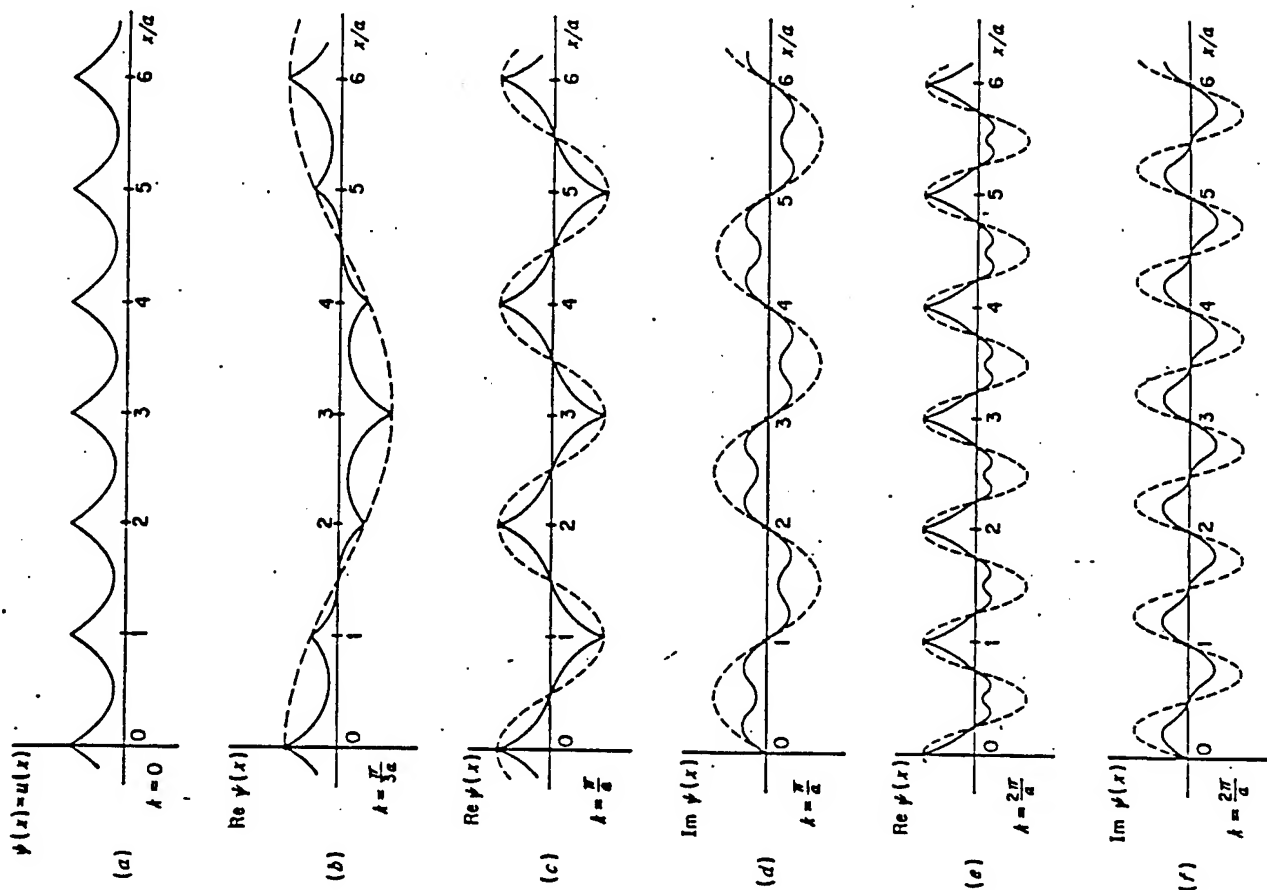
For a system with a periodic potential or impedance, the eigenfunctions are extended:

$$\Psi_{k,n}(x) = e^{ikx} u_n(x)$$

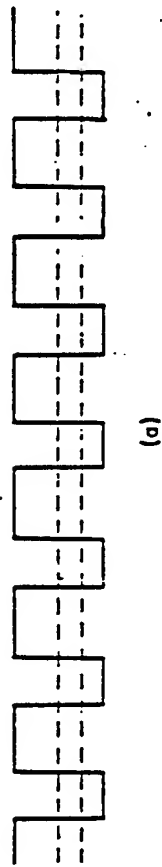
where $u_n(x+l) = u_n(x)$

$$|\Psi_{k,n}(x)| \sim \text{constant for all } x$$

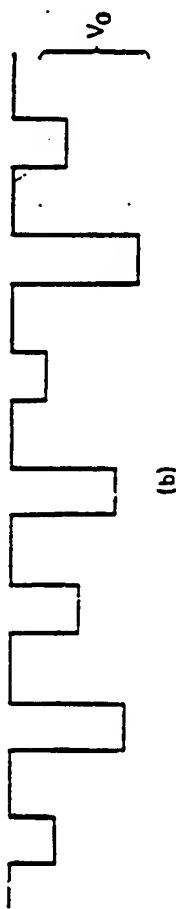
Solid state: Bloch wave functions \rightarrow



PERIODIC POTENTIAL $V_0(x+l) = V_0(x)$



$V_0(x) + \Delta V$ RANDOM

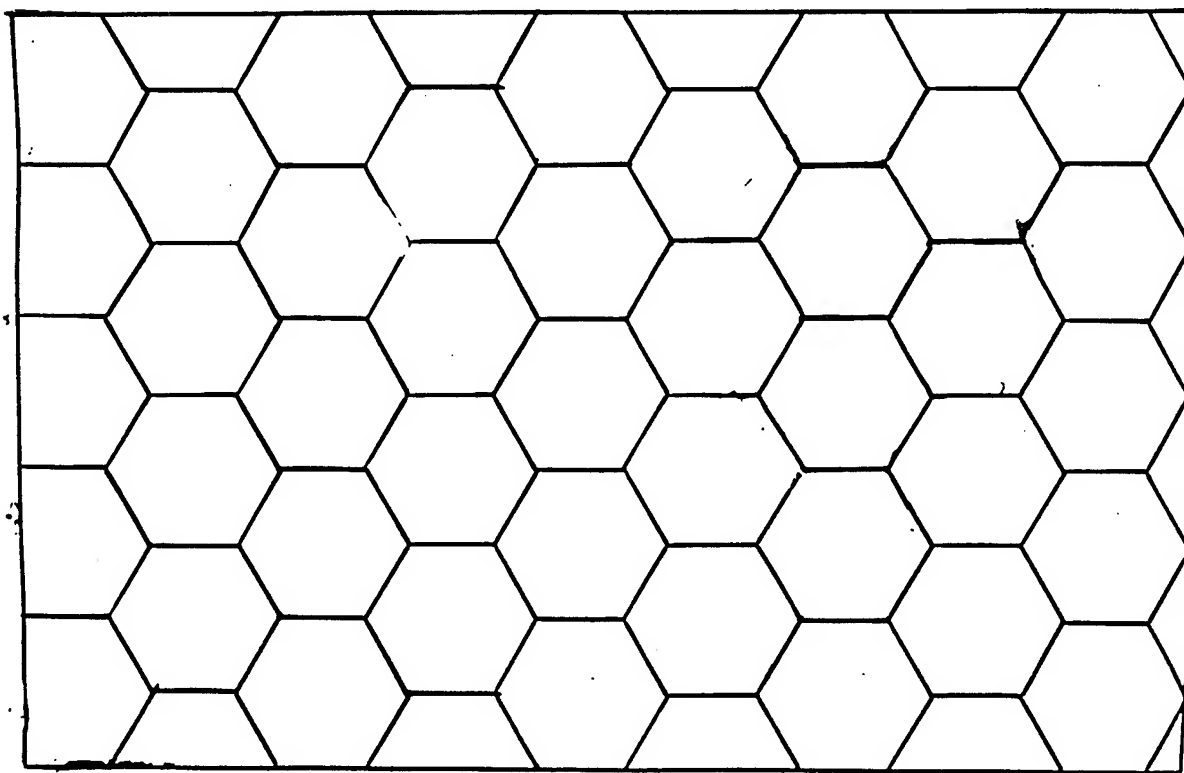
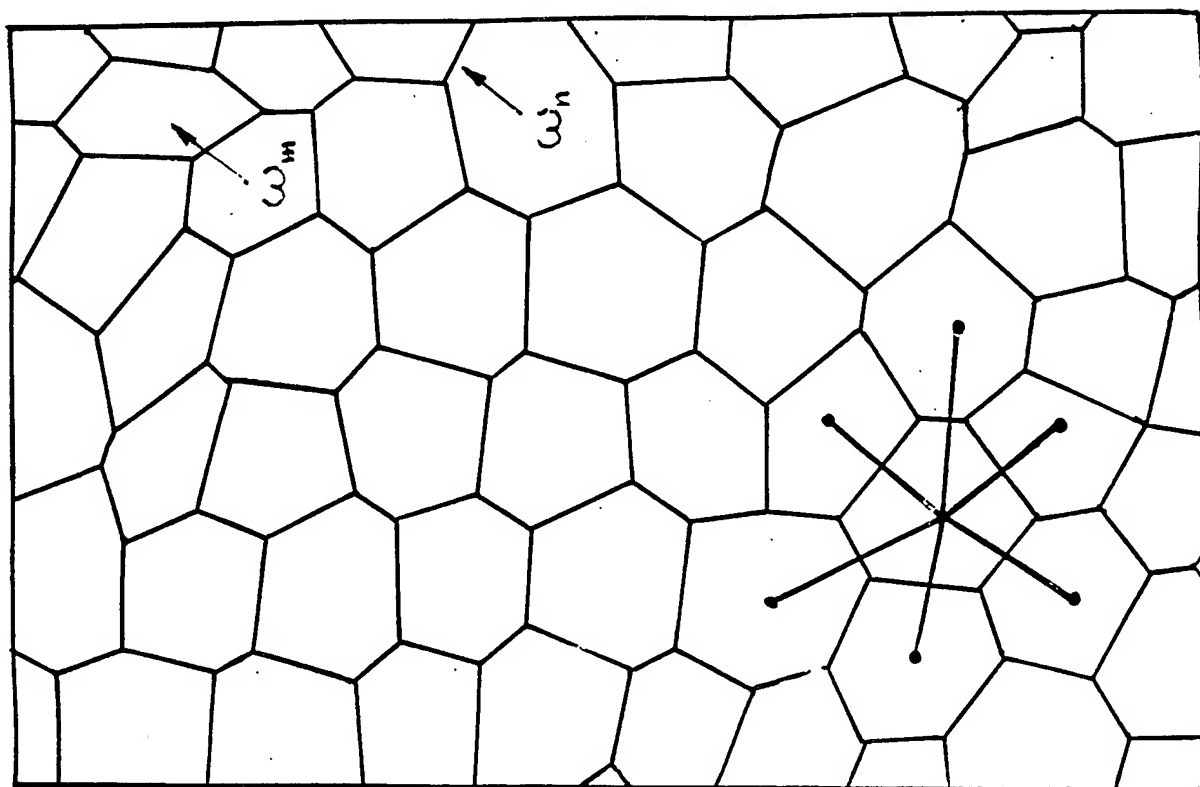


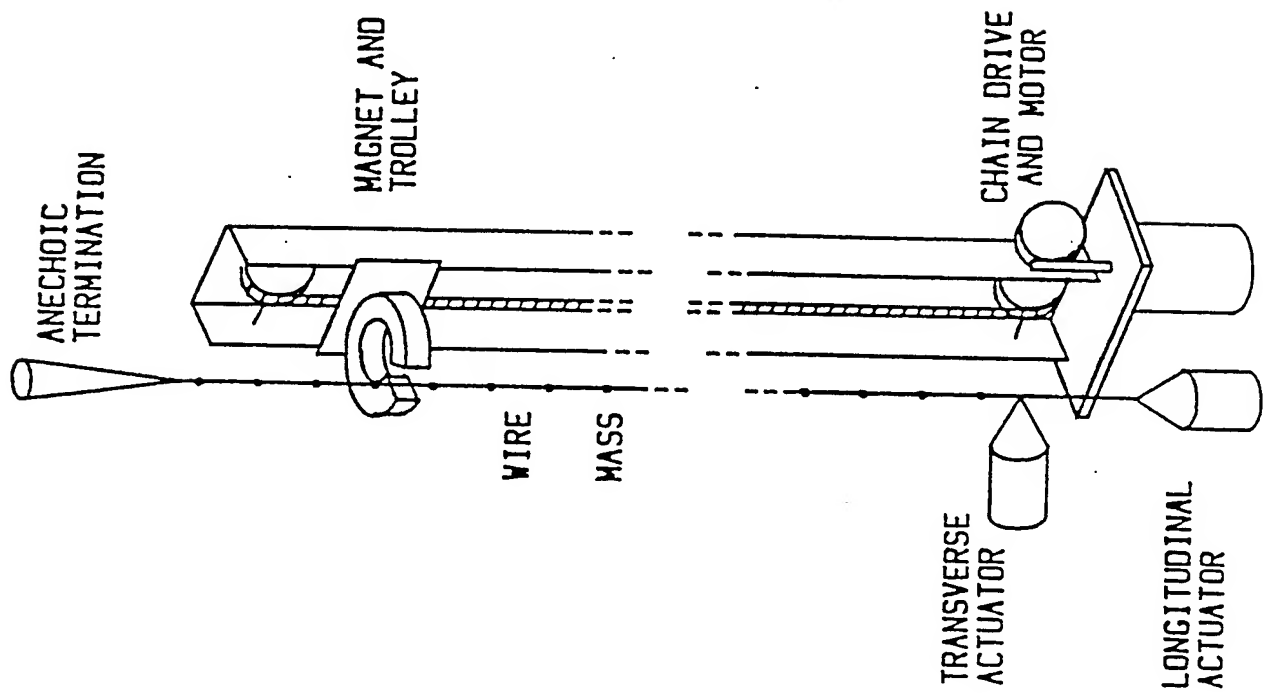
Random potential energy introduced by Anderson; (a) V_0 (b) $V_0 + \Delta V$

Wave function ψ of an electron when $l \sim a$. (a) Extended states
(b) localized states.

ANDERSON LOCALIZATION (1958)

★ M. Luban + J. Luscombe, Phys. Rev. B35, 9045 (1987)

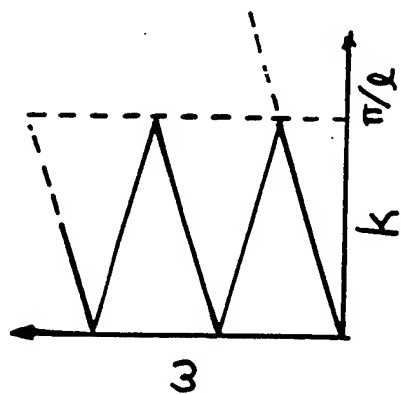




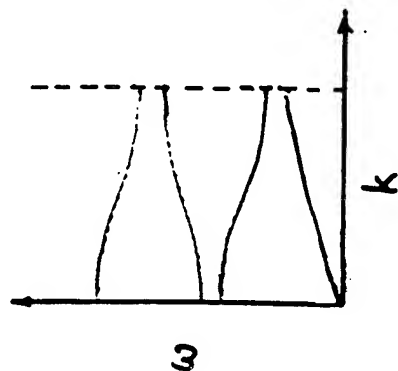


$$V_0(x) = \text{const}$$

Free electron e^{ikx}

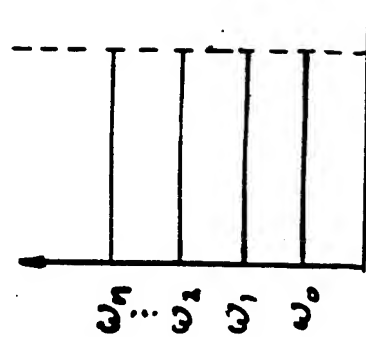


Periodic
Perturbation



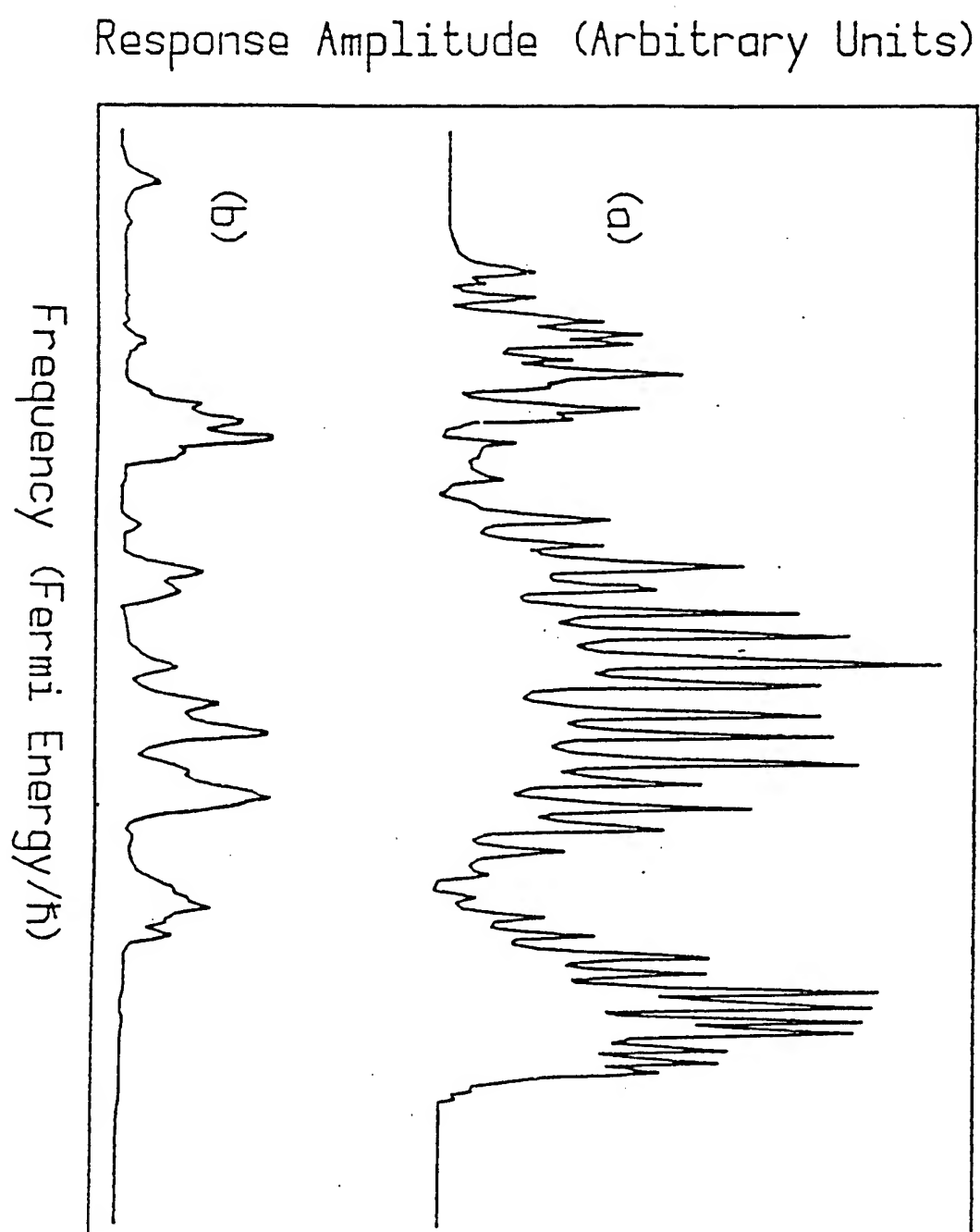
$$V_c(x) = \sum_n \delta(x-x_n)$$

Tight binding $u_n(x)$

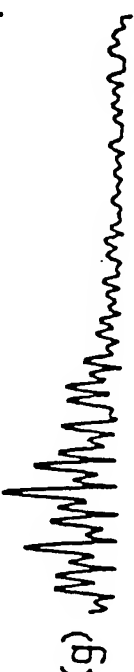


Coupling

Energy bands, gaps
Pass bands, stop bands



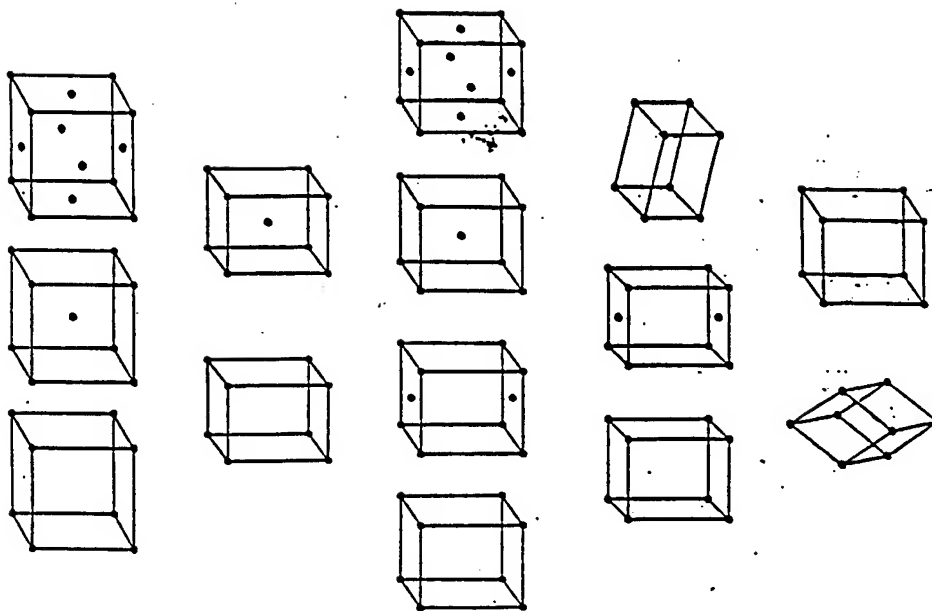
Transverse wave amplitude (Arbitrary units)



Position along wire

Solid States: Crystalline, Amorphous, Quasicrystalline

Crystal Bravais lattices



Kittel,
page 13:

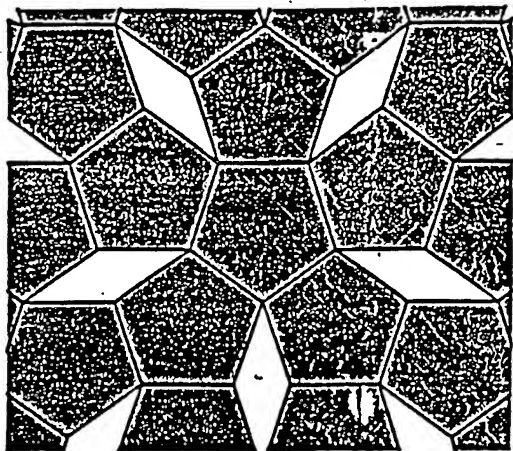
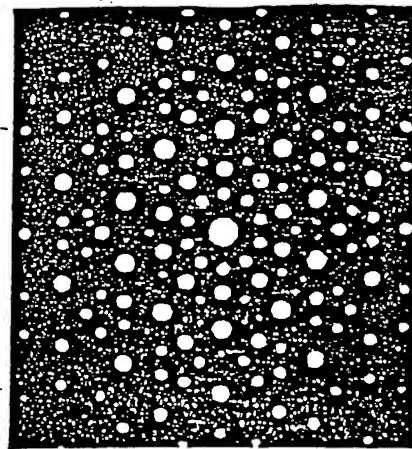
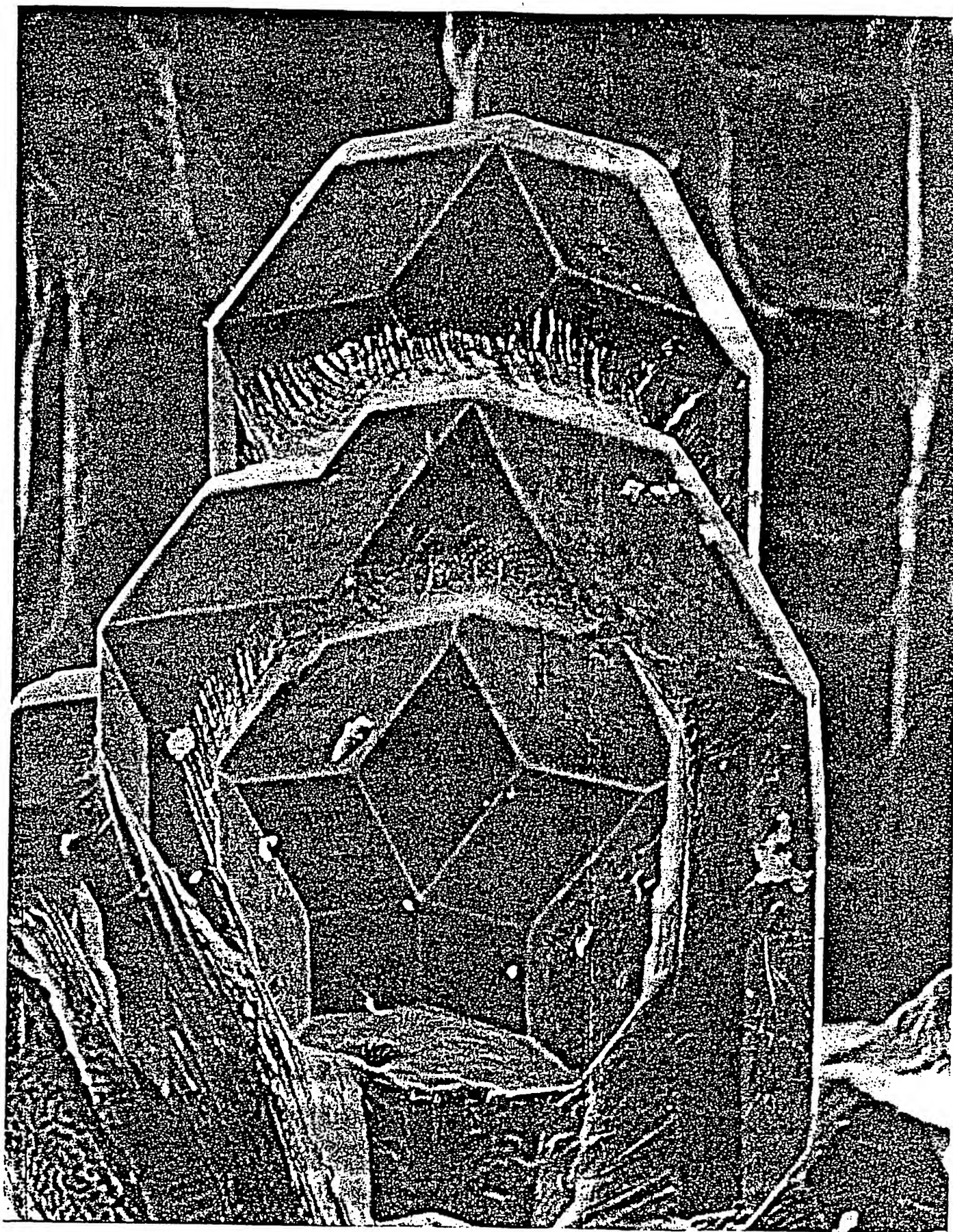
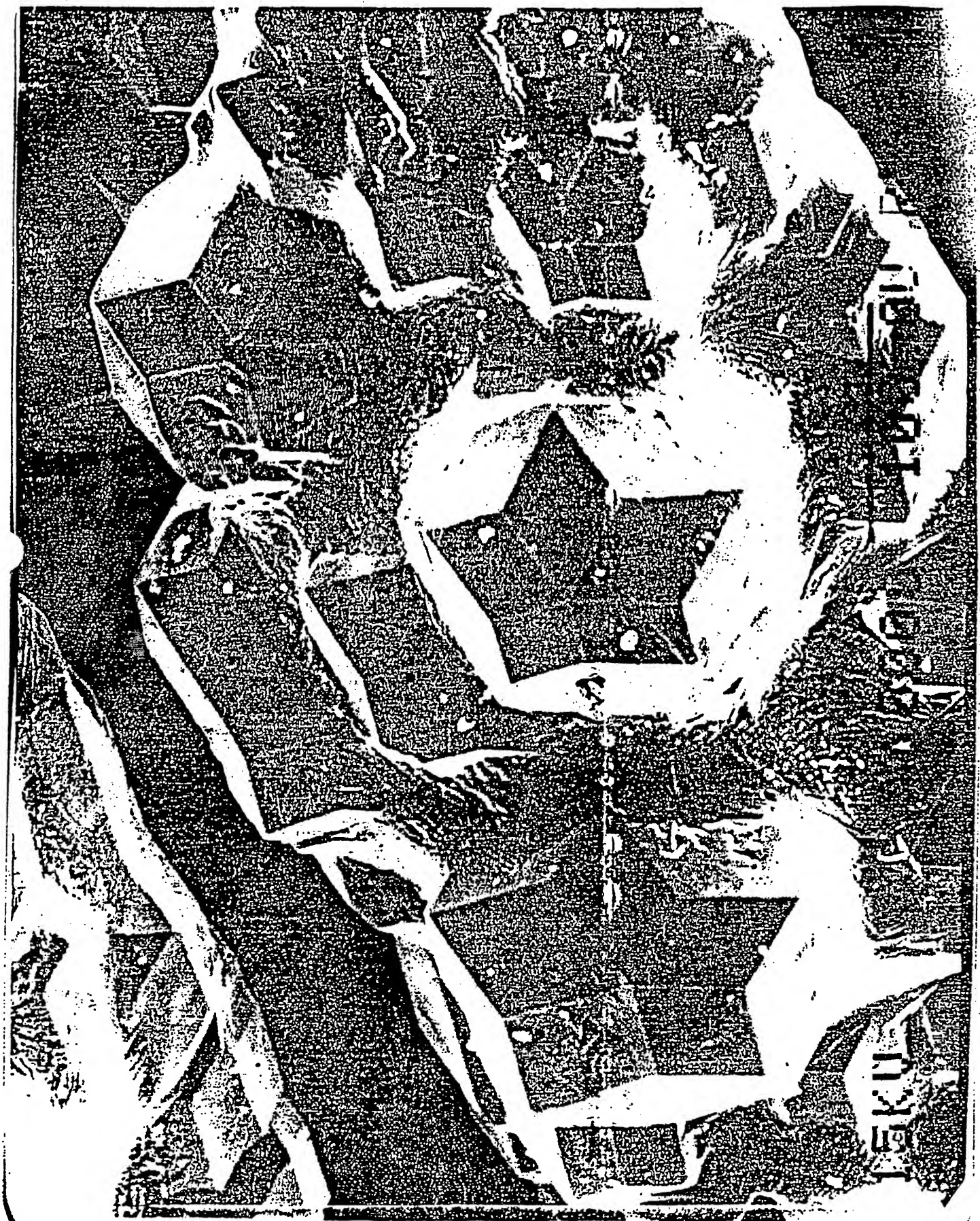


Figure 9a A five-fold axis of symmetry cannot exist in a lattice because it is not possible to fill all space with a connected array of pentagons.

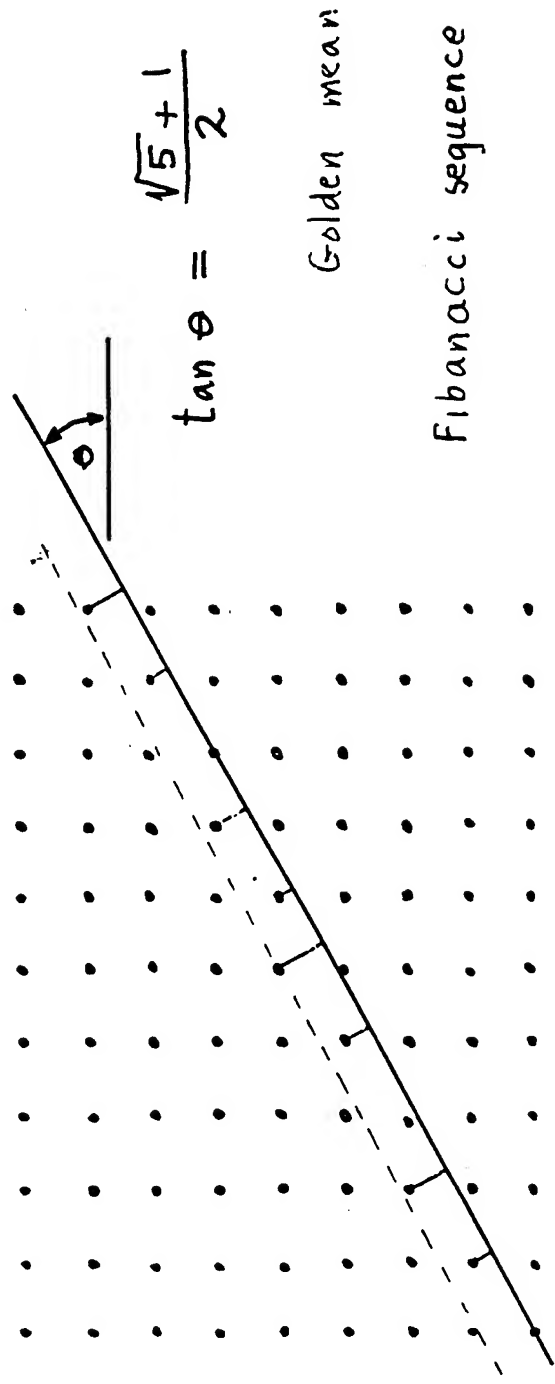
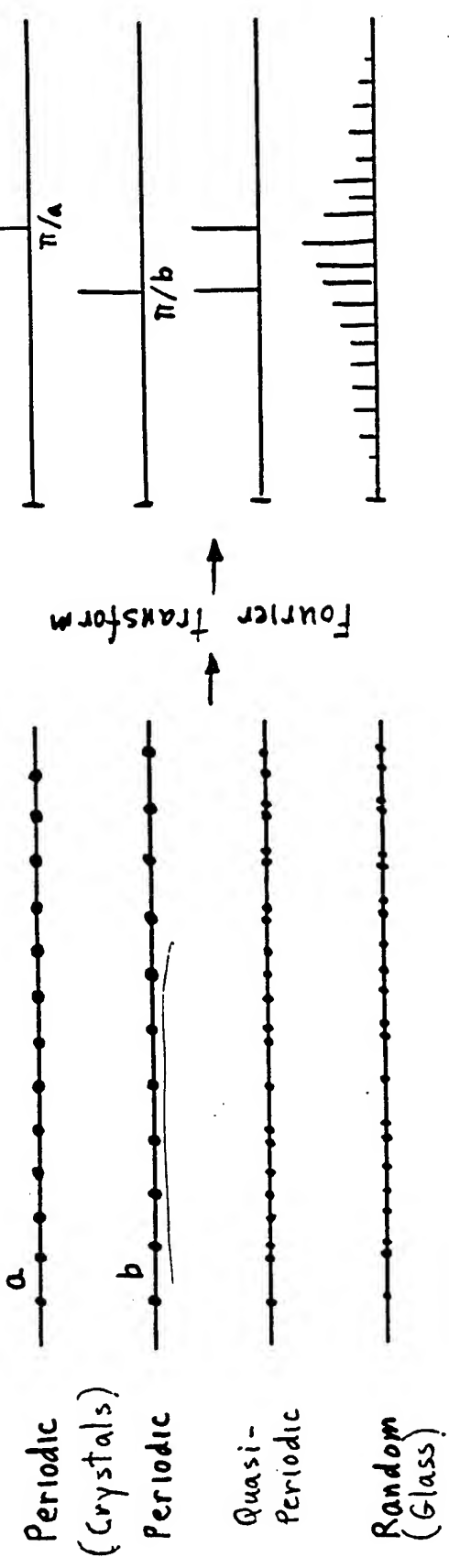


Shechtman
NBS, 1982

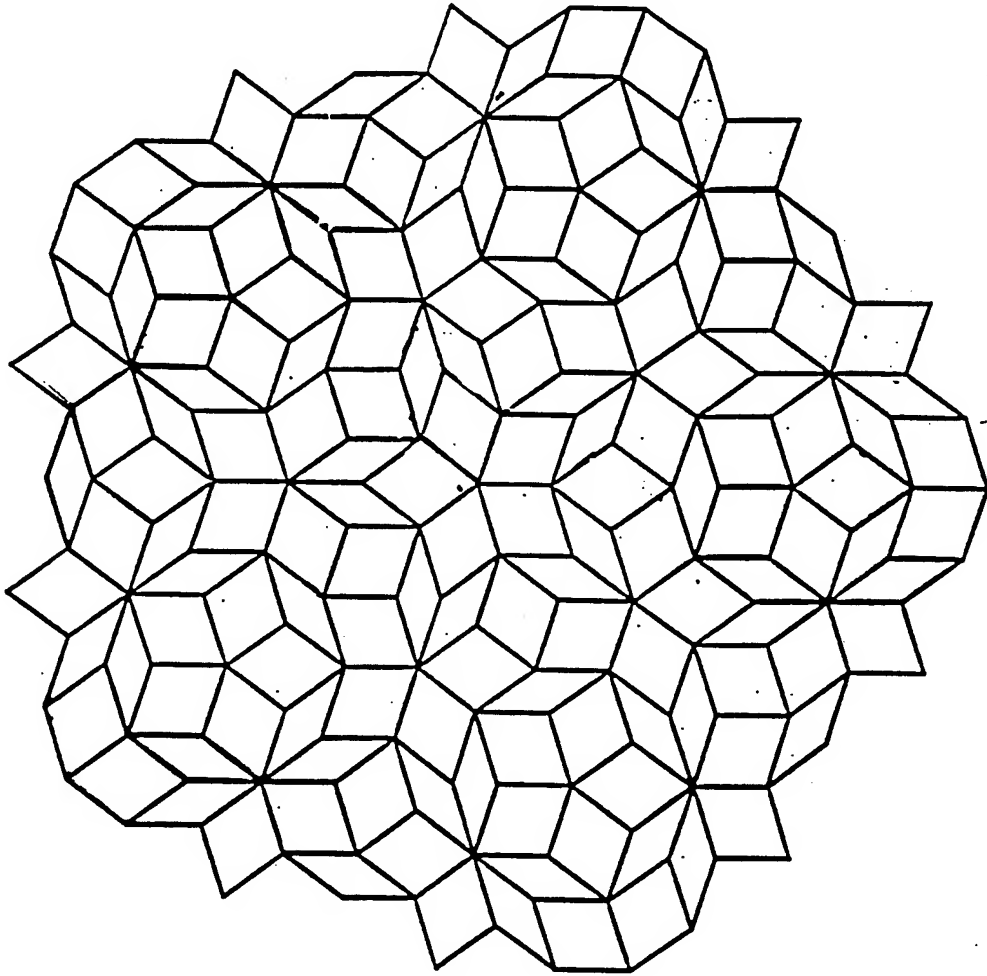




Quasi-periodicity

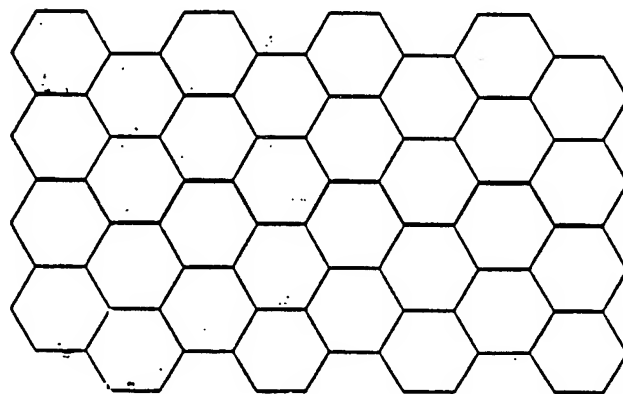


Penrose tile



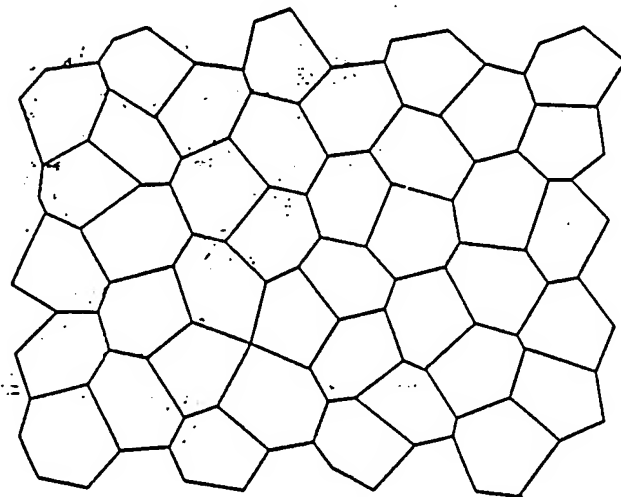
$$\text{Area of fat rhombus} / \text{Area of skinny rhombus} = (\sqrt{5} + 1) / 2$$

Acoustic Analog Studies of Quasicrystals



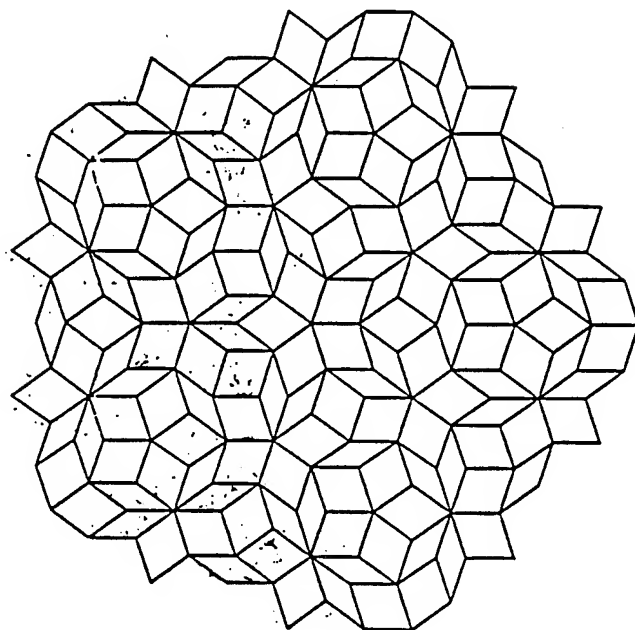
Periodic

Bloch's theorem



Random

Statistics

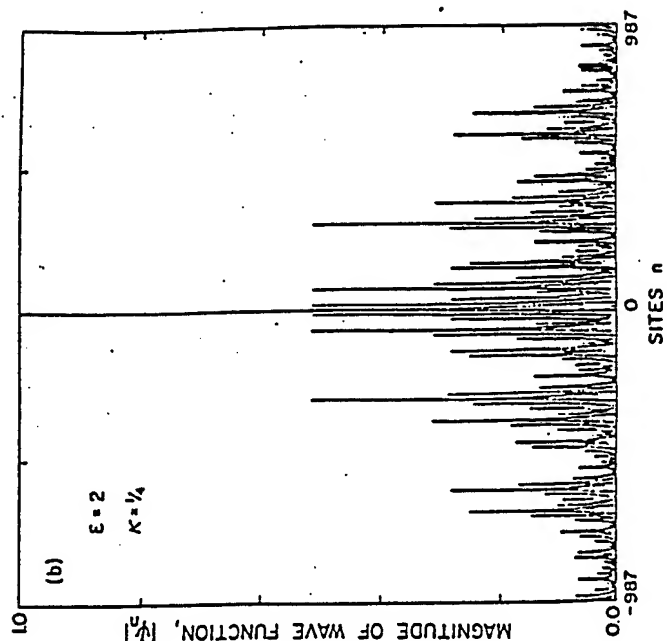
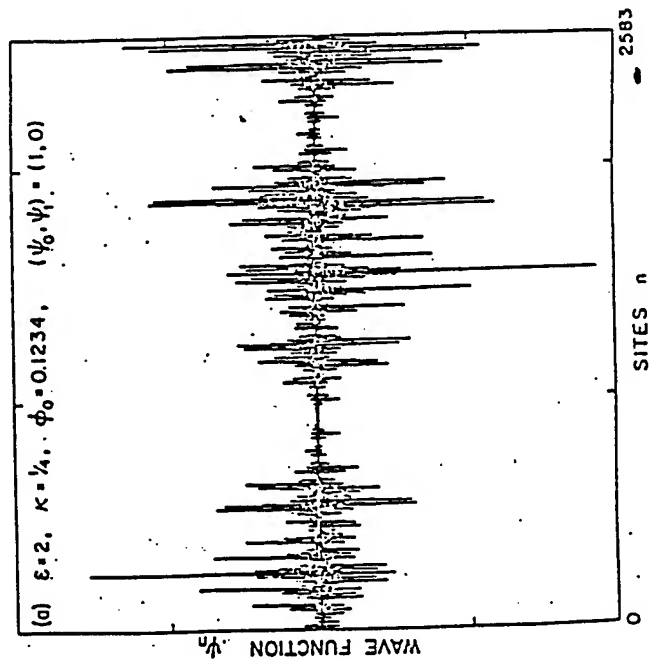
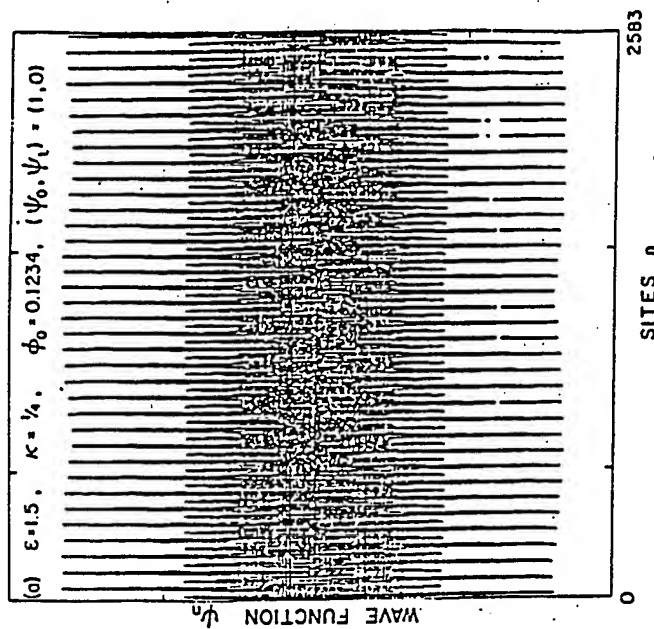
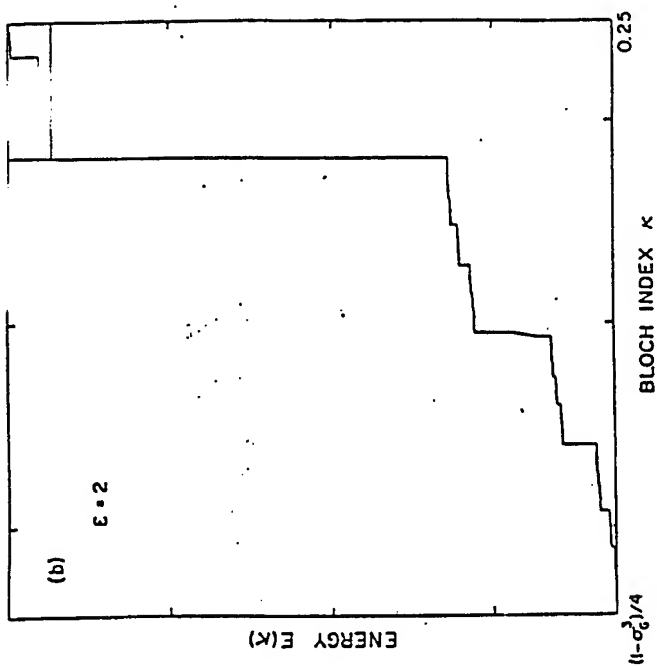


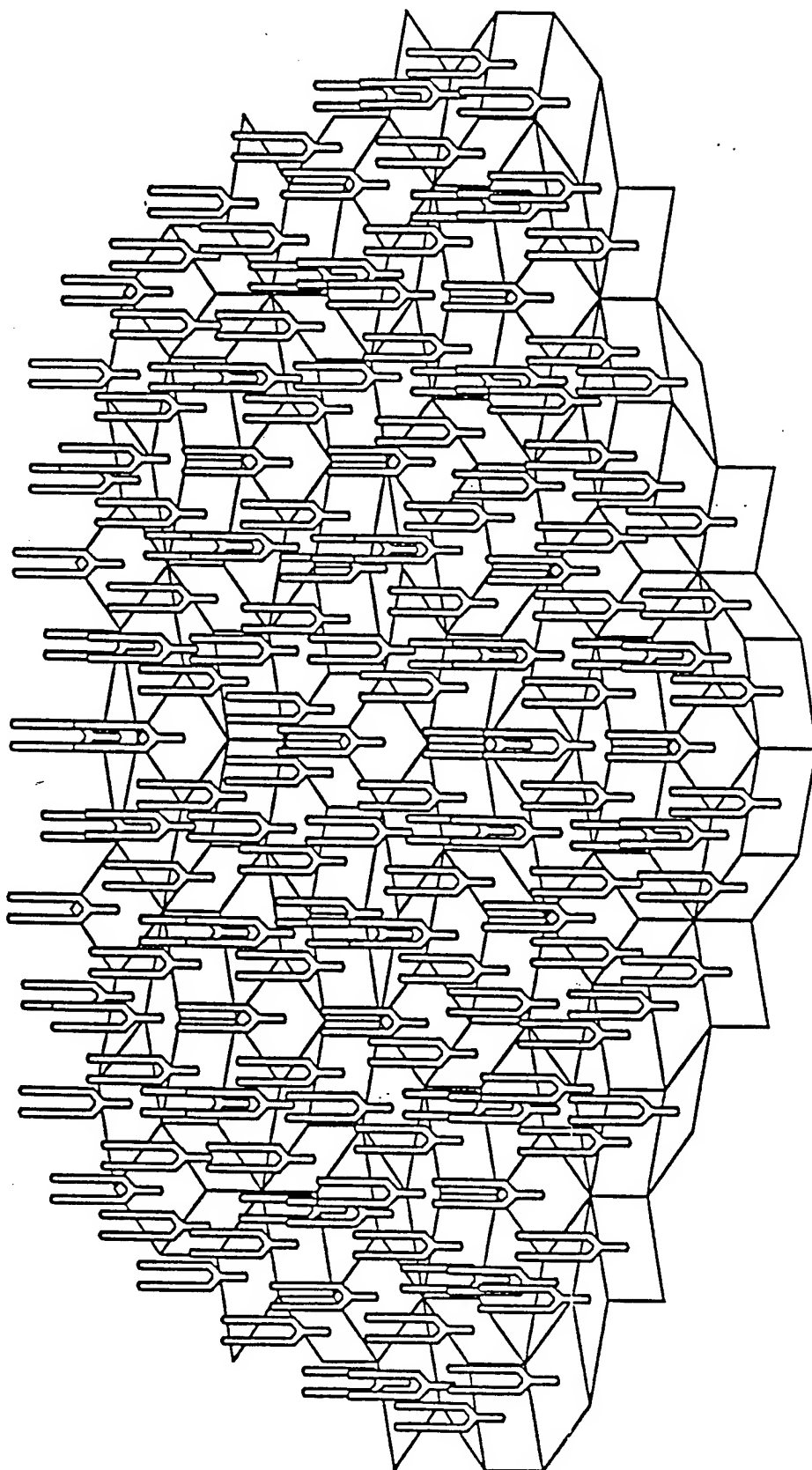
Quasicrystalline

?

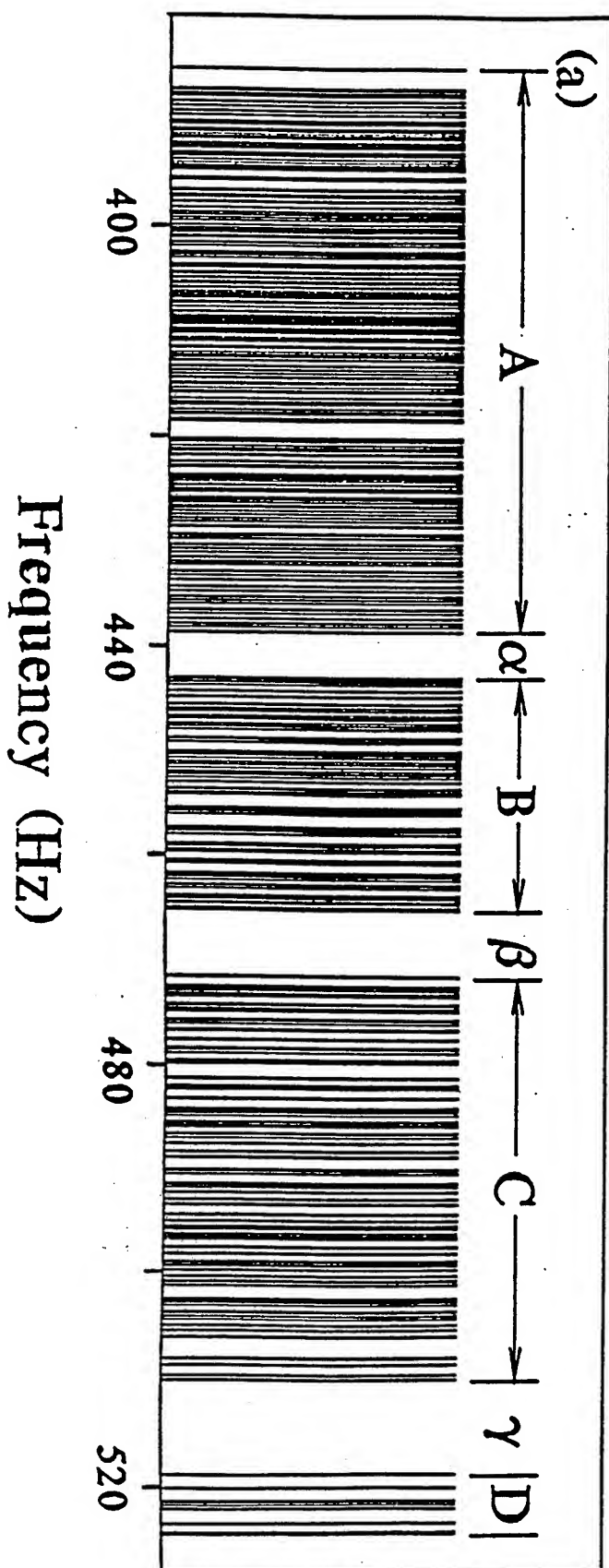
Effects of One-dimensional quasiperiodicity

Ostlund + Pandit
Phys Rev B 29
1394 (1984)

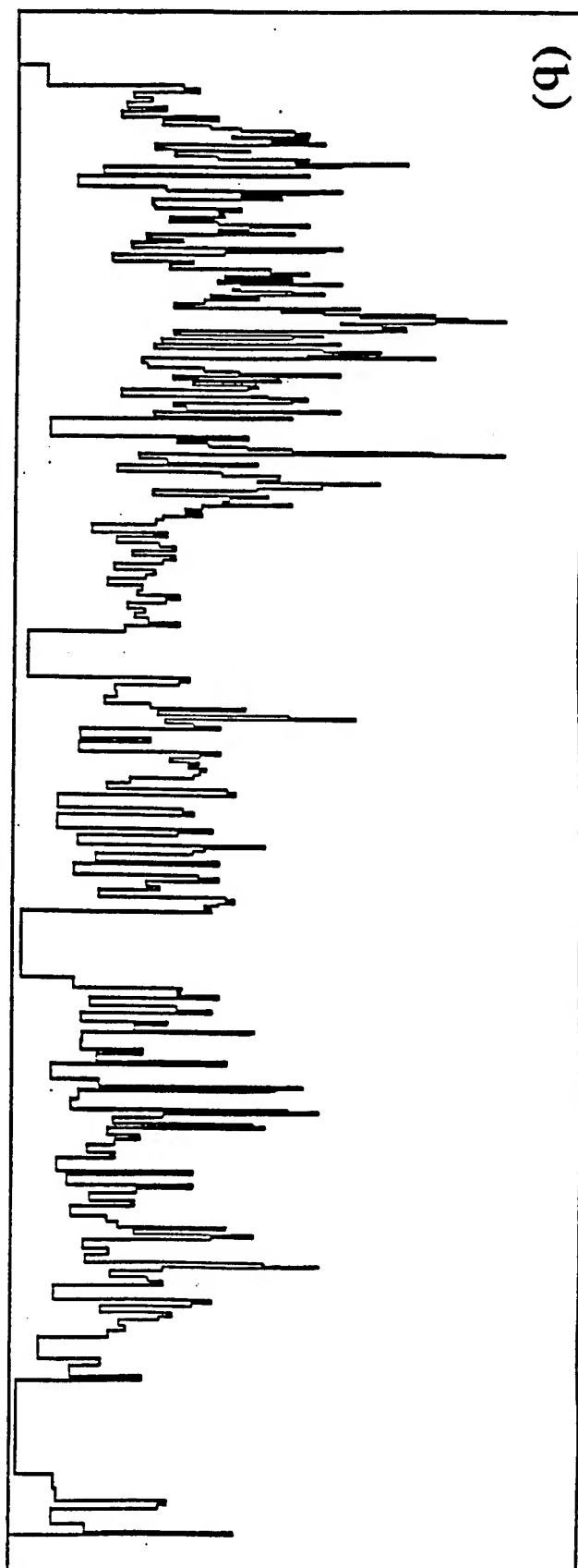




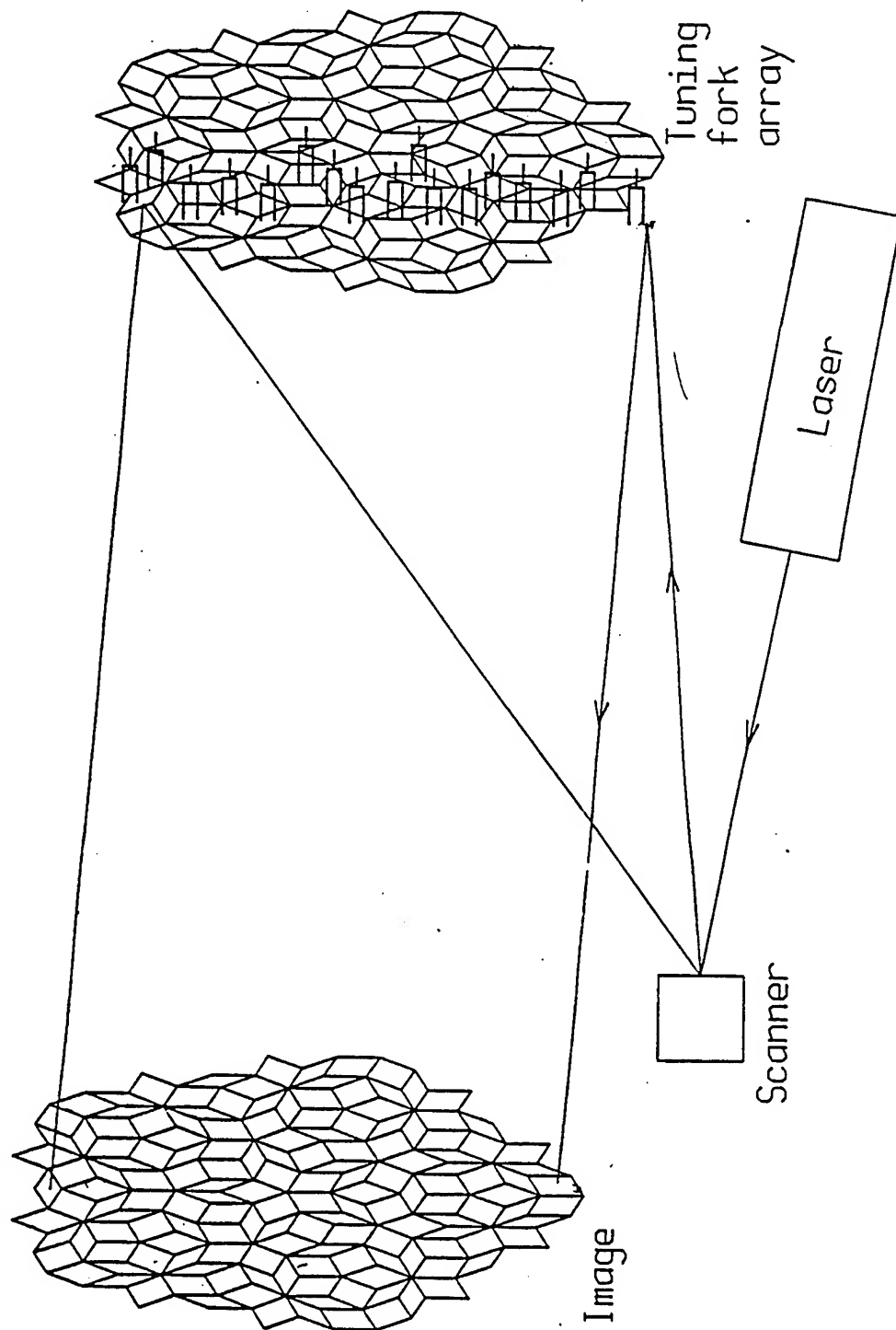
Spectrum



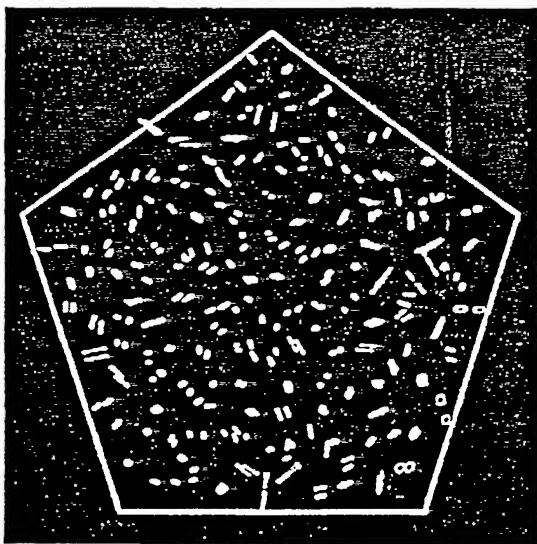
Density of states



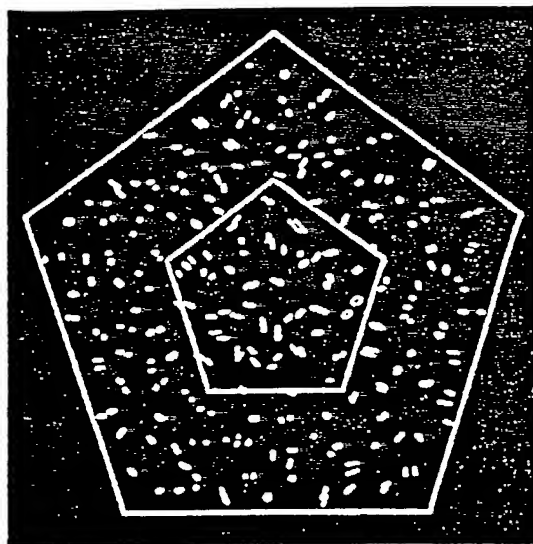
Measurement of Quasicrystal Eigenfunctions



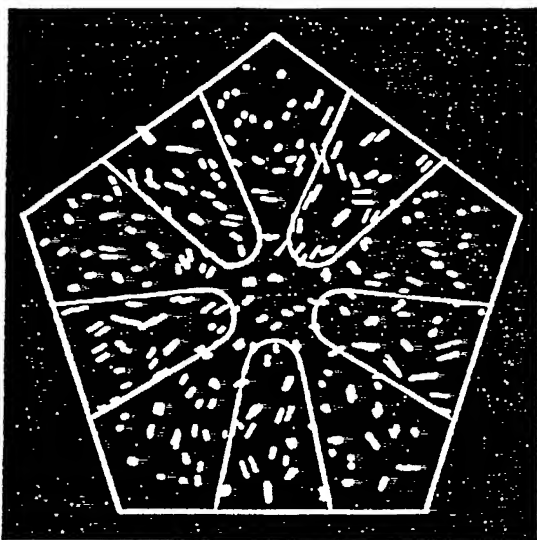
a



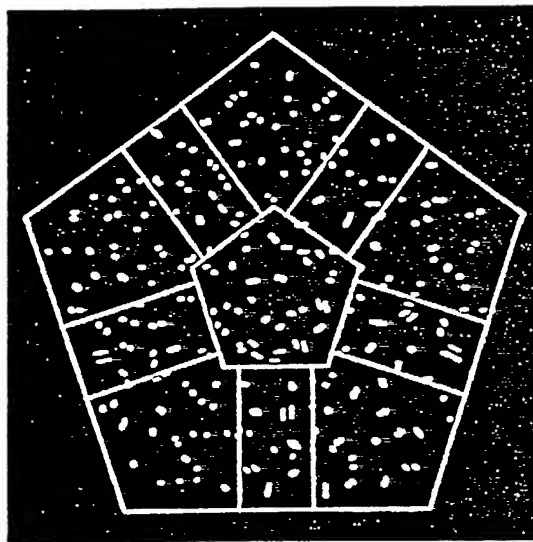
b



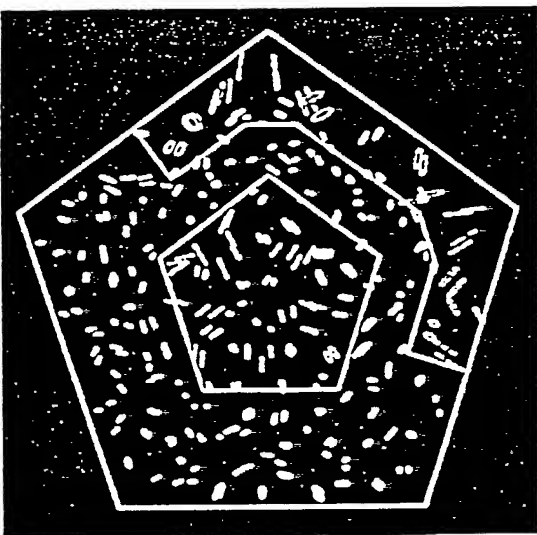
c



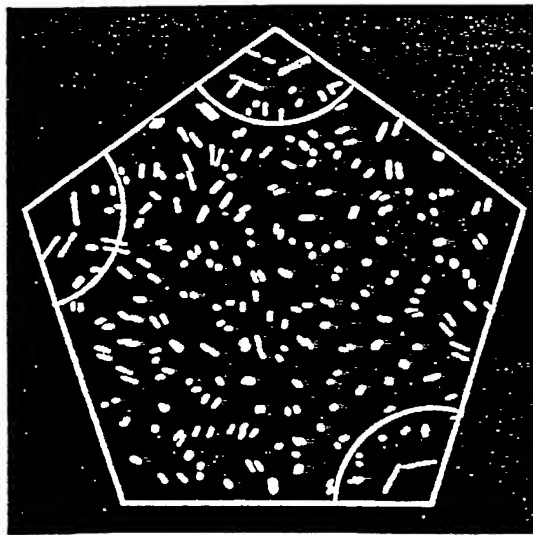
d



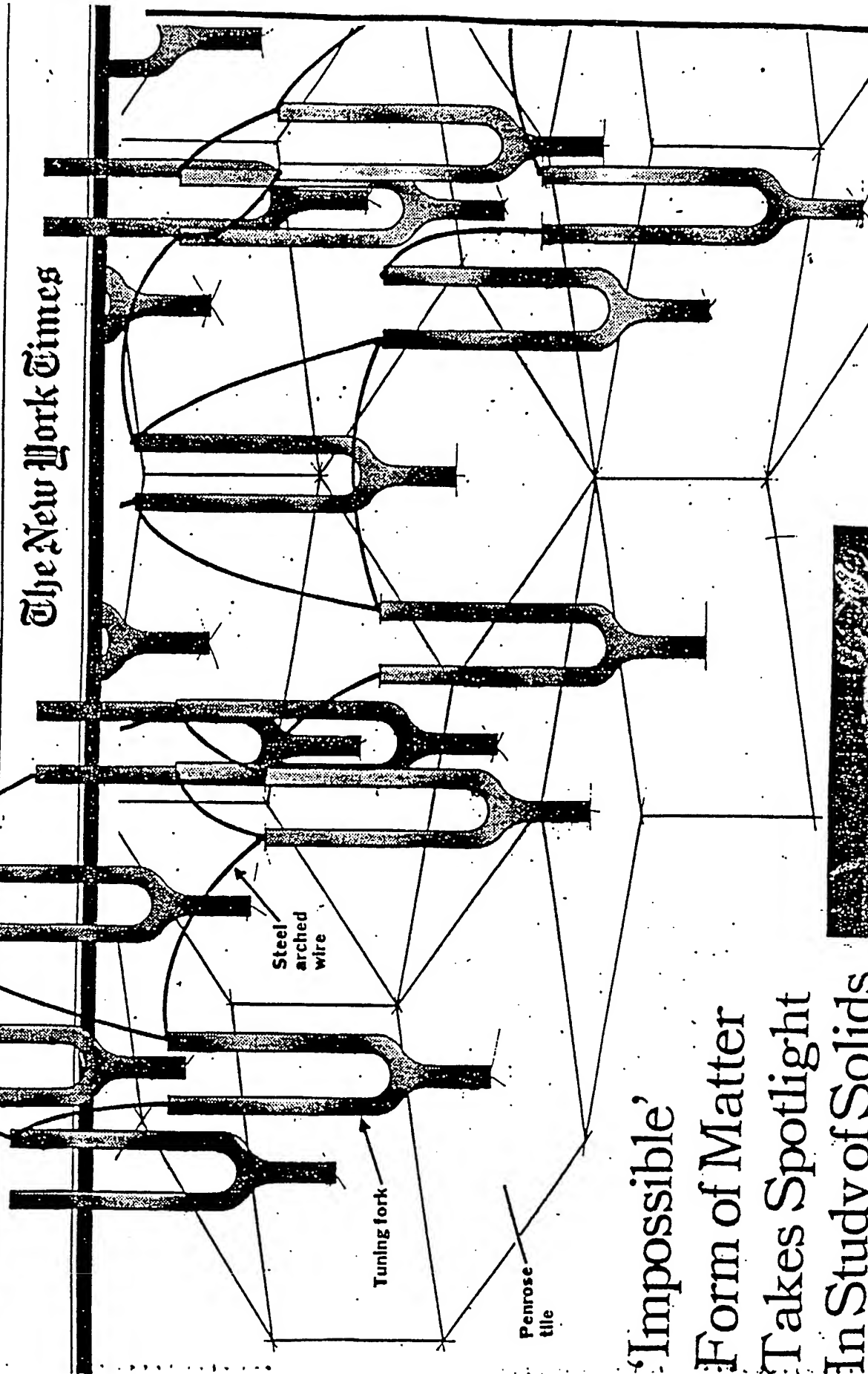
e



f



The New York Times



Penrose
tile

Steel
arched
wire

Tuning
fork

'Impossible' Form of Matter Takes Spotlight In Study of Solids

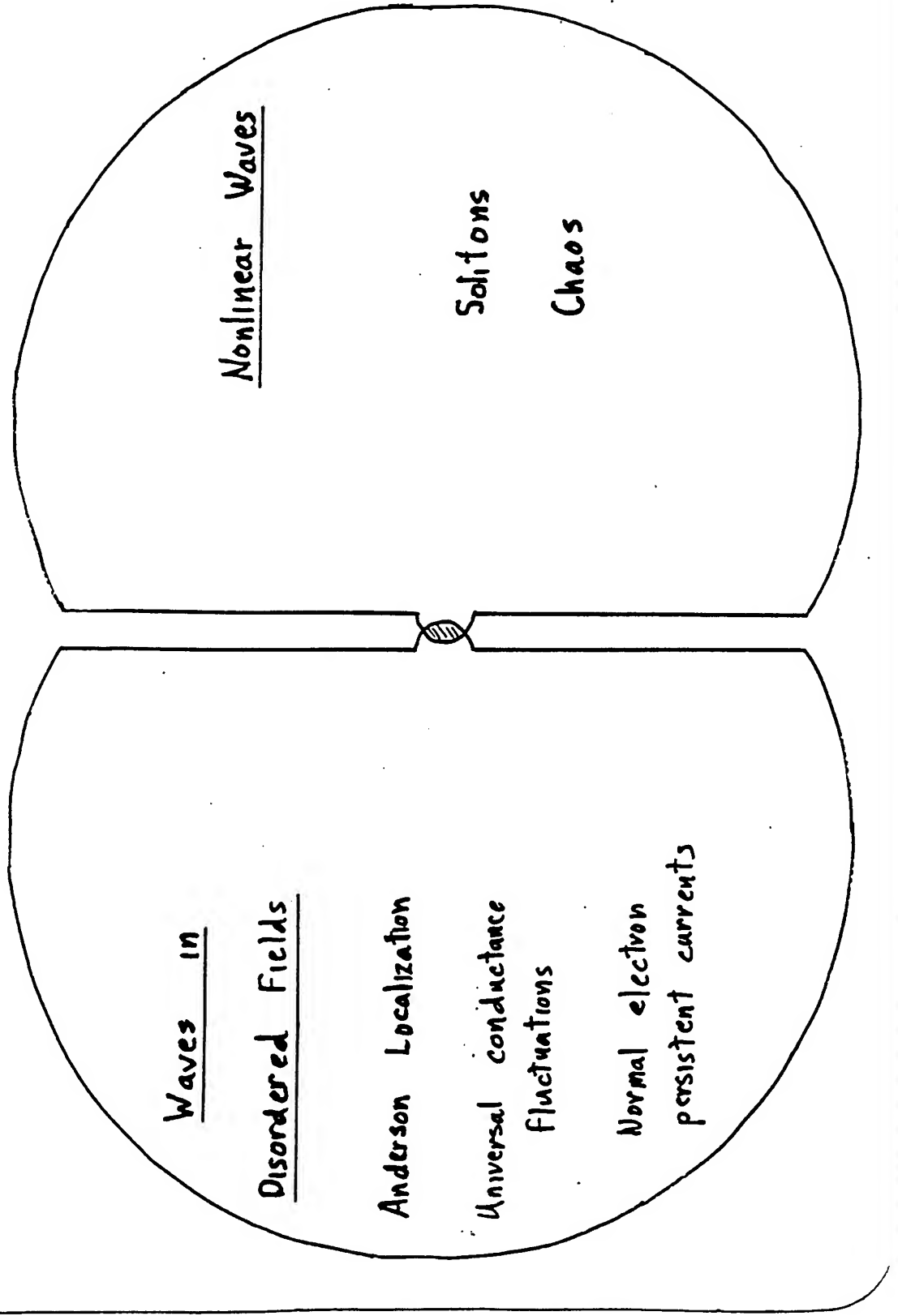
Th...sts seek clues to nature

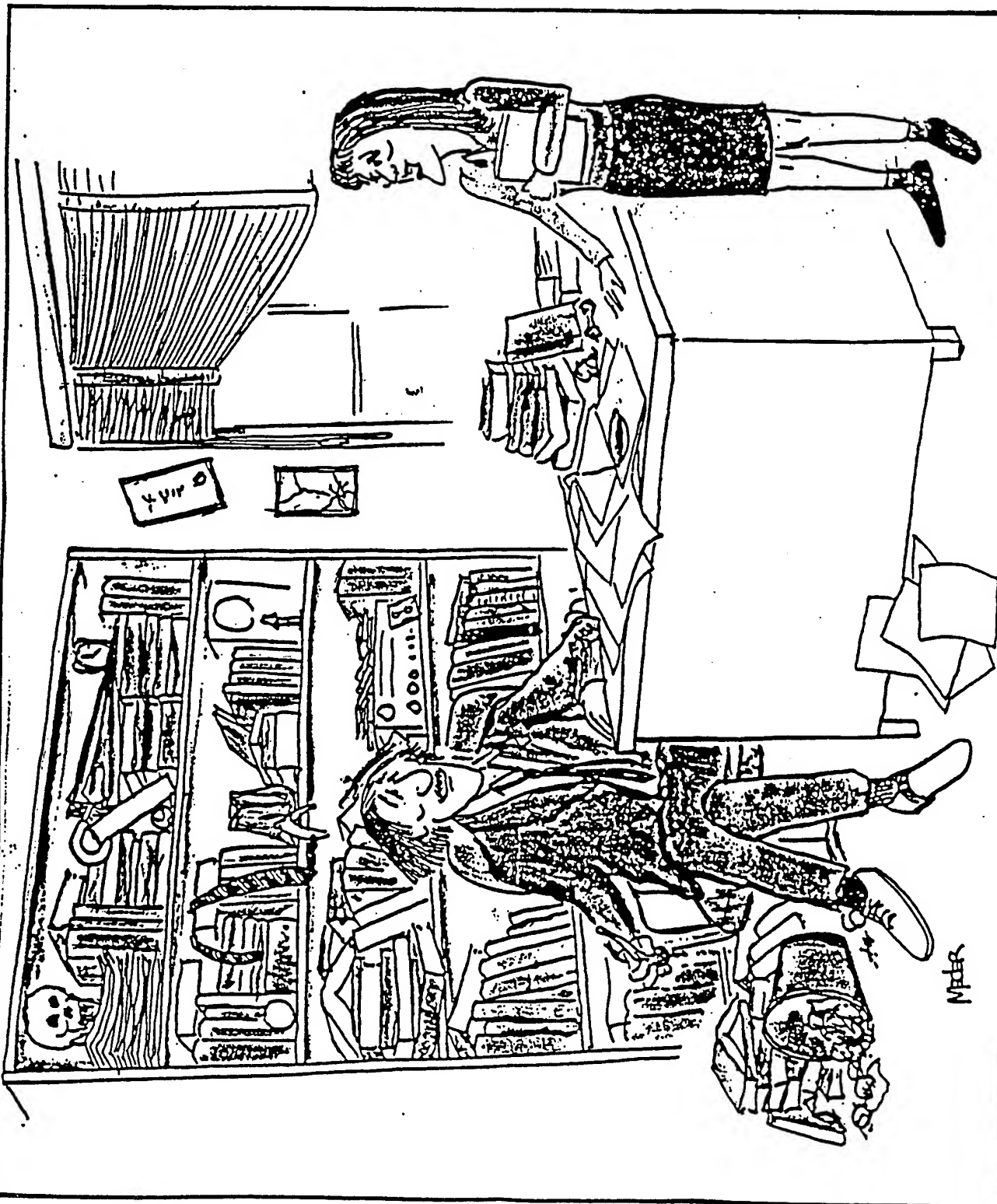


Source: Physical
Review Letters

The New York Times/Sept. 5, 1989; Illustration, Jana L.

Disorder and nonlinearity



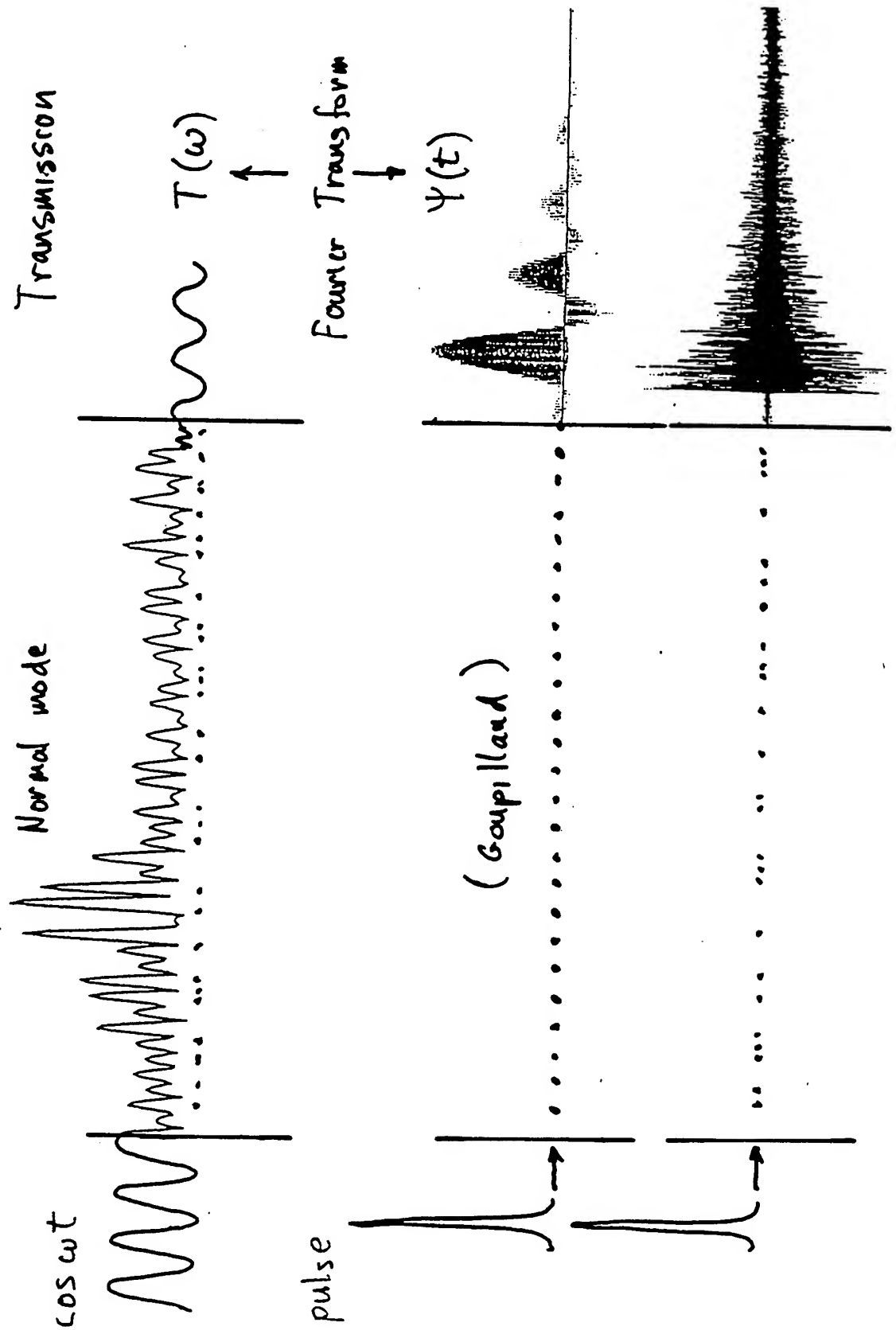


"What led you to the mathematics of chaos, Dr. Maynard?"

Does Nonlinearity Weaken Anderson Localization?

Reference:	<u>Yes</u>	<u>No</u>
1. P. Devillard and B. Souillard, J. Stat. Phys. 43, 423 (1986) Fixed output t, find t/r decays as power law for strong nonlinearity	X	
2. B. Doucot and R. Rammal, Europhysics Lett. 3, 969 (1987) Fixed output: power law decay - Fixed input: exponential decay	X	X
3. C. Albanese and J. Frohlich, Commun. Math. Phys. 116, 475 (1988) Rigorous theorem: Eigenstates of NLS eq. remain localized		X
4. Q. Li, C. M. Soukoulis St. Pnevmatikos, and E. N. Economou, Phys. Rev. B 38, 11888 (1988) A soliton can force its way through a binary alloy	X	
5. A. Soffer and M. I. Weinstein, Commun. Math. Phys. Same as 3.		X
6. R. Bourbonnais and R. Maynard, Phys. Rev. Lett. 64, 1397 (1990) Superpositions of localized states spread due to nonlinearity	X	
7. Yu. S. Kivshar, S. A. Gredeskul, A. Sanchez, and L. Vazquez, Phys. Rev. Lett. 64, 1693 (1990) Same as 4, but only for sufficiently strong soliton	X	X
8. R. Scharf and A. R. Bishop, "Nonlinearity with Disorder", ed. F. Abdullaev, A. R. Bishop, and S. Pnevmatikos (Springer, Berlin, 1992) The nonlinear Schrodinger equation on a disordered chain Numerical results; same as 7	X	X

Normal mode analysis versus Pulse analysis



Nonlinearity in a Stretched String

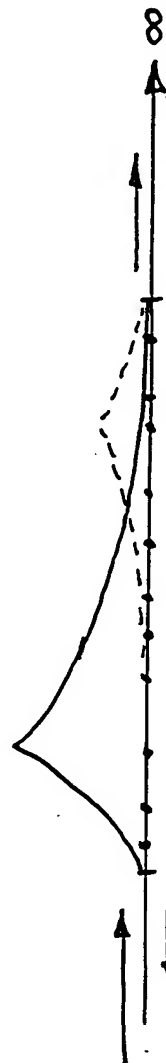
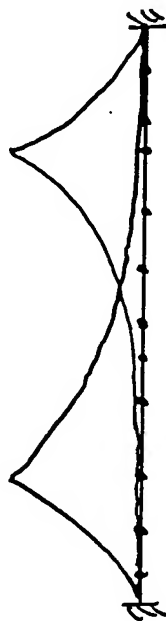
$\mu = \text{mass/length}$

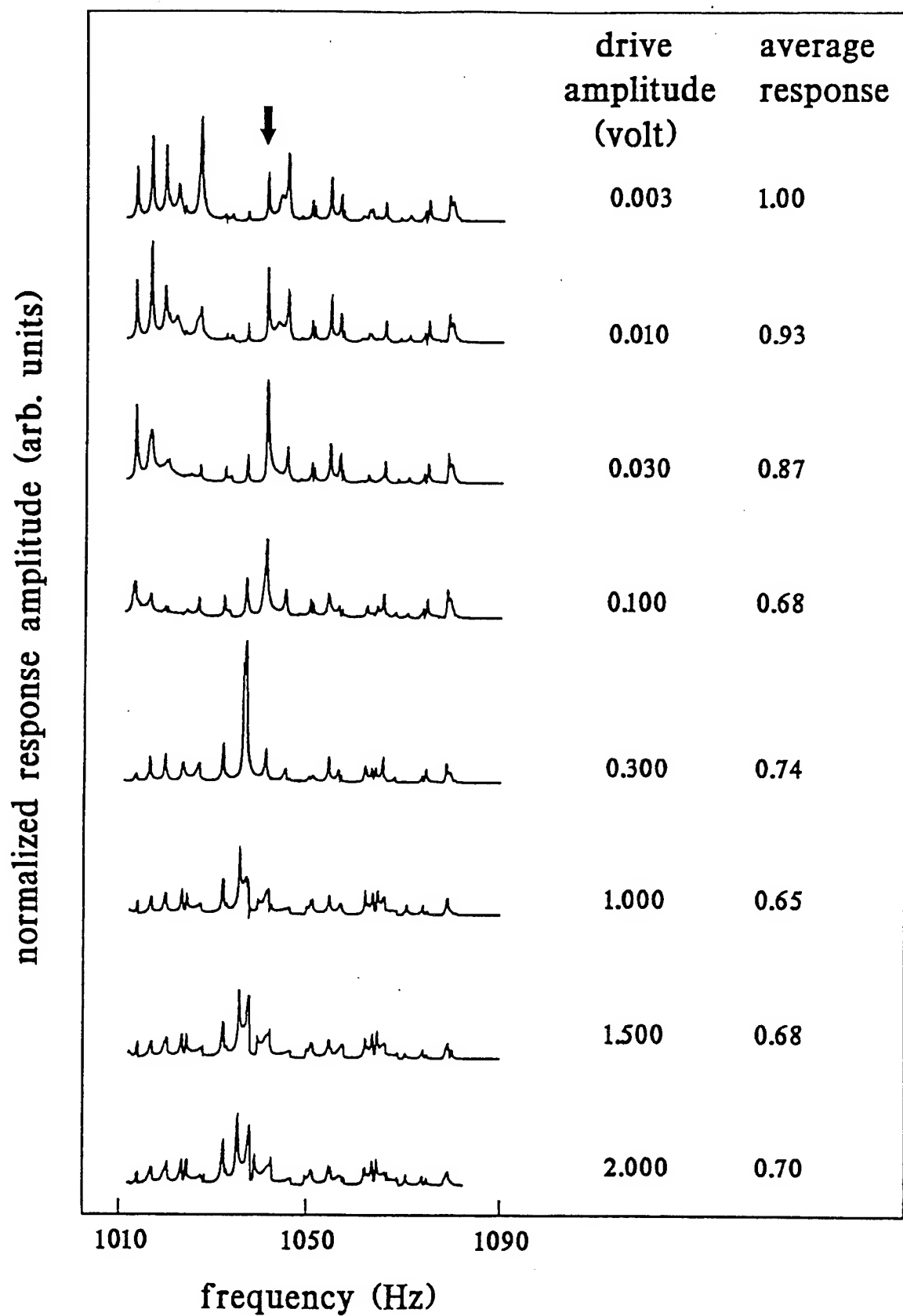


Newton: $\frac{\partial^2 \psi}{\partial x^2} - \frac{\mu}{T} \frac{\partial^2 \psi}{\partial t^2} = 0$ Wave speed $c_0 = \sqrt{T_0/\mu}$

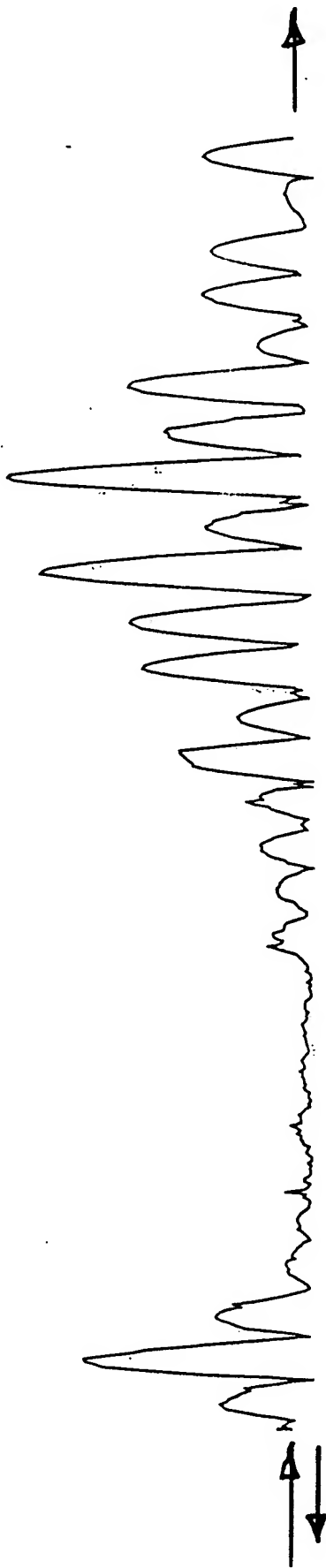
Are length correction: $T = T_0 \left\{ 1 + \left(\frac{\lambda}{\Delta x} \right) \left[\frac{1}{2} \int_0^{\lambda} \sqrt{1 + \left(\frac{\partial \psi}{\partial x} \right)^2} dx - 1 \right] \right\}$

Add masses: $\frac{\partial^2 \psi}{\partial x^2} + q^2 \psi - V(x) \psi - \left[\frac{1}{2} \left(\frac{\partial \psi}{\partial x} \right)^2 \int_0^{\lambda} \left(\frac{\partial \psi}{\partial x} \right)^2 dx \right] \psi = 0$

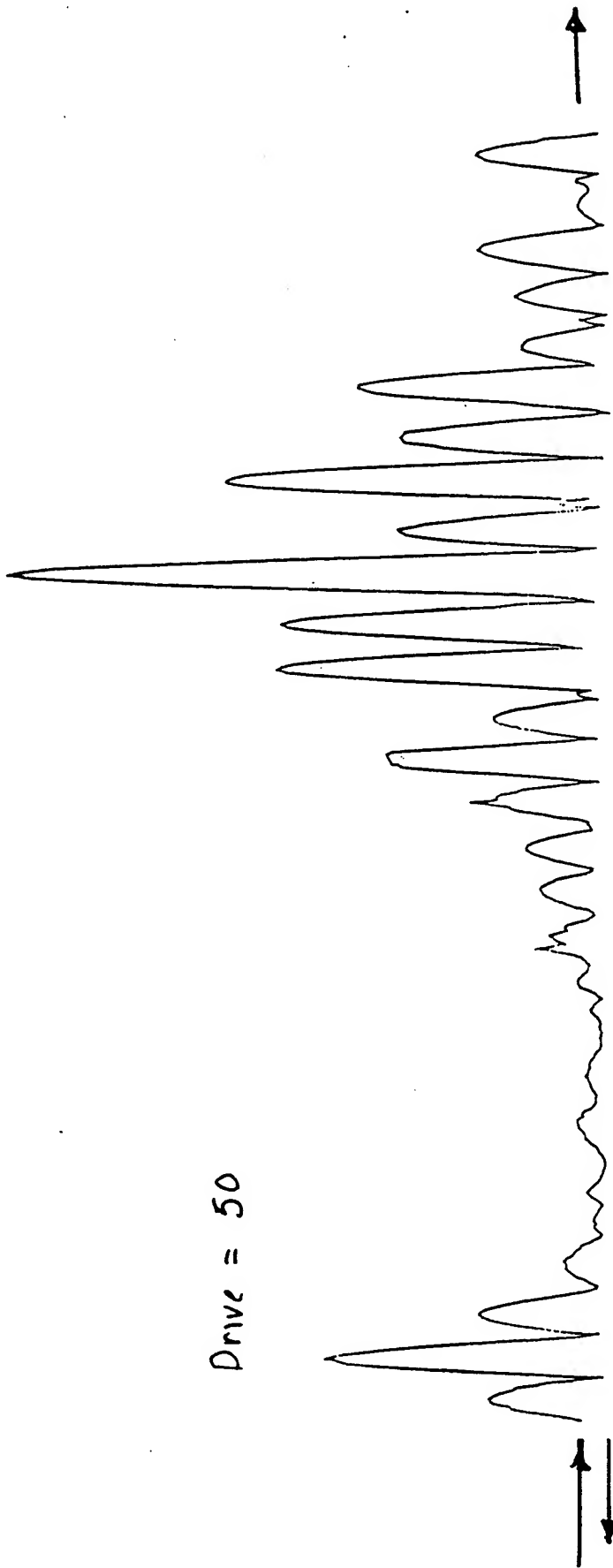




Drive = 1



Drive = 50



Theoretical Predictions for Nonlinear Pulse in Disordered Medium

Linear system \rightarrow 

Product of
Random Matrices $(\alpha_1 \beta_1) (\alpha_2 \beta_2) \dots (\alpha_N \beta_N) \Rightarrow T(\omega)$

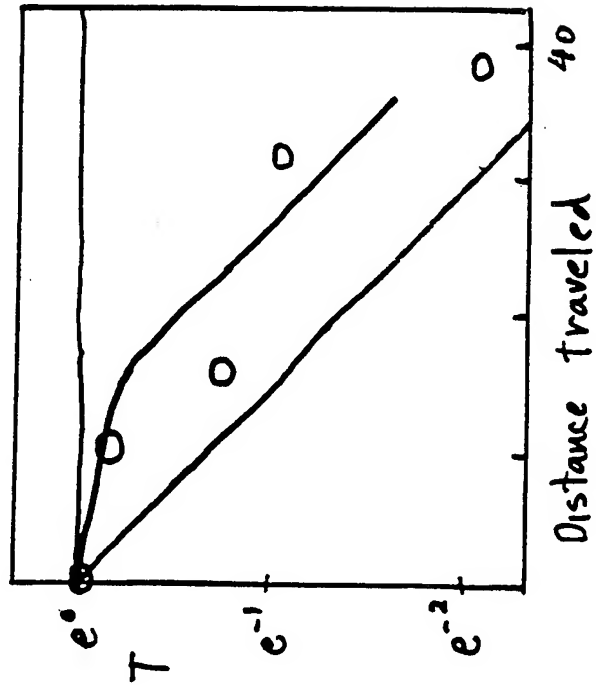
Nonlinear pulse has extra degree of freedom
 \Rightarrow satisfy conditions locally, within (second) length L_{NL}

Result:

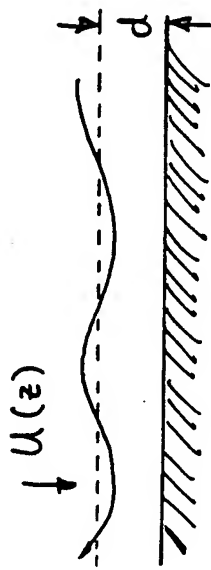
Strong soliton, $L_{NL} \ll L_A$

Intermediate, $L_{NL} \sim L_A$

Weak soliton $L_{NL} \gg L_A$



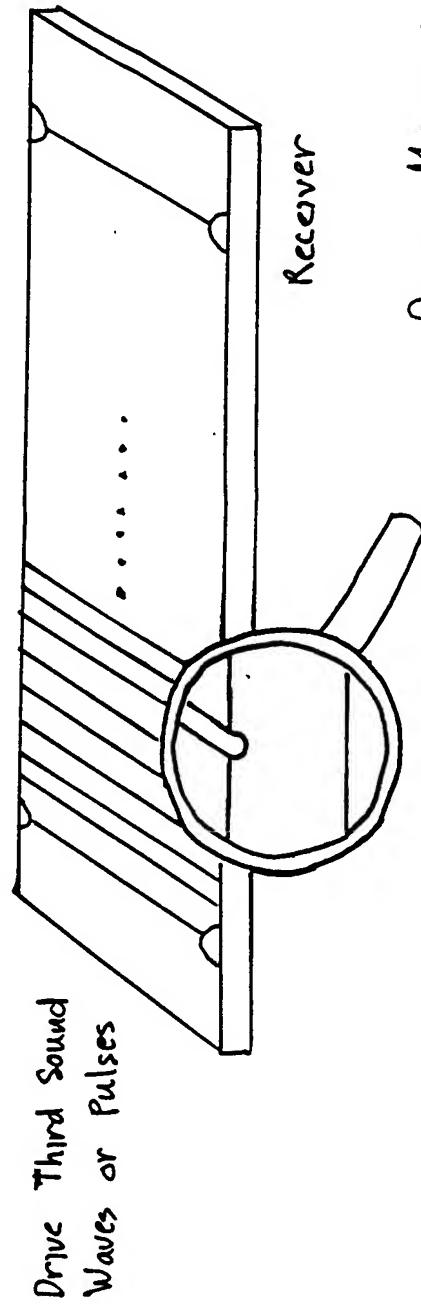
Nonlinear Waves and Pulses Surface Waves



Speed of wave = $\sqrt{d \frac{du}{dz}} = \sqrt{gd}$
 $c(d)$

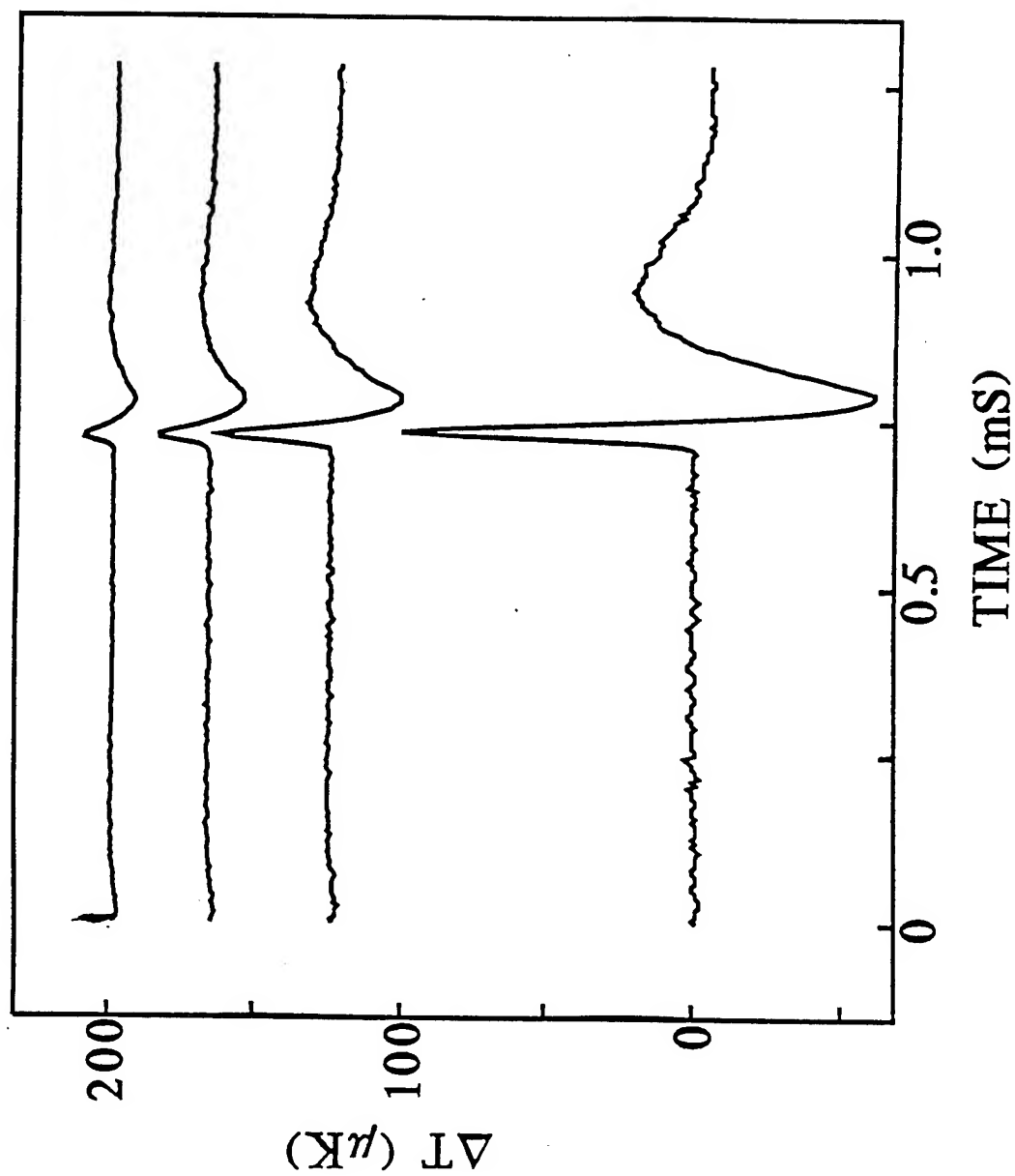
Finite amplitude: $C(d+\psi) \rightarrow$ Nonlinear Wave Eq.

Low attenuation: Superfluid Helium $U(z) = \text{Van der Waals } \frac{d}{z^3}$
 Third Sound

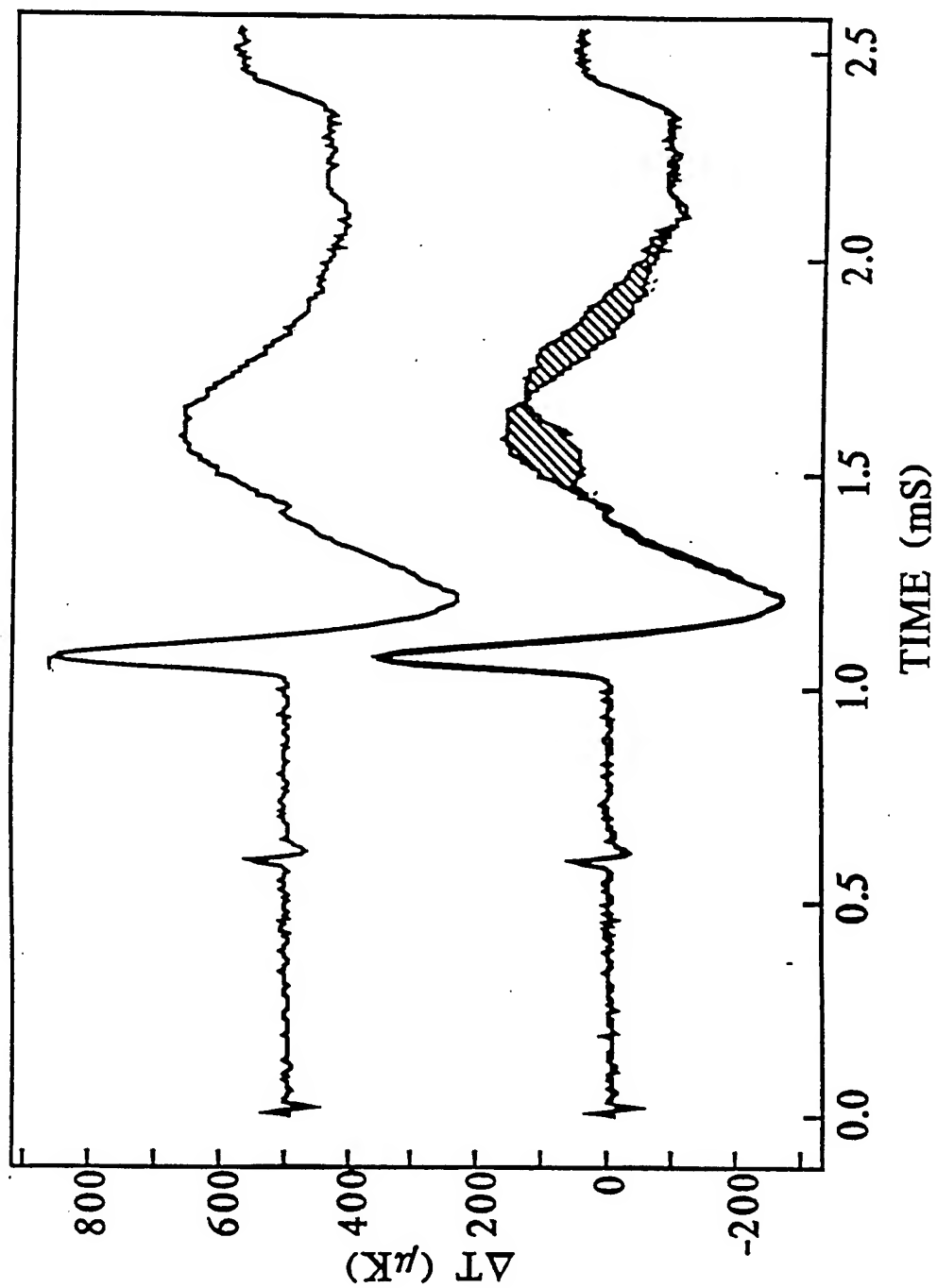


Doug Meegan

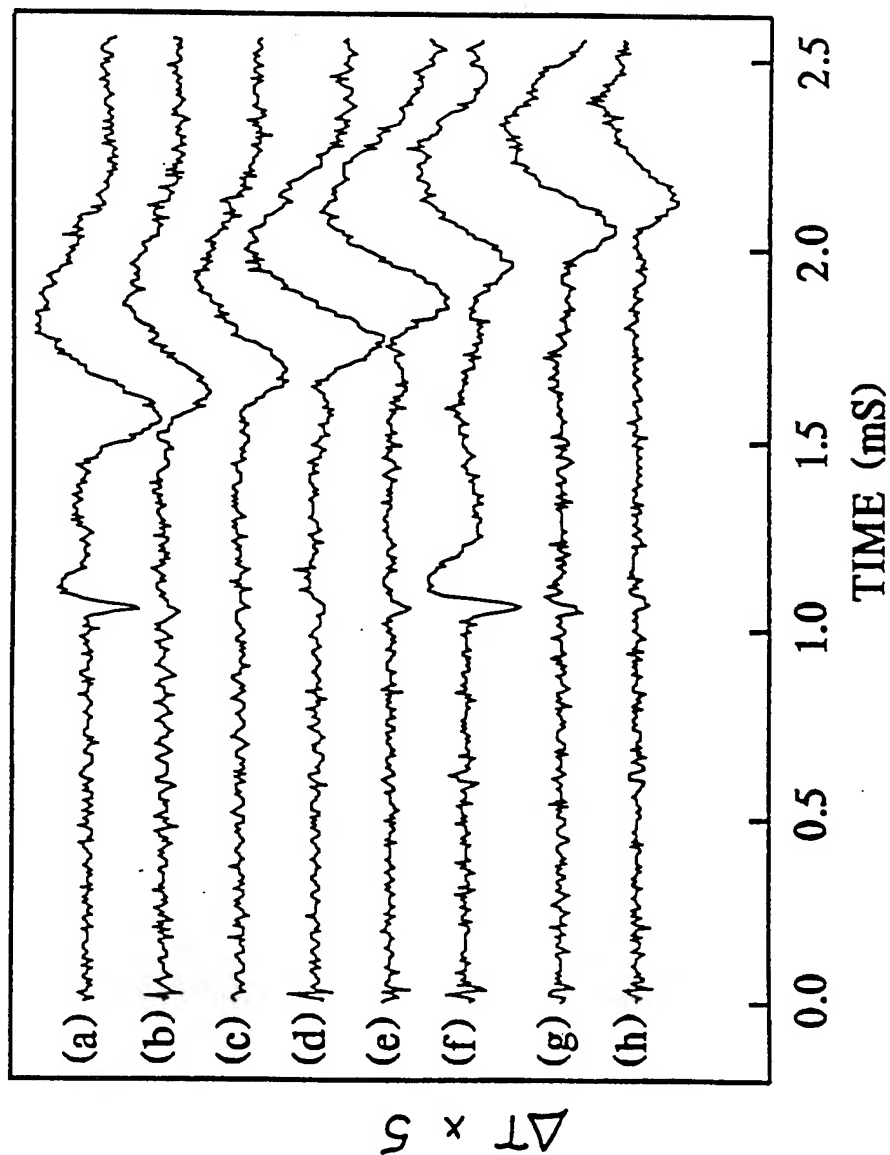
No scatterers (bare substrate)



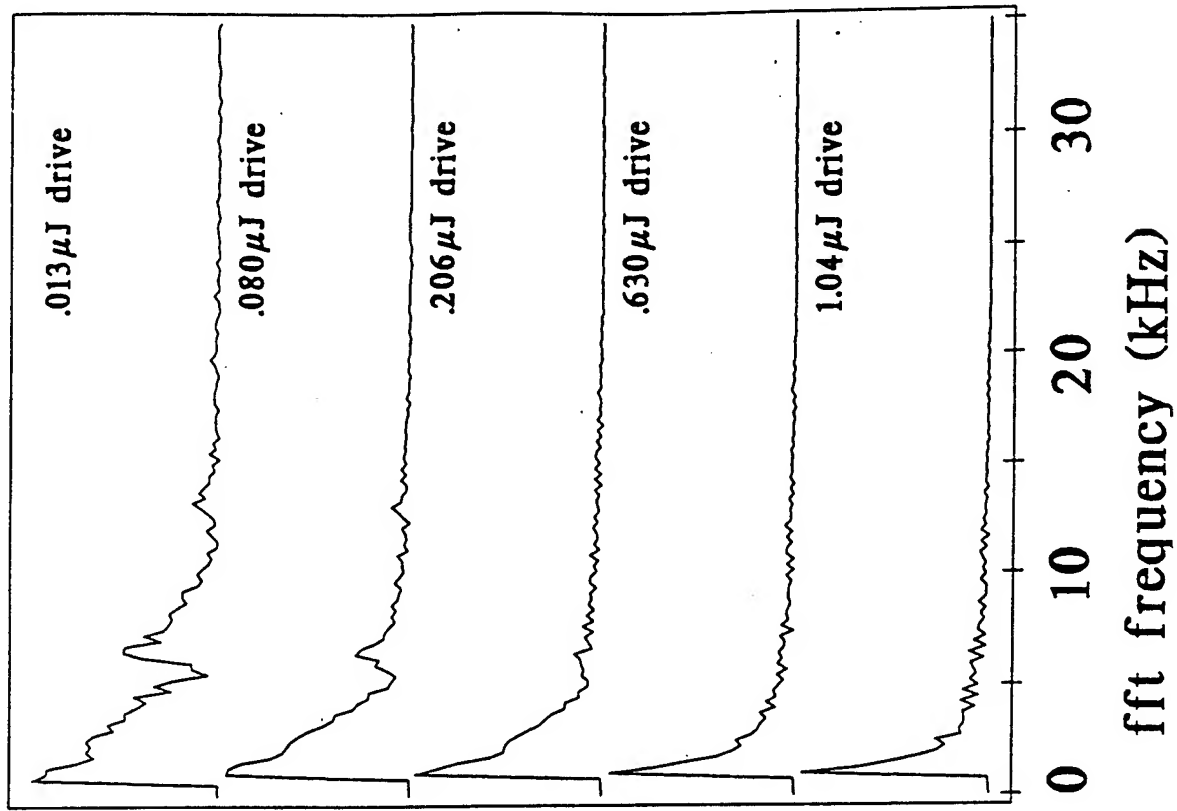
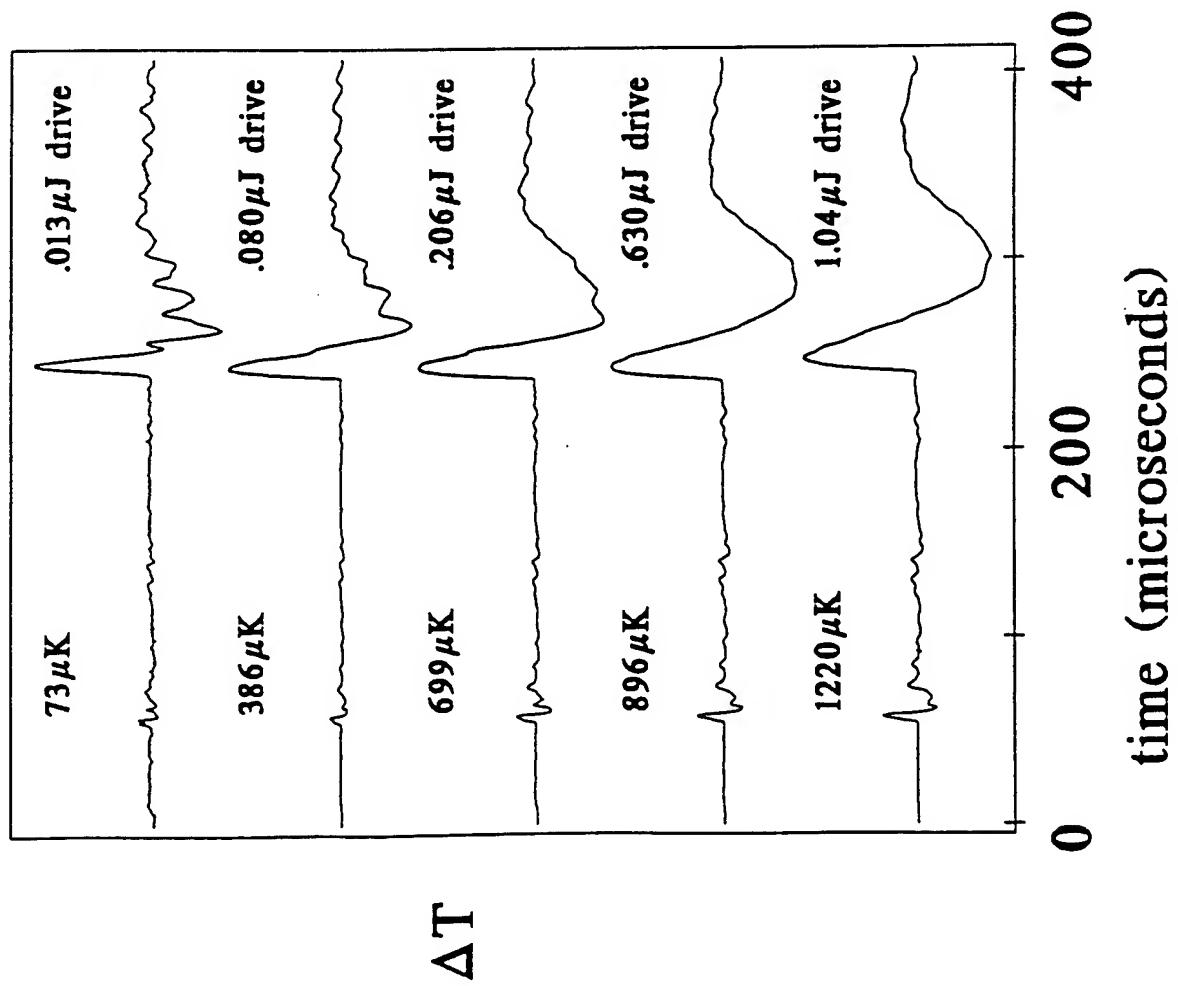
No scatters ; Appearance of nonlinear pulse

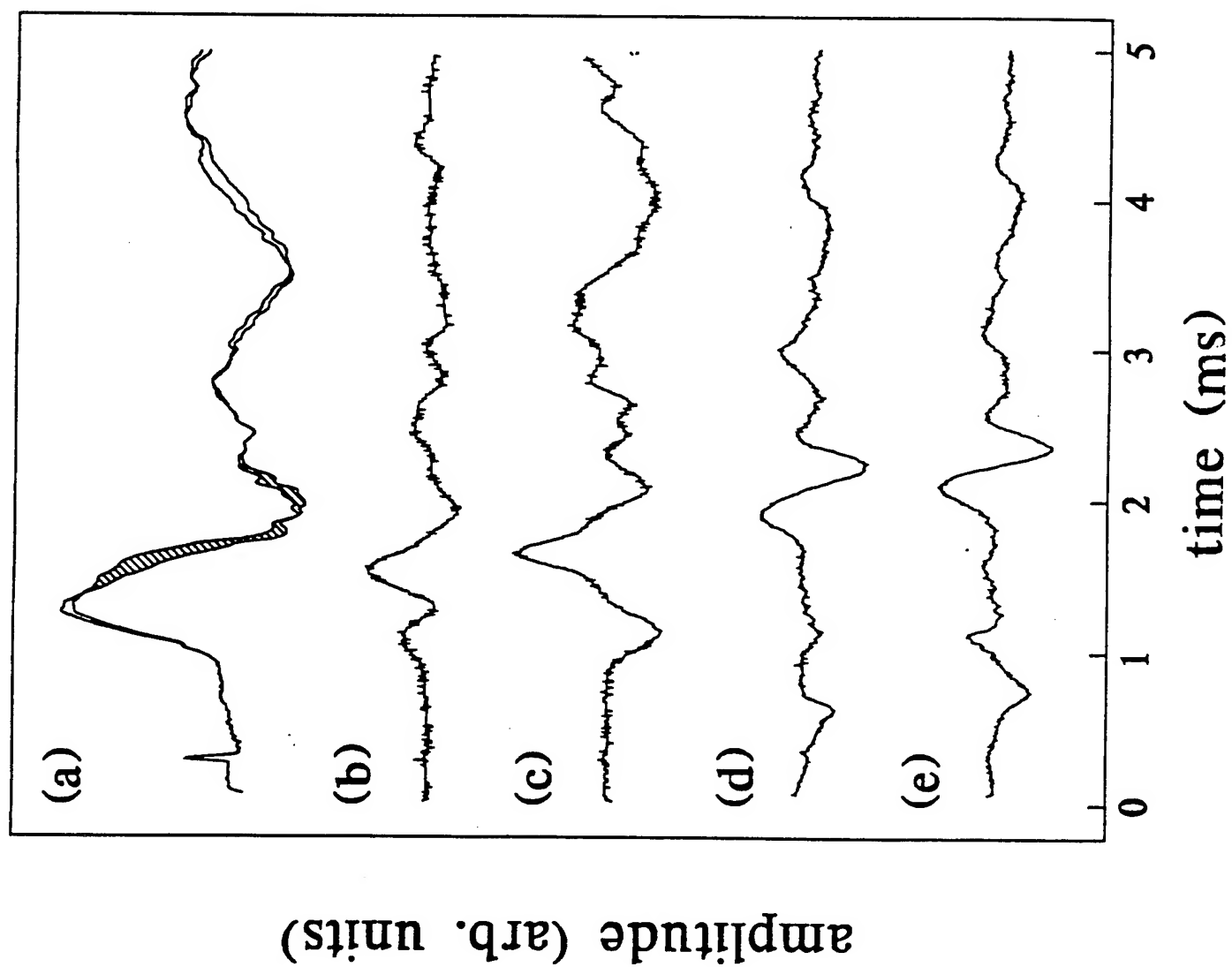


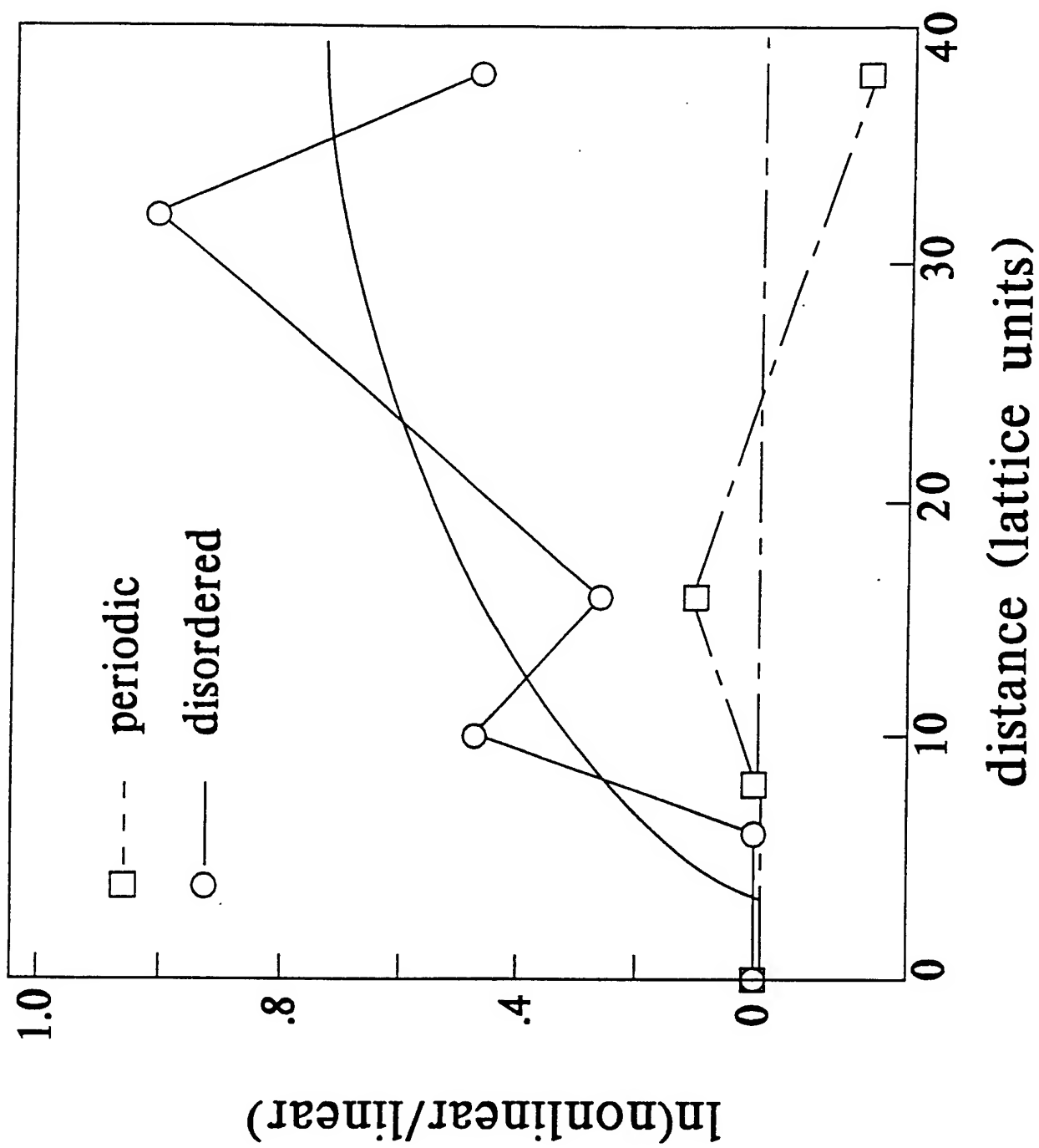
No scatterers; Nonlinear Pulse: C depends on amplitude



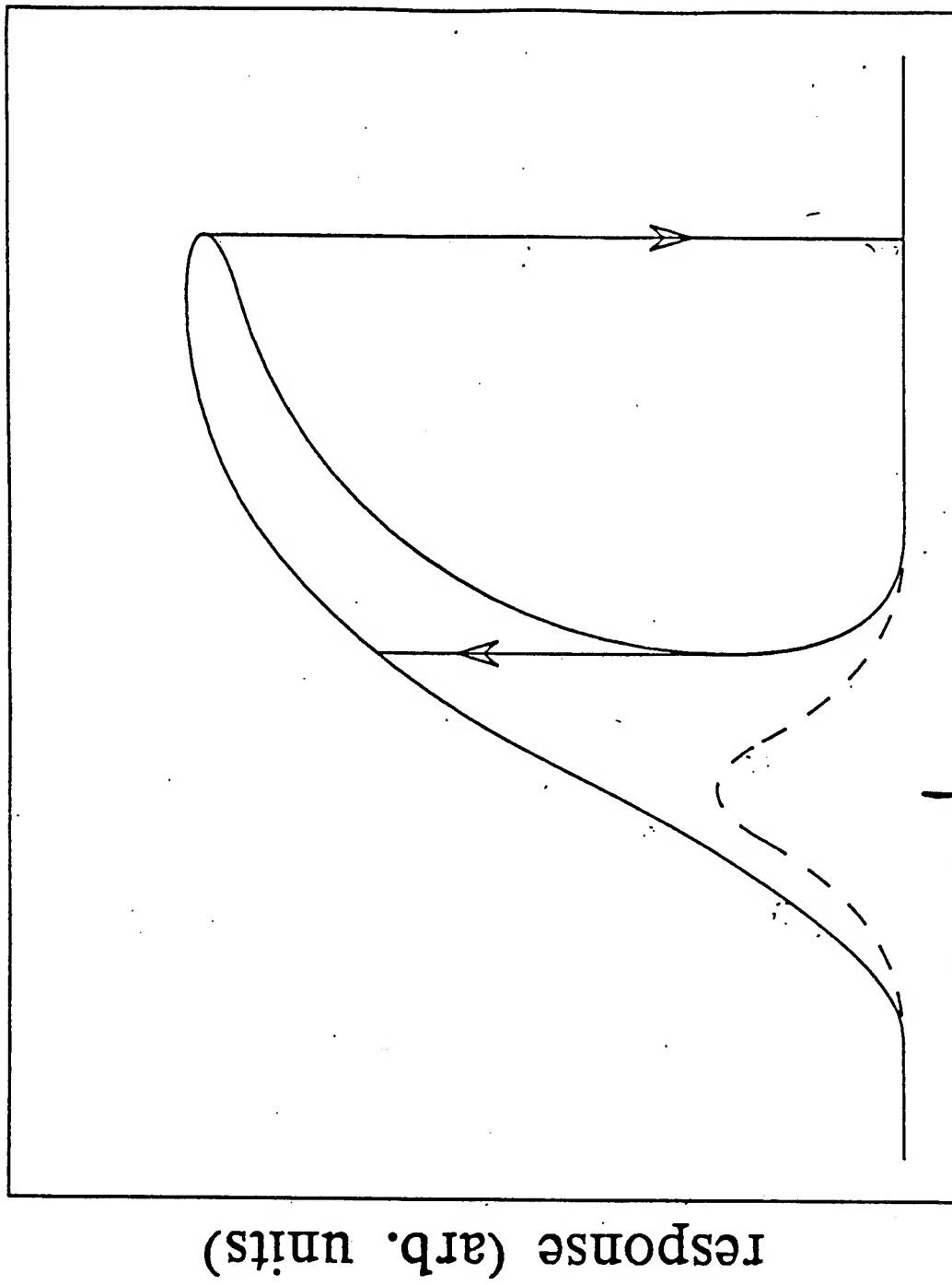
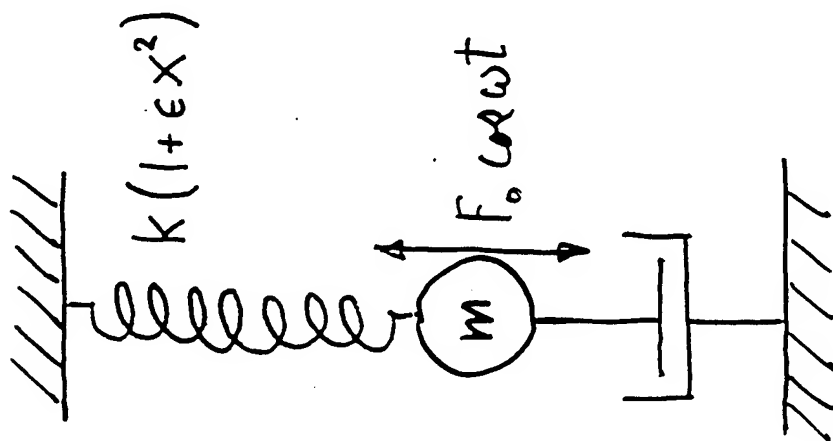
PERIODIC SUBSTRATE -- 1.1K, 7.5 layers

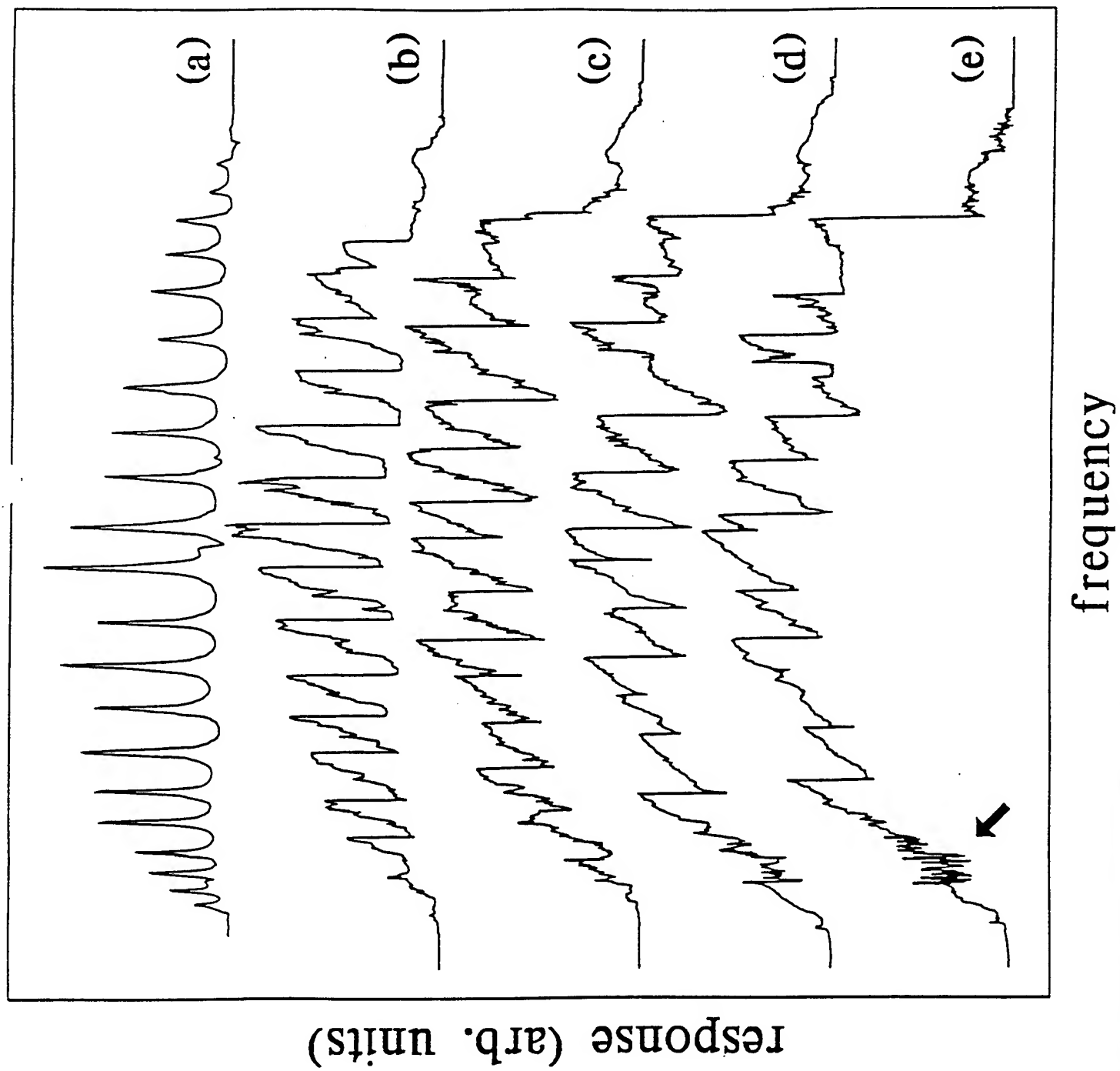


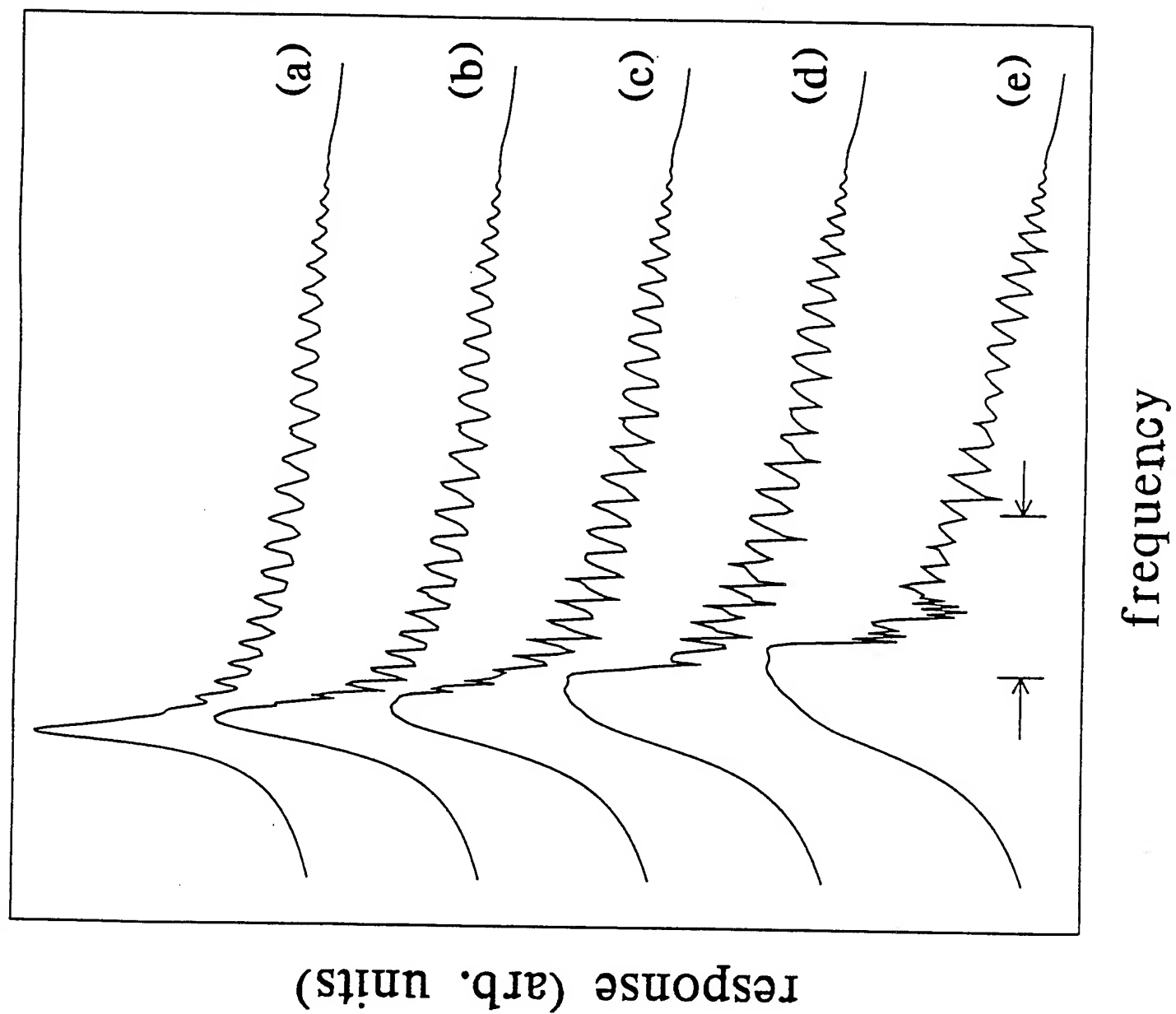


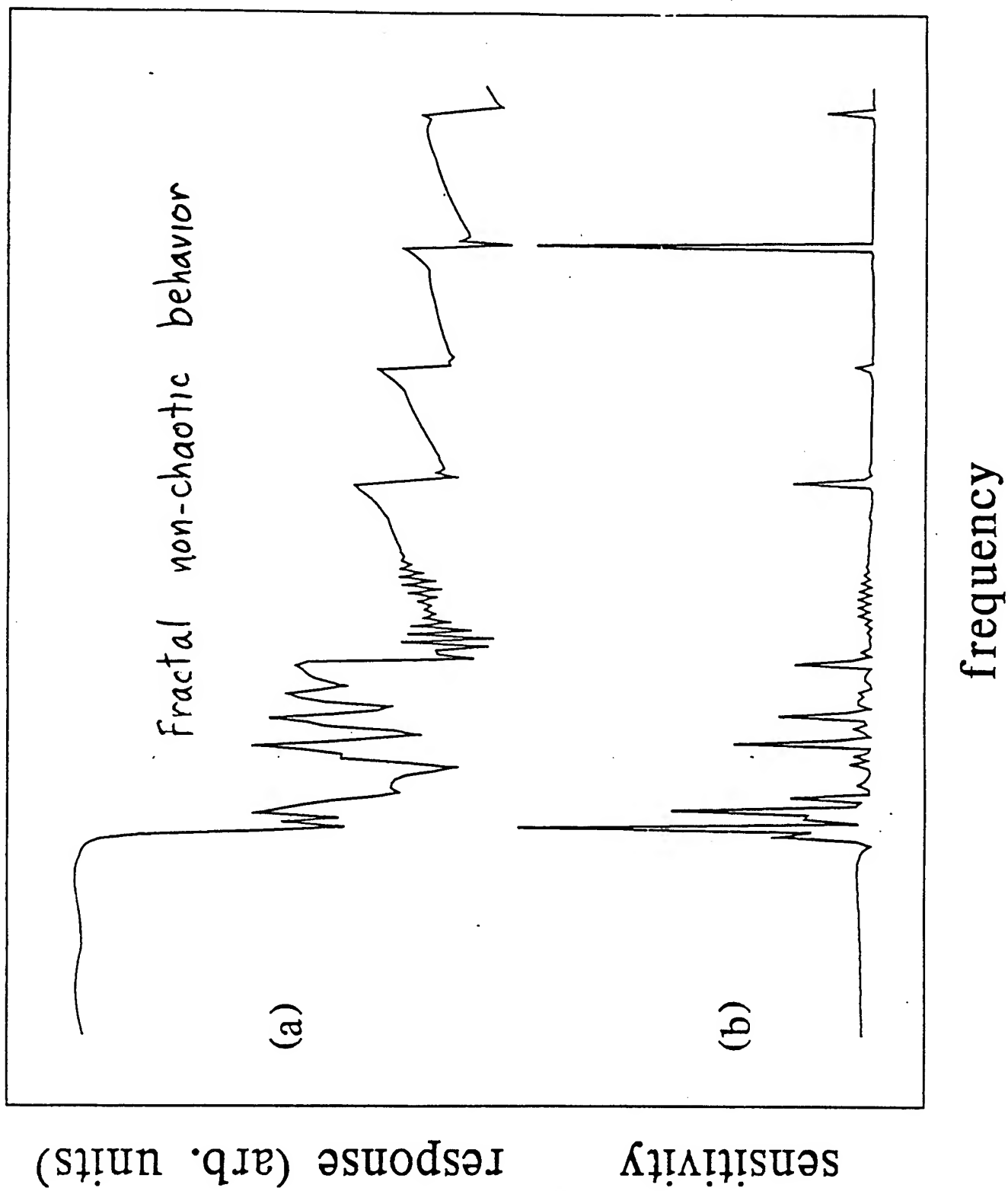


Driven mass on a nonlinear spring

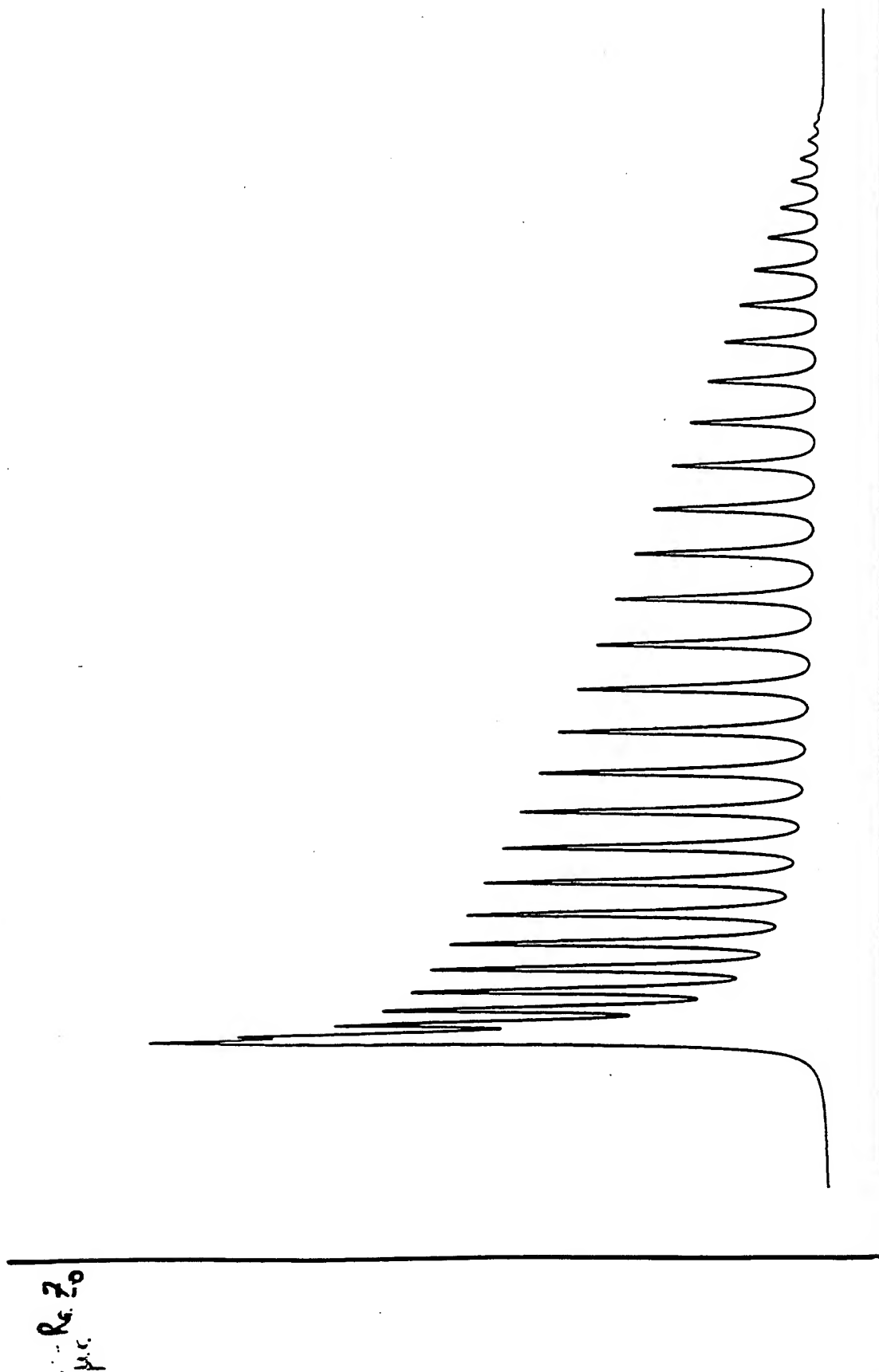




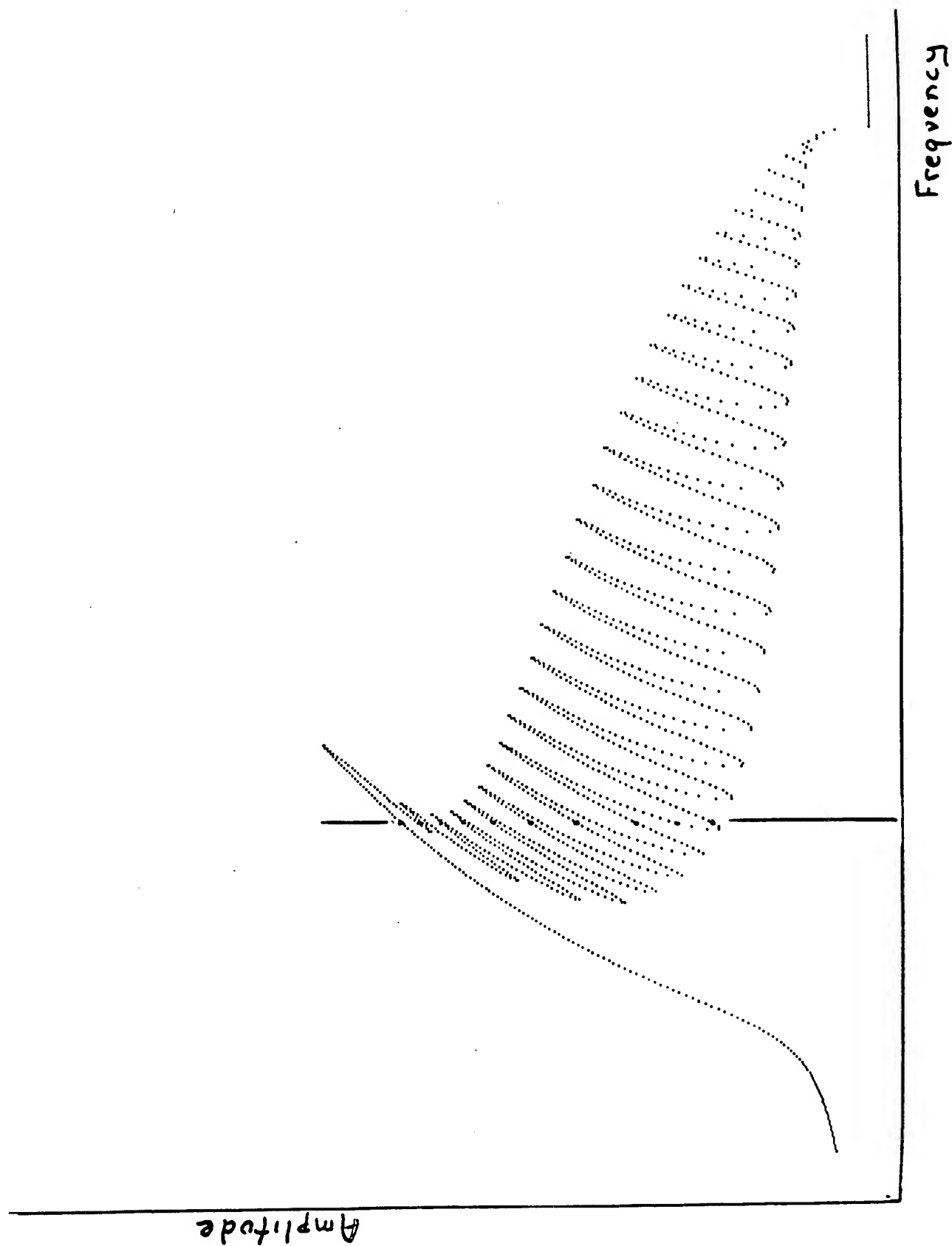




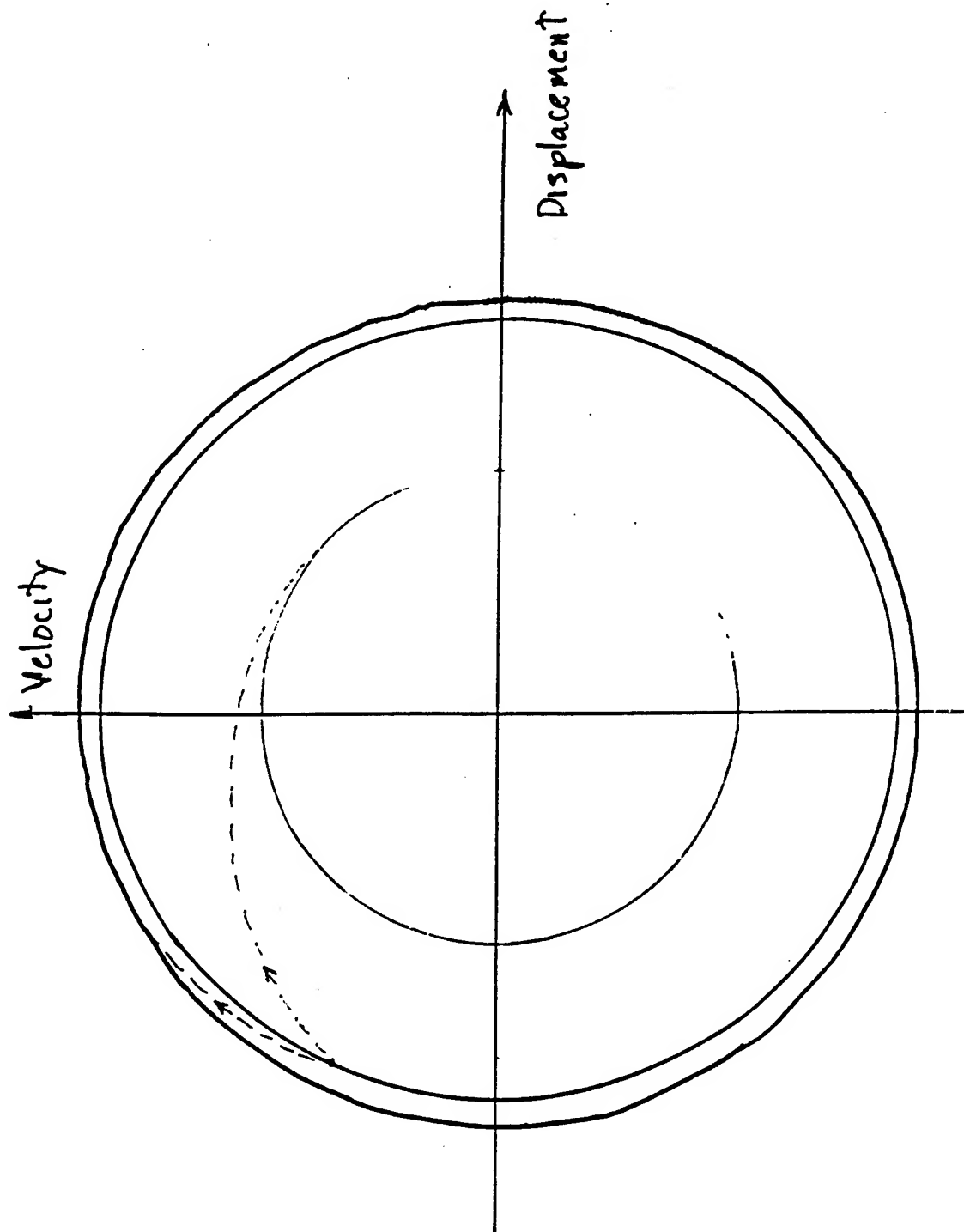
$$A = F \left(\frac{\omega}{c(a)} \right)$$



Nonlinearity $\epsilon = 0.005$



Basin Crowding and Noise



Magnetic Response of a Single, Isolated Gold Loop

V. Chandrasekhar, R. A. Webb, M. J. Brady, M. B. Ketchen, W. J. Gallagher, and A. Kleinsasser
IBM Research Division, T. J. Watson Research Center, P.O. Box 218, Yorktown Heights, New York 10598
 (Received 12 August 1991)

Measurements have been made of the low-temperature magnetic response of single, isolated, micron-size Au loops. The magnetic response is found to contain a component which oscillates with the applied magnetic flux with a fundamental period of $\Phi_0 = h/e$. The amplitude of the oscillatory component corresponds to a persistent current of $\approx (0.3-2.0)e v_F / L$, 1 to 2 orders of magnitude larger than predicted by current theories.

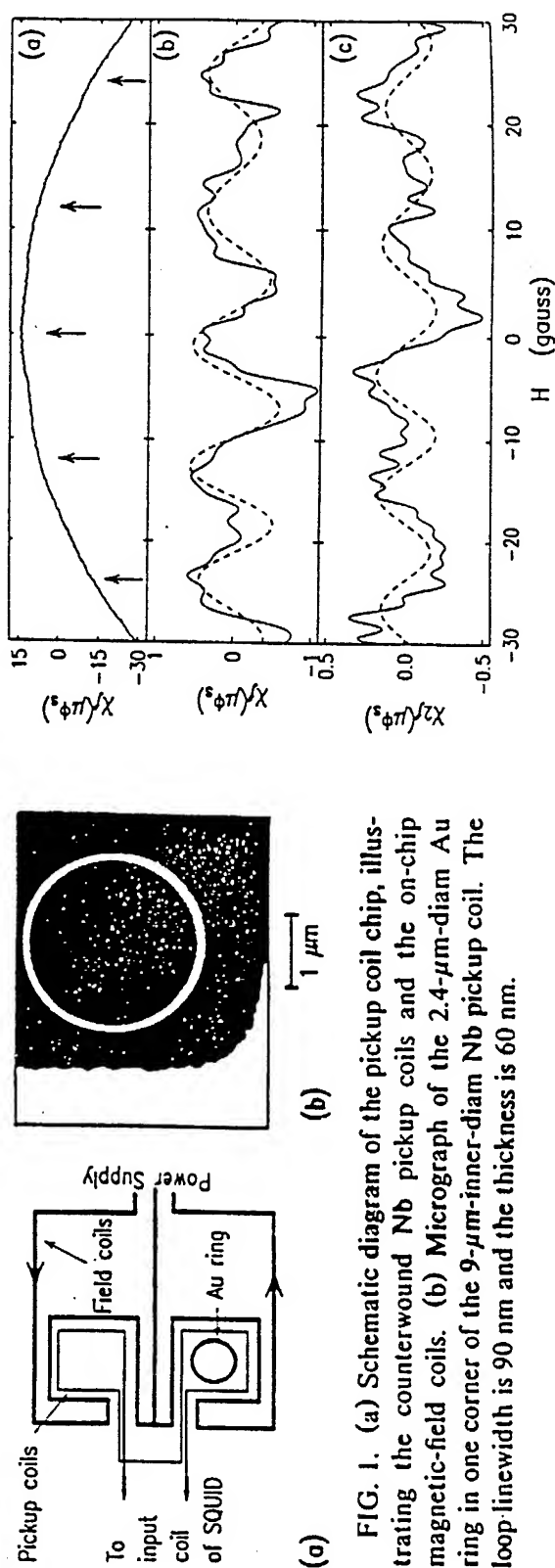
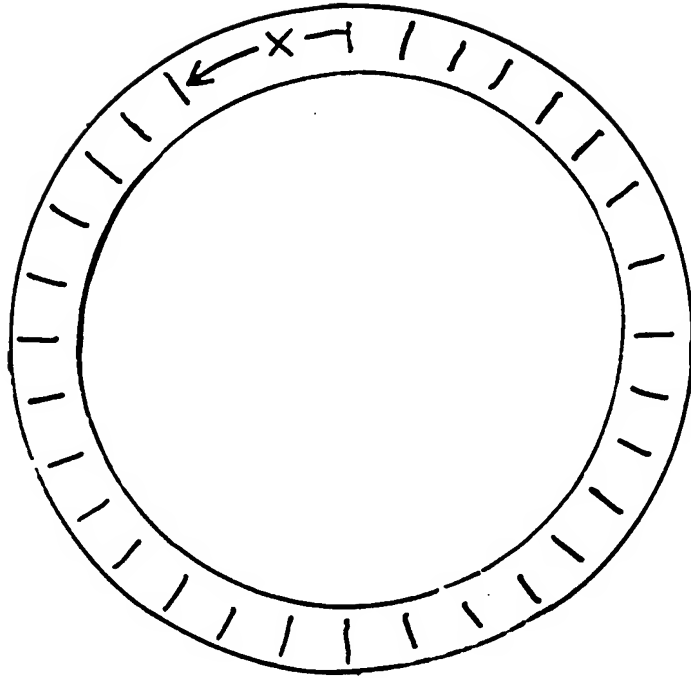


FIG. 1. (a) Schematic diagram of the pickup coil chip, illustrating the counterwound Nb pickup coils and the on-chip magnetic-field coils. (b) Micrograph of the 2.4- μ m-diam Au ring in one corner of the 9- μ m-inner-diam Nb pickup coil. The loop-line width is 90 nm and the thickness is 60 nm.

o o. No scattering - circular waveguide



Circumference = L

$$\psi \sim e^{i2\pi x/\lambda}$$

$$\begin{aligned} i &= ne \frac{-i\hbar}{2m} (\psi^* \nabla \psi - \psi \nabla \psi^*) \\ &= ne\hbar / [m\lambda] \\ &= ne\hbar / [m(\frac{L}{N})] \\ &= N ne\hbar / mL \end{aligned}$$

$$\begin{aligned} \Delta i &= ne\hbar / mL \\ &= \frac{e}{L} \left(\frac{n\hbar}{m} \right) \end{aligned}$$

$$\Delta i = \frac{e v_F}{L}$$

1. One electron, $T=0$, elastic scattering only.

Because of elastic scattering,
the electron follows a
Tortuous path, with length

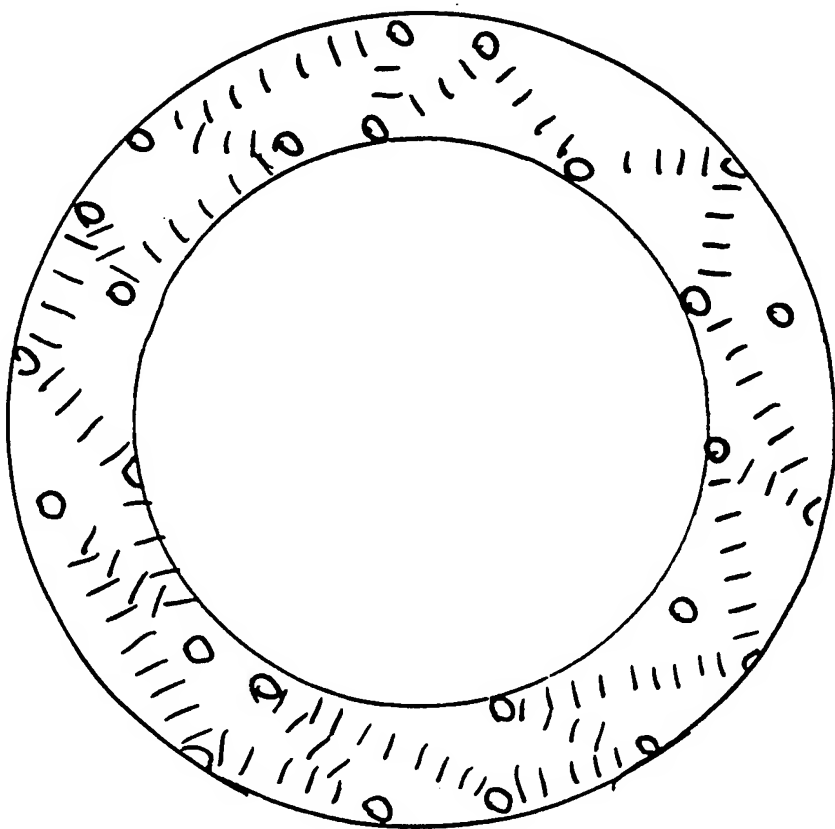
$$L' > L$$

Consequence:

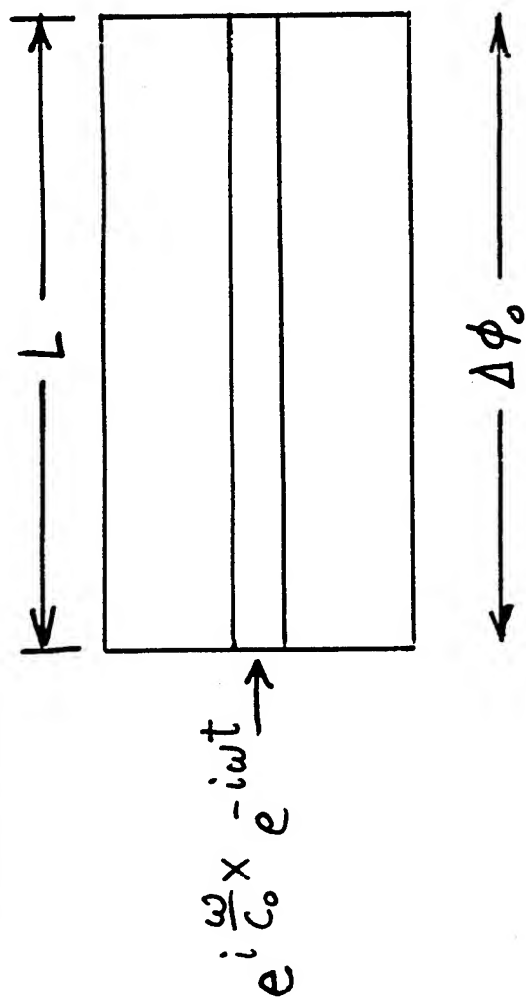
$$\Delta i = \frac{e v_F}{L'} = \frac{e v_F}{L} \left(\frac{L}{L'} \right)$$

$$= \frac{e v_F}{L} \left(\frac{L_e}{L} \right)$$

Analogous to acoustic tortuosity correction.

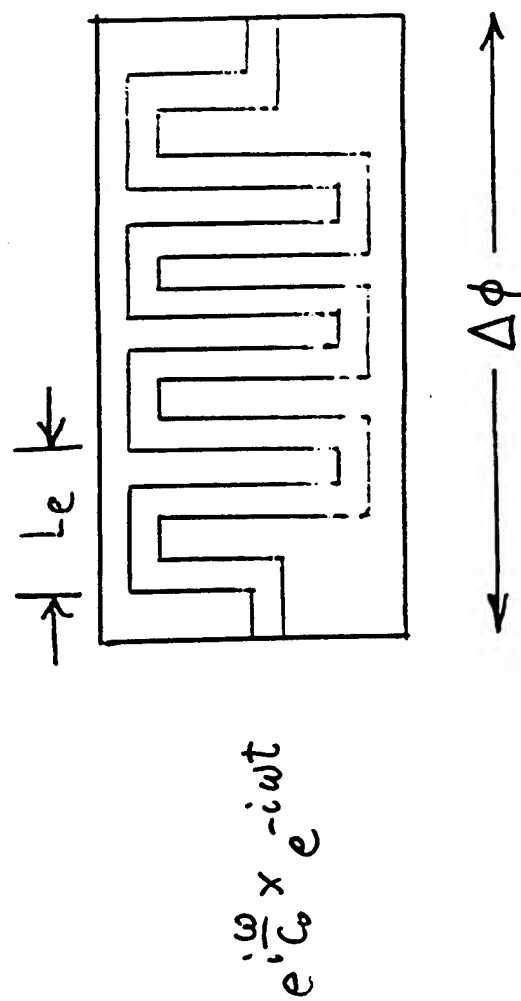


A useful model for the tortuosity correction:



$$\Delta\phi_0 = \frac{\omega L}{c_0}$$

$$c_0 = \frac{\omega L}{\Delta\phi_0}$$



$$\Delta\phi = \frac{\omega}{c_0} L'$$

$$c = \frac{\omega L}{\Delta\phi}$$

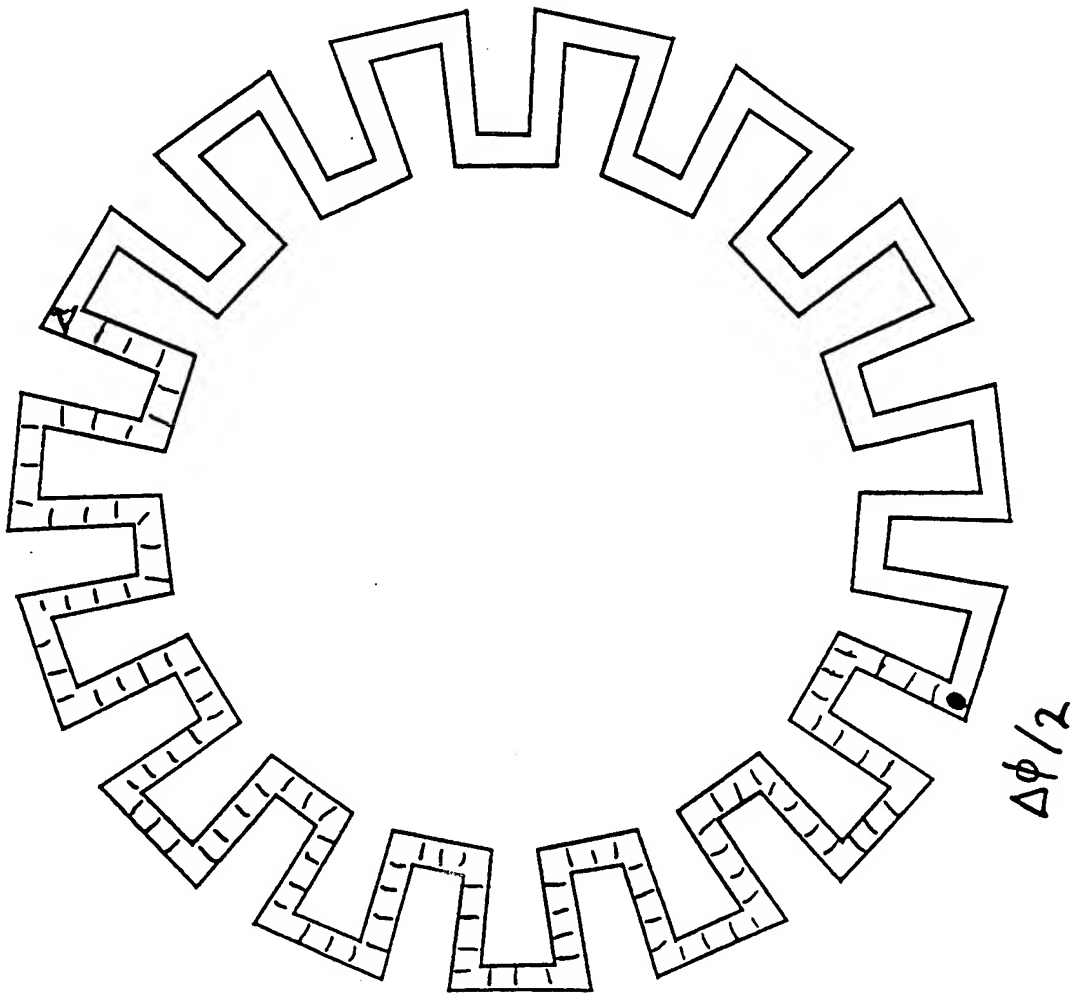
$$= c_0 \frac{L}{L'} = c_0 \frac{L_e}{L}$$

Circumference = L

Waveguide length = L'

$$C = \frac{\omega L}{\Delta\phi} = c_0 \frac{L}{L'}$$

But this would be
a transport measurement.



Persistent current
measurements are
made with an AC
axial magnetic field.

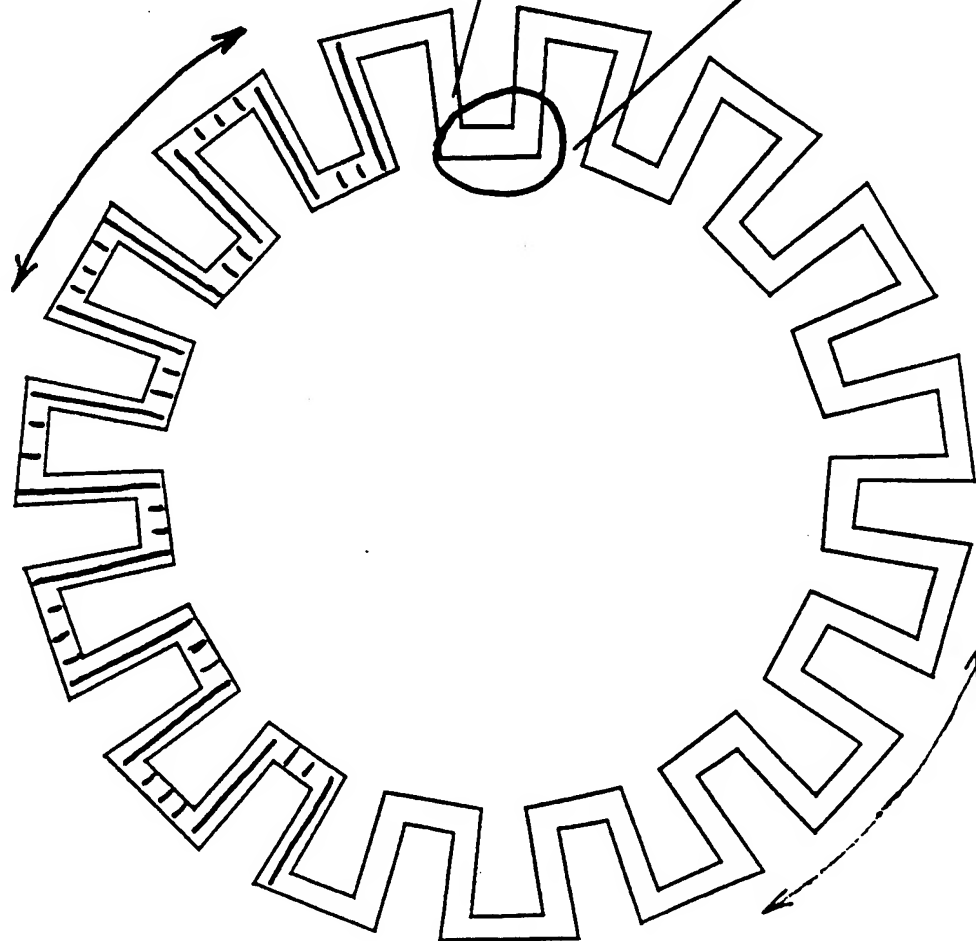
Effect of a purely azimuthal drive: Azimuthal modes are favored.



$$v_{\text{phase}} = \infty$$

$$\Delta\phi = \frac{\omega L}{c_0}$$

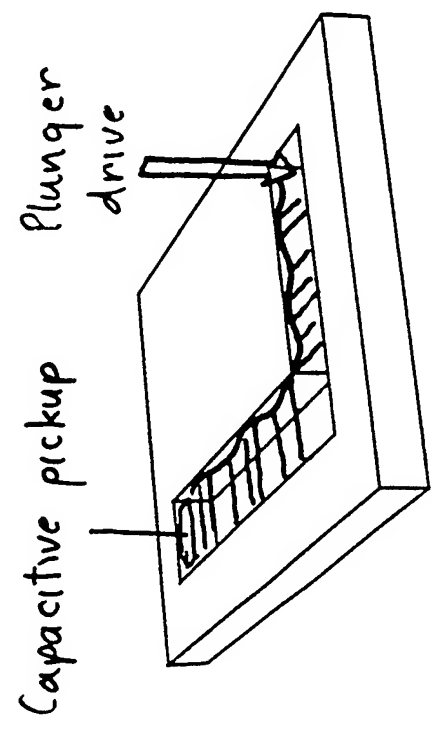
$$c = \frac{\omega L}{\Delta\phi} = c_0$$



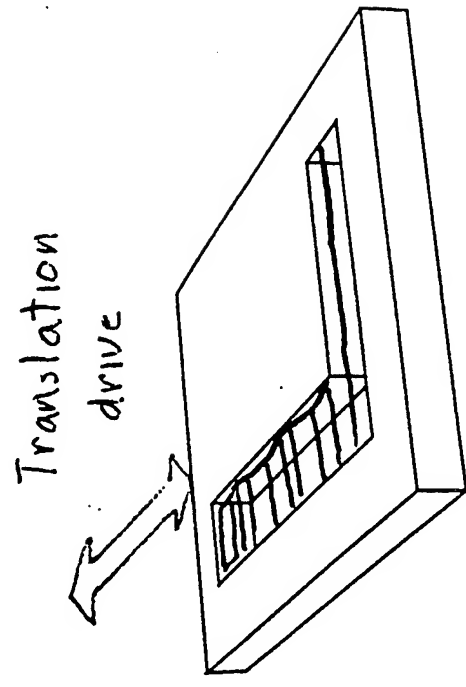
Distinguishing between L and L' - The L-shaped waveguide

Need low velocity wave to avoid resonances in waveguide structure.

Surface waves in a channel.

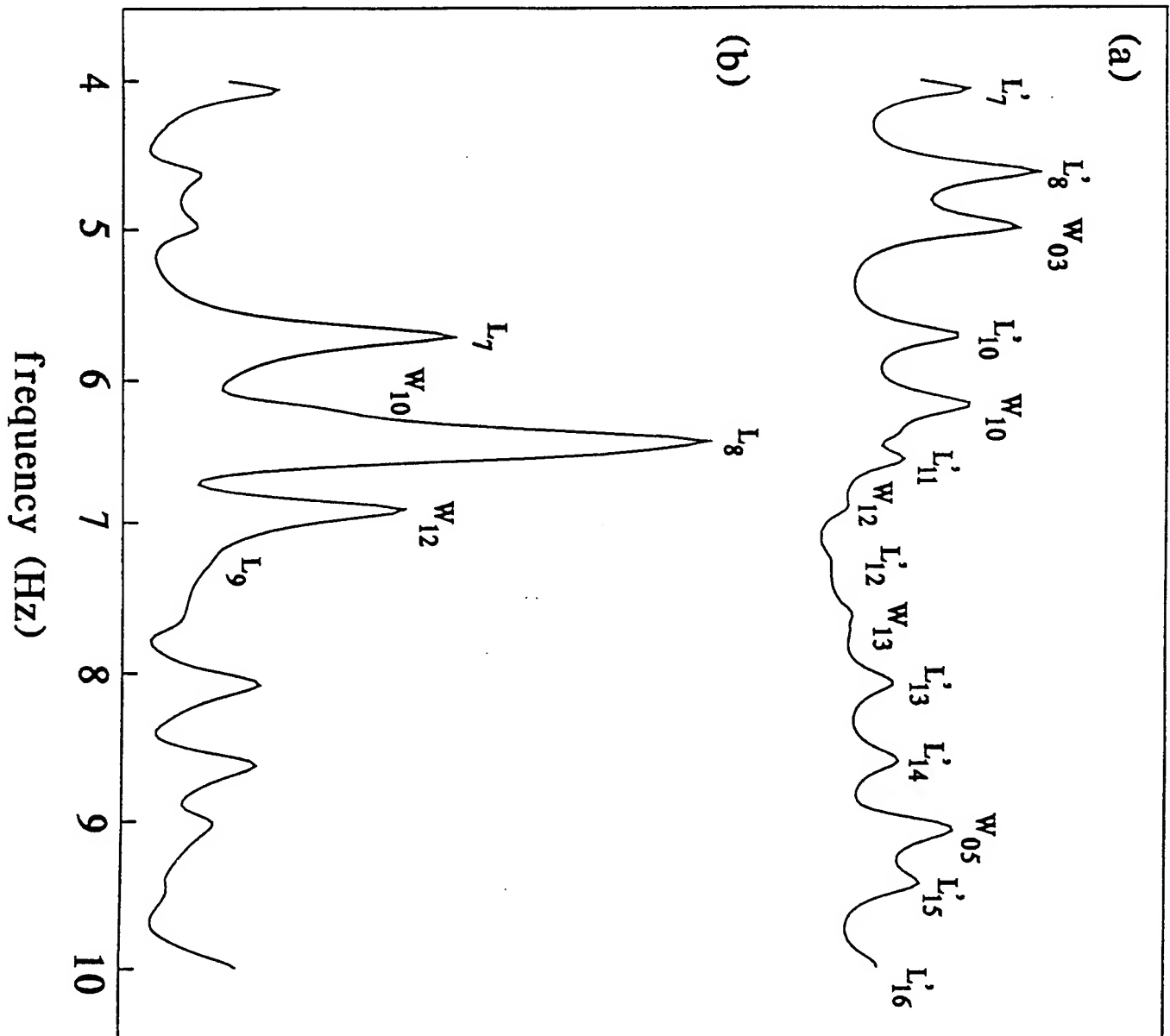


(a)



(b)

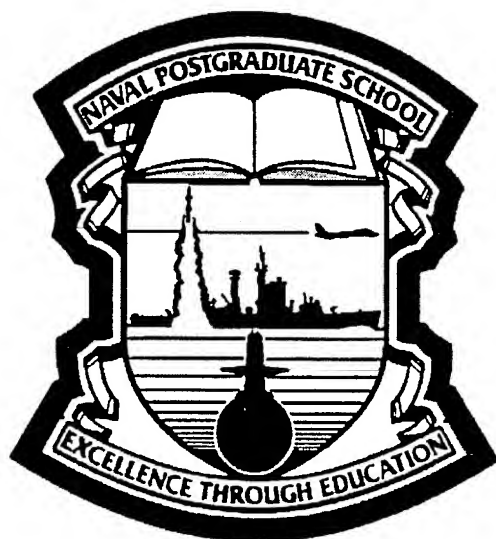
response amplitude (arb. units)



Physical Acoustics Summer School 1996

Sonoluminescence

Anthony A. Atchley
Physics Department
Naval Postgraduate School
Monterey, CA



Simplified Acoustic Levitation

Assume only two forces act on a gas bubble:

- 1) an acoustic force
- 2) buoyancy force

Also assume that any difficult problems can be ignored.

At equilibrium:

$$\langle F_{\text{acoustic}} \rangle_t = - \langle F_{\text{buoyancy}} \rangle_t$$

$$F_{\text{acoustic}} = -V(z,t) \nabla P(z,t)$$

$$F_{\text{buoyancy}} = \rho_L V(z,t) g \quad (\rho_L \neq \rho_L(t))$$

$$P(z,t) = P_m + P_A \cos(kz) \cos(\omega t)$$

$$V(z,t) = V_m - V_A(P_A, \omega) \cos(kz) \cos(\omega t)$$

$$F_{\text{acoustic}} = -[V_m - V_A(P_A, \omega) \cos(kz) \cos(\omega t)] \times [-k P_A \sin(kz) \cos(\omega t)]$$

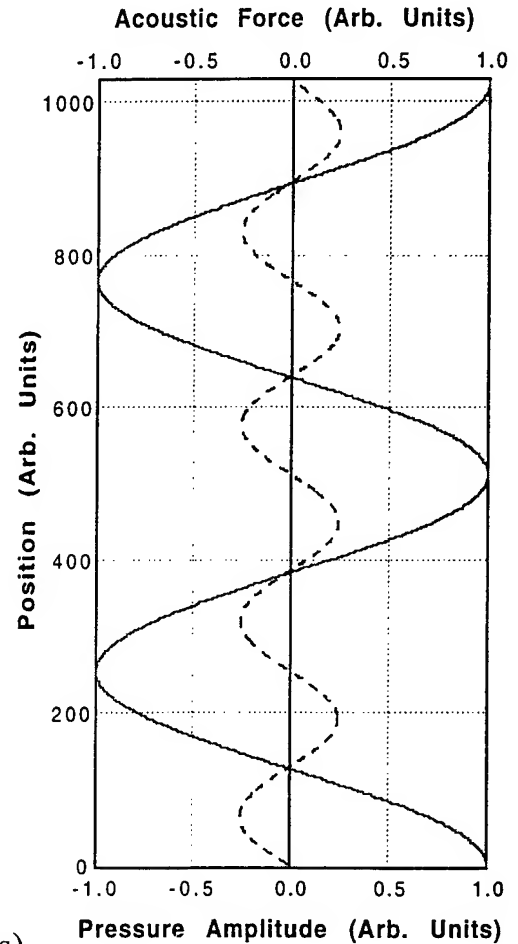
$$\begin{aligned} \langle F_{\text{acoustic}} \rangle_t &= -(1/2) k P_A V_A \sin(kz) \cos(kz) \\ &= -(1/4) k P_A V_A \sin(2kz) \end{aligned}$$

$$F_{\text{buoyancy}} = \rho_L [V_m - V_A(P_A, \omega) \cos(kz) \cos(\omega t)] g$$

$$\langle F_{\text{buoyancy}} \rangle_t = \rho_L V_m g \quad (\text{for linear oscillations})$$

$$(1/4) k P_A V_A \sin(2kz) = \rho_L V_m g$$

$$\sin(2kz) = 4 \rho_L V_m g / (k P_A V_A) = 4 \rho_L V_m g / (k f(P_A))$$

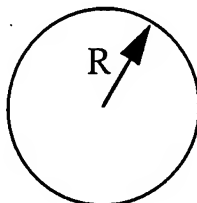


Bubble driven below
resonance.

Simplified Bubble Dynamics

Rayleigh - Plesset Equation

Bubble of instantaneous radius R
in an incompressible fluid.



Apply Conservation of Energy

$$KE + PE = \text{constant}$$

$$\dot{KE} = -\dot{PE}$$

Kinetic Energy

$$KE = \int_R^{\infty} \frac{1}{2} \rho_L u^2 dV$$

Consider the mass flux through a spherical surface centered on the bubble.
If the fluid is incompressible, then

$$4\pi r^2 u(r) = 4\pi R^2 u(R).$$

So,

$$u(r) = \frac{u(R)R^2}{r^2} = \frac{\dot{R}R^2}{r^2}.$$

Rayleigh Plesset Equation

$$\begin{aligned}
 KE &= \int_R^\infty \frac{1}{2} \rho_L \left[\frac{\dot{R} R^2}{r^2} \right]^2 4\pi r^2 dr \\
 &= 2\pi \rho_L \dot{R}^2 R^4 \int_R^\infty \frac{dr}{r^2} \\
 &= 2\pi \rho_L R^3 \dot{R}^2 \\
 &= \frac{1}{2} 3 \left(\frac{4}{3} \pi R^3 \rho_L \right) \dot{R}^2
 \end{aligned}$$

Recall that the effective mass of a small ($kR \ll 1$) bubble is

$$m_{eff} = 3 \left(\frac{4}{3} \pi R^3 \rho_L \right).$$

So,

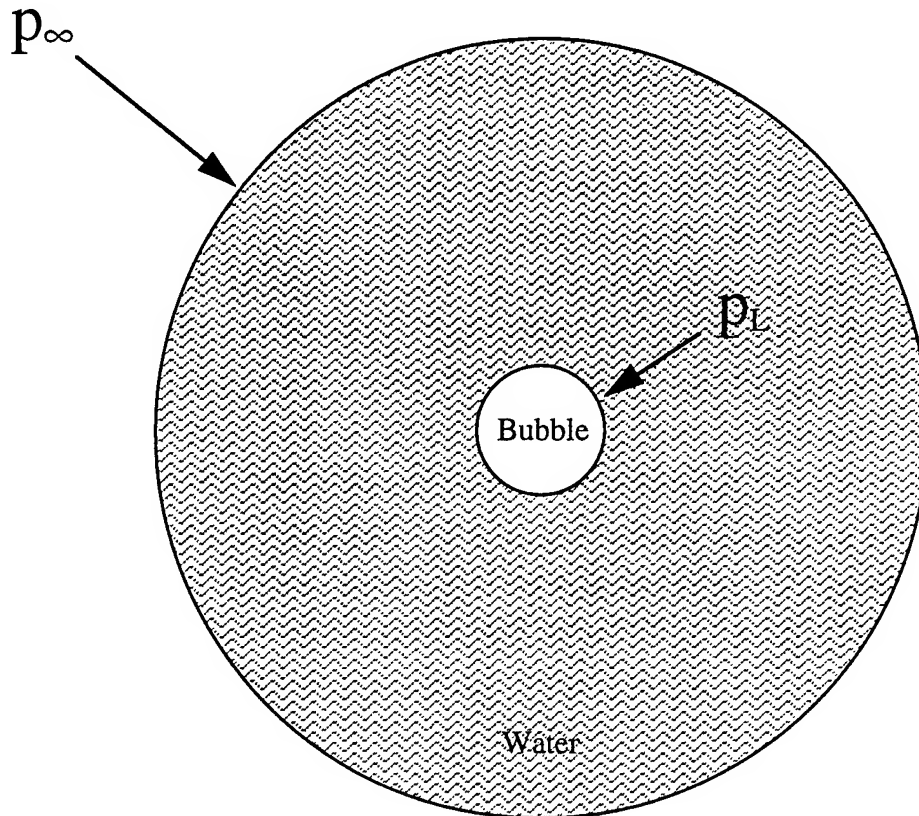
$$KE = \frac{1}{2} m_{eff} \dot{R}^2.$$

Taking the time derivative of the kinetic energy gives

$$\begin{aligned}
 \dot{KE} &= 2\pi \rho_L \left[R^3 \dot{R}^2 \right] \\
 &= 2\pi \rho_L \left[3R^2 \dot{R}^3 + 2R^3 \dot{R} \ddot{R} \right].
 \end{aligned}$$

Rayleigh - Plesset Equation

Potential Energy



p_{∞} = pressure in the water far from the bubble

p_L = pressure on the "wet" side of the bubble wall

If $p_{\infty} \neq p_L$, the bubble will change volume.

The time rate of change of the potential energy is

$$\begin{aligned} PE &= -(p_L - p_{\infty}) \frac{dV}{dt} \\ &= -(p_L - p_{\infty}) 4\pi R^2 \dot{R}. \end{aligned}$$

Rayleigh - Plesset Equation

Using

$$\dot{KE} = -\dot{PE}$$

gives the Rayleigh - Plesset equation

$$R\ddot{R} + \frac{3}{2}\dot{R}^2 = \frac{p_L - p_\infty}{\rho_L}$$

where

$$p_L = p_G + p_V - \frac{2\sigma}{R} - 4\mu \frac{\dot{R}}{R}$$

$$p_\infty = p_o + p_{acoustic}$$

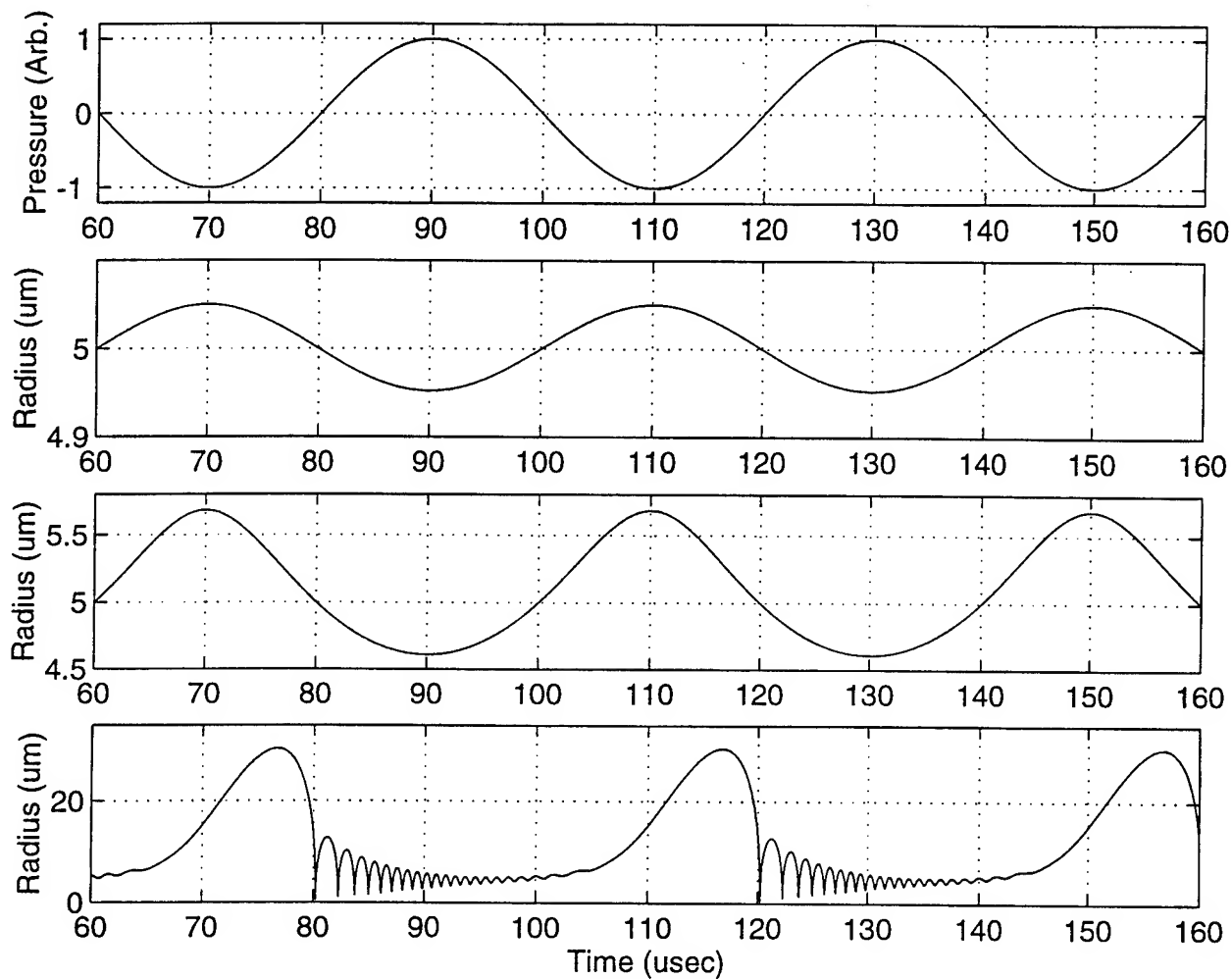
Refinments - Keller Equation

Adding the effects of compressibility leads to the Keller Equation

$$\left(1 - \frac{\dot{R}}{c}\right)R\ddot{R} + \frac{3}{2}\left(1 - \frac{1}{3}\frac{\dot{R}}{c}\right)\dot{R}^2 = \left(1 + \frac{\dot{R}}{c}\right)\frac{p_L - p_\infty - p_a}{\rho_L} + \frac{R}{\rho_L c} \frac{dp_L}{dt}$$

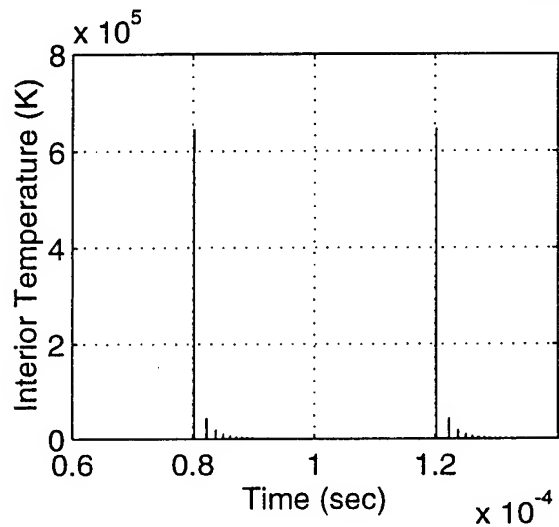
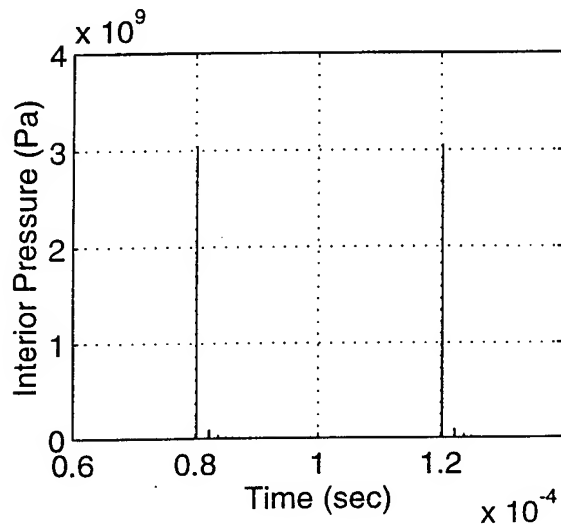
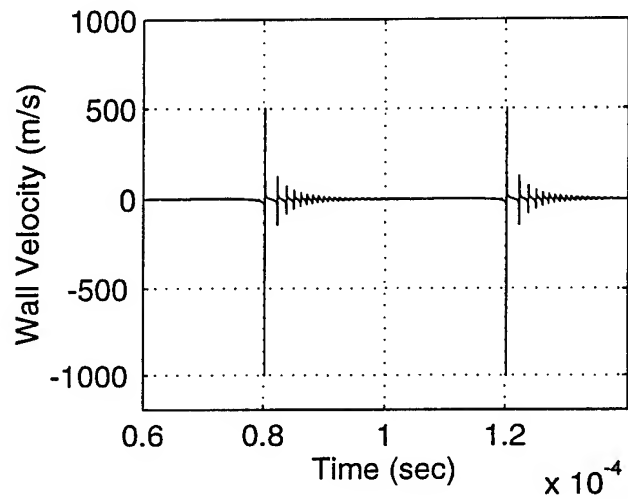
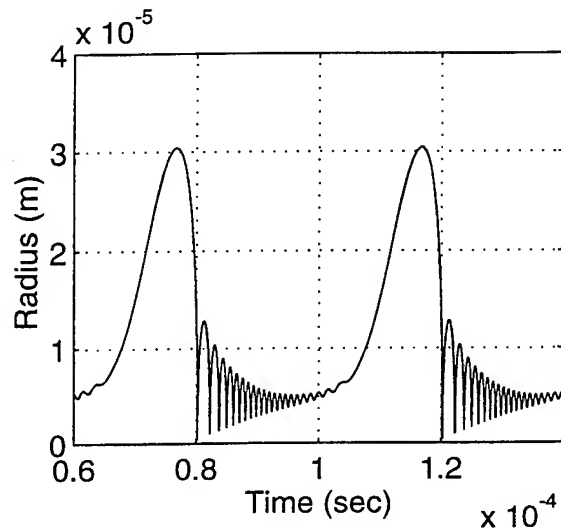
Predicted Bubble Response

$R_0 = 5 \mu\text{m}$ $P_A = 0.05, 0.5, 1.25 \text{ atm}$ $f = 25 \text{ kHz}$



A Closer Look Inside

$$R_o = 5 \mu\text{m} \quad P_A = 1.25 \text{ atm} \quad f = 25 \text{ kHz}$$



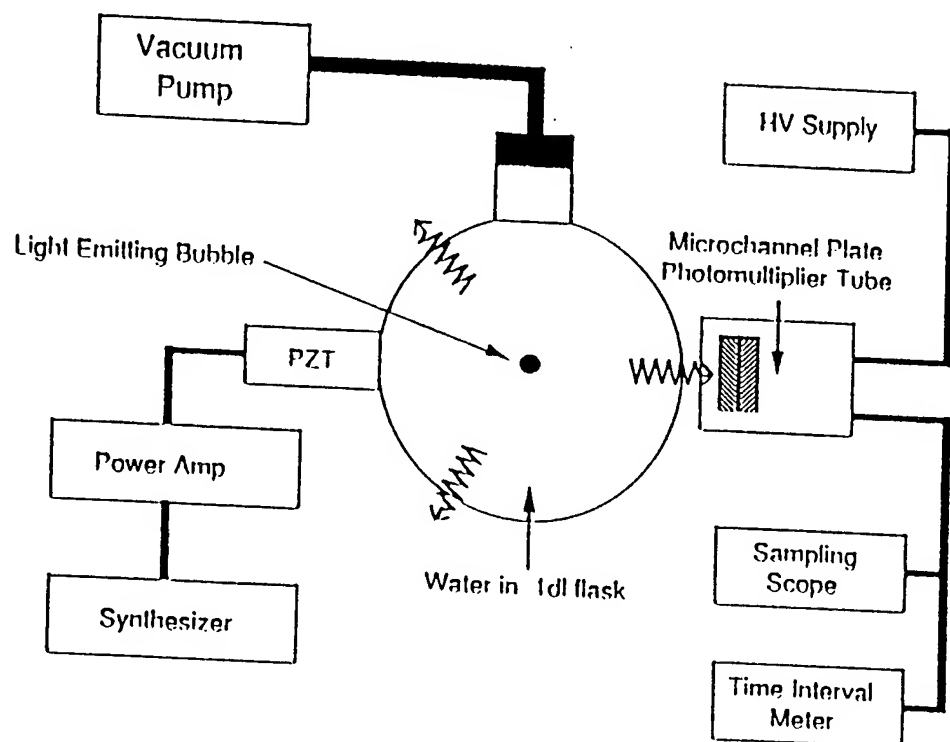


FIG. 2. Block diagram of the apparatus used to generate and observe SL. The sound field is driven with a piezoelectric transducer (PZT) and the emitted light is detected with a PMT biased by the high-voltage (HV) supply.

B. P. Barber, et. al., J. Acoust. Soc. Am. 91, 3061-3063 (1992).

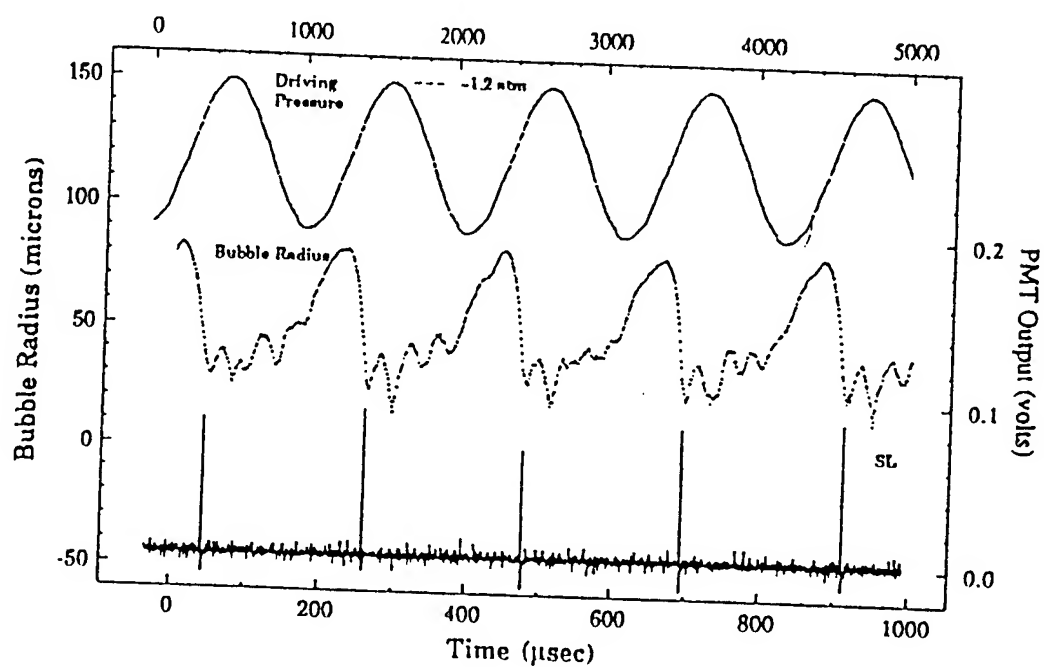


FIG. 18. Simultaneous plots of the sound field (top), bubble radius (middle) and sonoluminescence (bottom) in GLY21 at $P_{\text{at}} = 1.2 \text{ atm}$ and $f = 22.3 \text{ kHz}$.

D. F. Gaitan, et. al., J. Acoust. Soc. Am. 91, 3166-3183 (1992).

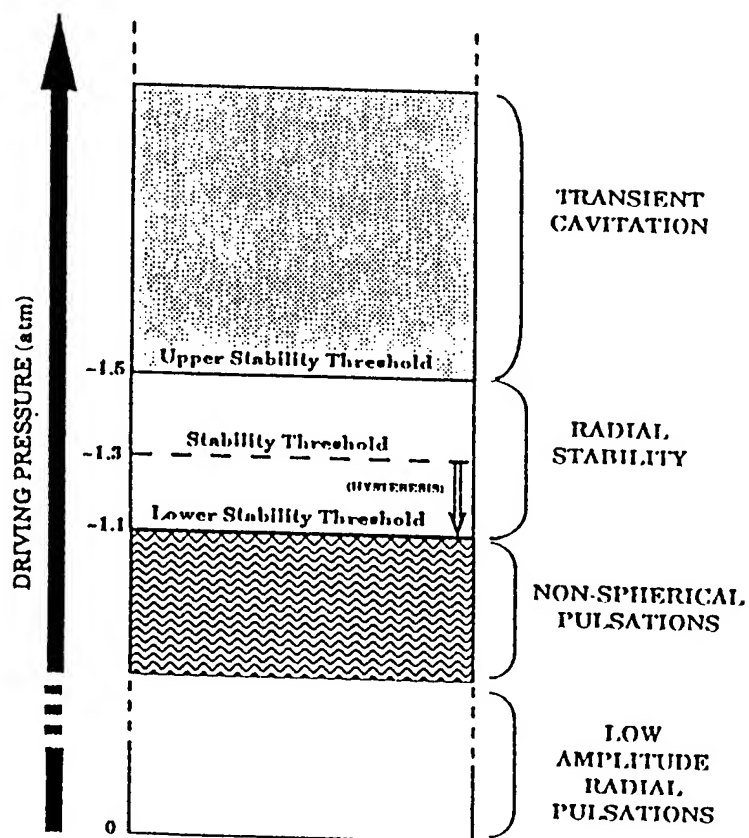


FIG. 10. Diagram of the observed radial stability thresholds for 15- to 20-mm bubbles in water/glycerine mixtures in an acoustic levitation system at $f = 21-25$ kHz.

D. F. Gaitan, et. al., J. Acoust. Soc. Am. 91, 3166-3183 (1992).

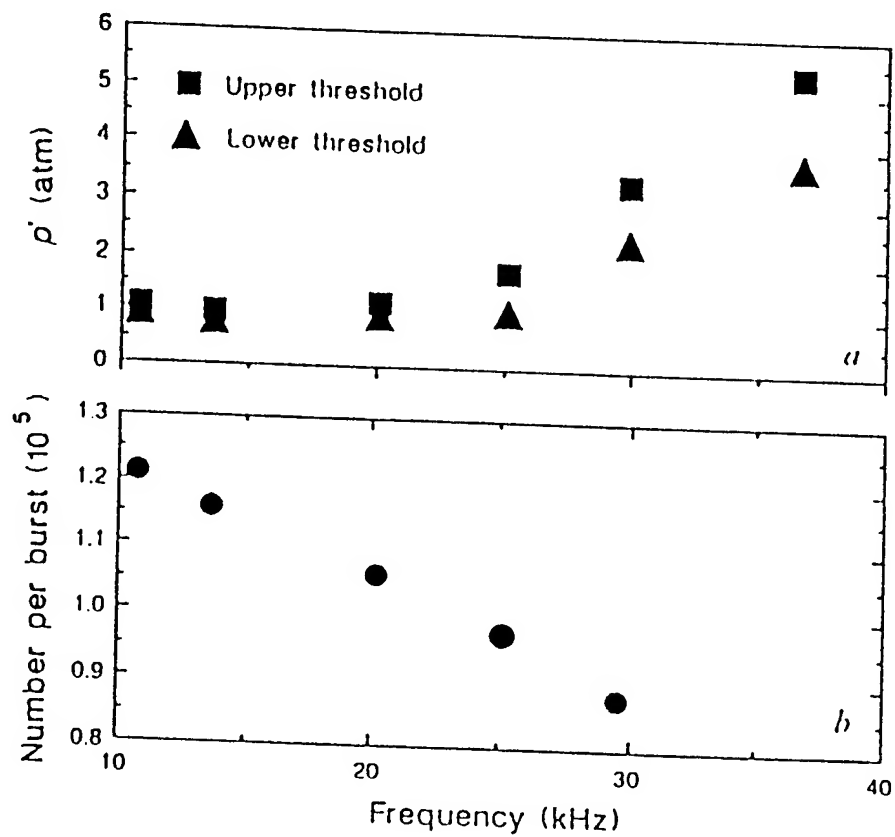


FIG. 1 *a*, Phase plane for continuous single-bubble sonoluminescence. The 20-kHz data point agrees with the measurement of Gaitan. *b*, Photons per burst as a function of acoustic frequency; p' has been chosen to maximize the light output.

B. P. Barber and S. J. Putterman, *Nature* 352, 318-320 (1991).

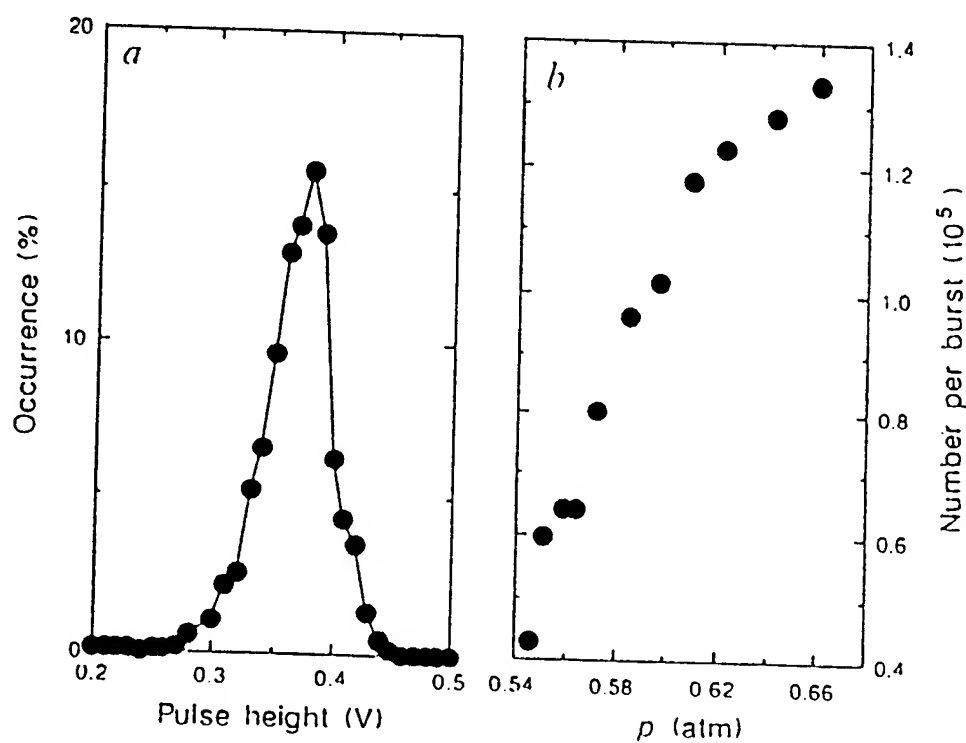


FIG. 3 *a*, Pulse height distribution. A pulse height of 0.1 V represents 1.1×10^4 photons emitted. $f_s = 20.193$ kHz. *b*, Photons per burst as a function of acoustic pressure amplitude. $f_s = 10.736$ kHz.

B. P. Barber and S. J. Putterman, *Nature* **352**, 318-320 (1991).

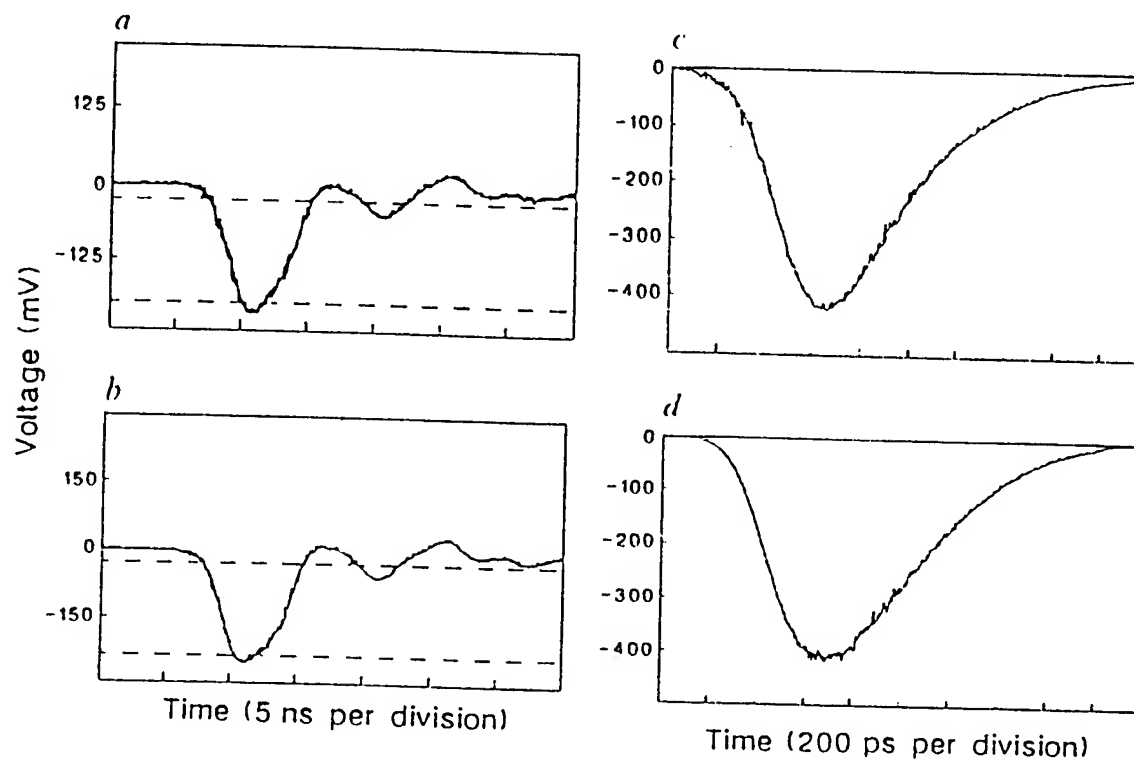


FIG. 2 The average of single-pulse outputs of the photomultiplier tube. *a*, SL data as recorded by a conventional (R928) PMT; *b*, same as *a*, but using a 34-ps laser pulser (Hamamatsu PLP-01) as the light source. *a* and *b* were obtained by running the PMT output into a digital sampling scope (HP 54201A). *c* and *d*, Data for a microchannel-plate PMT (Hamamatsu R1564U) running into a 20-GHz digital sampling scope (Tektronix 11802). *c* is for the SL source, and *d* for the 34-ps laser pulser.

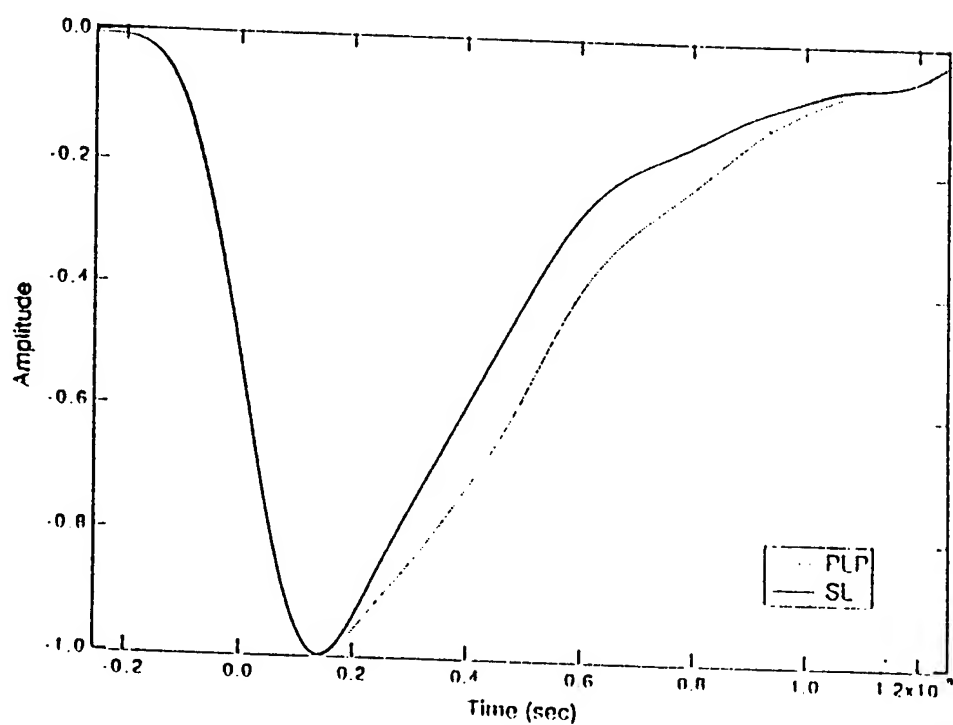


FIG. 1. Voltage versus time at the output of the PMT for SL and the PLP. The time scales are chosen so that the two curves pass through the 50% level at the same time. These curves correspond to the recording of about 25 photoelectrons. After passing through the delay line and 20-dB attenuator a single photoelectron corresponds to a peak amplitude of 2 mV.

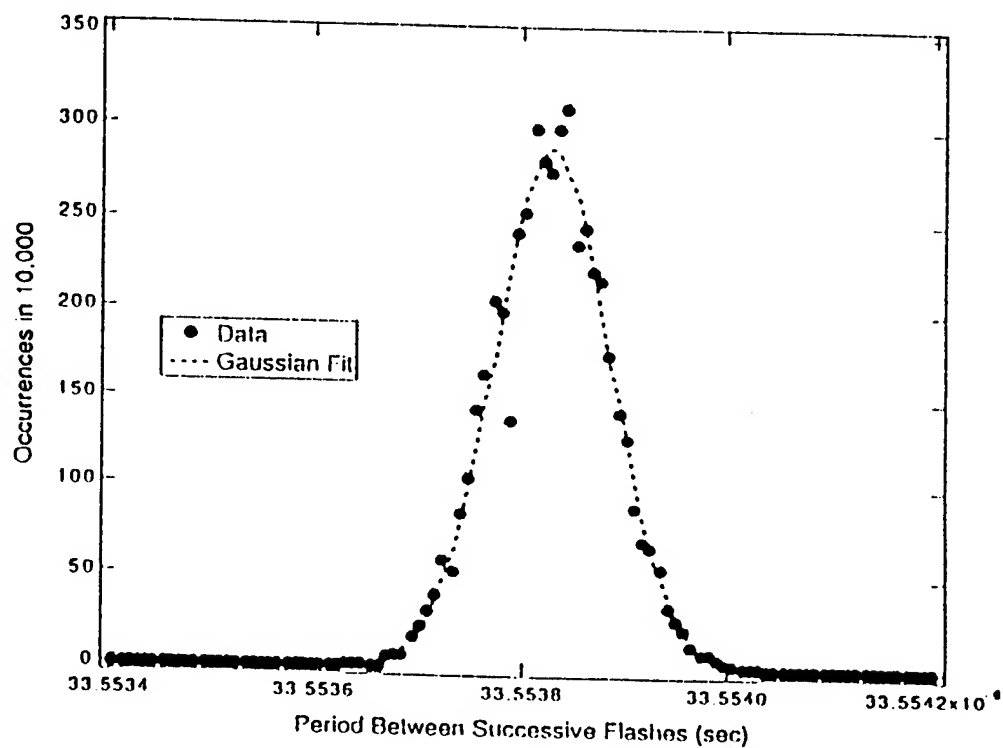
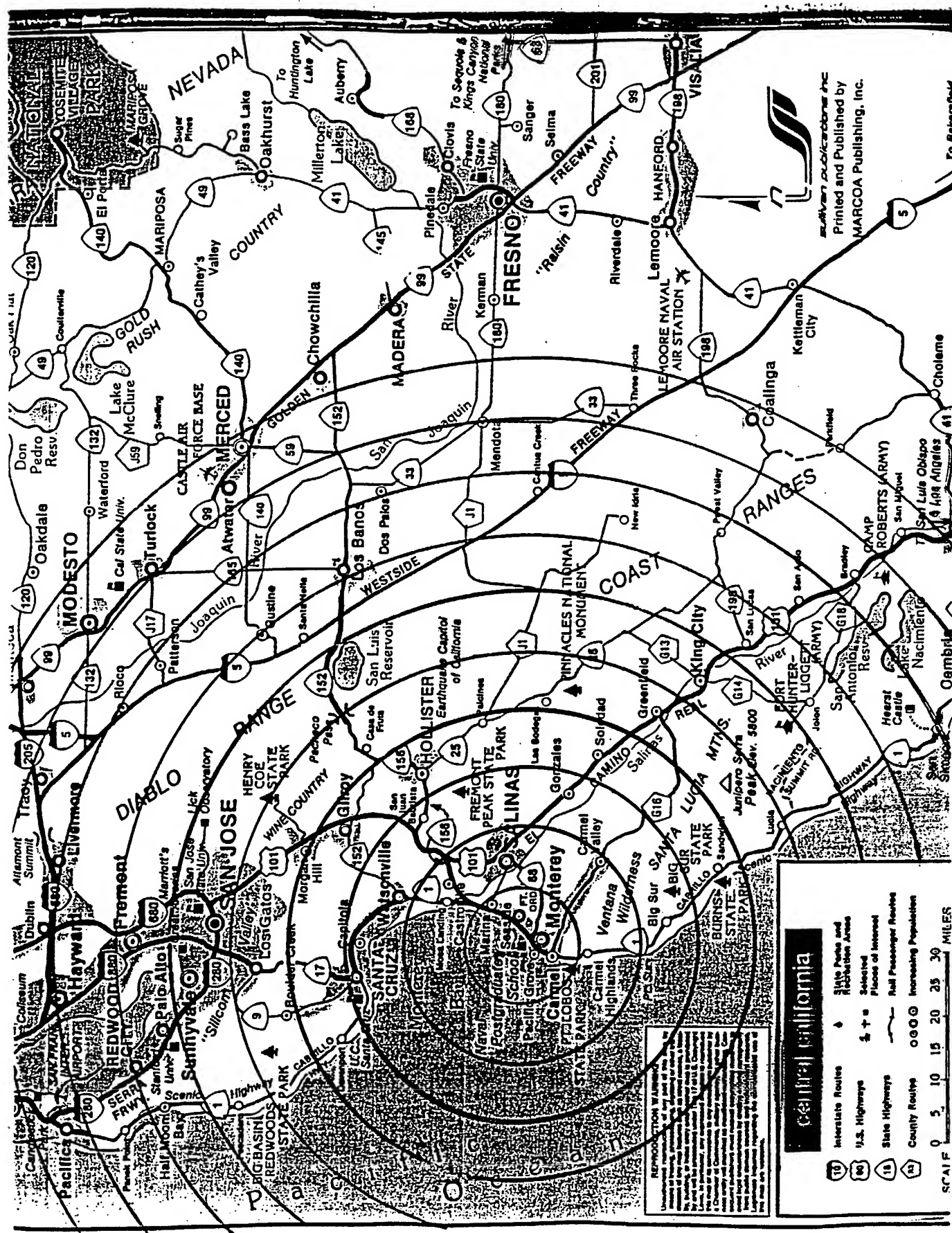


FIG. 3. Histogram of events versus period between flashes for sonoluminescence.

B. P. Barber, et. al., J. Acoust. Soc. Am. 91, 3061-3063 (1992).



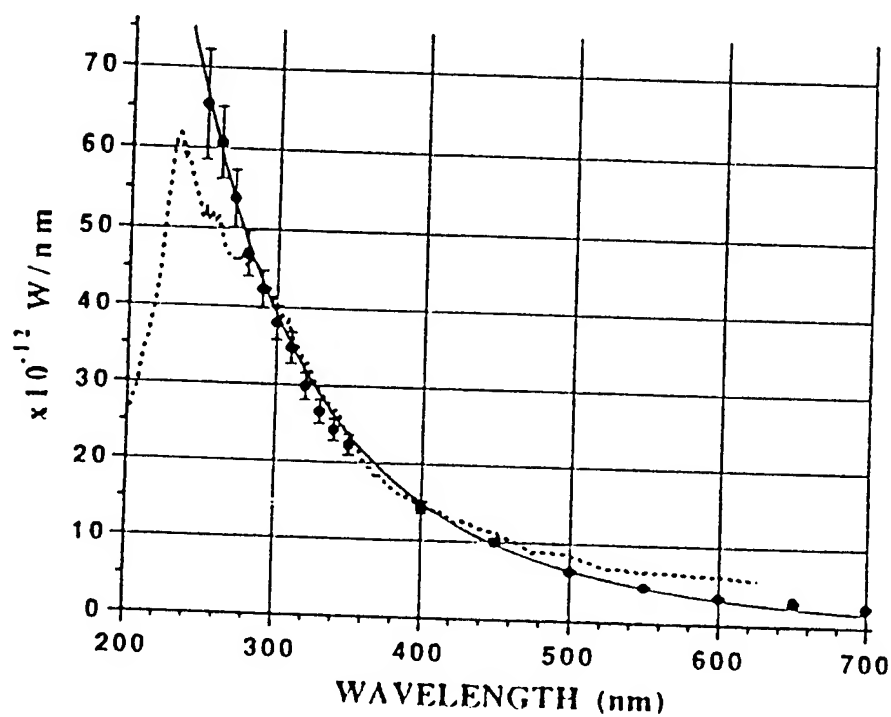
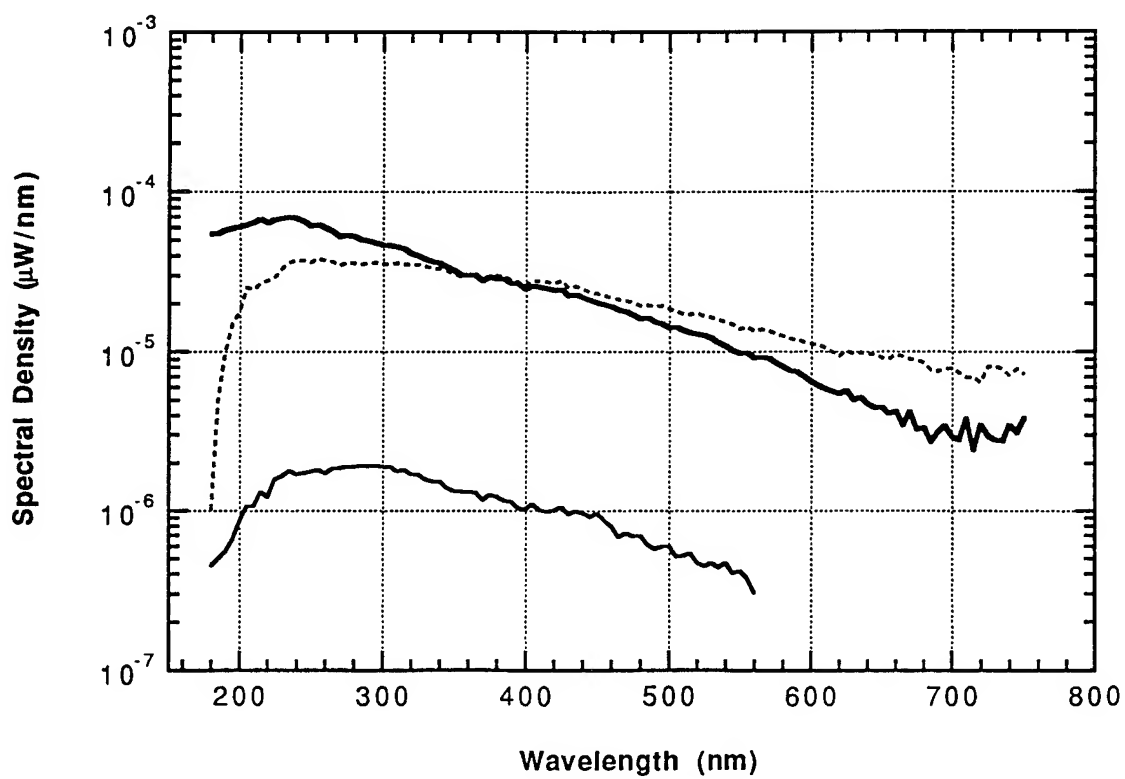
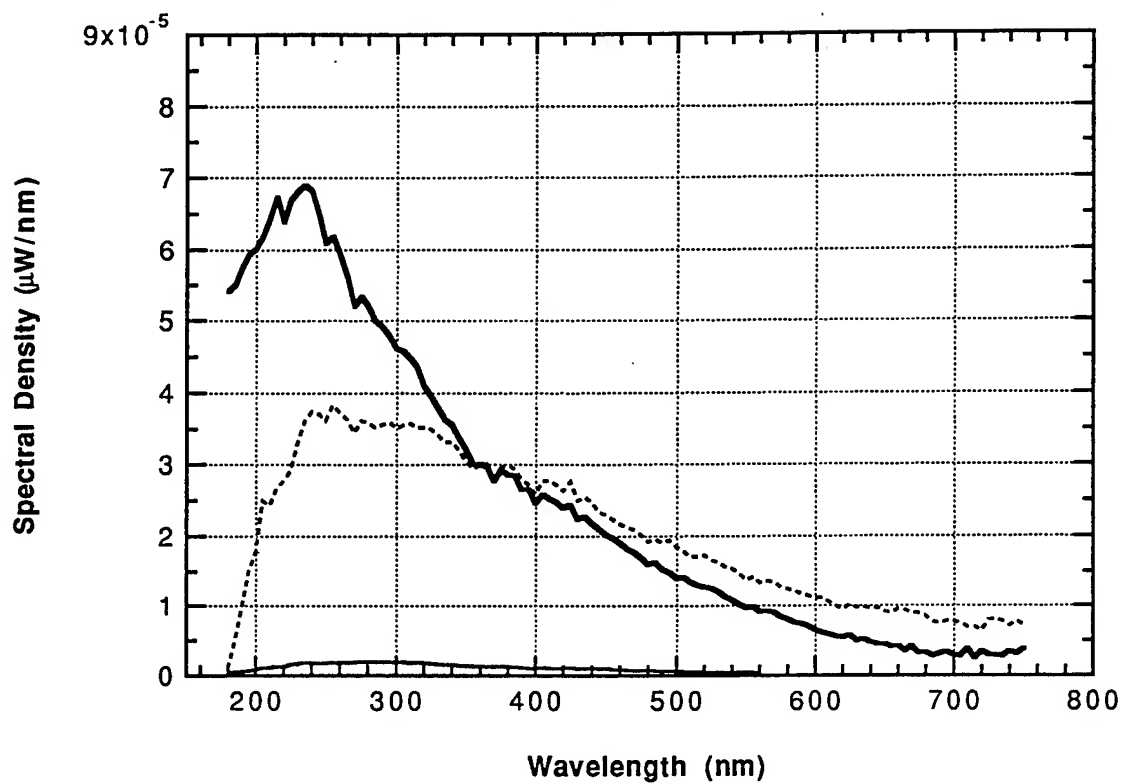


FIG. 1. Calibrated spectral density of the synchronous picosecond flashes of sonoluminescence at 22°C. The average spectral energy density of a single flash can be obtained by dividing by the acoustic frequency of 27 kHz. The dotted line was obtained via the D lamp calibration. The points with error bars were obtained by calibrating our apparatus with a QTH standard of spectral irradiance. The solid line is a 25000 K blackbody spectrum.

R. Hiller, et. al., Phys. Rev. Lett. 69, 1182-1184 (1992).



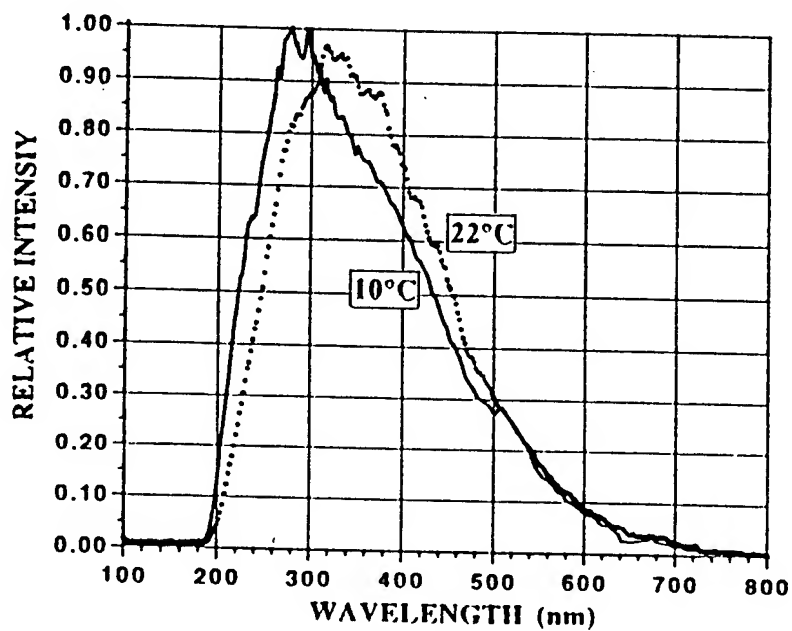
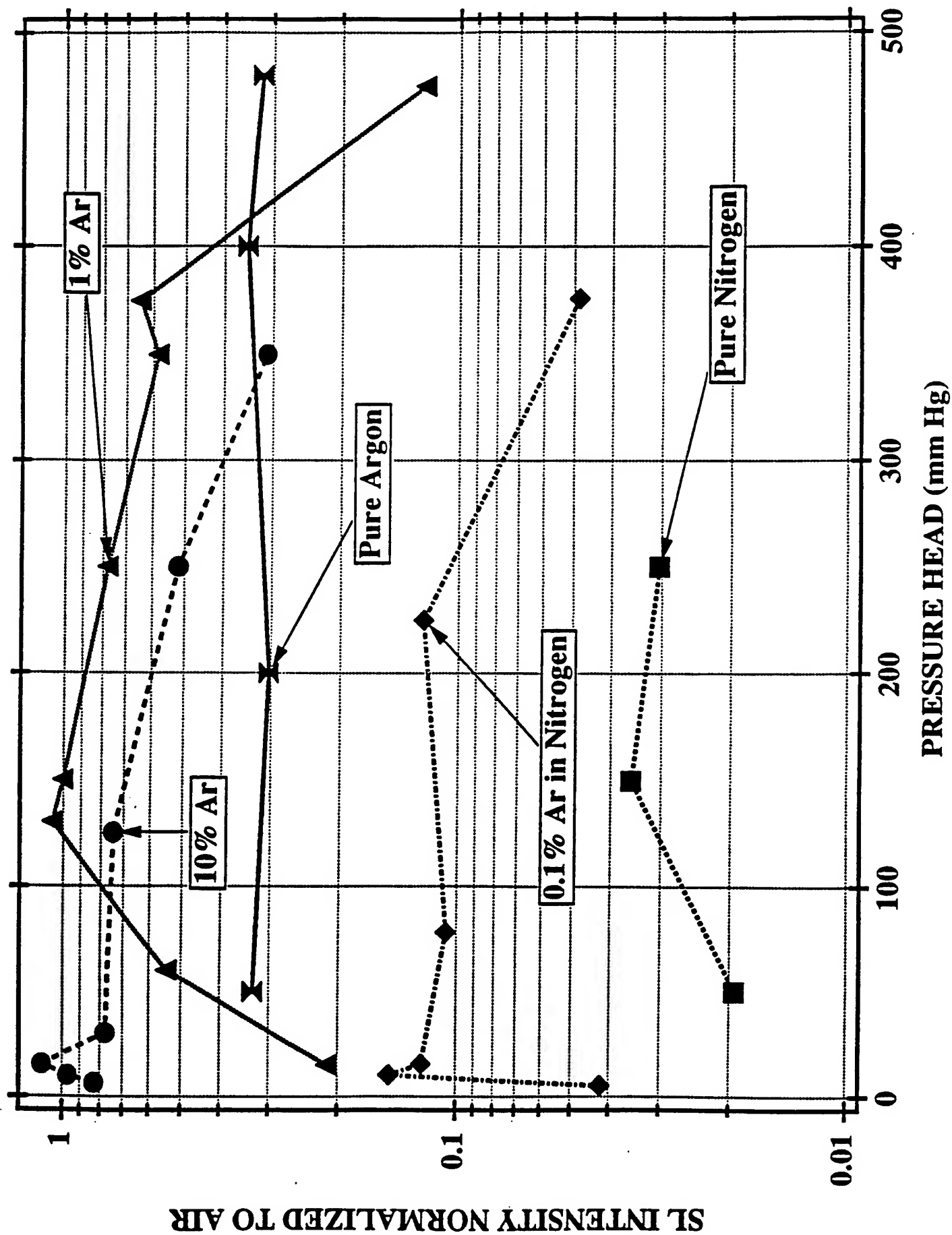
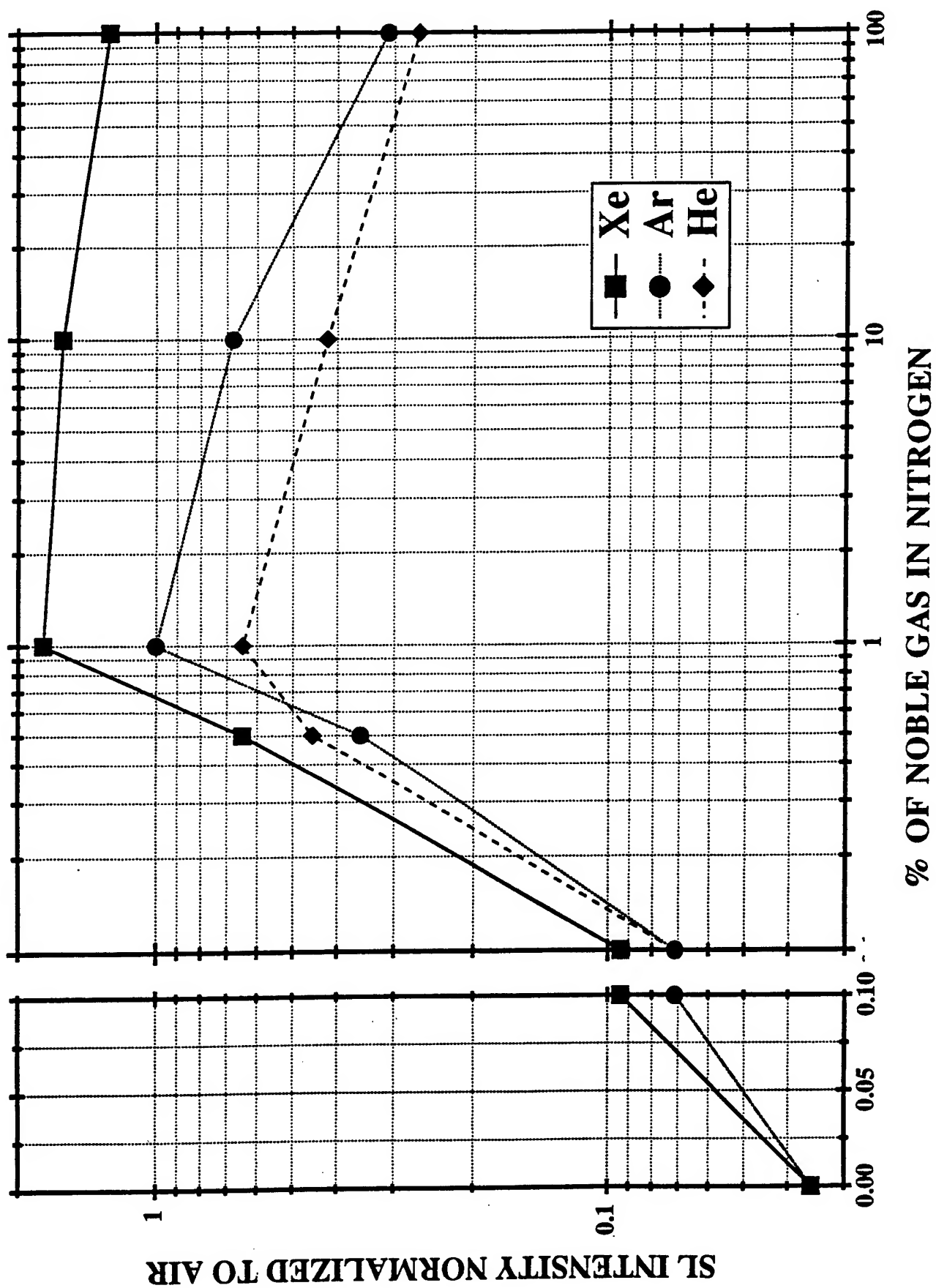
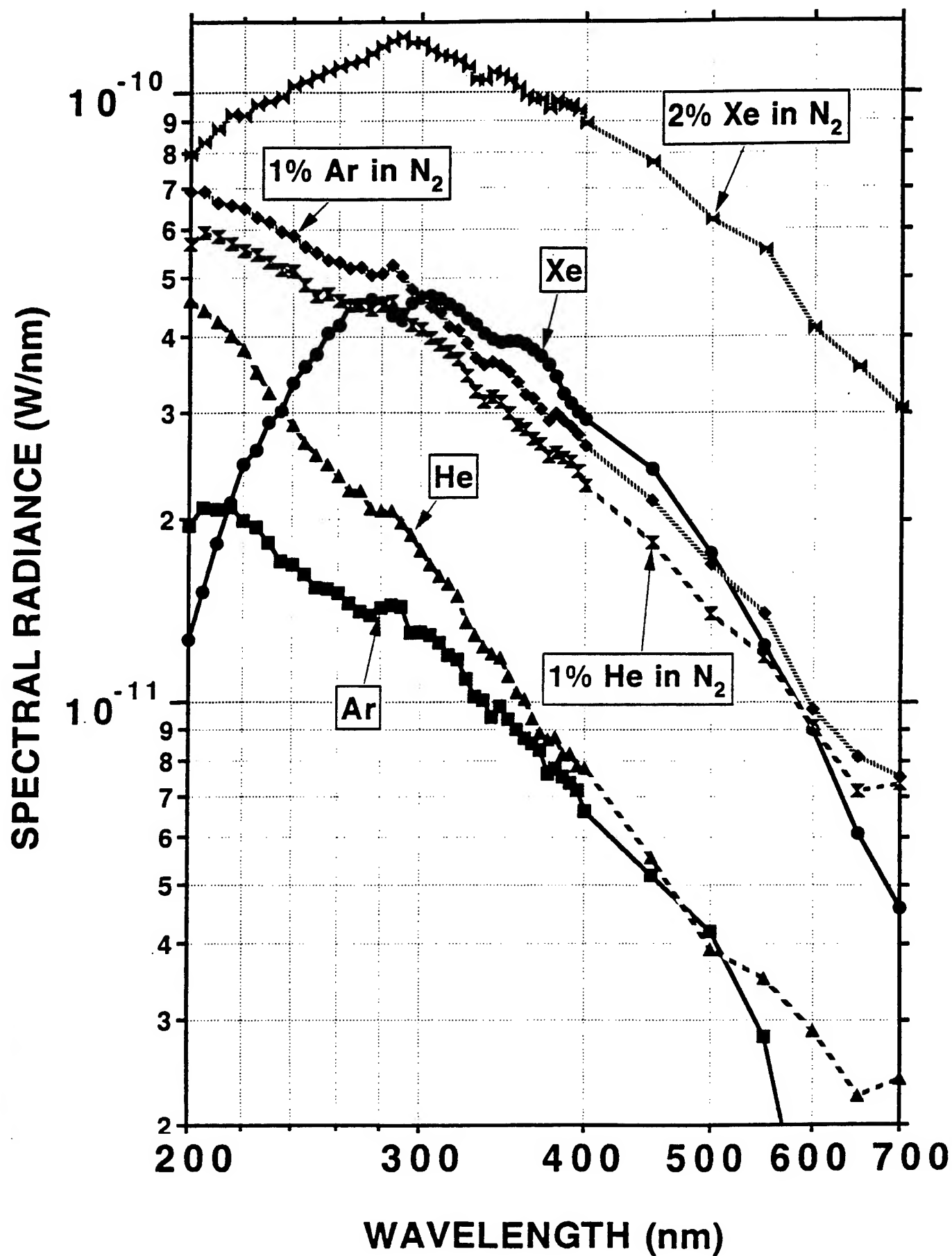


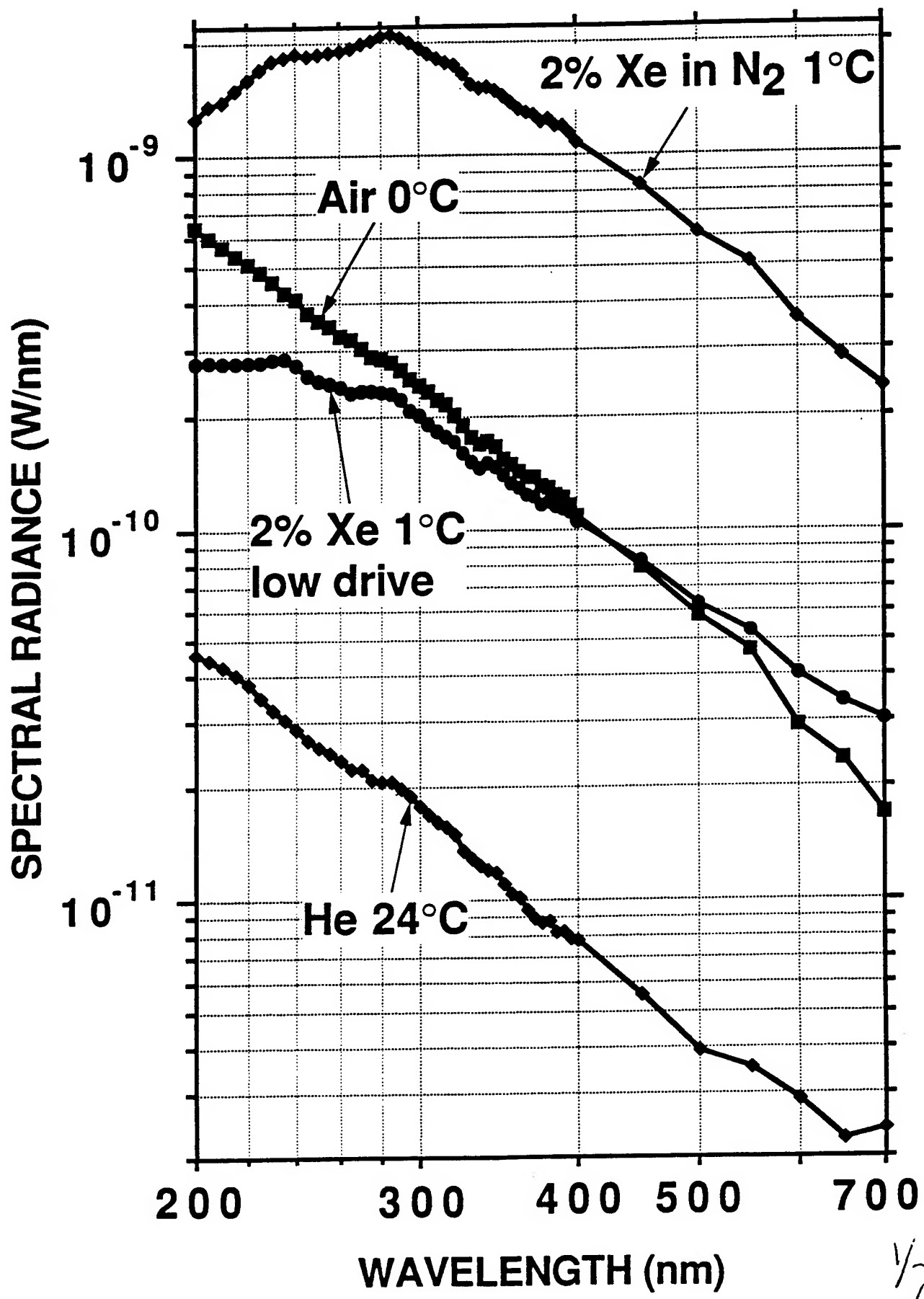
FIG. 4. Raw data for the spectral density of SL at 10 and 22°C. The peaks have been chosen so that the curves have equal area. These curves have not been corrected for the fiber grating, or PMT. The grating is blazed at 300 nm.

R. Hiller, et. al., Phys. Rev. Lett. 69, 1182-1184 (1992).









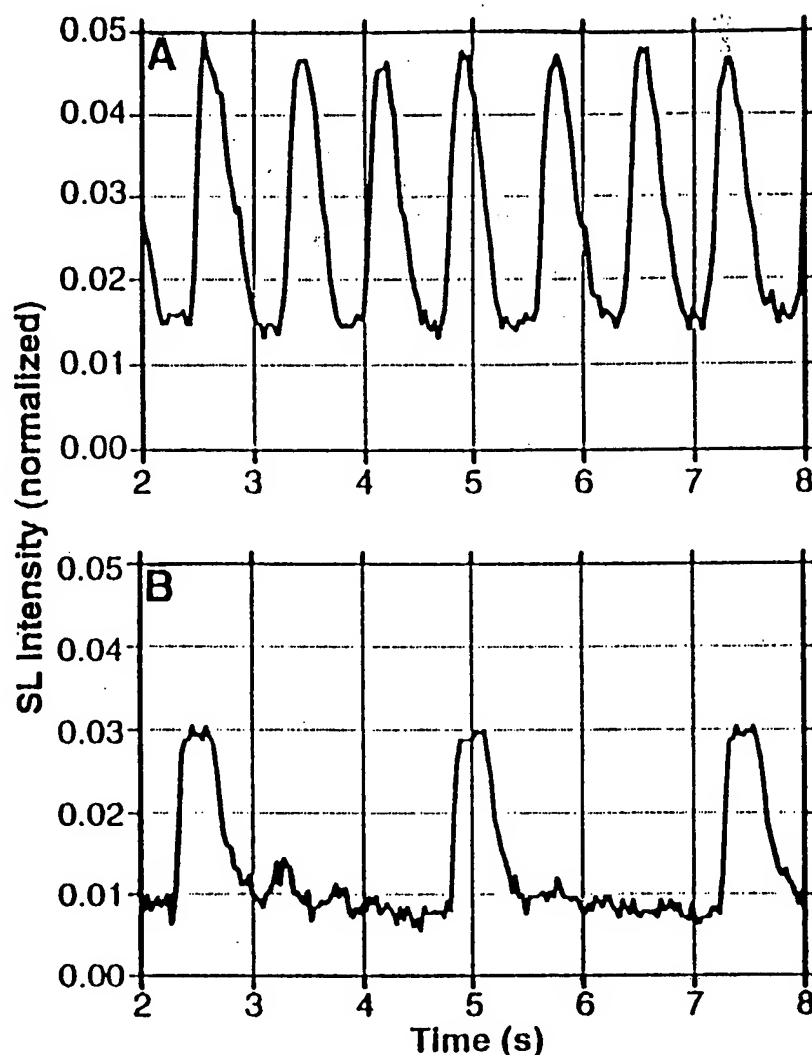
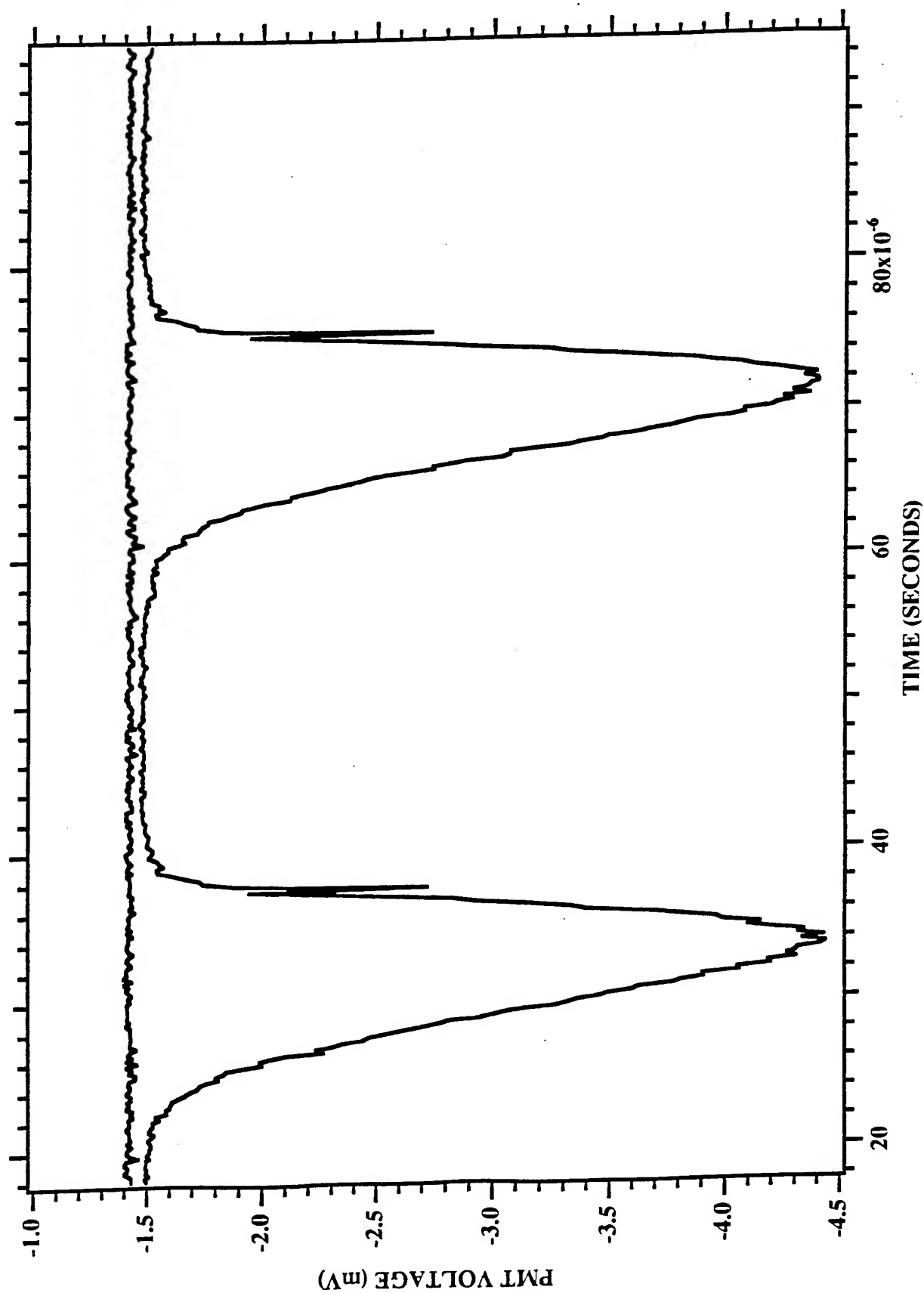
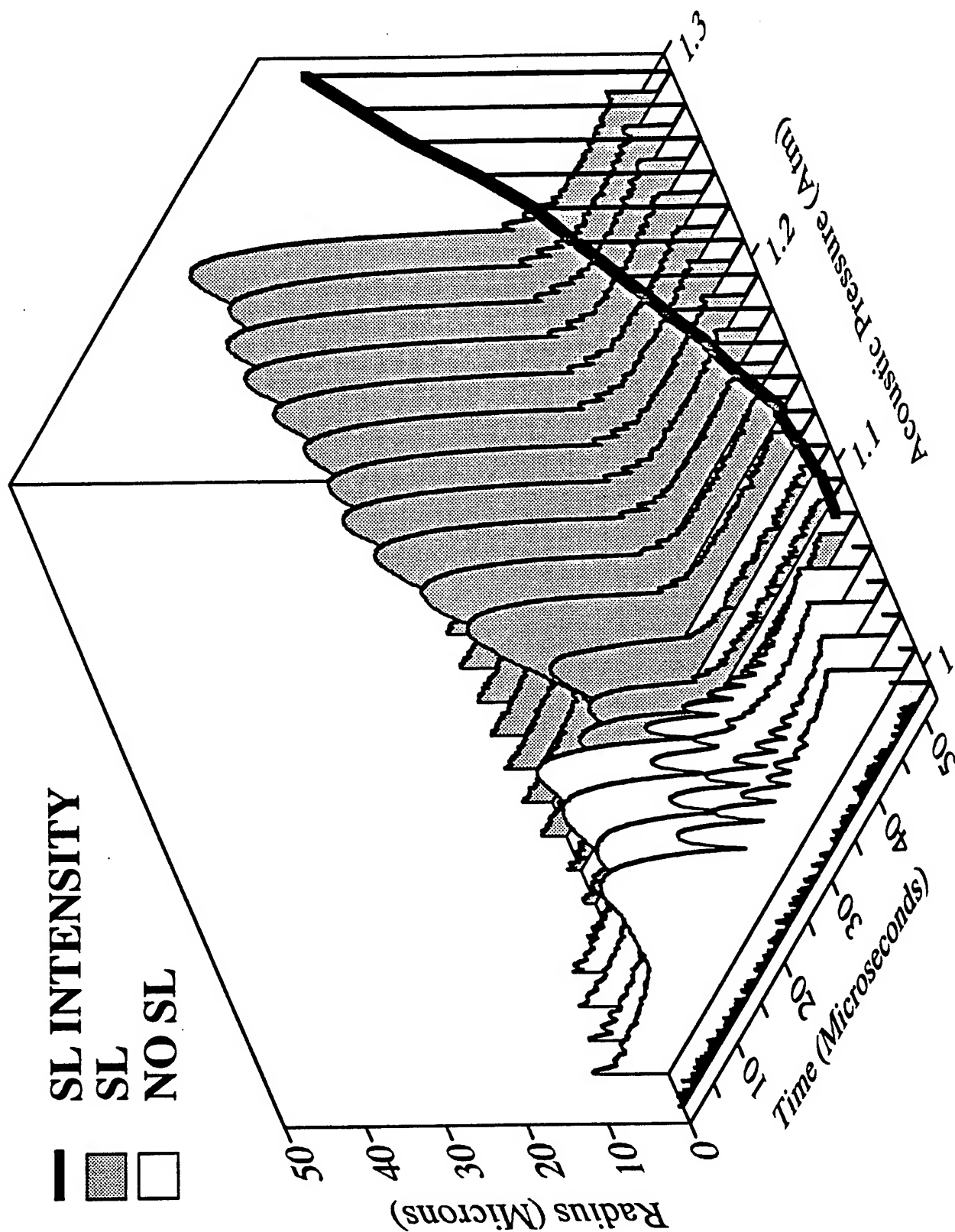


Fig. 5. Time dependence of SL from a pure N_2 bubble in water (with N_2 dissolved at 150 mmHg): (A) low drive, (B) high drive. The SL intensity has been normalized to the emission of an air bubble at the standard parameters delineated in Fig. 1. Uncertainty in the impurity concentration is about 0.05%. The long-term memory (over 100,000 cycles of sound) displayed in this data is indicative of an as yet unidentified physical process that is an essential aspect of the transition to SL. We were unable to observe steady SL from a single N_2 bubble. The average radius also drifts on the same time scales in these regimes. Because of this nonsteady motion and weak emission, we were unable to obtain a spectrum of a N_2 bubble.

Figure 1





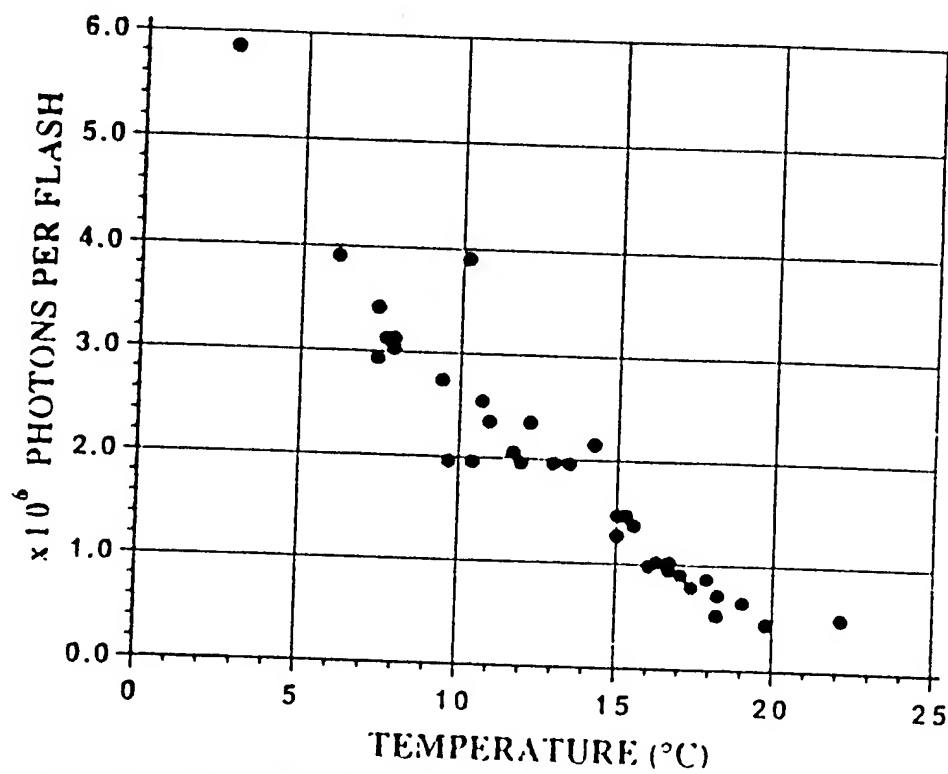


FIG. 3. Number of photons emitted per flash of SL as a function of temperature. At each temperature we recorded the output of the brightest bubble attainable.

R. Hiller, et. al., Phys. Rev. Lett. 69, 1182-1184 (1992).

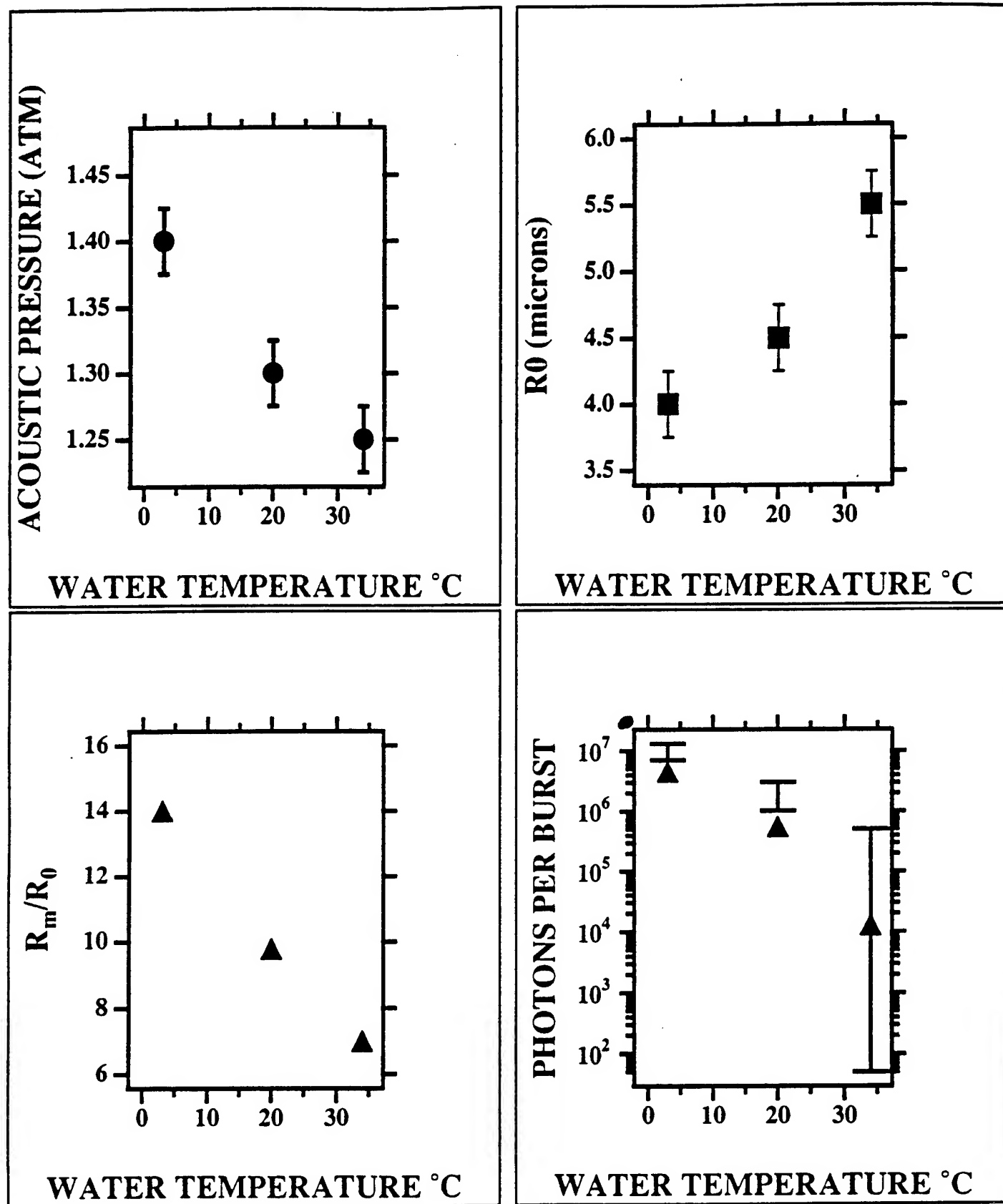


FIGURE 5: Values of the intensity of sonoluminescence, sound field level P_s , maximum bubble radius R_m and ambient radius R_0 as a function of water temperature for a trapped bubble of air. The number N of photons per burst (with wavelength greater than 200nm) is measured in each case near the maximum achievable value. The bars are the ranges of intensities calculated from the shock wave theory when the uncertainty in the experimental input parameters is allowed for.

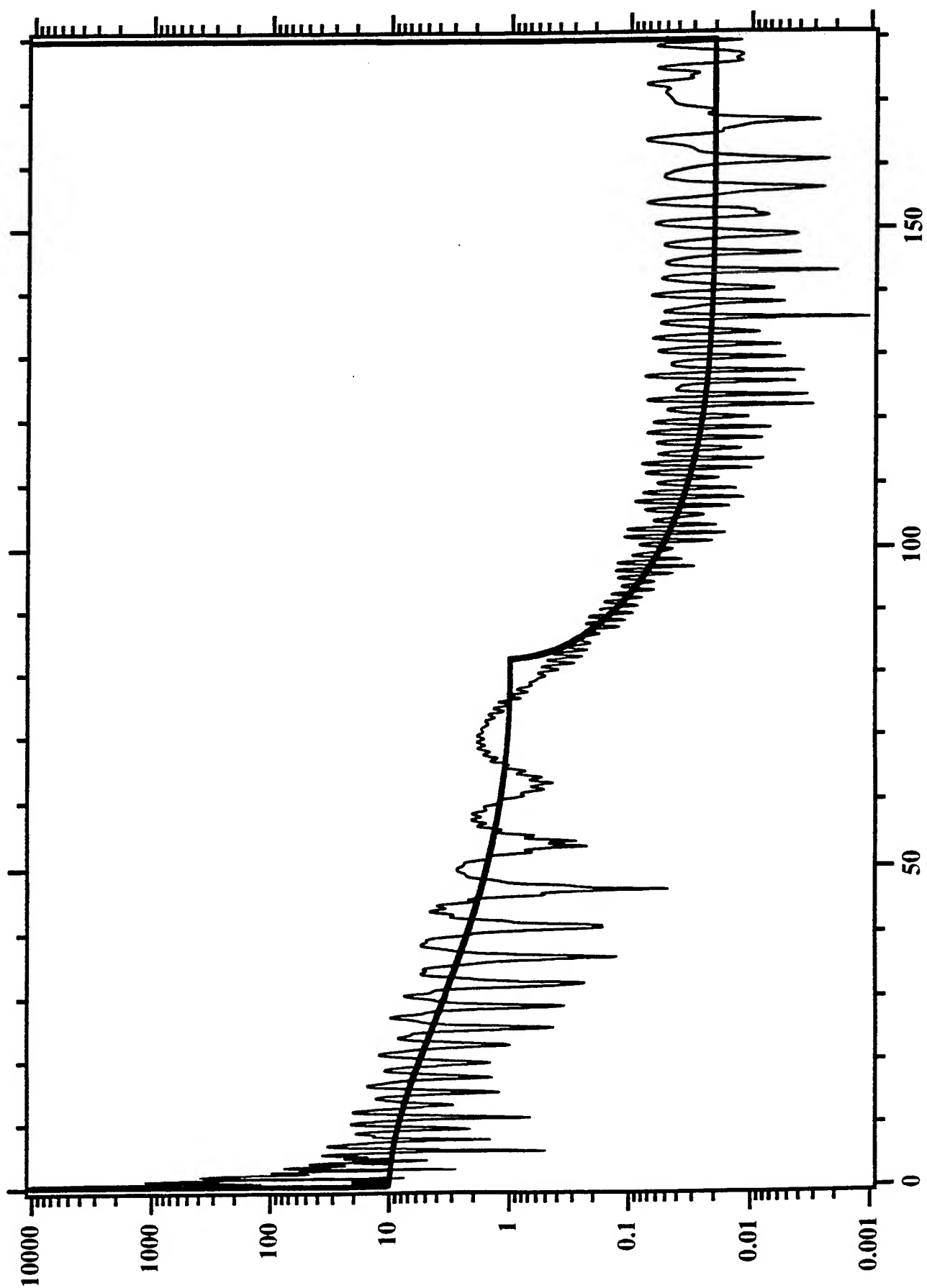
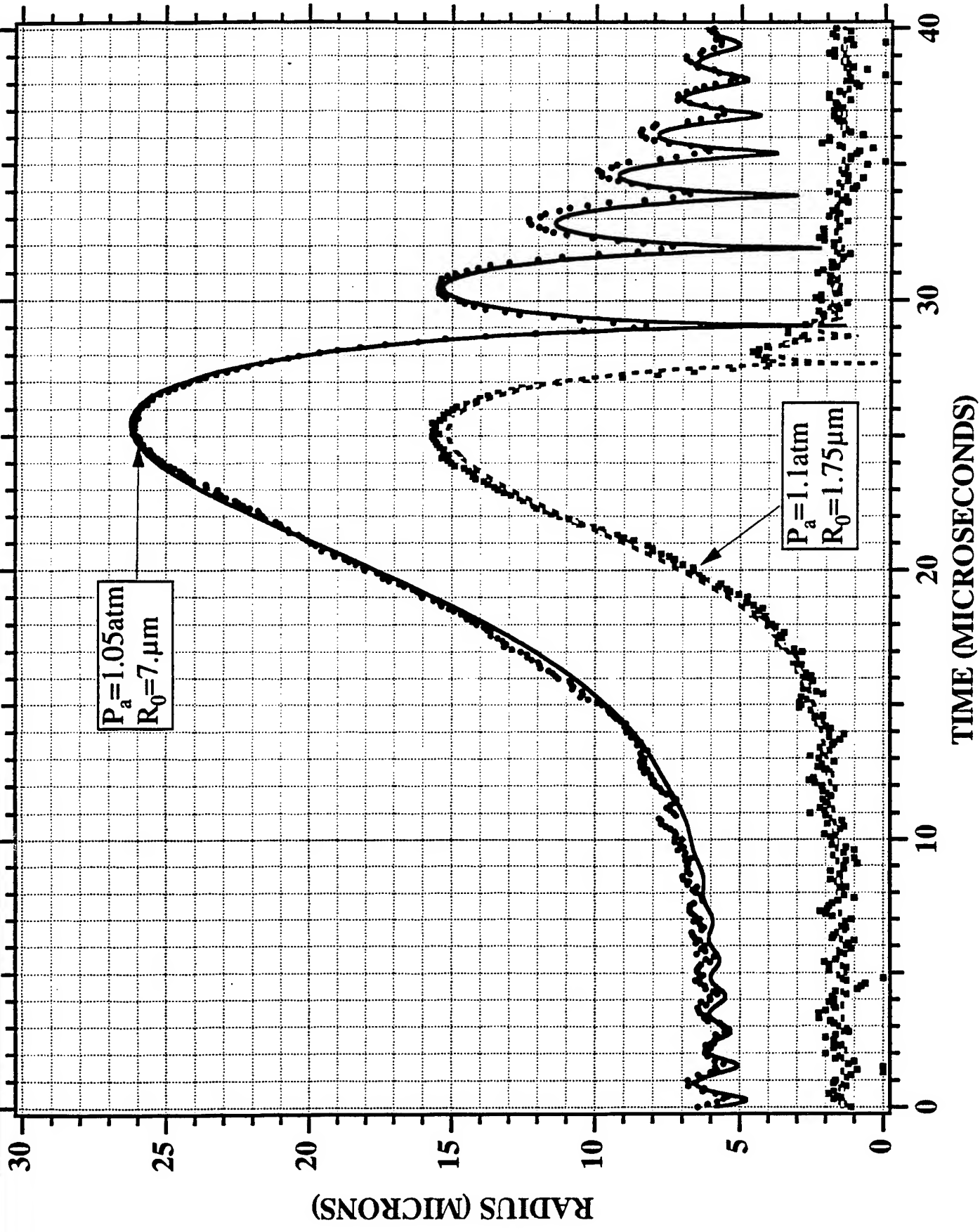


Figure 2



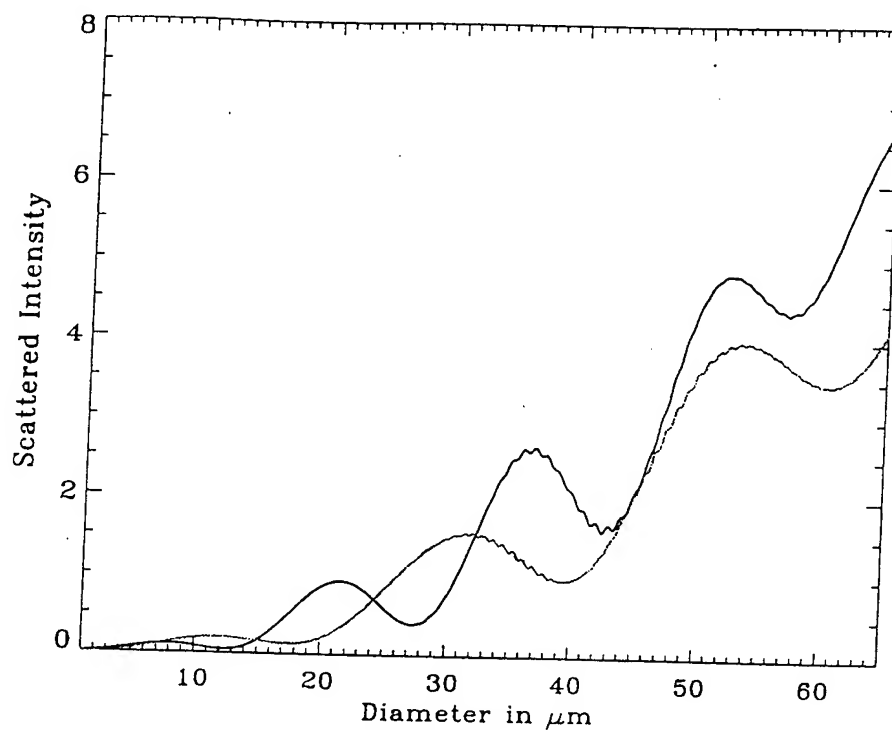


Fig. 1. Simultaneous LC scattering at scattering angles of 47° (dark curve) and 53° (light curve).

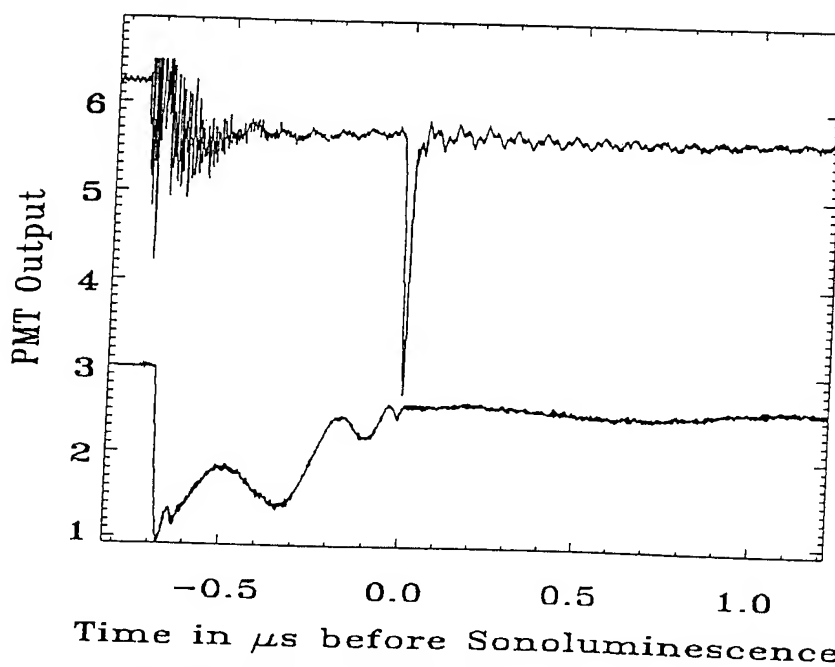


Fig. 6. SL and pulsed laser-scattering graph, showing the outputs of the PMT's used to monitor SL (upper trace) and scattering (lower trace) as functions of time. The laser pulse starts at -0.7 ms. The modulation in the scattered intensity corresponds to LC.

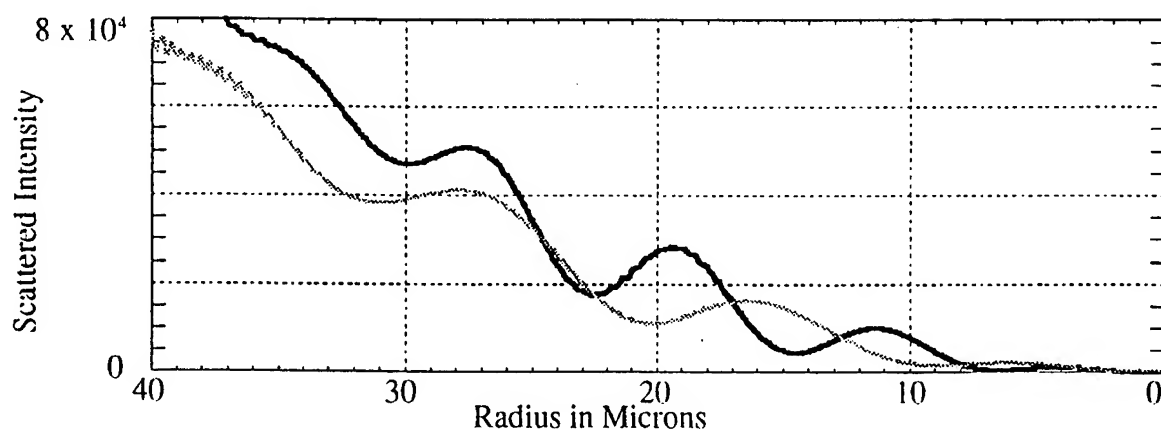


Figure 1. Theoretical scattered intensity for scattering angles of 48° (dark curve) and 53° (light curve) as a function of radius.

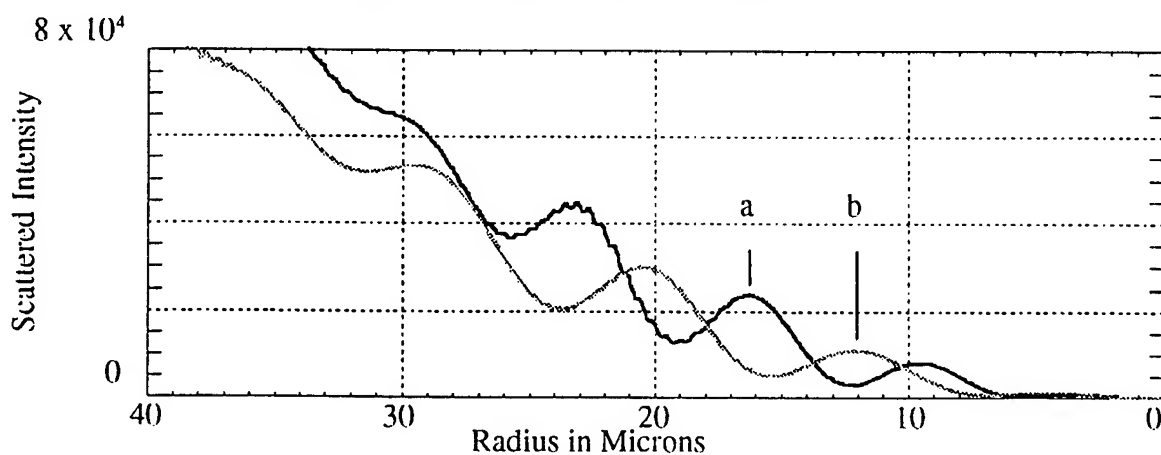


Figure 2a. Theoretical scattered intensity for scattering angles of 45° (dark curve) and 48° (light curve) as a function of radius.

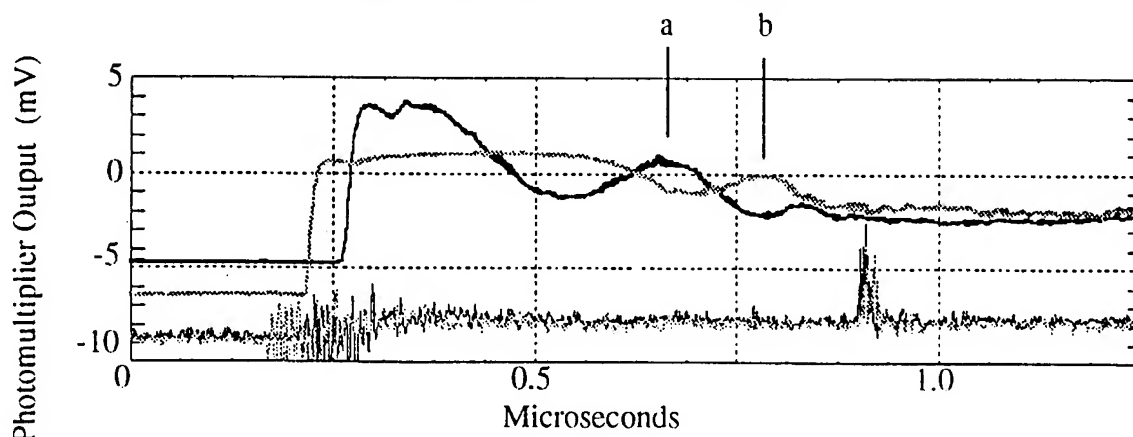


Figure 2b. Measured scattered intensity (upper traces) and output of SL monitor (lower traces) for the same angles as in Fig. 2a.

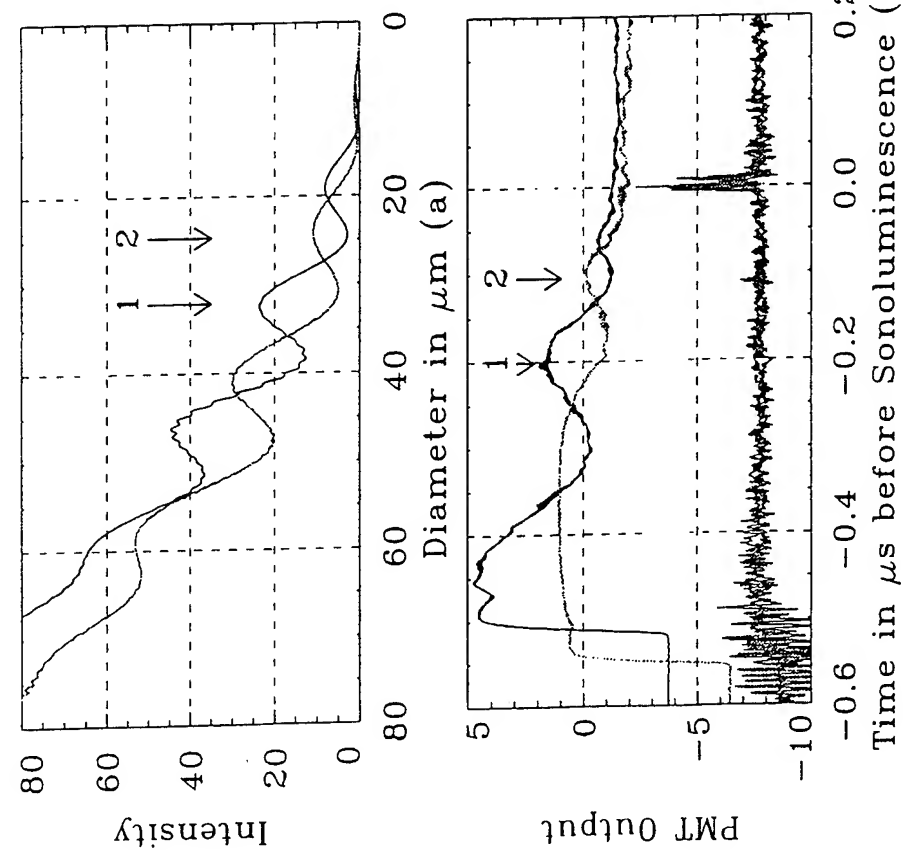


Fig. 7. LC identification by comparison of (a) theoretical and (b) experimental scattering at 45° (dark curve) and 48° (light curve). 1, scattering at $-0.2 \mu\text{m}$; 2, scattering at $24.4 \mu\text{m}$.

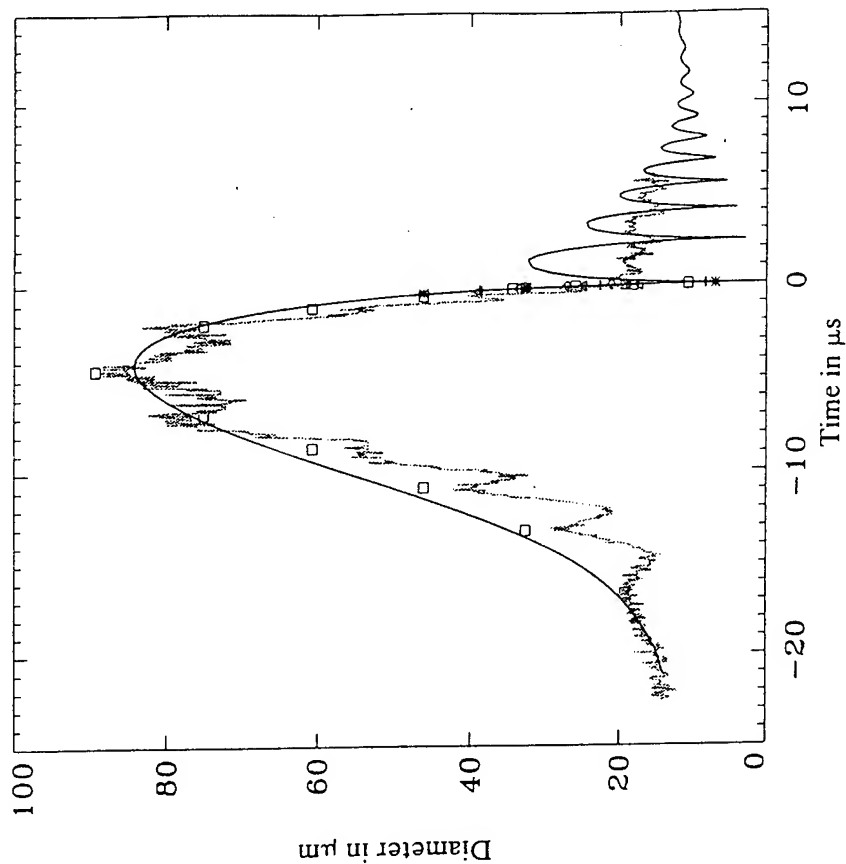


Fig. 8. Result of LC sizing (symbols) compared with hydrodynamic calculations (dark curve) and the square root of scattered intensity (light curve).

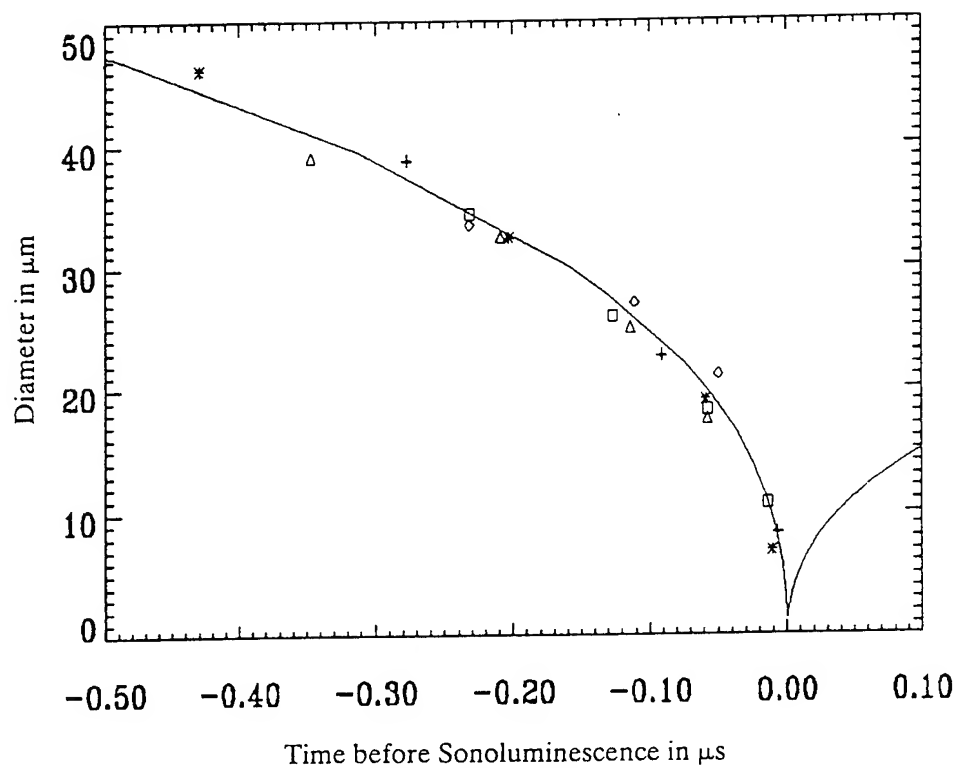


Fig. 9. Diameter near SL for several angles and bubbles over a three-day period compared with hydrodynamic calculations.

Comparison of Multibubble and Single-Bubble Sonoluminescence Spectra

Thomas J. Matula, Ronald A. Roy, and Pierre D. Mourad

Applied Physics Laboratory, University of Washington, 1013 NE 40th Street, Seattle, Washington 98105

William B. McNamara III and Kenneth S. Suslick

School of Chemical Sciences, University of Illinois at Urbana-Champaign, Urbana, Illinois 61801

(Received 12 July 1995)

Comparisons of the spectral characteristics of sonoluminescence from cavitation in bubble fields (MBSL) versus cavitation of single bubbles (SBSL) have been made for aqueous solutions under similar experimental conditions. In particular, alkali metal chloride solutions exhibit sonoluminescence emission from excited state Na or K atoms in MBSL, while SBSL exhibits no such emission. Since the metal ions are not volatile, participation of the initially liquid phase must occur in MBSL. Surface wave and microjet formation in cavitating bubble fields versus the high spherical symmetry of collapse of an isolated bubble may account for the observed differences.

PACS numbers: 78.60.Mq, 43.25.+y, 47.40.Nm

It has long been known that under certain conditions acoustic irradiation of a liquid can result in light emission, a phenomenon called sonoluminescence (SL) [1,2]. The process typically involves the application of high intensity ultrasound to a liquid by an immersed acoustic horn driven with a piezoelectric transducer. The resulting cavitation-bubble field is made up of a complex distribution of gas and vapor-filled bubbles of various equilibrium sizes that pulsate at various phases relative to the driving acoustic pressure field. The bubble dynamics is further complicated by interactions with neighboring bubbles [3] as well as with the vessel walls. Depending on the location within the pressure field and these other influences, some of the bubbles may grow dramatically during the negative portion of the sound field, followed by a quasi-adiabatic collapse that results in the heating of the bubble interior and the subsequent emission of light [4].

In spite of the complexity of cavitating bubble fields, many studies have been made of multibubble sonoluminescence (MBSL) and the influences of fluid and gas properties. The optical spectra of MBSL typically contains distinct, pressure broadened molecular or atomic emission bands. Of particular significance here is the identification of individual transitions from excited states of diatomic carbon (C_2) that contribute to the optical spectrum of MBSL in nonaqueous liquids. The fitting of the measured spectrum of C_2 permitted the measurement of an effective rotational and vibrational temperature of the excited states of C_2 of 5100 K [5].

Recent experimental advances [6] have also made it possible to examine both the temporal and spectral nature of sonoluminescence from a single bubble (SBSL). Here a single bubble is acoustically levitated in an aqueous solution that has been partially degassed. The bubble can be made to undergo large-amplitude, nonlinear, presumably radial pulsations during which light emission can occur. Some properties of SBSL include [7] the synchronous emission of light with each and every acoustic cycle, tem-

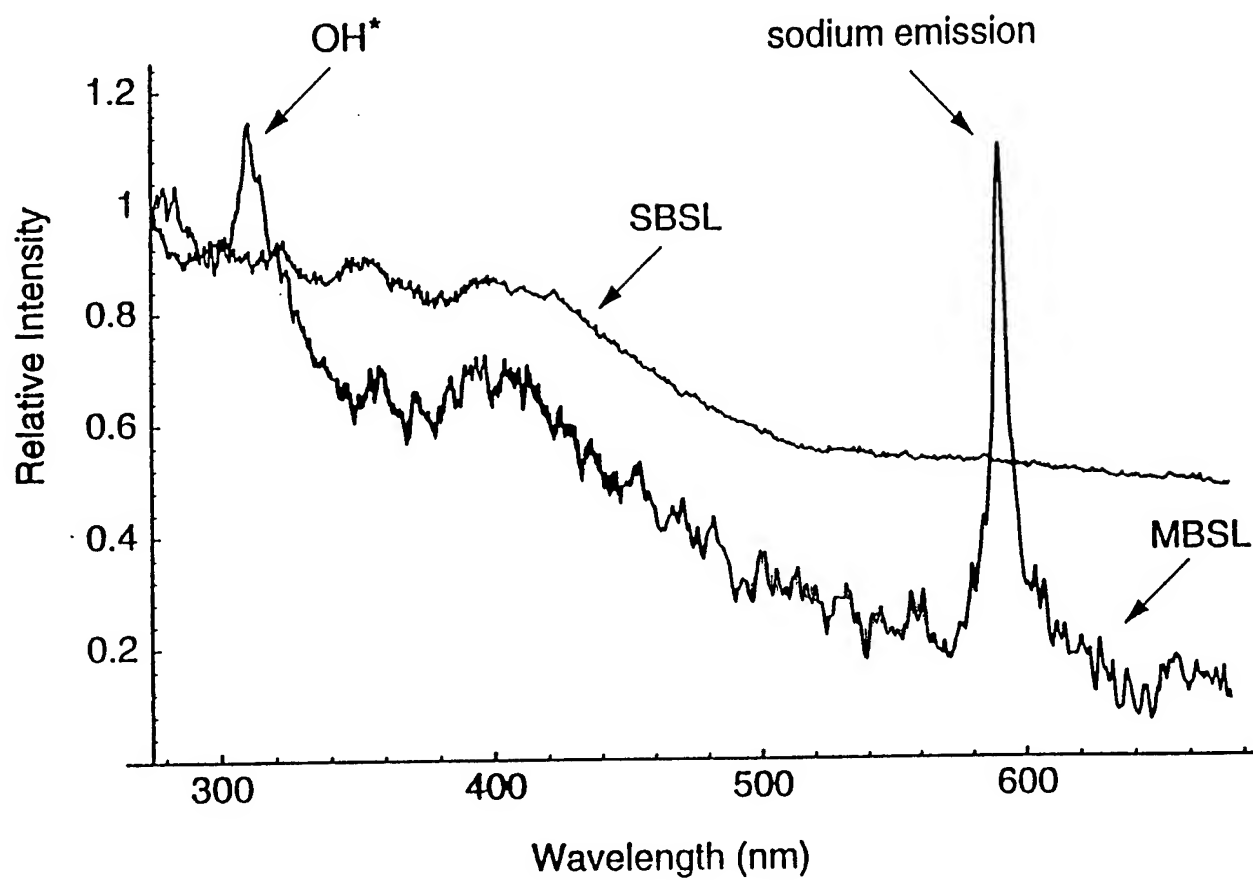
poral flash widths of less than 50 ps, and a continuous spectral energy density that increases from the visible into the UV, with eventual fall off due to UV absorption by the surrounding water. In addition, unlike in MBSL, there are little or no electronic or molecular bands associated with SBSL spectra. The shape of the spectrum of SBSL has led some researchers to suggest that SBSL is much "hotter" than MBSL, reaching temperatures as high as 50 000 K [8], and possibly much higher [9,10].

In order to probe the differences between MBSL and SBSL, we have explored emission from identical aqueous solutions containing potentially emissive, but nonvolatile solutes using the same spectrometer for both systems. Nonvolatile solutes provide a test of the involvement of the initially liquid phase surrounding the cavitating bubble in the sonoluminescent event [11,12]. An observation of an SL emission peak from a nonvolatile solute requires either that a fluid shell surrounding the bubble be heated sufficiently [13], or that liquid droplets containing the nonvolatile species become entrained and heated within the bubble [4,14].

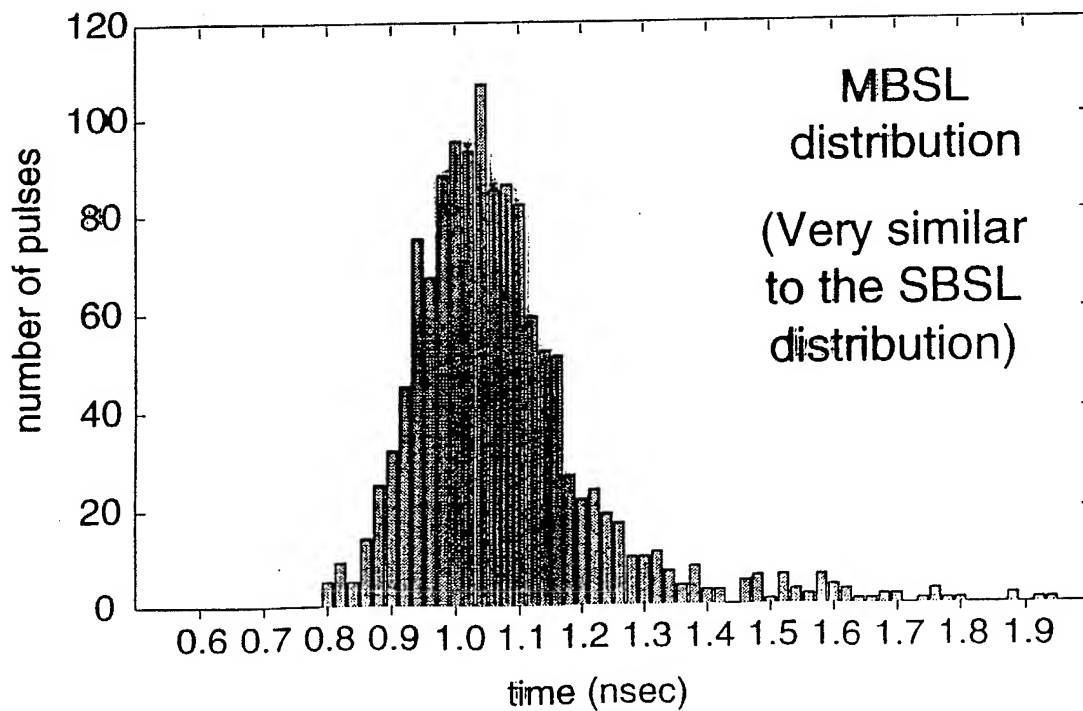
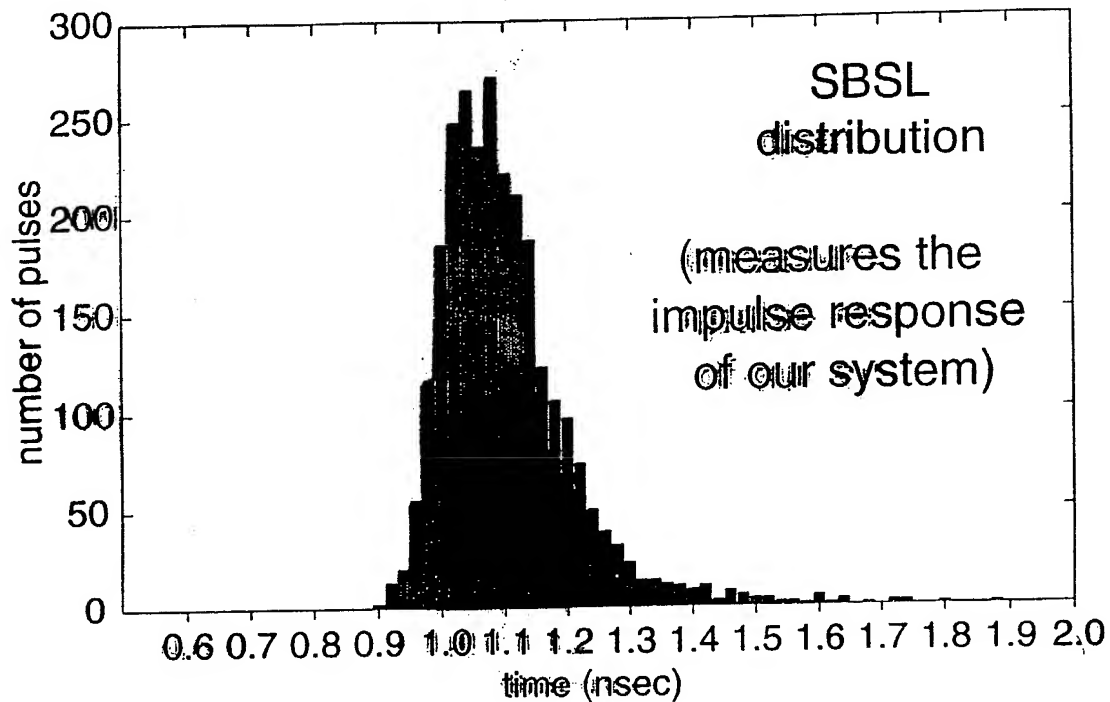
It was not possible to generate both MBSL and SBSL in a single apparatus, owing to the differences in techniques used to generate cavitation-bubble fields and isolated single bubbles. MBSL is generated using an ultrasonic horn, which produces large peak pressure within the liquid (around 10 bars), with high levels of gas saturation; while SBSL occurs with applied acoustic pressure amplitudes near 1 bar, and gas concentration levels that are a fraction of saturation. Nonetheless, comparison of the optical spectra can be made by using identical fluid preparation schemes under identical gas conditions with a single calibrated spectrometer.

The SBSL apparatus consisted of a quartz cylindrical levitation cell (8 cm tall by 4.5 cm diameter), as shown in Fig. 1(a). The cell was closed on top with a glass plate. A hollow cylindrical PZT transducer, cemented to the glass, was used to drive the levitator in tandem with a pow-

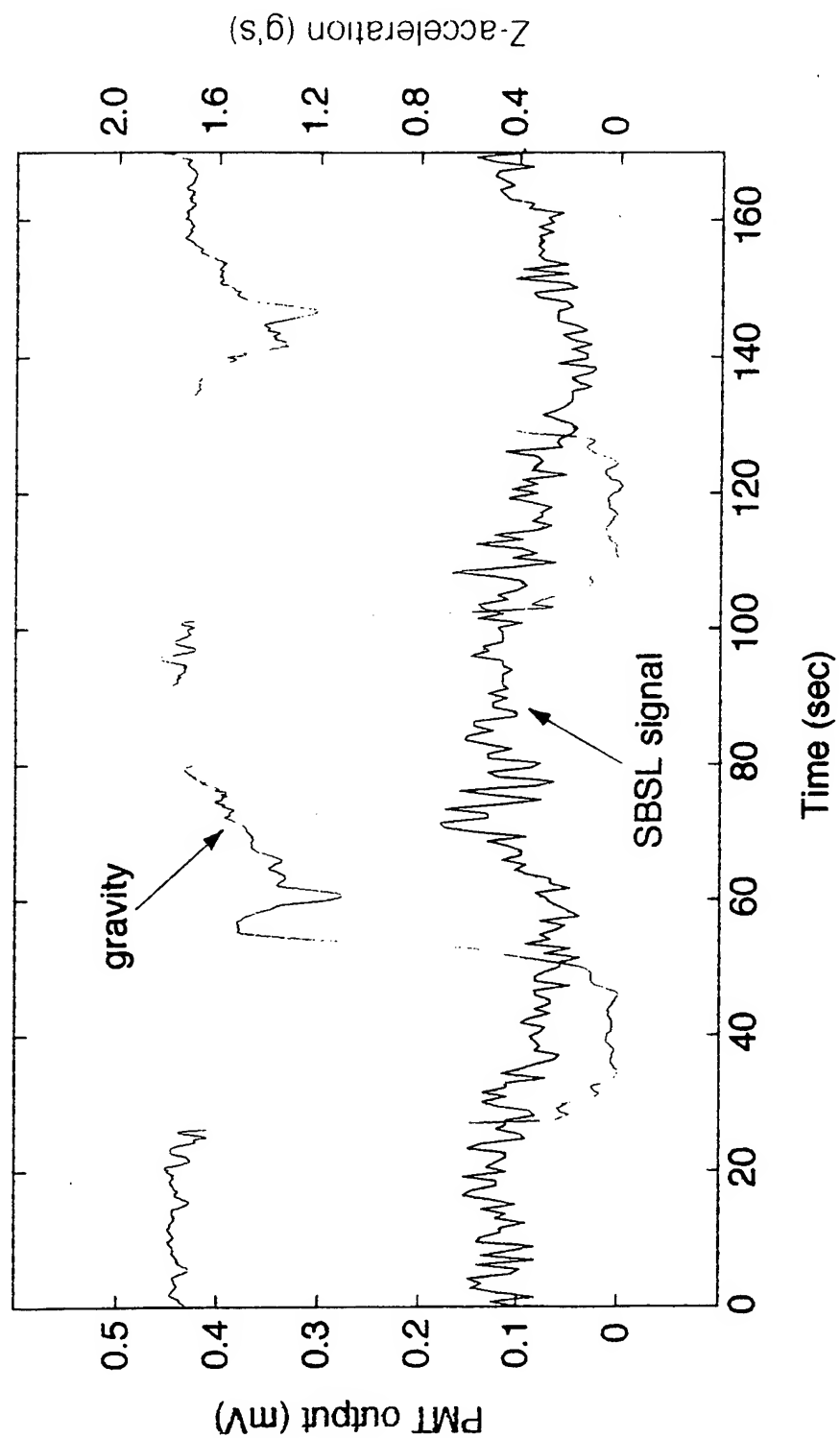
SL in 0.1 Molar NaCl / Water Solution
(air bubble)



How short are the pulses from sonoluminescence
from cavitation-bubble fields?



- The width of the distributions are due to the transit-time spread of electrons within the photomultiplier tube.



- Is mass diffusion playing a role here?

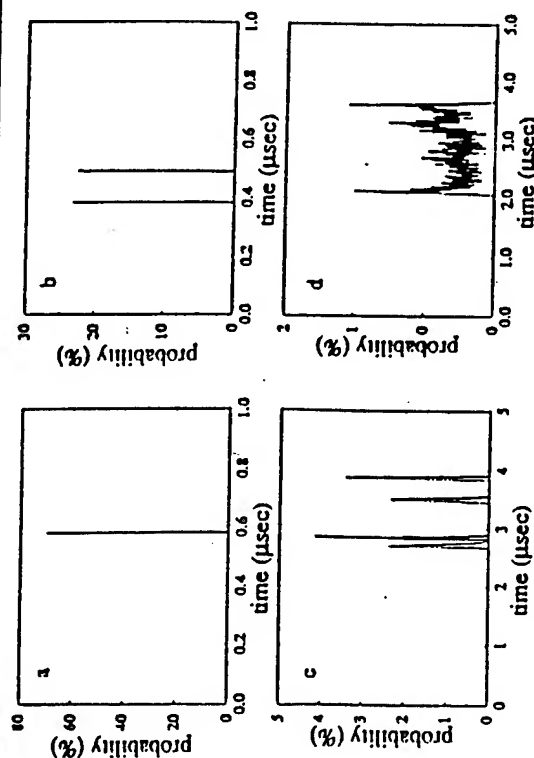


FIG. 2. Sequence of variation in time Δt between SL flashes from a single bubble. The data are histograms of the number of occurrences of a given Δt , measured sequentially during part of a bubble lifetime. The bin width is 0.25 nsec. Time zero is always defined as the time of the previous flash plus the ~ 36 μ sec delay. The histograms show (a) a single maximum, (b) 2 maxima, (c) 4 maxima, and (d) a broad distribution. The frequency was slowly detuned about 0.01 kHz to initiate the bifurcation. $R_0 \sim 5$ μ m, $P \sim 1.3$ atm, and $f_d = 27.0$ kHz.

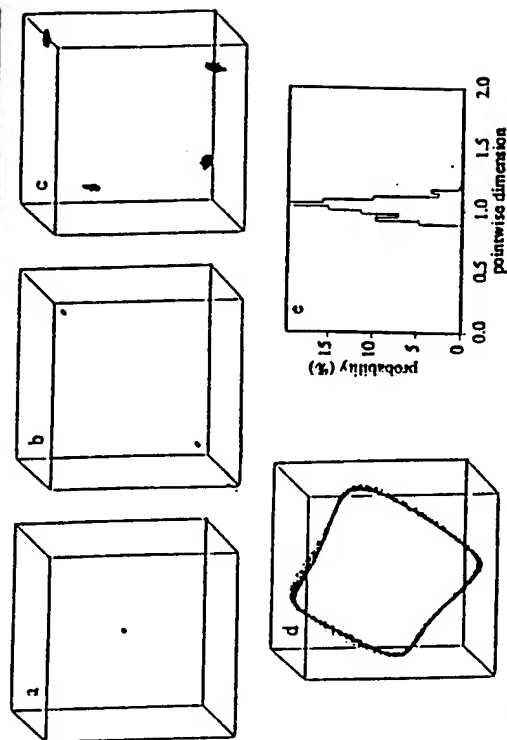


FIG. 3. Phase-space reconstruction of a typical bifurcation sequence of time series Δt . Each individual data point is a tuple of the form $(\Delta t_n, \Delta t_{n-1}, \Delta t_{n-2})$ generated using a single time series of flash data, where $3 \leq n \leq N$, and N is the number of data points (acoustic cycles) in each time series. Bifurcation of the variation Δt from period 1 (a) to 2 (b) to 4 (c) to a quasi-periodic state (d) is clearly shown. (a)-(d) are the attractors reconstructed from each of the Δt time series in Figs. 2(a)-2(d), respectively. (e) is the distribution of pointwise dimensions for (d).

Chaotic Sonoluminescence

R. Glynn Holt

Jet Propulsion Laboratory, MS 183-401, 4800 Oak Grove Drive, Pasadena, California 91109

D. Felipe Gaitan and Anthony A. Atchley

Department of Physics, Naval Postgraduate School, Monterey, California 93943

Joachim Holzfuss

Institut für Angewandte Physik, Technische Hochschule Darmstadt, Schlossgartenstrasse 7, D-64289 Darmstadt, Germany
(Received 12 November 1993)

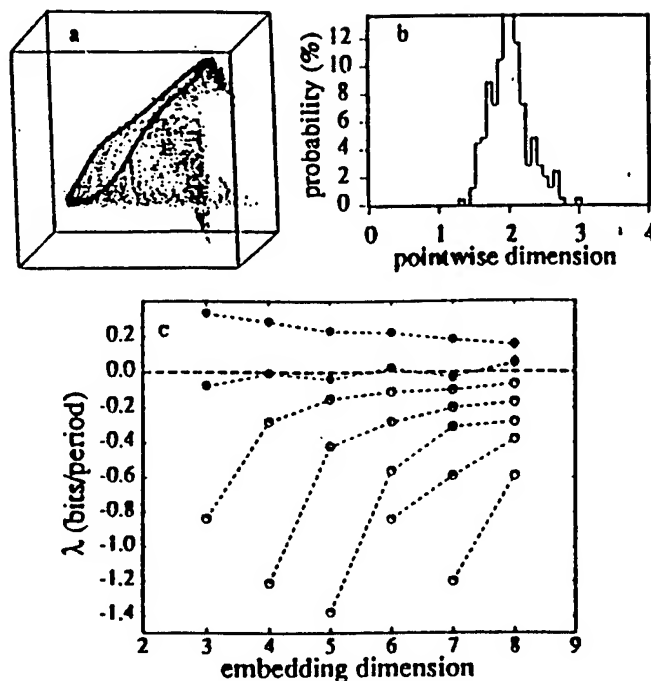


FIG. 4. Chaotic behavior in flash variation Δt . (a) is the attractor reconstructed from the flash time series. (b) is the distribution of pointwise dimensions for (a). (c) shows the results of calculation of the Lyapunov exponents for the attractor in (a).

Chaotic Sonoluminescence

R. Glynn Holt

Jet Propulsion Laboratory, MS 183-401, 4800 Oak Grove Drive, Pasadena, California 91109

D. Felipe Gaitan and Anthony A. Atchley

Department of Physics, Naval Postgraduate School, Monterey, California 93943

Joachim Holzfuss

Institut für Angewandte Physik, Technische Hochschule Darmstadt, Schlossgartenstrasse 7, D-64289 Darmstadt, Germany
(Received 12 November 1993)

Observation of a New Phase of Sonoluminescence at Low Partial Pressures

Bradley P. Barber, Keith Weninger, Ritva Löfstedt, and Seth Putterman

Physics Department, University of California, Los Angeles, California 90024

(Received 17 February 1995)

The acoustically driven pulsations of a gas bubble lead to 10^6 -fold changes in its volume and the emission of a light flash upon collapse. Mass diffusion between the bubble and the gas dissolved in the surrounding fluid maintains this steady-state bubble motion only at low partial pressures, around 3 Torr. This diffusion-controlled regime is uniquely favorable to sonoluminescence (SL) from hydrogenic gases and polyatomic gases with low adiabatic heating. Our analysis indicates that the previously investigated SL from bubbles at 200 Torr requires a nondiffusive mass flow mechanism.

PACS numbers: 78.60.Mq

A gas bubble trapped in water can transduce the energy of a macroscopic sound field down to the microscopic level where it is emitted as picosecond flashes [1] of ultraviolet light [2]. This phenomenon, sonoluminescence (or SL), is particularly sensitive to the amplitude of the imposed sound field, the ambient temperature of the water [3], and the gas composition of the bubble [4]. This last parameter depends on the concentration of the gas dissolved in the water. In particular, the observation of SL from a single bubble of air requires that the water be somewhat degassed [5], whereas with pure argon the intensity of the light emission is relatively independent of the dissolved concentration [4].

Here we report the observation of a new phase of SL which makes this phenomenon accessible to hydrogenic and polyatomic gases. As shown in Fig. 1, this phase is characterized by very low concentrations of dissolved gas (about 10 ppb for deuterium) or, equivalently, low partial pressures of solution of the gas in the water. In this region of parameter space, the steady-state motion of every trapped bubble is accompanied by light emission, as in Fig. 2, which shows the stable dynamics of an ethane bubble as a function of the acoustic drive level. Below the lowest drive level, the bubble is unstable against dissolution in the water, and when driven at an amplitude above the upper threshold the bubble disappears. We have also found that the stability of light emission from pure noble gas bubbles dramatically improves as the partial pressure is reduced to the level where light emission from polyatomic and hydrogenic gases is optimized.

The investigation in this region of parameter space was motivated by considering the mass flow between the pulsating bubble and the gas dissolved in the surrounding fluid [6–8]. When the bubble expands in response to the rarefaction of the driving pressure, the pressure of the gas inside it decreases and mass diffuses into it from the fluid; when the bubble collapses, the gas pressure inside it causes mass to diffuse out. Requiring the net mass flow per acoustic cycle to vanish specifies the steady-state solution of mass diffusion and the bubble dynamics. For sufficiently nonlinear bubble motion, diffusive equilibrium

requires that the partial pressure of gas dissolved in the fluid be given by [7,8]

$$P_{\infty}/P_0 \approx 3(R_0/R_m)^3, \quad (1)$$

where P_{∞} is the partial pressure, P_0 is the ambient pressure (1 atm), R_0 is the ambient radius where the pressure of the gas inside the bubble is the ambient pressure, and R_m is the maximum radius to which the bubble expands in response to the drive. The relation (1) is derived from coupling the measured radius-versus-time curves, $R(t)$, for driven bubble to the diffusion equation for gas dissolved

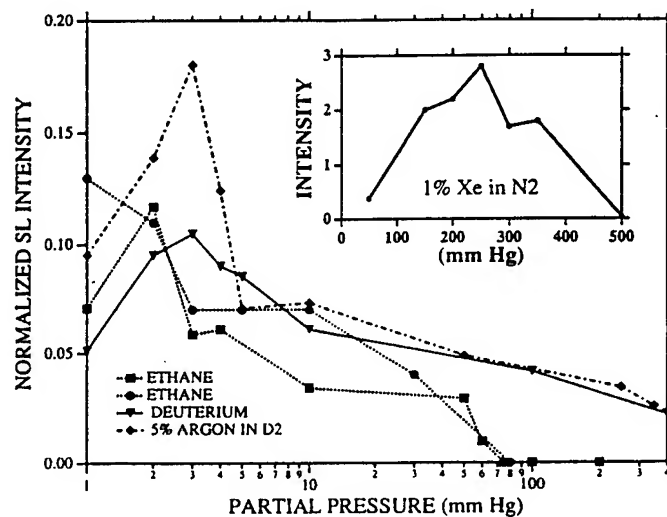


FIG. 1. Intensity of SL for ethane and deuterium as a function of partial pressure of the gas dissolved in the water. The intensities are normalized to air at 150 Torr. Air and xenon-doped nitrogen exhibit broad peaks centered near 200 mm. Inset: The intensities of D_2 and C_2H_6 peak at partial pressures of a few Torr. Between 50 and 150 mm of partial pressure, ethane gives intermittent light with an intensity of about 0.03 for a time scale of less than 25 s. These data points correspond to light-emitting states stable for over 1 min. The experiments were carried out in the acrylic resonators ($\omega_a \approx 35$ kHz) described elsewhere [4]. The saturated molar solubilities of D_2 , C_2H_6 , xenon, and nitrogen in water are about 15, 41, 88, and 13 ppm, respectively (at 1 atm). The two runs with ethane give a measure of the systematic variations.

Observation of Isotope Effects in Sonoluminescence

Robert A. Hiller and Seth J. Putterman

Physics Department, University of California, Los Angeles, California 90095

(Received 1 August 1995)

The spectrum of sonoluminescence emitted by single bubbles of H_2 , D_2 , He^3 , and He^4 trapped in H_2O and D_2O has been measured. We find that heavy water has a dramatic effect on the spectrum of hydrogenic gases, yielding a blackbody-type spectrum with a spectral peak at about 400 nm. The explanation of why such a small change in the driving fluid leads to such a large spectral shift is unknown.

PACS numbers: 78.60.Mq, 43.35.+d

The transduction of sound into light (sonoluminescence or "SL") is mediated by the extremely nonlinear pulsations of a trapped bubble of gas in water. Measurements indicate that the huge energy focusing involved in this process is accompanied by a number of unknowns. These include the light emitting mechanism [1-4], the origin of the upper and lower acoustic drive levels which delineate the SL regime [5], the mechanism of mass exchange between the bubble and gas dissolved in the liquid [6,7], the short duration of the flashes [8,9] (especially their fast turnoff), and the limits of energy concentration that can be achieved (i.e., what is the spectrum beyond the cutoff of water?). Finally, why is water the friendliest liquid for SL [10]?

The acoustic properties of the host liquid and the gas bubble are obviously key physical parameters for this phenomenon. Thus to learn about SL we have measured the effect of isotopic substitution [11] for the gas and for the host liquid. In this direction we have observed SL from H_2 , D_2 , He^3 , and He^4 bubbles driven by sound in H_2O and D_2O host liquids. In view of the (also unexplained) strong sensitivity of SL to the fluid temperature [5,12] these experiments were carried out near room temperature and the freezing point, which for D_2O is 3.8 °C.

Figure 1 shows the cold spectra of the stable helium isotopes in light and heavy water. A general feature of these measurements is that the spectrum of the light emitted by a bubble of He^3 is slightly more ultraviolet than that of a bubble of He^4 . Another feature is that bubbles in heavy water are somewhat dimmer and less strongly peaked in the ultraviolet than are bubbles in light water. This effect of heavy water on SL is particularly dramatic for hydrogenic gases as shown in Fig. 2. The appearance of a cutoff to the spectra of H_2 and D_2 bubbles driven by heavy water is pronounced and unexpected, and stands in marked contrast to previous spectral investigations of SL [12]. The rolloff from the spectral peak occurs at the peak efficiency of the photodetector [Hamamatsu photomultiplier (PMT) 2027] and monochromator (Acton Research 275, 1200 lines/mm grating blazed at 300 nm).

These experiments were carried out in a cylindrical quartz-walled flask (Heracus supracil) with stainless steel

end caps. Resonance frequencies ranged from 39.3 to 40.6 kHz for heavy water and 41.2 to 42.6 kHz for light water. The water was degassed of air and the gas of interest dissolved in to a partial pressure of 3 mm Hg in the water. The experimental procedure [13] involves seeding a bubble with a Nichrome boiler [14] into the sealed flask while driving the flask at its acoustic resonance. The bubble was aligned along the optic axis of the monochromator through the use of a laser beam trained on the output slit. Filters were used to suppress second order diffracted light. The monochromator slits were 3 mm for greatest throughput and result in a spectral resolution of about 10 nm FWHM. The radiance data has been corrected for the PMT, monochromator, and the sapphire window of the cold box. The data have

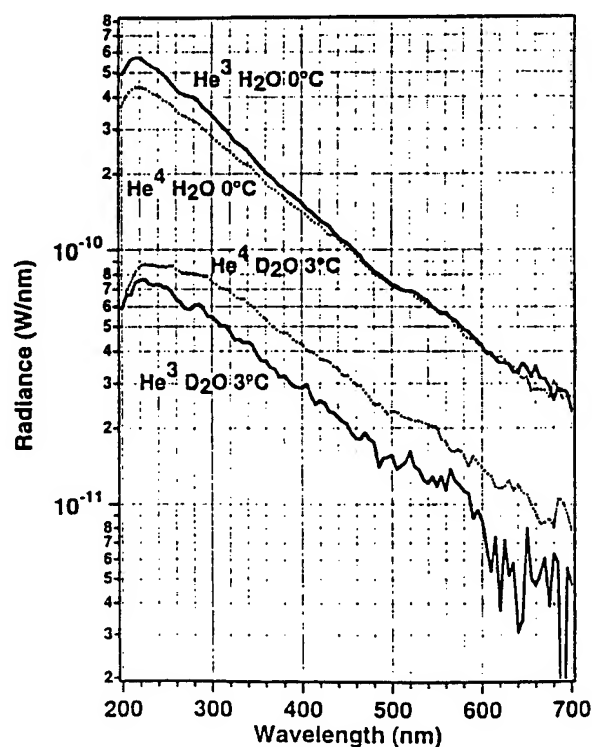


FIG. 1. Spectral radiance of helium isotopes in light and heavy water near the freezing point. Partial pressure of gas is 3 mm. Previous measurements of helium spectra [13] were carried out at 150 mm partial pressure.

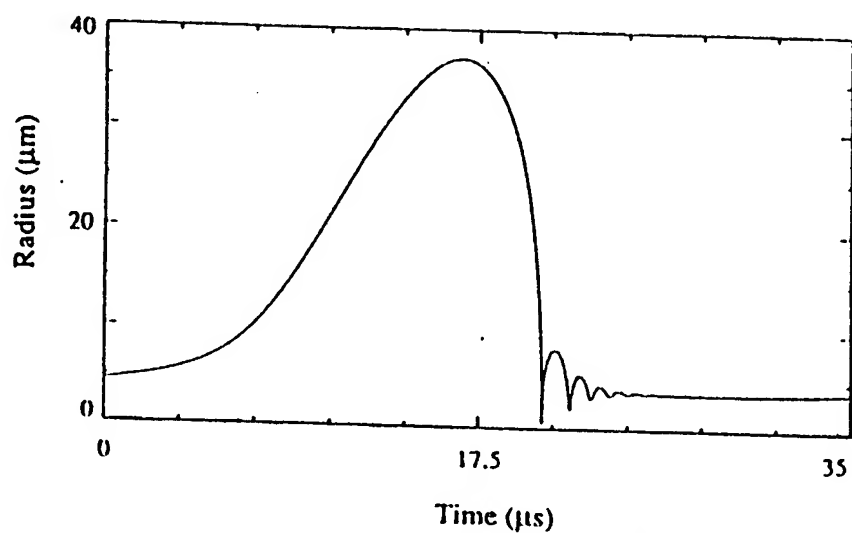


FIG. 1. Case (1): bubble radius vs time according to the adiabatic solution.

Wu and Roberts, Phys. Rev. Lett. 70, 3424-3427 (1993).

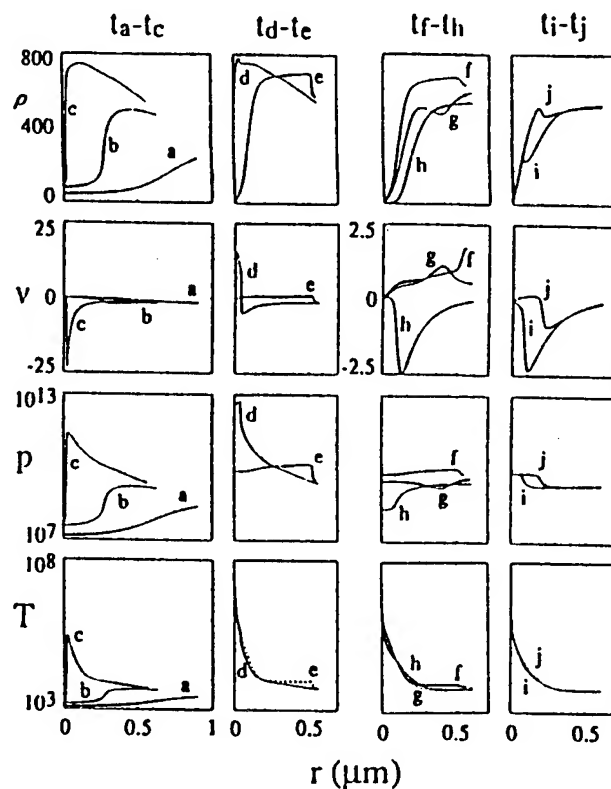


FIG. 2. Time evolution of case (1) from the nonadiabatic calculation. ρ is in kg m^{-3} , v in km s^{-1} , p in Pa, and T in K. Shown are solutions for (a) $t = t_a = 20.490257 \mu\text{s}$; (b) $t_b = t_a + 0.156 \text{ ns}$; (c) $t_c = t_a + 0.19864 \text{ ns}$; (d) $t_d = t_a + 0.19898 \text{ ns}$; (e) $t_e = t_a + 0.21641 \text{ ns}$; (f) $t_f = t_a + 0.22235 \text{ ns}$; (g) $t_g = t_a + 0.26172 \text{ ns}$; (h) $t_h = t_a + 0.377 \text{ ns}$; (i) $t_i = t_a + 0.396 \text{ ns}$; and (j) $t_j = t_a + 0.417 \text{ ns}$.

Wu and Roberts, Phys. Rev. Lett. 70, 3424-3427 (1993).

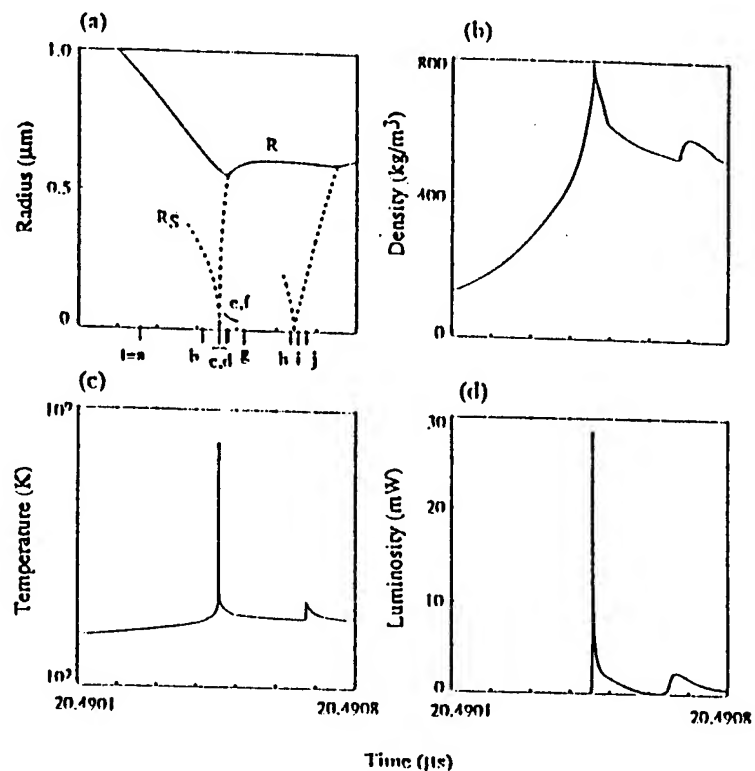
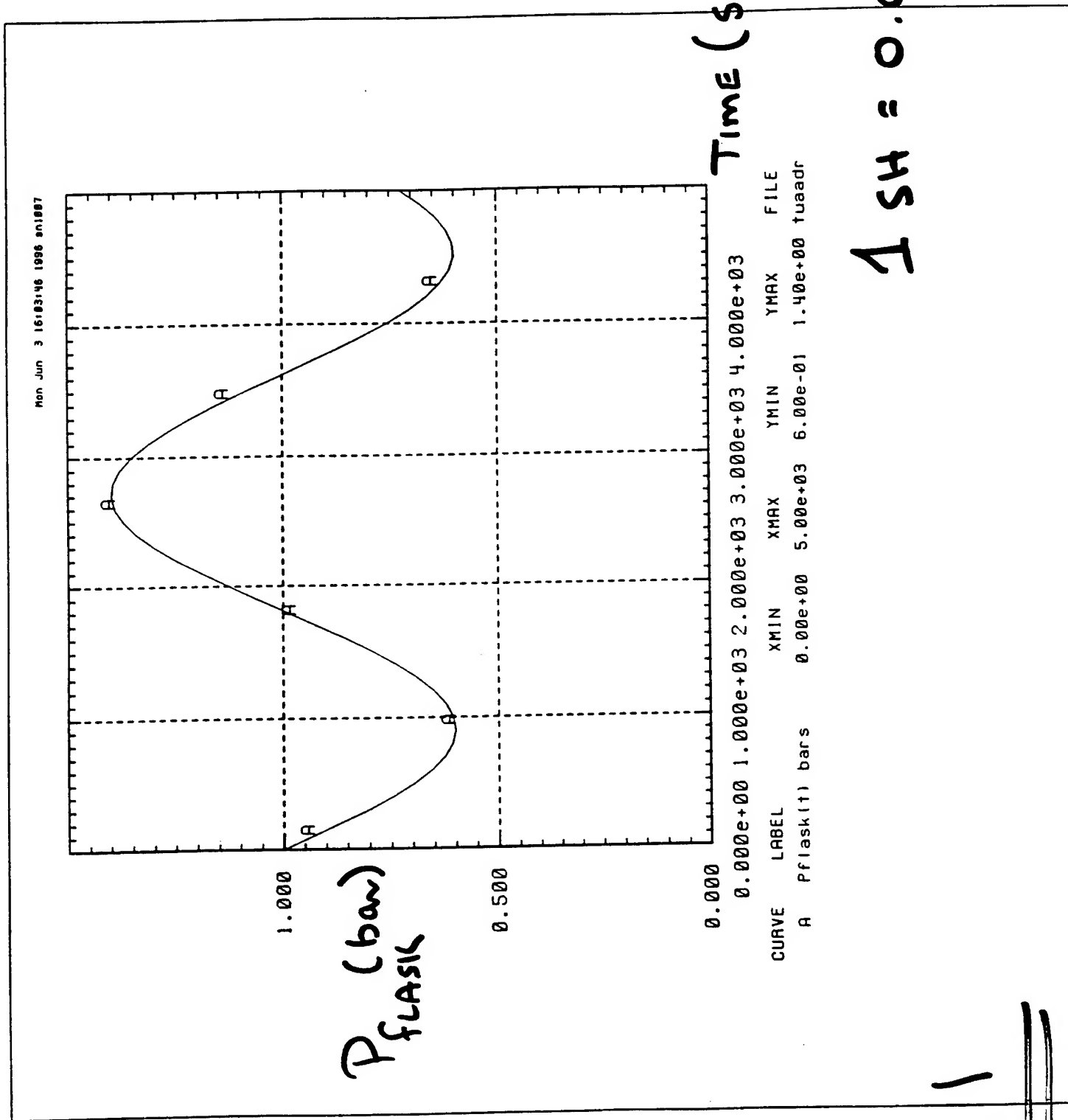


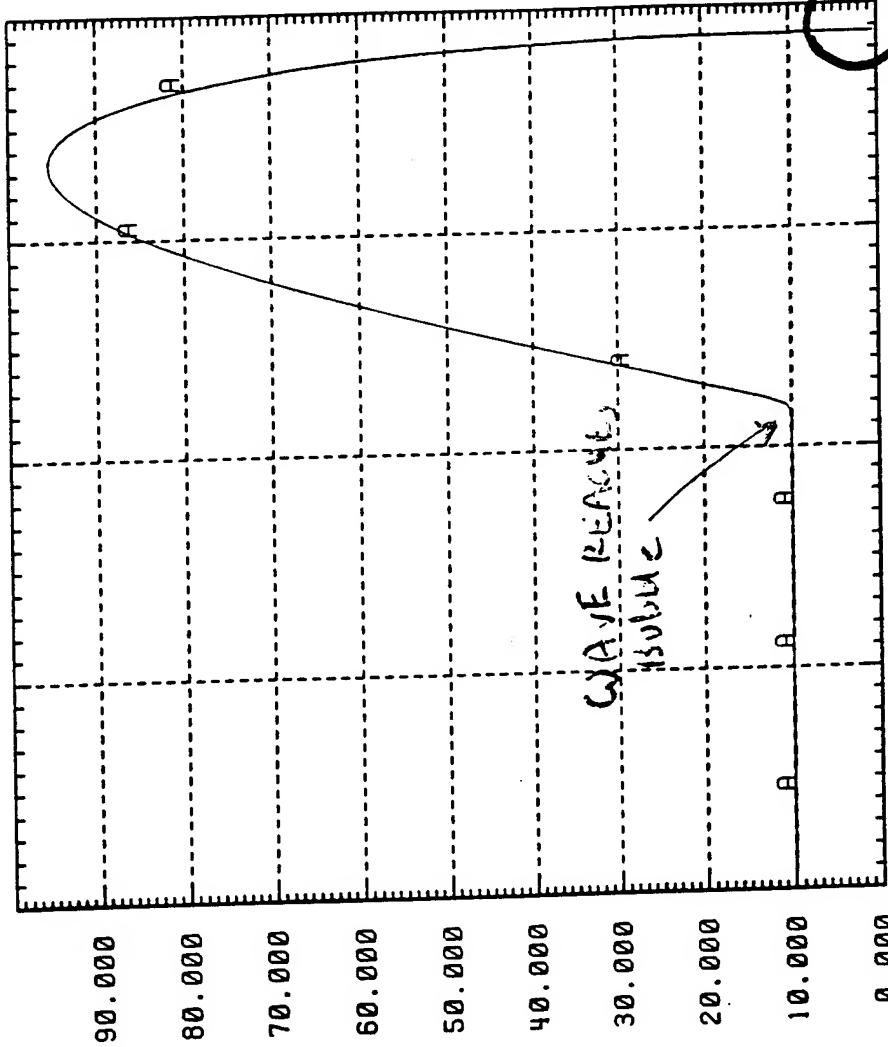
FIG. 3. Case (1): nonadiabatic solution. In (a), the bubble radius and the shock locations (dashed) are plotted as functions of time; the times $t_a - t_j$ employed in Fig. 2 are marked. In (b), (c), and (d), the maximum density, the temperature at maximum density, and the luminosity of the bubble are plotted as functions of time.

Wu and Roberts, Phys. Rev. Lett. 70, 3424-3427 (1993).



$$\Delta SH = 0.01 \mu s$$

Fig 1



CURVE	LABEL	XMIN	XMAX	YMIN	YMAX	FILE
A	R(t) um	0.00e+00	3.87e+03	5.11e-01	9.55e+01	tuaaplotr

RADIUS
(μm)

TIME (sh)

Fig 2

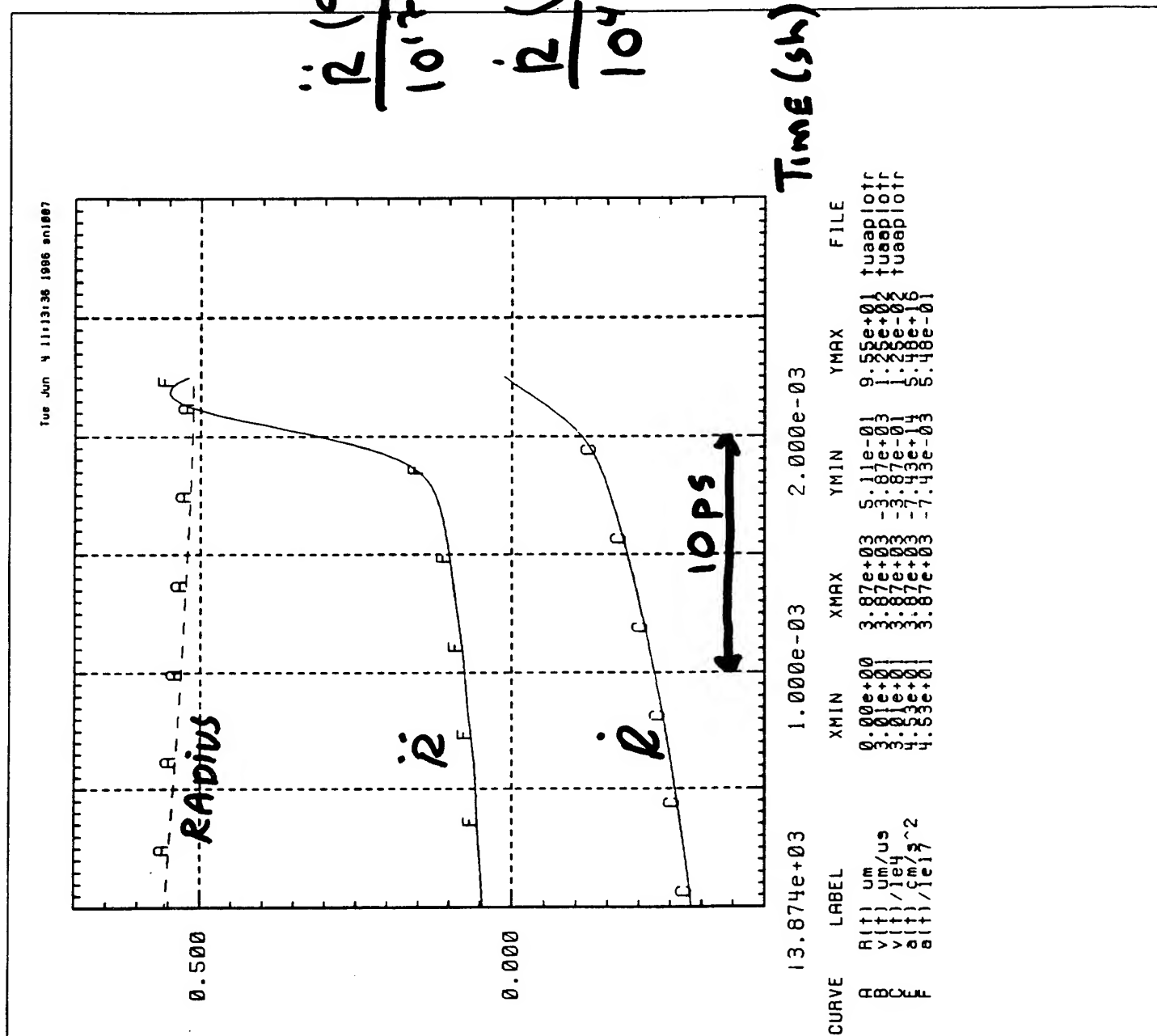
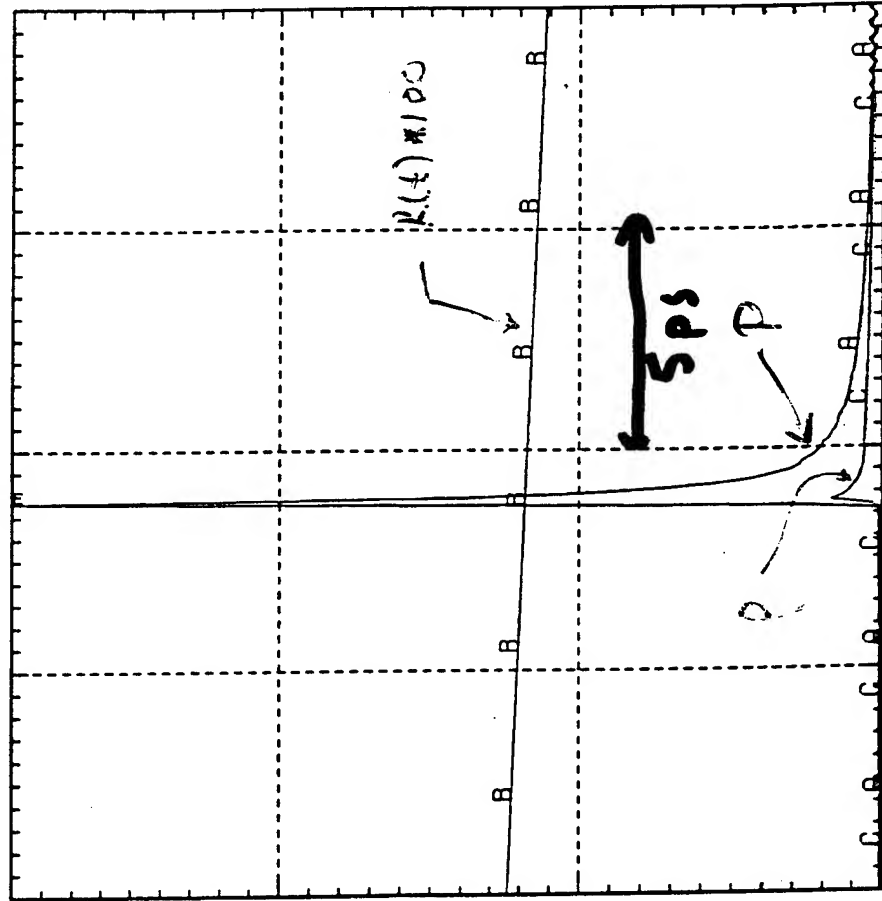
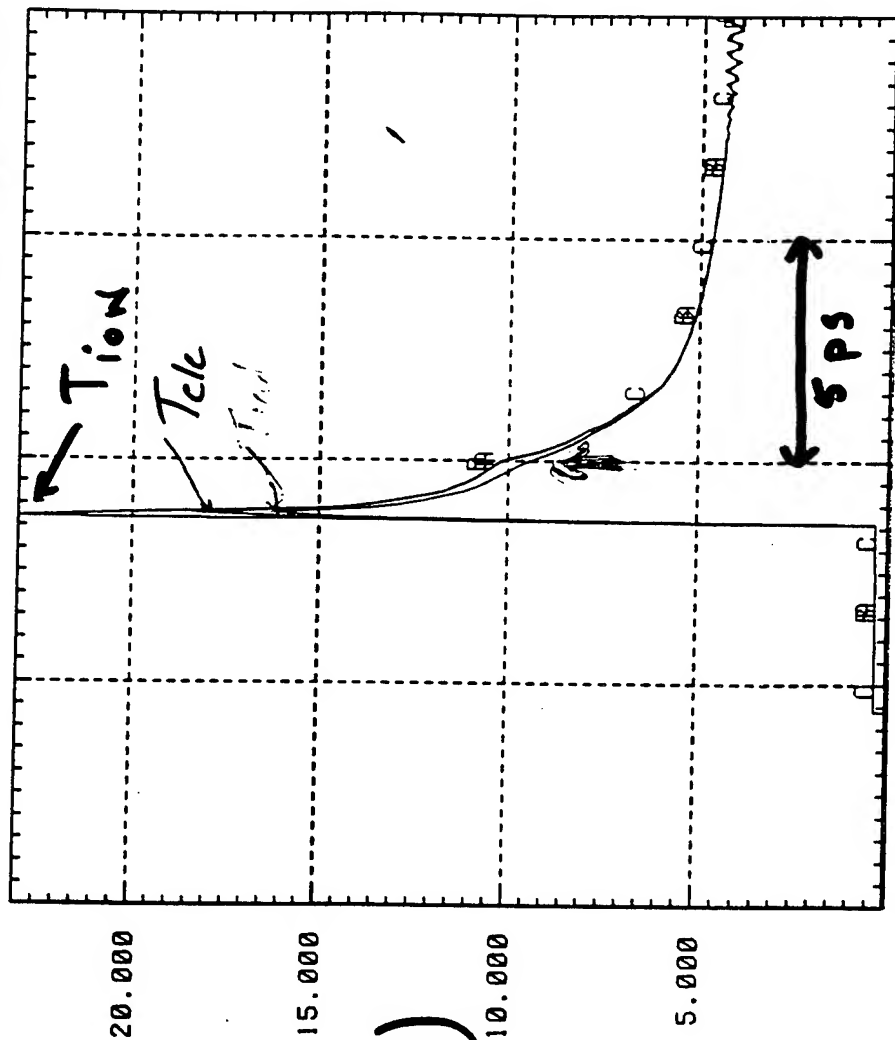


Fig 3



CURVE	LABEL	XMIN	XMAX	YMIN	YMAX	FILE
A	P(t) center Mbar	3.87e+03	3.87e+03	1.02e-03	1.45e+02	ulf77u00
B	P(t) 100 um	3.87e+03	3.87e+03	5.10e-01	1.42e+02	ulf77u00
C	P(t) center g/cc	3.87e+03	3.87e+03	5.40e-02	8.52e+00	ulf77u00

F_S4



Time (sh)

13.874e+03 5.000e-04 1.000e-03 1.500e-03

CURVE	LABEL	XMIN	XMAX	YMIN	YMAX	FILE
A	Tion center ev	3.87e+03	3.87e+03	2.50e-02	2.30e+01	ulf7tuaa
B	Tcle center ev	3.87e+03	3.87e+03	2.50e-02	1.84e+01	ulf7tuaa
C	Ttrad center ev	3.87e+03	3.87e+03	2.50e-02	1.63e+01	ulf7tuaa

Fig 5

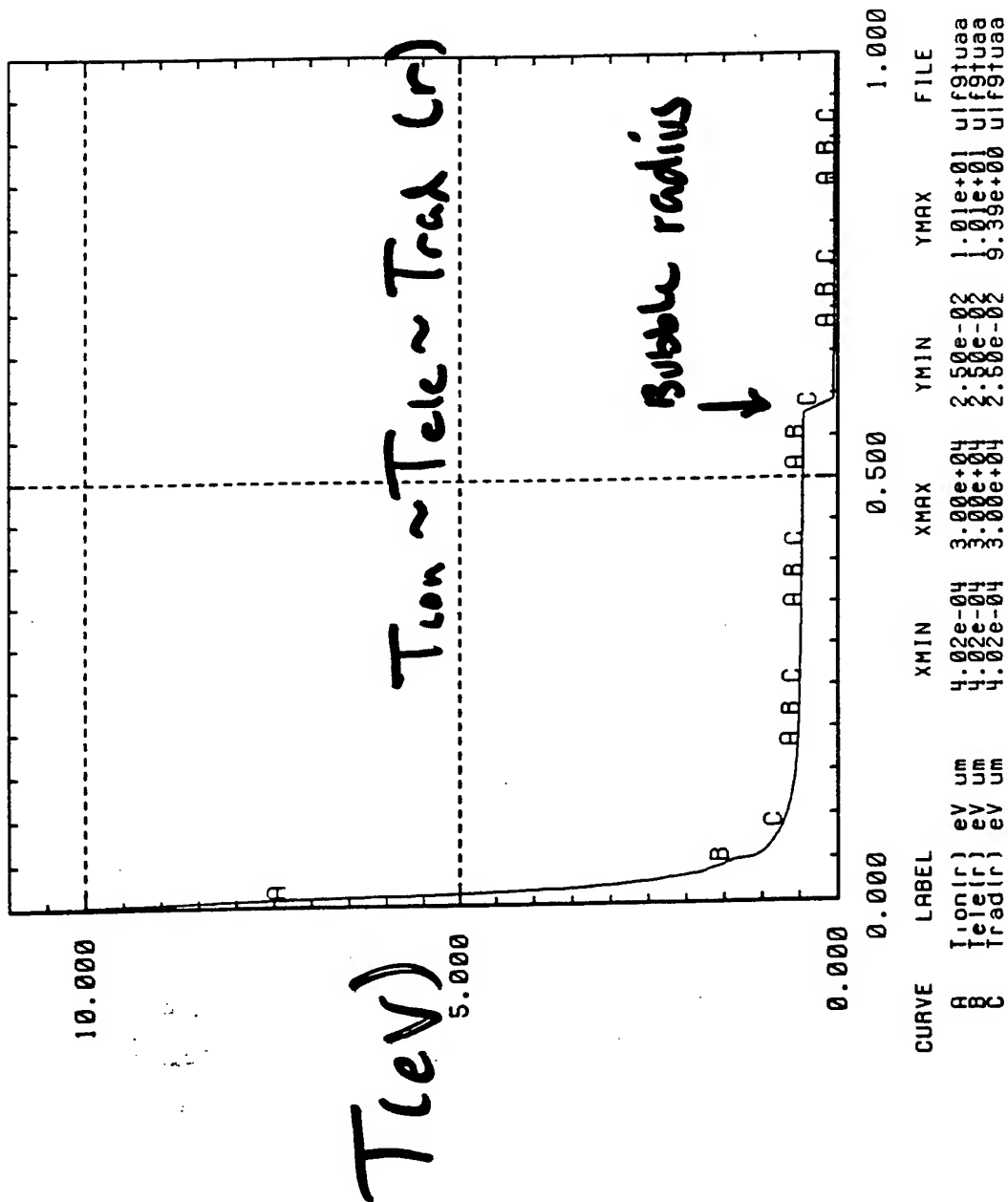
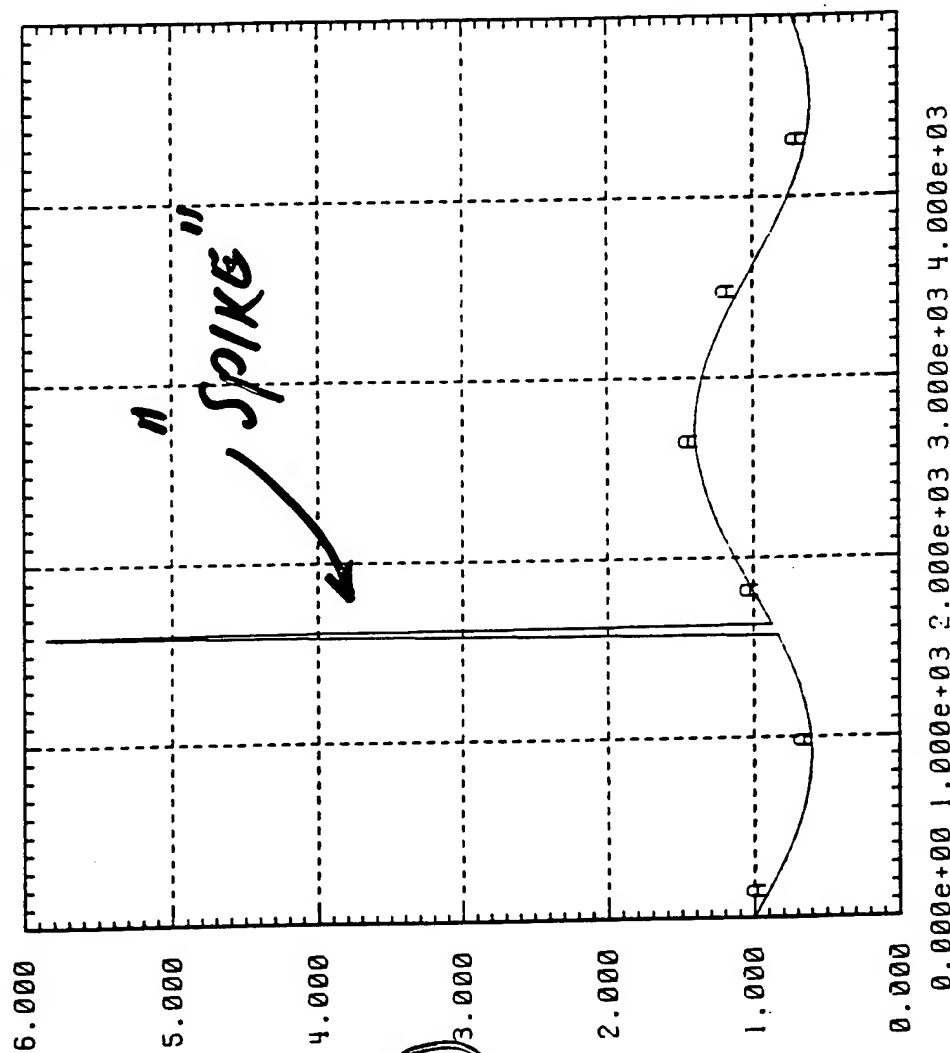


Fig 1.5 Sps after "flash"

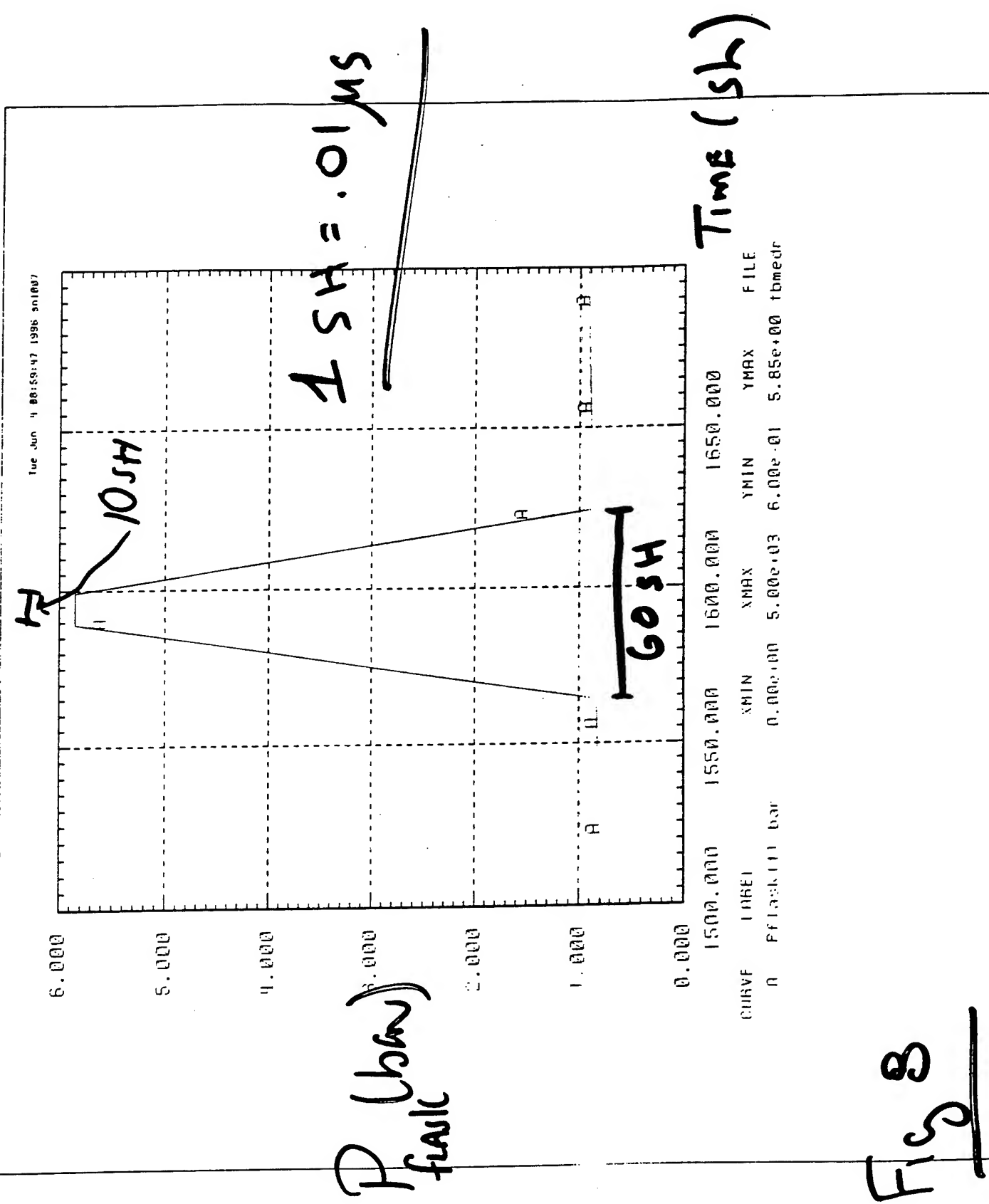
Tue Jun 4 00:59:08 1996 an1007



CURVE	LABEL	XMIN	XMAX	YMIN	YMAX	FILE
A	Pflask(t) bar	0.00e+00	5.00e+03	6.00e-01	5.85e+00	tbmedr

Fig 7

Fig 3



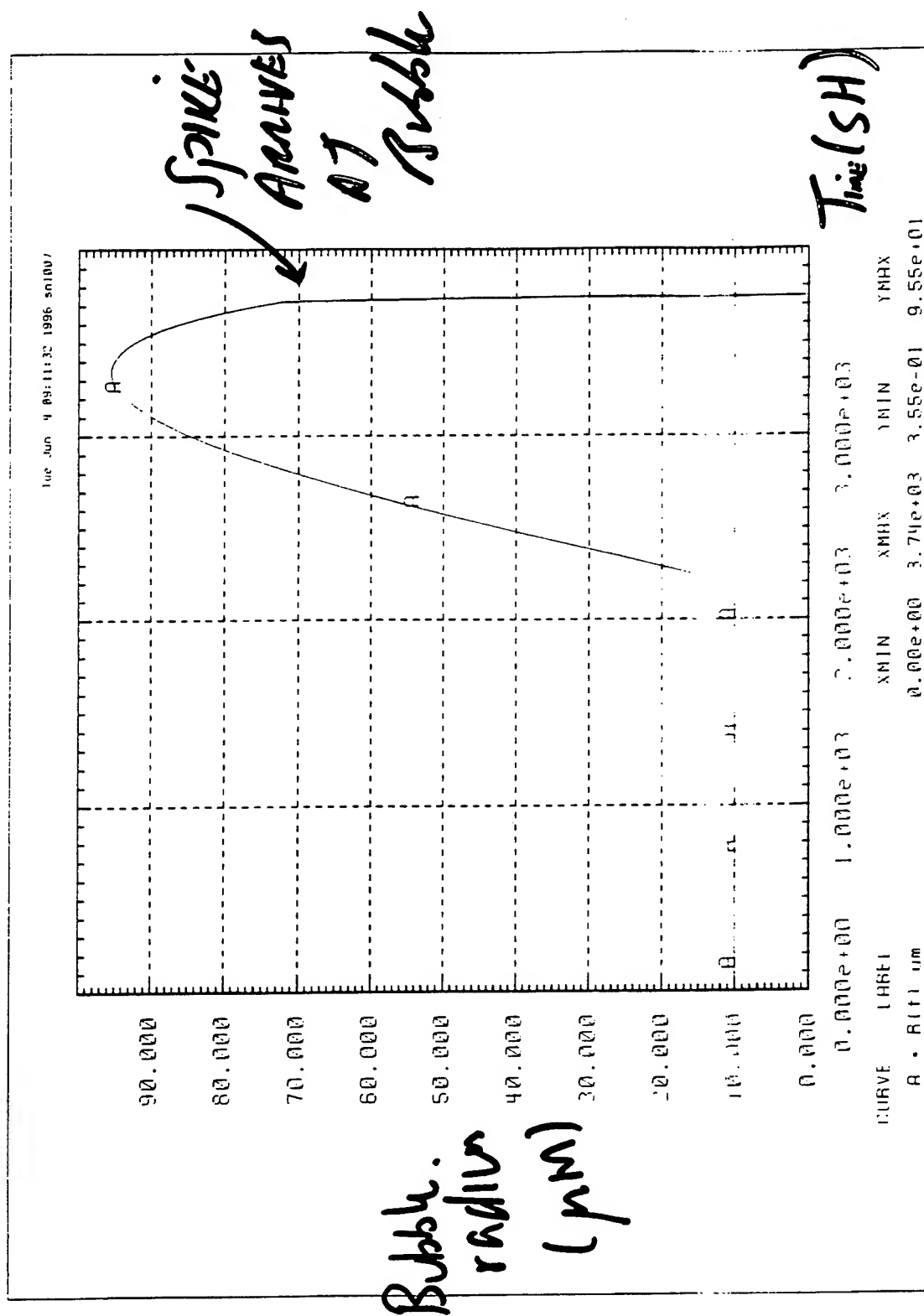
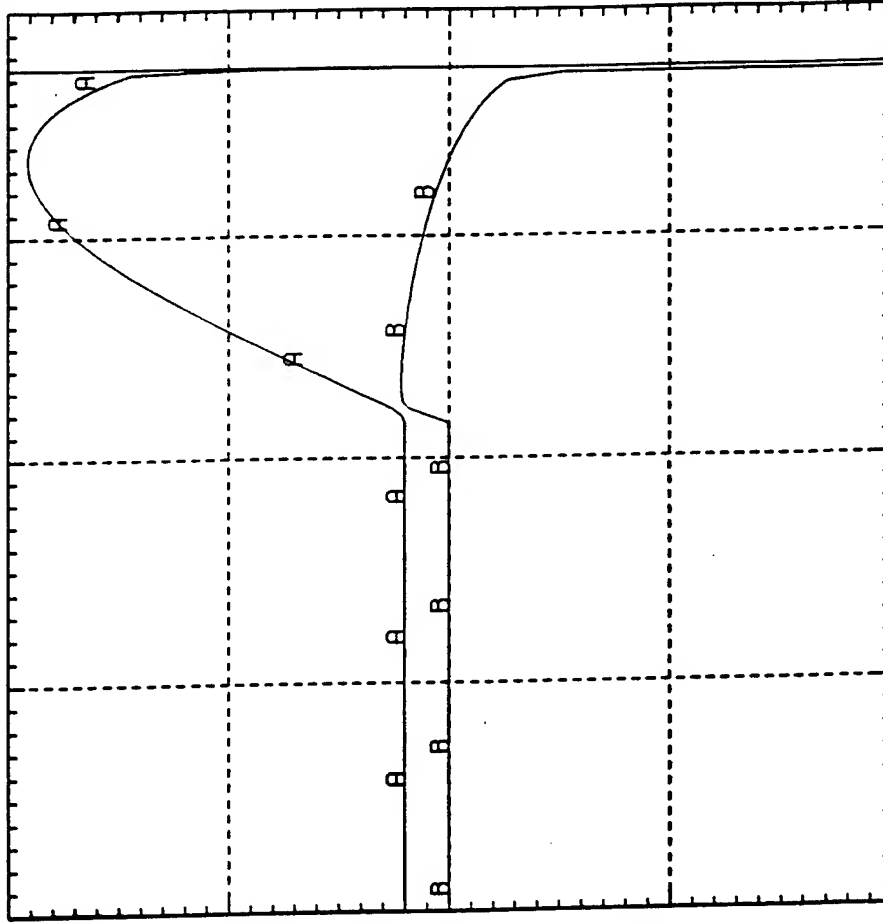


Fig 9



$R(\mu m)$
 $\dot{R}(\mu m/\mu s)$

Time(s)

CURVE	LABEL	XMIN	XMAX	YMIN	YMAX
A	R(t) μm	0.00e+00	3.74e+03	3.55e-01	9.55e+01
B	v(t) $\mu m/\mu s$	3.01e+01	3.74e+03	-1.29e+04	3.74e+03

Fig 10

Tue Jun 4 09:30:33 1986 sn1087

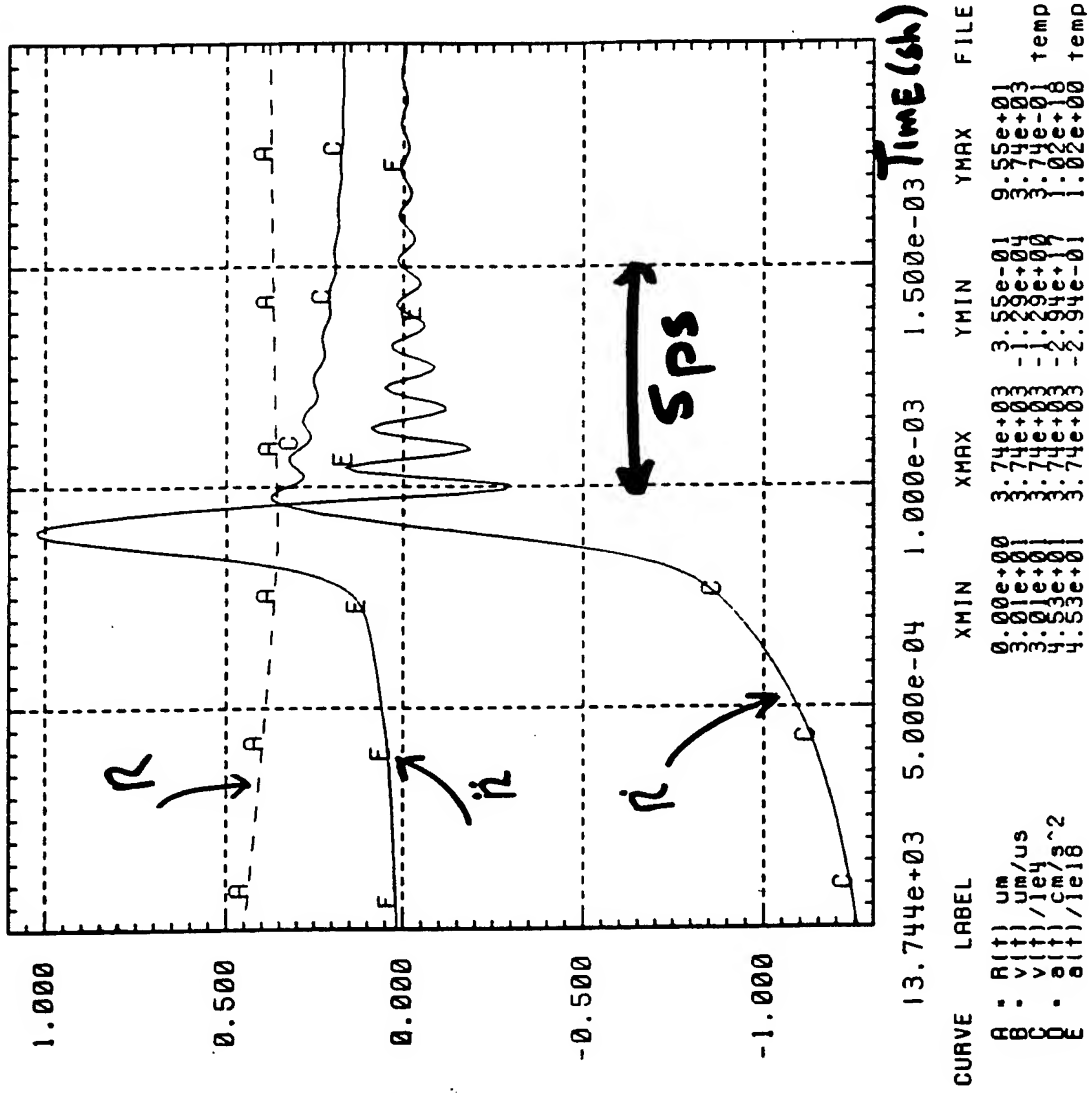
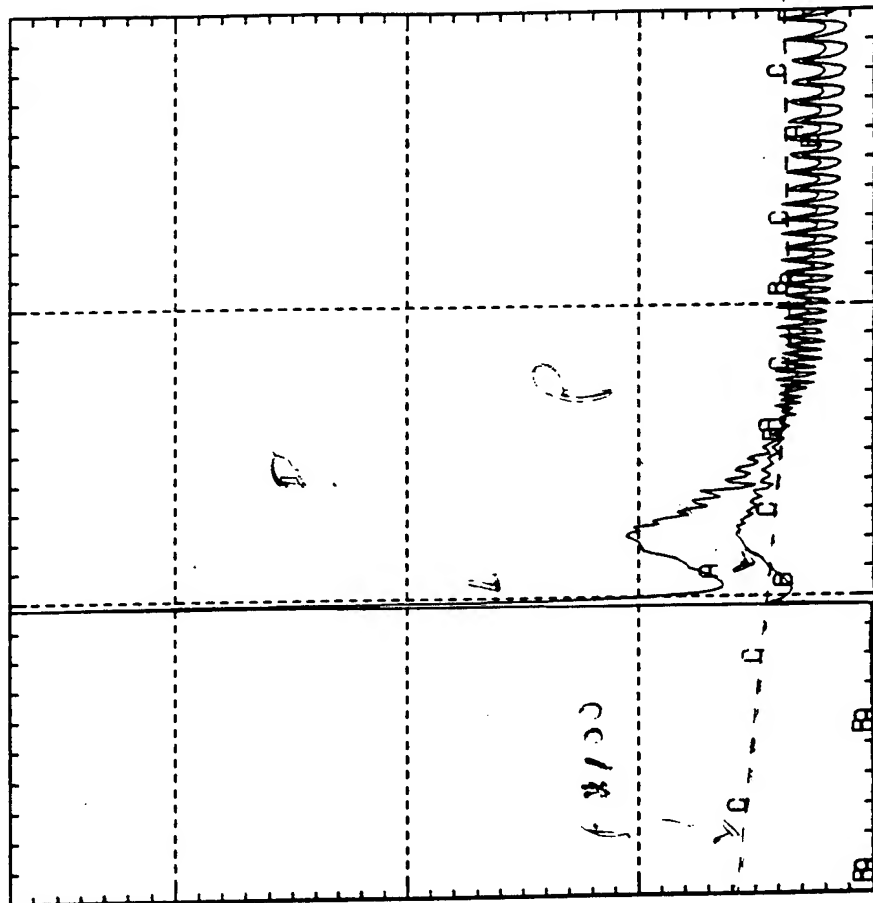


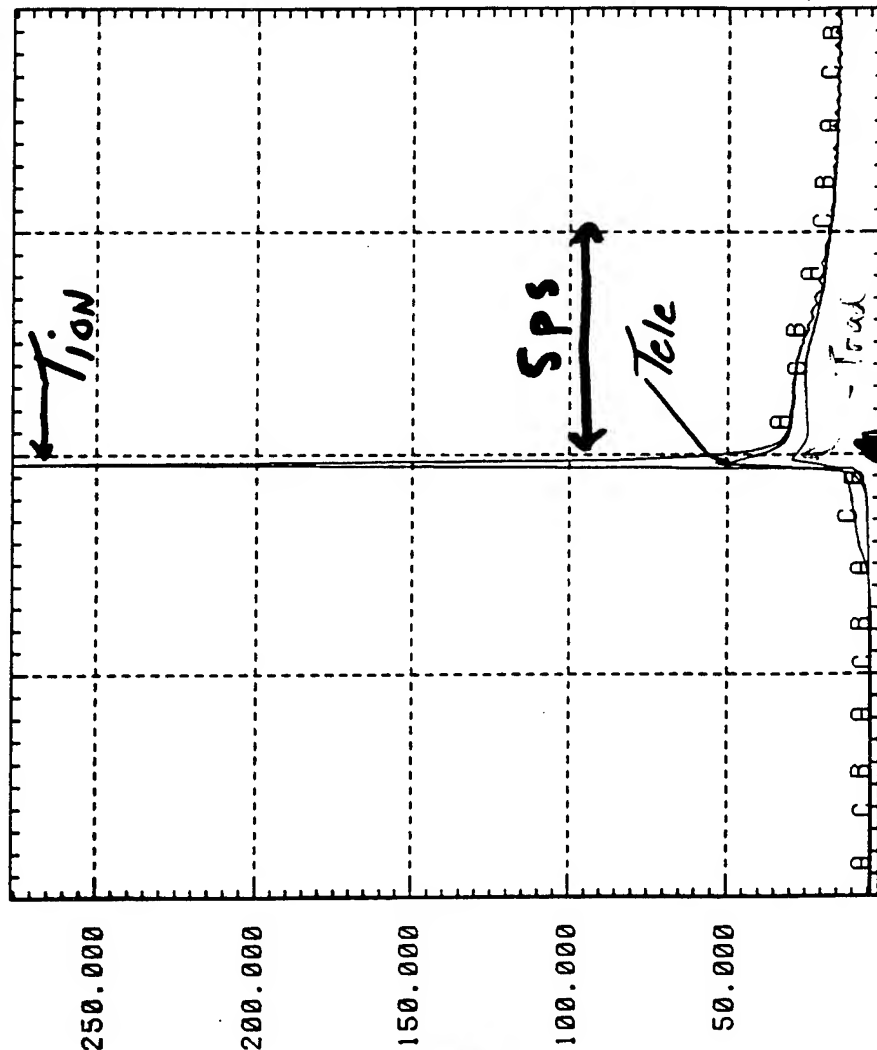
Fig 11



CURVE	LABEL	XMIN	XMAX	YMIN	YMAX	FILE
A	P(t) center Mbar	3.74e+03	3.74e+03	1.38e-04	3.70e+02	ulf7t.me
B	rho(t) 1.10 center	3.74e+03	3.74e+03	1.13e-03	5.80e+01	ulf7t.me
C	R(t) 1.00 um	3.74e+03	3.74e+03	3.55e+01	1.20e+02	ulf7t.me

Fig 12

1.000e-03
1.500e-03
2.000e-03

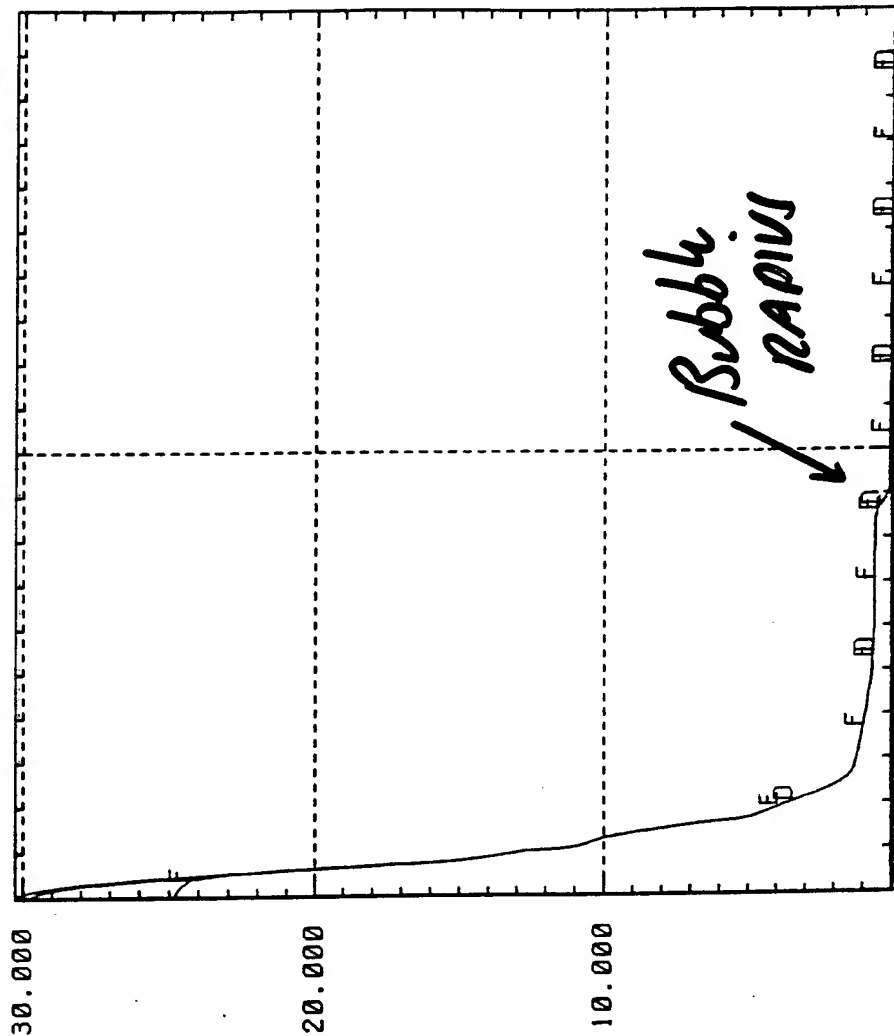


Time (sh)

13.744e+03 5.000e-04 1.000e-03 1.500e-03

CURVE	LABEL	XMIN	XMAX	YMIN	YMAX	FILE
A	Ion center	3.644e+03	3.744e+03	4.14e+00	2.76e+02	atchley/tmbetmp
B	Tele center	3.644e+03	3.744e+03	2.61e+00	4.98e+01	atchley/tmbetmp
C	Trad center	3.644e+03	3.744e+03	1.36e+00	2.98e+01	atchley/tmbetmp

Fig 13



CURVE	LABEL	XMIN	XMAX	YMIN	YMAX	FILE
D	T(ion(r))	ev 0.58e-04	3.00e+04	2.50e-02	3.03e+01	atchley/temps1
E	T(ele(r))	ev 0.58e-04	3.00e+04	2.50e-02	3.03e+01	atchley/temps1
F	T(rad(r))	ev 0.58e-04	3.00e+04	2.50e-02	3.03e+01	atchley/temps1

~ 1 ps after "flash"

Fig 14

Is sonoluminescence collision-induced emission?

Lothar Frommhold

Physics Department, University of Texas at Austin, Texas 78712-1081

Anthony A. Atchley

Physics Department, Naval Postgraduate School, Monterey, CA 93943

(August 16, 1994)

An estimate is attempted of the collision-induced emission (CIE) intensity and spectral profile in the visible and near UV region of the spectrum of N_2 -X pairs, where X represents another N_2 molecule or an argon atom, etc., for conditions that correspond to shock waves believed to exist in sonoluminescence experiments. Calculated profiles consist of superimposed high overtone bands and resemble measured profiles of sonoluminescence spectra. The intensities calculated on the basis of a few, simple assumptions concerning the induced dipole surface compare favorably with measurements. The agreement obtained suggests that collision-induced emission is a viable or even an attractive alternative to bremsstrahlung to explain sonoluminescence. According to the theory presented, the CIE source is optically thin so that the spectral emission profile is not related to Planck's radiation law.

43.20.+y,78.60.Mq,34.10.+x,33.70.-w

I. INTRODUCTION

A single bubble of air may be trapped in an acoustic standing wave setup in a water filled container. If the proper drive frequency and amplitude are applied, the bubble may emit short bursts of light, an effect called sonoluminescence. Some recent explanations of sonoluminescence have centered on the idea that a converging, spherically symmetric shock wave is launched in the gas in the interior of the bubble, as the bubble collapses under the influence of the acoustic standing wave. The assumption has been that the temperature in the (reflected) shock wave is so high that ionization and emission by electronic excitation and/or bremsstrahlung occur [1]. Temperatures in excess of 10^6 K are often assumed in such work.

Collision-induced absorption (CIA) and emission (CIE) arise from dipoles induced by intermolecular interactions ("collisions"). Especially the absorption spectra of the common, non-polar gases (e.g., hydrogen) have been studied in great detail in a number of laboratories; a recently published monograph summarizes the present knowledge [2]. Collision-induced emission, on the other hand, is less well studied but is thought to be an important source of electromagnetic radiation in the atmospheres of planets and cool stars [3,4]. Infrared emission of shockwaves has also been explained in terms of CIE [5]. In this letter, we want to explore the possible connections of sonoluminescence and collision-induced emission. CIE in the visible from shock waves at temperatures much lower than 10^6 K is expected at high gas densities.

Caledonia et al. reported studies of interaction-induced light emission in the H_2 fundamental band (near $2.4 \mu m$) at densities from 10 to 50 amagats behind reflected shock

Collision-induced emission in the fundamental vibration-rotation band of H_2

G. E. Caledonia and R. H. Krech

Physical Sciences Inc., Andover, Massachusetts 01810

T. D. Wilkerson

Institute of Physical Science and Technology, University of Maryland, College Park, Maryland 20742

R. L. Taylor

CVD Inc., Woburn, Massachusetts 08101

G. Birnbaum

National Institute of Standards and Technology, Gaithersburg, Maryland 20899

(Received 1 November 1990)

Measurements of collision-induced emission in the fundamental vibration-rotation band of hydrogen are presented for argon, xenon, and neon collision partners. These absolute, spectrally resolved infrared measurements were performed at high densities behind reflected shock waves over the temperature range of 900–3400 K. The emission was found to be dominated by Q -branch transitions at high temperature due primarily to the dipole moment induced by the overlap between the electron clouds of the collision pair. The strength of this interaction was evaluated from the data and compared with similar evaluations determined from low-temperature absorption studies.

I. INTRODUCTION

This paper reports studies of the collision-induced emission (CIE) in the fundamental vibration-rotation band of the hydrogen molecule. The spectrally resolved infrared emission of the H_2 band was measured at elevated temperatures and pressures using a high-density, moderate-temperature shock tube as the controlled light source. The measurements were performed for several rare-gas collision partners and were interpreted within the framework of existing theory.

Collision induction in hydrogen has been well characterized in absorption at temperatures below 400 K,^{1,2} but has only recently^{3,4} been studied at higher temperatures in emission. Collision-induced processes give rise to vibrational, rotational, and translational absorption and emission in molecules which by virtue of their symmetry do not have an electric dipole moment in their electronic ground state. The proximity of a collision partner makes possible the induction of a transient dipole in the colliding pair resulting from interactions due predominantly to the permanent quadrupole moment of H_2 and to the overlap of the molecular electron clouds. Such interactions produce relatively weak radiation signatures which, however, can be significant at high pressures. Indeed, CIE by H_2 has been found to be an important source of infrared radiation in planetary atmospheres,^{5–7} and its inverse process, collision-induced absorption, is the dominant source of infrared opacity in stellar atmospheres.⁸

The present study focused on the high-temperature band strength and spectral shape of the H_2 fundamental vibration-rotation band centered at 2.4 μm . The band emission was measured behind reflected shocks over the

temperature range of 900–3400 K. Gas mixtures of H_2 with Ne, Ar, and Xe were investigated. Since the emission is collision induced, its intensity scales as the square of the density; measurements were performed over the density range of 10–50 amagats.

A description of the experimental apparatus and techniques is provided in Sec. II. A brief review of the theory of Van Kranendonk,^{9,10} and how it was applied to the present data, is presented in Sec. III. The data are summarized in Sec. IV and analyzed to evaluate the induced dipole parameters. The summary and conclusions of the study are given in Sec. V.

II. EXPERIMENTAL APPARATUS AND PROCEDURES

The measurements were performed in the Physical Sciences Inc. (PSI) shock tube facility. The shock tube is a valuable tool for this type of study because it can readily heat and equilibrate a large volume of gas at steady chemical and thermal conditions. Furthermore, the thermodynamic properties of the gas can be calculated accurately from measurements of the initial gas pressure and shock velocity. On the negative side, a measurement must be performed during a relatively short test time (≤ 1.5 ms) and thus there is little opportunity for time averaging the signal.

The emission measurements were performed behind reflected shocks in a polished stainless steel shock tube with an interior diameter of 6 $\frac{1}{2}$ in. The driver and test sections were 9 and 18 ft long, respectively, with $\frac{1}{4}$ -in.-thick walls. A schematic diagram of the apparatus is shown in Fig. 1. The optical measurements were made

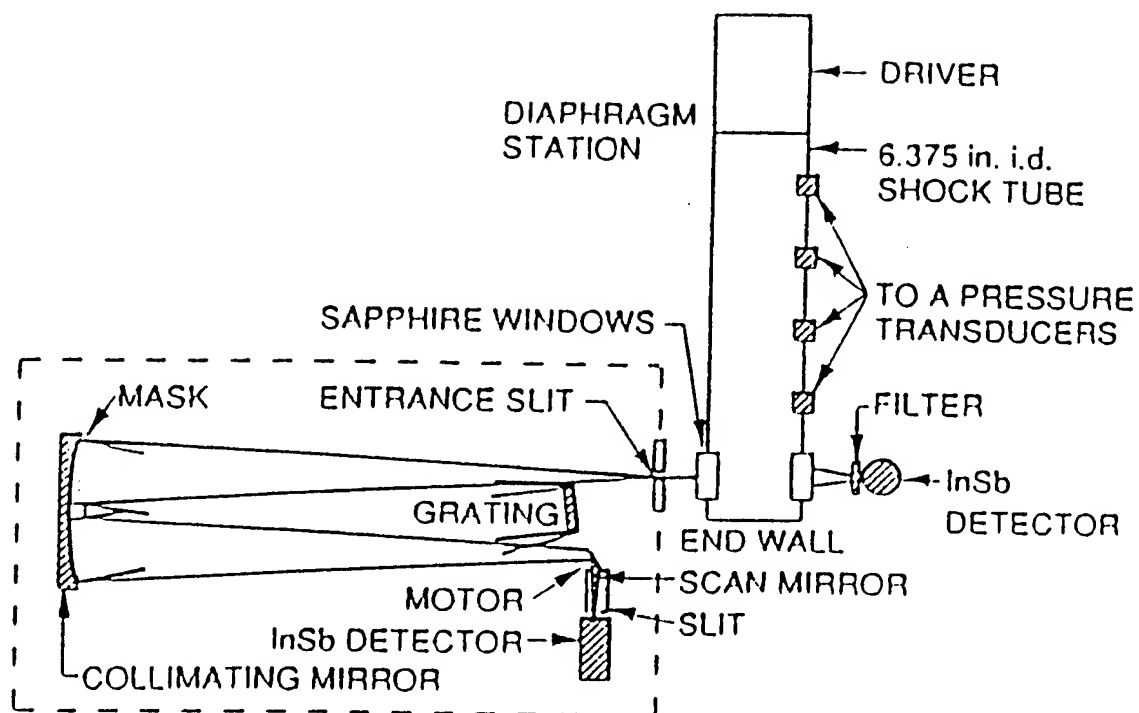


FIG. 1. Schematic of shock tube and ir instrumentation.

- [16] A. Borysow, M. Moraldi, and L. Frommhold. *J.Q.S.R.T.*, **31**, 235 (1984).
- [17] R. Hiller, S. J. Putterman, and B. Barber. *Phys. Rev. Letters* **60**, 1182 (1992).
- [18] J. T. Carlson, S. D. Lewis, A. A. Atchley, D. F. Gaitan, X. K. Maruyama, M. E. Lowry, M. J. Moran, and D. R. Sweider. In *Advances in Nonlinear Acoustics*, H. Hobaek, ed., World Scientific, River Edge, N.J., pp. 406 – 411.
- [19] S. P. Reddy. In G. Birnbaum, ed., *Phenomena Induced by Intermolec. Interactions*, p. 129. Plenum Press, New York, 1985.
- [20] G. Herzberg. *Astrophys. J.*, **115**, 337 (1952).
- [21] H. Spinrad. *Astrophys. J.*, **140**, 1639 (1964).

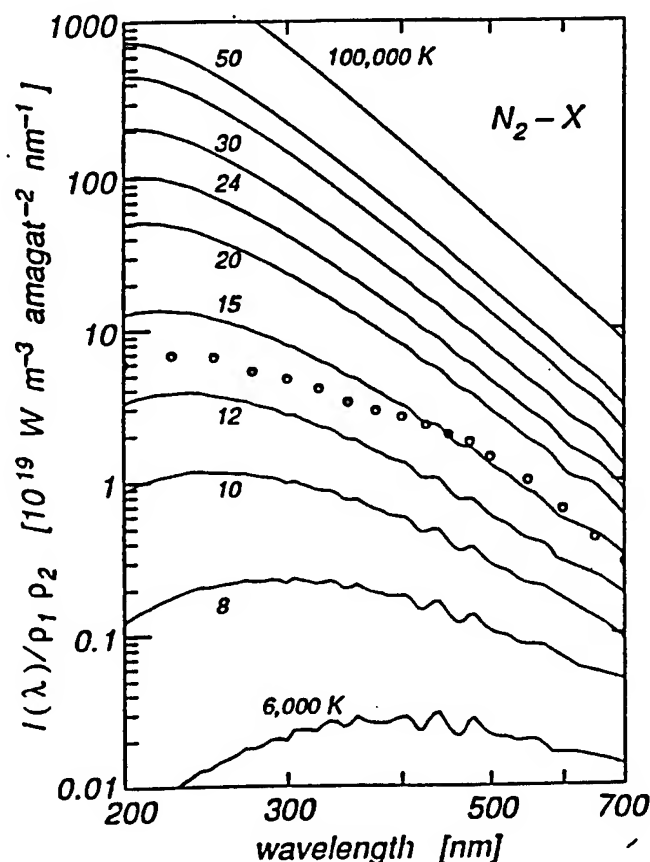


FIG. 1. Total emission in Watt per unit source volume, over gas densities of N_2 and X, per 1 nm wavelength, for eleven temperatures from 6,000 to 100,000 K; the numbers 8 ... 50 are short for 8,000 K ... 50,000 K; continuous wave emission is assumed. Also shown is a measurement [18] (circles). The structures discernible at low temperature are artifacts.

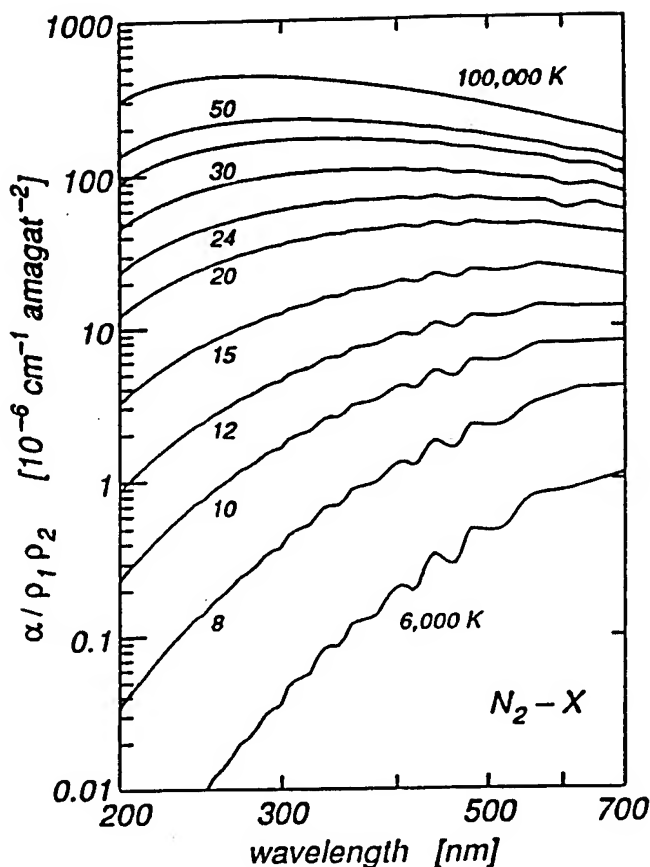
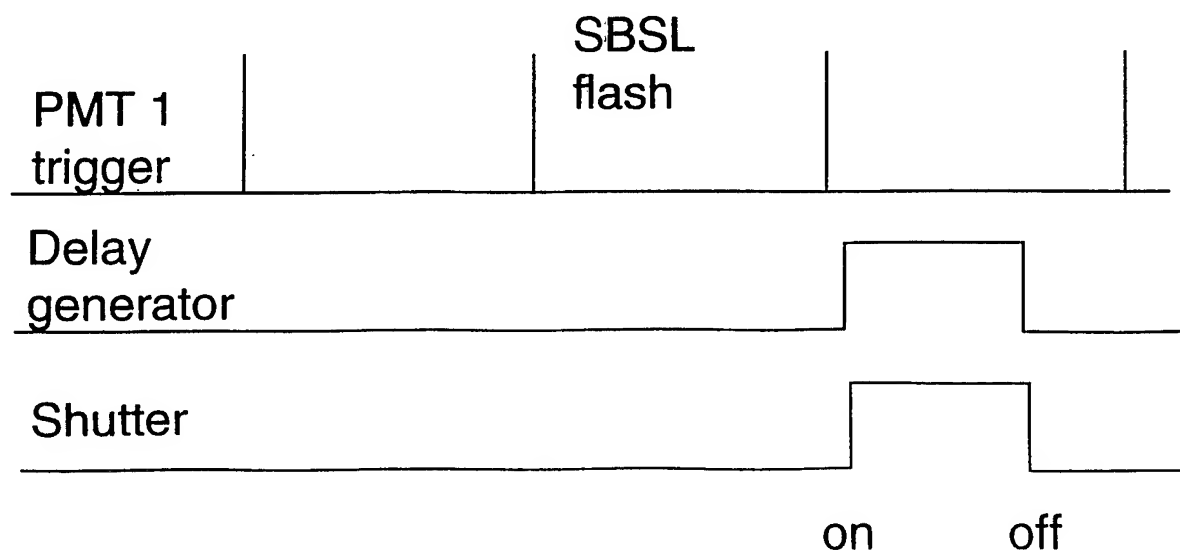
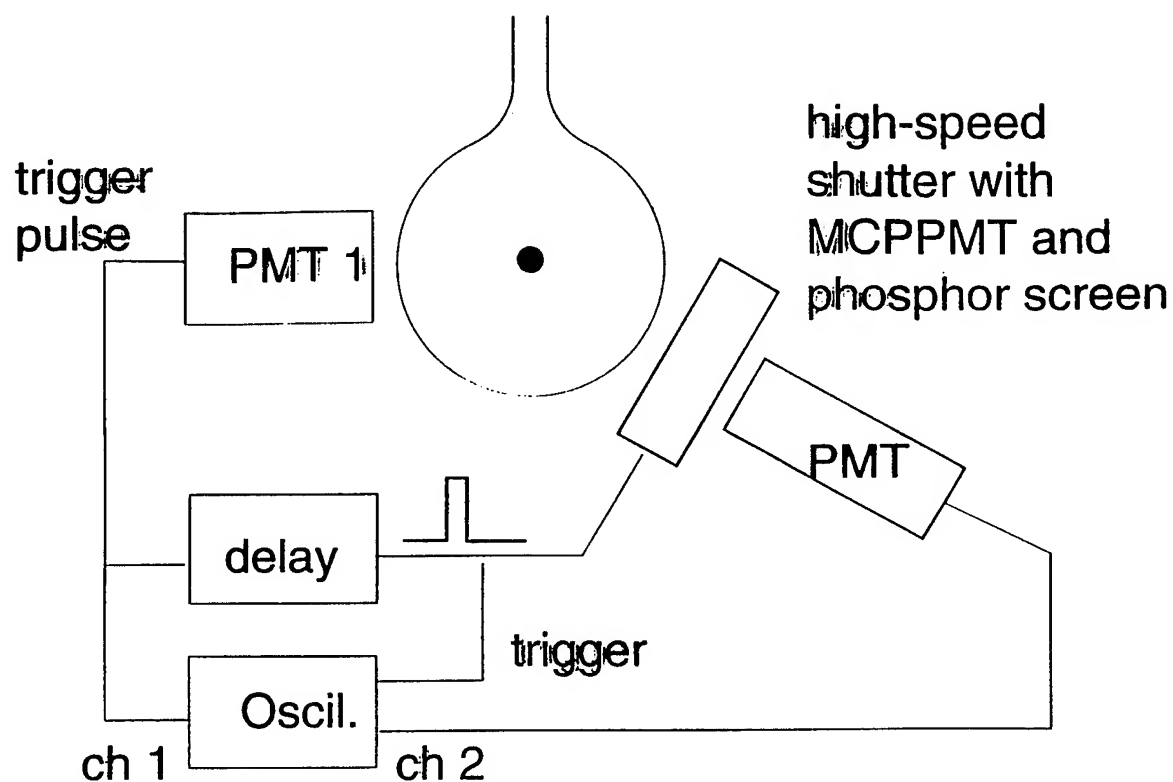
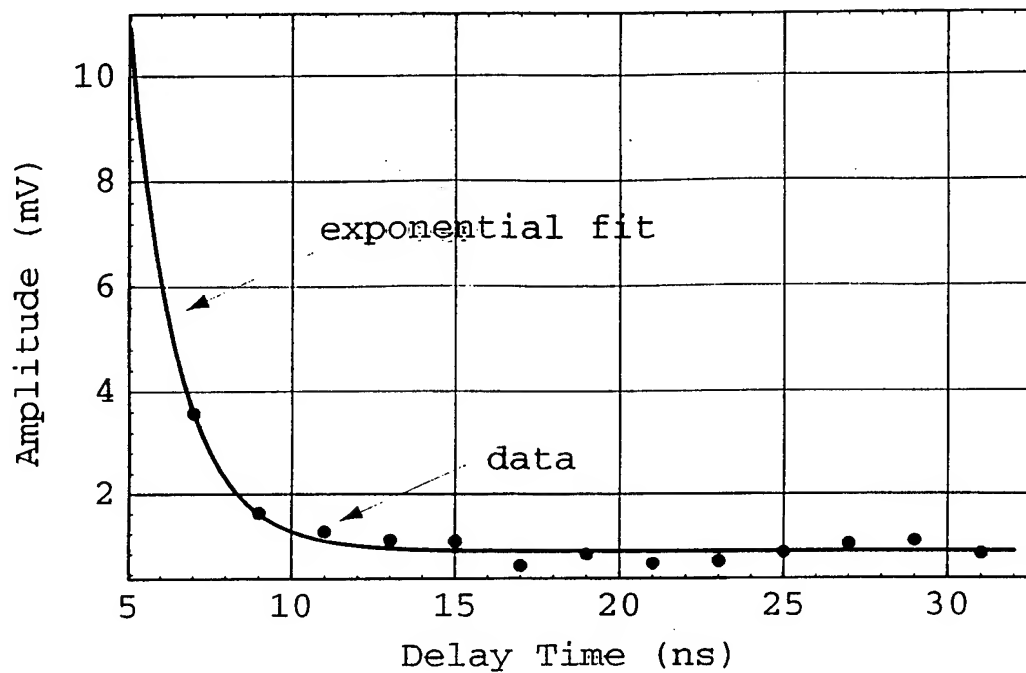


FIG. 2. The calculated absorption coefficient α over gas densities of N_2 and X, for eleven temperatures from 6,000 to 100,000 K; the numbers 8, ... 50 are short for 8,000 K ... 50,000 K. Structures discernible at low temperatures are artifacts.

Is there an afterglow to SBSL?





- Average of 1000 waveforms, background subtracted.
- Some signal, even 9 ns after main bang.
- Jitter in system is ≈ 5 ns, but not yet quantitative!
- Preliminary data - Is there a preglow as well?

Sonoluminescence as Quantum Vacuum Radiation

Claudia Eberlein*

Department of Physics, University of Illinois at Urbana-Champaign, Urbana, Illinois 61801-3080

(Received 2 June 1995; revised manuscript received 11 December 1995)

Sonoluminescence is explained in terms of quantum vacuum radiation by moving interfaces between media of different polarizability. It can be considered as a dynamic Casimir effect, in the sense that it is a consequence of the imbalance of the zero-point fluctuations of the electromagnetic field during the noninertial motion of a boundary. The transition amplitude from the vacuum into a two-photon state is calculated in a Hamiltonian formalism and turns out to be governed by the transition matrix element of the radiation pressure. Expressions for the spectral density and the total radiated energy are given. [S0031-9007(96)00240-2]

PACS numbers: 78.60.Mq, 03.70.+k, 42.50.Lc

Sonoluminescence is a phenomenon that has so far resisted all attempts of explanation. A short and intense flash of light is observed when ultrasound-driven air or other gas bubbles in water collapse. This process has been known for more than 60 years to occur randomly when degassed water is irradiated with ultrasound [1]. Recently interest has been revived by the contriving of stable sonoluminescence [2,3] where a bubble is trapped at the pressure antinode of a standing sound wave in a spherical or cylindrical container and collapses and re-expands with the periodicity of the sound. With a clock-like precision a light pulse is emitted during every cycle of the sound wave; the jitter in the sequence of pulses is almost unmeasurably small. Shining laser light upon the bubble and analyzing the scattered light on the basis of the Mie theory of scattering from spherical obstacles one has been able to record the time dependence of the bubble radius [4]; these experiments showed that the flash of light is emitted shortly after the bubble has collapsed, i.e., shortly after it has reached its minimum radius. This and the fact that the spectrum of the emitted light resembles radiation from a black body at several tens of thousands degree kelvin have led to the conjecture that the light could be thermal radiation from the highly compressed and heated gas contents of the bubble after the collapse [5]. It has also been argued that the experimentally observed spectrum would equally well be compatible with the idea of a plasma forming at the bubble center after the collapse and radiating by means of bremsstrahlung [6]. An alternative suggestion has tried to explain the sonoluminescence spectrum as pressure-broadened vibration-rotation lines [7], but although this theory has been very successful in the case of randomly excited (multibubble) sonoluminescence seen in silicone oil it has been inefficacious for sonoluminescence in water.

All of the above theories have serious flaws. Both blackbody radiation and bremsstrahlung would make a substantial part of the radiated energy appear below 200 nm where the surrounding water would absorb it. If one estimates the total amount of energy to be absorbed

corresponding to the observed number of photons above the absorption edge, one quickly convinces oneself that this would be far too much to leave no macroscopically discernible traces in the water, as, for instance, dissociation [8]; however, nothing the like is observed. Another very strong argument against all three of the above theories is that the processes involved in each of them are far too slow to yield pulse lengths of 10 ps or less, but which are observed. Moreover, if a plasma were formed in the bubble, one should see at least remnants of slow recombination radiation from the plasma when the bubble reexpands. As to the theory involving vibration-rotation excitations, the line broadening required to model the observed spectrum seems rather unrealistic.

In its concept the theory to be presented here has been loosely inspired by Schwinger's idea [9] that sonoluminescence might be akin to the Casimir effect, in the sense that the zero-point fluctuations of the electromagnetic field might lie at the origin of the observed radiation. More closely related to this is the Unruh effect well known in field theory [10]; its original statement is that a uniformly accelerated mirror in vacuum emits photons with the spectral distribution of blackbody radiation. However, the phenomenon is far more general than that and in particular not restricted to perfect mirrors. This kind of quantum vacuum radiation has been shown to be generated also by moving dielectrics [11]. Whenever an interface between two dielectrics or a dielectric and the vacuum moves noninertially photons are created. In practice this effect is very feeble, so that it has up to now been far beyond any experimental verification. Sonoluminescence might be the first identifiable manifestation of quantum vacuum radiation.

The mechanism by which radiation from moving dielectrics and mirrors in vacuum is created is understood most easily by picturing the medium as an assembly of dipoles. The zero-point fluctuations of the electromagnetic field induce these dipoles and orient and excite them. However, as long as the dielectric stays stationary or uniformly moving such excitations remain virtual; real photons are created only when the dielectric or mirror moves

NONLINEAR ACOUSTICS

OUTLINE

- I. NONLINEARITY AND WAVEFORM DISTORTION
- II. WEAK SHOCK THEORY
- III. MODEL EQUATIONS
- IV. SOUND BEAMS
- V. DISPERSION
- VI. ACOUSTIC STREAMING
- VII. RADIATION PRESSURE

I. NONLINEARITY AND WAVEFORM DISTORTION

WHAT IS NONLINEAR ACOUSTICS?

Sources of nonlinearity in fluids:

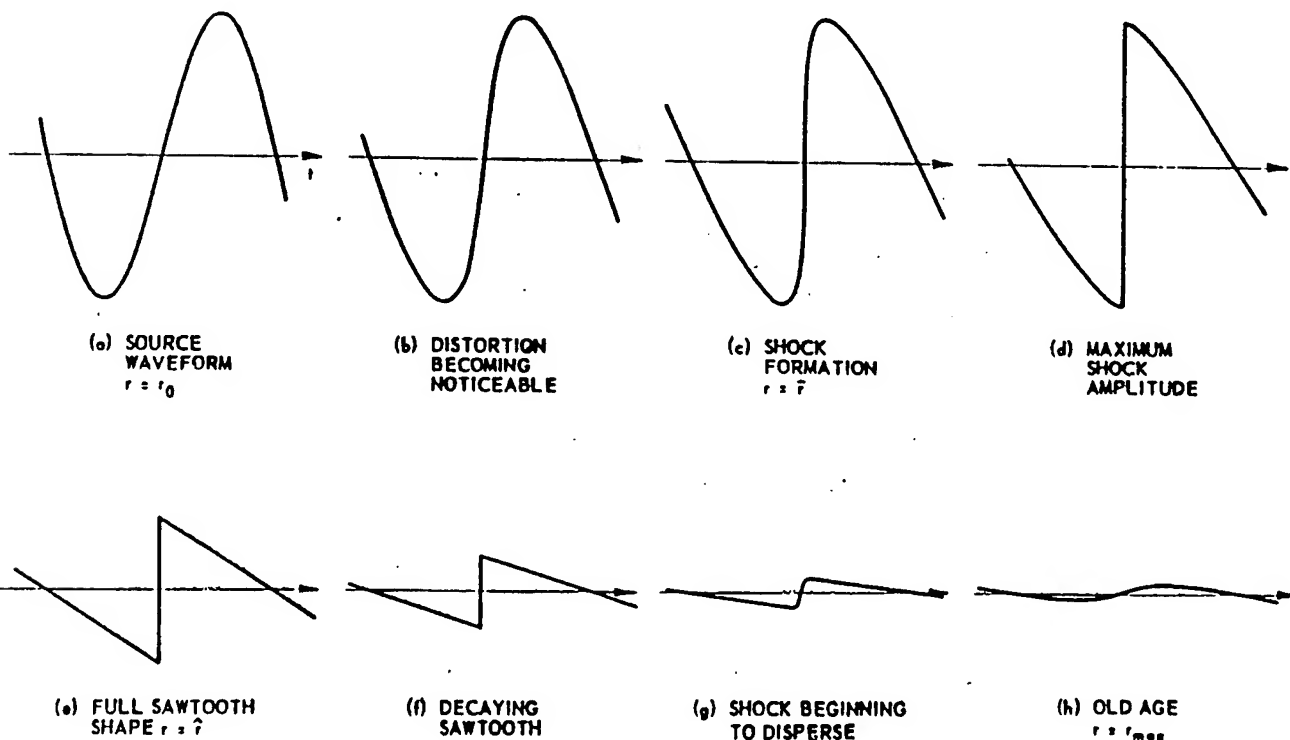
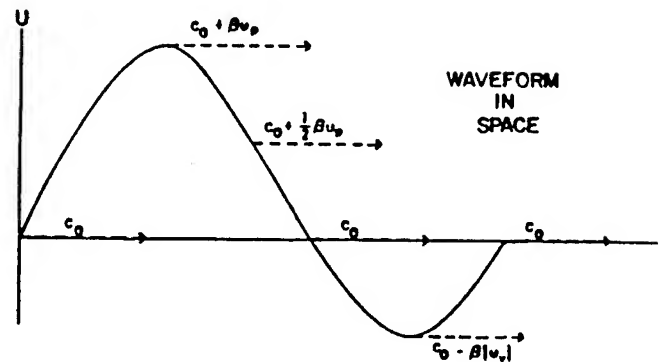
- 1) Equation of state
- 2) Convection

Effects on plane waves:

- Propagation speed varies along waveform

Consequences:

- Wave distortion
- New frequencies
- Radiation pressures
- Acoustical streaming
- Shock waves



PROGRESSIVE PLANE WAVES

Exact equations for an isentropic gas:

Continuity: $\frac{\partial \rho}{\partial t} + u \frac{\partial \rho}{\partial x} + \rho \frac{\partial u}{\partial x} = 0$

Momentum: $\rho \frac{\partial u}{\partial t} + \rho u \frac{\partial u}{\partial x} + \frac{\partial p}{\partial x} = 0$

State: $\frac{p}{p_0} = \left(\frac{\rho}{\rho_0}\right)^\gamma$

Progressive waves (one direction):

$$\boxed{\frac{\partial u}{\partial t} + (c_0 + \beta u) \frac{\partial u}{\partial x} = 0}$$

where

$$c_0 = \sqrt{\frac{\gamma p_0}{\rho_0}} = \text{small signal sound speed}$$

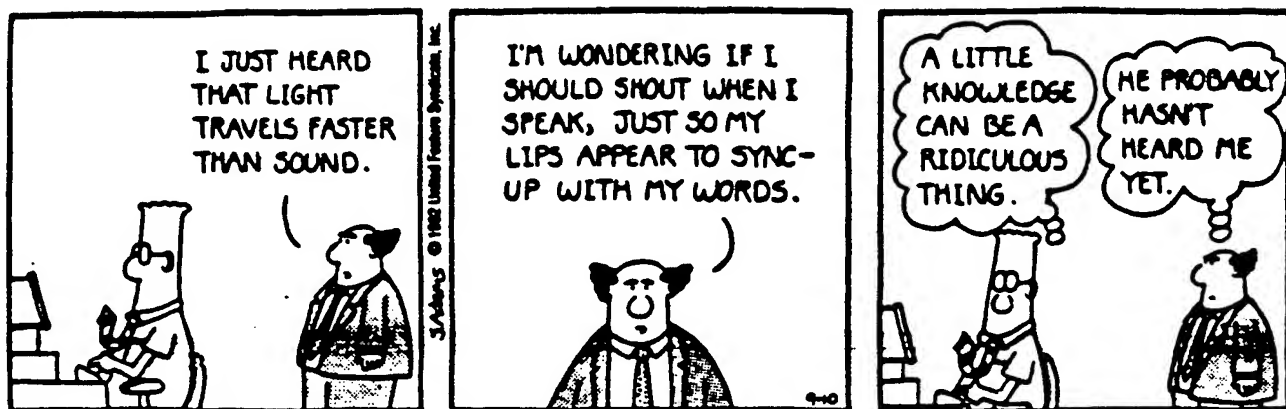
$$\beta = \frac{\gamma+1}{2} = \text{coefficient of nonlinearity}$$

Exact solution:

$$\boxed{u = f\left(t - \frac{x}{c_0 + \beta u}\right)} \quad \text{Poisson, 1808}$$

Propagation speed:

$$\boxed{\frac{dx}{dt} = c_0 + \beta u}$$



PROPAGATION SPEED IN LIQUIDS

Expand general isentropic state equation $p = p(\rho)$:

$$p = p_0 + \left(\frac{\partial p}{\partial \rho}\right)_{s, p_0} (\rho - \rho_0) + \frac{1}{2!} \left(\frac{\partial^2 p}{\partial \rho^2}\right)_{s, p_0} (\rho - \rho_0)^2 + \dots$$

Let $p' = p - p_0$, $\rho' = \rho - \rho_0$:

$$p' = A \frac{\rho'}{\rho_0} + B \frac{1}{2!} \left(\frac{\rho'}{\rho_0}\right)^2 + C \frac{1}{3!} \left(\frac{\rho'}{\rho_0}\right)^3 + \dots$$

where

$$\frac{B}{A} = \frac{\rho_0}{C_0^2} \left(\frac{\partial^2 p}{\partial \rho^2}\right)_{s, p_0} \quad C_0^2 = \left(\frac{\partial p}{\partial \rho}\right)_{s, p_0}$$

Liquids: $5 \lesssim \frac{B}{A} \lesssim 10$

Diatomic Gases: $\frac{B}{A} \approx 0.4 \quad (= \gamma - 1)$

Propagation speed:

$$\frac{dx}{dt} = c_0 + \beta u$$

$$\beta = 1 + \frac{B}{2A}$$

$$= 1.2 \text{ in air}$$

$$= 3.5 \text{ in water}$$

R.T. Beyer
JASA 32
719 (1960)

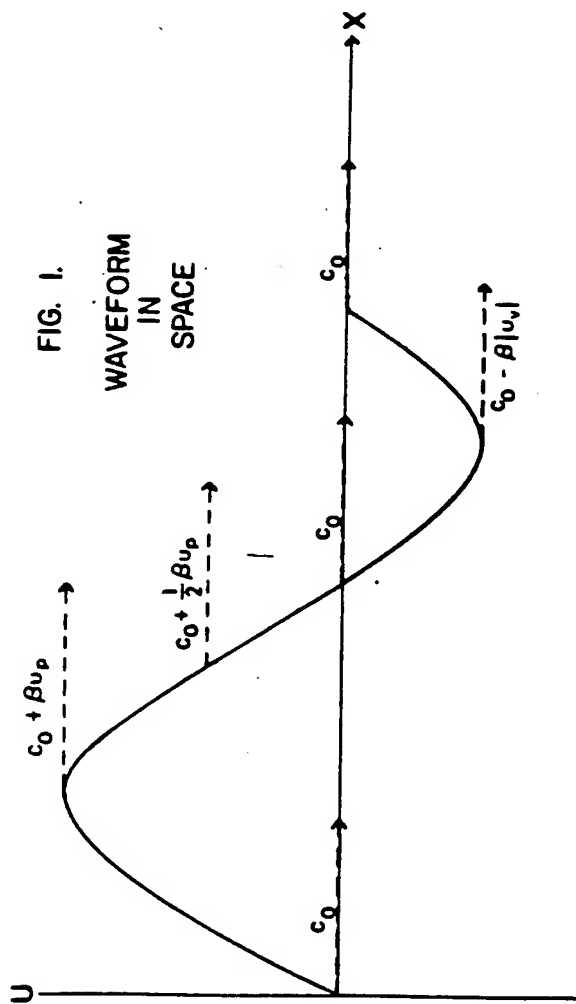
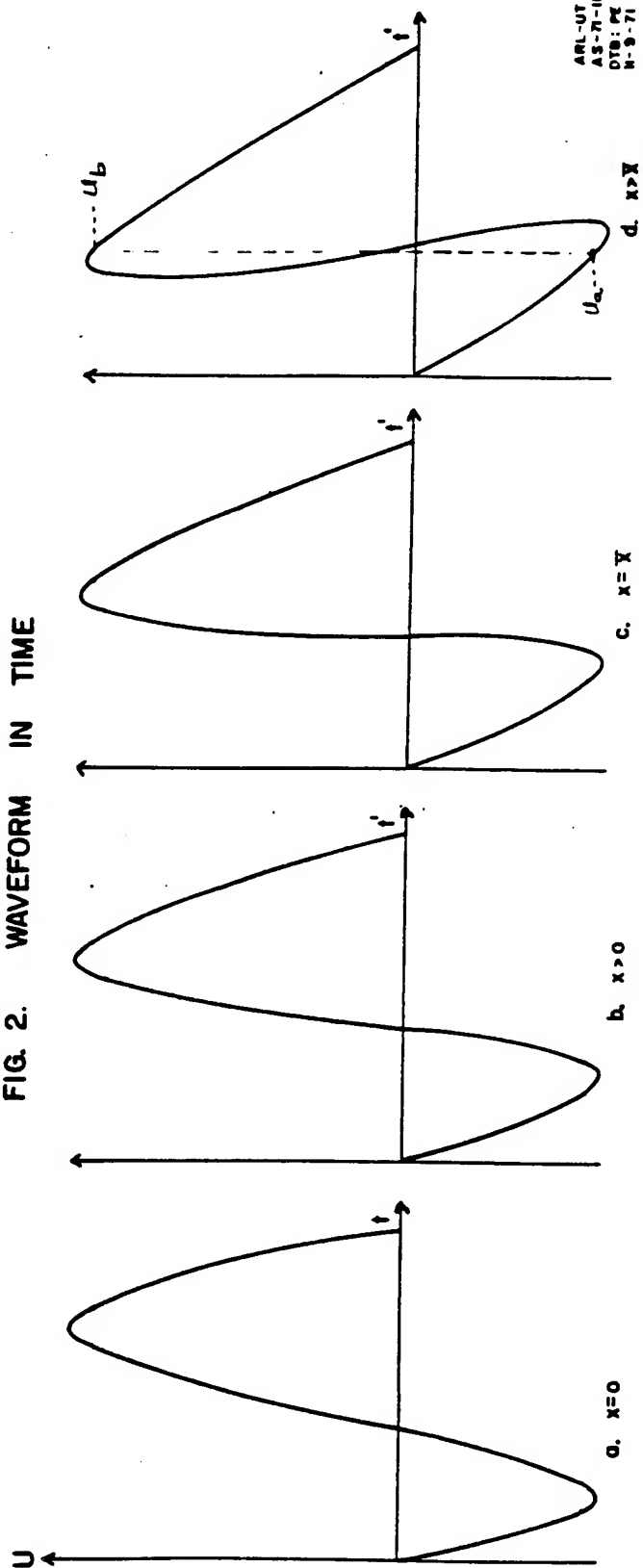


FIG. 2. WAVEFORM IN TIME



ALTERNATIVE FORMS OF B/A, C/A

Basic definitions:

$$A = \rho_0 \left(\frac{\partial P}{\partial \rho} \right)_{s, \rho_0} = \rho_0 c_0^2, \quad B = \rho_0^2 \left(\frac{\partial^2 P}{\partial \rho^2} \right)_{s, \rho_0}, \quad C = \rho_0^3 \left(\frac{\partial^3 P}{\partial \rho^3} \right)_{s, \rho_0}$$

Alternative isentropic forms:

$$\frac{B}{A} = 2 \rho_0 c_0 \left(\frac{\partial c}{\partial P} \right)_{s, \rho_0}$$

$$\frac{C}{A} = \frac{3}{2} \left(\frac{B}{A} \right)^2 + 2 \rho_0^2 c_0^3 \left(\frac{\partial^2 c}{\partial P^2} \right)_{s, \rho_0}$$

- easier to measure change in sound speed as function of pressure
- sound waves can be used to produce the isentropic pressure variations ("finite amplitude method")

"Thermodynamic method":

$$\frac{B}{A} = 2 \rho_0 c_0 \left(\frac{\partial c}{\partial P} \right)_{T, \rho_0} + \frac{2 \alpha_T T_0 c_0}{c_p} \left(\frac{\partial c}{\partial T} \right)_{P, \rho_0}$$

- most accurate method of measurement

[Coppens et al., JASA 38, 797 (1965)]

TABLE I

Values of B/A.
Except Where Indicated, All Values are at Atmospheric Pressure

<u>Substance</u>	<u>T, °C</u>	<u>B/A</u>	<u>Substance</u>	<u>T, °C</u>	<u>B/A</u>
distilled water	0	4.2	methyl acetate	30	9.7
	20	5.0	cyclohexane	30	10.1
	40	5.4	nitrobenzene	30	9.9
	60	5.7	mercury	30	7.8
	80	6.1	sodium	110	2.7
	100	6.1	potassium	100	2.9
<u>Pressure</u>			tin	240	4.4
1 atm	30	5.2	indium	160	4.6
200 kg/cm ²	30	6.2	bismuth	318	7.1
4000	30	6.2			
8000	30	5.9	monatomic gas	20	0.67
			diatomic gas	20	0.40
sea water					
(3.5%)	20	5.25	methyl iodide	30	8.2
methanol	20	9.6	sulfur	121	9.5
ethanol	0	10.4	glycerol (4% H ₂ O)	30	9.0
	20	10.5	1,2 - dichloro-	30	11.8
	40	10.6	hexafluoro-		
n-propanol	20	10.7	cyclopentene		
N-butanol	20	10.7	(DHCP)		
acetone	20	9.2			
beneze	20	9.0			
chlorobenzene	30	9.3			
liquid nitrogen	b.p.	6.6			
benzyl alcohol	30	10.2			
diethylamine	30	10.3			
ethylene glycol	30	9.7			
ethyl formate	30	9.8			
heptane	30	10.0			
hexane	30	9.9			

R.T. Beyer, Nonlinear Acoustics (1974)

Table 1 Some B/A values for biological materials

	Biological material (and state)	Method ^a	B/A (and uncertainty)	Reference
1.	Bovine serum albumin (BSA) (20 g/100 cm ³ , 25°C)	Therm.	6.23 (\pm 0.25)	31
	BSA (22 g/100 cm ³ , 30°C)	F.A.	6.45 (\pm 0.30)	21
	BSA (38.9 g/100 cm ³ , 30°C)	F.A.	6.64	30
	BSA (38.9 g/100 cm ³ , 30°C)	Therm.	6.68 (\pm 0.2)	30
2.	Haemoglobin (50%, 30°C)	F.A.	7.6	22
3.	Whole porcine blood (12% haemoglobin, 7% plasma proteins, 30°C)	F.A.	6.2 (\pm 0.25)	22
4.	Beef liver (Whole, 23°C)	F.A.	7.75 (\pm 0.4)	22
	Beef liver (Homogenized, 23°C)	F.A.	6.8 (\pm 0.4)	22
	Beef liver (Whole, 30°C)	F.A.	6.42	30
	Beef liver (Whole, 30°C)	Therm.	6.88	30
	Beef liver (Whole, 30°C)	Therm.	6.54 (\pm 0.2)	32
	Dog liver (30°C)	F.A.	7.6 - 7.9 (\pm 0.8)	35
	Pig liver (25°C)	F.A.	6.7 (\pm 1.5)	36
	Human liver (Normal, 30°C)	F.A.	7.6 (\pm 0.8)	35
	Human liver (Congested, 30°C)	F.A.	7.2 (\pm 0.7)	35
5.	Pig fat	Therm.	10.9	27
	Pig fat	F.A.	11.0-11.3	27
	Human breast fat (22°C)	Therm.	9.21	32
	Human breast fat (30°C)	Therm.	9.91	32
	Human breast fat (37°C)	Therm.	9.63	32
6.	Canine spleen	F.A.	6.8	37
	Dog spleen	F.A.	6.8 (\pm 0.7)	35
	Human spleen (Congested)	F.A.	7.8	37
	Human spleen (Normal, 30°C)	F.A.	7.8 (\pm 0.8)	35
7.	Beef brain (30°C)	F.A.	7.6	27
8.	Beef heart (30°C)	F.A.	6.8-7.4	27
9.	Pig muscle (30°C)	F.A.	7.5-8.1	27
	Pig muscle (25°C)	F.A.	6.5 (\pm 1.5)	36
10.	Dog kidney (Normal, 30°C)	F.A.	7.2 (\pm 0.7)	35
	Canine kidney (30°C)	F.A.	7.2	37
11.	Human multiple myeloma (22°C)	F.A.	5.6	32
	Human multiple myeloma (30°C)	F.A.	5.8	32
	Human multiple myeloma (37°C)	F.A.	6.2	32

^aTherm. = thermodynamic method; F.A. = finite amplitude method

the state of the tissue. Cancerous tissue normally shows a higher water fraction than normal tissue. The water fraction goes from 0.76 in normal liver tissue to 0.90 for multiple myeloma³². In general, water in tissue may be found as bound water and as free water in equilibrium with one another and expressed by

$$(H_2O)_n \rightleftharpoons n H_2O \quad (12)$$

where $(H_2O)_n$ is referred to as bound water while H_2O is generally referred to as free water. An increase in the bound state means that, on average, molecules have a greater degree of association with the neighbouring molecules which means that they are held more strongly together. This stronger binding also makes a larger ultrasonic pressure necessary in order to stretch the intermolecular bonds into their non-linear region, which macroscopically is being felt as decreased non-linearity of the water according to Equation (3). This suggests that the magnitude of B/A in water-like media may be related to the relative amounts of bound and free water.

The equilibrium between these two water states, for instance expressed through the ratio of bound to free water, is closely related to the state and the nature of the tissue as shown by NMR studies³³. Prospective relations between the ratio of bound to free water and the non-linear parameter B/A , have recently been suggested³⁹. It was concluded by Yoshizumi *et al.*³⁹ that the temperature dependence of B/A , of water for instance, could be due to

the change in the ratio of the bound to the free water with the change in temperature. Whether the estimates of the ratios of bound to free water determined from B/A measurements can be used for characterization of biological media such as human tissue is still an open question which has to be studied more closely.

The existence of several possible relationships between B/A of biological media and other physical qualities such as intermolecular potentials, macrostructure, water fraction and ratio of bound to free water of the biological media emphasize the need for further systematic studies. This will probably demand an internationally funded research programme where several qualified laboratories in various countries share a research programme over several years on advanced modelling of biological media.

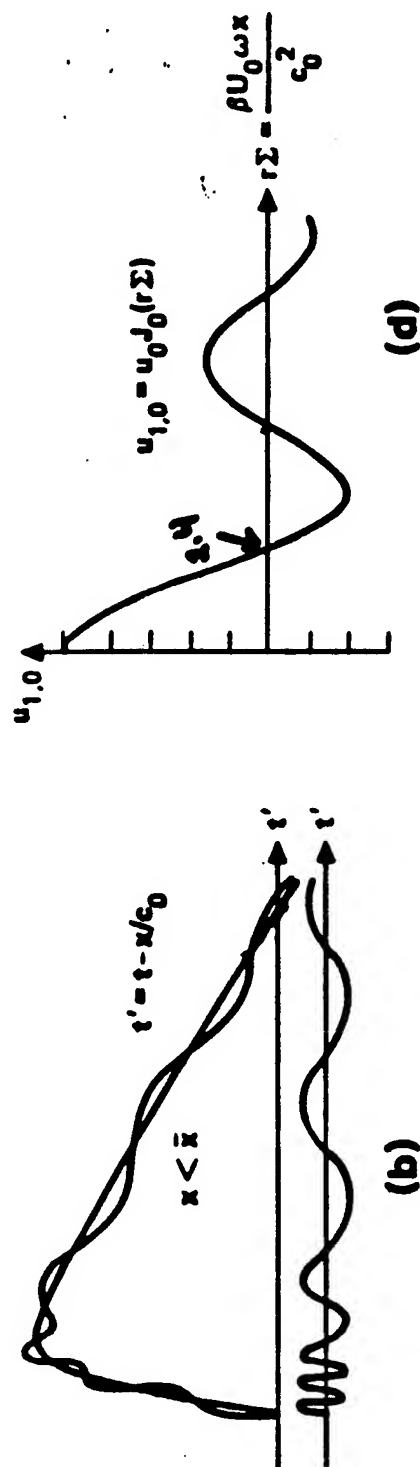
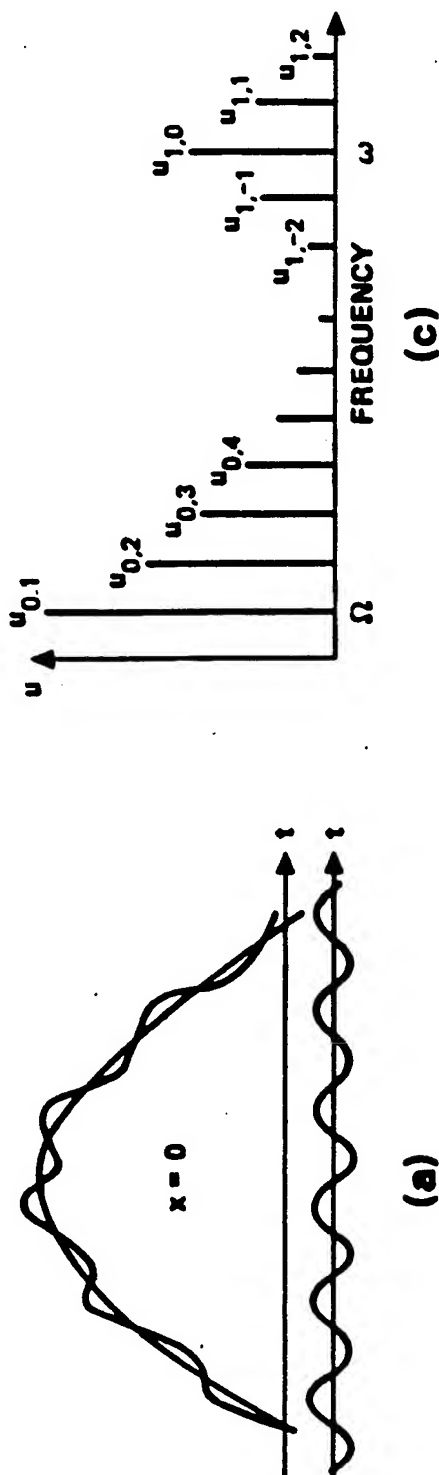
In spite of the inhomogeneous character of biological materials such as tissues, where scattering, phase cancellations, dispersion, etc. influence the ultrasonic wave propagation, a reliable experimental procedure leading to reproducible B/A data should be developed to prove, *in vitro*, that B/A may be used for the characterization of biological media. If the uncertainties found in relation to the experimental data could be reduced for the thermodynamic or for the finite amplitude method - or maybe for both - an answer to the question of applicability of B/A for characterization of biological media may be found.

The prospective development of a clinically applicable

in vivo method picture of the using non-in towards a ge of biological ultrasonic qu Research present going world⁴⁰, but wide collabor problems. T creation of distortion e ultrasonic e future not on physics, the may be found reproducible place. This co-ordinated will, undout

Reference

1. Bjørnø, L. objective 83 Butter
2. Bjørnø, L. Progress Chapma
3. Dunn, F. absorptio
4. Muir, T. acoustic sound in
5. Carstens Demon-frequen 359
6. Goss, S. focused absorptio (1981) St
7. Carstens Finite an in tissue 302
8. Beyer, R. (1960) 3
9. Bjørnø, paramo (Eds N FRG (
10. Rao, M. molecu
11. Carstens sound p (1955) 2
12. Hartma liquids.
13. Apfel, R. liquid 1
14. Apfel, I. measur 148
15. Goss, compil tissue J
16. Hama,



SUPPRESSION OF SOUND BY SOUND

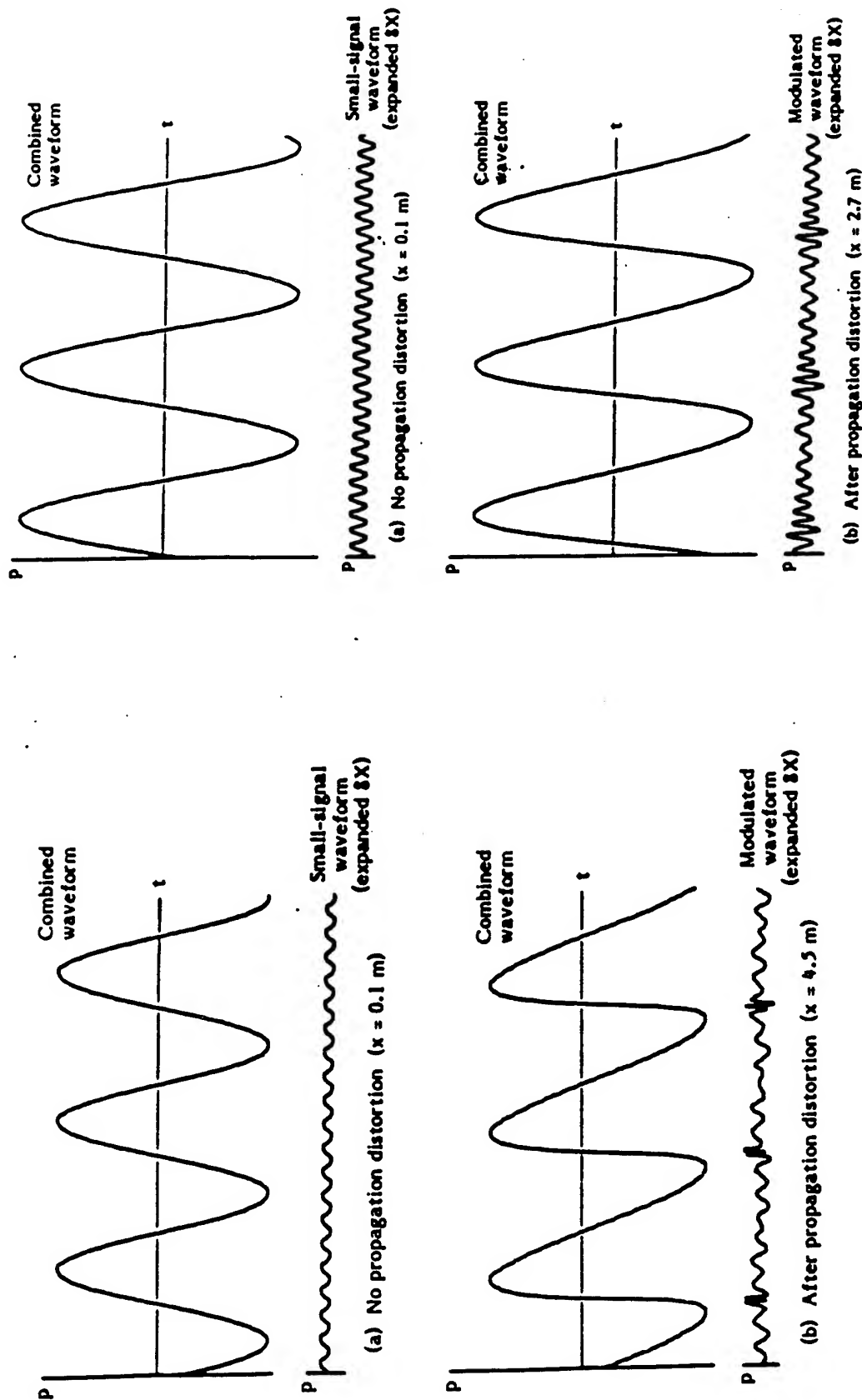


Figure 4.3
Demonstration of the noncollinear
modulation of sound by sound

Figure 4.1
Demonstration of the collinear
modulation of sound by sound

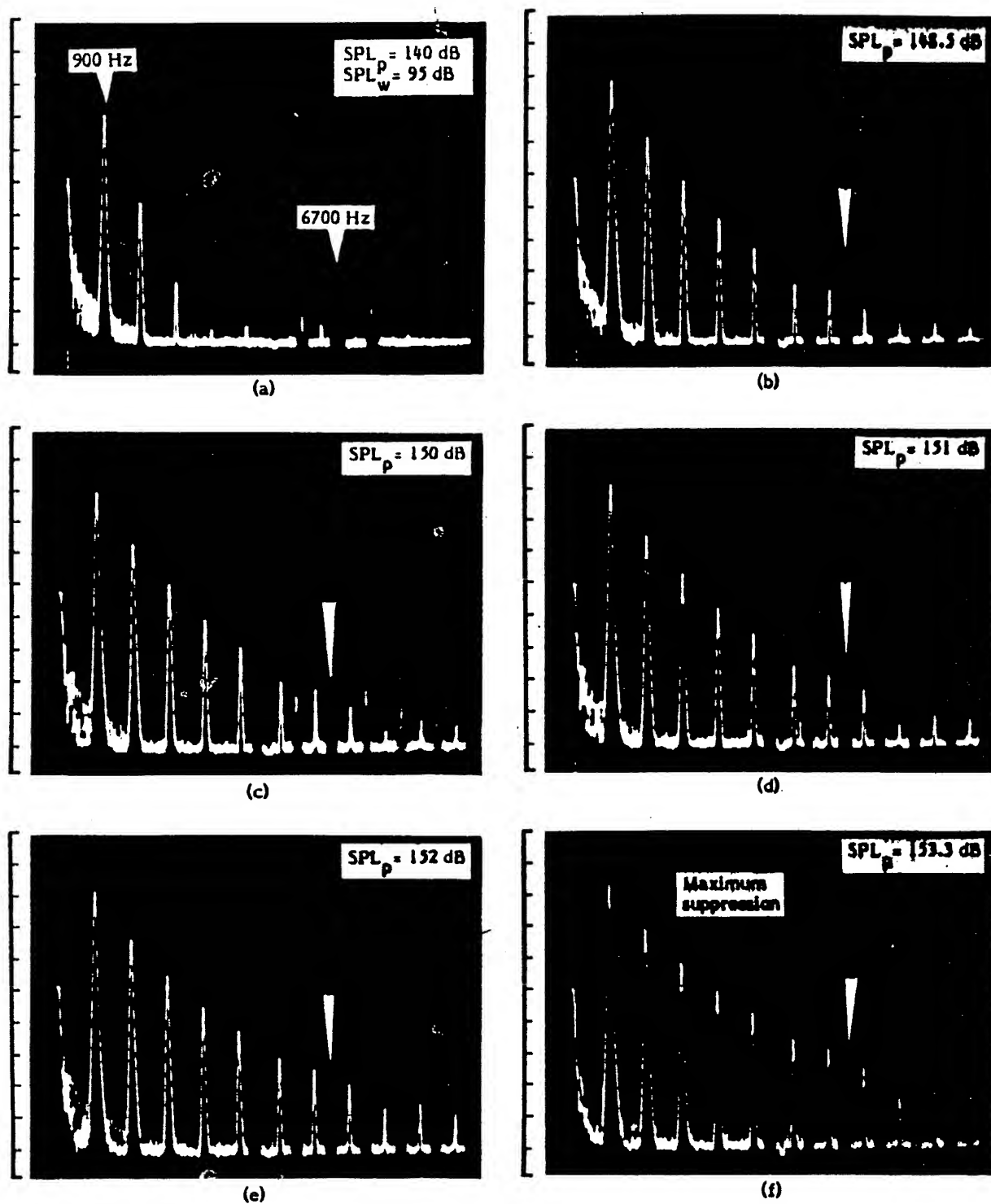


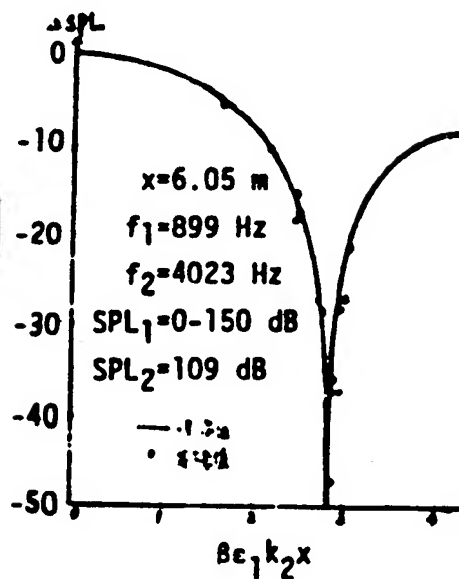
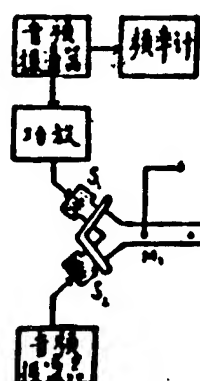
Figure 4.4
 Observation of the
 modulation of sound by sound
 in the frequency domain

GONG, ZHU, DU (1979)

有限振幅与小振幅平面声波的

非线性相互作用研究

(Nonlinear Interaction of a Finite-Amplitude Wave
with a Small-Signal Wave in Air)



Ref. 59

COEFFICIENT OF NONLINEARITY FOR COMPRESSION WAVES IN ELASTIC SOLIDS

Shock Formation Distance:

$$\bar{x} = \frac{1}{\beta \epsilon k}$$

where

ϵ = Mach number or strain

k = wavenumber

β = coefficient of nonlinearity

$$= - \left(\frac{3}{2} + \frac{A + 3B + C}{\rho c_l^2} \right)$$

substance	β
air	1.2
water	3.5
iron	4.4
plastic foam	~ 100
marble	~ 800
sediment	$\sim 10^2 - 10^3$
rock	$> 10^4$

L. A. Ostrovsky, *J. Acoust. Soc. Am.* **90**, 3332 (1991)

Nonlinear Energy of Deformation

- Isotropic solid to cubic order in strain is (Landau's notation)

$$E = \mu e_{ik}^2 + \left(\frac{1}{2}K - \frac{1}{3}\mu\right) e_{jj}^2 + \frac{1}{3}\mathcal{A}e_{ik}e_{ij}e_{kj} + \mathcal{B}e_{ik}^2e_{jj} + \frac{1}{3}\mathcal{C}e_{jj}^3,$$

where

$$e_{ik} = \frac{1}{2} \left(\frac{\partial u_i}{\partial X_k} + \frac{\partial u_k}{\partial X_i} + \frac{\partial u_j}{\partial X_i} \frac{\partial u_j}{\partial X_k} \right)$$

is the Lagrangian strain tensor. Thus,

$$\begin{aligned} E &= E_2 + E_3, \\ E_2 &= \frac{1}{4}\mu \left(\frac{\partial u_i}{\partial X_k} + \frac{\partial u_k}{\partial X_i} \right)^2 + \left(\frac{1}{2}K - \frac{1}{3}\mu \right) \left(\frac{\partial u_j}{\partial X_j} \right)^2, \\ E_3 &= \left(\mu + \frac{1}{4}\mathcal{A} \right) \frac{\partial u_i}{\partial X_k} \frac{\partial u_j}{\partial X_i} \frac{\partial u_j}{\partial X_k} + \left(\frac{\mathcal{B}}{2} + \frac{K}{2} - \frac{\mu}{3} \right) \frac{\partial u_j}{\partial X_j} \left(\frac{\partial u_i}{\partial X_k} \right)^2 \\ &\quad + \frac{\mathcal{A}}{12} \frac{\partial u_i}{\partial X_k} \frac{\partial u_k}{\partial X_j} \frac{\partial u_j}{\partial X_i} + \frac{\mathcal{B}}{2} \frac{\partial u_i}{\partial X_k} \frac{\partial u_k}{\partial X_i} \frac{\partial u_j}{\partial X_j} + \frac{\mathcal{C}}{3} \left(\frac{\partial u_j}{\partial X_j} \right)^3. \end{aligned}$$

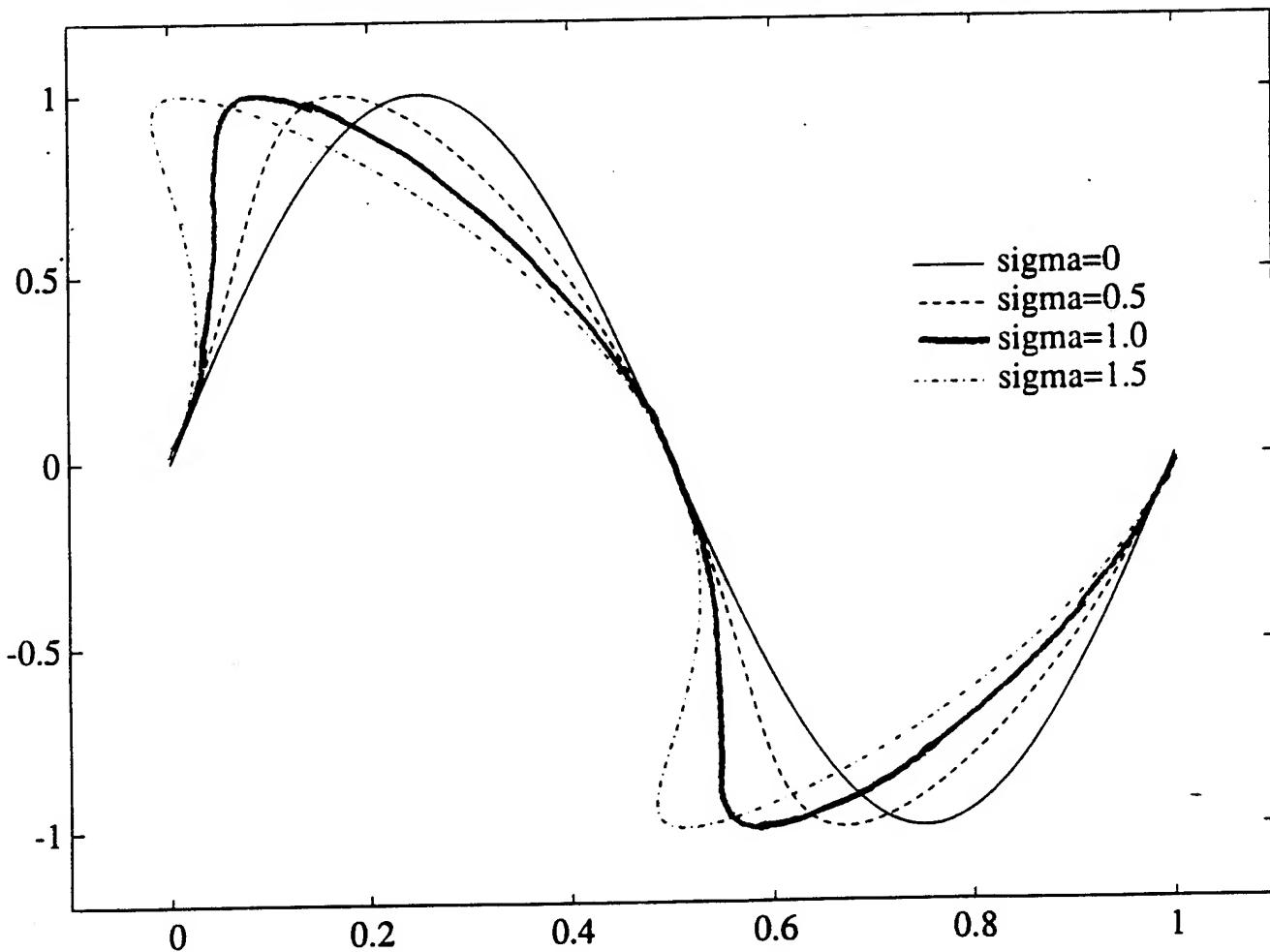
SHEAR WAVES

Model Equation for Plane Waves:

$$\frac{\partial v}{\partial x} = v^2 \frac{\partial v}{\partial \tau} \quad \left(\frac{dx}{dt} = c_t + \beta v^2 \right)$$

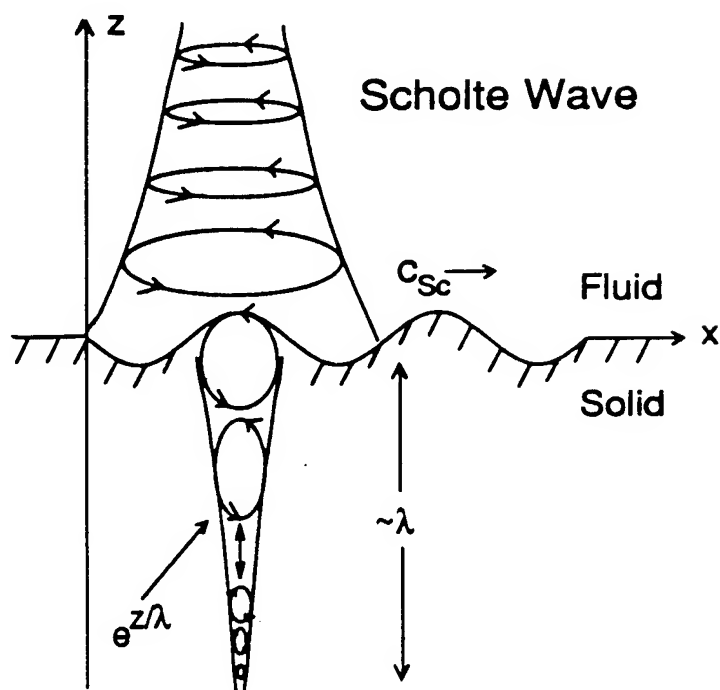
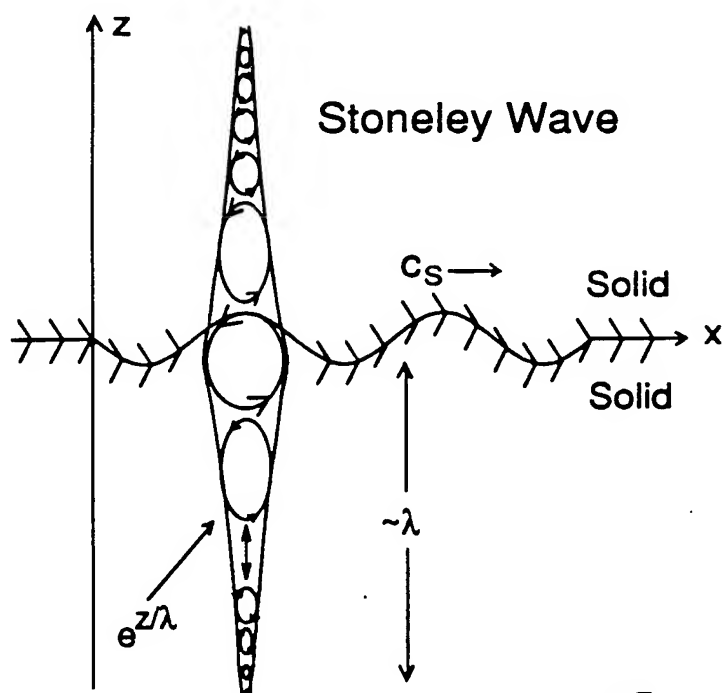
- cubic nonlinearity

Shear wave distortion of a sine wave in retarded time.

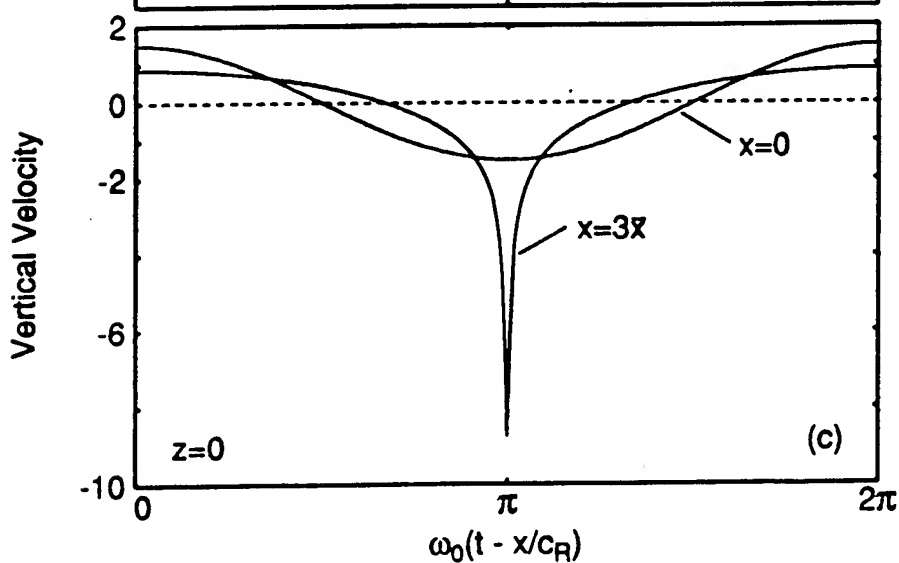
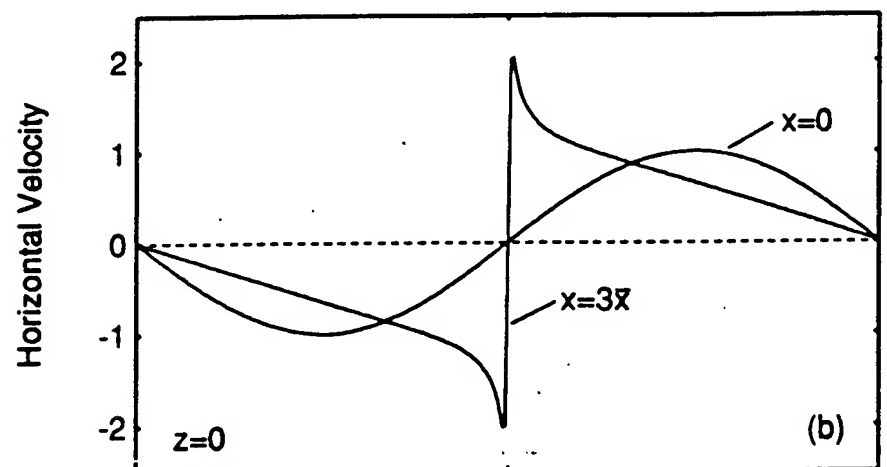
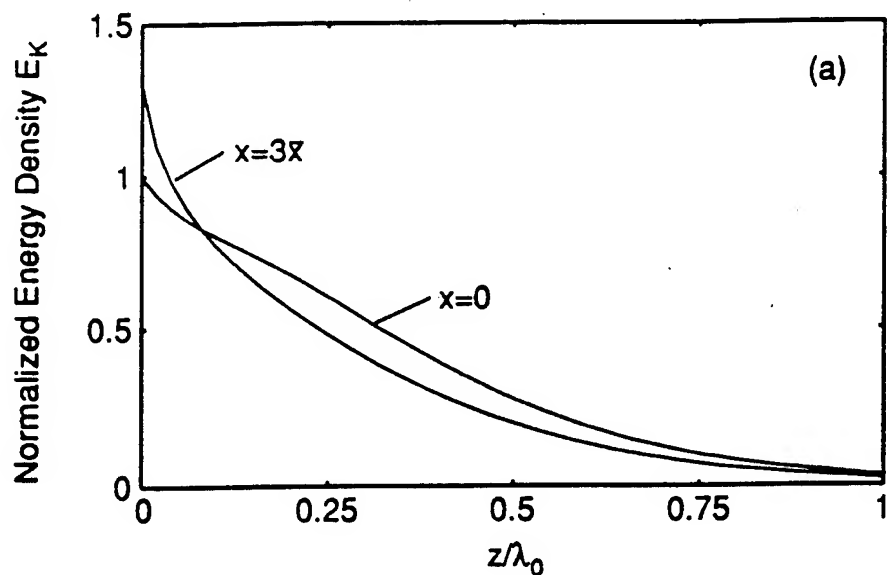


Linear Surface Waves

- Rayleigh (1885)
- Stoneley (1924)
- Scholte (1942)

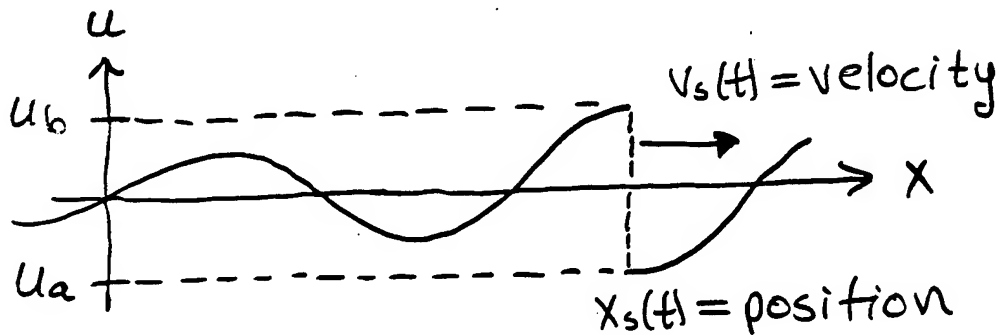


Nonlinear Rayleigh Wave Distortion



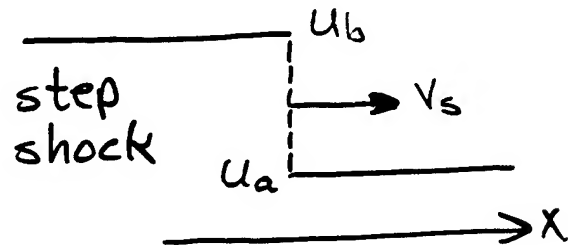
II. WEAK SHOCK THEORY

WEAK SHOCK THEORY



I. Weak Shock Limit of Rankine-Hugoniot Relations

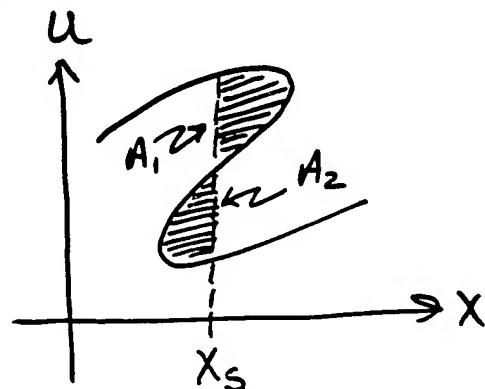
$$V_s = c_0 + \frac{\beta}{2} (u_a + u_b)$$



II. Landau's Equal Area Rule

Determine position x_s of shock by equating "areas"

$$A_1 \equiv A_2$$



- Perfect discontinuities (jumps) assumed; shock structure (e.g., rise time) not described

Finally
since that

Since (v/v_0)
limits from
rangement

which show
periodic v
of the init

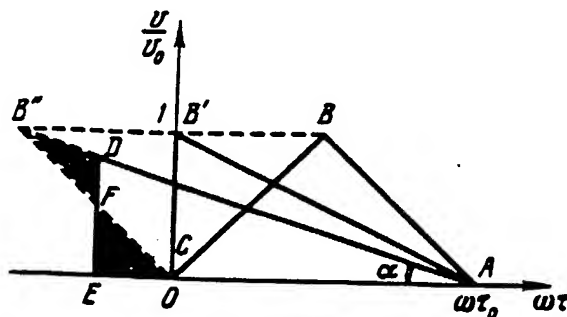


Fig. 1.13. Change in the shape of a single triangular pulse.

Everything that has been said in this section applies to the behavior of a periodic signal in a nonlinear medium, which is harmonic at the input to the system. As a conclusion, we consider the progress of the propagation of a uniform disturbance.

Let the profile of the initial disturbance have the form of an isosceles triangle ABC, drawn in Fig. 1.13. The discontinuity is formed here at the point $\sigma = \omega_0 \tau / 2$. It is easy to see that in the region $0 < \sigma < \omega_0 \tau / 2$, the area of the profile does not change and is equal to $\omega_0 \tau / 2$. When the pulse passes the point $\sigma = \omega_0 \tau / 2$, its leading edge CB takes the position CN' and then at some $\sigma > \omega_0 \tau / 2$, the position CB''.

As we already know, in place of CB'' we have the discontinuity ED, constructed so that the areas of the triangles CEF and FDB'' are equal. But this means that the areas of the triangles ABC and ADE are also equal, i.e., the conservation of momentum holds in lowest approximation. The formation of a discontinuity consequently leads to the spreading out of the disturbance and a "smearing out" of its amplitude throughout the medium.

From the condition of equality of the areas ABC and ADE, $\frac{\omega_0 \tau}{2} = \frac{1}{2} AE^2 \tan \alpha = \frac{1}{2} \frac{AE^2}{\sigma + \omega_0 \tau / 2}$, we can establish the formulas which describe the spreading out at $\sigma > \omega_0 \tau / 2$:

$$AE = \omega_0 \tau \sqrt{\frac{1}{2} + \frac{\sigma}{\omega_0 \tau}} \quad (5.21)$$

and the decrease in the amplitude of the discontinuity $ED = AE \tan \alpha$:

$$ED = \frac{1}{\sqrt{\frac{1}{2} + \frac{\sigma}{\omega_0 \tau}}} \quad (5.22)$$



N WAVES

Sources:

- sonic booms
- sparks
- lithotripters
- thunder
- explosions
- bullets

(rise time)

10^{-3} sec

(duration)

10^{-1} sec

10^{-6} sec

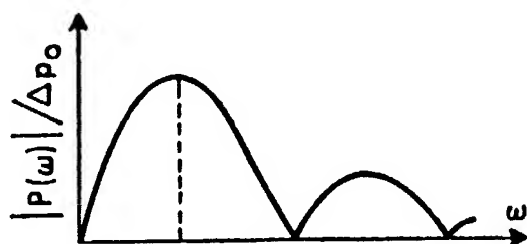
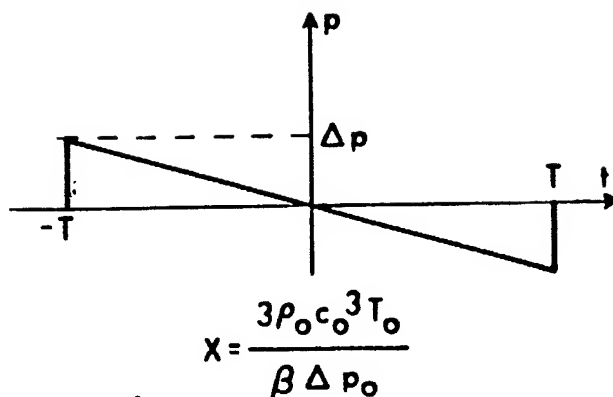
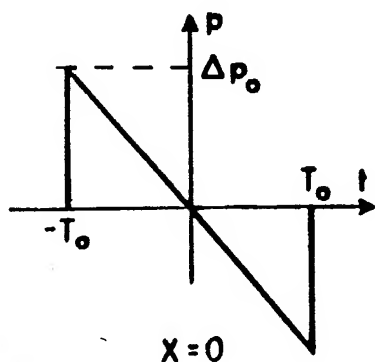
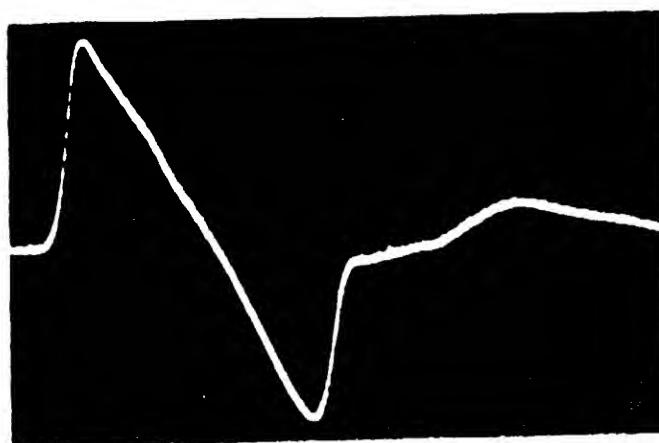
10^{-5} sec

10^{-9} sec

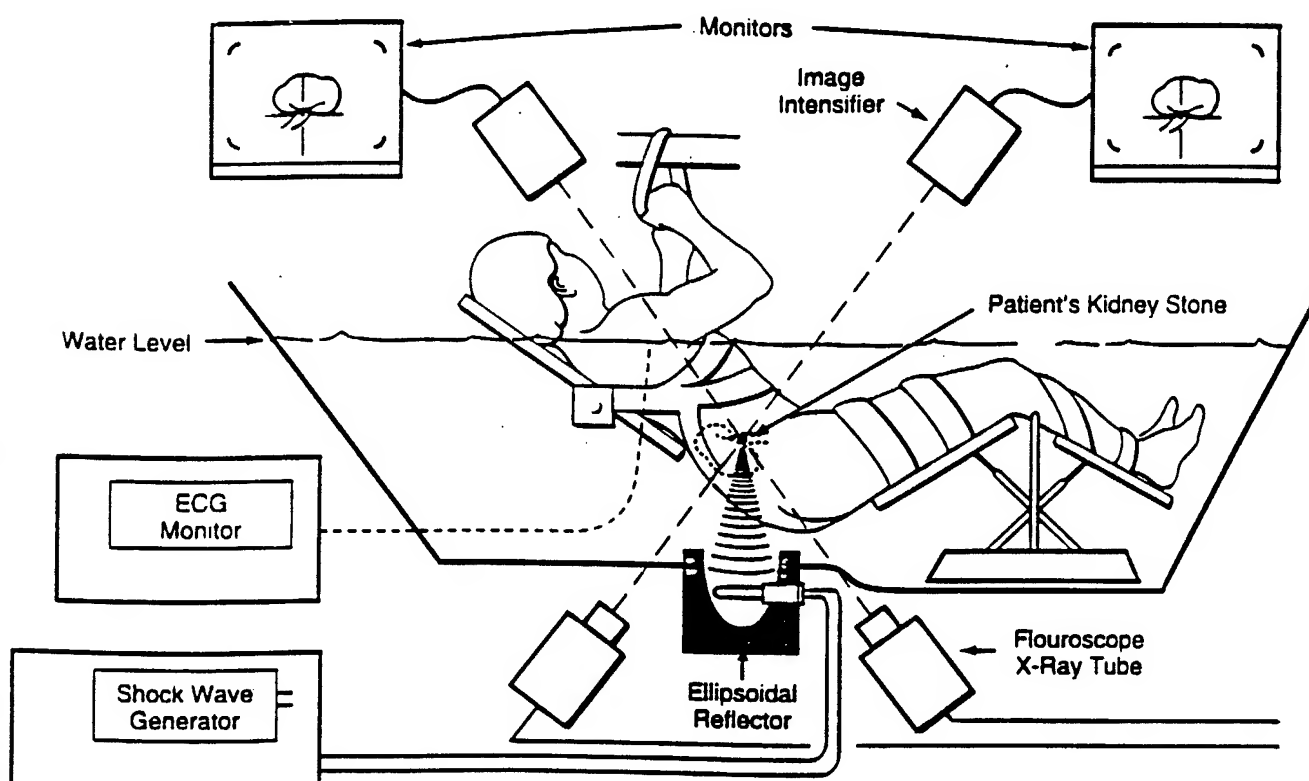
10^{-6} sec

$$\Delta p \sim \frac{1}{\sqrt{x}}$$

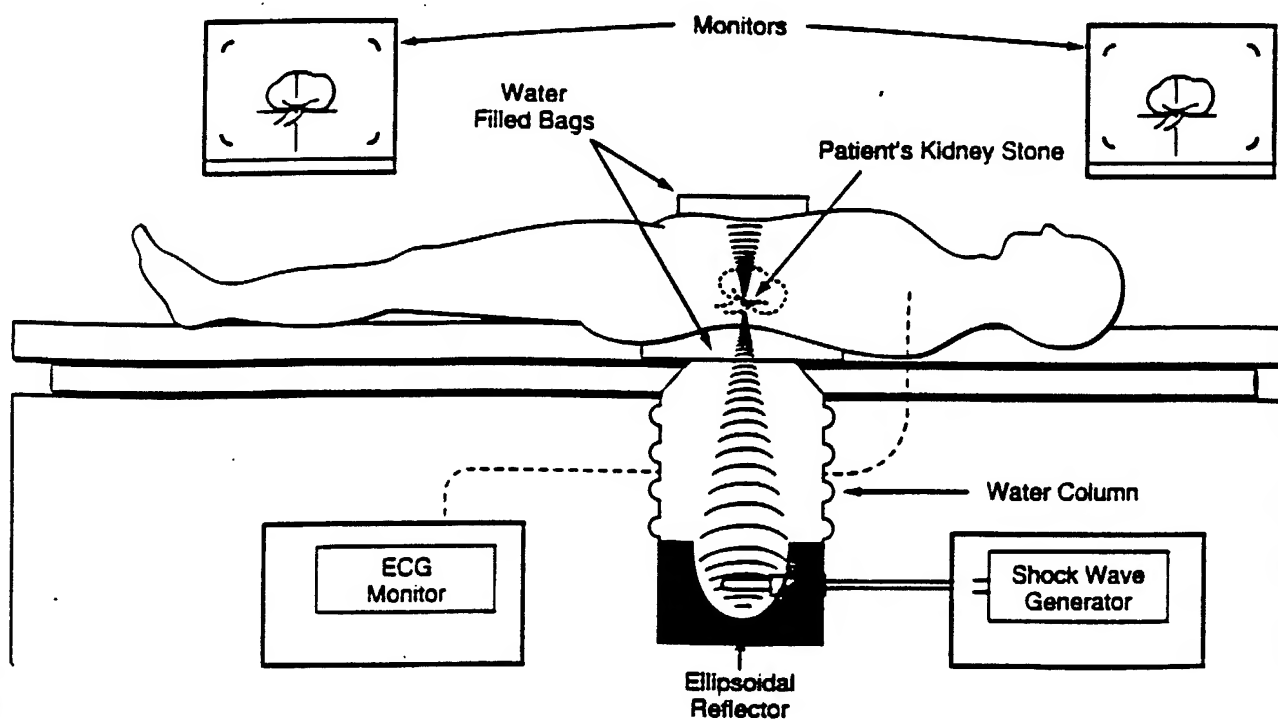
$$T \sim \sqrt{x}$$



First-Generation Extracorporeal Shock Wave Lithotripter



Second-Generation Extracorporeal Shock Wave Lithotripter



THEORETICAL PREDICTIONS OF THE ACOUSTIC PRESSURE GENERATED BY A SHOCK WAVE LITHOTRIPTER

A. J. COLEMAN, M. J. CHOI and J. E. SAUNDERS
Medical Physics Department, St. Thomas' Hospital, London SE1 7EH, UK

(Received 5 July 1990; in final form 1 October 1990)

Ultrasound in Med. & Biol. Vol. 17, No. 3, pp. 245-255, 1991
Printed in the U.S.A.

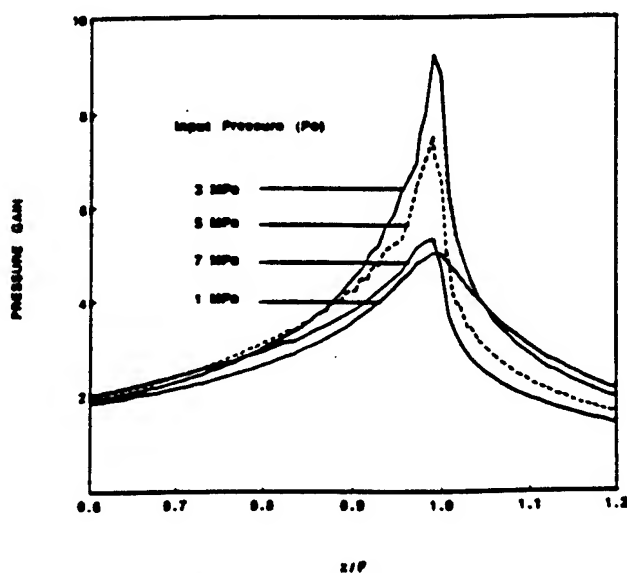
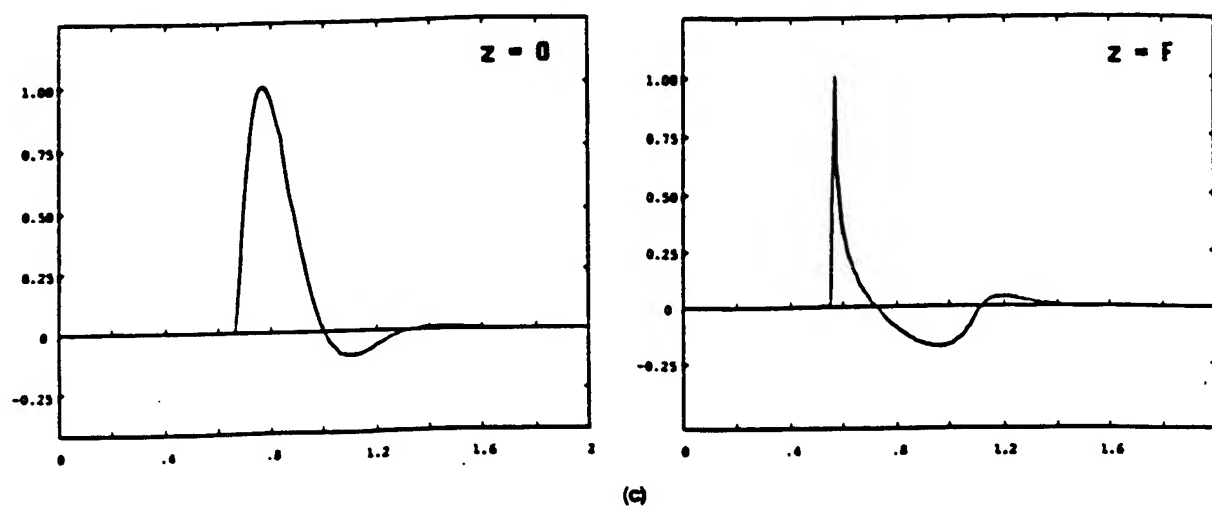


Fig. 4. Plots of the peak positive pressure gain (p^+/p_a) along the beam axis, z/F , calculated for a pulsed (exponentially damped sinusoidal) aperture waveform with peak pressures, p_a , of 1, 3, 5 and 7 MPa ($n_{\text{max}} \geq 384$). The curve for 5 MPa is shown as a dotted line and corresponds to that predicted for the Dornier HM3 operated at around 20 kV

FOURIER ANALYSIS

Source Condition:

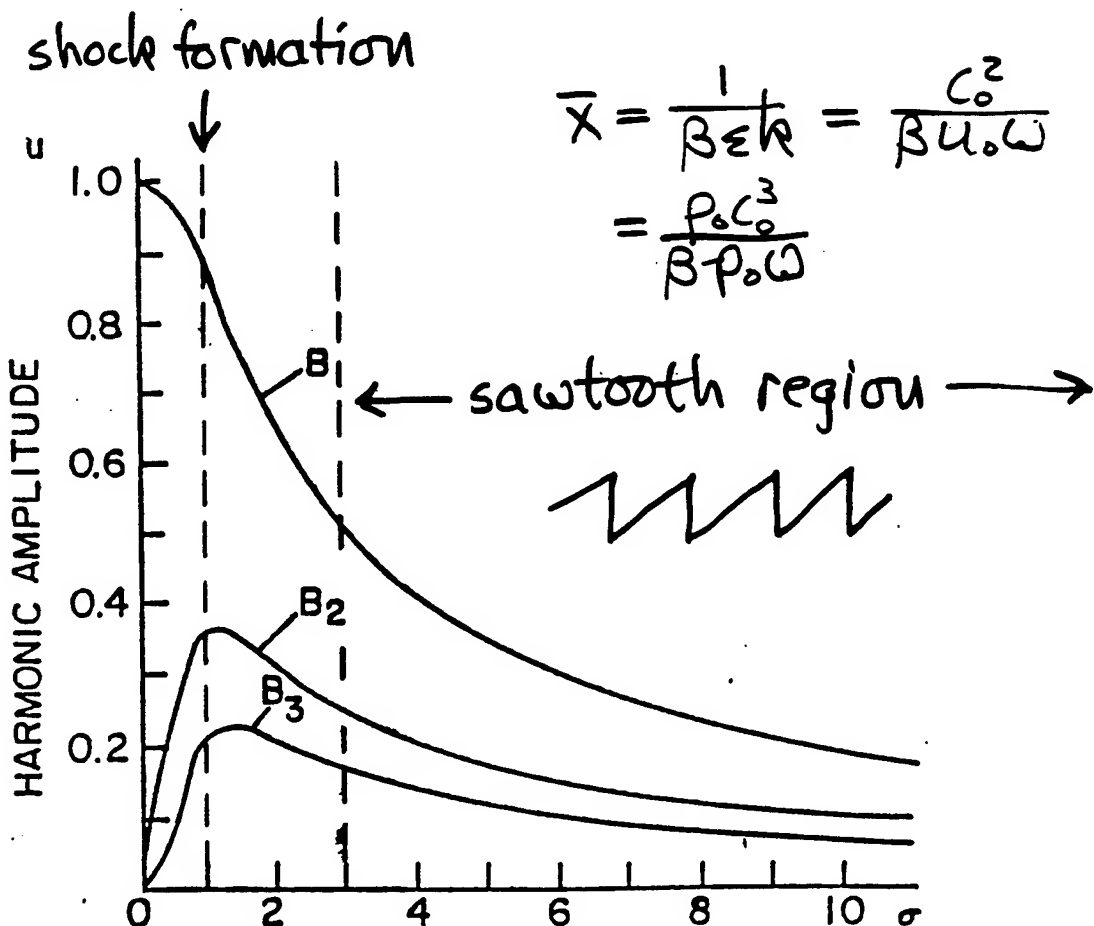
$$u(0, \tau) = u_0 \sin \omega \tau$$

Fourier Series Solution:

$$u(\sigma, \tau) = u_0 \sum_{n=1}^{\infty} B_n(\sigma) \sin n\omega \tau, \quad \sigma = \frac{\beta \omega u_0 x}{c_0^2}$$

$$B_n(\sigma) = \frac{2 J_n(n\sigma)}{n\sigma}, \quad \sigma < 1 \quad (= x/\bar{x})$$

$$= \frac{2}{n(1+\sigma)}, \quad \sigma \geq 1 \quad (\text{sawtooth})$$



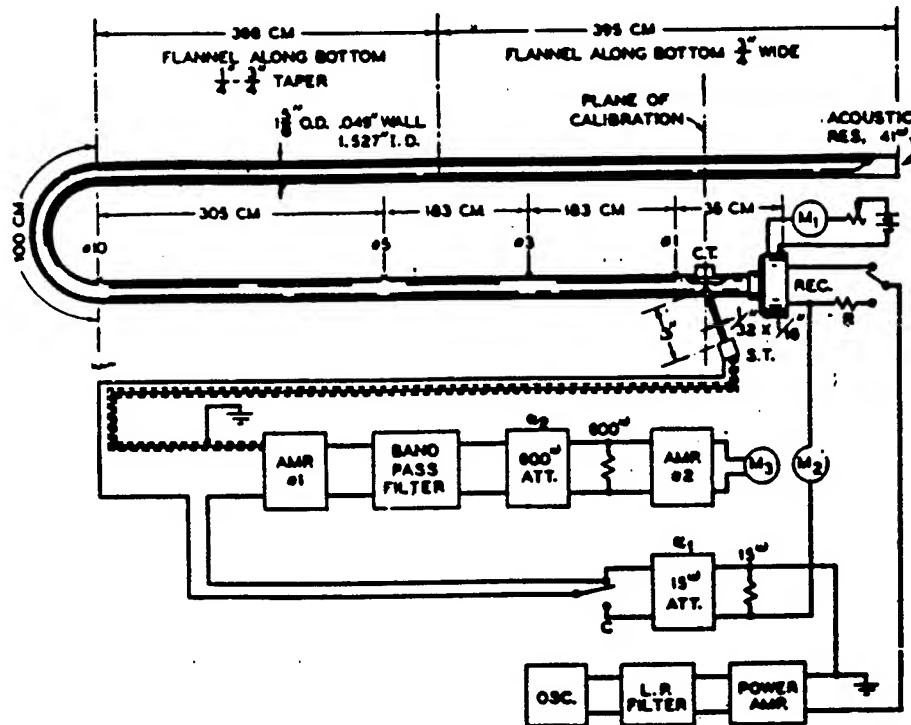


FIG. 2. Apparatus for measuring extraneous frequencies generated in air carrying intense sound waves. C.T., calibrating transmitter; S.T., search transmitter; R, resistance substitute for receiver.

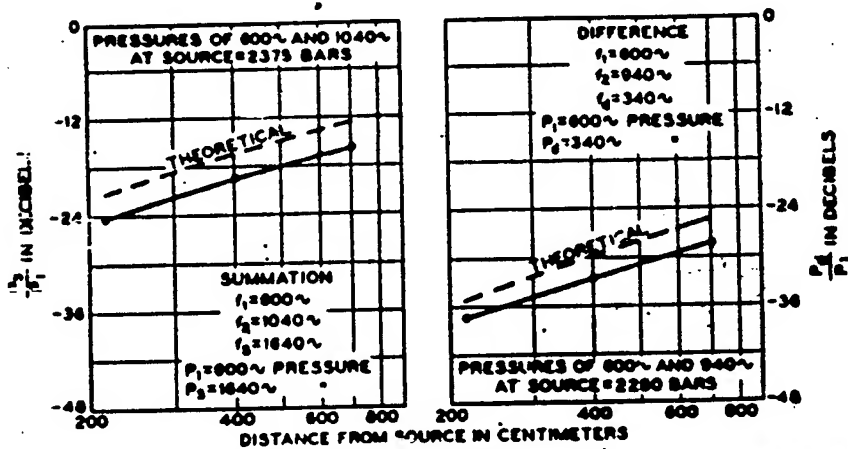


FIG. 6. Magnitude of summation and difference frequencies vs. distance from source.

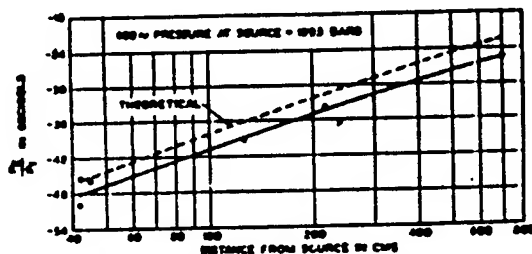


FIG. 3. Magnitude of 2nd harmonic vs. distance from source.

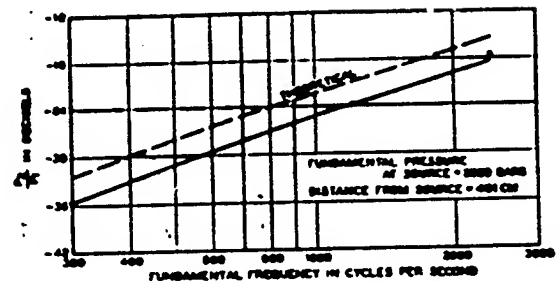


FIG. 4. Variation of 2nd harmonic magnitude with frequency of fundamental.

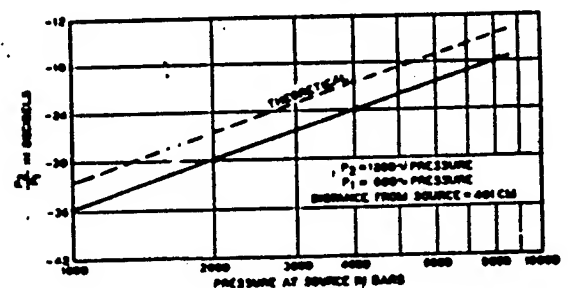


FIG. 5. Variation of 2nd harmonic pressure with fundamental pressure.

ACOUSTIC SATURATION

Use sawtooth solution ($\sigma \geq 3$)

$$u = u_0 \sum_{n=1}^{\infty} \frac{2}{n(1+\sigma)} \sin n\omega t, \quad \sigma = \frac{\beta \omega u_0 X}{c_0^2}$$

and let $\sigma \gg 1$:

$$\begin{aligned} u &\sim u_0 \sum_{n=1}^{\infty} \frac{2}{n \beta \omega u_0 X / c_0^2} \sin n\omega t \\ &= \frac{2c_0^2}{\beta \omega X} \sum_{n=1}^{\infty} \frac{1}{n} \sin n\omega t \end{aligned}$$

→ No dependence on u_0 !

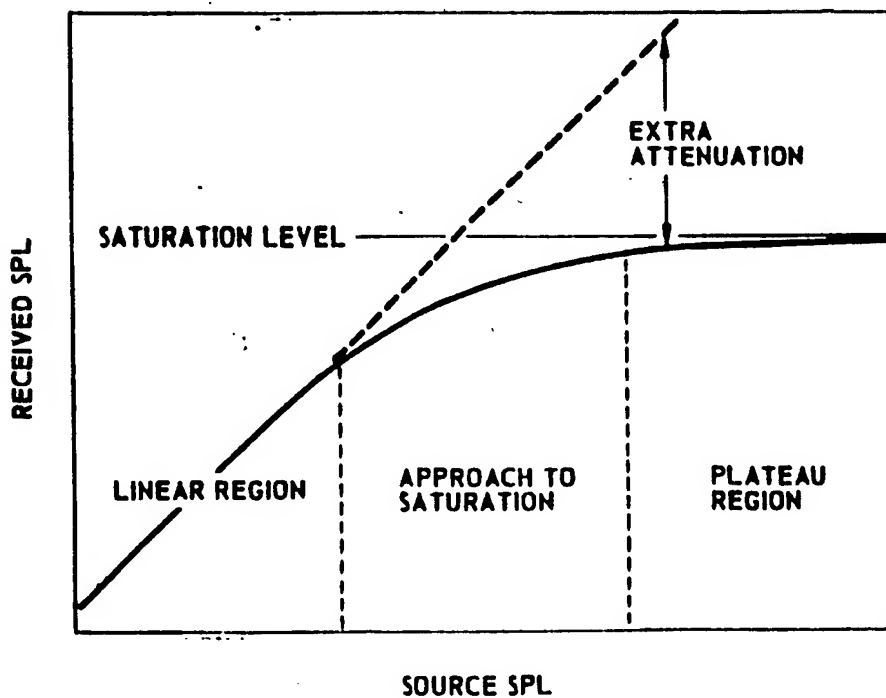


FIGURE 1.1
THE DEVELOPMENT OF SATURATION

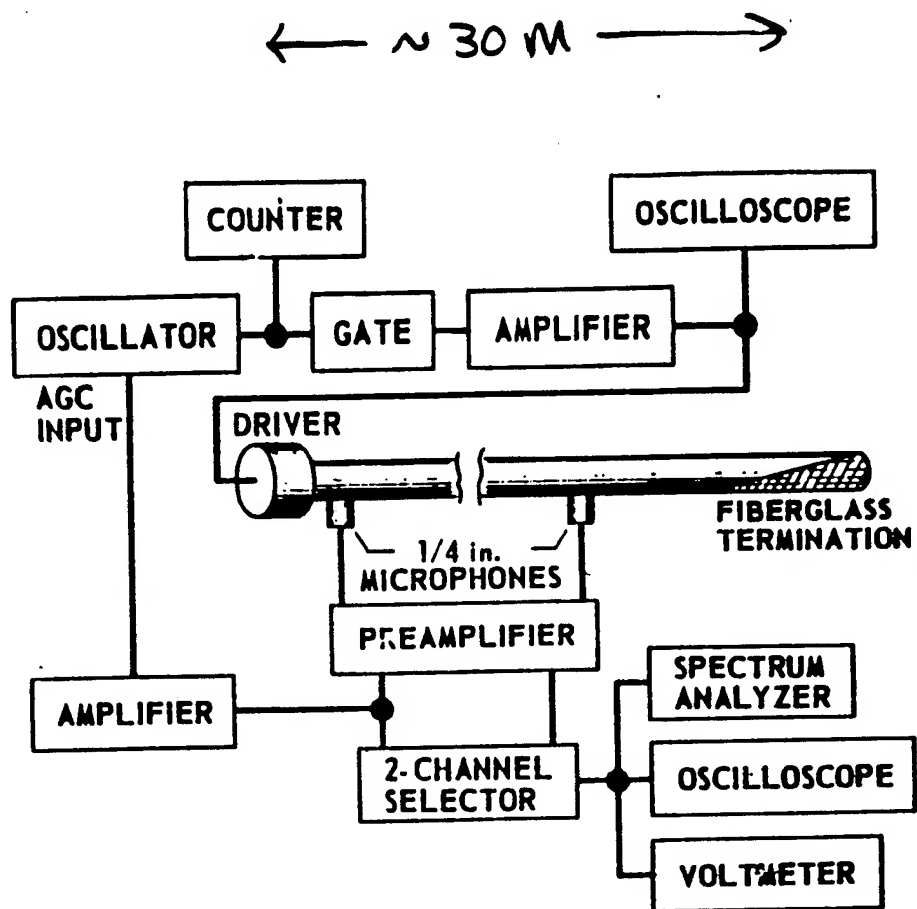


FIGURE 4-1
BLOCK DIAGRAM OF THE EXPERIMENTAL APPARATUS

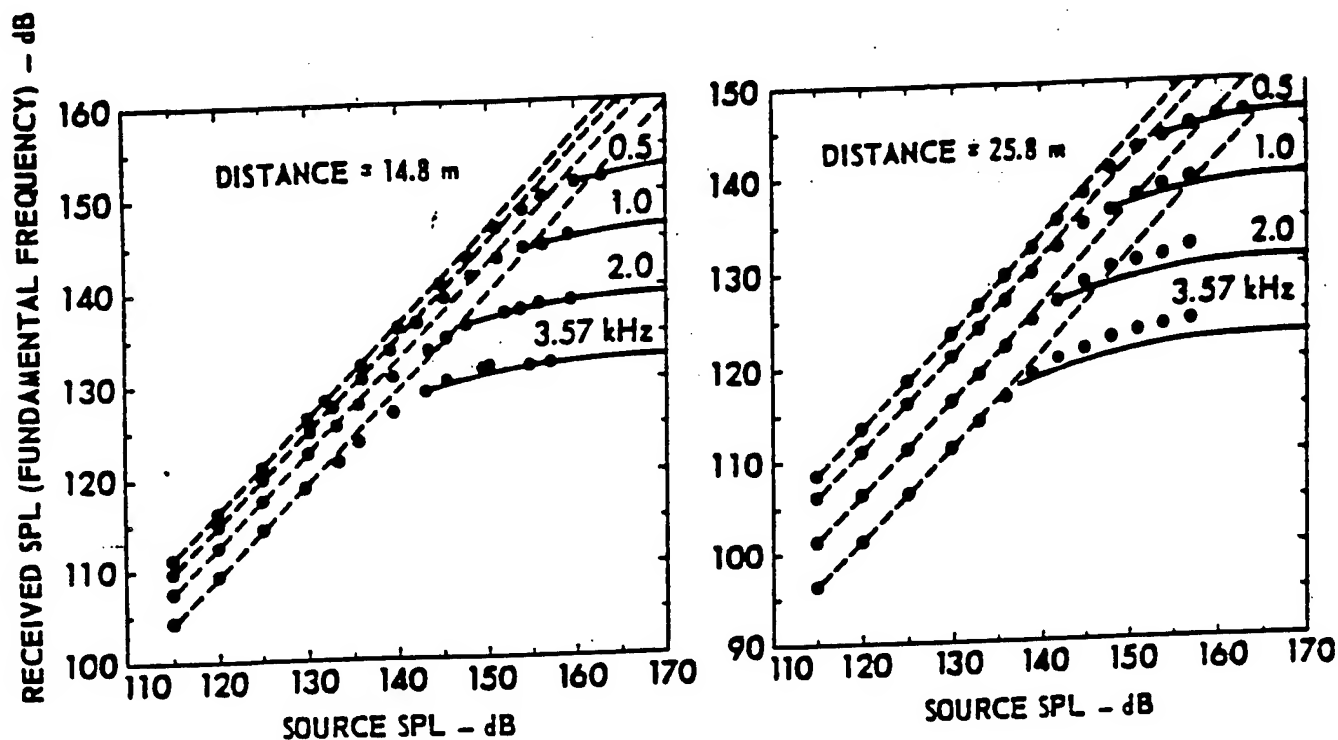


FIGURE 5-5
AMPLITUDE RESPONSE CURVES AT
FUNDAMENTAL FREQUENCY

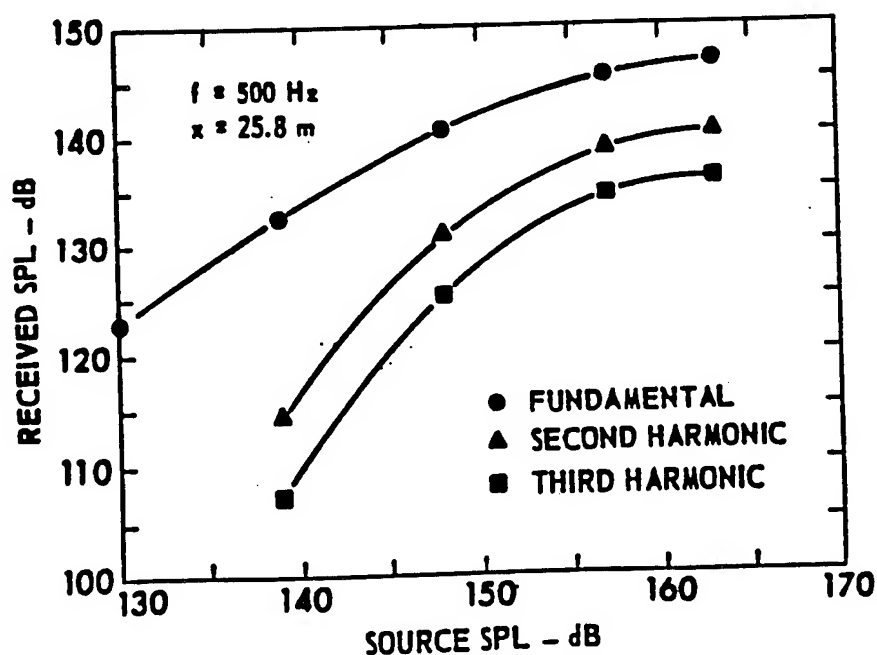


FIGURE 5-6
AMPLITUDE RESPONSE CURVES FOR
THE FIRST THREE HARMONICS OF
AN INITIALLY SINUSOIDAL WAVE

Webster
& Blackstock,
JASA 62,
518 (1977)

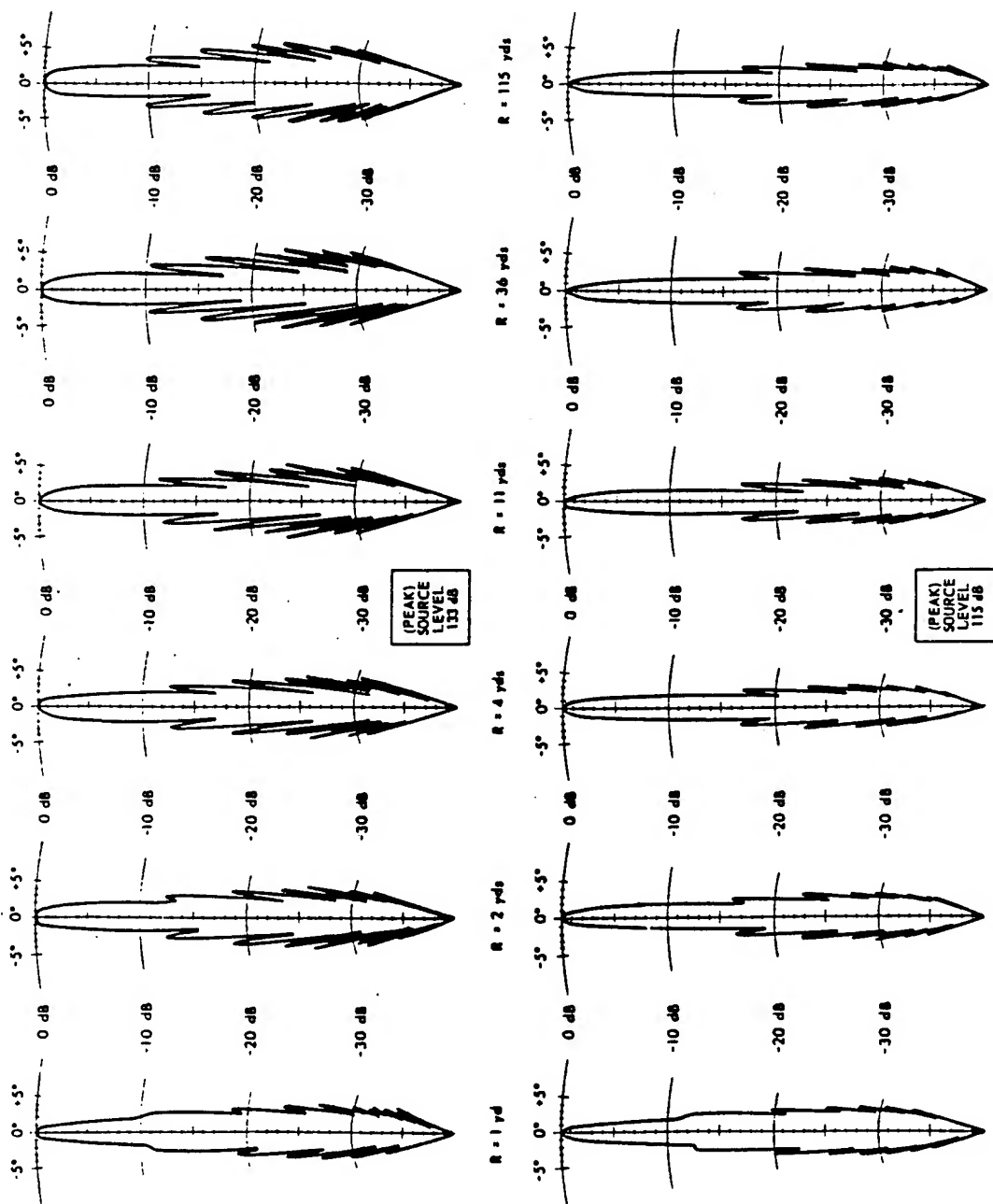


FIG. 9
BEAM PATTERNS (FUNDAMENTAL) AT VARIOUS RANGES FOR A STRONG AND A WEAK WAVE
(3 in. diam PISTON PROJECTOR, $f = 434$ kHz, $DI = 36.5$ dB, $\eta = 40^\circ$)

ARL - UT
85-70-1155
TGM - RFO
10 - 1 - 70

Shooter, Hair & Blackstock, JASA 55, 54 (1974)

NUMERICAL MODELING

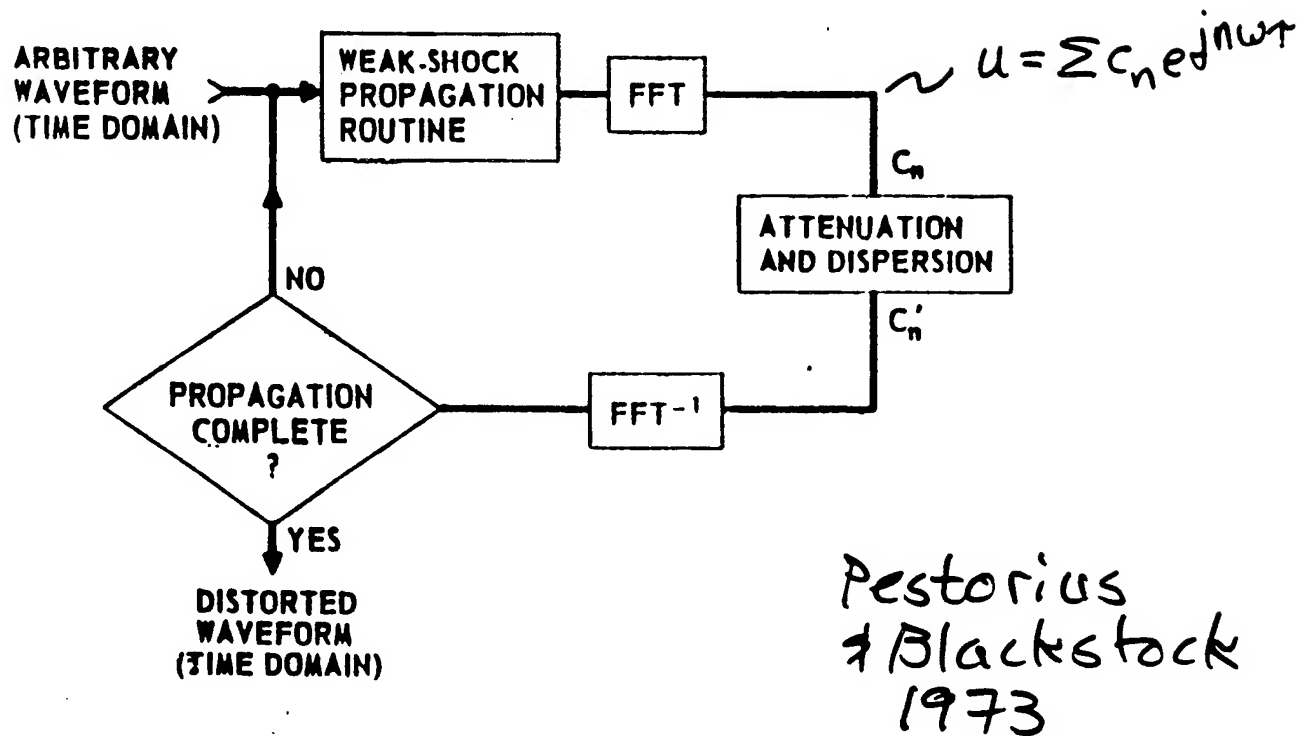


FIGURE 3-8
A SCHEMATIC DIAGRAM OF MODIFIED WEAK-SHOCK THEORY

Time Domain Steps:

$$\frac{dx}{dt} = c_0 + \beta u \quad , \text{ continuous waves}$$

$$= c_0 + \frac{\beta}{2}(u_a + u_b) \quad , \text{ shocks}$$

Frequency Domain steps:

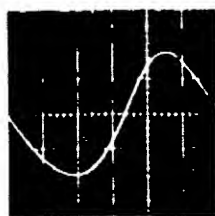
$$c_n' = c_n e^{-(\alpha_n + j\delta_n)\Delta x}$$

α_n = attenuation coefficient

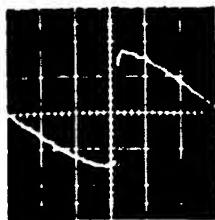
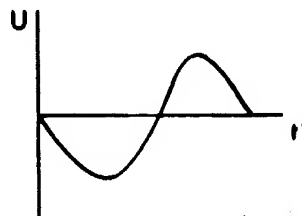
δ_n = dispersion coefficient

EXPERIMENTAL

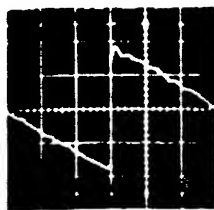
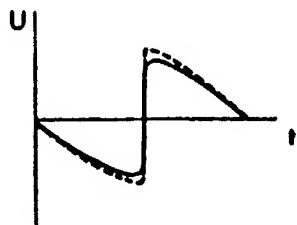
COMPUTED



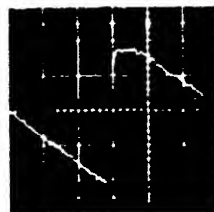
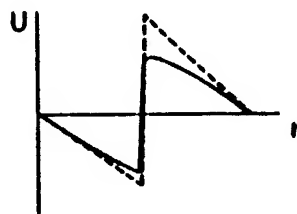
$X = 1 \text{ ft}$
 $VA = 1$



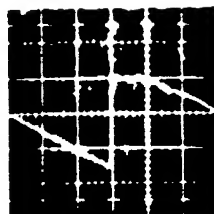
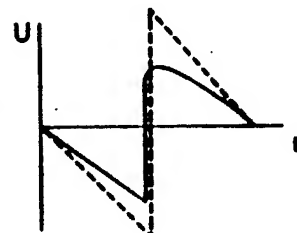
$X = 13 \text{ ft}$
 $VA = 1$



$X = 37 \text{ ft}$
 $VA = 2$



$X = 61 \text{ ft}$
 $VA = 4$



$X = 85 \text{ ft}$
 $VA = 4$

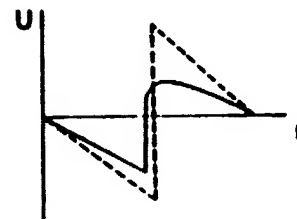


Figure 14 A comparison of experimental and computed time waveforms for a wave produced by an 800 Hz source at one end of a 96 ft progressive wave tube. The source SPL is 159 dB (re 0.0002 μ bar); VA stands for the vertical amplification of the oscilloscope. The dashed-line predictions are given by weak-shock theory alone, that is, without any account taken of tube wall attenuation and dispersion.

CS-72-425-P

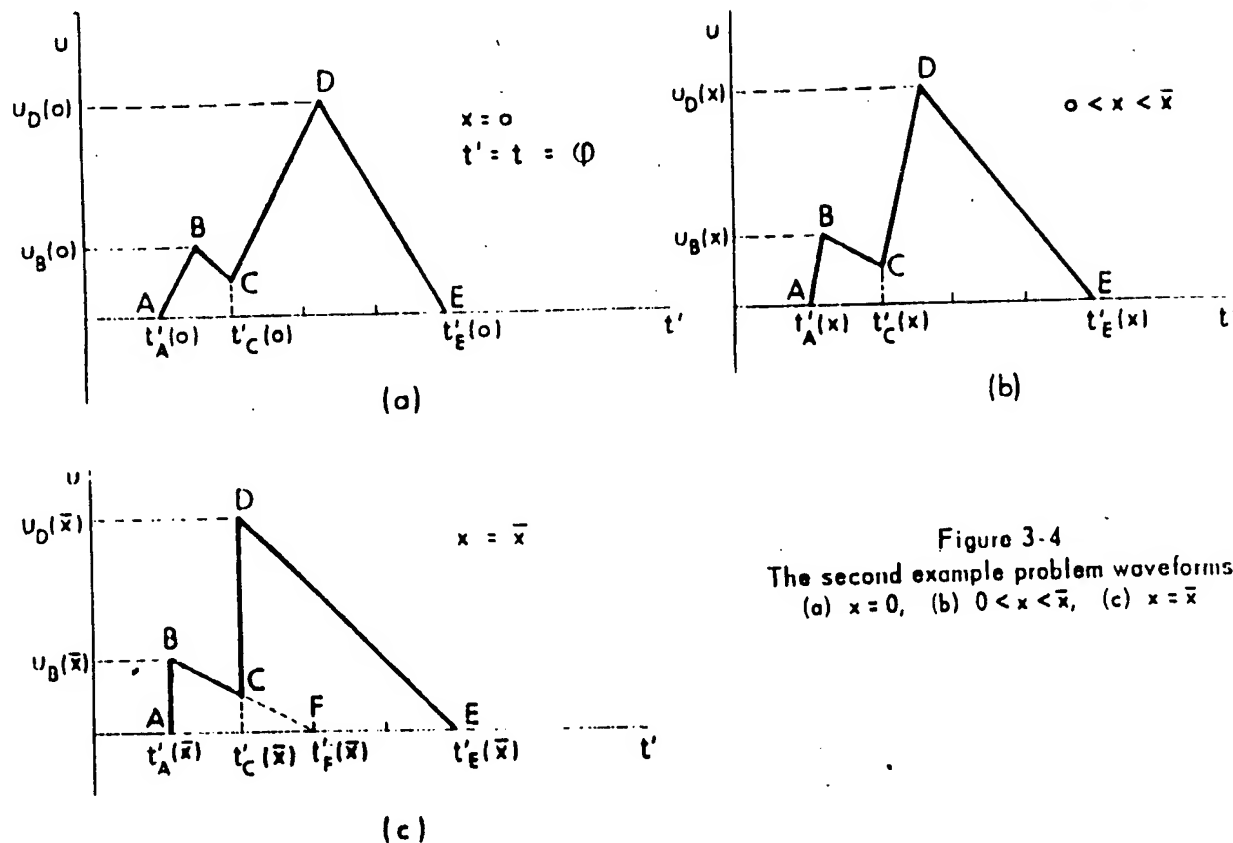


Figure 3-4
The second example problem waveforms
(a) $x = 0$, (b) $0 < x < \bar{x}$, (c) $x = \bar{x}$

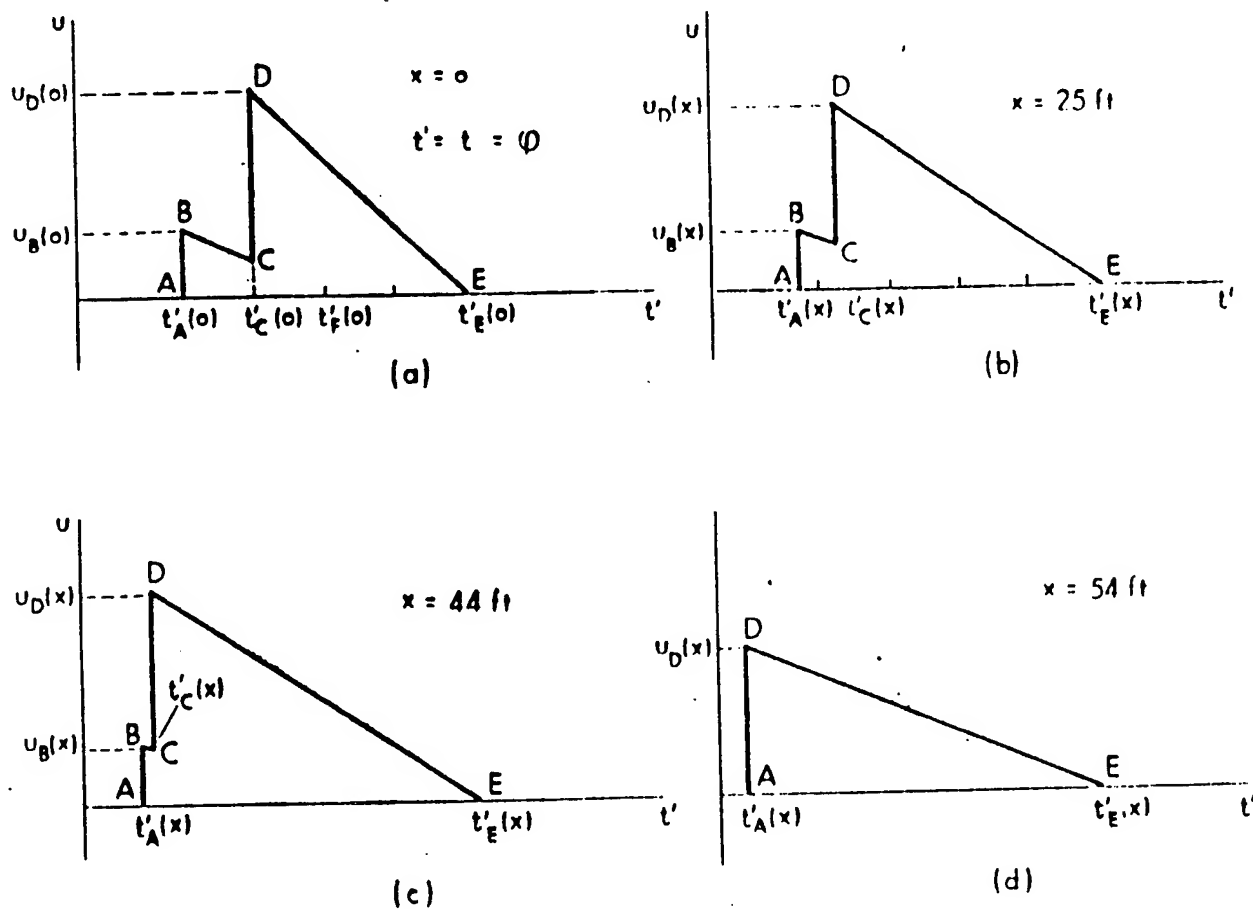


Figure 3-5
The second example problem (cont'd)

- (a) The source waveform in the shifted coordinate system.
- (b) The source waveform after propagating 25 ft.
- (c) Just prior to shock merger.
- (d) The simplified waveform after shock merger.

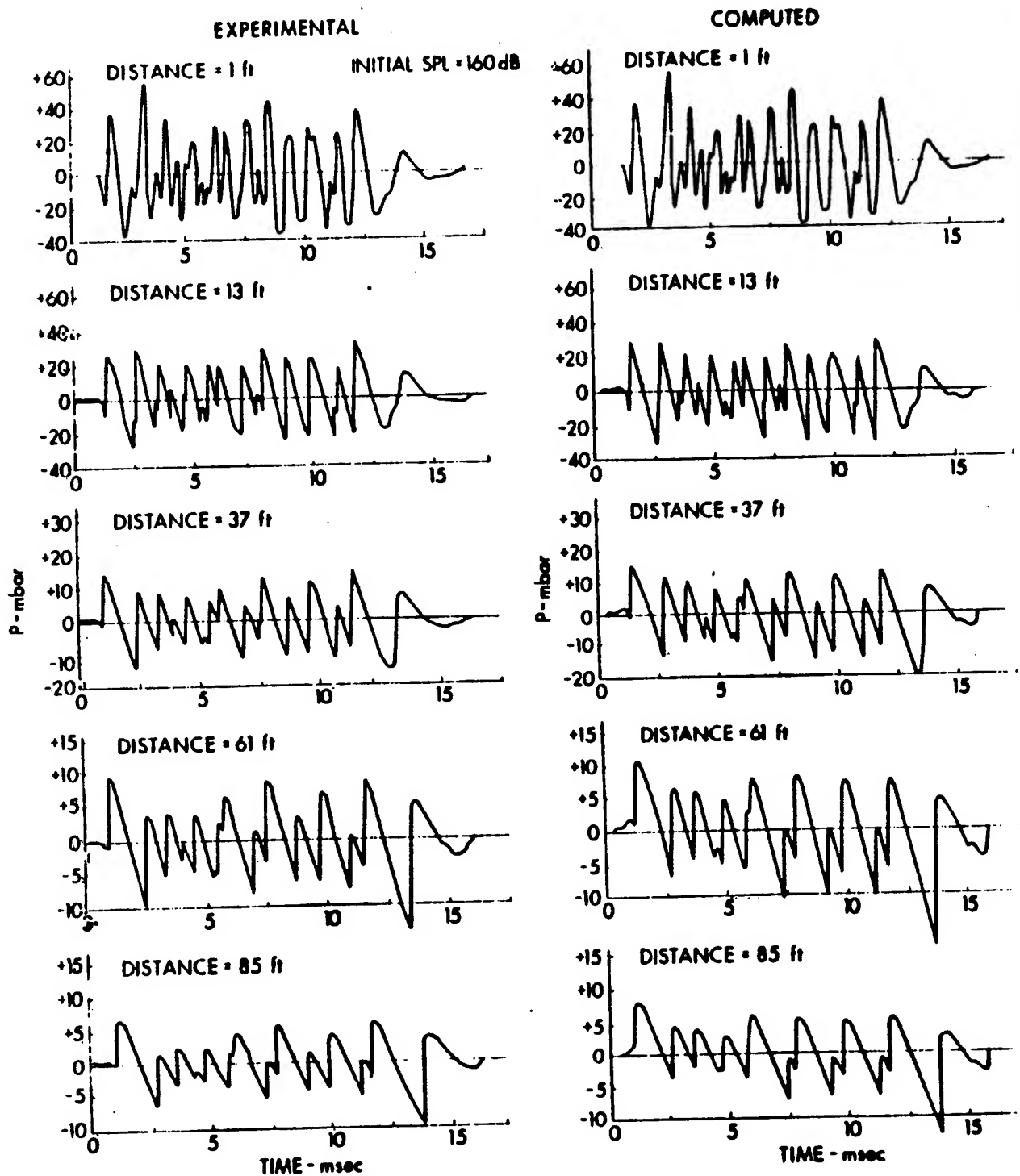


FIGURE 6-9
NOISE PULSE 1 AT VARIOUS DISTANCES

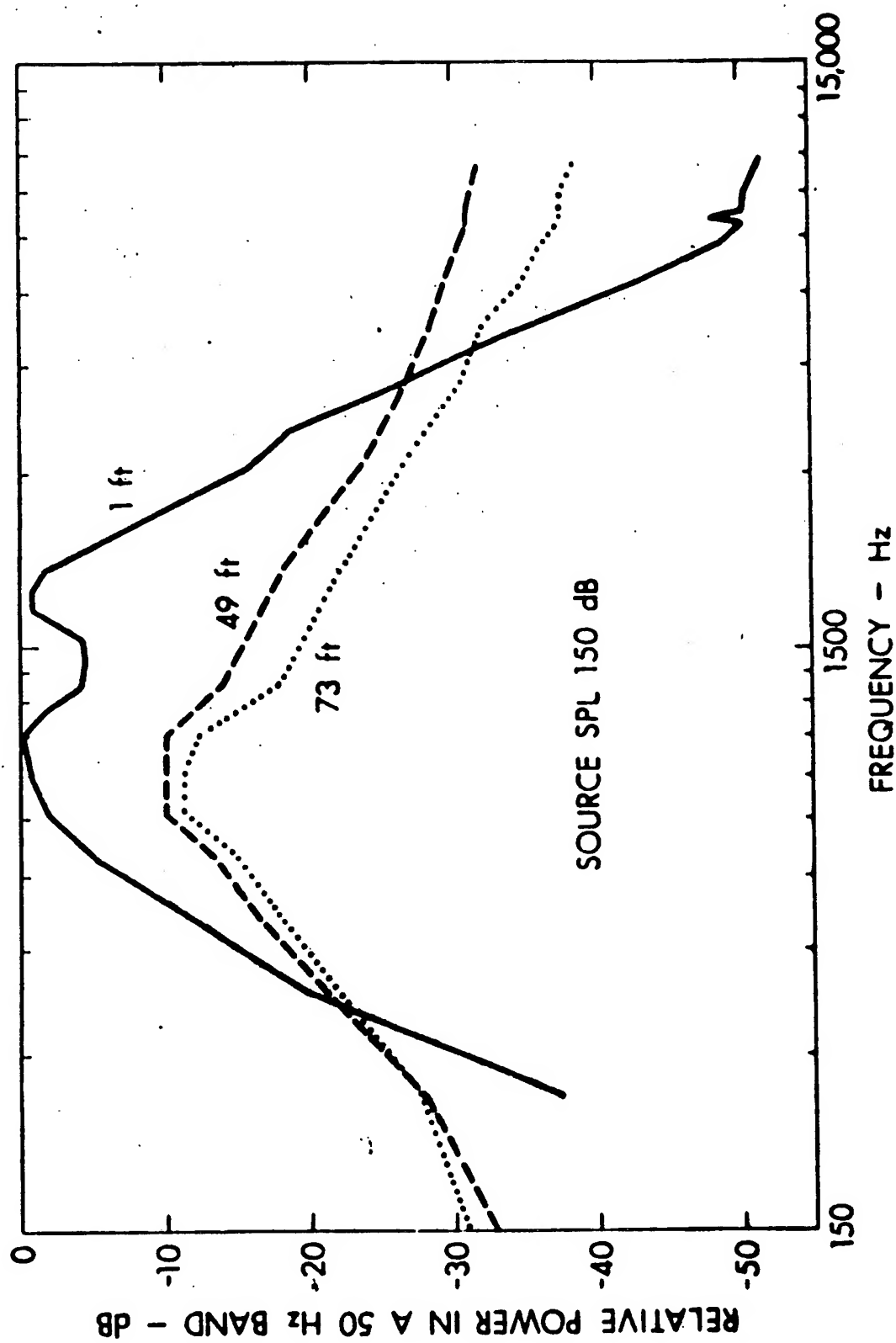


FIGURE 6-15
EXPERIMENTAL SPECTRUM AT VARIOUS DISTANCES

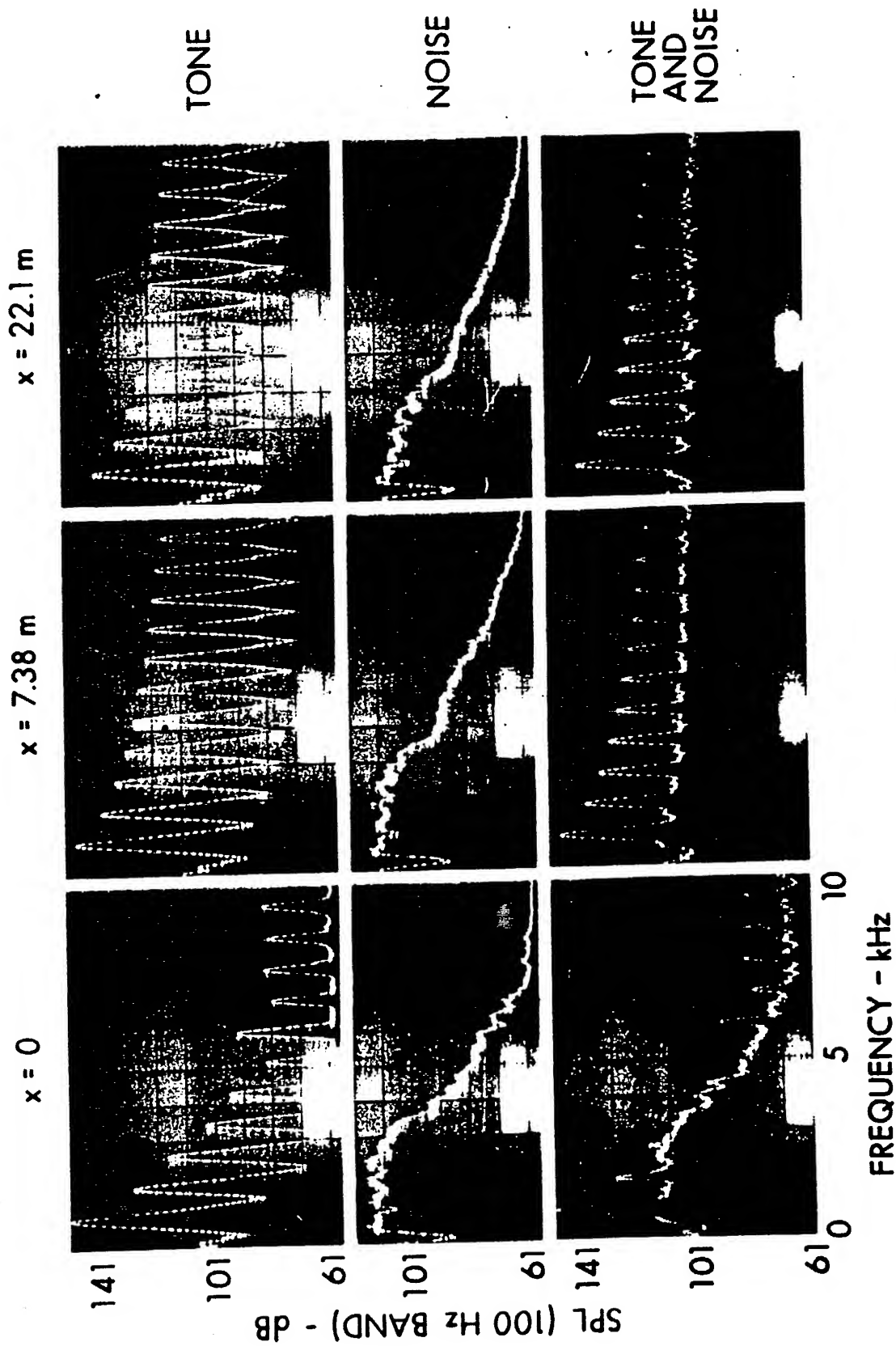


FIGURE 3

Interaction of tone with noise.

From Refs. 77-2, 77-6, and 78-1.

Webster & Blackstock
JASA 83, 657 (1978)

D. A. Webster and D. T. Blackstock: Collinear interaction of noise with a tone

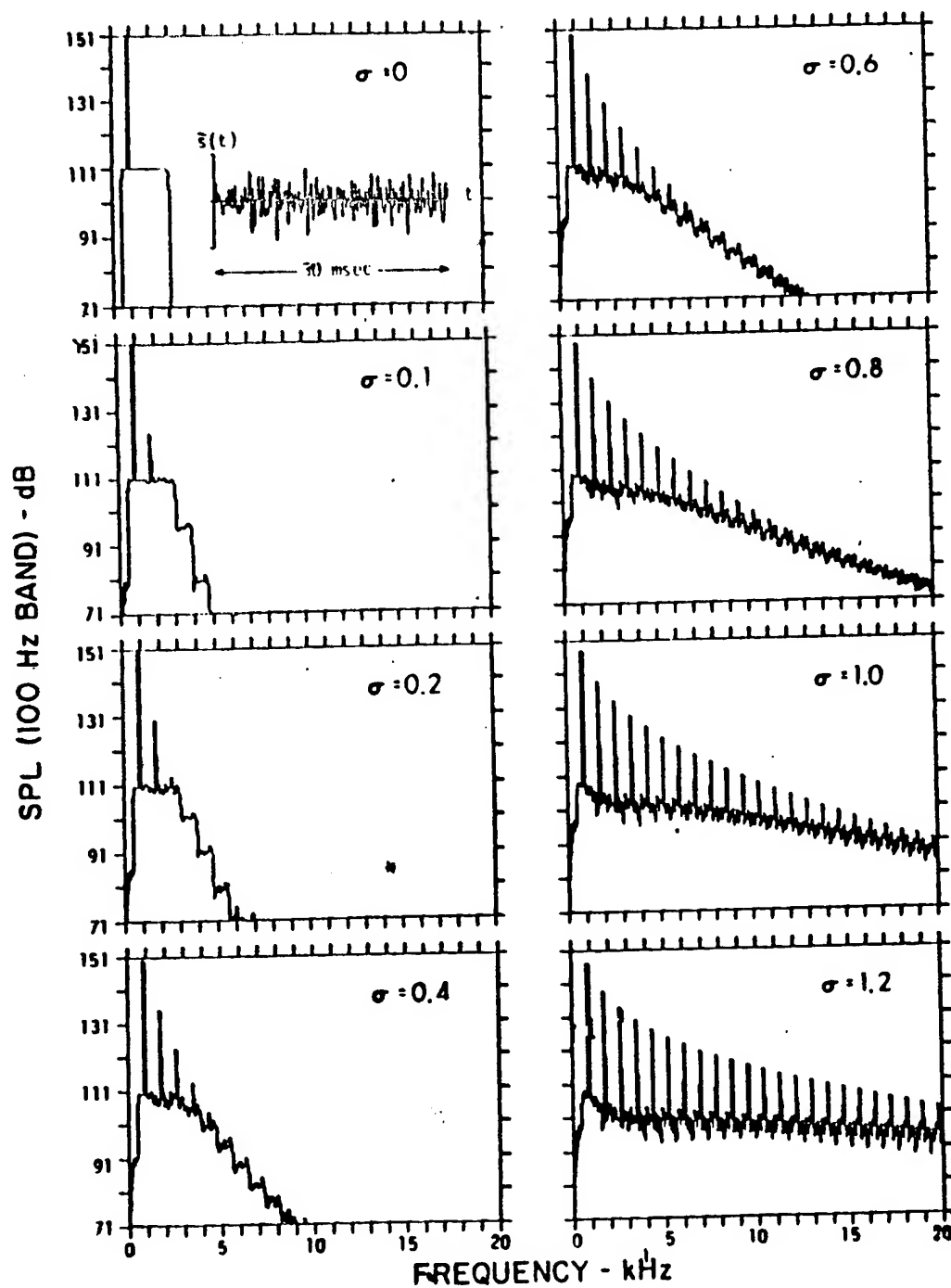


FIG. 8. Computed tone-noise interaction spectra. Symbols: $\sigma \equiv x/\bar{x}$, $\bar{x} = 7.45$ m. The conditions are roughly those of experiment I.

III. MODEL EQUATIONS

VISCOUS, HEAT CONDUCTING FLUIDS

309

Continuity:

$$\frac{D\rho}{Dt} + \rho \vec{\nabla} \cdot \vec{u} = 0 \quad \left(\frac{D}{Dt} = \frac{\partial}{\partial t} + \vec{u} \cdot \vec{\nabla} \right)$$

Momentum:

$$\rho \frac{D\vec{u}}{Dt} + \vec{\nabla} p = \left(\zeta + \frac{4}{3}\eta \right) \nabla^2 \vec{u} + \left(\zeta + \frac{1}{3}\eta \right) \vec{\nabla} \times \vec{\nabla} \times \vec{u}$$

Entropy:

$$\rho T \frac{Ds}{Dt} = \kappa \nabla^2 T + \zeta (\vec{\nabla} \cdot \vec{u})^2 + \frac{\eta}{2} \left(\frac{\partial u_i}{\partial x_j} + \frac{\partial u_j}{\partial x_i} - \frac{2}{3} \delta_{ij} \frac{\partial u_k}{\partial x_k} \right)^2$$

State:

$$P = P(p, s) \\ = P_0 \left(\frac{p}{p_0} \right)^\gamma \exp \left(\frac{s - s_0}{c_v} \right), \text{ perfect gas}$$

[see Landau & Lifshitz, Fluid Mechanics]

MODEL EQUATIONS OF NONLINEAR ACOUSTICS

- Exact equation for lossless ($\beta, \gamma, \kappa = 0$) perfect gas ($P \propto \rho^\gamma$) in terms of velocity potential ϕ :

$$c_0^2 \nabla^2 \phi - \phi_{tt} = \left(2 \vec{\nabla} \phi_t + \frac{1}{2} \vec{\nabla} |\vec{\nabla} \phi|^2 \right) \cdot \vec{\nabla} \phi + (\gamma - 1) \left(\phi_t + \frac{1}{2} |\vec{\nabla} \phi|^2 \right) \nabla^2 \phi$$

- Common starting point in aeroelasticity, and for perturbation techniques used in nonlinear acoustics.

- ADVANTAGE: It's exact

- DISADVANTAGES:

1) restricted to lossless gases

2) no exact solutions known (except Poisson solution for progressive plane waves)

LIGHTHILL'S ORDERING SCHEME

- All lossless linear terms (e.g., $\vec{\nabla} p$) are $O(\varepsilon)$, where

$$\varepsilon \sim \frac{u}{c_0} = \text{acoustic Mach number}$$

- All loss coefficients are $O(\mu)$:

$$\zeta, \eta, \kappa = O(\mu)$$

- 1) First-order terms:

$$O(\varepsilon), \text{ lossless linear}$$

- 2) Second-order terms:

$$O(\varepsilon^2), \text{ lossless quadratic}$$

$$O(\mu\varepsilon), \text{ lossy linear}$$

- 3) Higher-order terms:

$$O(\varepsilon^3), O(\mu\varepsilon^2), O(\mu^2\varepsilon), \text{ etc.}$$

- • Discard all higher-order terms in derivations of all model equations

SECOND-ORDER BASIC EQUATIONS

Let $p = P - P_0$, $p' = p - p_0$, etc., use first-order relations to simplify second-order terms, and ignore vorticity ($\vec{\nabla} \times \vec{u}$) to obtain:

Continuity

$$\frac{\partial p'}{\partial t} + p_0 \vec{\nabla} \cdot \vec{u} = \frac{1}{p_0 c_0^4} \frac{\partial p^2}{\partial t} + \frac{1}{c_0^2} \frac{\partial \mathcal{L}}{\partial t}$$

Momentum

$$p_0 \frac{\partial \vec{u}}{\partial t} + \vec{\nabla} p = -\frac{1}{p_0 c_0^2} \left(1 + \frac{4}{3} \eta \right) \vec{\nabla} \frac{\partial p}{\partial t} - \vec{\nabla} \mathcal{L}$$

Entropy & state

$$p' - \frac{p}{c_0^2} = -\frac{\kappa}{p_0 c_0^4} \left(\frac{1}{c_v} - \frac{1}{c_p} \right) \frac{\partial p}{\partial t} - \frac{1}{p_0 c_0^4} \frac{B}{2A} p^2$$

$$\mathcal{L} = \frac{p_0 u^2}{2} - \frac{p^2}{2 p_0 c_0^2} = \text{Lagrangian density}$$

Note: For progressive plane waves we have $p = p_0 c_0 u$ at first order and therefore $\mathcal{L} = 0$ at second order, in which case the momentum equation is linear!!

- Full second-order wave equation

[Aanonsen et al., JASA 75, 749 (1984)]

$$\left(\nabla^2 - \frac{1}{c_0^2} \frac{\partial^2}{\partial t^2}\right) p + \frac{\delta}{c_0^4} \frac{\partial^3 p}{\partial t^3} = -\frac{\beta}{\rho_0 c_0^4} \frac{\partial^2 p^2}{\partial t^2} - \left(\nabla^2 + \frac{1}{c_0^2} \frac{\partial^2}{\partial t^2}\right) d$$

- Westervelt equation

[Westervelt, JASA 35, 535 (1963)]

$$\left(\nabla^2 - \frac{1}{c_0^2} \frac{\partial^2}{\partial t^2}\right) p + \frac{\delta}{c_0^4} \frac{\partial^3 p}{\partial t^3} = -\frac{\beta}{\rho_0 c_0^4} \frac{\partial^2 p^2}{\partial t^2}$$

The approximation $d \approx 0$ to obtain Westervelt equation restricts it to quasiplane progressive waves.

$$\beta = 1 + \frac{B}{2A} = \text{coefficient of nonlinearity}$$

$$\delta = \frac{1}{\rho_0} \left(\frac{4}{3} \eta + \zeta \right) + \frac{\kappa}{\rho_0} \left(\frac{1}{c_v} - \frac{1}{c_p} \right)$$

= sound diffusivity

$$\alpha_\omega = \frac{\delta \omega^2}{2c_0^3} = \text{thermoviscous attenuation}$$

• Burgers Equation

[Khokhlov et al., Acustica 14, 248 (1964)]

Begin with Westervelt equation for 1-D:

$$\left(\frac{\partial^2}{\partial x^2} - \frac{1}{c_0^2} \frac{\partial^2}{\partial t^2}\right)p = -\frac{\delta}{c_0^4} \frac{\partial^3 p}{\partial t^3} - \frac{\beta}{2\rho_0 c_0^4} \frac{\partial^2 p^2}{\partial t^2}$$

Two approximate sol'ns for limiting cases:

$$p \approx \exp\left(-\frac{\omega^2}{2c_0^3} \delta z\right) \sin \omega \tau, \quad \beta = 0$$

$$\approx \sin\left(\omega \tau + \frac{\beta k}{2\rho_0 c_0^2} p z\right), \quad \delta = 0 \text{ (Poisson)}$$

Both solutions are of the form

$$p = p(x_1, \tau)$$

$$\tau = t - \frac{x}{c_0} = \text{retarded time}$$

$$x_1 = \varepsilon x = \text{"slow" length scale } [\delta = O(\varepsilon)]$$

$$\Rightarrow \frac{\partial^2}{\partial t^2} = \frac{\partial^2}{\partial \tau^2}$$

$$\frac{\partial^2}{\partial x^2} = \frac{1}{c_0^2} \frac{\partial^2}{\partial \tau^2} - \varepsilon \frac{2}{c_0} \frac{\partial^2}{\partial x_1 \partial \tau} + \varepsilon^2 \frac{\partial^2}{\partial x_1^2}$$

Keep only second-order terms on slow scale:

$$\frac{\partial p}{\partial x} = \frac{\delta}{2c_0^3} \frac{\partial^2 p}{\partial \tau^2} + \frac{\beta}{2\rho_0 c_0^3} \frac{\partial p^2}{\partial \tau}$$

SPECTRAL NUMERICAL SOLUTION

Dimensionless Burgers Equation:

$$\frac{\partial P}{\partial \sigma} = \frac{1}{\Gamma} \frac{\partial^2 P}{\partial \tau^2} + P \frac{\partial P}{\partial \tau}$$

$$P = \frac{p}{p_0}, \quad \sigma = \frac{x}{\lambda}, \quad \tau = \omega(t - \frac{x}{c_0}), \quad \Gamma = \frac{1}{\alpha \bar{x}}$$

Fourier Series Expansion:

$$P(\sigma, \tau) = \frac{1}{2} \sum_{n=-N}^N P_n(\sigma) e^{jn\tau}$$

Resulting Coupled First-Order ODE's:

$$\frac{dP_n}{d\sigma} = \underbrace{-\frac{n^2}{\Gamma} P_n}_{\text{absorption}} + \underbrace{j\frac{n}{4} \left(\sum_{m=1}^{n-1} P_m P_{n-m} \right)}_{\text{sum freqs.}} + \underbrace{2 \sum_{m=n+1}^N P_m P_{m-n}^*}_{\text{diff. freqs.}}$$

Simple modification for arbitrary absorption and dispersion relations:

$$\frac{n^2}{\Gamma} \rightarrow A_n + jD_n$$

***** Choose absorption law (ABSTV, ABSREL or ABSBL) for A(N) *****

```

DO 10 N=1,NHAR
  P(N) = CMPLX(0.,0.)
  A(N) = ABSTV(N)
10  CONTINUE
  P(1) = CMPLX(0.,-1.)

```

***** Second order Runge-Kutta *****

```

20  DO 30 N=1,NHAR
    K1(N) = STEP * ( (J*N/4.) * SUM(P,N,NHAR) - A(N) * P(N) )
    P2(N) = P(N) + K1(N)
30  CONTINUE
    DO 40 N=1,NHAR
        K2 = STEP * ( (J*N/4.) * SUM(P2,N,NHAR) - A(N) * P2(N) )
        P(N) = P(N) + (K1(N)+K2)/2.
40  CONTINUE

    X = X + STEP
    IF (X.LT.XOUT(I)) GO TO 20

    DO 50 N=1,NHAR
        POUT(I,N) = P(N)
50  CONTINUE
    I = I + 1
    IF (I.LE.IOUT) GO TO 20

```

***** Write complex harmonic amplitudes to file "Harmonics" *****

```

DO 60 N=1,NHAR
  WRITE(12,*) N, ( POUT(I,N), I=1,IOUT )
60  CONTINUE
  CLOSE(12)

```

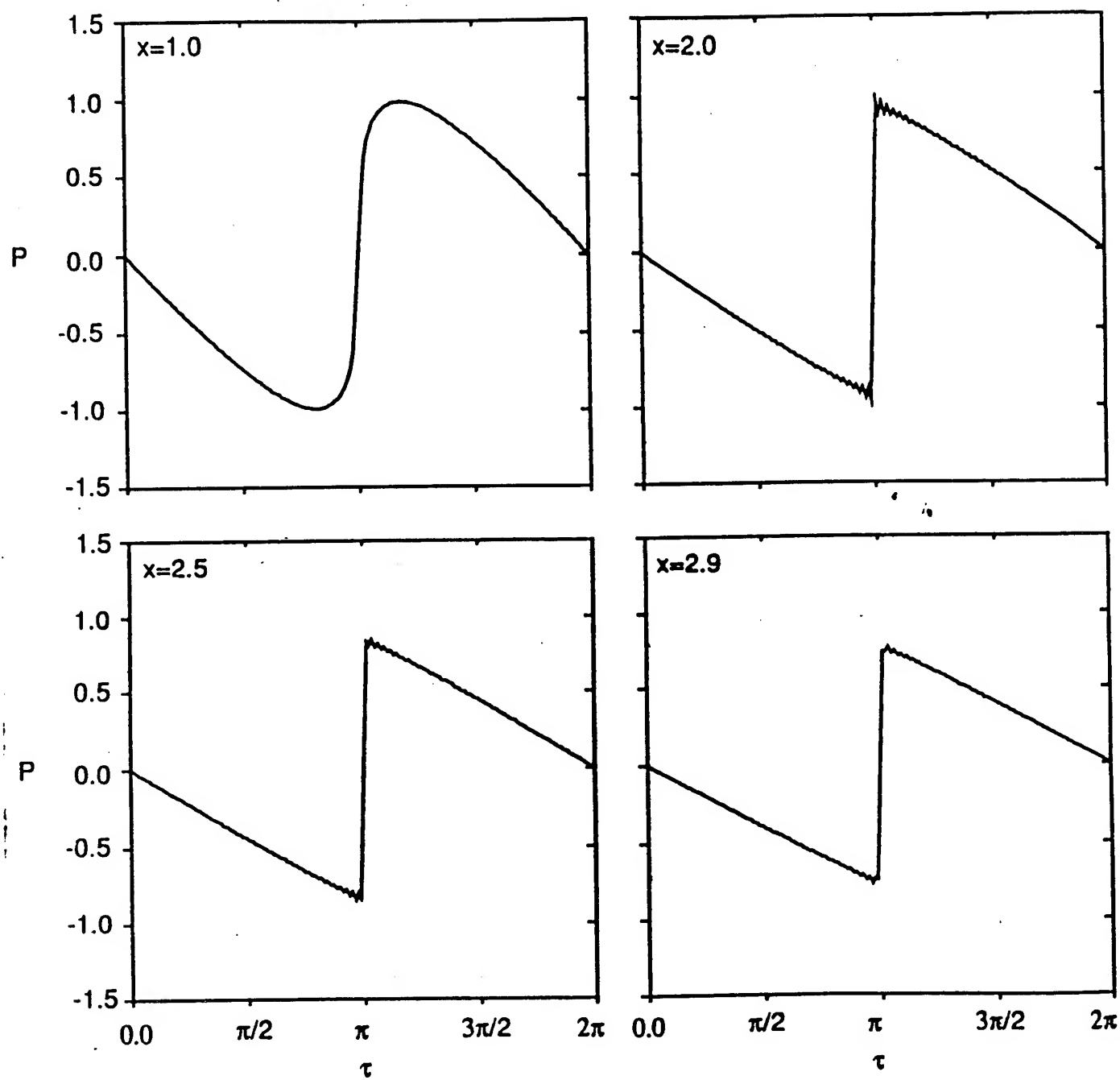
***** Subroutine for nonlinearity (discrete convolution) *****

```

COMPLEX FUNCTION SUM(P,N,NHAR)
COMPLEX P(900)
  SUM = CMPLX(0.,0.)
  DO 400 M=1,N-1
    SUM = SUM + P(M)*P(N-M)
400  CONTINUE
  DO 410 M=NHAR,N+1,-1
    SUM = SUM + 2.*P(M)*CONJG(P(M-N))
410  CONTINUE
  RETURN

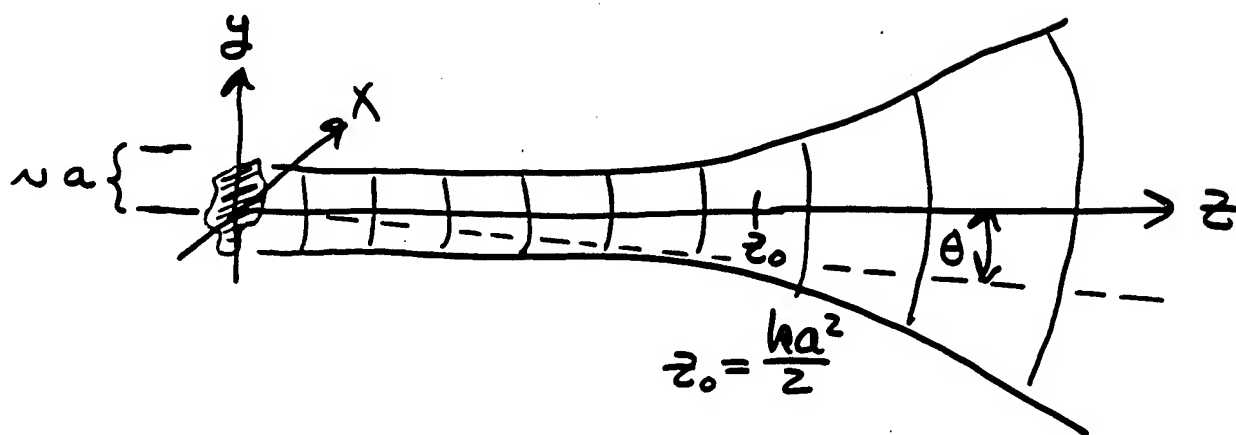
```

Number of harmonics= 75

 $G=1/\Gamma=0.01$ 

IV. SOUND BEAMS

SOUND BEAMS



KZK Equation:

$$\underbrace{\frac{\partial^2 p}{\partial z \partial t} - \frac{c_0}{z} \nabla_{\perp}^2 p}_{\text{diffraction}} - \underbrace{\frac{\delta}{z c_0^3} \frac{\partial^3 p}{\partial t^3}}_{\text{absorption}} = \underbrace{\frac{\beta}{2 \rho_0 c_0^3} \frac{\partial^2 p^2}{\partial t^2}}_{\text{nonlinearity}}$$

$$\nabla_{\perp}^2 = \frac{\partial^2}{\partial x^2} + \frac{\partial^2}{\partial y^2}$$

Assumptions:

Burgers equation recovered for $\nabla_{\perp}^2 p = 0$

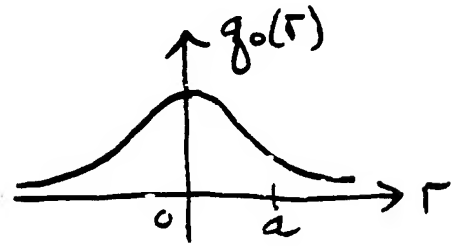
- $ka \gg 1$ (directive beams)
- $\frac{z}{a} \gtrsim (ka)^{1/3}$ (not too near source)
- $\theta \lesssim 20^\circ$ (not too far off axis)

Zabolotskaya & Khokhlov, Sov. Phys. Acoust. 15, 35 (1969)]

GAUSSIAN BEAMS

Source function:

$$q_0(r) = p_0 \exp \left[-(r/a)^2 \right]$$



Primary wave ($z_0 = ka^2/2$):

$$q_1(r, z) = \frac{p_0 e^{-\alpha_1 z}}{1 - jz/z_0} \exp \left[-\frac{(r/a)^2}{1 - jz/z_0} \right]$$

Farfield directivity ($z \gg z_0$):

$$D_1(\theta) = \exp[-(ka/2)^2 \tan^2 \theta]$$

Second harmonic pressure:

$$P_0 = \frac{\beta p_0^2 k^2 a^2}{4 \rho_0 c_0^2}$$

$$q_2(r, z) = \frac{j P_0 e^{-\alpha_2 z + j(2\alpha_1 - \alpha_2)z_0}}{1 - jz/z_0} \exp \left[-\frac{2(r/a)^2}{1 - jz/z_0} \right] \\ \times \{ E_1[j(2\alpha_1 - \alpha_2)z_0] - E_1[j(2\alpha_1 - \alpha_2)(z_0 - jz)] \}$$

Lossless limit:

$$q_2(r, z) = \frac{j P_0 \ln(1 - jz/z_0)}{1 - jz/z_0} \exp \left[-\frac{2(r/a)^2}{1 - jz/z_0} \right]$$

Farfield:

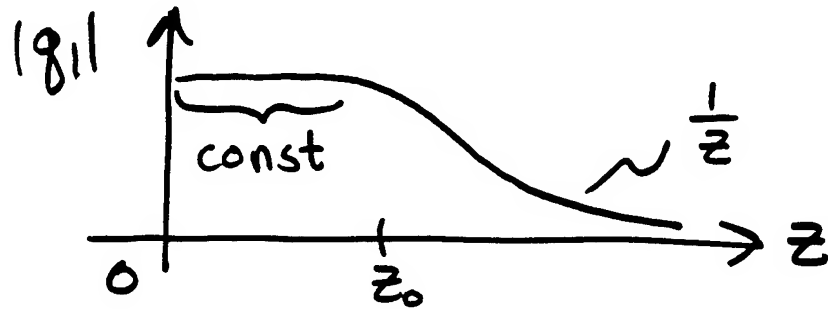
$$q_2(\theta, z) = -P_0 \frac{\ln(z/z_0) - j\pi/2}{z/z_0} D_1^2(\theta) \exp(-jkz \tan^2 \theta)$$

$$p = p_1 + p_2, \quad |p_2| \ll |p_1|, \quad p_2(r, z, t) = q_2(r, z) e^{-in\omega t}$$

LOSSLESS SECOND HARMONIC GENERATION

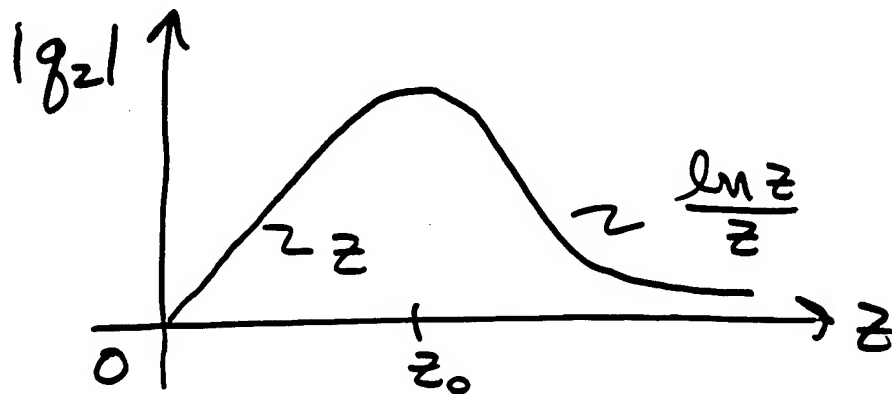
Fundamental Component:

$$g_1(r, z) = \frac{p_0}{1 + iz/z_0} \exp \left\{ -\frac{(r/a)^2}{1 + iz/z_0} \right\}$$

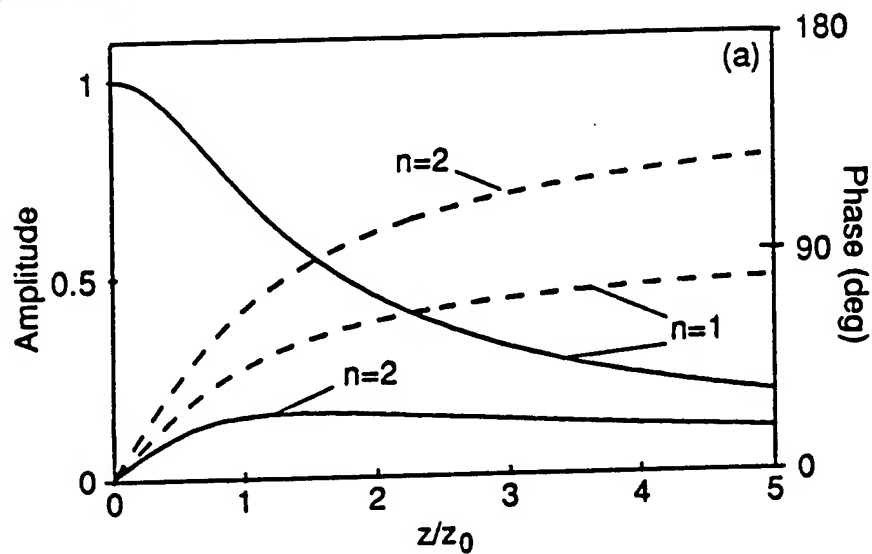


Second Harmonic Component:

$$g_2(r, z) = \frac{p_0^2 \beta k^2 a^2}{4i p_0 c_0^2} \frac{\ln(1 + iz/z_0)}{1 + iz/z_0} \exp \left\{ -\frac{2(r/a)^2}{1 + iz/z_0} \right\}$$



unfocused:



Focused:

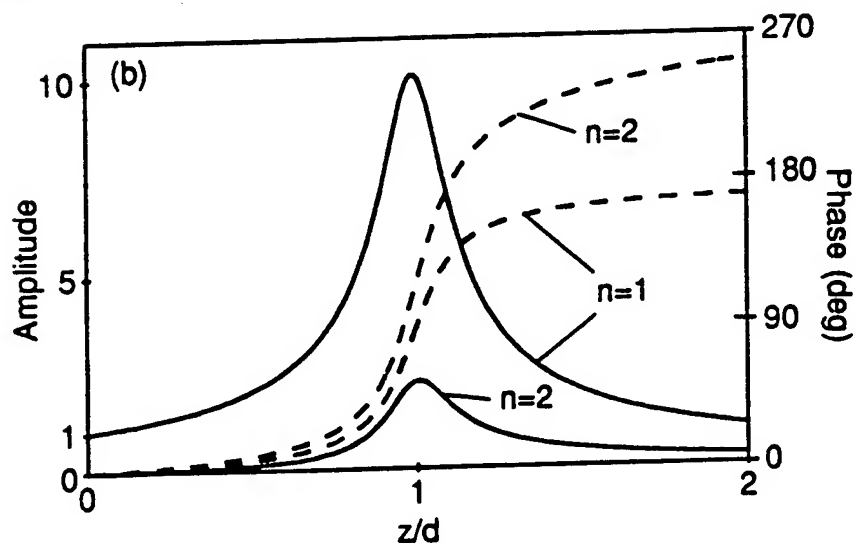


Figure 8.1

UNIFORM CIRCULAR SOURCES

Source condition:

$$q_0(r) = p_0 H(a - r)$$

where H is the Heaviside step function.

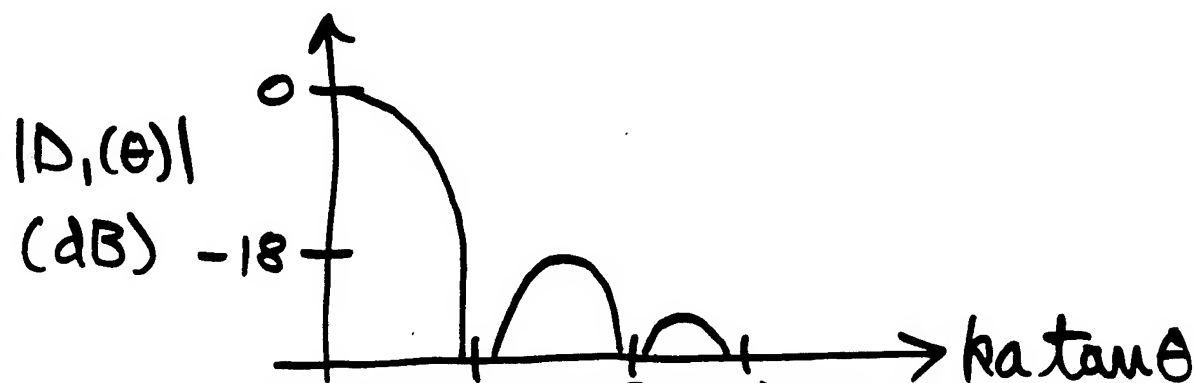
Axial solution for primary beam [valid for $z \gtrsim a(ka)^{1/3}$]:

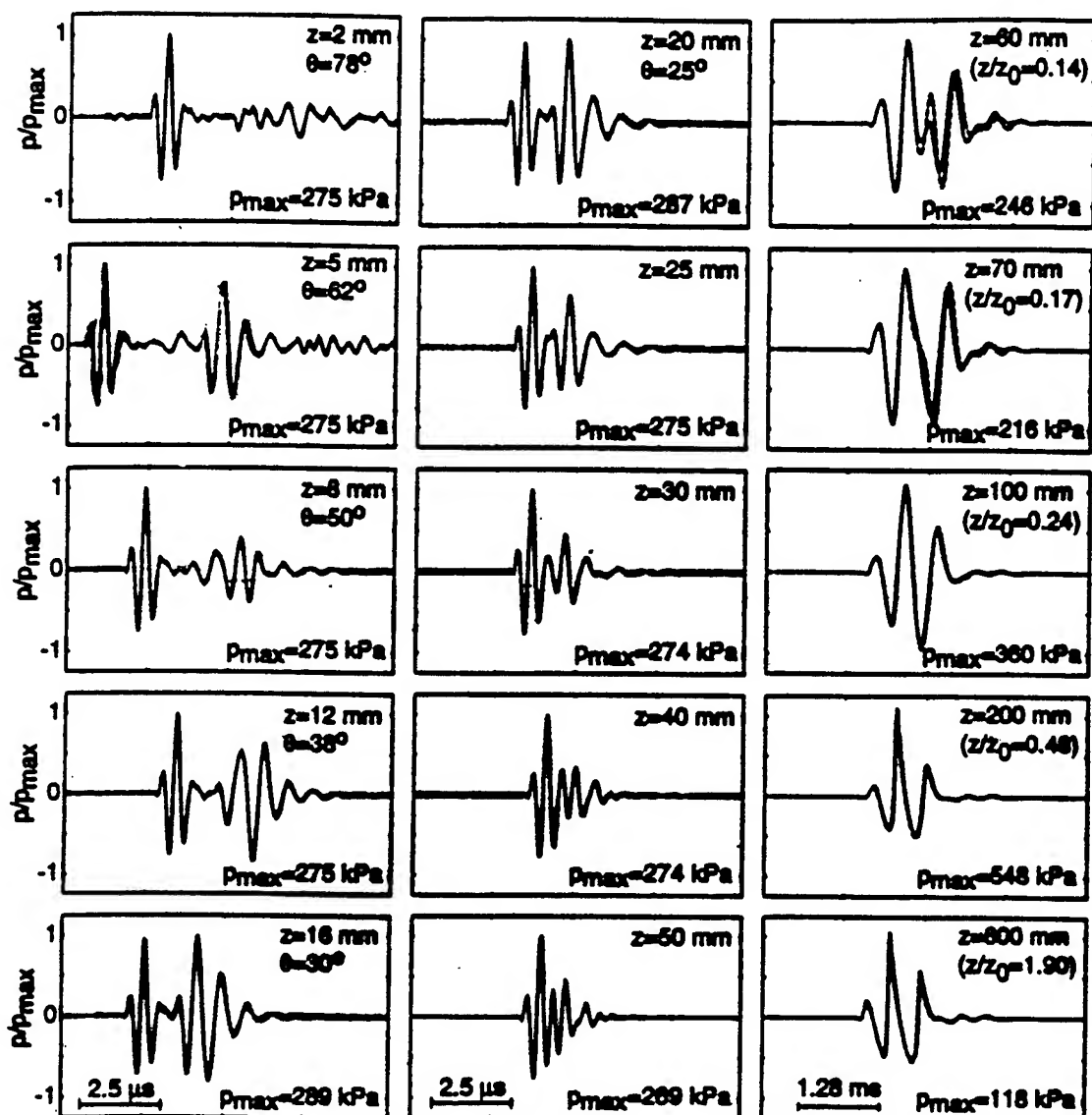
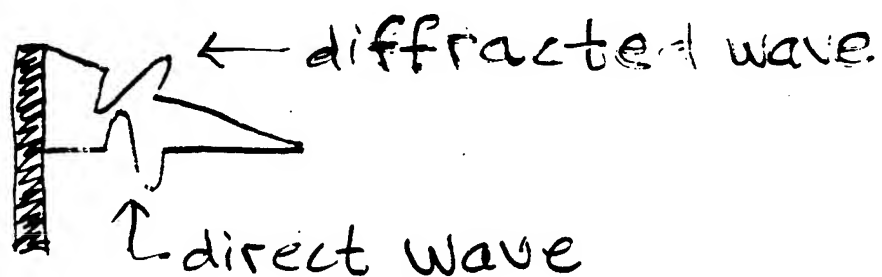
$$\begin{aligned} q_1(0, z) &= j2p_0 \sin(z_0/2z) \exp(-\alpha_1 z - jz_0/2z) \\ &= 0 \quad z = z_0/2n\pi, \quad n = 1, 2, \dots \end{aligned}$$



Farfield directivity (valid for $\theta \lesssim 20^\circ$):

$$D_1(\theta) = \frac{2J_1(ka \tan \theta)}{ka \tan \theta}$$





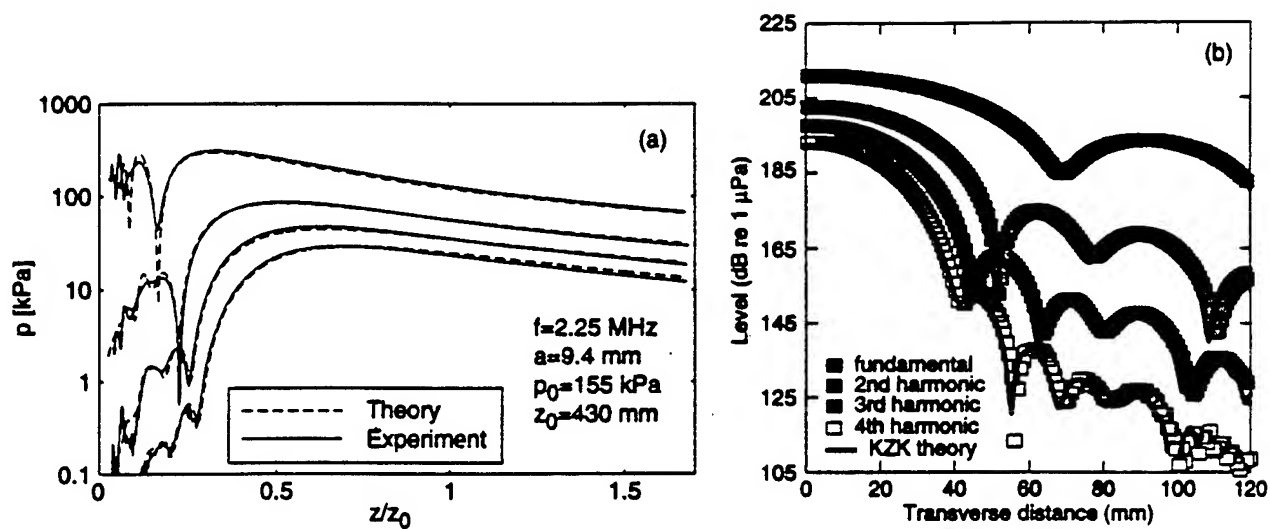
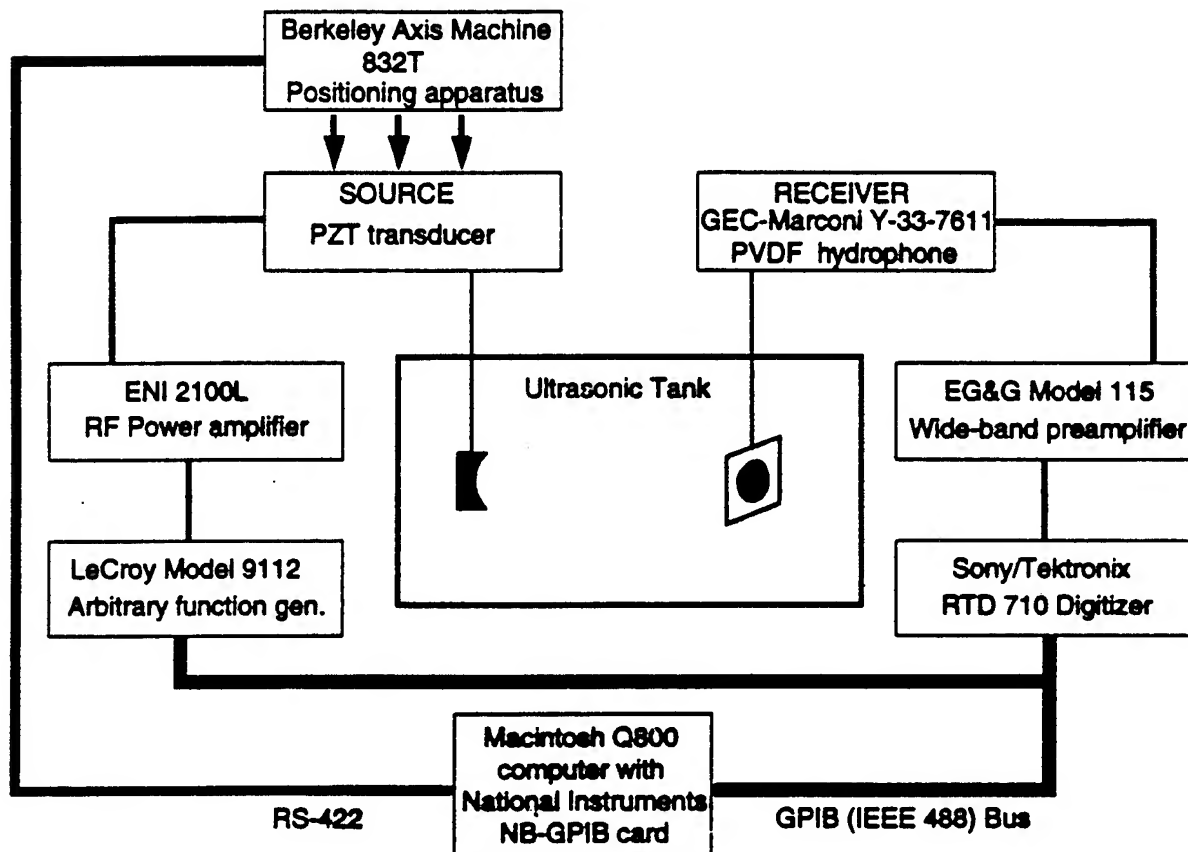


Figure 4 (Chapter 8)



1
Figure 2

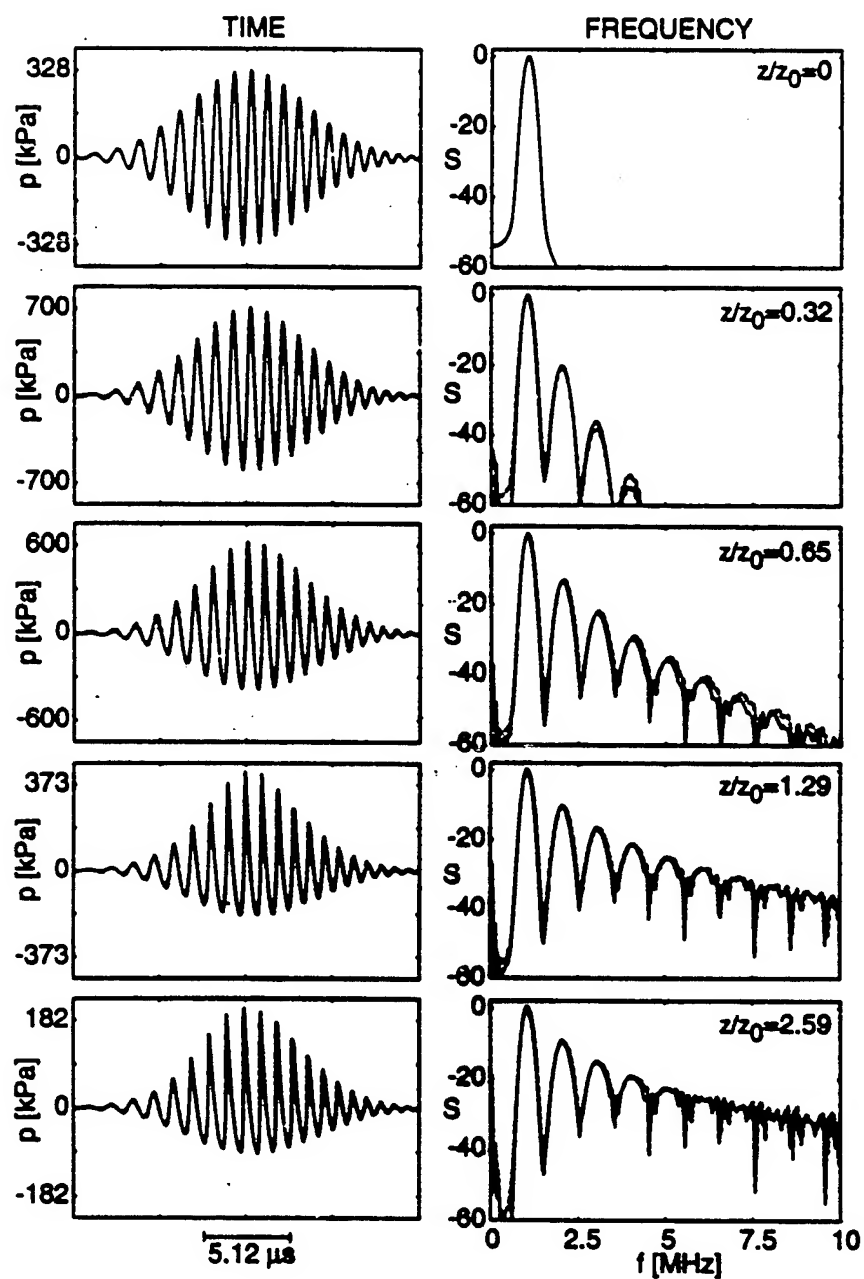
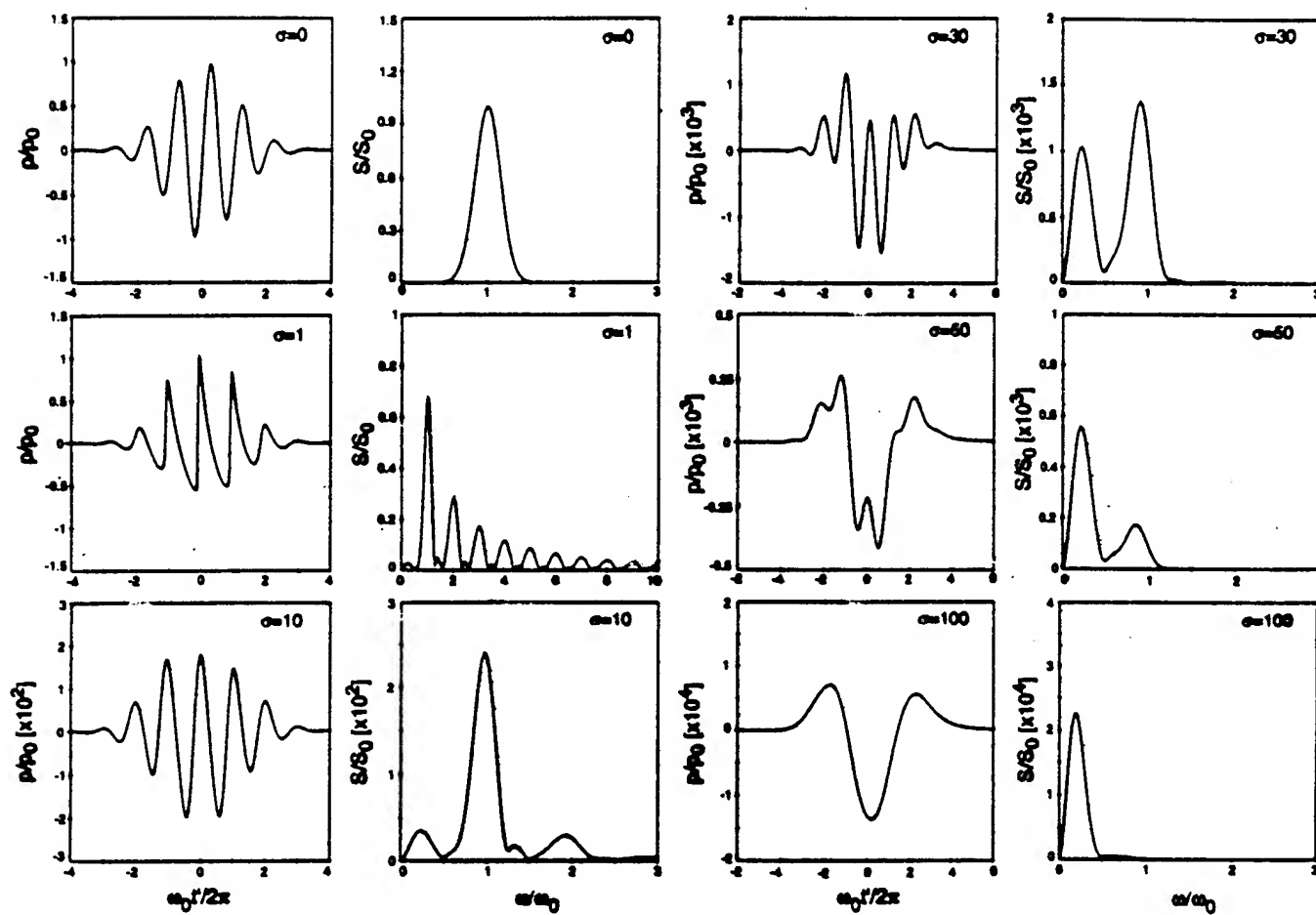


Figure 7



$$\sigma = \frac{v}{v_0}$$

Figure 6 (Chapter 8)

SELF-DEMODULATION (BERKTAY—1965)

Given the source pressure

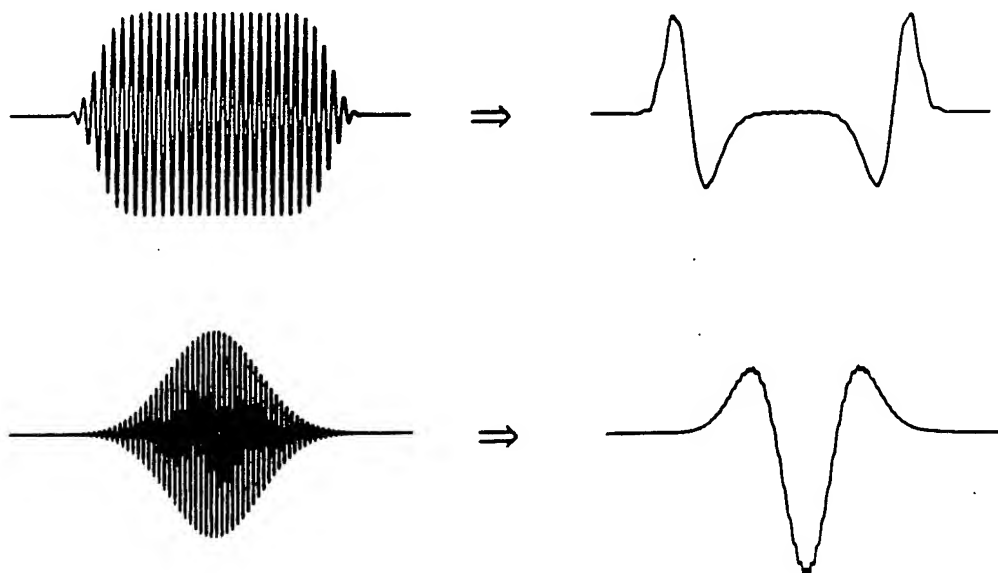
$$P = E(t) \sin \omega_0 t$$

where

$E(t)$ = slowly varying modulation envelope

Berktag predicted that in the farfield ($\sigma \gg 1$) and for strong absorption ($A > 1$), the pressure on axis varies as

$$P \propto \frac{\partial^2 E^2(t)}{\partial t^2}$$



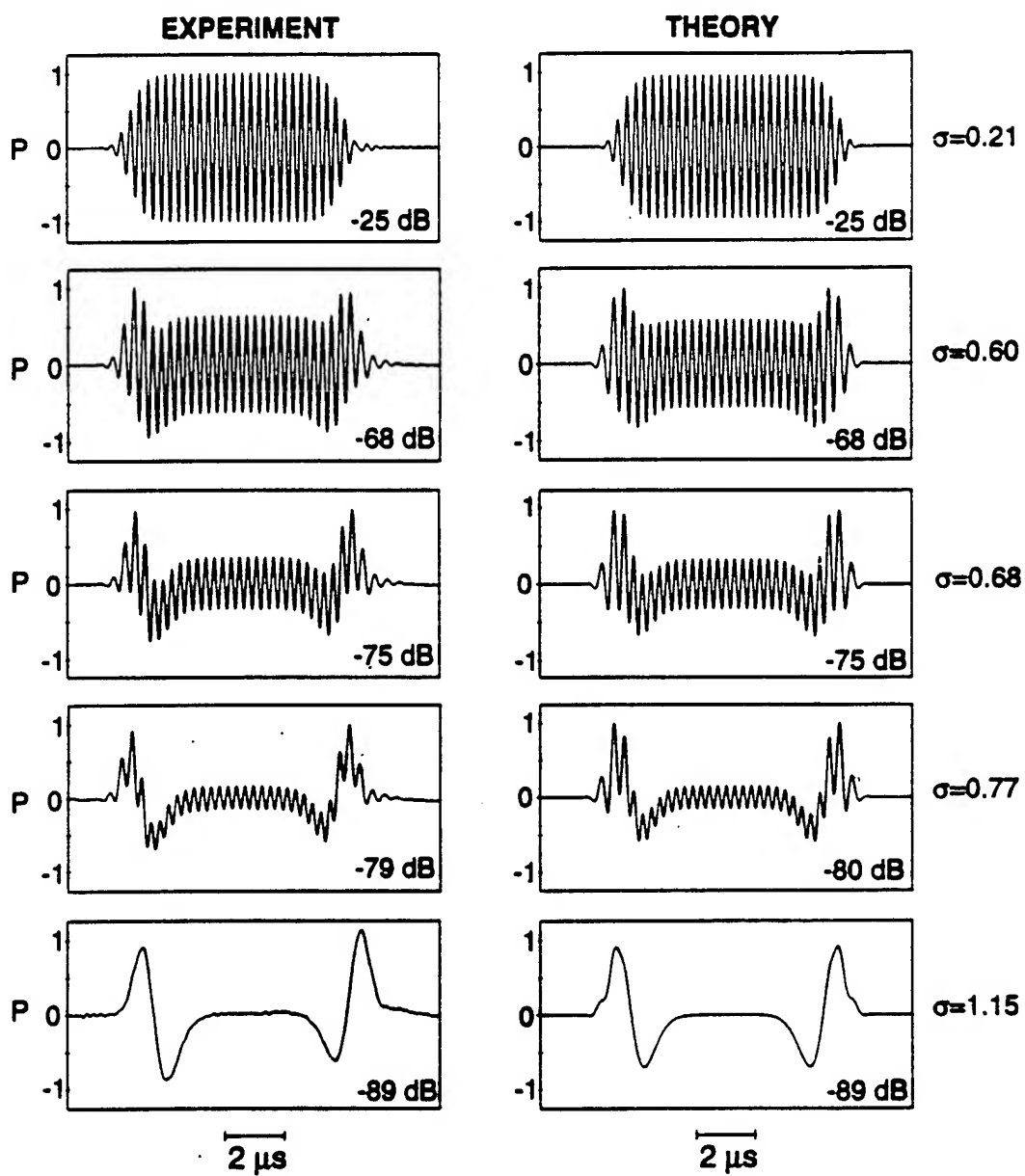


Figure 3 (Chapter 8)

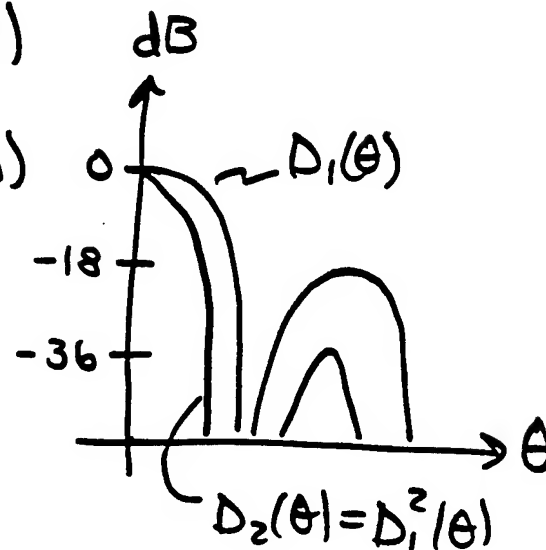
BEAM PATTERNS (Lossless Theory)

FARFIELD:

$$D_n(\theta) = D_1^n(\theta)$$

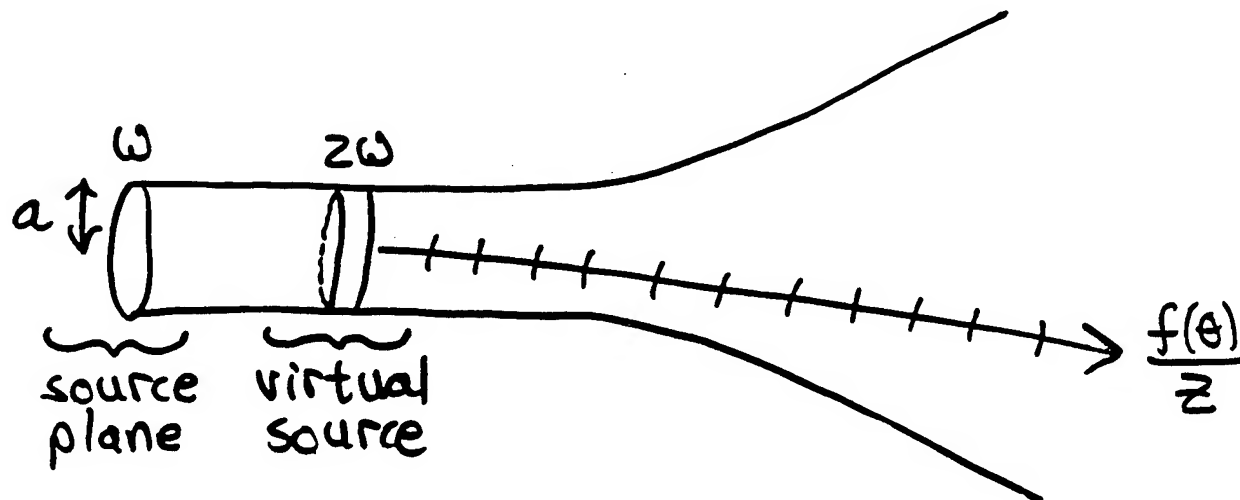
$D_1(\theta)$ = linear directivity (ω)

$D_n(\theta)$ = directivity at $n\omega$



NOT-SO-FARFIELD:

$$p_2(\theta, z) \sim A \frac{\ln z}{z} D_1^2(\theta) + B \frac{1}{z} f(\theta) + \text{H.O.T.}$$

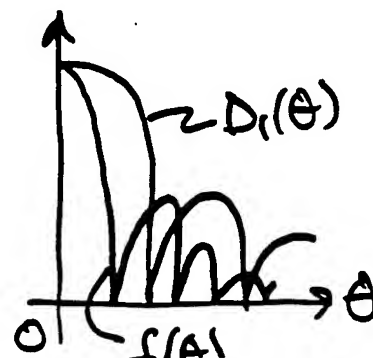


If

$$D_1(\theta) = \frac{2J_1(ka \tan \theta)}{ka \tan \theta}$$

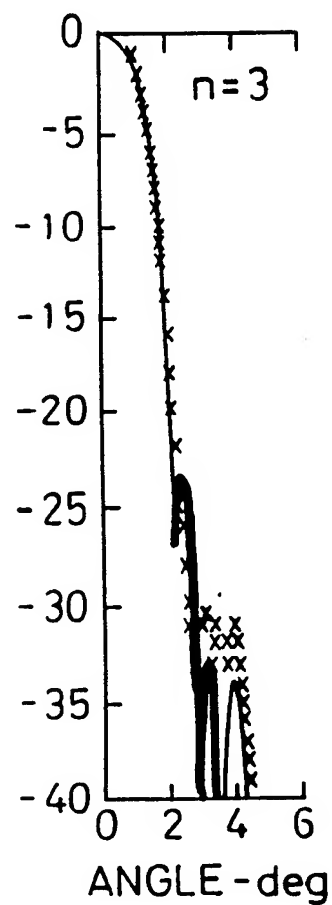
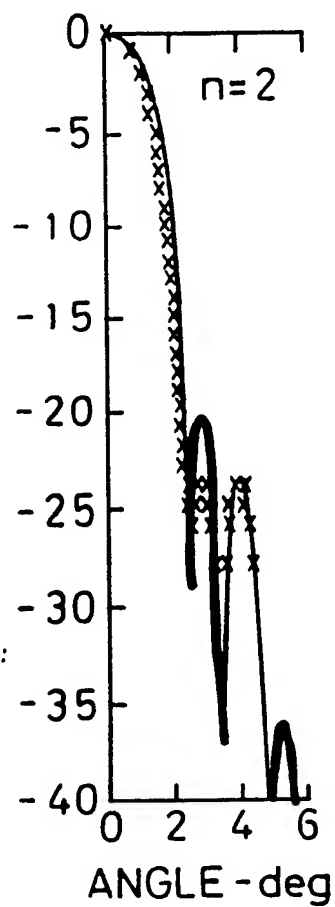
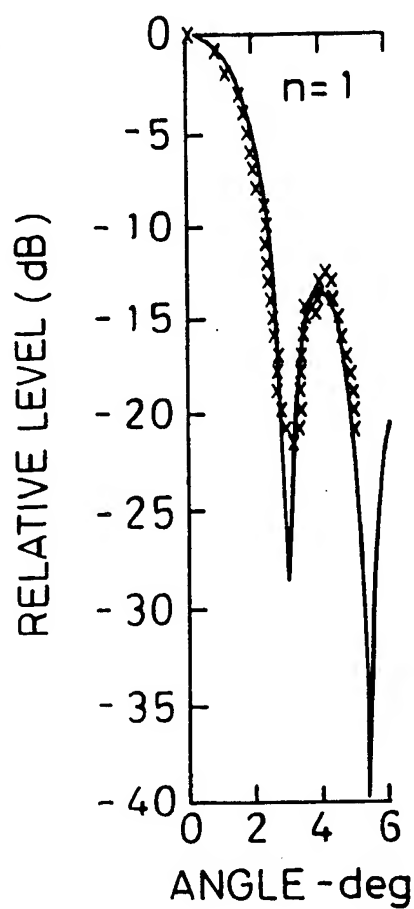
Expect

$$f(\theta) \sim \frac{2J_1(2ka \tan \theta)}{2ka \tan \theta}$$



$$Z = 7.1 Z_0, \quad \frac{\Gamma_0}{Z_0} = 0.88, \quad \alpha \Gamma_0 = 0.01$$
$$f = 450 \text{ kHz}$$

x LOCKWOOD
— THEORY



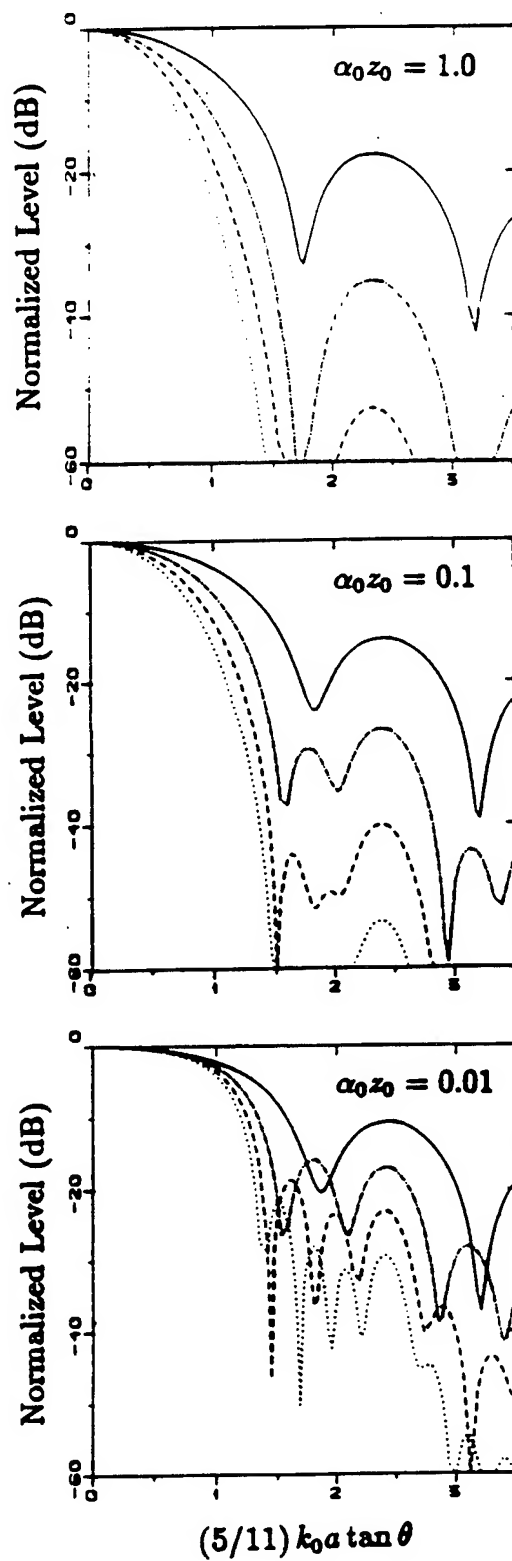
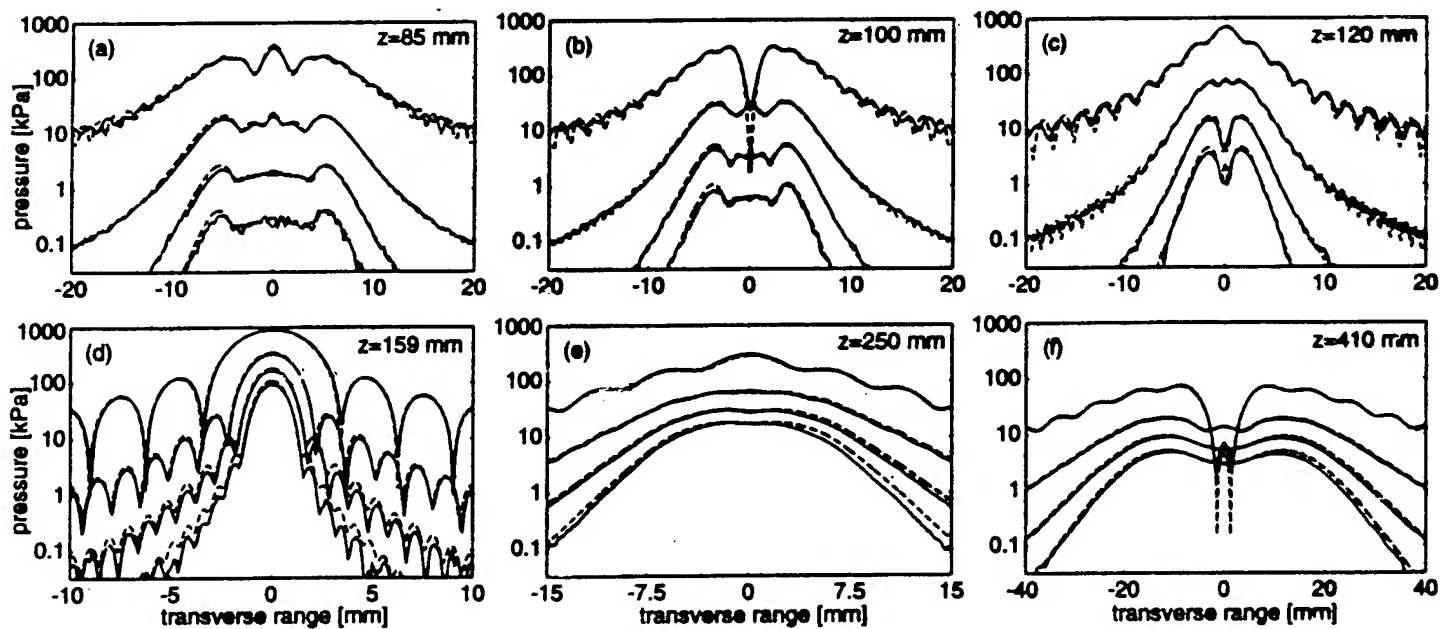
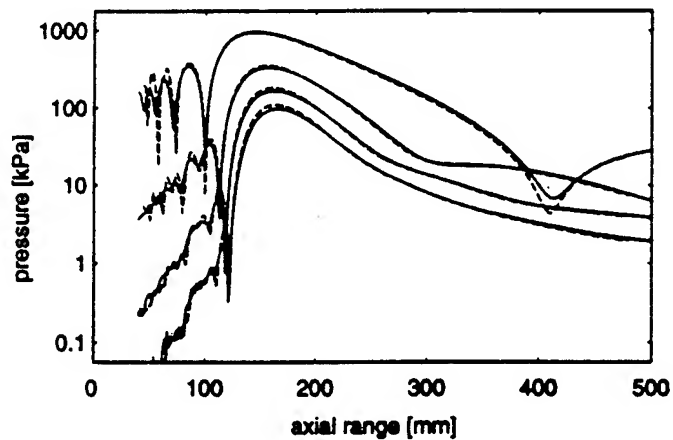


Figure 8.4

FOCUSED BEAM



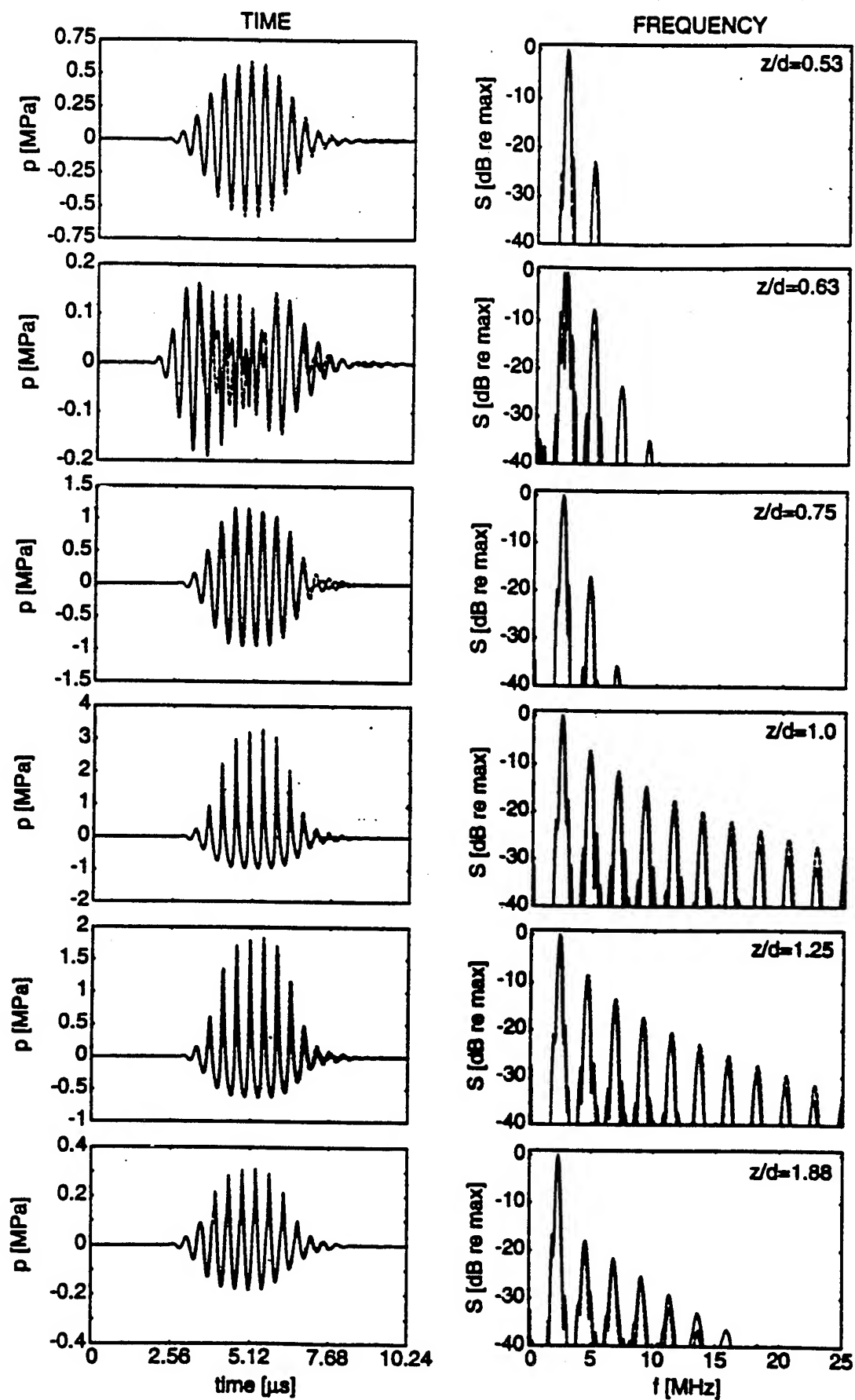
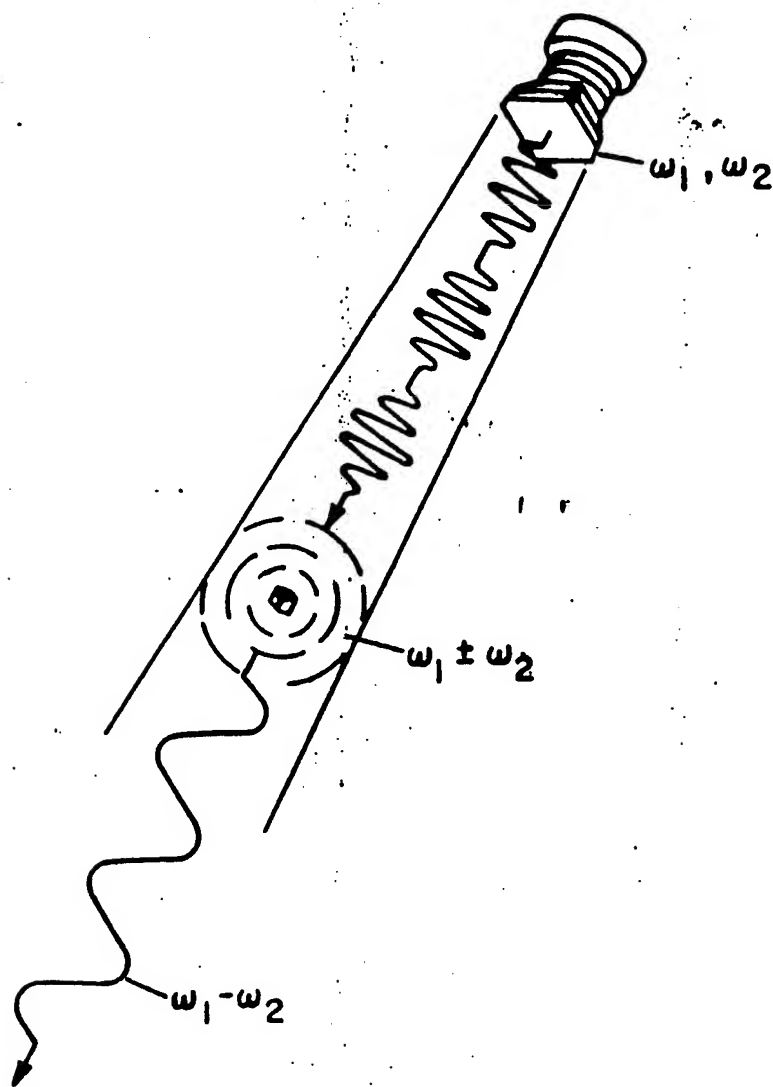
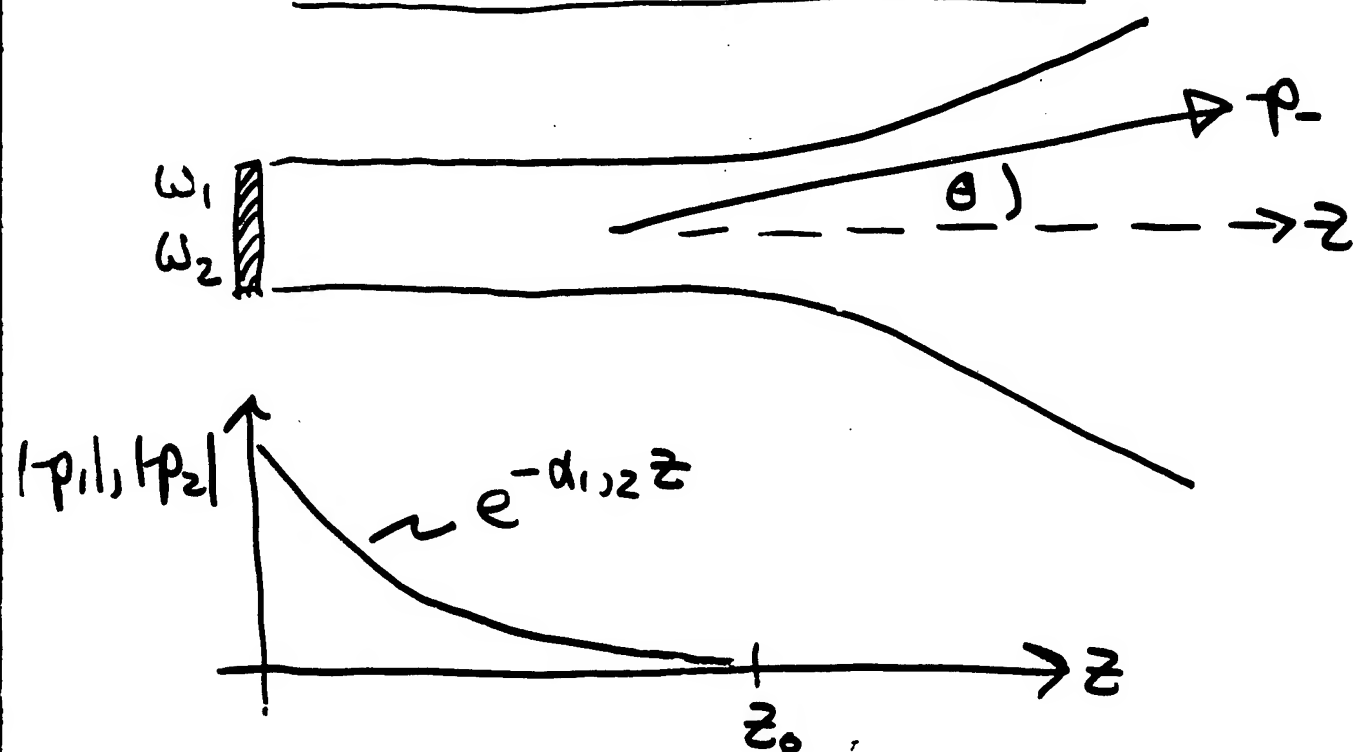


Figure 9

PROCESSES IN A PARAMETRIC TRANSMITTING ARRAY



WESTERVELT DIRECTIVITY



Collimated primary waves in nearfield:

$$p \simeq p_{01} e^{-\alpha_1 z} \sin(\omega_1 t - k_1 z) + p_{02} e^{-\alpha_2 z} \sin(\omega_2 t - k_2 z)$$

Difference frequency generation in nearfield behaves like exponentially tapered line array:

$$D_-(\theta) = \frac{1}{1 + jz(k_-/\alpha_T) \sin^2(\theta/2)}$$

Half-power angle:

$$(\alpha_T = \alpha_1 + \alpha_2 - \alpha_-)$$

$$\theta_{HP} \simeq \sqrt{\frac{2\alpha_T}{k_-}} \propto \sqrt{\frac{\lambda_-}{L_a}}$$

$$D(\theta) \approx \frac{1}{1 + jz(k_r/\alpha_T)\sin^2(\theta/2)}$$

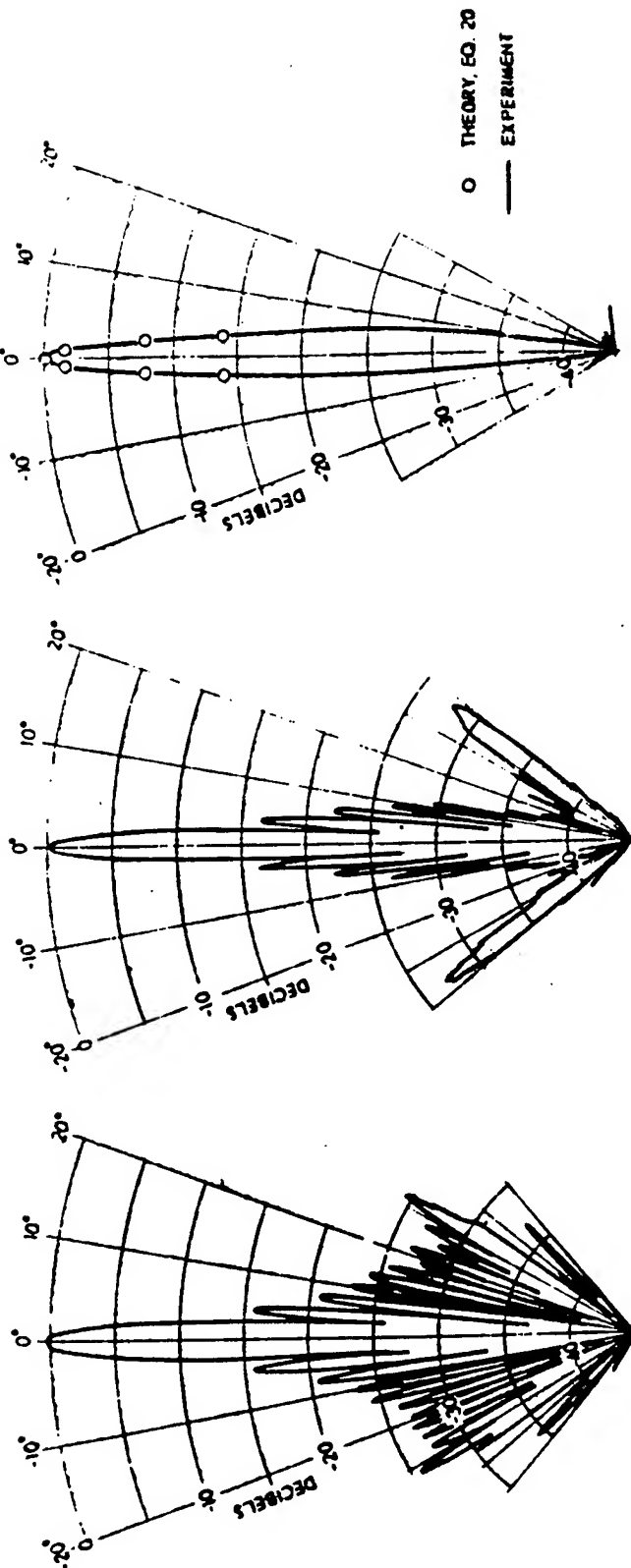


FIGURE 12
PARAMETRIC TRANSMITTING
ARRAY DIRECTIVITY PATTERNS

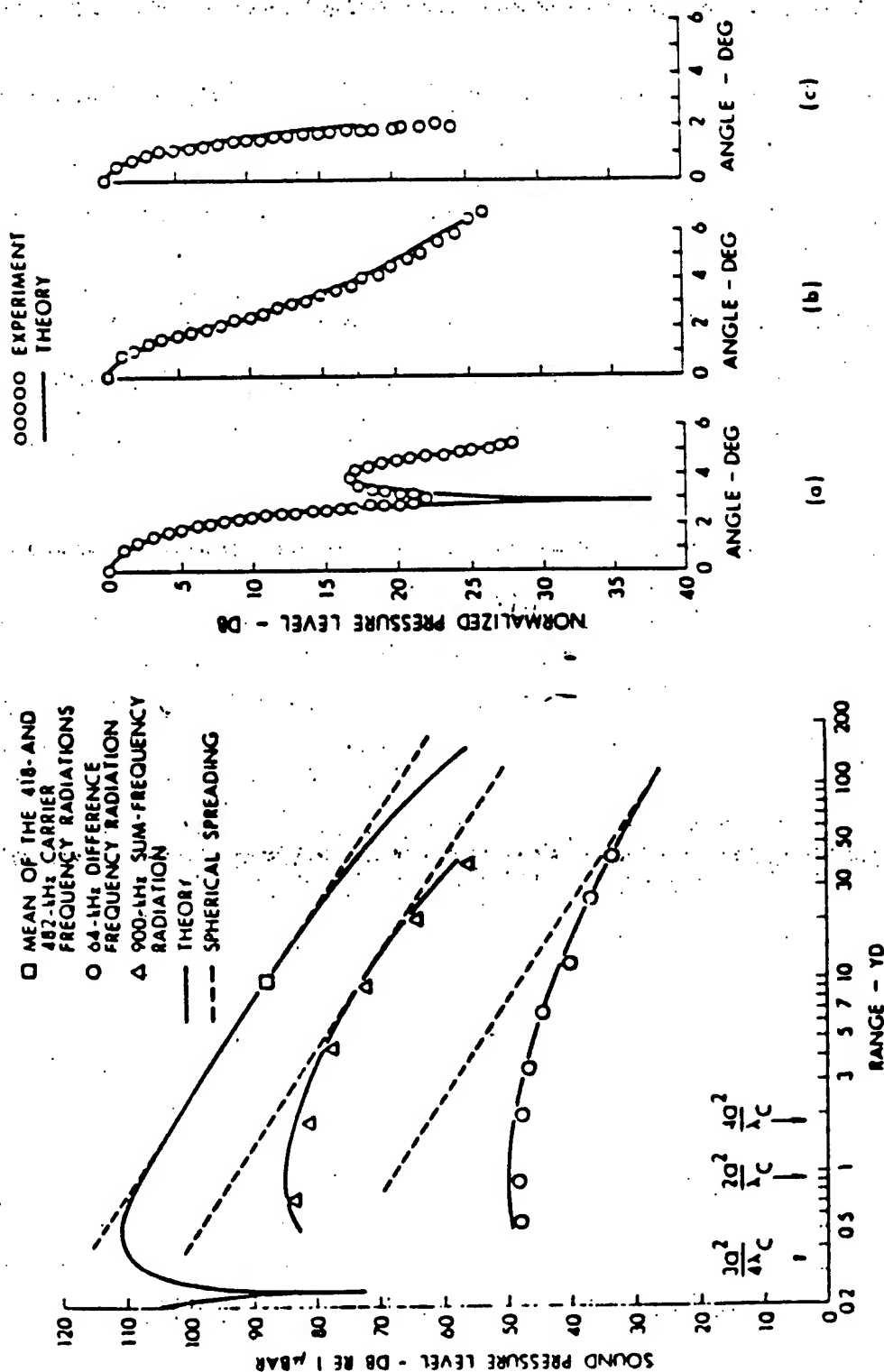


Fig. 8—Propagation curves for a parametric array.

Fig. 9—Beam patterns for the (a) 482 kHz primary, (b) 64 kHz difference frequency, and (c) 900 kHz sum frequency waves.

Ref. 85 $d=3''$

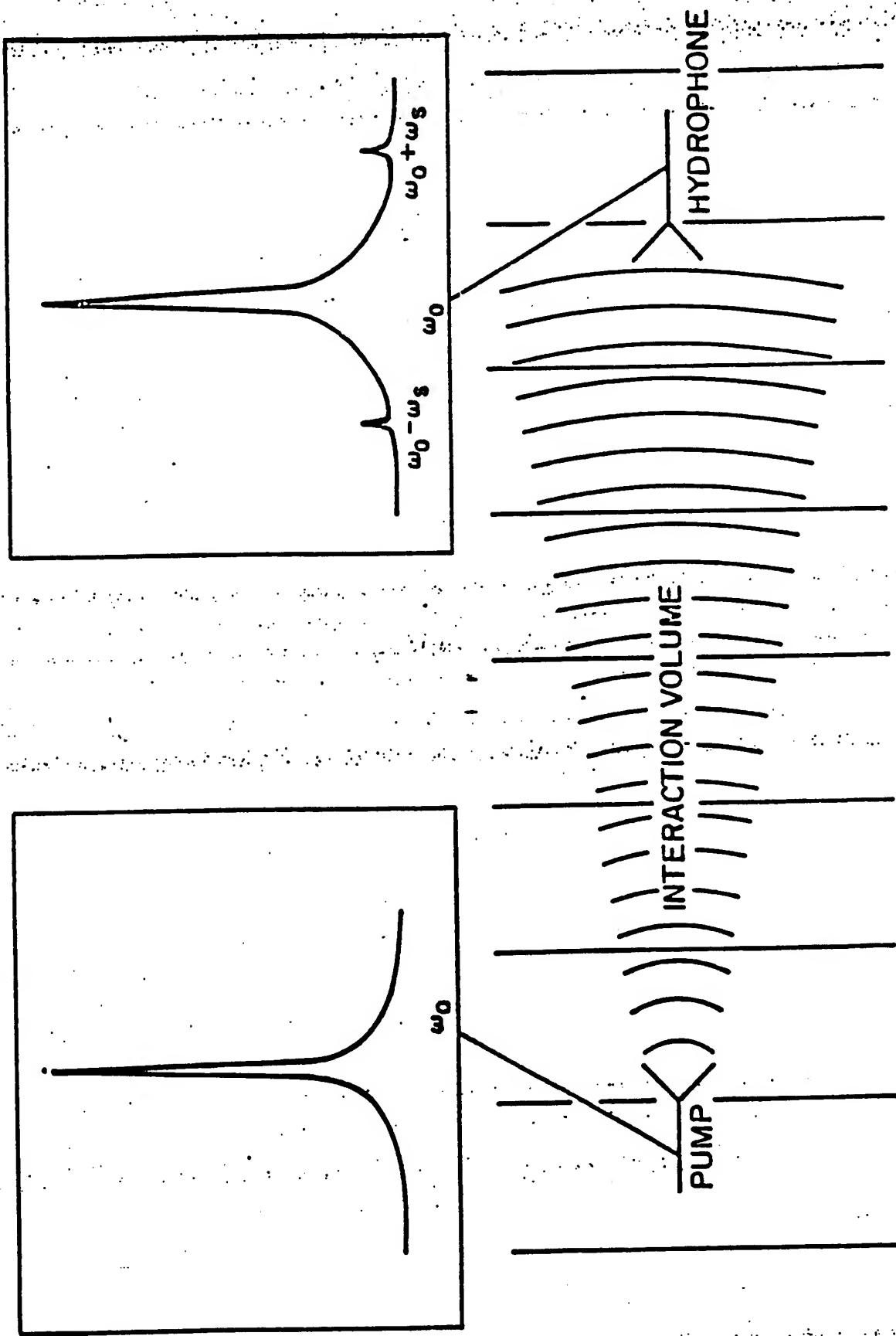


Figure 26. Parametric Receiving Array

Experimental Verification of Parametric Reception

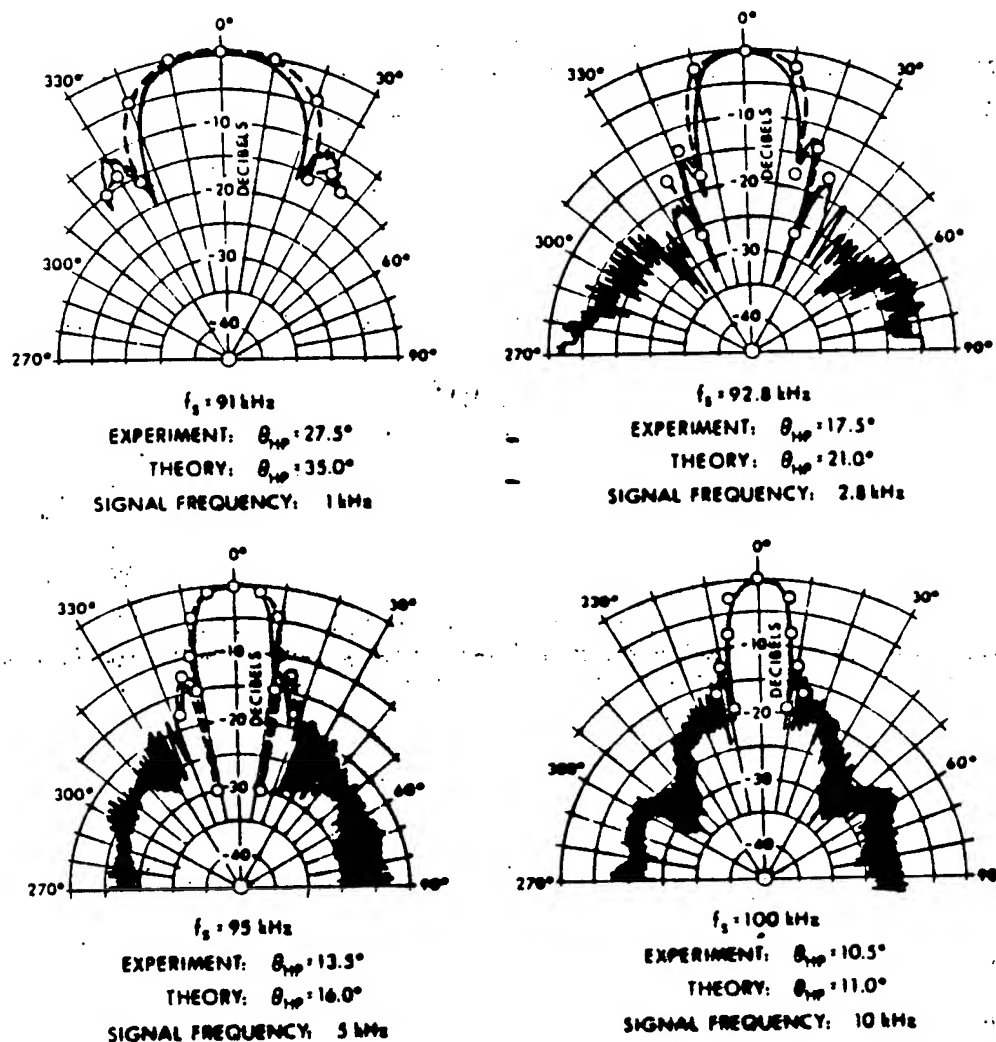


Figure 10-16.—Sum frequency patterns for a pump-receiver separation of 48 ft. Theoretical values $\circ - \circ$, experimental values —, $F_1 = 90 \text{ kHz}$, $P_1 = 101 \text{ dB re } 1 \mu\text{bar at } 1 \text{ yd}$, $P_2 = 85 \text{ dB re } 1 \mu\text{bar at input to parametric receiving array}$, $f_2 = 1.0, 2.8, 5 \text{ and } 10 \text{ kHz}$ (from Barnard et al. [16]).

Barnard, Willette, Truchard, & Shooter,
 JASA 52, 1437 (1972)

V. DISPERSION

RELAXATION

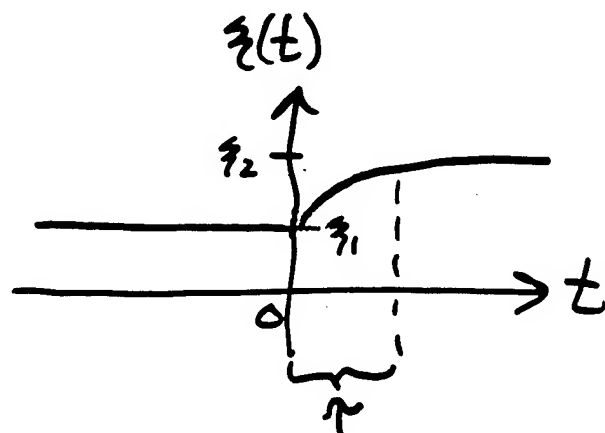
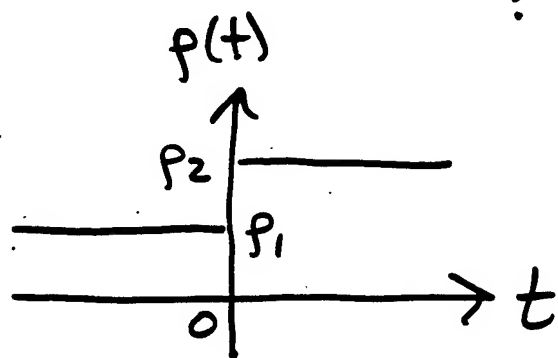
Let

$$p = p(p, \xi)$$

$$\xi = \xi(p) = \text{"internal" coordinate}$$

ξ provides macroscopic characterization of:

- chemical reactions
- molecular vibrations
- phase transitions
- \vdots



Assume:

$$\frac{d\xi}{dt} = -\frac{\xi - \xi_1}{\tau} = O(\varepsilon) \quad (\tau = \text{"relaxation time"})$$

Second order state equation:

$$p' = \underbrace{C_0^2 p'}_{O(\varepsilon)} + \underbrace{\frac{B}{2A} \frac{C_0^2}{P_0} p'^2}_{O(\varepsilon^2)} + \underbrace{M C_0^2 \int_{-\infty}^t \frac{\partial p'}{\partial t'} e^{-(t-t')/\tau} dt'}_{O(\varepsilon^2)}$$

$$M = \frac{C_\infty^2 - C_0^2}{C_0^2} = \text{dispersion} = O(\varepsilon)$$

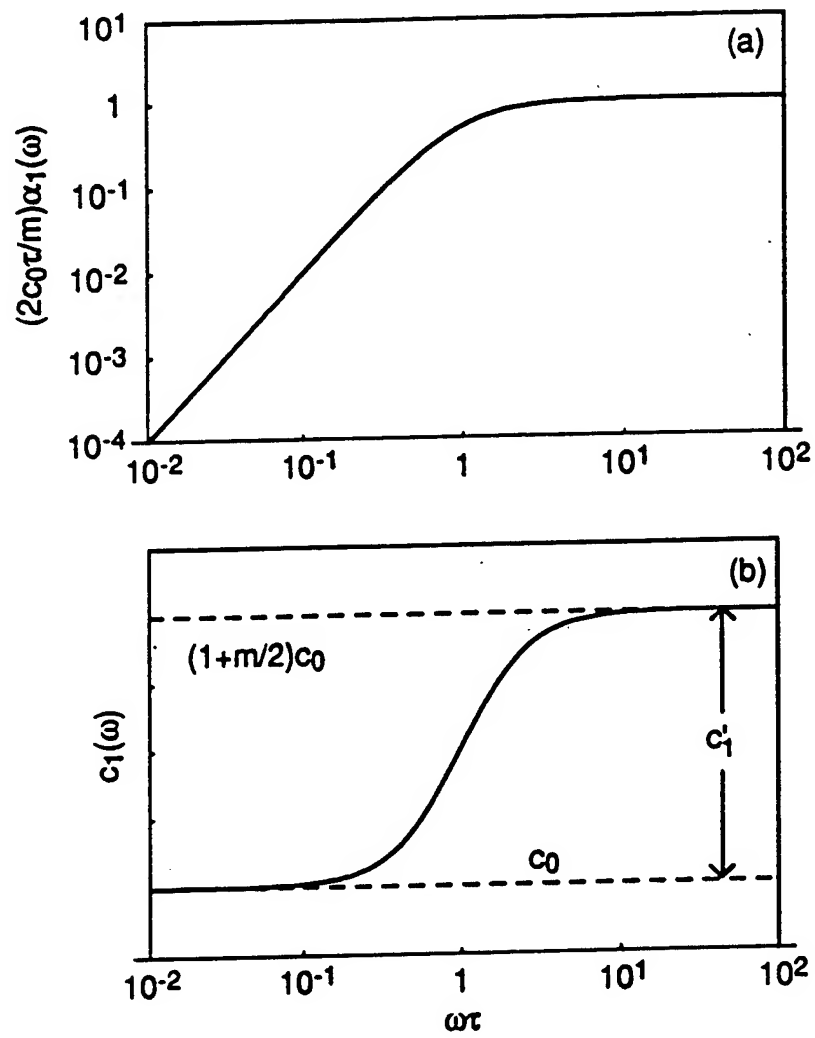


Figure 5.1

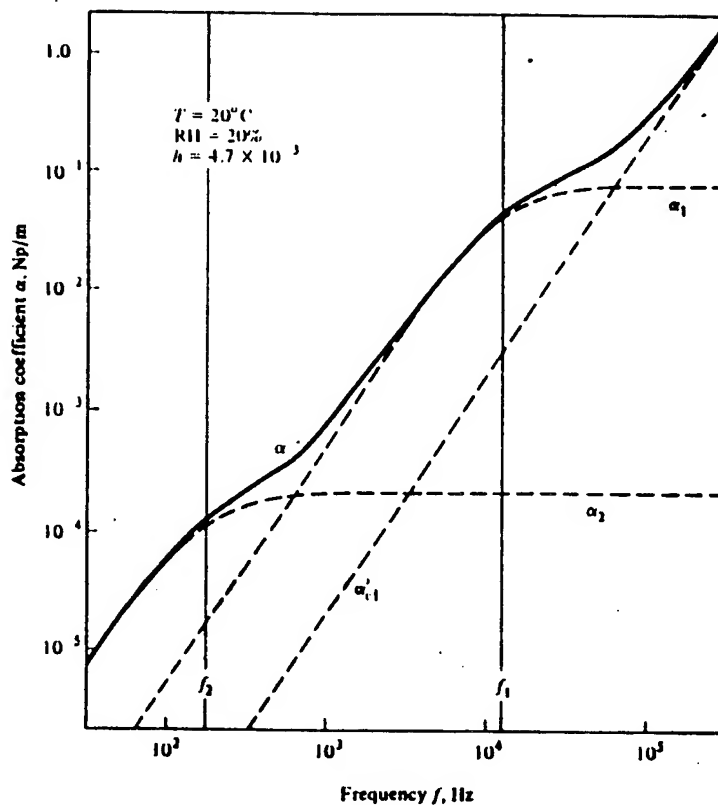
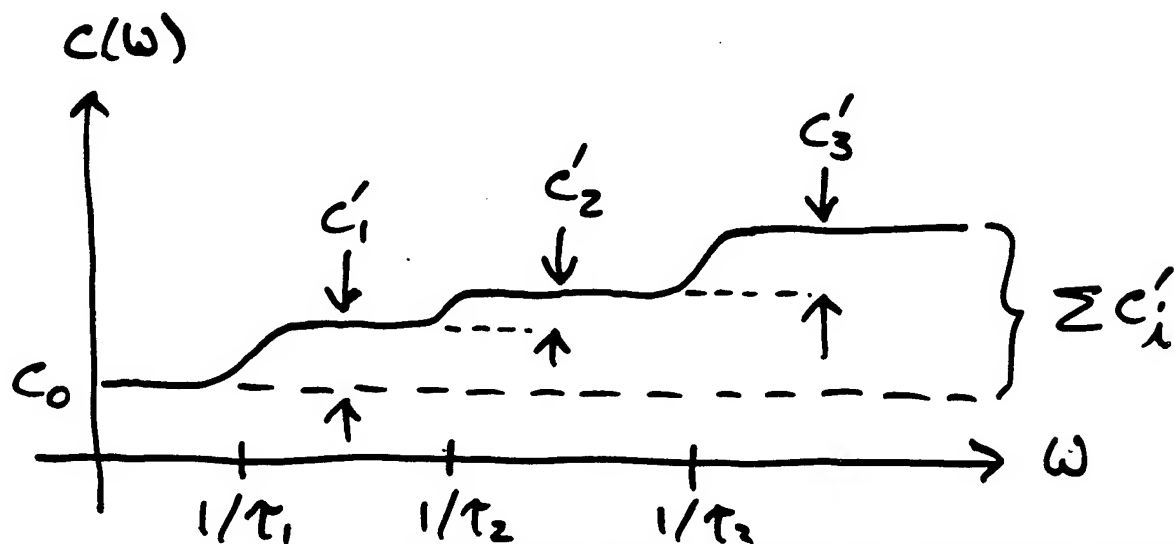


Figure 10-13 Log-log plot of sound-absorption coefficient versus frequency for sound in air at 20°C at 1 atm pressure and with a water-vapor fraction h of 4.676×10^{-3} ($\text{RH} = 20\%$). The two relaxation frequencies are 12,500 Hz (O_2) and 173 Hz (N_2).



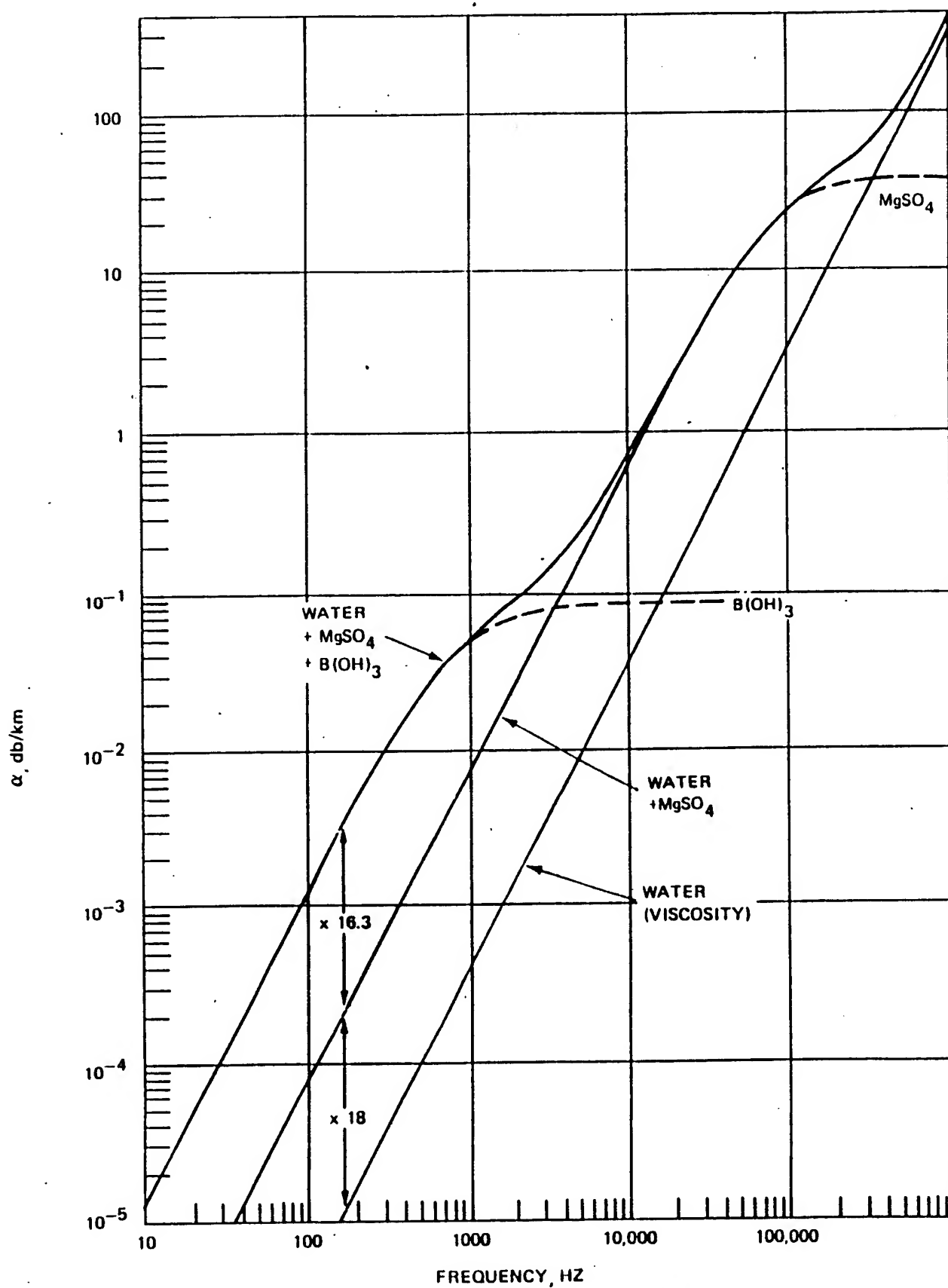


Fig. 7. Sound Absorption in Sea Water at 4°C, Pressure 1 atm (zero depth). Fisher and Simmons (27).

35 ppt salinity
pH = 8

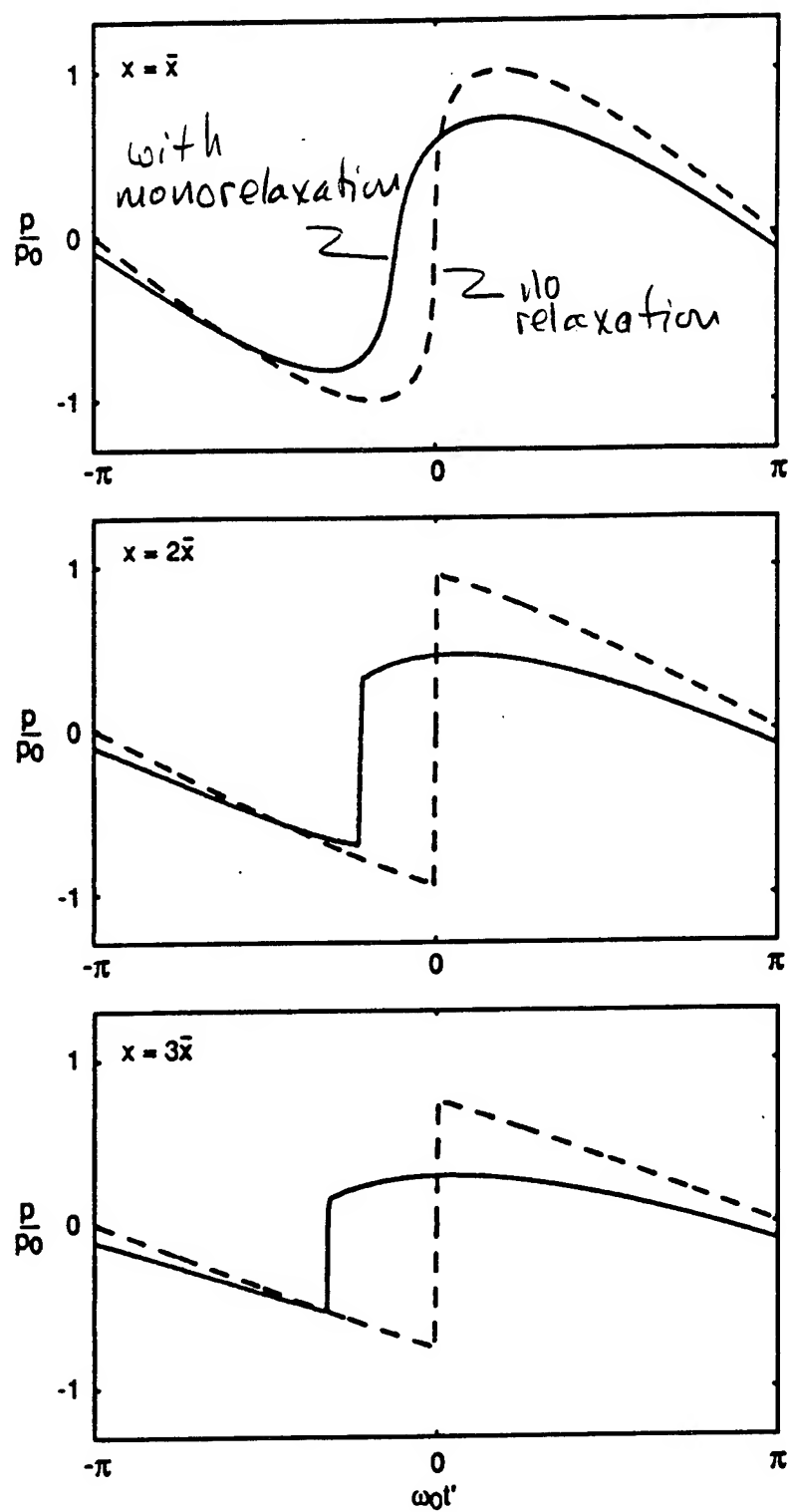
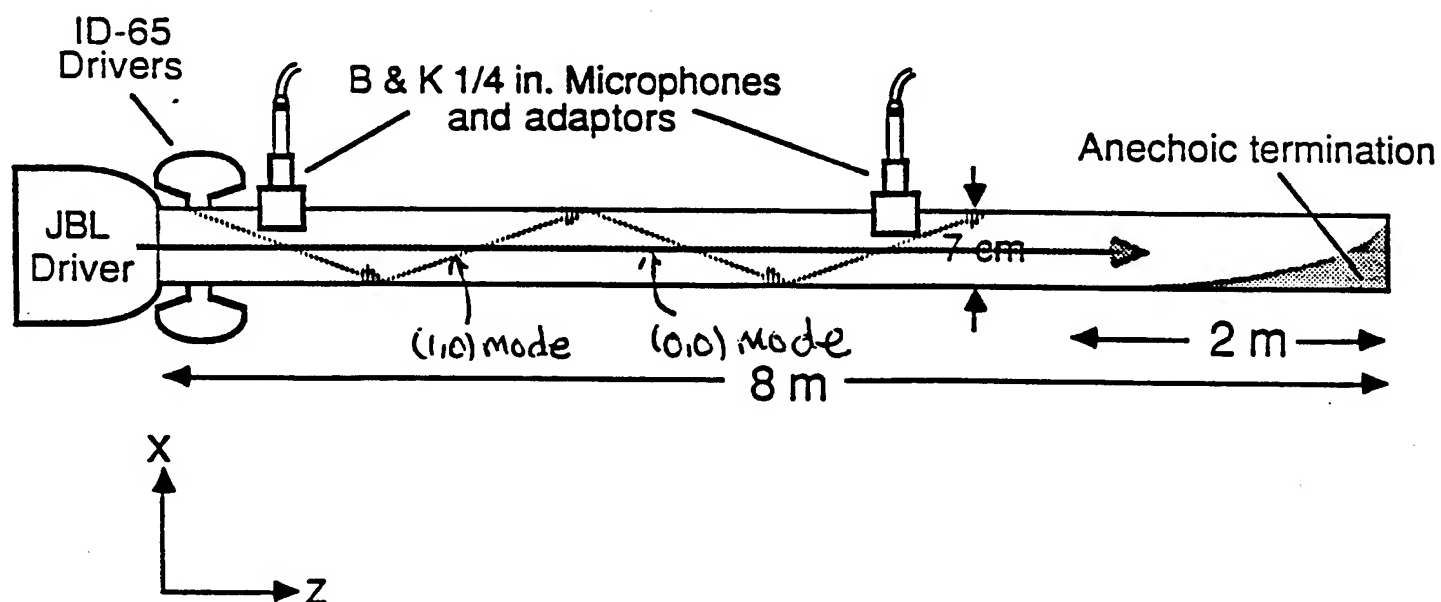
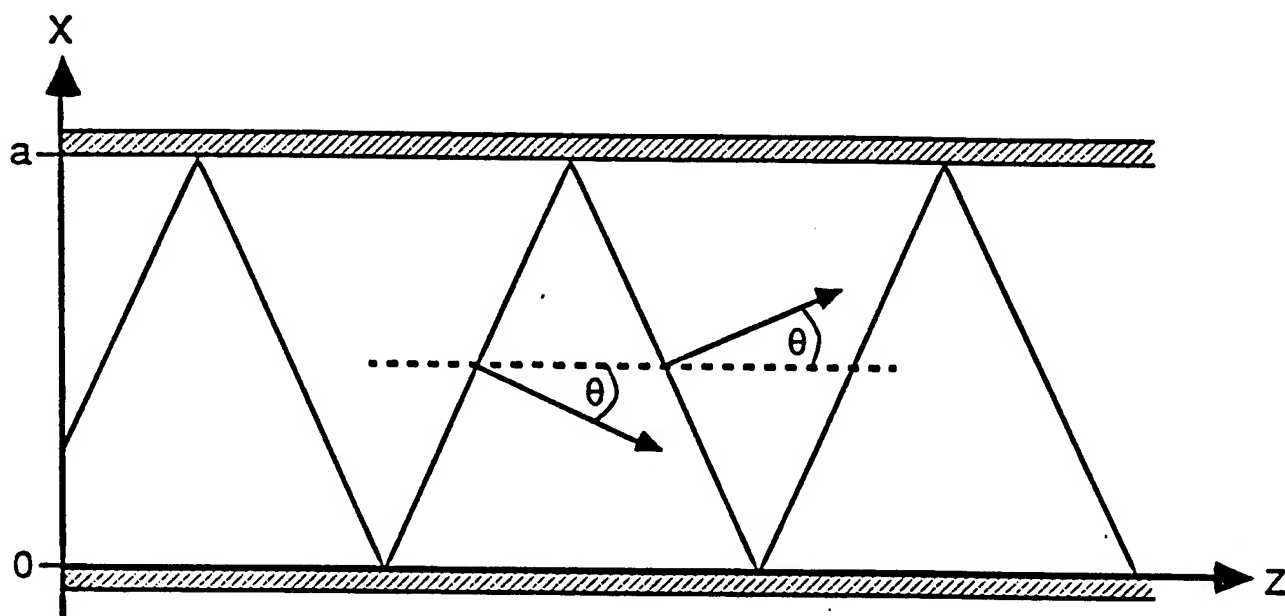


Figure 5.3

WAVEGUIDE DISPERSION



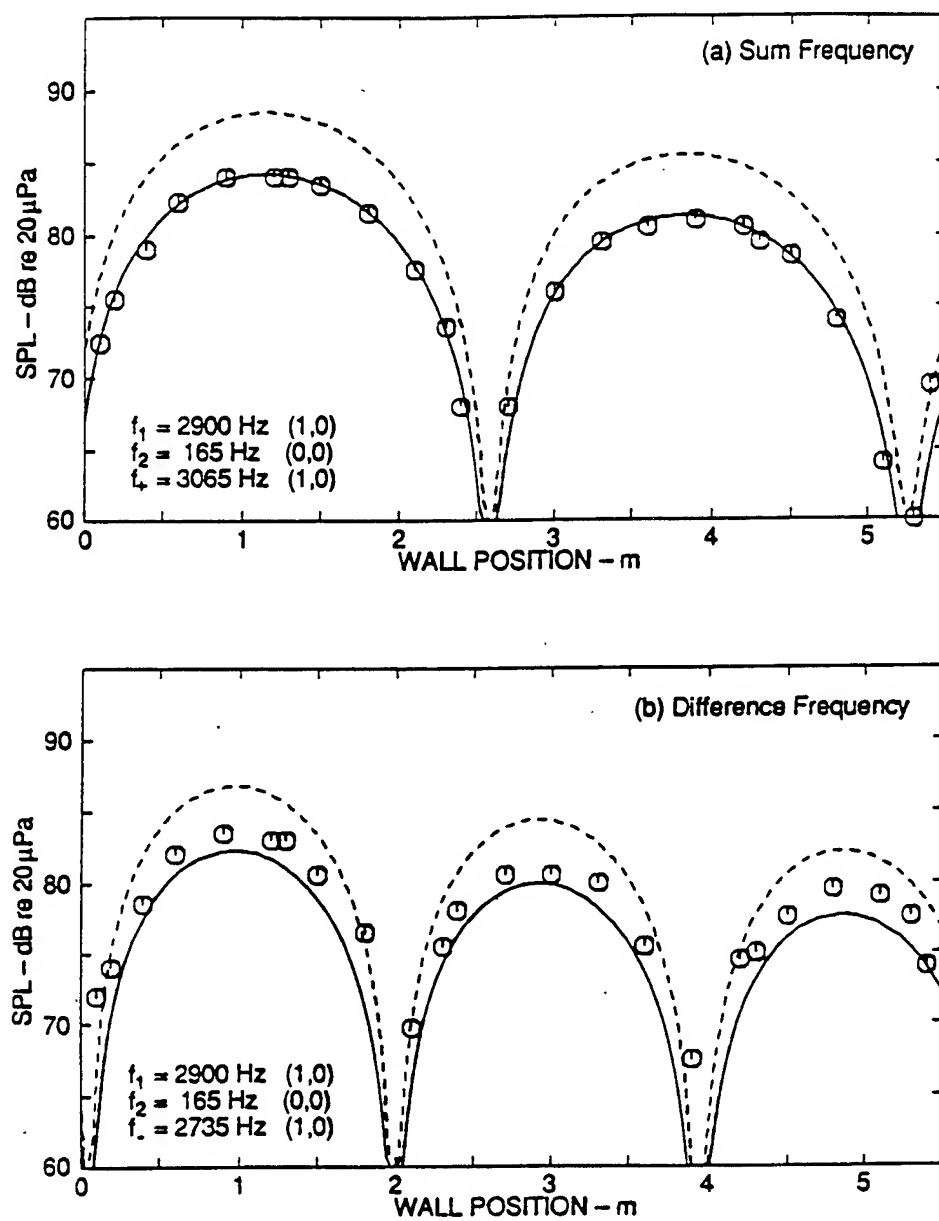


Figure 5.5

Hamilton & TenCate, JASA 81, 1703 (1987)

BASIC EQUATIONS FOR BUBBLY LIQUIDS

Assume uniform distribution of identical bubbles, each of volume $V = V_0 + v$ and number/volume N . Average density ρ of mixture:

$$\rho_0/\rho = NV + (1 - NV_0)\rho_{l0}/\rho_l$$

Expand densities ($\rho = \rho_0 + \rho'$, $\rho_l = \rho_{l0} + \rho'_l$, $\rho_g = \rho_{g0} + \rho'_g$) and linearize:

$$\frac{\rho'}{\rho_0} = \frac{p}{\rho_0 c_0^2} - Nv$$

Linear wave equation:

$$\nabla^2 p - \frac{1}{c_0^2} \frac{\partial^2 p}{\partial t^2} = -\rho_0 N \frac{\partial^2 v}{\partial t^2} \quad (1)$$

Rayleigh-Plesset equation [$V = (4\pi/3)R^3$]:

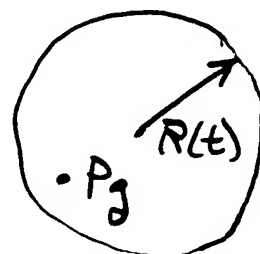
$$R\ddot{R} + \frac{3}{2}\dot{R}^2 + 4\nu\frac{\dot{R}}{R} = \frac{P_g - P}{\rho_0}$$

Adiabatic gas law:

$$P_g/P_0 = (V_0/V)^\gamma$$

Quadratic equation for bubble volume:

$$\ddot{v} + \delta\omega_0\dot{v} + \omega_0^2 v + \eta p = av^2 + b(2v\ddot{v} + \dot{v}^2) \quad (2)$$



• P

LINEAR THEORY

$$\omega_0 = \sqrt{\frac{3\gamma P_0}{\rho_0 R_0^2}} = \text{bubble resonance}$$

$$\delta = \frac{4\nu}{\omega_0 R_0^2} = \text{viscous damping}$$

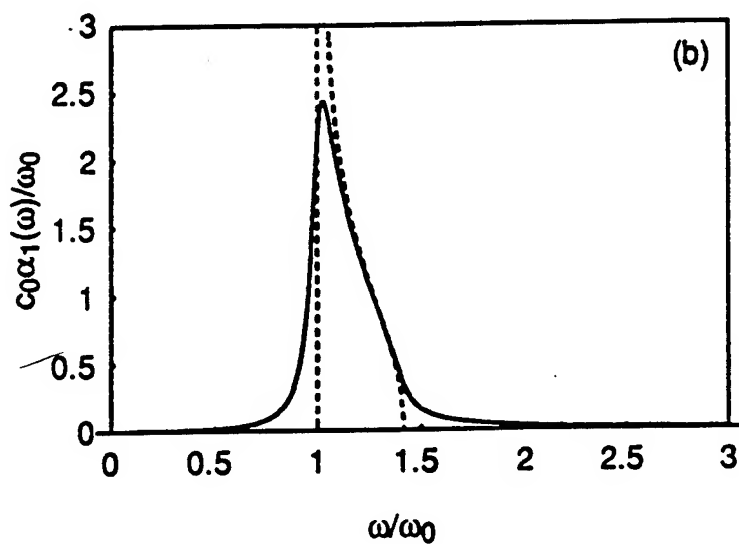
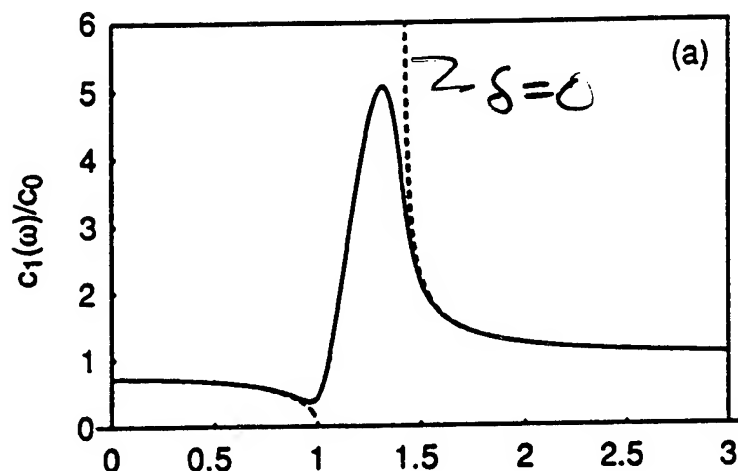
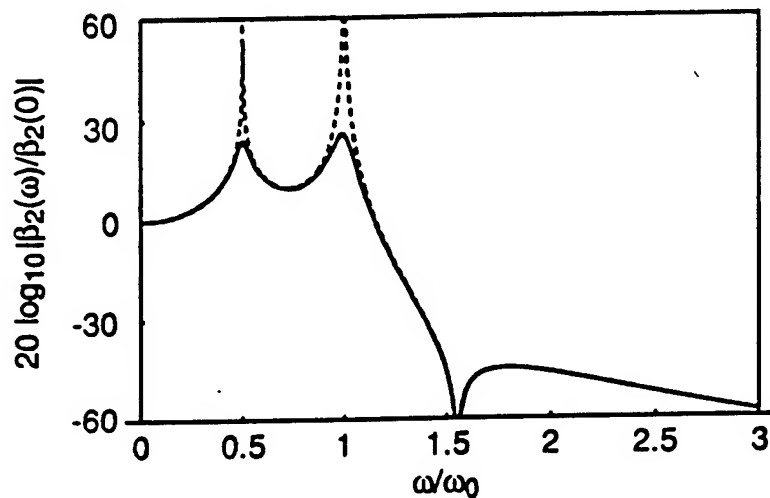


Figure 5.6

SECOND HARMONIC GENERATION

$$p = \frac{1}{2} (p_1 e^{j\omega t} + p_2 e^{j2\omega t}) + \text{c.c.}$$

$$\left(\nabla^2 + \frac{4\omega^2}{c_2^2} \right) p_2 = \beta_2(\omega) \frac{2\omega^2}{\epsilon_0 c_0^4} p_1^2$$



$\beta_2(\omega)$ = effective coefficient of nonlinearity

Figure 5.7

KdV-BURGERS EQUATION

Plane wave equation:

$$\frac{\partial^2 p}{\partial x^2} - \frac{1}{c_0^2} \frac{\partial^2 p}{\partial t^2} = -\rho_0 N \frac{\partial^2 v}{\partial t^2}$$

Below resonance ($\omega^2 \ll \omega_0^2$), bubble equation reduces to:

$$v = -\frac{\eta}{\omega_0^2} p - \frac{\delta}{\omega_0} \dot{v} - \frac{1}{\omega_0^2} \ddot{v} + \frac{a}{\omega_0^2} v^2$$

Volume terms are second order, so use $v = -\eta p / \omega_0^2$:

$$v = -\frac{\eta}{\omega_0^2} p + \frac{\delta \eta}{\omega_0^3} \dot{p} + \frac{\eta}{\omega_0^4} \ddot{p} + \frac{a \eta^2}{\omega_0^6} p^2$$

Substitute in wave equation, with $c_{00}^2 = c_0^2 / (1 + \mu C)$:

$$\frac{\partial^2 p}{\partial x^2} - \frac{1}{c_{00}^2} \frac{\partial^2 p}{\partial t^2} = -\frac{\mu \rho_0 \eta}{\omega_0^4 V_0} \left(\delta \omega_0 \frac{\partial^3 p}{\partial t^3} + \frac{\partial^4 p}{\partial t^4} + \frac{a \eta}{\omega_0^2} \frac{\partial^2 p^2}{\partial t^2} \right)$$

Introduce slow scales:

$$t' = t - x/c_{00} \quad x_1 = \epsilon x$$

$O(\epsilon^2)$ relation on slow scale:

$$\frac{\partial p}{\partial x} = a' p \frac{\partial p}{\partial t'} + b' \frac{\partial^3 p}{\partial t'^3} + c' \frac{\partial^2 p}{\partial t'^2}$$

KdV SOLITONS

Ignore losses:

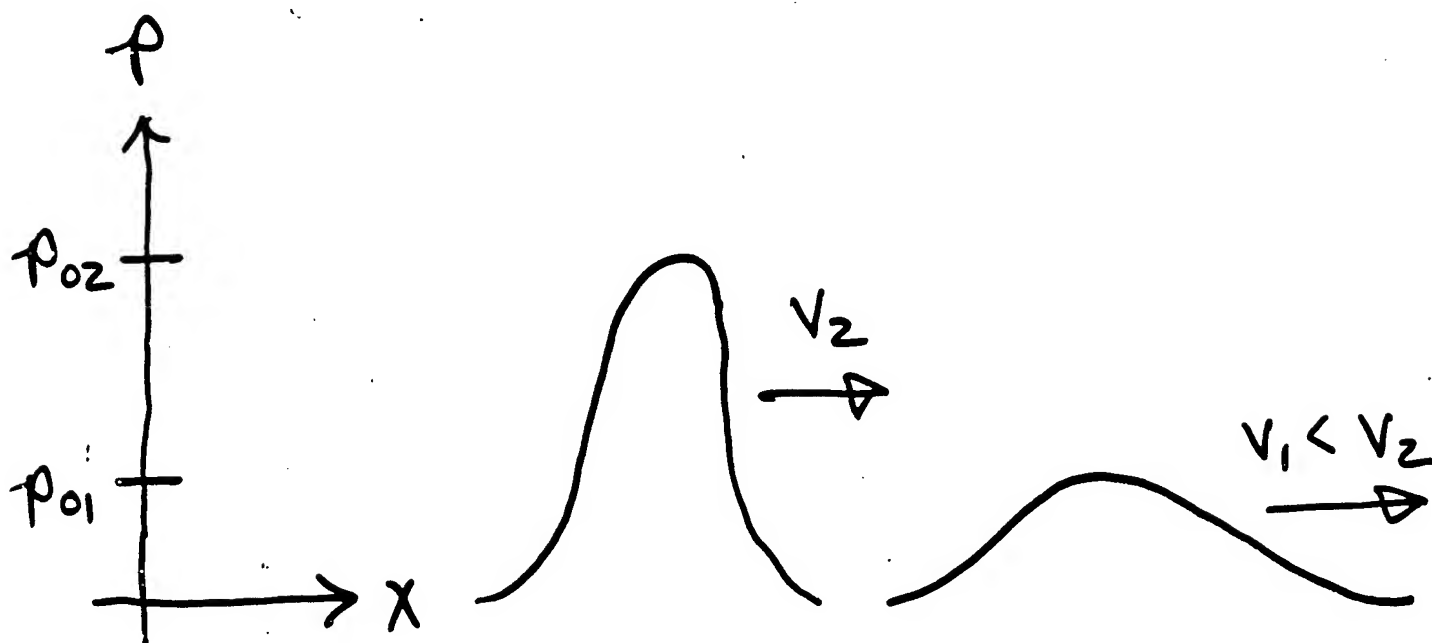
$$\frac{\partial p}{\partial x} = a' p \frac{\partial p}{\partial t'} + b' \frac{\partial^3 p}{\partial t'^3}$$

Single soliton solution:

$$p = p_0 \operatorname{sech}^2 \left(\frac{t - x/v}{T} \right)$$

where

$$(v - c_{00}) \propto p_0 \quad T \propto \frac{1}{\sqrt{p_0}}$$



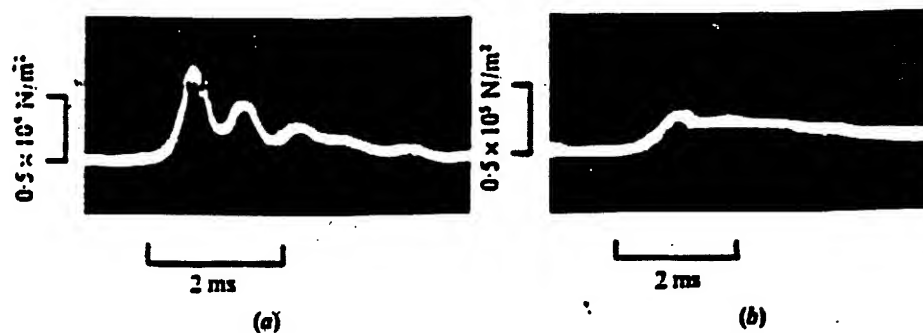


FIGURE 13. Evolution of the multi-soliton perturbation in a liquid with He bubbles.
 $\sigma = 36$; $\sigma/Re = 0.14$; $\Delta P_0 = 1.74 \times 10^5 \text{ N/m}^2$; $L_0 = 0.15 \text{ m}$.

	$L \text{ (m)}$	$P_0 \times 10^{-5}$ (N/m^2)	$\phi_0 \times 10^2$	$R_0 \times 10^2 \text{ (m)}$	$\Delta P_0/\Delta P_0$
(a)	0.6	1.07	1.03	1.24	0.47
(b)	1.4	1.16	0.95	1.21	0.16

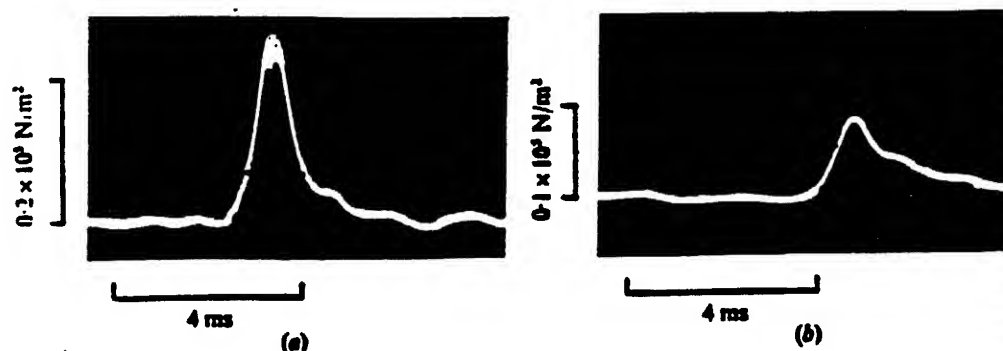


FIGURE 14. Evolution of a single soliton in a liquid with He bubbles.
 $\sigma = 13.1$; $\sigma/Re = 0.21$; $\Delta P_0 = 0.628 \times 10^5 \text{ N/m}^2$; $L_0 = 0.09 \text{ m}$.

	$L \text{ (m)}$	$P_0 \times 10^{-5}$ (N/m^2)	$R_0 \times 10^2 \text{ (m)}$	$\phi_0 \times 10^2$	$\Delta P_0/\Delta P_0$
(a)	0.6	1.07	1.24	1.03	0.415
(b)	1.4	1.16	1.21	0.95	0.149

VI. ACOUSTIC STREAMING

STREAMING PARAMETERS

$$p = p_0 + p_1 + p_{dc}$$

$$p = p_0 + p_1 + p_{dc}$$

$$\vec{u} = \underbrace{\quad}_{O(1)} \underbrace{\vec{u}_1}_{O(\epsilon)} + \underbrace{\vec{u}_{dc}}_{O(\epsilon^2)}$$

where

$$f_{dc} \triangleq \frac{1}{T} \int_T f dt$$

Mass Flow Rate:

$$\begin{aligned} \left\langle \frac{\text{mass}}{\text{unit time}} \right\rangle &= \int_S \langle p \vec{u} \rangle \cdot d\vec{S} \\ &= p_0 \int_S \left(\vec{u}_{dc} + \frac{\langle p_1 \vec{u}_1 \rangle}{p_0} \right) \cdot d\vec{S} + O(\epsilon^3) \end{aligned}$$

Define:

$$\begin{aligned} \vec{U} &= \vec{u}_{dc} + \frac{\langle p_1 \vec{u}_1 \rangle}{p_0} \\ &= \text{mass transport velocity} \end{aligned}$$

See Nyborg, "Acoustic Streaming",
Physical Acoustics, Academic (1965)

FIELD EQUATIONS

Combine continuity and momentum to eliminate density, and time average:

where

$$\mu \nabla^2 \vec{u}_{dc} = \vec{\nabla} p_{dc} - \vec{F}$$

$$\vec{F} = -\rho_0 \langle (\vec{u}_i \cdot \vec{\nabla}) \vec{u}_i + \vec{u}_i (\vec{\nabla} \cdot \vec{u}_i) \rangle$$

= driving force (per unit volume)

Plane Waves:

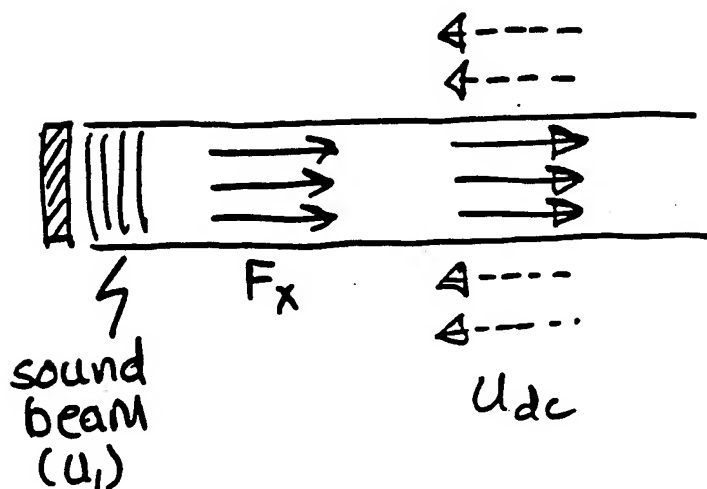
$$F_x = -\rho_0 \frac{\partial \langle u_i^2 \rangle}{\partial x}$$

Example:

$$u_i = u_0 e^{-\alpha x} \sin(\omega t - kx)$$

$$F_x = \alpha \rho_0 u_0^2 e^{-2\alpha x}$$

$$= 0 \text{ if } \alpha = 0$$



ACOUSTIC STREAMING

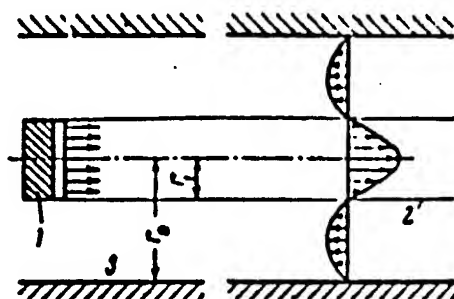


Figure 7-6.—Acoustic streaming for a sawtooth wave
(from Statnikov [13]).

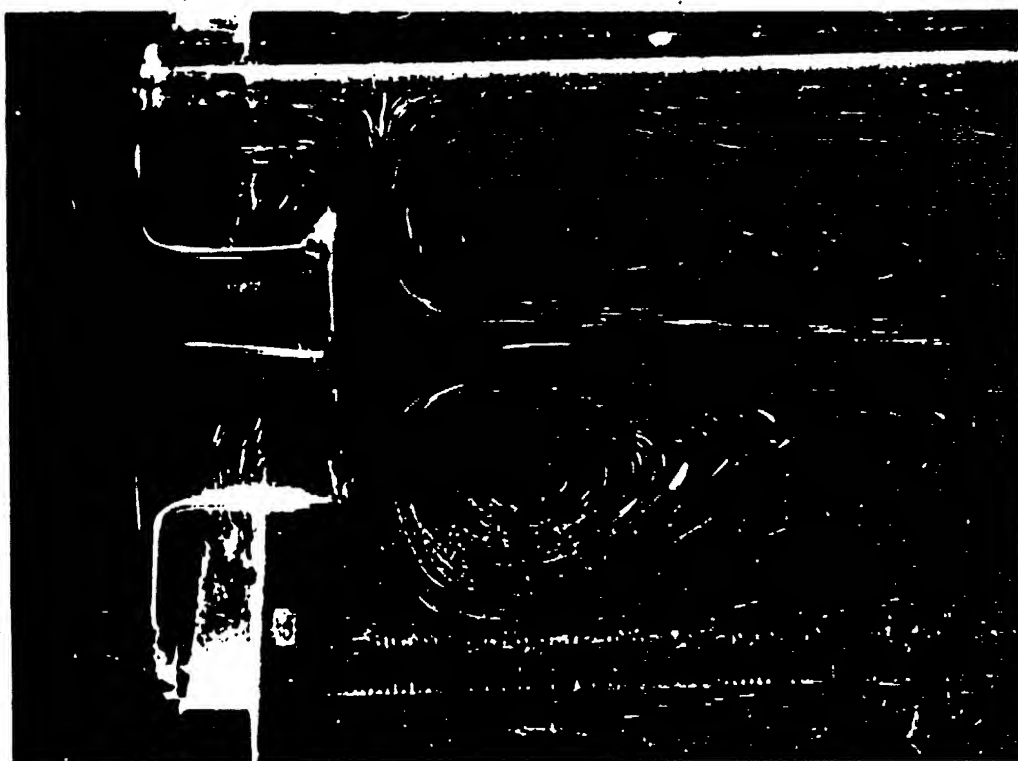


Figure 7-4.—Acoustic streaming from a sound source in water. The motion is made visible by a suspension of finely divided aluminum (from Liebermann [11]).

Matsuda et al. (1993):

$$Re = \frac{u_0 l}{\nu}$$

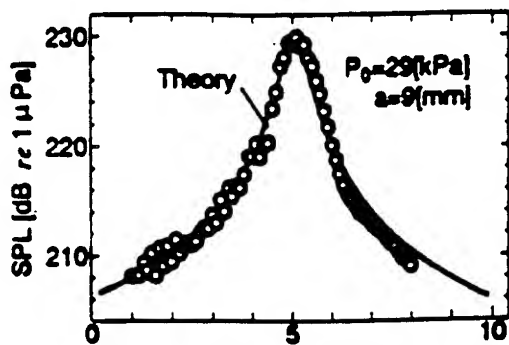


Fig. 1. Axial sound field.

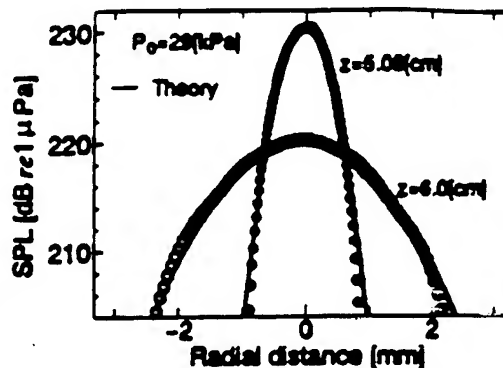


Fig. 2. Radial sound profile.

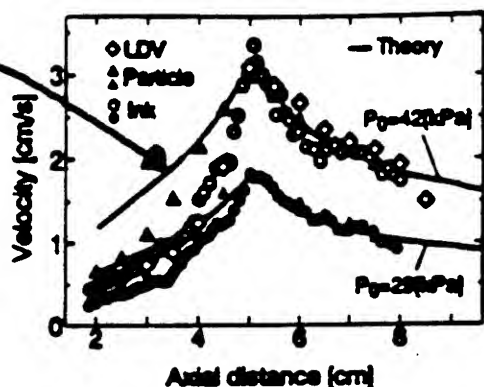


Fig. 3. Velocity profiles on axis.

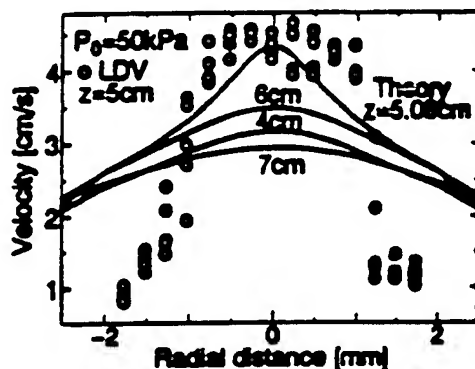


Fig. 4. Off-axis velocity profile.

Starritt et al. (1989):

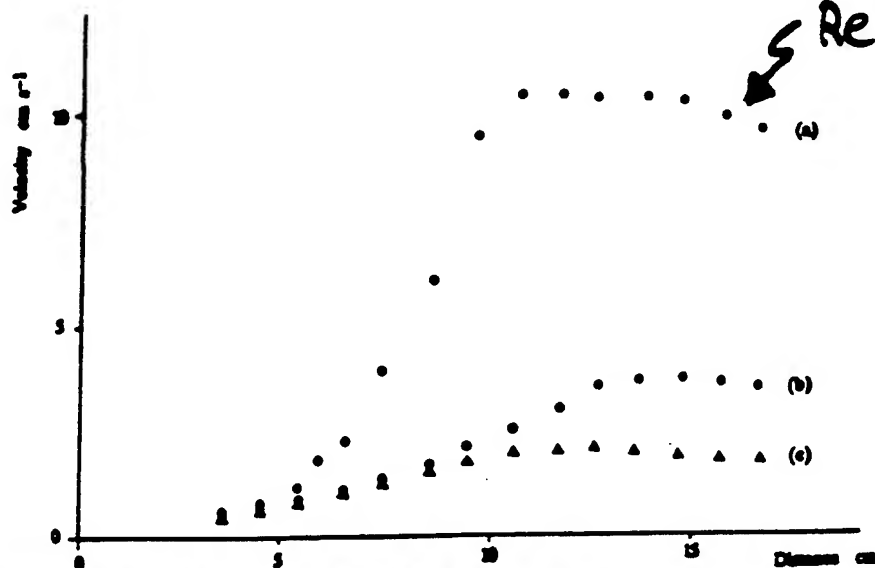
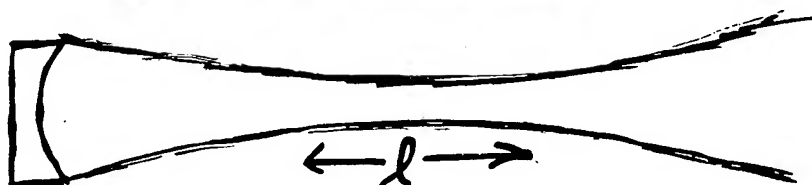
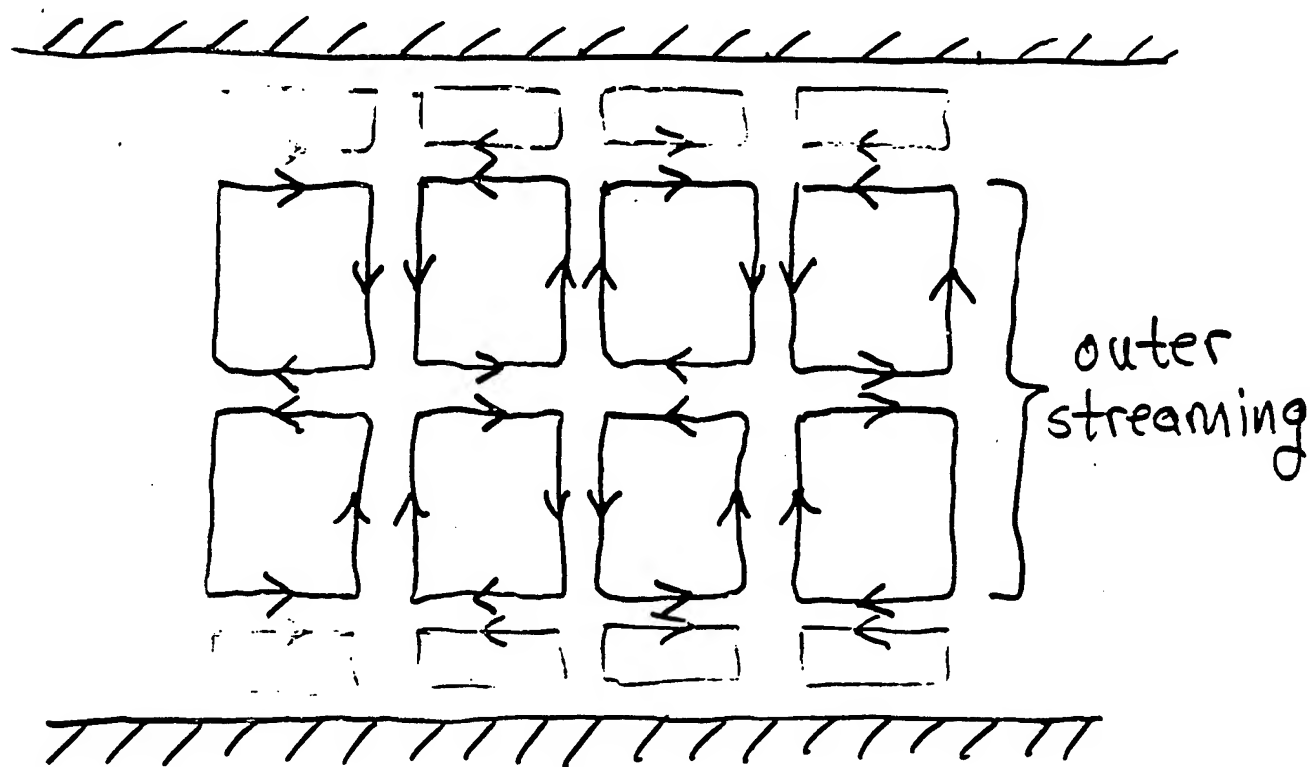
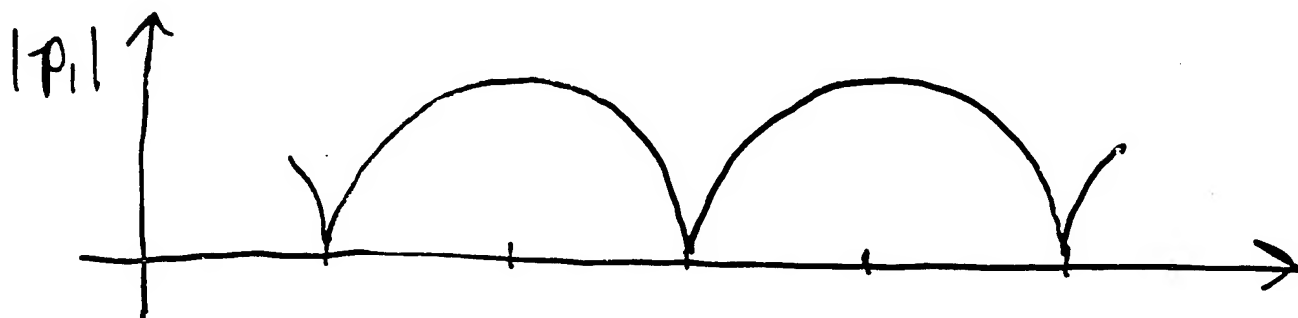
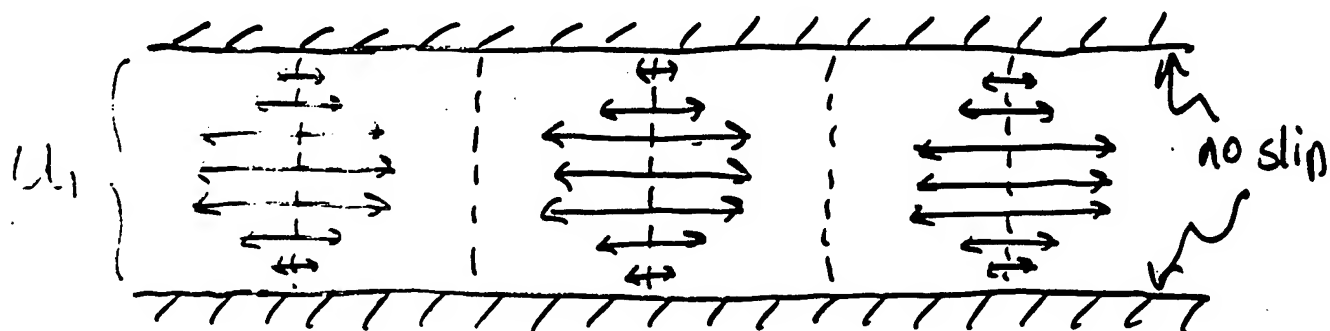


Fig. 5. Variation in streaming velocity with distance from transducer. 3.5 MHz, pulse length 3 μ s, total acoustic power 100 mW. (a) peak positive pressure, $p^* = 3.4$ MPa, prf 2 kHz. (b) $p^* = 1.4$ MPa, prf 20 kHz. (c) $p^* = 0.2$ MPa, cw.



STANDING WAVES BETWEEN PARALLEL PLATES



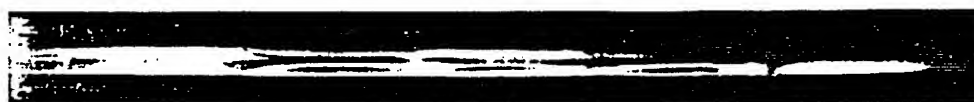


FIG. 9.—Five sections of the node-antinode circulation. Wave-length 56.5 cm.

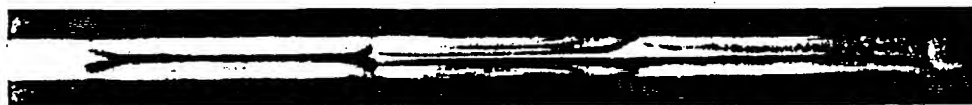


FIG. 10.—Three sections of the node-antinode circulation.



FIG. 11.—Two sections of the node-antinode circulation.

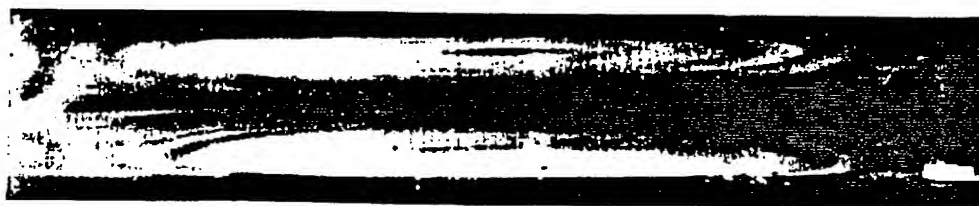


FIG. 12.—One section, node to antinode, of the circulation. Wave-length 56.5 cm.

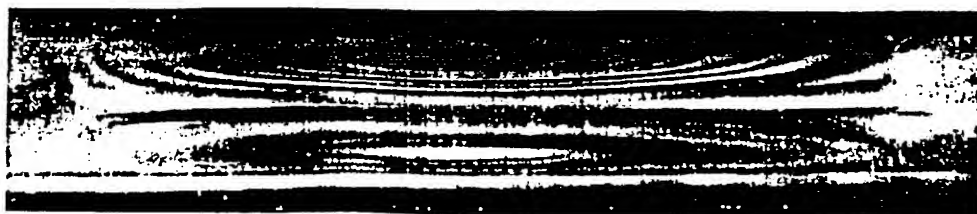


FIG. 13.—Another photograph of a node to antinode action of the circulation.



31. Secondary streaming induced by an oscillating cylinder. A long circular cylinder is oscillated normal to its axis by a loudspeaker in a mixture of water and glycerine. Suspended glass beads are illuminated in a cross plane by a stroboscope. The amplitude of oscillation is 0.17 of the

radius, and the Reynolds number based on frequency and radius is 70. The steady second-order streaming motion is directed toward the body along the axis of oscillation (indicated by arrows) in the inner region, and opposite in the outer region. Photograph by Masakazu Tatsumo

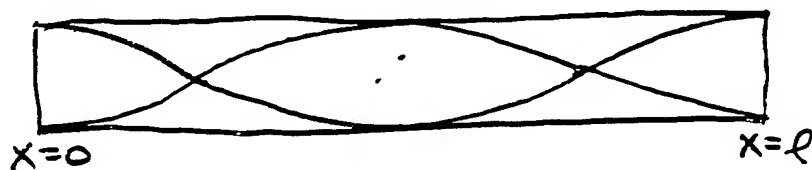
VII. RADIATION PRESSURE

RADIATION PRESSURE

[See Lee & Wang, JASA 94, 1099 (1993)]

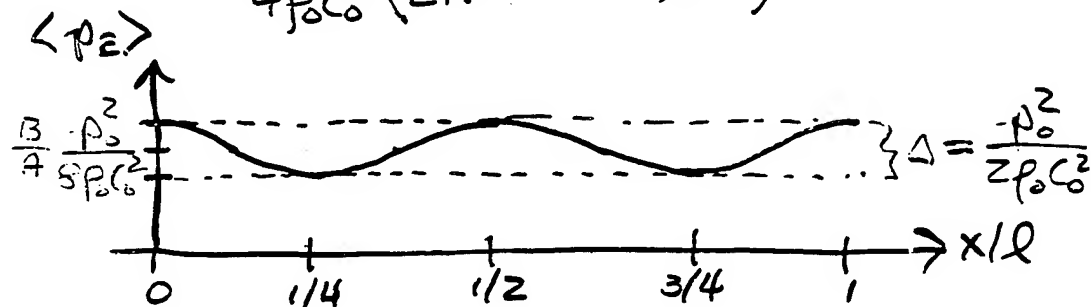
- Primary Field: Standing Wave

$$p_1 = p_0 \cos\left(\frac{n\pi x}{\ell}\right) \sin(\omega_n t)$$



- DC Pressure Field:

$$\begin{aligned} \langle p_E \rangle &= \left\langle \frac{p_1^2}{2\rho_0 c_0^2} - \frac{\rho_0 u_1^2}{2} \right\rangle + \text{const} \\ &= \frac{p_0^2}{4\rho_0 c_0^2} \left(\frac{B}{2A} + \cos^2 \frac{2n\pi x}{\ell} \right) \quad (\text{Eulerian}) \end{aligned}$$



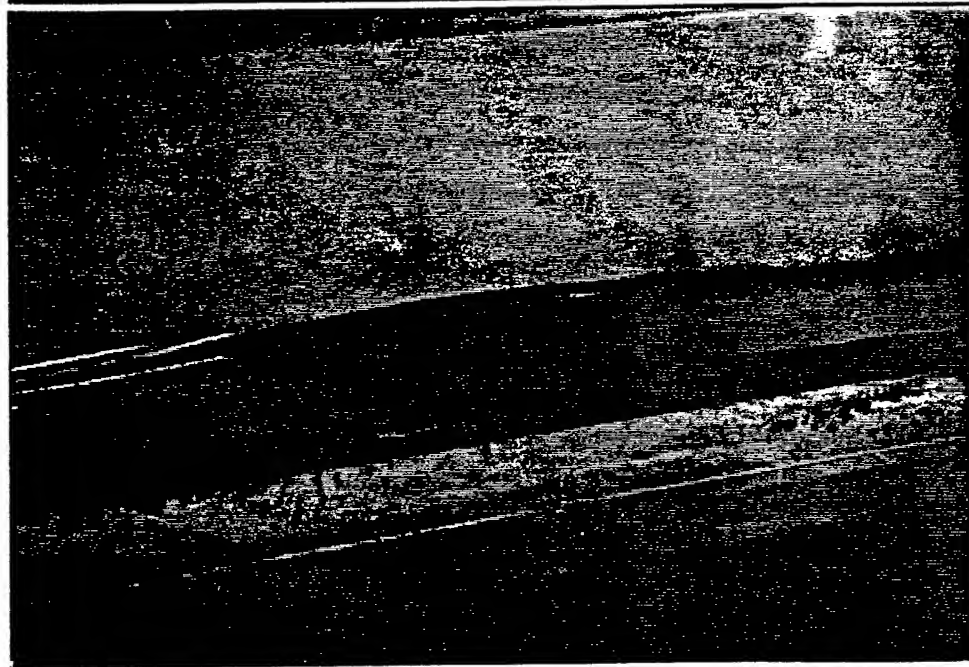
- Lagrangian DC Pressure:

$$\begin{aligned} \langle p_L \rangle &= \left\langle \frac{p_1^2}{2\rho_0 c_0^2} + \frac{\rho_0 u_1^2}{2} \right\rangle + \text{const} \\ &= \left(1 + \frac{B}{2A} \right) \frac{p_0^2}{4\rho_0 c_0^2} \quad (\neq \text{function of } x) \\ &= \langle p_E \rangle \text{ at particle velocity nodes} \end{aligned}$$

Water deflection due to
D.C. pressure at 161 dB.



Pre-fountain ripple at
161.5 dB.



Water fountain at
161.5 dB



Brand, O., and Freund, H. (1934).
Zeitschrift Fur Physik. 92, 385-389.

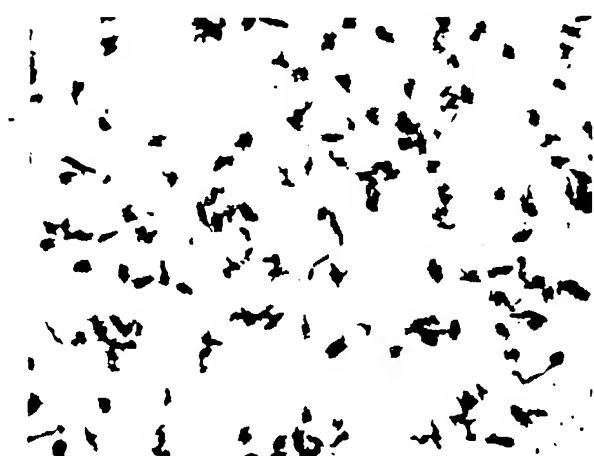


FIG. 5. $\times 50$.



FIG. 6.

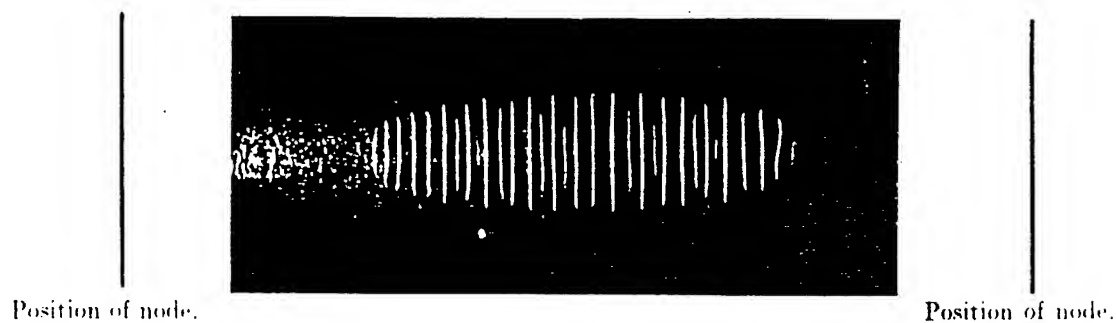


FIG. 7.



FIG. 8.

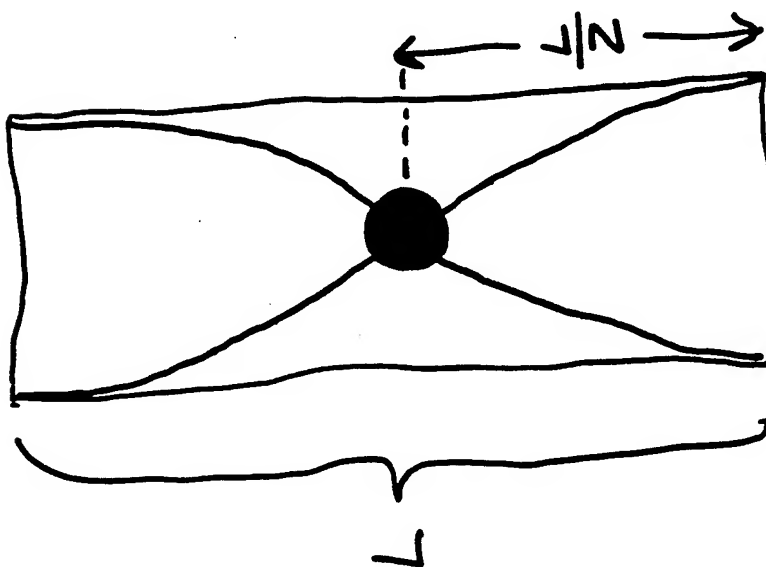


FIG. 9.



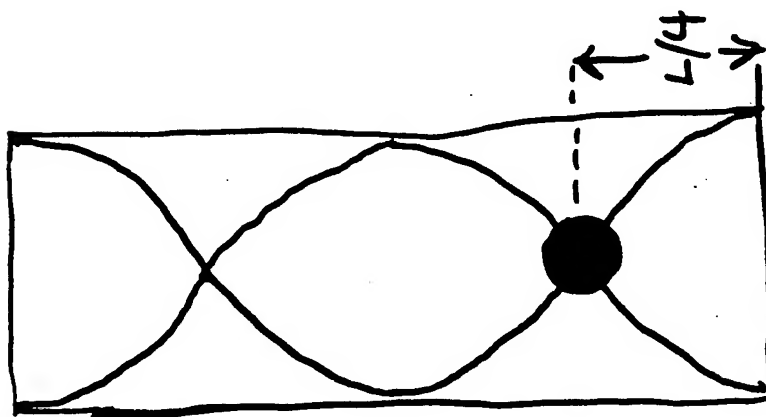
ACOUSTIC ELEVATOR

Lowest
Resonance



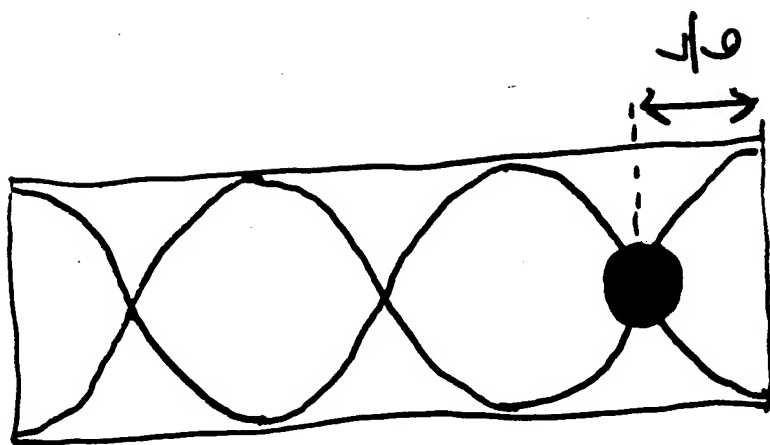
$$f = f_0$$

First
overtone



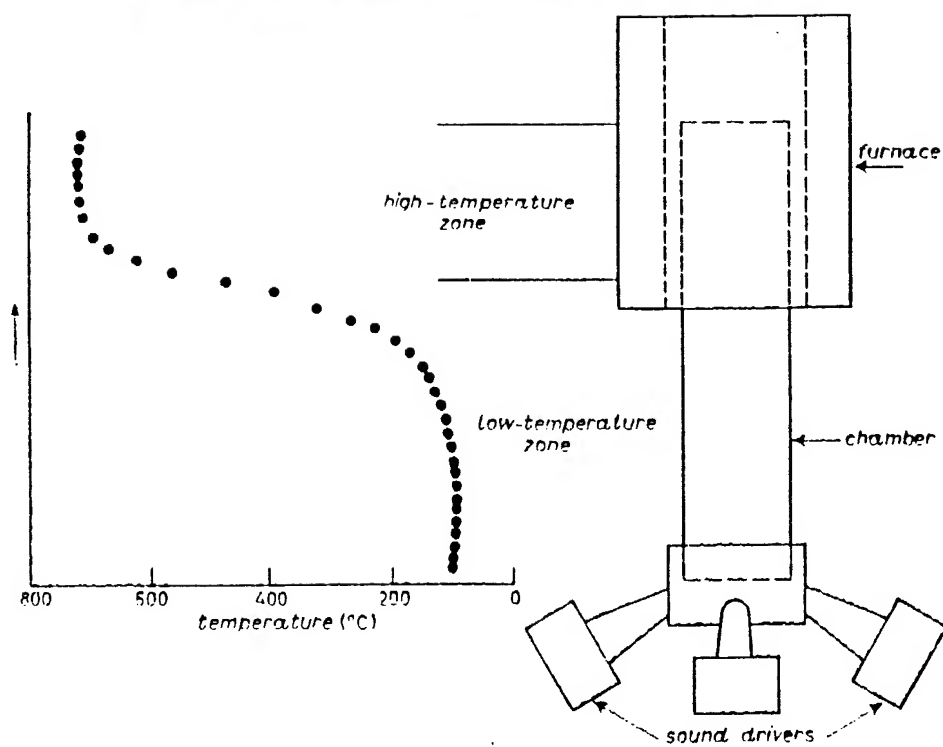
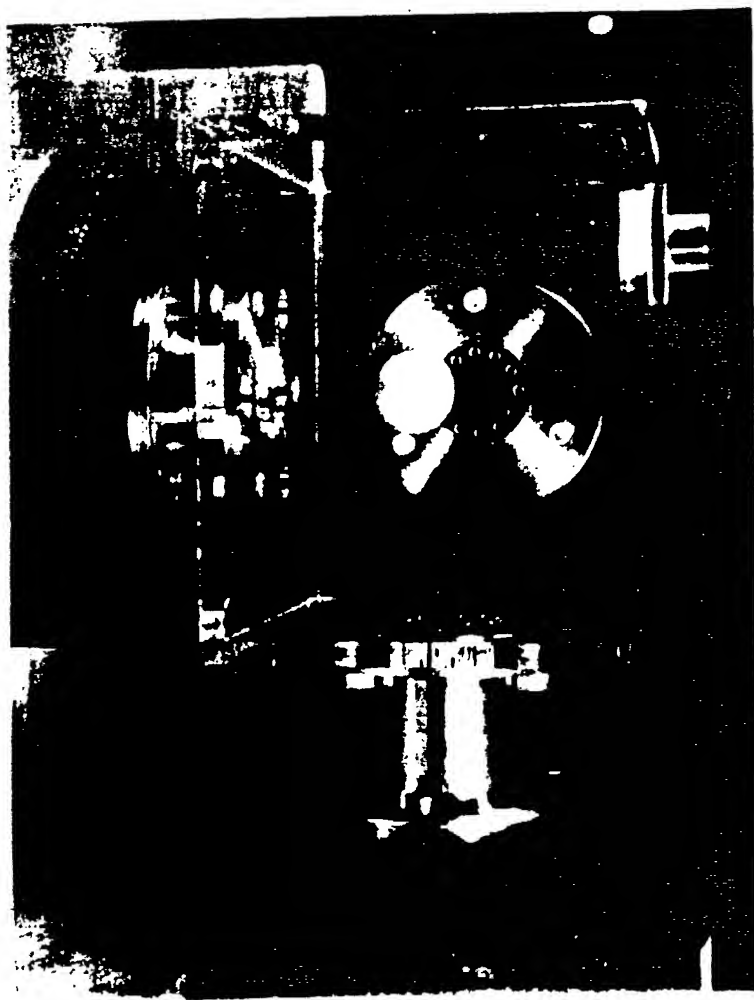
$$f = 2f_0$$

Second
overtone



$$f = 3f_0$$





Atmospheric Refraction of Sound

I. Basics

Introduction

Mechanisms

Wave equation (speed of sound)

Reflection

Ground models

Meteorology

Ray tracing

Ray tracing lab

Break

II. Advanced

Problems with the above

Spherical wave reflection

Fast field program

Residue series

Normal mode

III. Graduate

3-D FFP, winds, density

Introduction

- **Understanding our world**
- **Noise**
- **Detection/location**

Research

- **Solution oriented**
- **Cyclical**
- **Low level**

Mechanisms affecting sound propagation

- **Spherical spreading**
- **Atmospheric attenuation**
- **Refraction**
- **Diffraction**
- **Ground absorption**
- **Scattering**
- **Non-linear effects**

Atmospheric sound propagation

- **Wavelength long**
- **Non-linear effects**
- **Ground surface effects**
- **Wind**
- **Meteorological variability**
- **Turbulence**

Wave Equation

Continuity

$$1. \quad \frac{\partial \rho}{\partial t} + \rho_0 \nabla \cdot \vec{v} = 0$$

Newton's second law (Euler eq)

$$2. \quad \rho_0 \frac{\partial \vec{v}}{\partial t} = -\nabla p$$

Equation of state

$$3. \quad p = \left(\frac{\partial p}{\partial \rho} \right)_0 \rho = c^2 \rho$$

$$\frac{\partial \textcircled{1}}{\partial t} = \nabla \cdot \textcircled{2} \quad \text{using } \frac{p}{c^2} = \rho$$

Gives

$$\nabla^2 p - \frac{1}{c^2} \frac{\partial^2 p}{\partial t^2} = 0$$

For single frequencies

$$\nabla^2 p - k^2 p = 0; \quad k = \frac{\omega}{c}$$

Solution for k constant is plane waves:

$$p = \hat{p} e^{i(\vec{k} \cdot \vec{r} - \omega t)}$$

From Euler eq

$$\vec{v} = \vec{n} \frac{\hat{p}}{\rho c} \quad \vec{n} = \frac{\vec{k}}{k}$$

Reflection from ground

Specific acoustic impedance

Uniform surface, plane waves, invariance under translation

$$\left(\frac{\hat{p}}{\hat{v}_{\text{in}}} \right) = Z_s(\omega) = \rho c \zeta(\omega)$$

Ground Impedance

Delany - Bazeley

Embleton, Piercy and Daigle

Attenborough

Stinson and Champoux

Allard

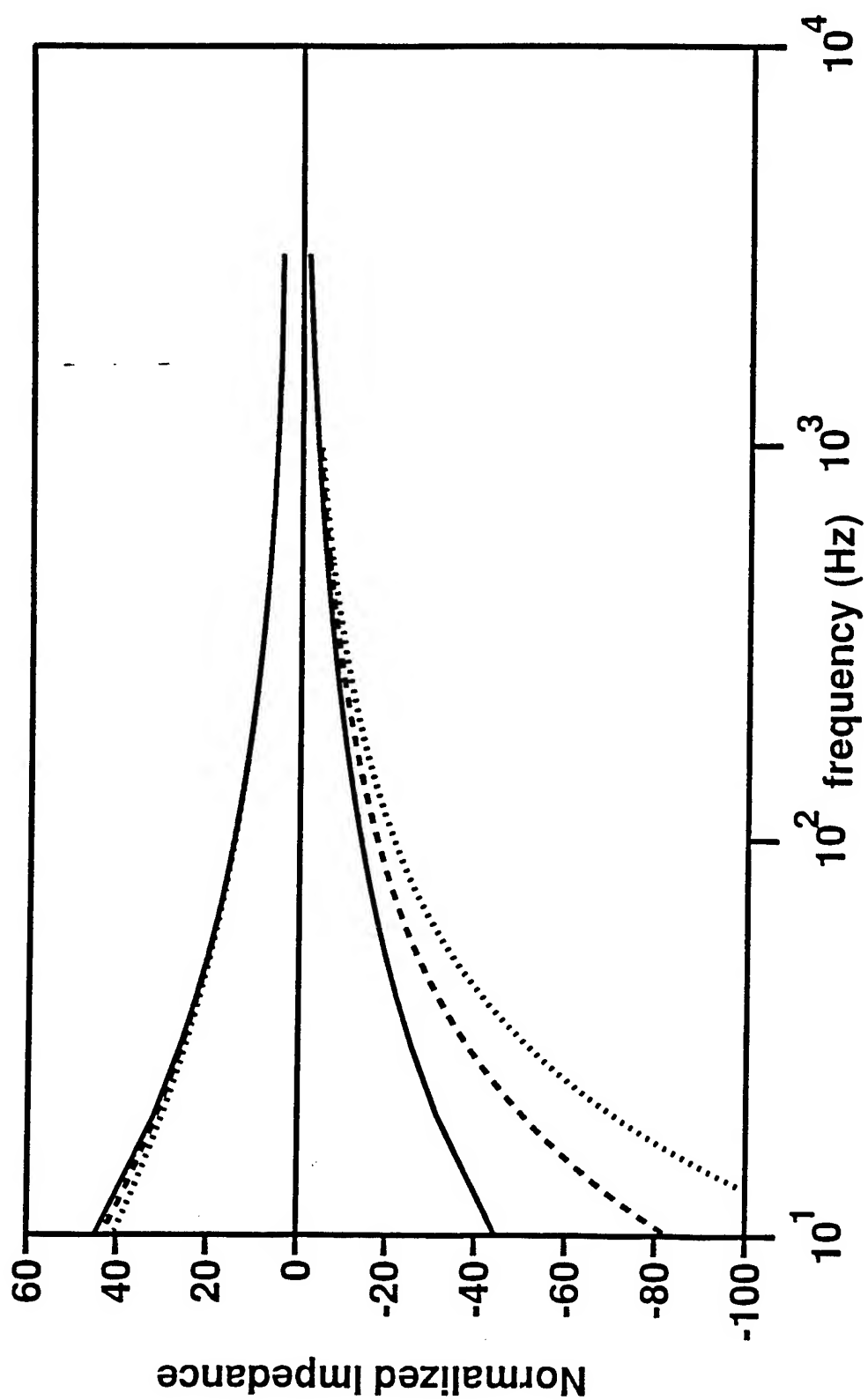
Sabatier and Bass

Variables

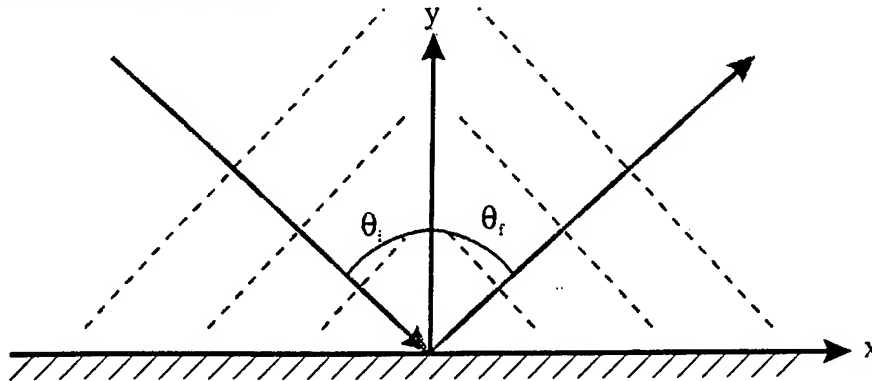
Porosity

Flow Resistance

Shape Factors



Invariance along x



$$k_I \sin \Theta_I = k_R \sin \Theta_R$$

$$\text{But } k_I = k_R = \frac{\omega}{c} \text{ so } \Theta_I = \Theta_R$$

y dependence then - $k \cos \Theta_I, k \cos \Theta_I$

Amplitude of reflected wave $R(\Theta_I) \hat{f}$

Total pressure and velocity

$$\hat{p} = \hat{f} e^{ik_x x} [e^{-i\hat{k}_y y} + R(\Theta_I) e^{i\hat{k}_y y}]$$

$$\hat{v}_y = \frac{\cos \Theta_I}{\rho c} \hat{f} e^{ik_x x} [-e^{-i\hat{k}_y y} + R(\Theta_I) e^{i\hat{k}_y y}]$$

So at $y = 0$

$$\left(\frac{Z(\omega)}{\rho c} \right) \cos \Theta_I = \frac{1 + R(\Theta_I)}{1 - R(\Theta_I)}$$

and

$$R(\Theta_I) = \frac{\zeta(\Theta_I) \cos \Theta_I - 1}{\zeta(\Theta_I) \cos \Theta_I + 1}$$

Special Cases

Fluid-Fluid $\rho_{\text{II}}, c_{\text{II}} ; \frac{c_{\text{I}}}{\sin \Theta_{\text{I}}} = \frac{c_{\text{II}}}{\sin \Theta_{\text{II}}}$

$$\zeta(\Theta_{\text{I}}) = \frac{\rho_{\text{II}} c_{\text{II}}}{\rho_{\text{I}} c_{\text{I}} \cos(\Theta_{\text{II}})}$$

Rigid surface: $v_{\text{in}} = 0$

$$R = 1$$

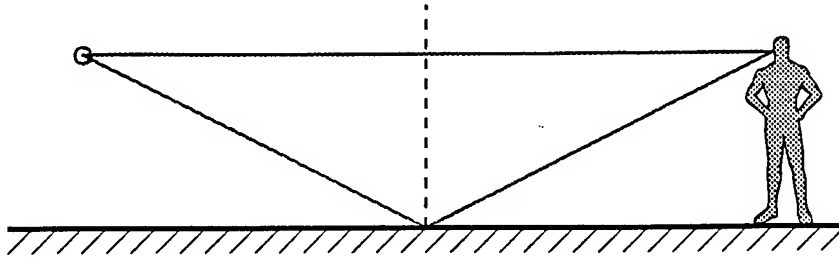
Pressure release: $p = 0$

$$R = -1$$

Grazing Incidence:

$$R = -1$$

First Problem:



Lloyd's Mirror

FM vs AM radio

Second problem:

Is grazing same as pressure release?

Sound Speed not Uniform

$$c = \sqrt{\frac{\gamma RT}{M}}$$

Temperature and relative humidity affect c

$$M = 29(1-h) + 18h$$

$$\gamma = (d+2)/d = c_p/c_v$$

$$d = 5(1-h) + 6h$$

Plug in

$$c = (331 + 0.6 T_c)(1 + .16h)$$

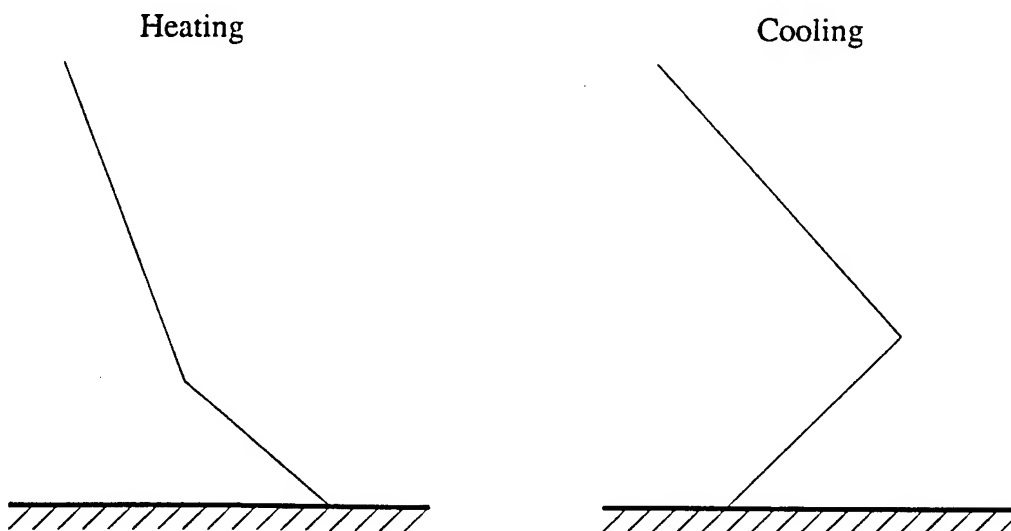
Meteorology

Average Temperature Profile:

Adiabatic lapse rate: -9.8 K/km

(120 km Thermosphere)

Diurnal Variation



Wind Profiles

Close to logarithmic near to ground

Decoupled by inversions

For the simple picture we say

$$c = c(z) + w(z) \cos \phi$$

ϕ **Angle between direction of propagation and
direction of wind flow**

RAY TRACING

Eikonal Equation

Simplest Case:

$$\nabla^2 p = \frac{1}{c^2} \frac{\partial^2 p}{\partial t^2}$$

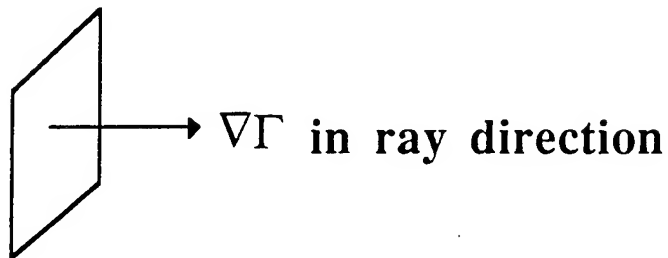
Try

$$p(x,y,z) = A(x,y,z) \exp \left(i\omega \left[t - \Gamma(x,y,z)/c_0 \right] \right)$$

$A(x,y,z)$ Amplitude

$\Gamma(x,y,z)$ Phase

$\Gamma(x,y,z) = C$ is surface of constant phase



Plug into wave equation

$$\nabla^2 A(\mathbf{x}, \mathbf{y}, \mathbf{z}) - 2i\omega \nabla A \cdot \nabla \Gamma / c_0$$

$$-\omega^2 A \frac{\nabla \Gamma}{c_0} \cdot \frac{\nabla \Gamma}{c_0}$$

$$2i\omega A \frac{\nabla^2 \Gamma}{c_0} + \frac{\omega^2 A}{c^2} = 0$$

If A and $\nabla \Gamma$ slowly varying so that

$$\frac{\nabla^2 A}{A} < < \frac{\omega^2}{c^2} \nabla^2 \Gamma < \frac{c_0}{c} \frac{\omega}{c} = n \frac{\omega}{c}$$

$$\nabla^2 \Gamma < \frac{c_0}{c} \frac{\omega}{c} = n \frac{\omega}{c}$$

$$\frac{\nabla A}{A} \cdot \nabla \Gamma < \frac{\omega}{c} \cdot n$$

Then

$$\omega^2 A \frac{\nabla \Gamma}{c_o} \cdot \frac{\nabla \Gamma}{c_o} = \frac{\omega^2}{c^2} A$$

or

The Eikonal Equation

$$\nabla \Gamma \cdot \nabla \Gamma = n^2$$

$$n = n(x, y, z) = \frac{c_o}{c(x, y, z)}$$

Note Limits !

$$\lambda \frac{1}{c} \frac{dc}{dz} \ll 1$$

$$\lambda \frac{1}{A} \frac{dA}{dz} \ll 1$$

Snell's Law

Express Eikonal in terms of direction cosines.

Express direction cosines in terms of ds.

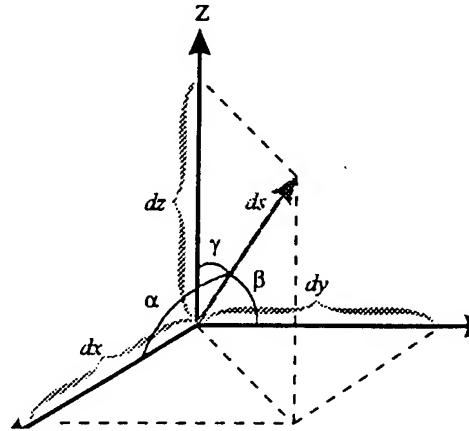
Note $|\nabla\Gamma| = n$ so Eikonal equation can be written

$$\alpha^2 + \beta^2 + \gamma^2 = 1$$

where
$$\alpha = \frac{(\nabla\Gamma)_x}{|\nabla\Gamma|} = \frac{1}{n} \frac{\partial\Gamma}{\partial x}$$

$$\beta = \frac{1}{n} \frac{\partial\Gamma}{\partial y}, \quad \gamma = \frac{1}{n} \frac{\partial\Gamma}{\partial z}$$

Direction cosines in terms of ds



$$\alpha = \frac{dx}{ds} ; \quad \beta = \frac{dy}{ds} ; \quad \gamma = \frac{dz}{ds}$$

So combining solutions for γ

$$n \frac{dx}{ds} = n \frac{1}{n} \frac{\partial \Gamma}{\partial x} = \frac{\partial \Gamma}{\partial x}$$

$$n \frac{dy}{ds} = n \frac{1}{n} \frac{\partial \Gamma}{\partial y} = \frac{\partial \Gamma}{\partial y}$$

$$n \frac{dz}{ds} = n \frac{1}{n} \frac{\partial \Gamma}{\partial z} = \frac{\partial \Gamma}{\partial z}$$

Note:

$$\frac{d\Gamma}{ds} = \alpha \frac{\partial \Gamma}{\partial x} + \beta \frac{\partial \Gamma}{\partial y} + \gamma \frac{\partial \Gamma}{\partial z}$$

so

$$\frac{d\Gamma}{ds} = \alpha n \alpha + \beta n \beta + \gamma n \gamma = n$$

Taking $\frac{d}{ds}$ of both sides of each equation:

3-D Snell's Laws

$$\frac{d}{ds} \left(n \frac{dx}{ds} \right) = \frac{\partial n}{\partial x}$$

$$\frac{d}{ds} \left(n \frac{dy}{ds} \right) = \frac{\partial n}{\partial y}$$

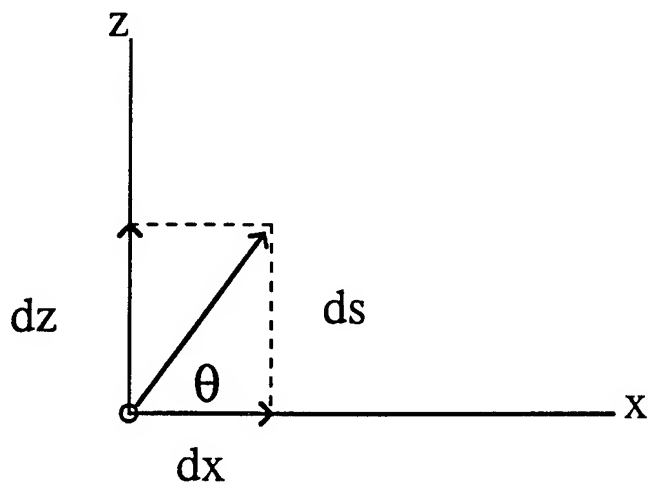
$$\frac{d}{ds} \left(n \frac{dz}{ds} \right) = \frac{\partial n}{\partial z}$$

Specialize to $n = n(z)$ only

$$n \frac{dx}{ds} = \text{constant} = n \alpha_0$$

$$n \frac{dy}{ds} = \text{constant} = n \beta_0$$

Choose x, z plane



$$n \cos \theta = n_0 \cos \theta_0$$

$\frac{\cos \theta}{c(z)} = \frac{\cos \theta_0}{c(o)} = p, \text{ constant}$

$$\gamma = \frac{dz}{ds} = \sin \theta$$

Radius of Curvature

Put $\frac{dz}{ds} = \sin \Theta$ into 3rd Snell's Law

$$\frac{d}{ds} (n \sin \Theta) = \frac{dn}{dz}$$

$$\text{use } \frac{dn}{ds} = \frac{dn}{dz} \frac{dz}{ds} = \frac{dn}{dz} \sin \Theta$$

$$\frac{d\Theta}{ds} = \frac{\cos \Theta}{n} \frac{dn}{dz} = -\frac{\cos \Theta}{c} \frac{dc}{dz}$$

$$\text{so curvature } \left| \frac{d\Theta}{ds} \right| = pg$$

$$R = \frac{c}{\cos \Theta} \frac{1}{dc/dz} = \frac{1}{pg}$$

For linear sound speed change

R is constant in layer

$$R = \frac{c}{\cos \Theta} \frac{dz}{dc}$$

$$c = c_i (1 + az) = c_i + gz$$

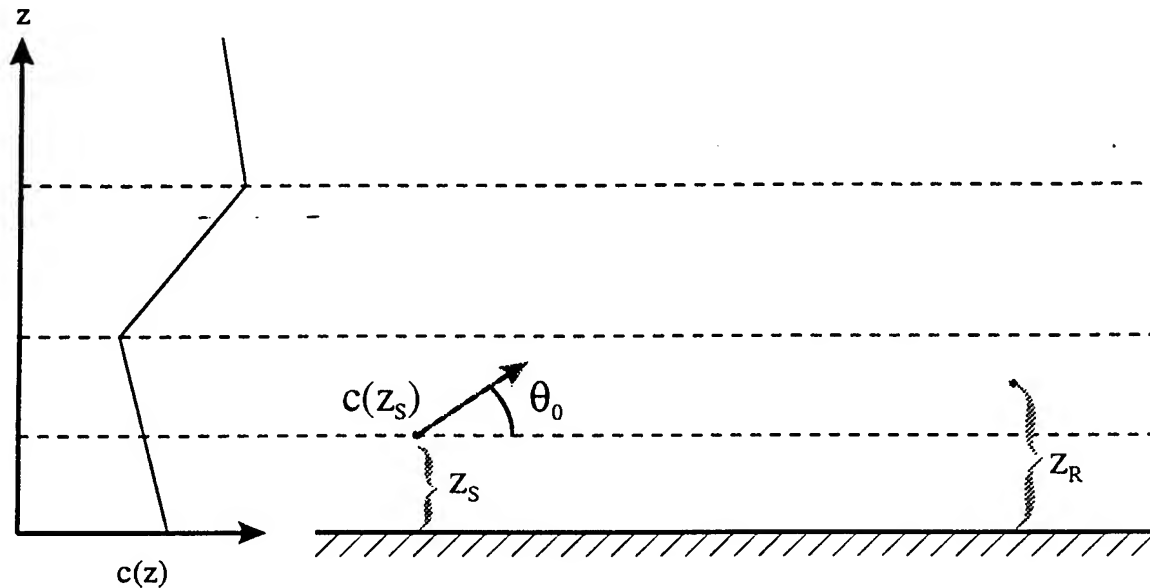
$$R = \frac{1}{pg};$$

p constant in atmosphere, g constant in layer

Example: Huge - 1m/s/m

$$R \cong \frac{340}{1} \text{ m/s} \frac{1}{1 \text{ m/s/m}} = 340\text{m}$$

Construction of Rays for Linear Gradient Layers



What happens?

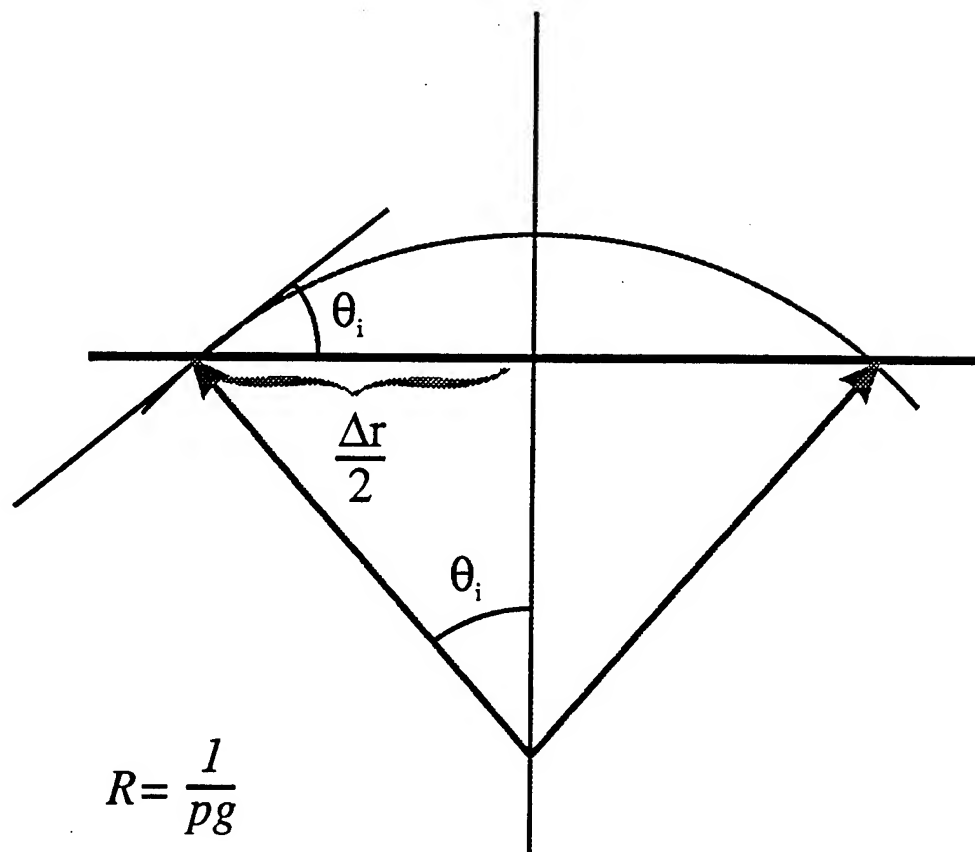
Becomes horizontal at z s.t.

$$\frac{\cos \Theta}{c(z)} = \frac{1}{c(z)} = \frac{\cos \Theta_0}{c(z_s)} = p$$

$$c(z) = \frac{c(z_s)}{\cos (\Theta_0)}$$

If no $c(z) > \frac{c(z_s)}{\cos (\Theta_0)}$ doesn't come back

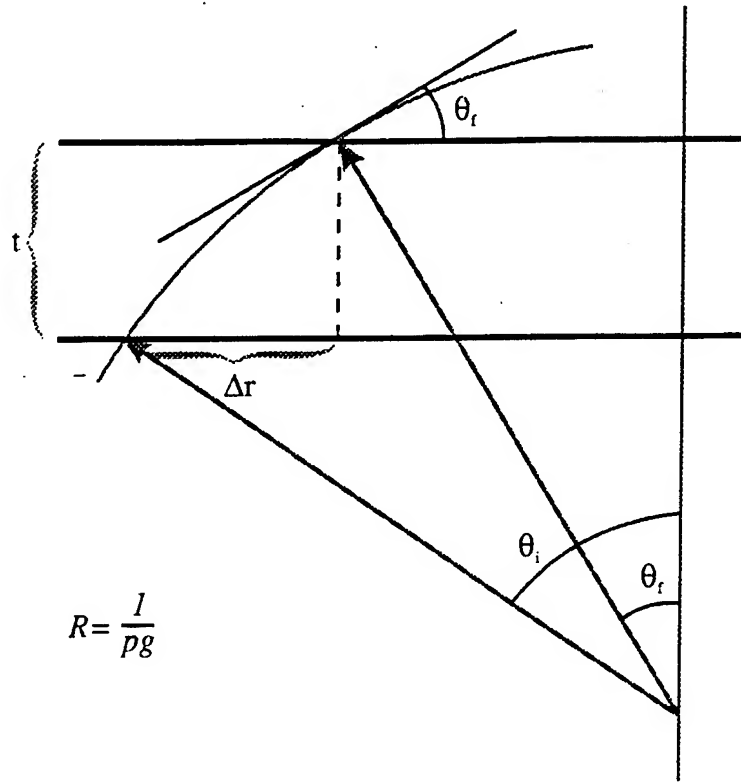
Ray turning in a layer



$$\Delta r = 2 \frac{\sin \Theta_i}{pg}$$

$$h = \frac{1}{pg} - \frac{1}{pg} \cos \Theta_i \cong \frac{\Theta_i^2}{2pg}$$

Rays through a Layer:



$$\Theta_i, \Theta_f \text{ calculated from } p = \frac{\cos \Theta}{c(z)}$$

$$\Delta r = R |\sin \Theta_f - \sin \Theta_i|$$

$$t = R |\cos \Theta_f - \cos \Theta_i|$$

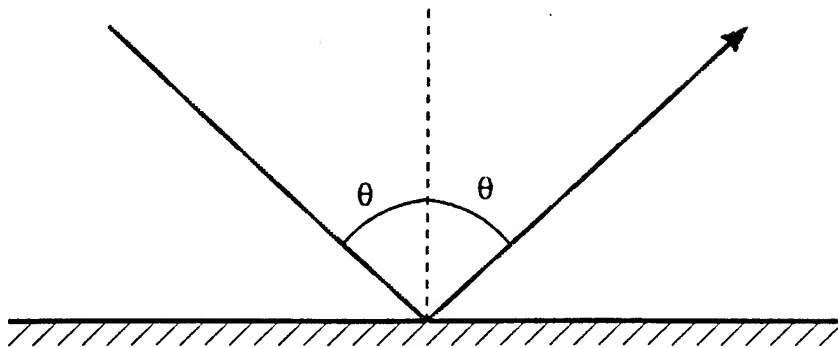
So

$$\Delta r = t \frac{|\sin \Theta_f - \sin \Theta_i|}{|\cos \Theta_f - \cos \Theta_i|}$$

$$= t \frac{|\cos \Theta_f + \cos \Theta_i|}{|\sin \Theta_f + \sin \Theta_i|}$$

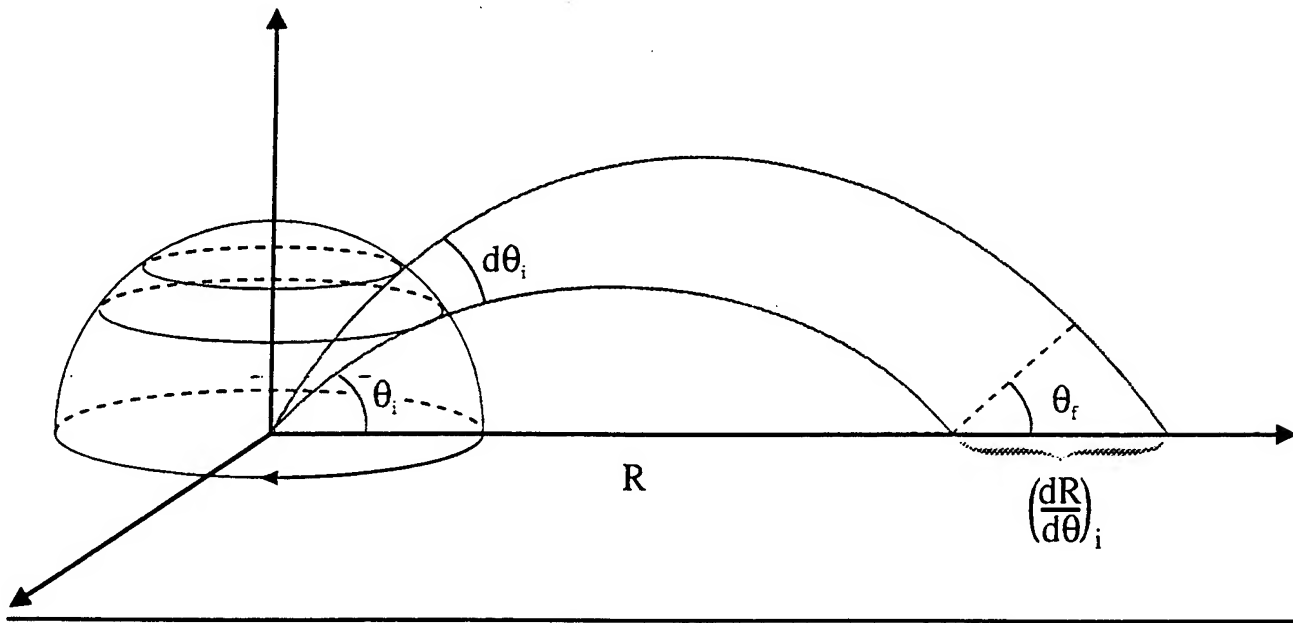
What about the ground?

$$\Theta = \Theta'$$



We use a mirror atmosphere.

Geometry for Focus Factor



Area for straight rays =

$$2\pi R \cos \Theta_i R d\Theta_i$$

Area for refracted rays =

$$2\pi R \sin \Theta_f \left(\frac{dR}{d\Theta} \right)_i d\Theta_i$$

Intensity is higher if area smaller

$$\text{focus factor} = \frac{\perp \text{ Area without refraction}}{\perp \text{ Area with refraction}}$$

$$= \frac{2\pi R \cos\Theta_0 R d\Theta_0}{2\pi R \left(\frac{dR}{d\Theta}\right)_{\Theta_0} d\Theta_0 \sin\Theta}$$

$$f = \frac{R \cos\Theta_0}{\left(\frac{dR}{d\Theta}\right)_0 \sin\Theta}$$

What if $\left(\frac{dR}{d\Theta}\right)_0 = 0!$

Fermat's Principle:

**Rays travel in a path which is stationary
with respect to travel time**

Identifies rays above plus

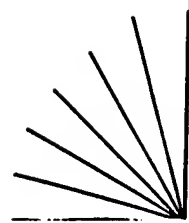
PASS 96

Outdoor Sound Laboratory

June 26, 1996

- I. Draw rays coming from the source using the following rules:
 - A. Ray paths are circles tangent to the initial direction – radii are given on worksheet
(+ is downward curving; – is upward)
 - B. Angle of reflection = angle of incidence at the ground.
 - C. At a layer interface the different circle radii are tangent to the same line.
 - D. If $R = \infty$ rays are straight lines.
- II. Add additional ray paths as needed to understand the ray field.
- III. Think about what a listener would hear at different positions.

CASE I



$R = 3''$

$R = \infty$

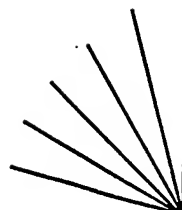
TRANS 34

CASE II

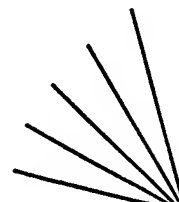
TRANS '35

$$R = \infty$$

$$R = -5''$$



CASE III



$$R = 5''$$

$$R = 3''$$

$$R = \infty$$

TRANS 36

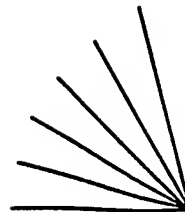
CASE IV

TRANS 37

$$R = \infty$$

$$R = 5''$$

$$R = -5''$$



Problems

- CASE I** **Lots of energy close to ground**
- CASE II** **No sound audible by ray trace**
- CASE III** **Lots of energy at caustics**
- CASE IV** **No sound heard since sound speed
never higher than that at source
but _____**

And

Lloyd's Mirror Effect

And

Caustics - $\pi/2$ phase change

Computer Program

Rays only come back if $c(z) \geq c(z_s)$

Rays turn in a layer if $g(z+) > g(z-)$

Ground treated as a mirror

$\frac{dR}{d\Theta}$ and time of flight

Newton's method used for each class of eigenrays

Helmholtz Equation in Cylindrical Coordinates

$$\frac{\partial^2 p}{\partial r^2} + \frac{1}{r} \frac{\partial p}{\partial r} + \frac{\partial^2 p}{\partial z^2} + k^2 p = \frac{-2}{r} \delta(r') \delta(z - z_s)$$

Separate variables with an integral transform

$$\hat{p}(K, z) = \int_0^\infty p(r, z) J_0(Kr) r dr$$

$$p(r, z) = \int_0^\infty \hat{p}(K, z) J_0(Kr) K dK$$

Boundary Conditions

1. Complex impedance ground

$$Z_c = \frac{p}{v_n}$$

2. Pressure continuous at z_s . Particle velocity discontinuous.

3. Pressure goes to zero at ∞

Applications

Spherical wave reflection

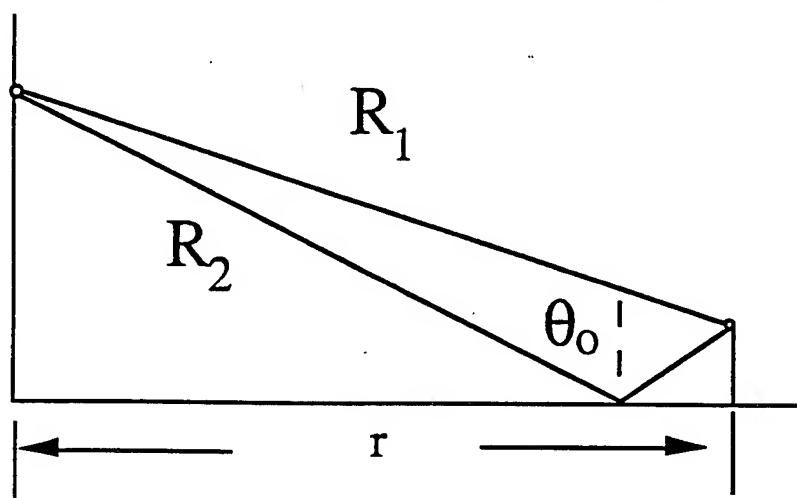
Fast field program

Residue series solution for upward refraction

**Normal mode solution for downward
refraction**

Spherical Wave Reflection

Point source, complex impedance ground



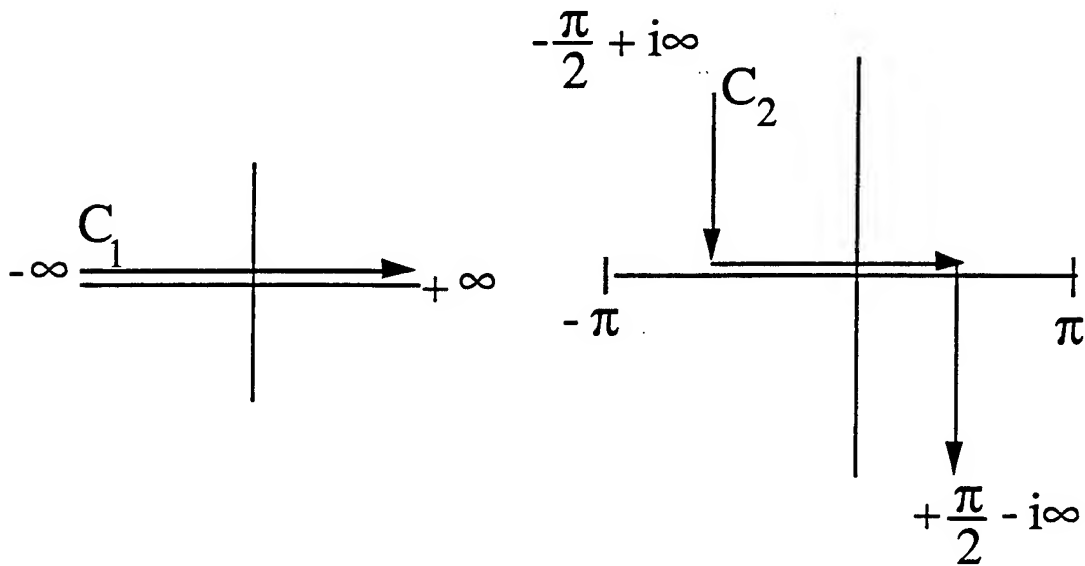
Uniform atmosphere - e^{ikr}

How does this differ from plane wave reflection?

$$R(\theta) = \frac{Z_c \cos\theta - 1}{Z_c \cos\theta + 1}$$

Brekhovskikh

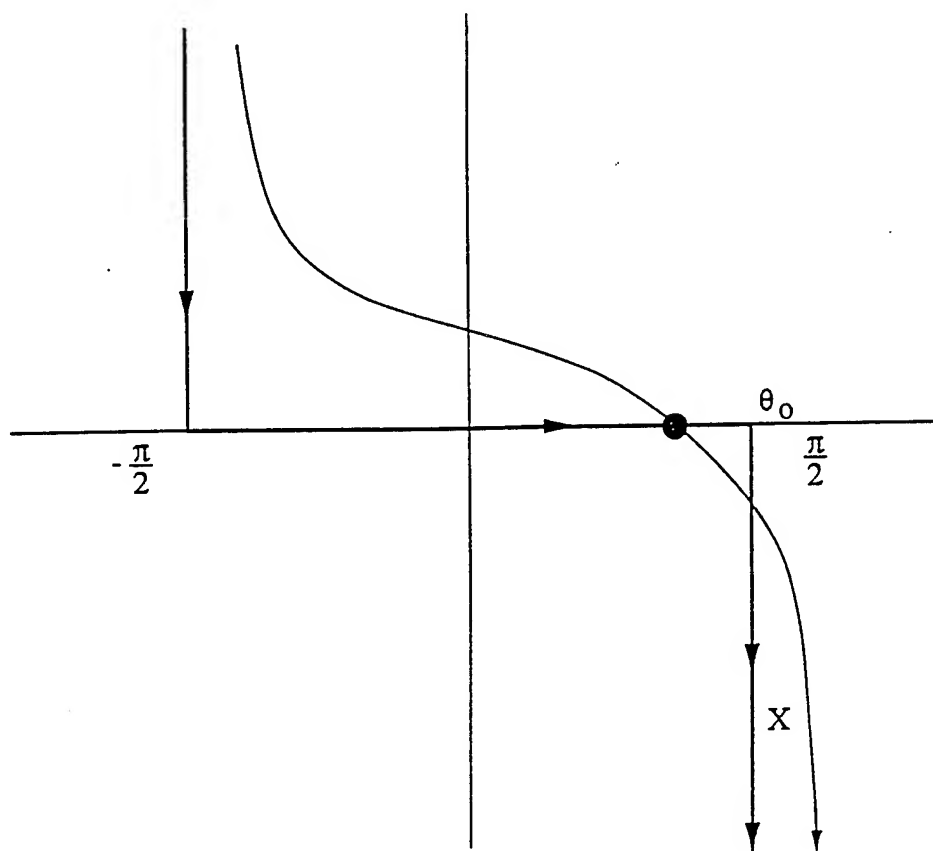
Converts to θ space



$$\phi = \phi_{\text{direct}} + \phi_{\text{reflected}}$$

$$\phi_{\text{reflected}} = \sqrt{\frac{k}{2\pi r}} e^{i\pi/4} \int_{C_2} e^{ikr \cos(\theta - \theta_0)} R(\theta) \sqrt{\sin\theta} d\theta$$

Solution by Steepest Descents



Biggest contribution at θ_0 - falls off rapidly

Lloyd's mirror

x - possible pole at $Z \cos \theta + 1 = 0$

Spherical Wave Reflection (Donato)

(Attenborough, Hayek, Lawther)

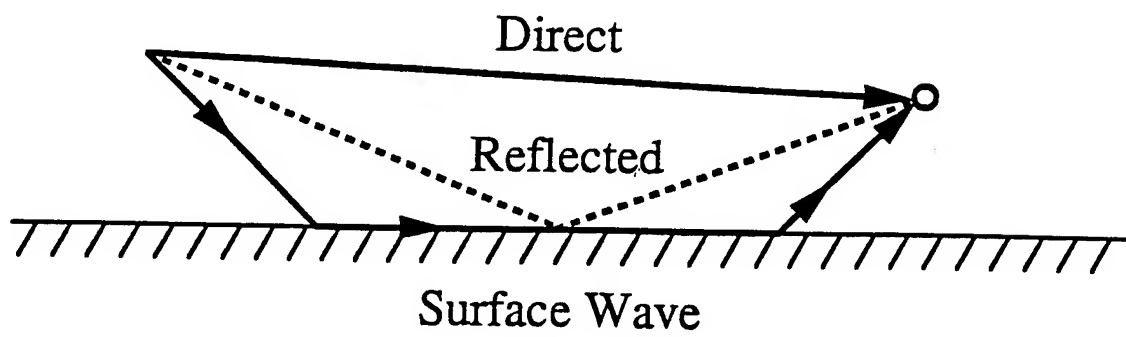
$$\Phi = \frac{e^{-ik_0 R_1}}{R_1} + \frac{e^{-ik_0 R_2}}{R_2}$$

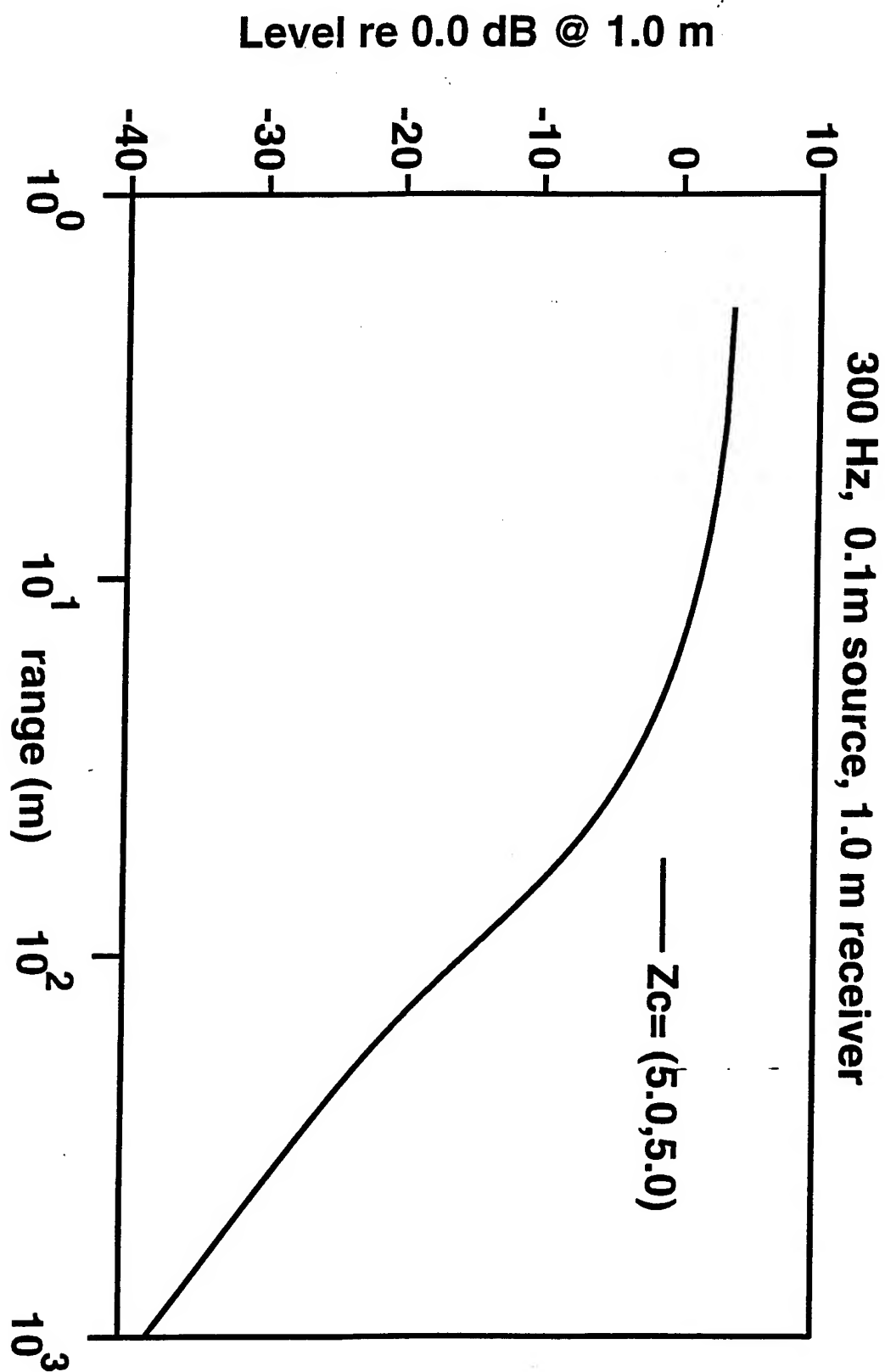
$$- \left[\frac{2}{Z_c \cos \Theta_0 + 1} \right] \frac{e^{-ik_0 R_2}}{\sqrt{r R_2}} \left[1 + \frac{i(Z_c^2 - 1/8)}{k_0 R_2} \right]$$

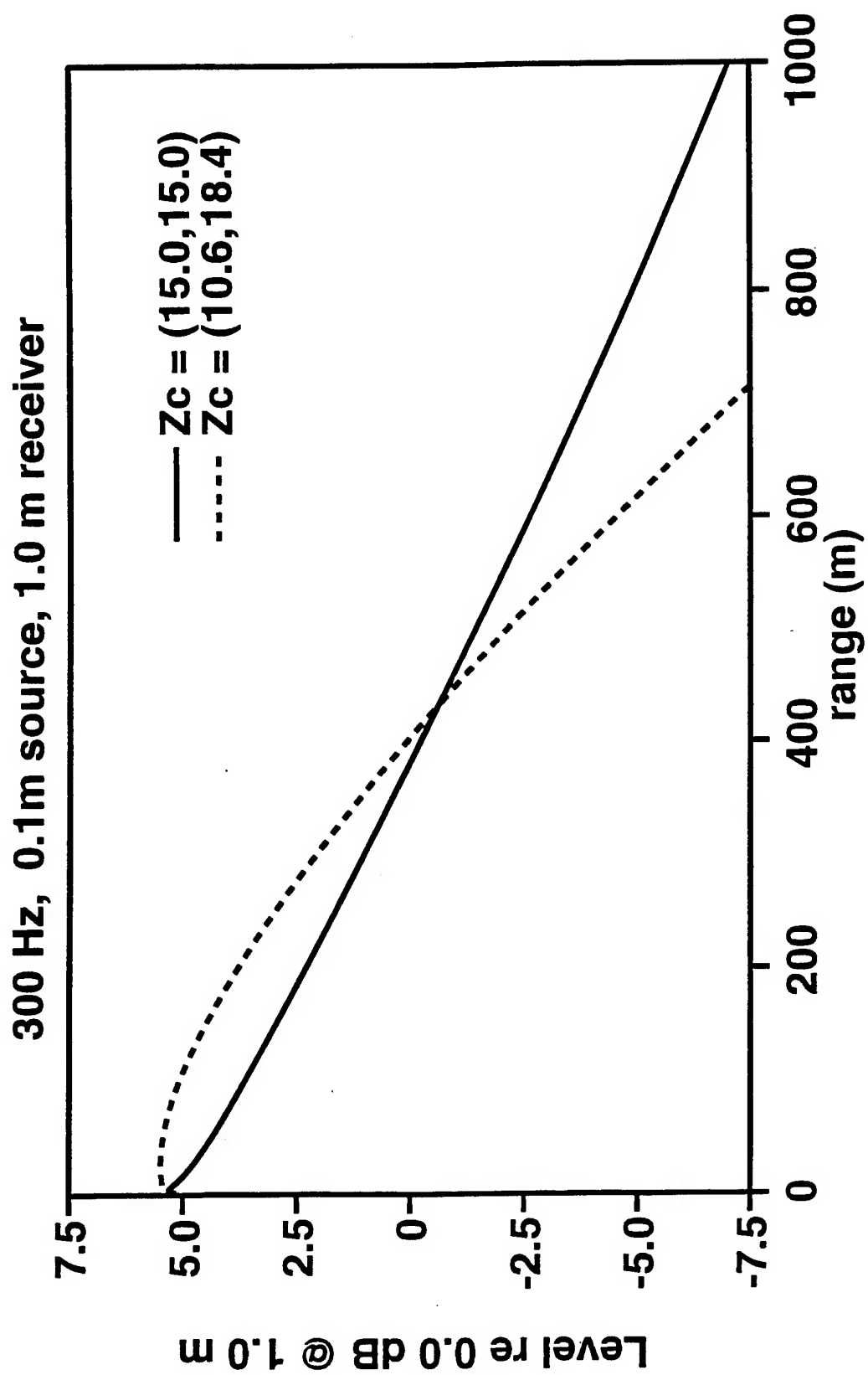
$$+ \sqrt{\frac{k_0}{2\pi d}} \frac{4\pi}{Z_c} \sqrt{\sin \Theta_p} \exp [i\pi/4 - ik_0 R_2 \cos (\Theta_p - \Theta_0)].$$

$$; \Theta_p \text{ solution of } \cos \Theta_p = \frac{1}{Z_c}$$

RESULT







Break Up The Equation for P

$$\frac{dP}{dz} = -i \omega \rho_0 U_z$$

$$\frac{dU_z}{dz} = \frac{-i(k^2(z) - K^2)}{\omega \rho_0} P + \frac{2}{\omega \rho_0} \delta(z - z_s)$$

Two Ways To Solve For P(k,z)

- 1) Propagator Matrix Method
- 2) Transmission Line Analogy

Advantages Of Each Approach

Propagator Matrix - Can Do Solid Layers

Transmission Line - Can Have Reflectionless Terminations And
Numerically Stable

Evaluating the integral

$$p(r,z) = \int_0^{\infty} \hat{p}(K,z) J_0(Kr) K \, dK$$

$$J_0(Kr) = \frac{1}{2} [H_0^1(Kr) + H_0^2(Kr)]$$

$$H_0^1(Kr) \cong \sqrt{\frac{2}{\pi K}} \frac{e^{i(Kr - \pi/4)}}{\sqrt{r}}$$

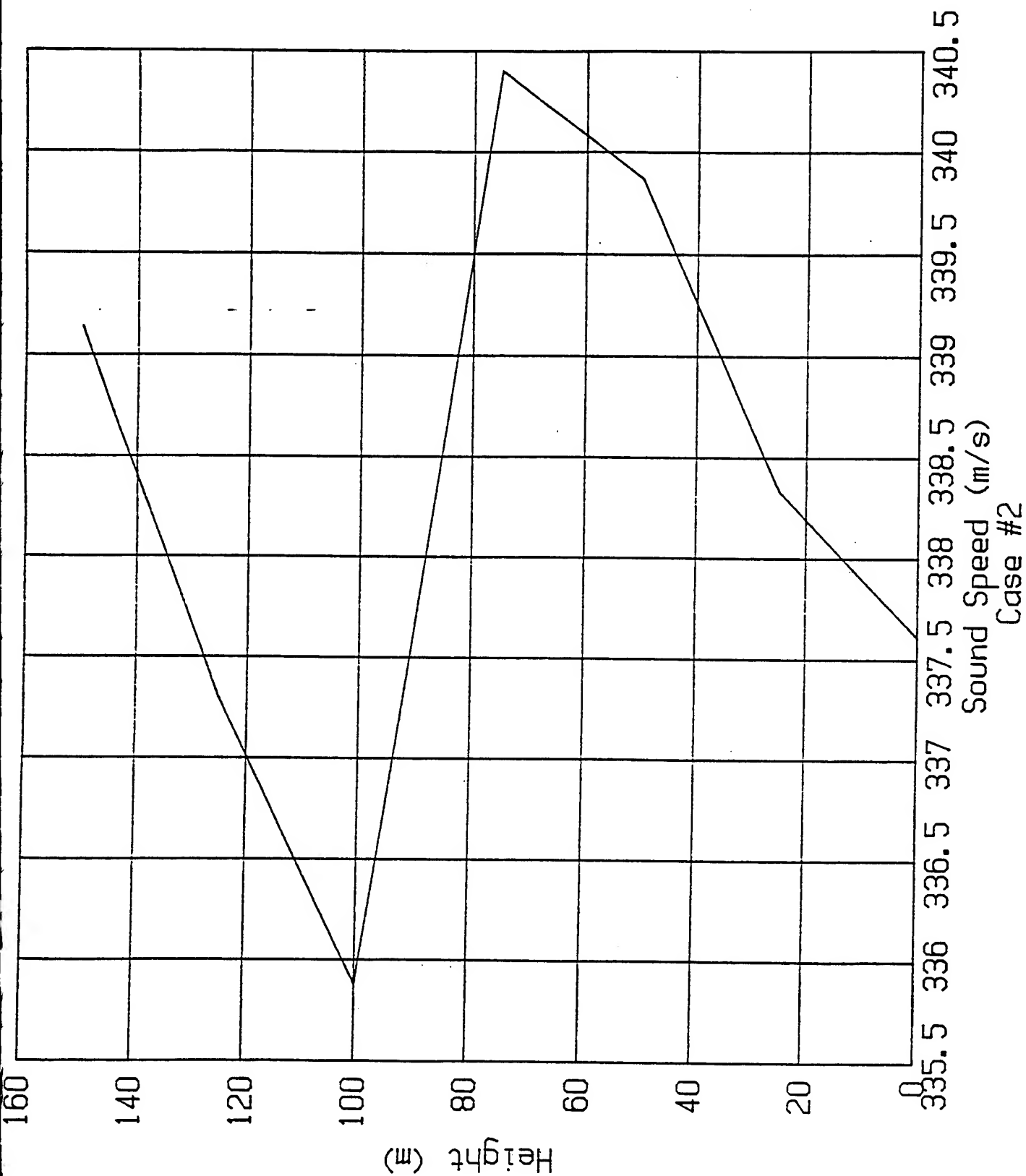
so

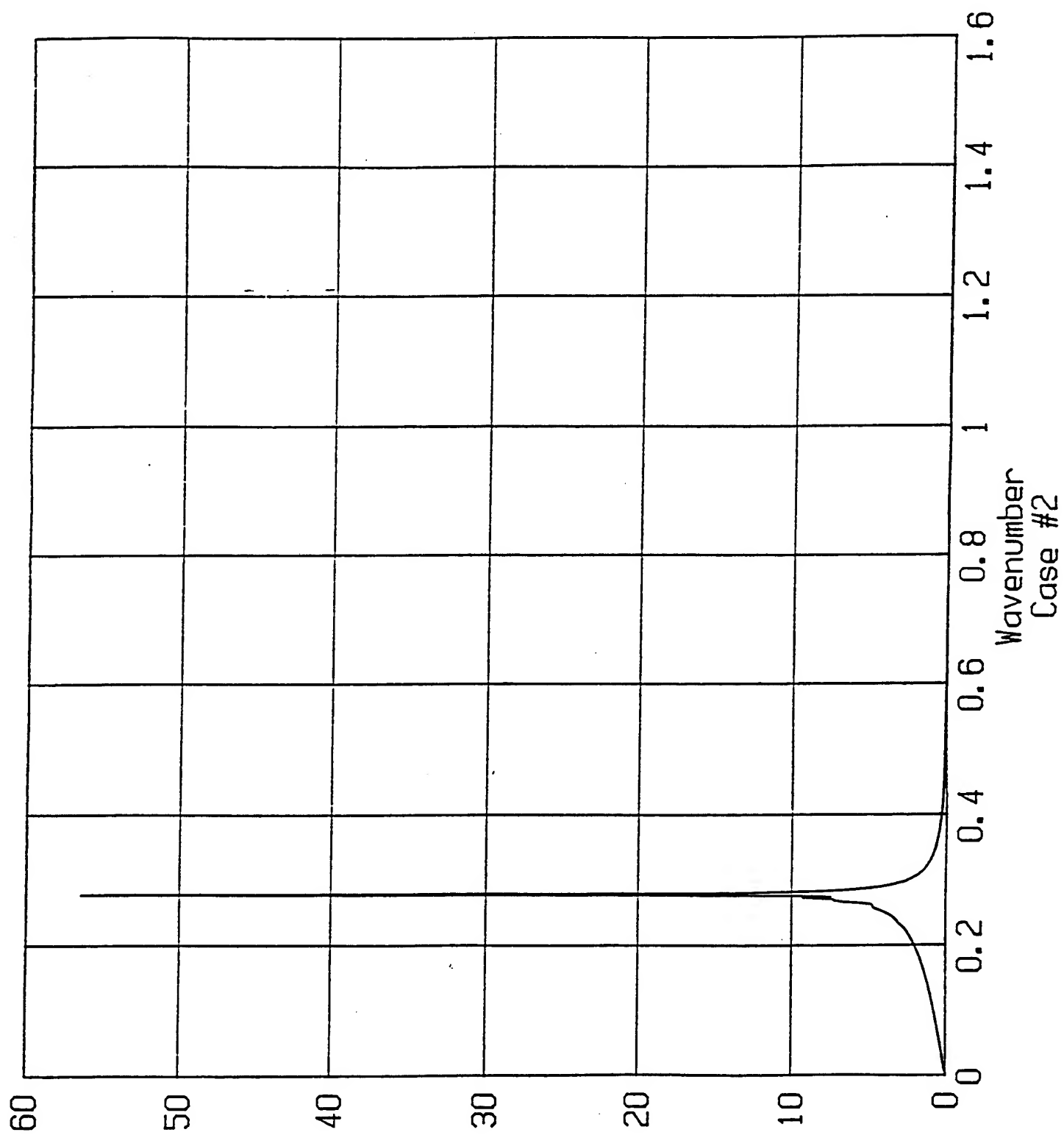
$$p(r,z) = \frac{1+i}{\sqrt{2\pi r}} \int_0^{\infty} \hat{p}(K,z) e^{iKr} \sqrt{K} \, dK$$

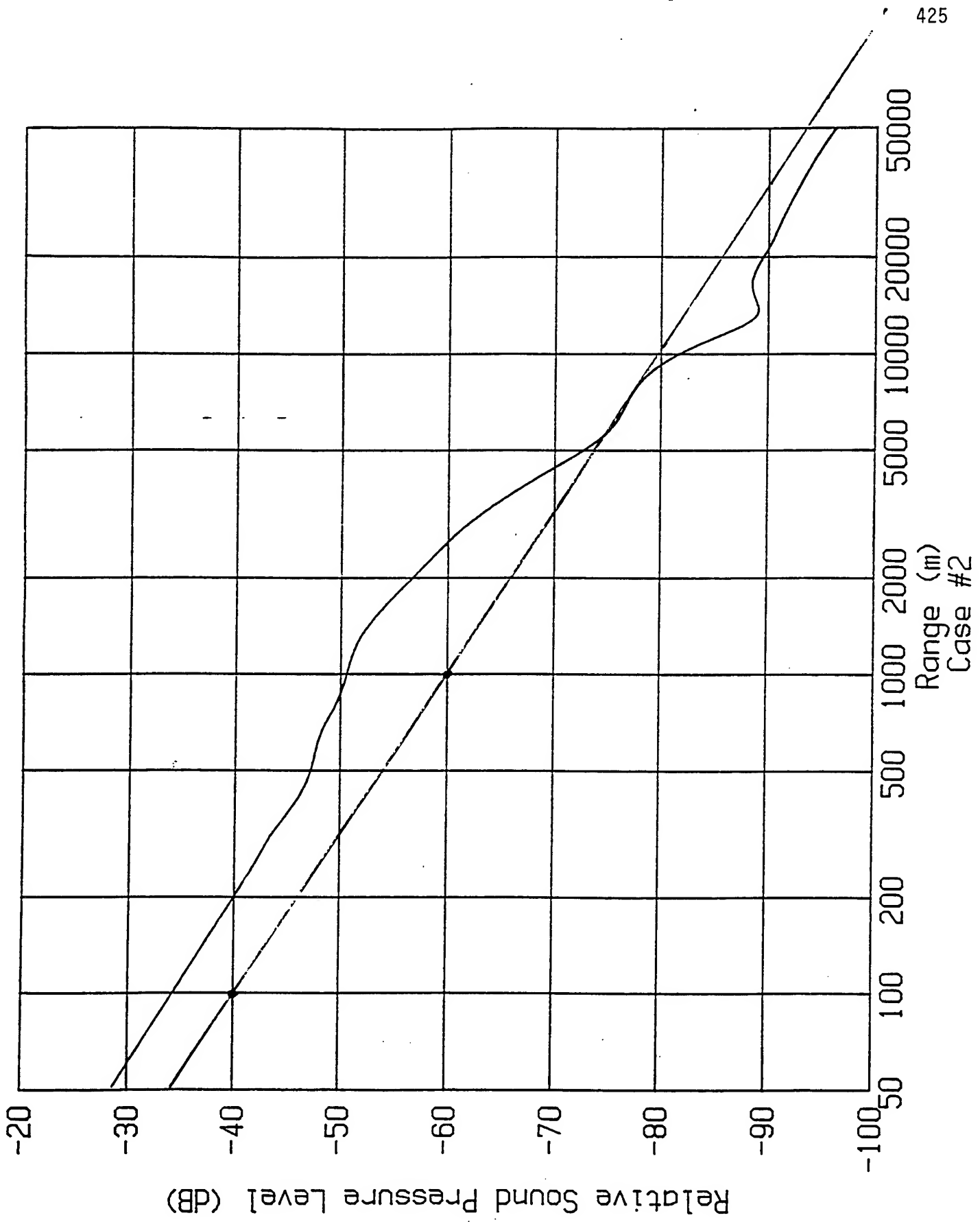
This is Fourier transform of

$$\hat{p}(K,z) \sqrt{K}$$

Use F.F.T to give $p(r_m)$; $m = 0, N-1$







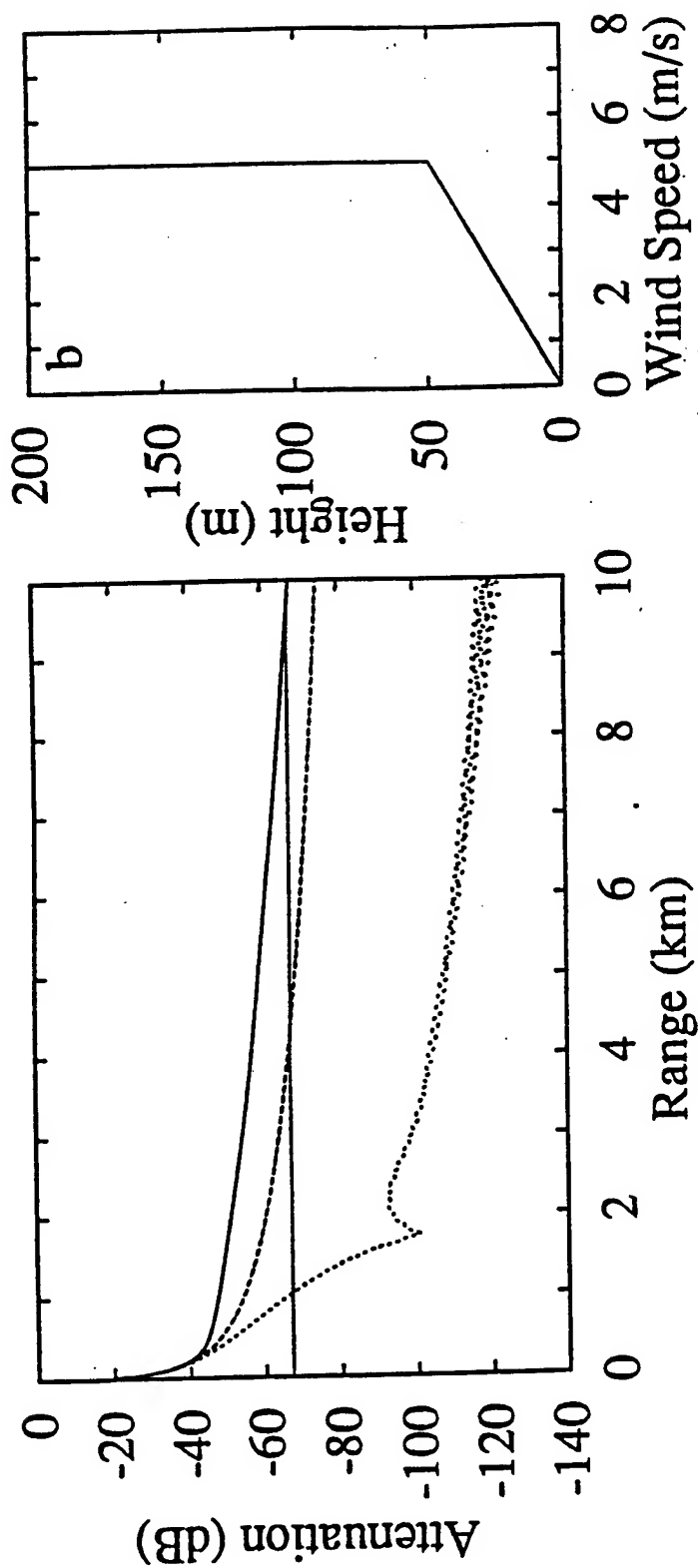


Figure 0.1: 15 Hz attenuation excess (a) predicted by FFP for a simple model of low-level wind shear (b). Short dashes, upwind. Long dashes, crosswind. Solid line, downwind. Atmosphere assumed to be thermally homogeneous ($\partial T / \partial z = 0$).

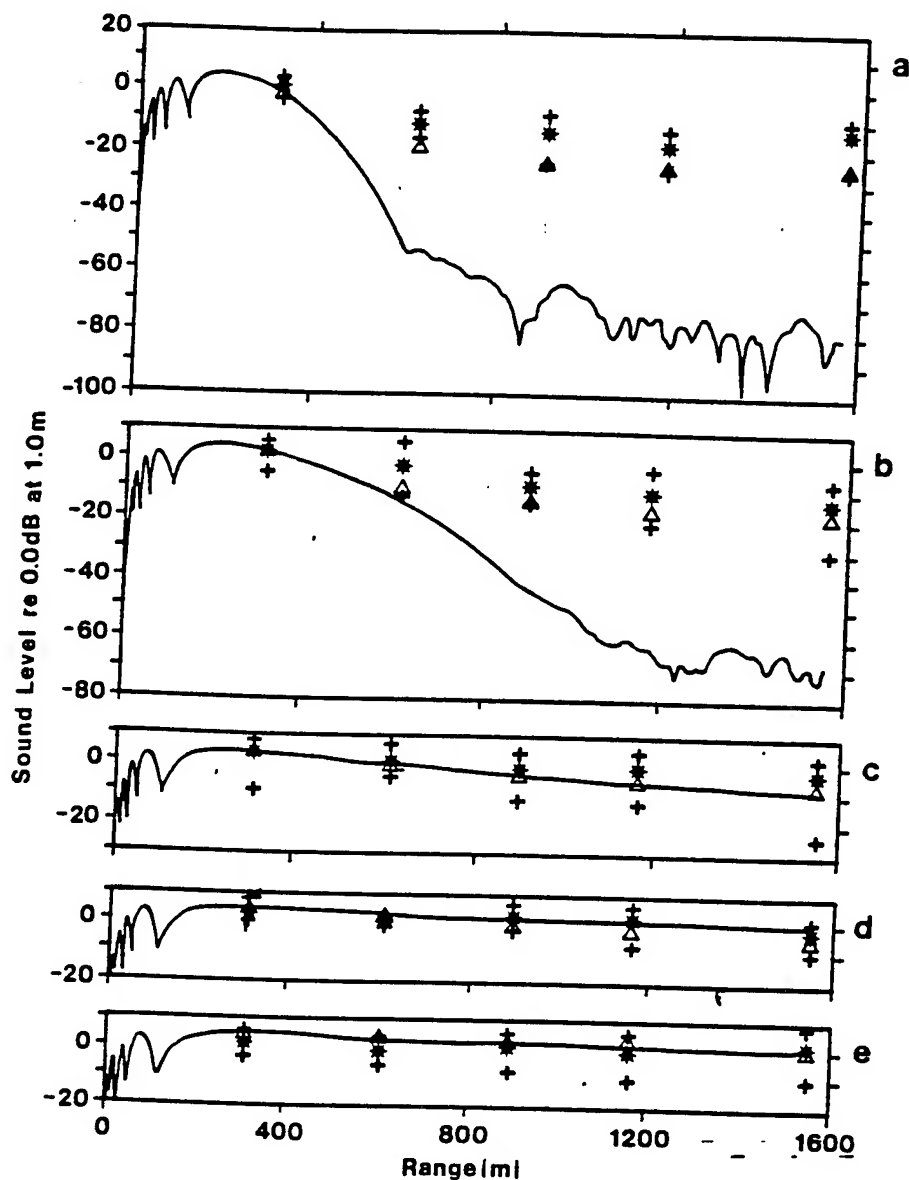


FIG. 6. Comparison of the data for Bondville, IL with coherent parabolic equation predictions and with the turbulent FFP calculation. $f=630$ Hz. (a) $a=-0.8$ m/s, (b) $a=-0.4$ m/s, (c) $a=0$ m/s, (d) $a=0.4$ m/s, and (e) $a=0.8$ m/s. * are data points with error limits; Δ —turbulent FFP calculation. The continuous line is the coherent parabolic equation calculation.

Questions

Accuracy of FFP for upward refraction

Role of surface wave for upward refraction

Criteria for downwind refraction

Residue Series for Upward Propagation

Point source, complex impedance ground
upward refracting atmosphere.

We pick a special atmosphere

$$c(z) = \frac{c(o)}{\left[1 + \frac{2z}{R}\right]^{1/2}}$$

Equation for $\hat{p}(K, z)$:

$$\frac{d^2 \hat{p}}{dz^2} + \left(k_o^2 - K^2 + \frac{2k_o^2 z}{R} \right) \hat{p} = 0$$

Solution are Airy functions

BILINEAR PROFILE

$$c = c_0 \left(1 + \frac{2z}{R}\right)^{-1/2}$$

$$P = -2\pi l e^{i\pi/6} \text{Ai}\left[\left(\tau - \frac{z_{>}}{l}\right) \exp\left(\frac{i2\pi}{3}\right)\right] \\ \times \left[\text{Ai}\left(\tau - \frac{z_{>}}{l}\right) - \frac{\left[\text{Ai}'(\tau) - q \text{Ai}(\tau)\right] \text{Ai}\left[(\tau - z_{<})/l \exp(i2\pi/3)\right]}{\text{Ai}'[\tau \exp(i2\pi/3)] - q \text{Ai}[\tau \exp(i2\pi/3)]} \right]$$

$$l = (R/2k_0^2)^{1/3}, q = ik_0 l/Z_c$$

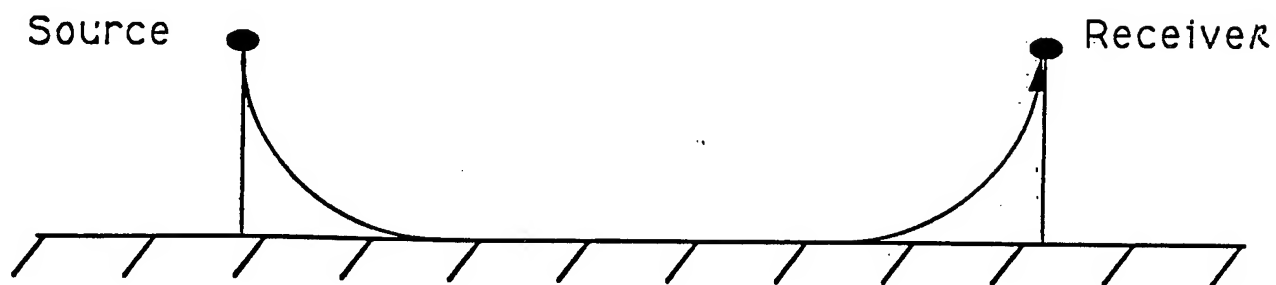
$$\tau = (k^2 - k_0^2) l^2$$

Zeroes of $\text{Ai}' - q \text{Ai}$ give Residue Series.

$$q = 0 \quad \text{zero of } \text{Ai}'$$

$$q \rightarrow \infty \quad \text{zero of } \text{Ai}$$

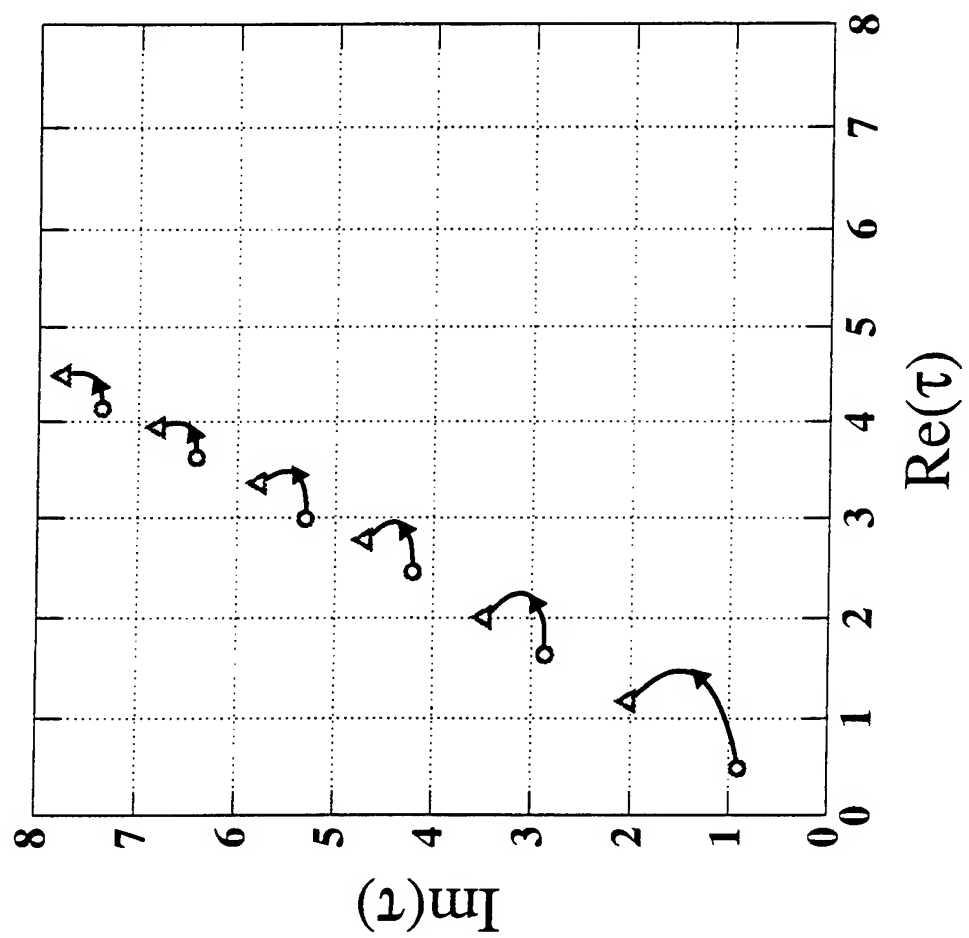
General Behavior



$$\hat{p} = w^{\frac{1}{2}} e^{-\alpha w} e^{i\beta w} e^{i(kw - \omega t)}$$

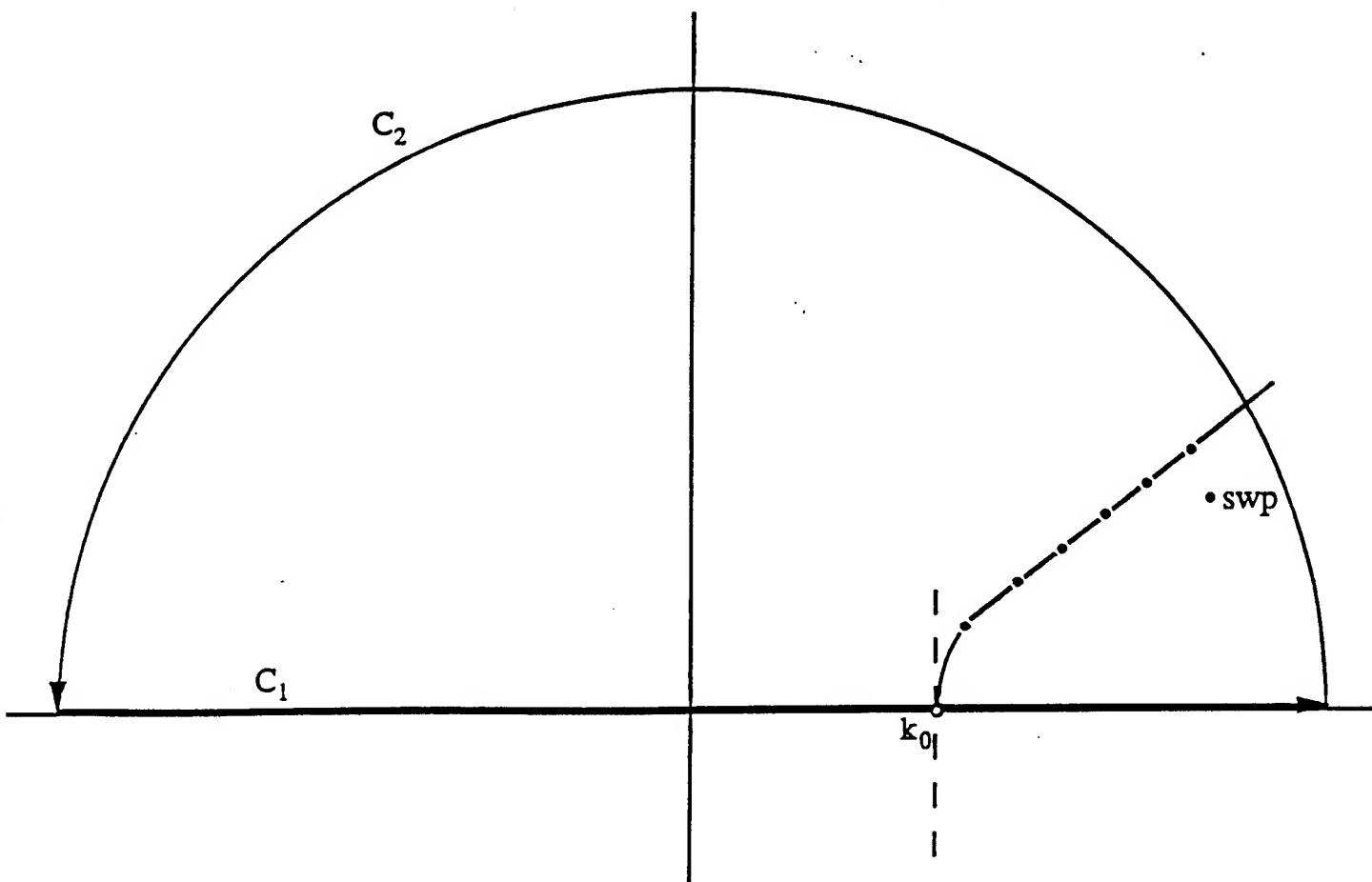
$$\alpha = \text{Re} \left[\left(-e^{-\frac{i\pi}{6}} b_1 \right) \left(\frac{k_0}{2R^2} \right)^{\frac{1}{3}} \right]$$

$$\beta = \text{Im} \left[\left(-e^{-\frac{i\pi}{6}} b_1 \right) \left(\frac{k_0}{2R^2} \right)^{\frac{1}{3}} \right]$$



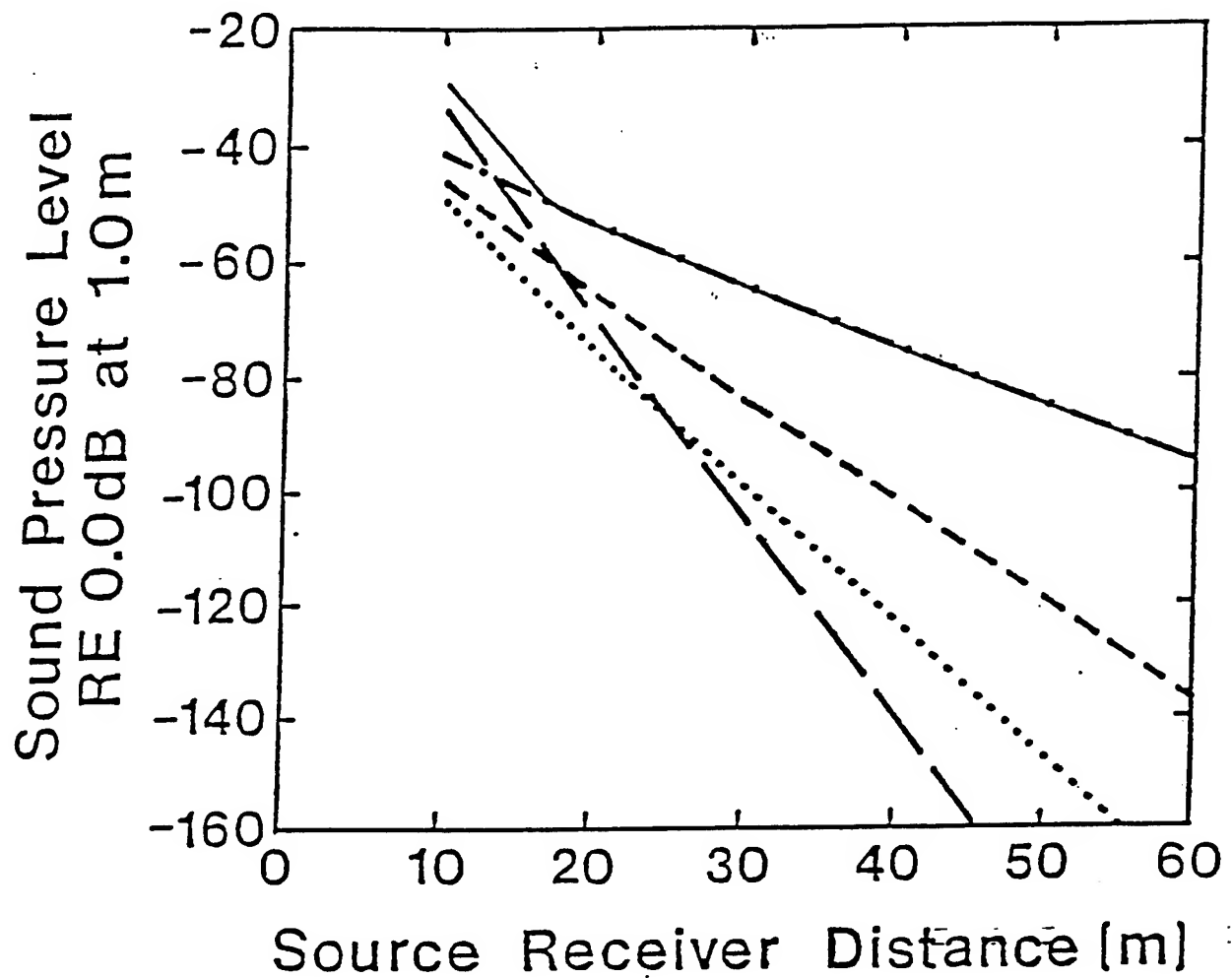
Residue Solution: Upward Refraction

$$k_n = \sqrt{k_0^2 + \frac{\tau_n}{l}}$$



Pole at: $k + i\alpha$;

$$e^{i(k + i\alpha)r} = e^{ikr}e^{-\alpha r}$$

**b**

Spherical Wave \Leftrightarrow Upward Refraction \Leftrightarrow FFP

- **Surface wave contributes to residue series**
- **Arises from zero of Airy function**
- **SWP Only important in transition region**
- **FFP Accurate to -120dB**
- **Turbulence contributes to levels in the shadow zone**

Normal Mode Method for Downward Refraction

Point source, complex impedance
boundary, downward refracting
atmosphere.

Bilinear profile

$$c = \frac{c(o)}{\left[1 - \frac{2z}{R}\right]^{1/2}}$$

Three boundary conditions

Normal Mode Solution:

$$\hat{P}(z,k) = -2\pi e^{i\pi/6} l \text{Ai}(\tau + y >) \times$$

$$\left(\text{Ai}[(\tau + y <)] e^{i2\pi/3} \left[\frac{\text{Ai}'(\tau e^{i2\pi/3}) + q \text{Ai}(\tau e^{i2\pi/3})}{\text{Ai}'(\tau) + q \text{Ai}(\tau)} \right] \times \text{Ai}(\tau + y <) \right).$$

$$l = (R/2k_0^2)^{1/3}$$

$$q = ik_0 l / Z_c$$

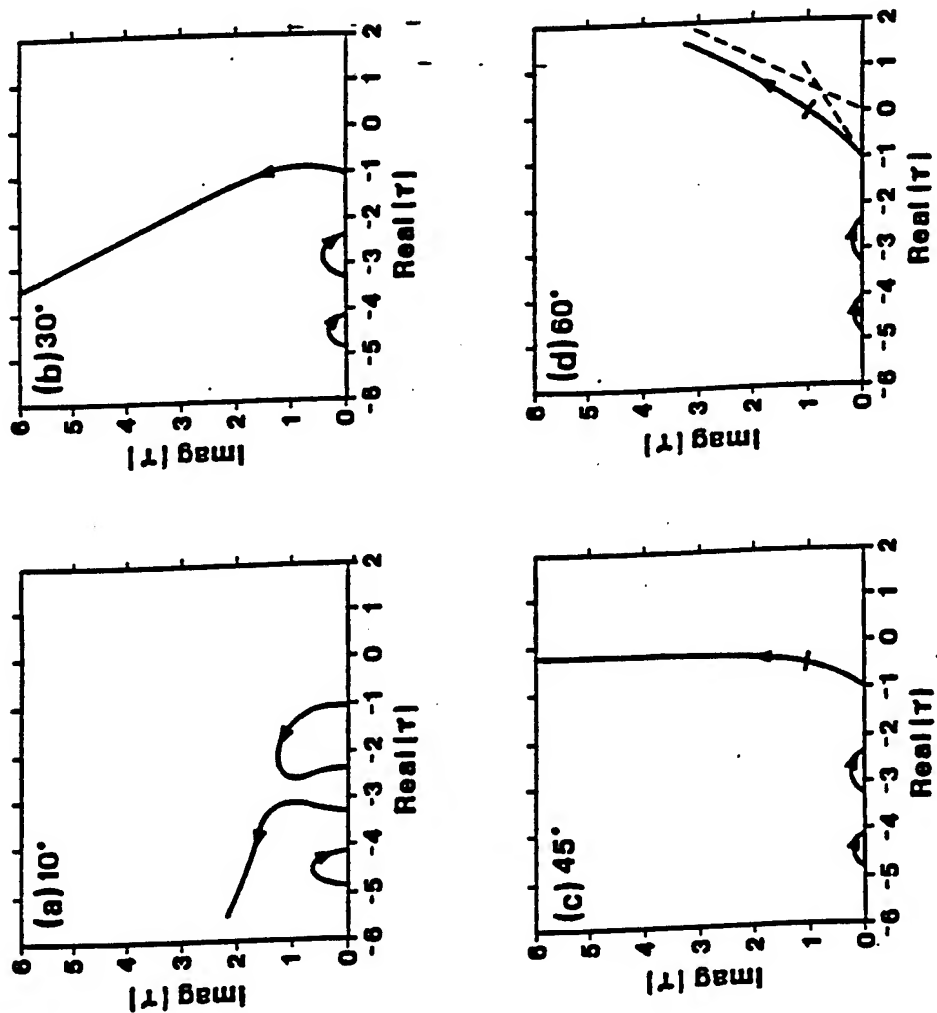
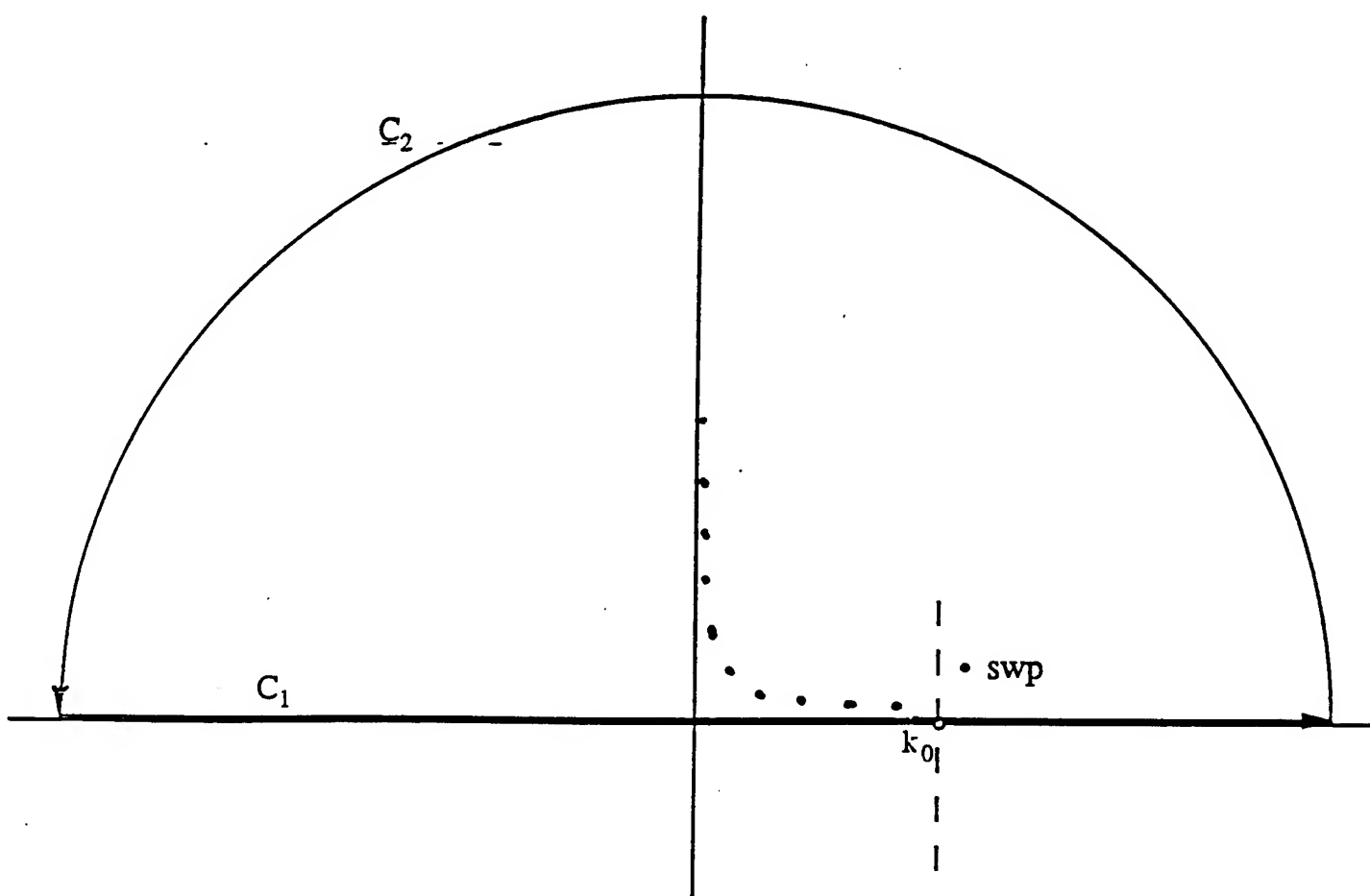


FIG. 4. Behavior of the zeros of Eq. (5) as q varies from zero to infinity for four phases of the impedance: (a) 10° , (b) 30° , (c) 45° , and (d) 60° . The point at which $q = 1.0$ is marked on Fig. 4(c) and (d). The asymptotes for small and large q are the dashed lines in Fig. 4(d).

Residue Solution: Downward Refraction

$$k_n = \sqrt{k_0^2 + \frac{\tau_n}{l}}$$



swp - Subsonic if impedance angle large
and curvature small.

THE HIGHER f , THE MORE POLES

Numerical Example:

$$R = 200 \text{ m}$$

$$f = 10 \text{ Hz}$$

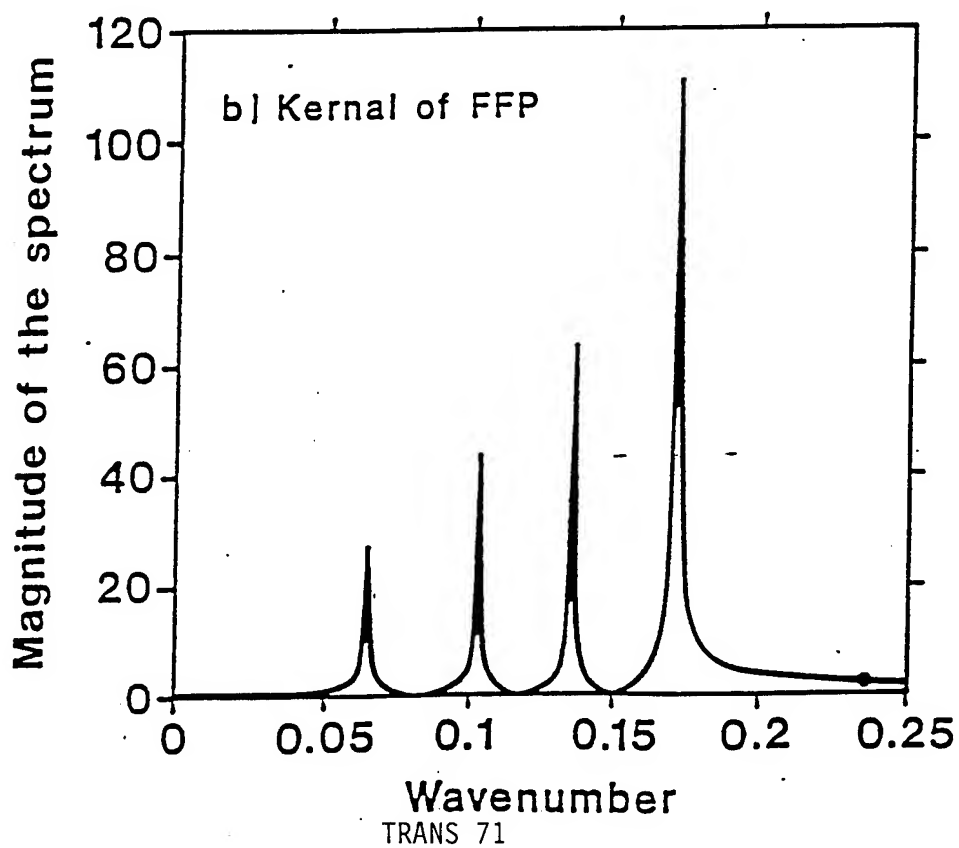
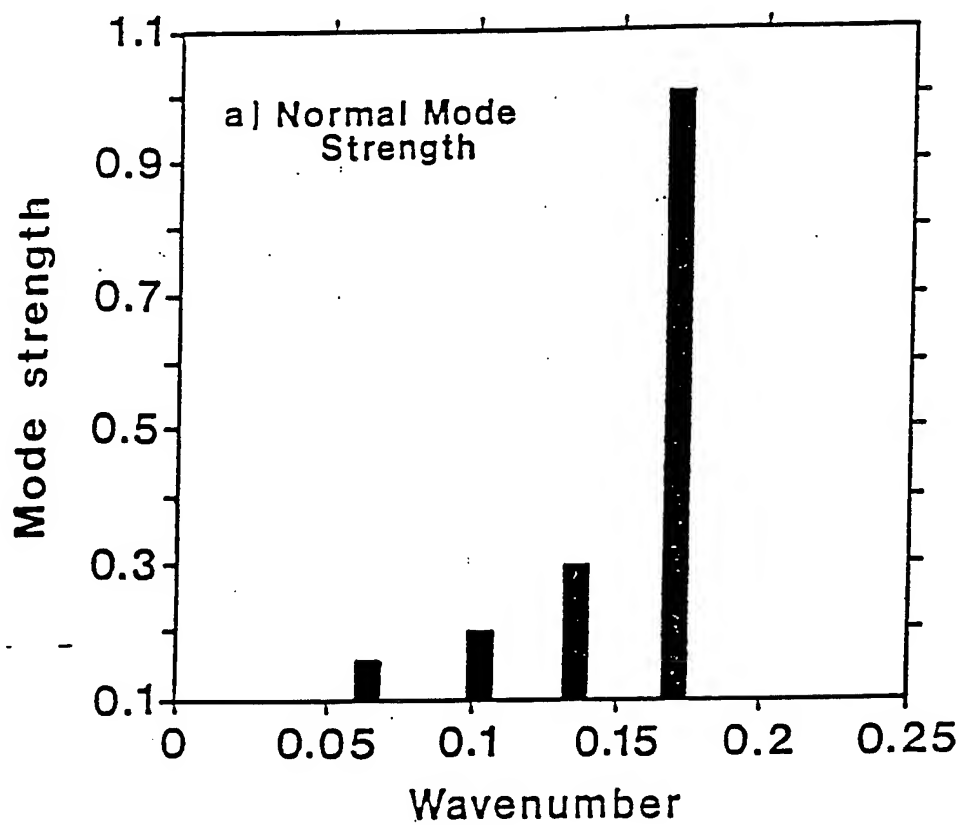
$$\sigma_{\text{eff}} = 300,000 \text{ cgs units}$$

Impedance Model:

Attenborough low frequency approximation

$$q = .035 + i .035$$

$\text{Re}(\tau)$	$\text{Im}(\tau)$	$\text{Re}(k_n)$	$\text{Im}(k_n)$	h_n
-0.984440794E+00	0.355343751E-01	0.171293223E+00	0.506772578E-03	14.0831
-0.323741681E+01	0.108113171E-01	0.135401576E+00	0.195056080E-03	46.3159
-0.481283475E+01	0.727297229E-02	0.103133024E+00	0.172273623E-03	68.8546
-0.615762629E+01	0.568480551E-02	0.637657608E+01	0.217787361E-03	88.0938



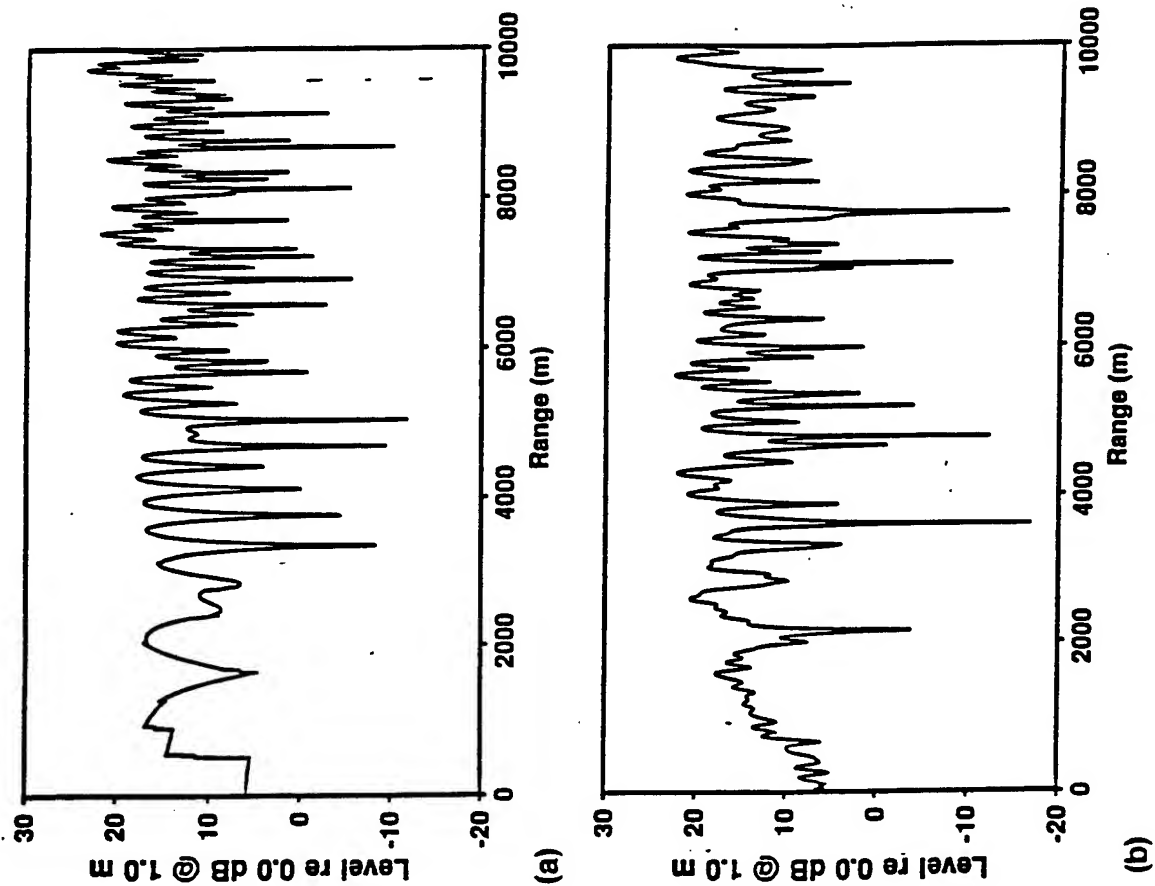


FIG. 2. Sound-pressure level versus range for the standard case for $f=10$ Hz calculated using (a) the heuristic model, (b) the fast field program. $\sigma=366\ 000\ \text{Pa s/m}^2$.

Normal Mode \Leftrightarrow Spherical Wave \Leftrightarrow FFP

- **Impedance pole always contributes**
- **Only a true surface wave for mild refraction**
- **Normal mode strength and attenuation related to the FFP spectrum**
- **Low inversions don't lead to large enhancement**

Conclusions

- Full wave needed at caustics, in shadow zones, and near to ground
- Determining parameter is $l = (R/2k_0^2)^{1/3}$
- Surface wave behavior does not lead to enhancement at long range
- Ideal cases help us to understand FFP results

Physical Acoustics Summer School - 1996

**Sensor Physics:
Signals and Noise**

Thomas B. Gabrielson
NAWC Aircraft Division
Code 4554 MS07
Warminster, PA 18974-0591
tbgabr@nadc.navy.mil

Thomas B. Gabrielson
Applied Research Laboratory
The Pennsylvania State University
P.O. Box 30
State College, PA 16804

Physical Acoustics Summer School 1996

Sensor Physics: Signals and Noise

Introduction

Equilibrium-Thermal Noise

Relation of fluctuations to dissipation

Total-energy methods; frequency distribution

Examples

Shot and Nonequilibrium Noise

Basic theory

Molecular collisions

Metals and semiconductors

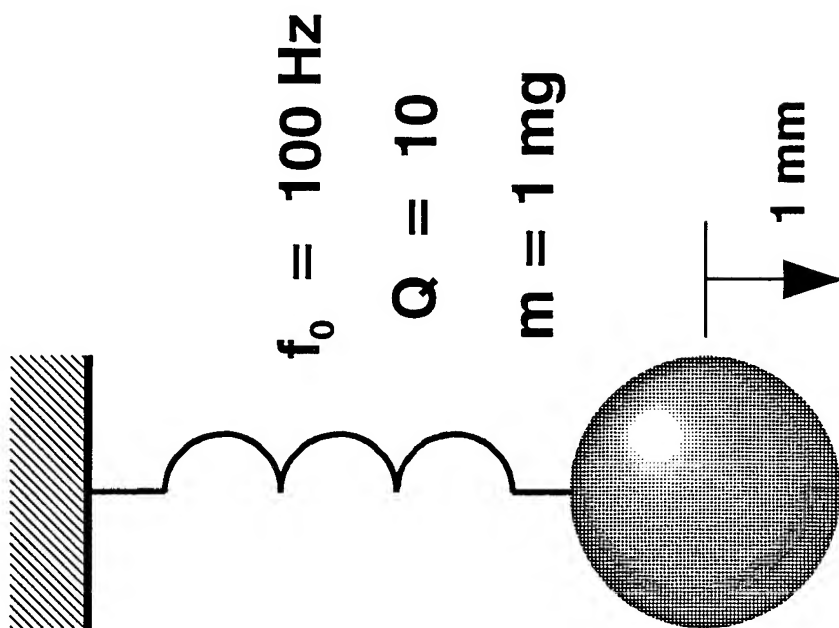
Sensor Calibration

Reciprocity calibration

Bessel-null methods

Summary

QUIZ: Question #1



Given an initial displacement of 1mm,
how long will it take for the
amplitude to decay to 0.1\AA ?

(This level is equivalent to an
acceleration of 0.5 micro-g's.)

Q in Resonant Systems:

- (1) 2π times the number of cycles required for energy to decay by e^{-1} ; π times the number of cycles for the amplitude to decay by e^{-1} . Alternately, $Q = \pi N / 0.693$ where N is the number of cycles for the amplitude to decay by a factor of 2.
- (2) Ratio of the resonance frequency to the width of the resonance peak. The width must be measured as the full width from one half-power point to the other.
- (3) Ratio of mass reactance (or stiffness reactance) at resonance to the resistance for series-connected elements; the reciprocal of that ratio for parallel-connected elements.
- (4) 2π times the energy stored in the system divided by the energy dissipated per cycle; 2π times the resonance frequency times the stored energy divided by the power dissipated.
- (5) The reciprocal of 2 times the damping factor; the reciprocal of the loss tangent.
- (6) If the damping is high (small Q), the resonance is isolated from other resonances, and there is no other mechanism to generate a changing phase, the Q can be determined from the rate-of-change of the phase (in radians per hertz) at the resonance frequency:

$$Q = \frac{f_0}{2} \left(\frac{d\phi}{df} \right)_{f_0}$$

Q in Resonant Systems:

- (7) From curve-fit on HP3562 dynamic signal analyzer: the curve-fit produces a conjugate set of poles for a resonance peak, $f_r \pm if_i$. The resonance frequency, f_0 , and the Q are as follows:

$$\begin{aligned} f_0 &= \sqrt{f_r^2 + f_i^2} \approx f_i \\ Q &= \frac{1}{2f_r} \sqrt{f_r^2 + f_i^2} \approx \frac{f_i}{2f_r} \end{aligned}$$

where the approximations are valid for large Q .

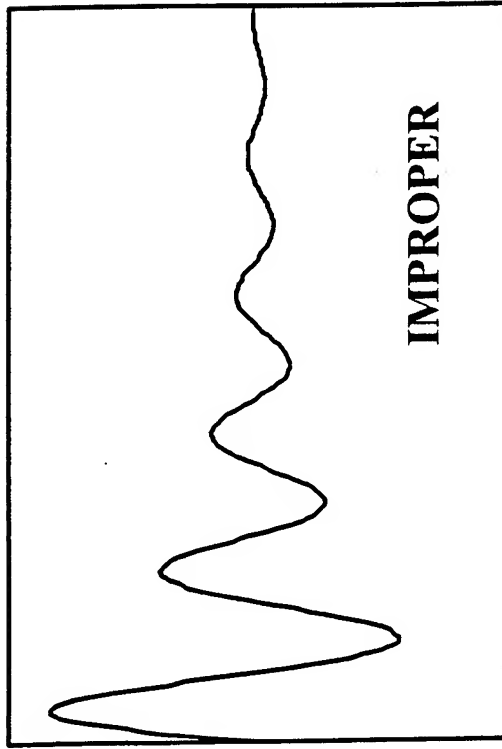
- (8) Drive the system with a square wave and observe the ringing at the edge transitions of the square wave. If the peak-to-peak amplitude of the first half-cycle of the ringing is a and the peak-to-peak amplitude of the second half-cycle is b , then the damping factor is:

$$\zeta = \frac{1}{2Q} = \frac{\ln(a/b)}{\sqrt{\ln^2(a/b) + \pi^2}}$$

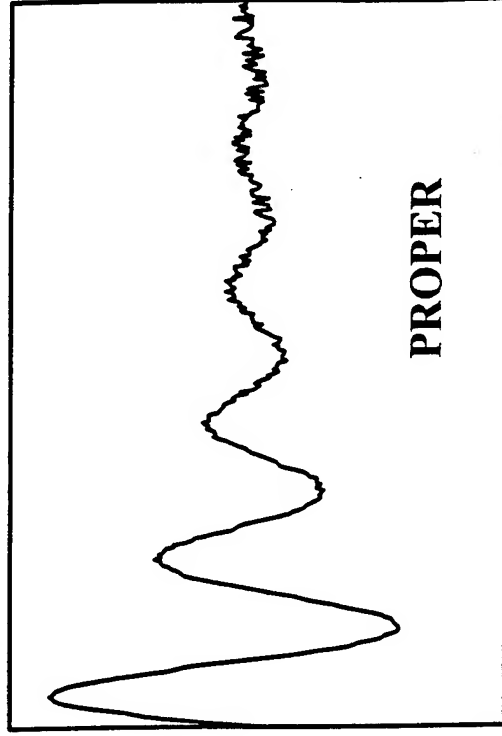
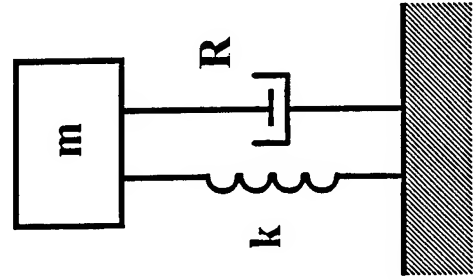
Note: The equivalent noise bandwidth of a resonant system is:

$$\Delta f_{NB} = \frac{\pi f}{2Q}$$

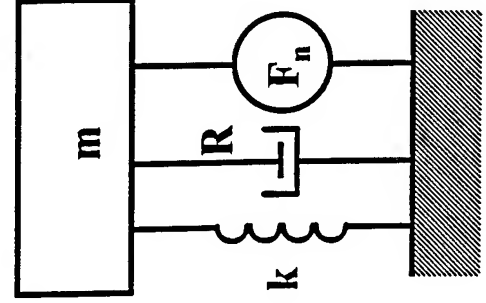
Proper Dynamics for Damped Mass-Spring:



$$m\ddot{x} + R\dot{x} + kx = 0$$

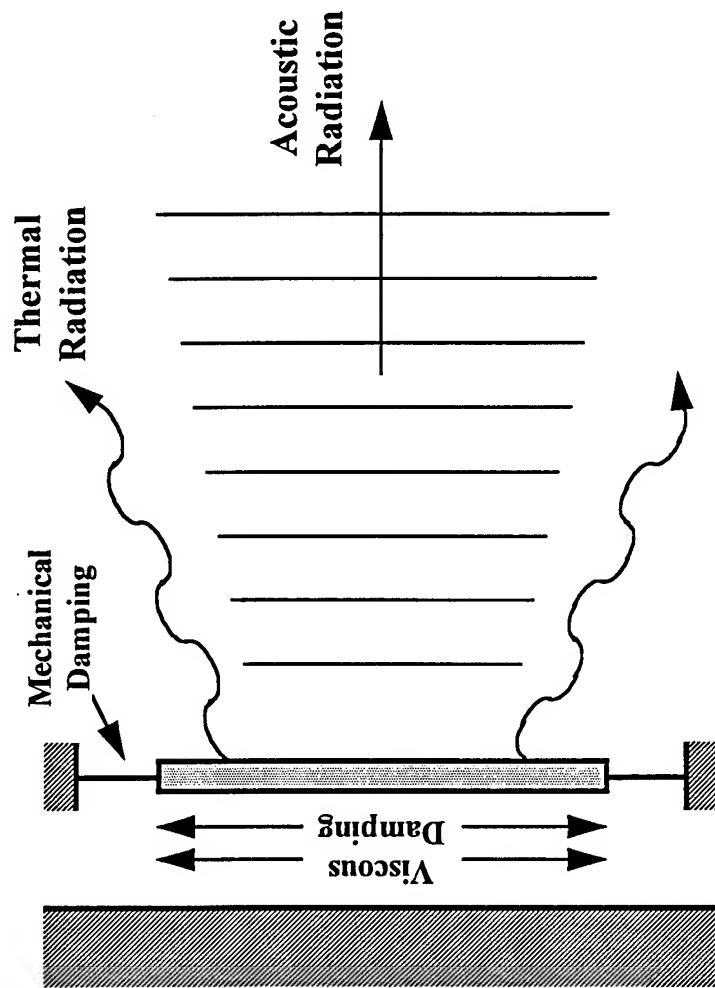


$$m\ddot{x} + R\dot{x} + kx = f_n(R,t)$$



Fluctuation-Dissipation Theorem:

If there is a path along which energy can flow from a system to its environment, *then energy from the environment can flow back into the system*. Dissipation is a measure of the energy that leaves the system (either as ordered energy in the case of radiation or as disordered energy in the case of damping); thermal fluctuations are a measure of the disordered energy that enters the system from the environment. *In thermal equilibrium, the presence of dissipation guarantees the presence of fluctuations.*



Equilibrium Thermal Fluctuations:

Total Energy

Each degree-of-freedom of a system has a “thermal” energy of $\frac{1}{2}k_B T$ where k_B is Boltzmann’s constant (1.38×10^{-23} joules/kelvin) and T is the absolute temperature.

There is such a thermal energy associated with each of the components of kinetic energy ($\frac{1}{2}mv_x^2$, $\frac{1}{2}mv_y^2$, $\frac{1}{2}mv_z^2$), spring-potential energy ($\frac{1}{2}kx^2$), rotational kinetic ($\frac{1}{2}I\omega^2$), capacitive ($\frac{1}{2}CV^2$), etc.

A molecule in a liquid has

$$\frac{1}{2} m v_x^2 = \frac{1}{2} k_B T$$

A ball-bearing in a liquid has

$$\frac{1}{2} m v_x^2 = \frac{1}{2} k_B T$$

An atom in a solid OR a mass on a spring has

$$\frac{1}{2} k x^2 = \frac{1}{2} k_B T$$

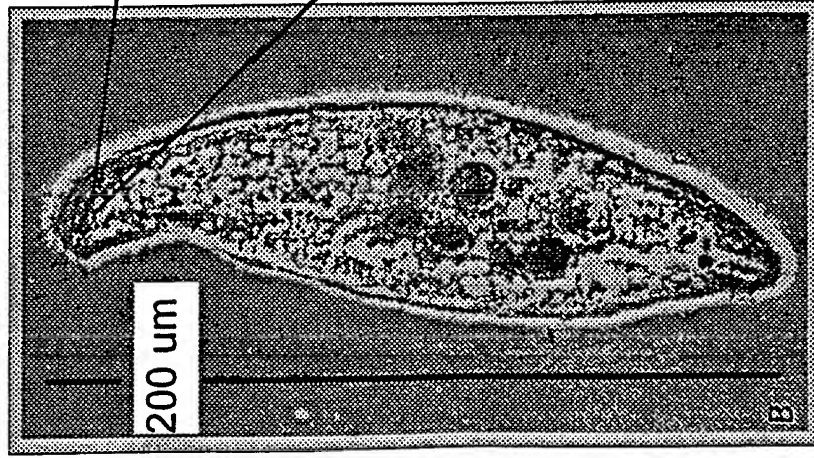
Energy Levels:

$k_B T$ at room temperature:	0.025 eV
hf at optical frequencies:	1.5 - 3 eV
acoustic wave (100 μ Pa in air):	0.4 eV/cm ³
acoustic wave (100 μ Pa in water):	30 μ eV/cm ³
chemical bonds	
covalent:	4 eV
ionic:	2 eV
hydrogen:	0.2eV

$$(1 \text{ eV} = 1.6 \times 10^{-19} \text{ joules})$$

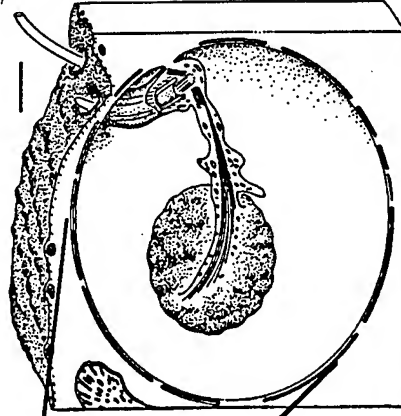
Sensing of Gravity by Protozoa

1. Fenchel and Finlay, "Geotaxis in the ciliated protozoon *Loxodes*," J. Exp. Biol. 110, 17-33 (1984)
2. Fenchel and Finlay, "The structure and function of Muller vesicles in *Loxodid* ciliates," J. Protozool. 33, 69-76 (1986)



(reprinted with permission
from Ref. 1)

Loxodes striatus



7 μm

(reprinted with permission
from Ref. 2)

proof mass, $m = 45$ picograms
range of mass motion, $L = 3$ micrometers

sensor's potential energy = mgL
sensor's thermal energy = kT

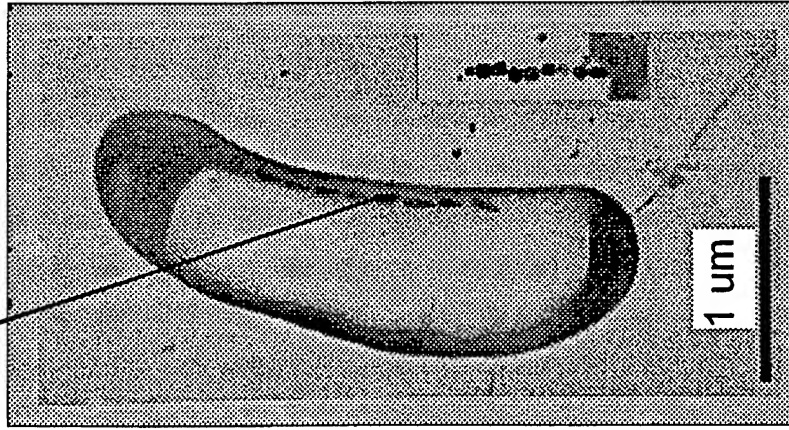
$$mgL / kT = 330$$

If linear dimensions of vesicle were reduced by a factor of 4, then $mgL / kT = 1$ and the organism would be unable to distinguish up from down!

Sensing of Magnetic Fields by Bacteria

1. Frankel, Blakemore, and Wolfe, "Magnetite in freshwater magnetotactic bacteria," Science 203, 1355 (1979)
2. Blakemore, Frankel, and Kalmijn, "South-seeking magnetotactic bacteria in the Southern Hemisphere," Nature 286, 384 (1980)

magnetite



magnetotactic bacterium

magnetic dipole moment, $M = 1.3 \text{ fA m}^2$
magnetic flux density, $B = 50 \text{ microtesla}$

sensor's potential energy = MB
sensor's thermal energy = kT

$$MB / kT = 16$$

(reprinted with permission
from Ref. 2)

Equilibrium Thermal Fluctuations:

Distribution of Energy

The distribution of thermal energy is given by Nyquist:

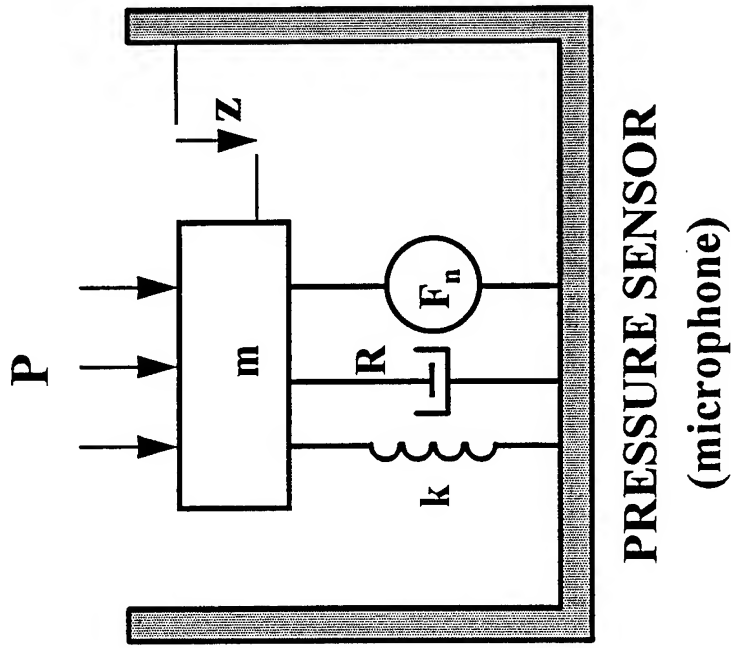
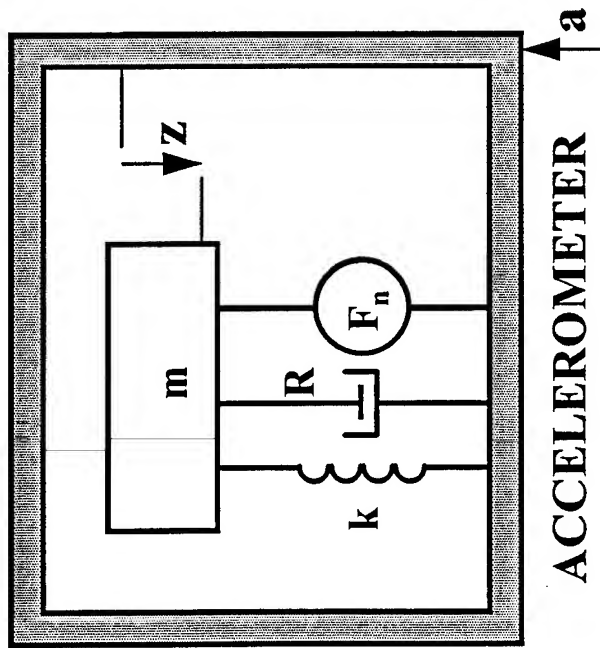
$$F_n^2 = 4 k_B T R_{\text{mechanical}} df$$

$$V_n^2 = 4 k_B T R_{\text{electrical}} df$$

R is resistance: force per velocity for mechanical resistance, volts per ampere for electrical resistance. In general, the real part of the relevant impedance is used for R (which may be a function of frequency). df is the increment of bandwidth.

Since the noise power is distributed over frequency, the noise is described by a power density (watts per hertz), or an amplitude-squared per hertz (newtons² per hertz, volts² per hertz), or an amplitude per root hertz (pascals per root hertz, meters per second per root hertz).

Noise Equivalent Signal:



Set noise to zero and solve for signal response: $a = g(z)$

Set signal to zero and solve for output due to noise: $z_n = h(F_n)$

Calculate noise-equivalent signal: $a_n = g(z_n)$

Noise Equivalent Signal:

ACCELEROMETER

$$(ma_n)^2 = 4k_B T R df$$

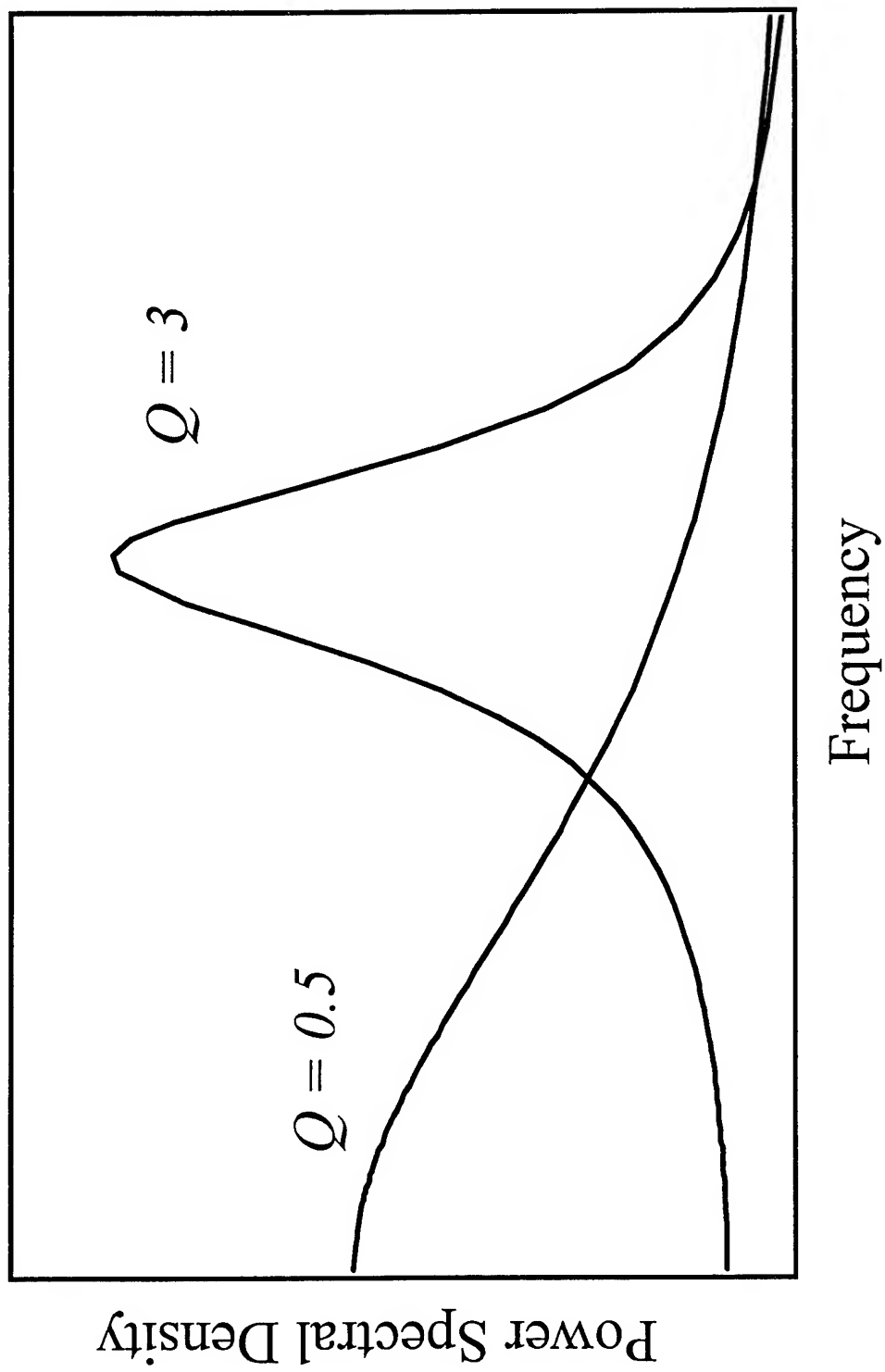
$$a_n^2 / df = 4k_B T \frac{R}{m^2} = 4k_B T \left[\frac{\omega_0}{mQ} \right]$$

PRESSURE SENSOR

$$(p_n A)^2 = 4k_B T R df$$

$$p_n^2 / df = 4k_B T \frac{R}{A^2} = 4k_B T \left[\frac{\omega_0 m}{A^2 Q} \right]$$

Frequency Distribution of Noise:



Noise Associated with Radiation:

Spherical wave (spherical source):
$$p = \frac{A}{r} e^{i(kr - \omega t)}$$

Compute radial particle velocity from Newton's Law in fluid:
$$-\nabla p = \rho \frac{\partial u}{\partial t} \Rightarrow u_r = \left(1 + \frac{i}{kr}\right) \frac{p}{\rho c}$$

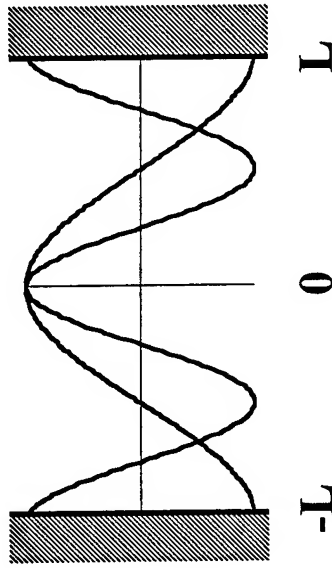
Mechanical radiation resistance (ratio of force to velocity):
$$Z = \frac{p A}{u_r} = \rho c A \left\{ \frac{(kr)^2}{1 + (kr)^2} - i \frac{kr}{1 + (kr)^2} \right\}$$

Radiation resistance for a point source ($A = 4\pi r^2$):
$$\Re\{Z\}|_{r \rightarrow 0} \rightarrow \rho c A (kr)^2 = \pi \frac{\rho f^2}{c} A^2$$

Pressure fluctuations associated with "loss" by radiation:

$$\boxed{p_n^2 = 4 k_B T \frac{\Re\{Z\}}{A^2} = 4 k_B T \pi \frac{\rho f^2}{c} df}$$

Noise Associated with Radiation:



Start with a rigid-walled box, side = $2L$, sensor in the middle.

Modes have max pressure at walls and at center:

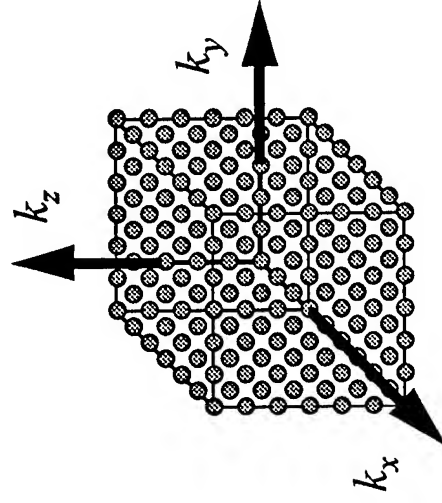
$$\cos(l\pi x/L), \cos(m\pi y/L), \cos(n\pi z/L)$$

Wavenumbers are then:

$$k_x = l\pi/L, k_y = m\pi/L, k_z = n\pi/L$$

(spacing between k 's = π/L)

$$\text{and } k^2 = k_x^2 + k_y^2 + k_z^2$$



Cell "volume" in k -space is $(\pi/L)^3$ with one k -point per cell.
Each mode gets $k_B T$ (1/2 for kinetic, 1/2 for potential) therefore,

$$\textbf{k-space density of thermal energy} = k_B T (L/\pi)^3$$

Noise Associated with Radiation:

Energy in dk is energy in a spherical shell between k and $k+dk$.

$$\begin{aligned}\text{Volume of shell in } k\text{-space} &= (4\pi/3)[(k + dk)^3 - k^3] \\ &= 4\pi k^2 dk \text{ for small } dk.\end{aligned}$$

Therefore, $dE = k_B T (L/\pi)^3 4\pi k^2 dk$, or, since $k = 2\pi f/c$,

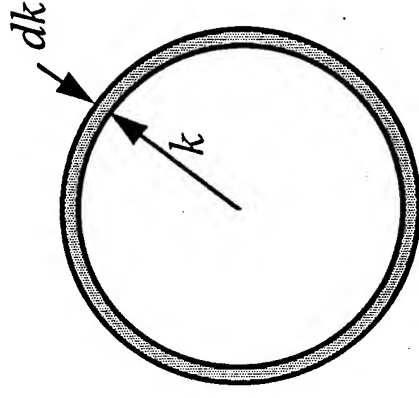
$$dE = 32\pi k_B T L^3 f^2 df/c^3$$

Divide by the spatial volume, $(2L)^3$, to get the true energy density:

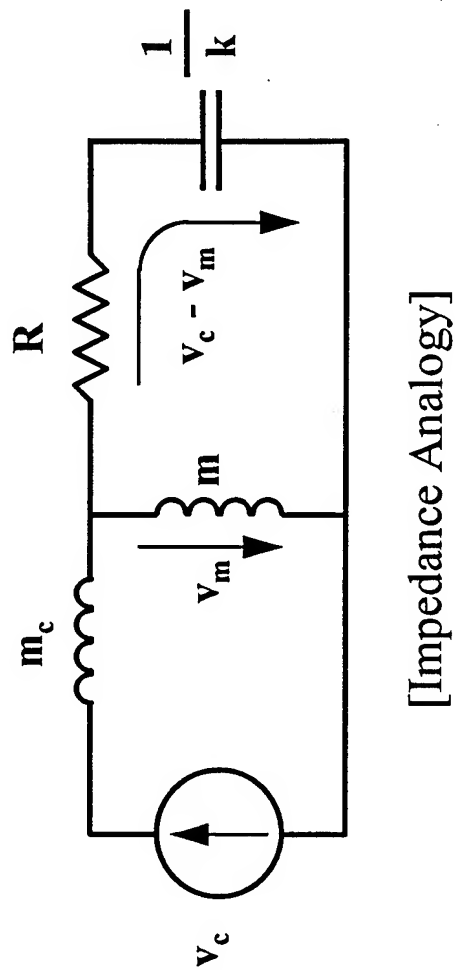
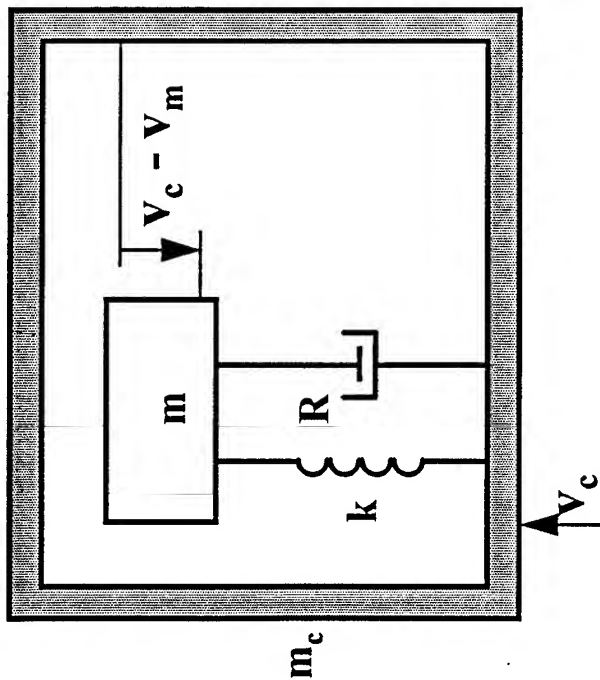
$$\mathcal{E} = 4\pi k_B T f^2 df/c^3$$

Another way to write the energy density is $\mathcal{E} = p^2/\rho c^2$ so the pressure fluctuations associated with the radiation are given by

$$p_n^2 = 4k_B T \pi \frac{\rho f^2}{c} df$$



The Simple Accelerometer:



[Impedance Analogy]

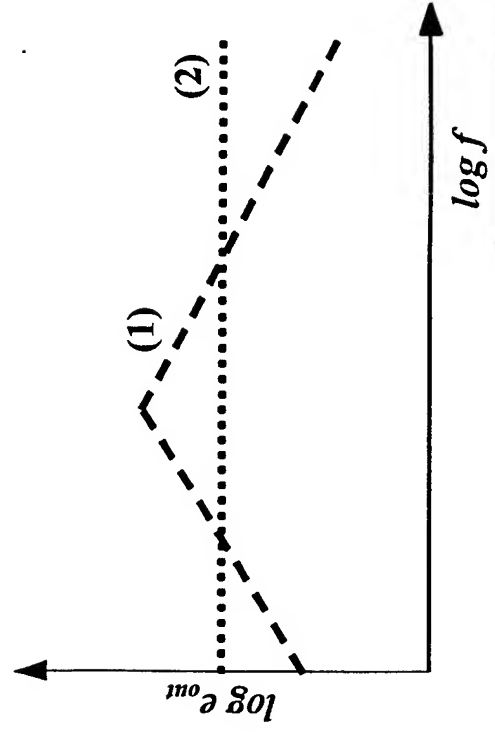
$$\frac{v_c - v_m}{v_c} = \frac{\left(\frac{\omega}{\omega_0}\right)^2}{\left(\frac{\omega}{\omega_0}\right)^2 - 1 - j\left(\frac{\omega}{\omega_0}\right)\left(\frac{1}{Q}\right)}$$

Equilibrium Noise in a Geophone (velocity transducer):

$$a_n^2 = 4k_B T \frac{\omega_0}{mQ} \Rightarrow v_n^2 = 4k_B T \frac{\omega_0}{\omega^2 mQ}$$

$$e_{out} = \text{const.} * (v_c - v_m)$$

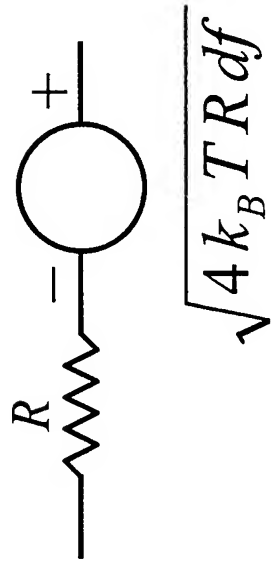
For the simple accelerometer, $(v_c - v_m)/v_c$ is proportional to ω^2 below ω_0 and to ω^0 above ω_0 . The noise velocity (referenced to the case) is proportional to ω^{-1} . Therefore, the output noise voltage (1) is proportional to ω' below ω_0 and to ω^{-1} above ω_0 .



The equilibrium -thermal noise associated with the electrical resistance in the sense coil produces an output voltage noise (2) that is independent of frequency:

$$e_{out} = \sqrt{4k_B T R_{coil}}$$

Equivalent Noise Generators:



MECHANICAL:

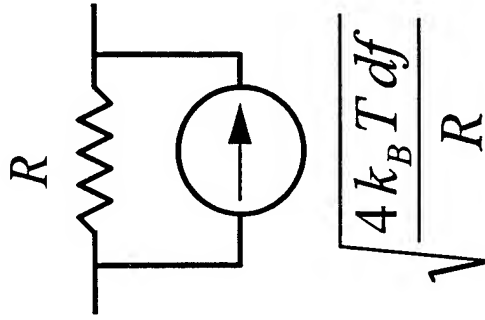
force

velocity

ELECTRICAL:

voltage

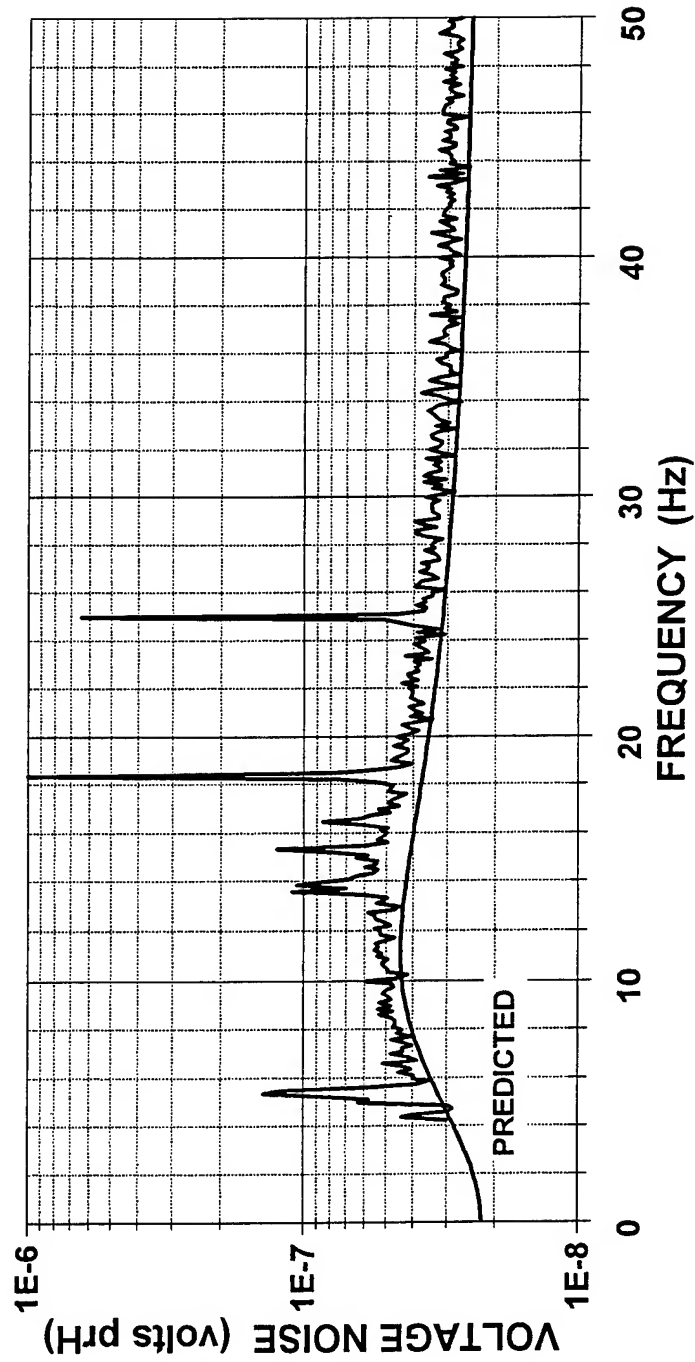
current



NAWC Aircraft Division
Code 4554
Warminster, PA 18974

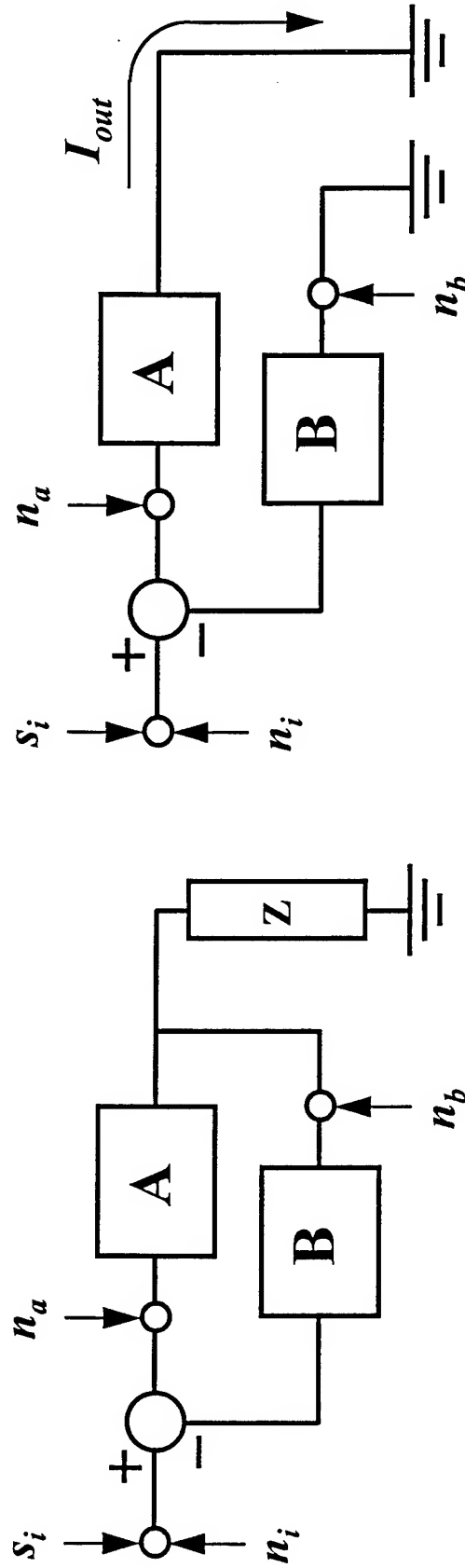
Noise-Floor Measurement

x4 Array 5/21/95



Signal-to-Noise Ratio: A Useful Theorem

The signal-to-noise ratio at the output of a linear circuit does not depend on the value of the output load.

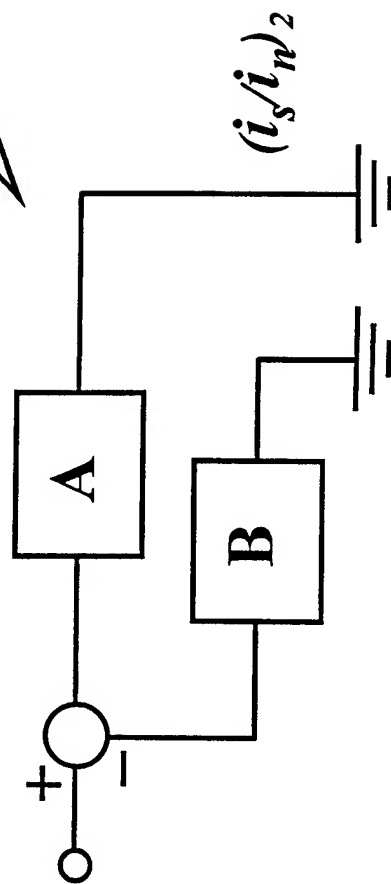
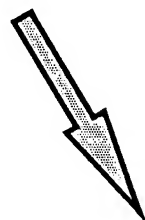
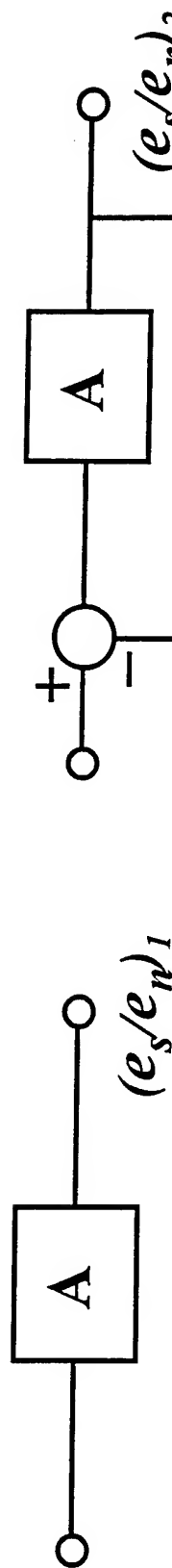


Analysis of complicated circuits can often be simplified by setting the output load to zero and calculating the ratio of signal current to noise current.

Signal-to-Noise Ratio and Feedback:

The effective Q of a system can be changed by adding feedback.
Positive feedback increases the Q ; negative feedback decreases the Q .

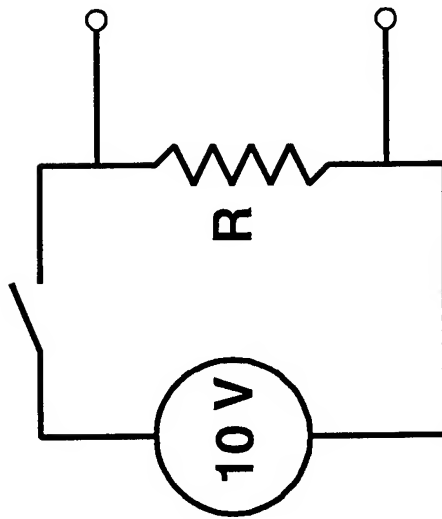
Can the noise of a system be reduced by adding feedback?



$$(e_s/e_n)_2 = (i_s/i_n)_2 > (e_s/e_n)_1$$

Not this way!

QUIZ: Question #2:



Measure the spectral density of the voltage noise across a resistor.

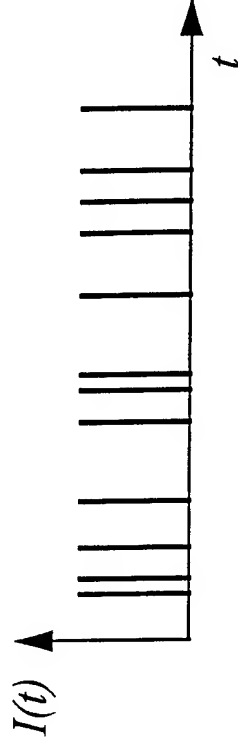
Put 10 VDC across the resistor to induce a current.

By what factor does the noise voltage increase? (Ignore $1/f$ noise.)

Shot Noise:

Given a current consisting of impulses:

$$I(t) = q \sum_{i=1}^{\infty} \delta(t - t_i)$$



Expand current as a Fourier series:

$$I(t) = \sum_{k=0}^{\infty} [a_k \cos(2\pi f_k t) + b_k \sin(2\pi f_k t)]$$

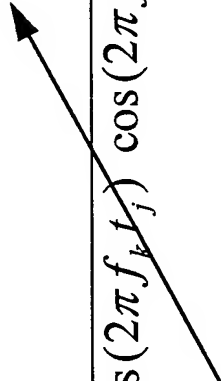
$$\text{where } a_k = \frac{2}{T} \int_0^T I(t) \cos(2\pi f_k t) dt = \frac{2q}{T} \sum_{i=1}^N \cos(2\pi f_k t_i)$$

(The period, T, is long enough to encompass many (N) events.)

One component of the expansion covers a band of $\Delta f (= 1/T)$. The mean-square value in that band is:

$$\overline{i_k^2} = \overline{a_k^2 \cos^2(2\pi f_k t)} + \overline{b_k^2 \sin^2(2\pi f_k t)} + \overline{a_k b_k \cos() \sin()} = \frac{1}{2} (\overline{a_k^2} + \overline{b_k^2})$$

Shot Noise:

$$\overline{a_k^2} = \frac{4q^2}{T^2} \left\{ \sum_{i=1}^N \overline{\cos^2(2\pi f_k t_i)} + \sum_{j \neq k} \overline{\cos(2\pi f_k t_j) \cos(2\pi f_k t_k)} \right\} = \frac{4q^2}{T^2} N \frac{1}{2}$$


The second summation is zero *only if the impulses are statistically independent*.

If the events are not independent, then the cross-terms must be evaluated!

(For independent events, the mean-square value of b_k is identical to that of a_k .)

$$\text{Since } \bar{I} = \frac{N}{T} \quad \text{and} \quad \Delta f = \frac{1}{T}$$

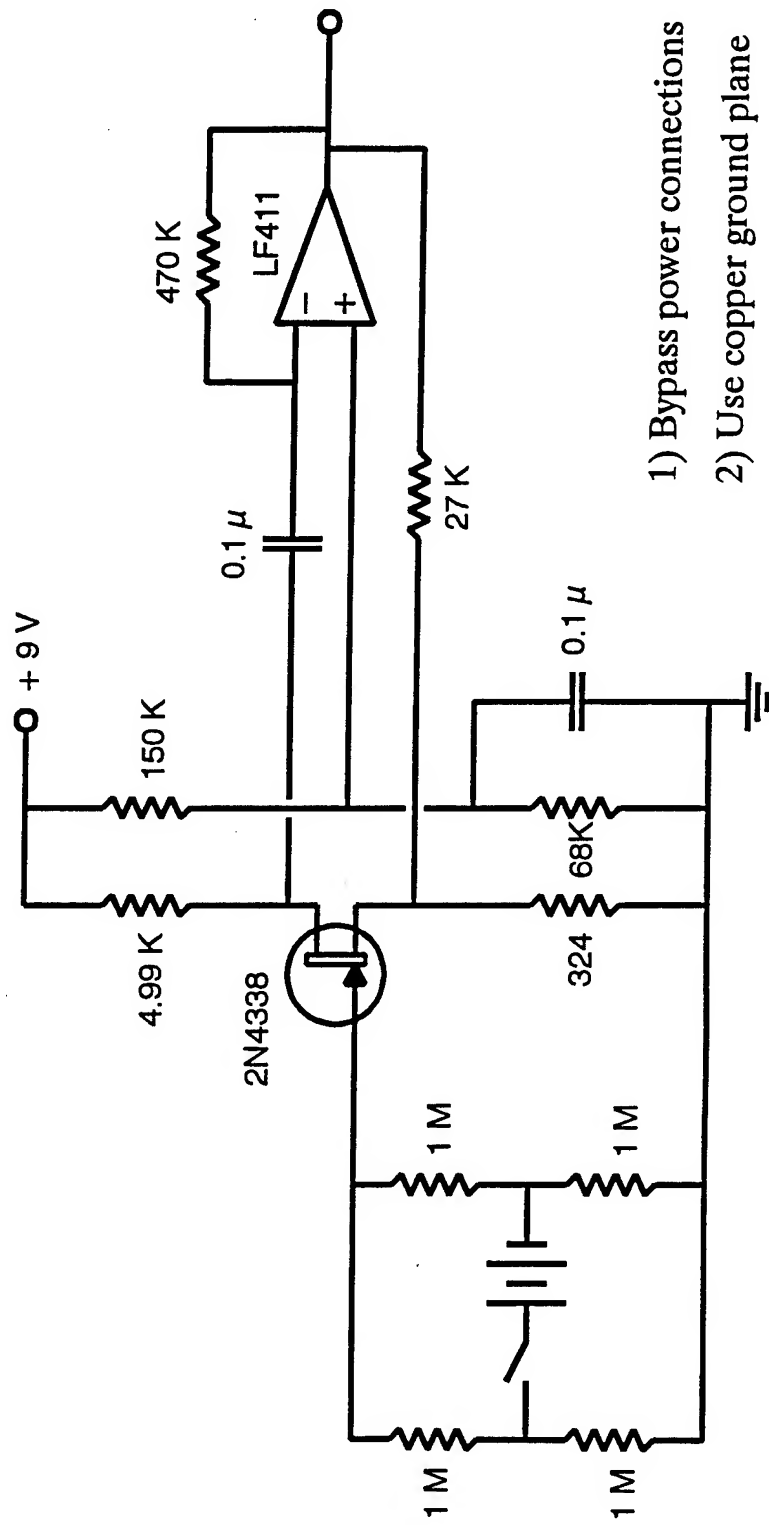
$$\overline{i_k^2} = 2q \bar{I} \Delta f$$

Applies to processes consisting of events that are:

- (1) impulse-like
- (2) independent

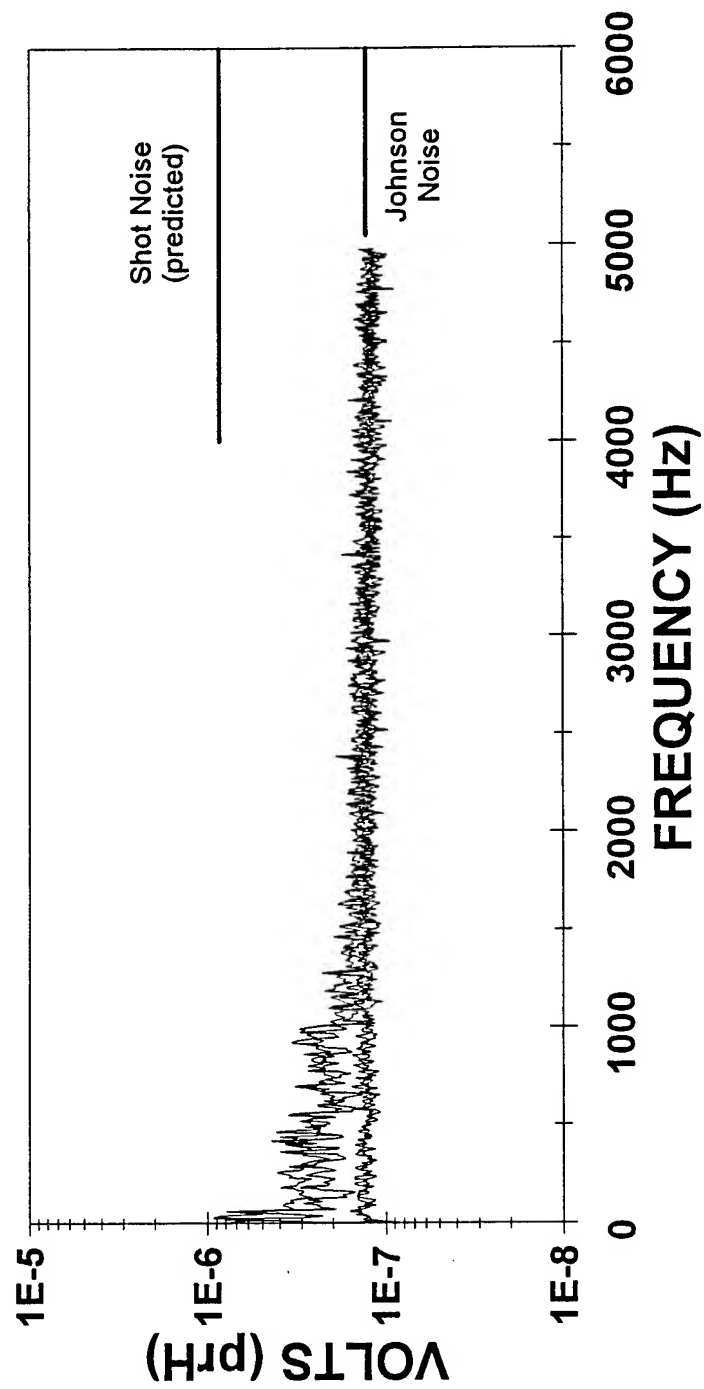
Circuit for Basic Noise Experiment:

Gate-resistance bridge allows noise measurement of input resistance with and without current. Bridge rejects common-mode noise from battery and permits measurement to zero frequency.



Resistor Noise

with and without current flow



Noise From Molecular Collisions (Free-Molecular Flow):

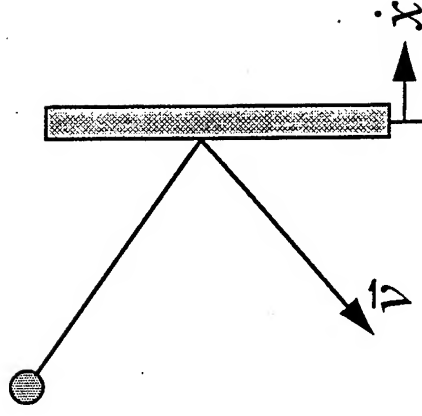
$$\text{Force} = \sum_{\text{molecules}} \left\{ \begin{array}{l} \text{rate of change in momentum of a molecule} \\ \text{initially traveling to the right and hitting the} \\ \text{disk from behind} \end{array} \right\}$$

= (molecular flux) (momentum change per collision)

$$= \frac{n}{2} A (v_x - \dot{x}) \cdot 2m(v_x - \dot{x})$$

$$= nmv_x^2 A - 2nmv_x A\dot{x} + \cancel{nm(\dot{x})^2 A}$$

$$= P_0 A - R_{mech} \dot{x}$$



$$R_{mech} = 2nmv_x A$$

Noise From Molecular Collisions (Free-Molecular Flow):

$$p_n^2 = \frac{F_n^2}{A^2} = \frac{4k_B T R_{\text{mech}} df}{A^2} = 8nmk_B T v_x df / A$$

$$P_0 = nk_B T$$

$$\bar{v} = 2\bar{v}_x$$

$$p_n^2 = 2[2m\bar{v}] \frac{P_0}{A} df$$

Looks like a shot-noise expression!

Generalized Forms for Shot Noise:

$$\left[\begin{array}{c} \text{mean-square} \\ \text{fluctuation in} \\ \text{flux density} \end{array} \right] = 2 \left[\begin{array}{c} \text{quantity} \\ \text{per} \\ \text{carrier} \end{array} \right] \left[\begin{array}{c} \text{average} \\ \text{flux} \\ \text{density} \end{array} \right] \left[\begin{array}{c} \text{bandwidth} \\ \text{[area]} \end{array} \right]$$

electric-charge flux density:

$$j_n^2 = 2 [q] J_0 \Delta f / A$$

photon flux density:

$$I_n^2 = 2 [hf] I_0 \Delta f / A$$

momentum flux density:

$$p_n^2 = 2 [2mv] P_0 \Delta f / A$$

Pressure-fluctuation noise power is proportional
(3/2 power) to STATIC PRESSURE.

Molecular-Impact Noise:

Equilibrium thermal fluctuations in force (Nyquist):

$$F_n^2 = 4 k_B T R_{MECH} \Delta f$$

$$R_{MECH} = 16 \eta a \quad (\text{Stokes' flow: disk, radius } a)$$

$$p_n^2 = 4 k_B T 16 \eta a / A^2$$

Pressure-fluctuation noise power is almost
INDEPENDENT of static pressure.

Molecular-Impact Noise:

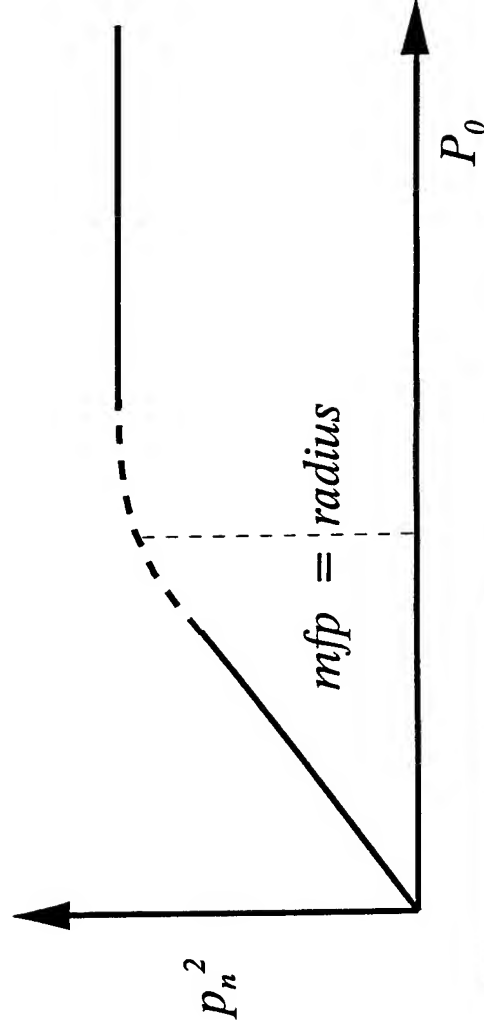
Shot-noise form requires that collisions be INDEPENDENT. As long as the mean-free-path is smaller than the disk radius, the molecular collisions are highly DEPENDENT.

Add some kinetic theory:

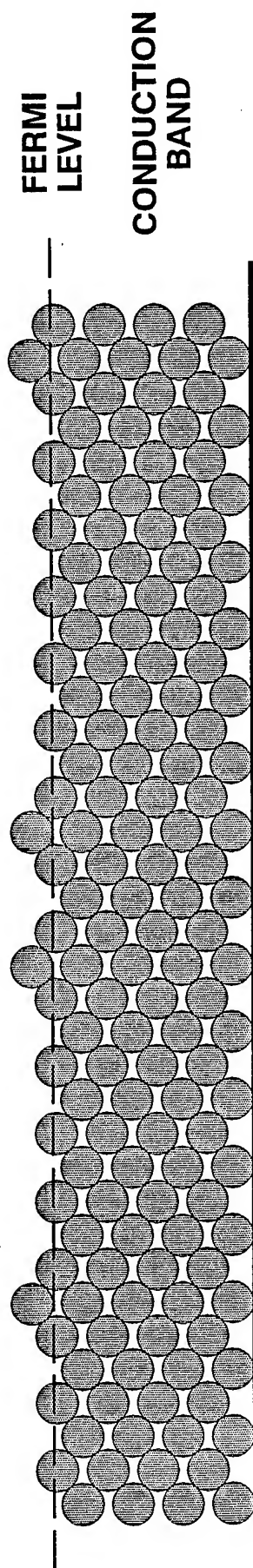
$$P_0 = n k_B T$$

$$\eta = n m v (mfp) / 3$$

$$(p_{n1}^2) / (p_{n2}^2) = 3\pi/8 \text{ (radius)} / \text{(mean-free-path)}$$



Noise in Metallic Conductors:

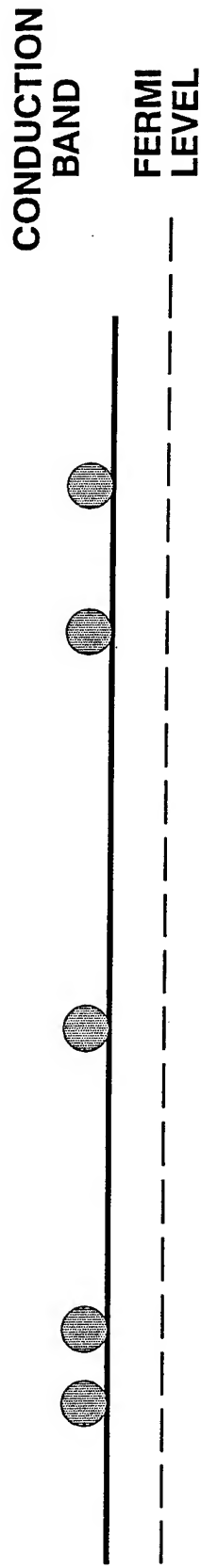


Carriers (electrons) are highly correlated

Noise is independent of flow volume (current)

$$i_n^2 = 4 k_B T / R$$

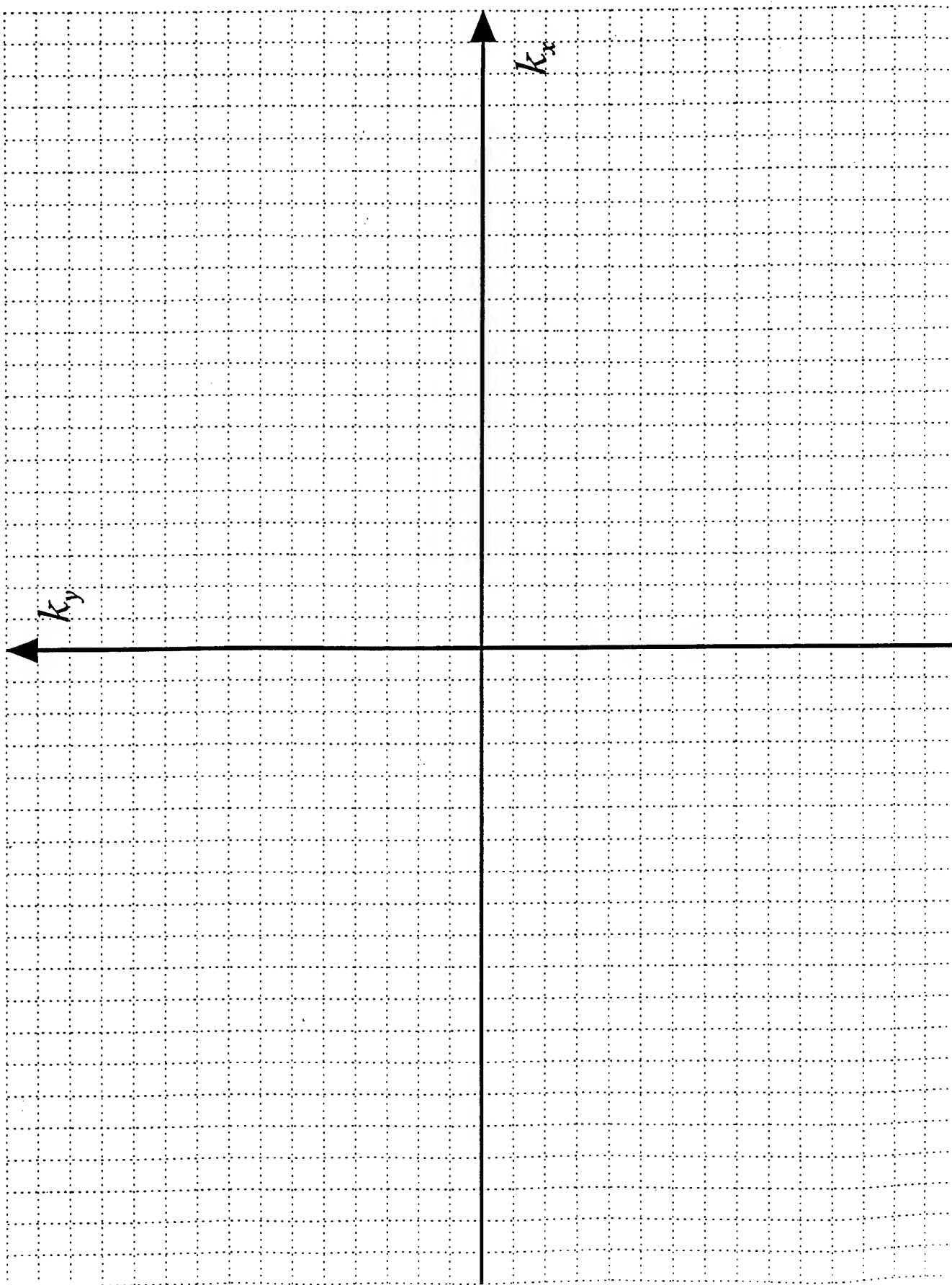
Noise in Semiconductors:



Carriers (holes or electrons) are independent

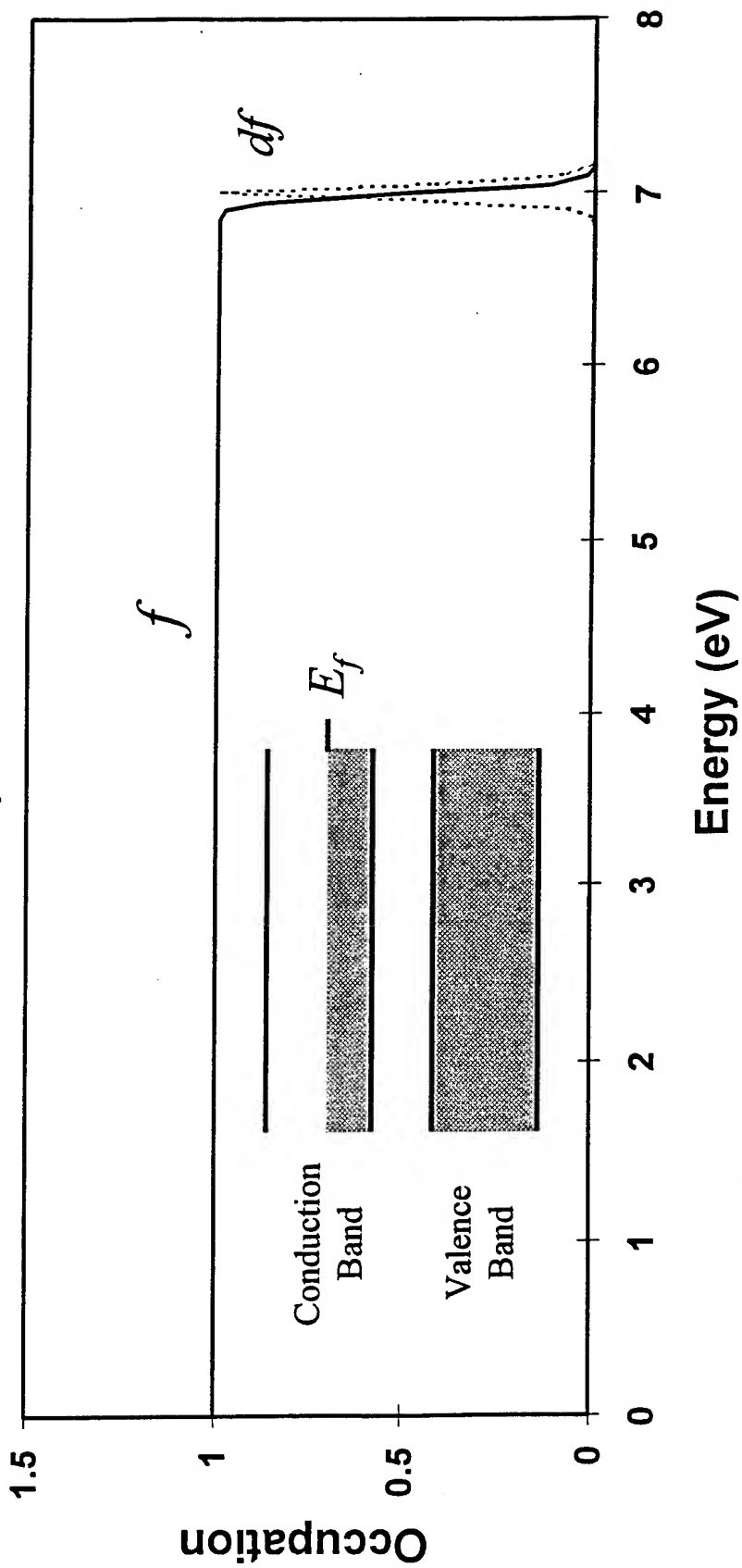
Noise is dependent on flow volume (current)

$$i_n^2 = 2qI_0$$



Occupation (f) and Fluctuation (df):

Normal Metal ($E_f = 7 \text{ eV}$; $k_B T = 0.025 \text{ eV}$)

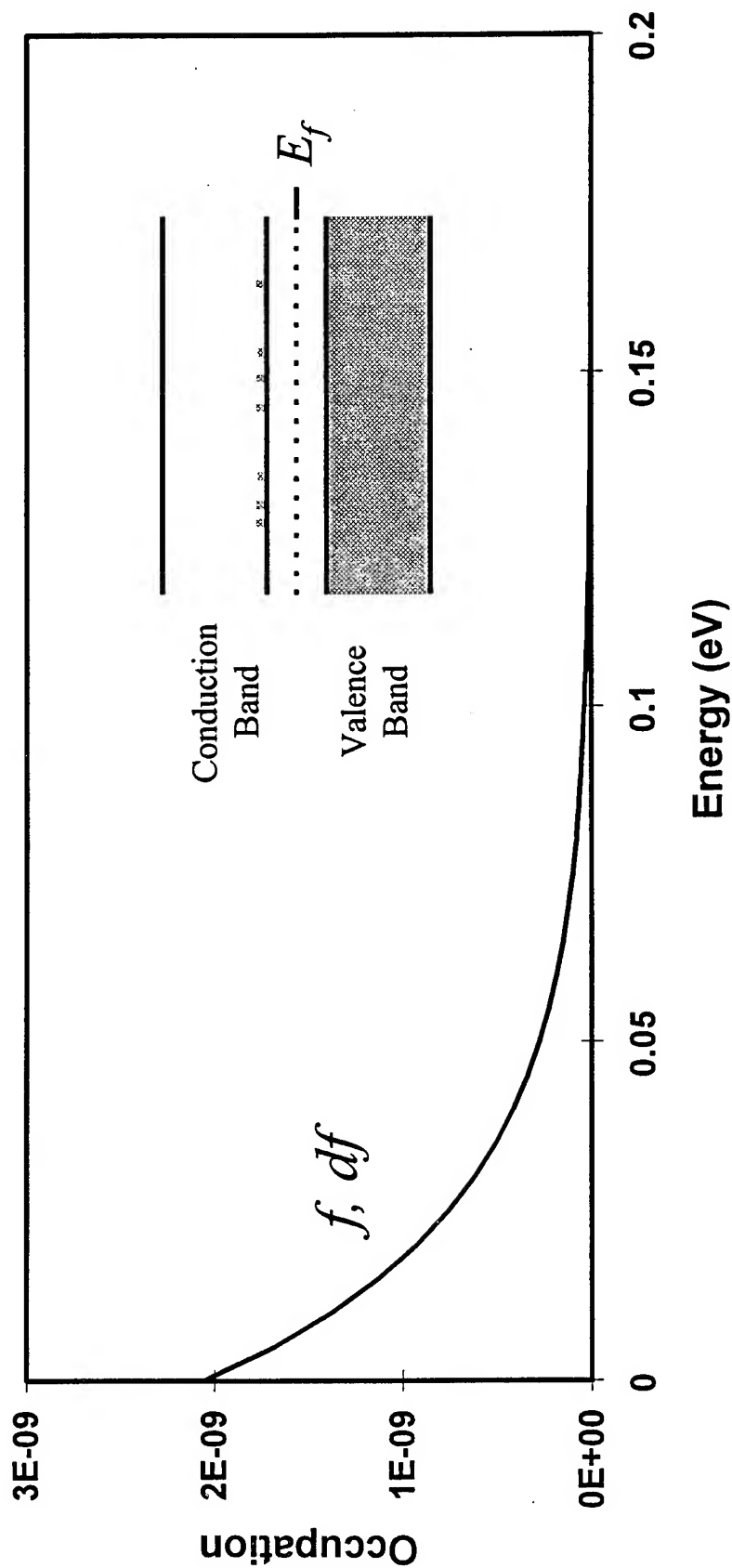


$$f = \frac{1}{1 + e^{\frac{E - E_f}{k_B T}}}$$

$$df = k_B T \frac{\partial f}{\partial E}$$

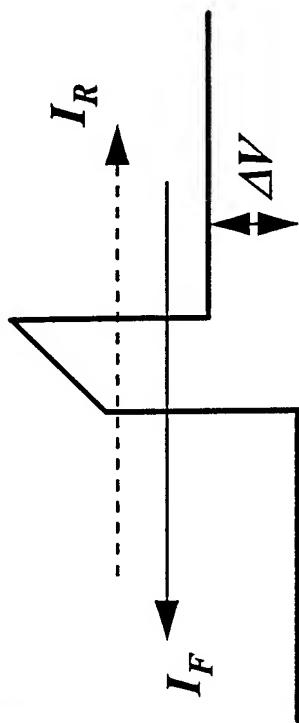
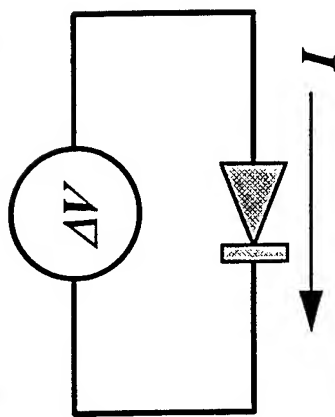
Occupation (f) and Fluctuation (df):

Semiconductor ($E_f = -0.5 \text{ eV}$; $k_B T = 0.025 \text{ eV}$)



$$f \approx e^{\frac{-(E-E_f)}{k_B T}}$$

Noise as a Function of Applied Voltage:



$$I_R = I_F e^{-\frac{q\Delta V}{k_B T}}$$

$$I = I_F - I_R = I_F \left[1 - e^{-\frac{q\Delta V}{k_B T}} \right] = \frac{\Delta V}{R}$$

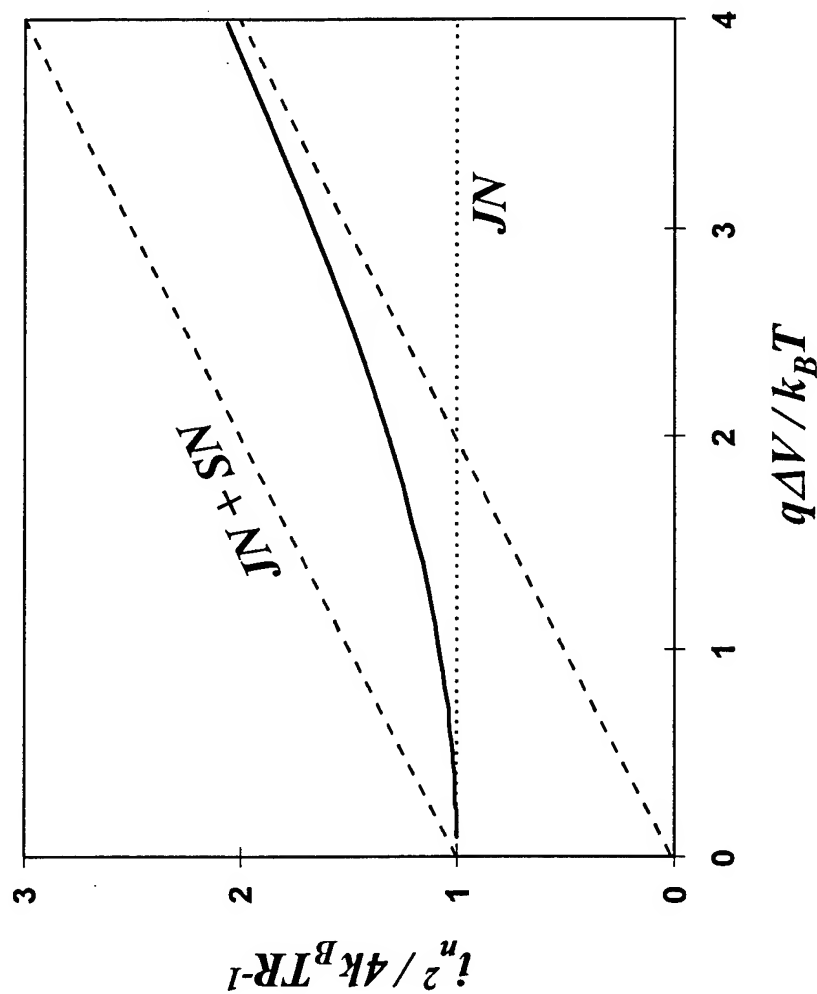
$$i_n^2 = 2qI_R df + 2qI_F df = 2qI_F \left[1 - e^{-\frac{q\Delta V}{k_B T}} \right] df$$

$$i_n^2 = 2 \frac{q\Delta V}{R} \left(\frac{1 + e^{-\frac{q\Delta V}{k_B T}}}{1 - e^{-\frac{q\Delta V}{k_B T}}} \right) df$$

Noise as a Function of Applied Voltage:

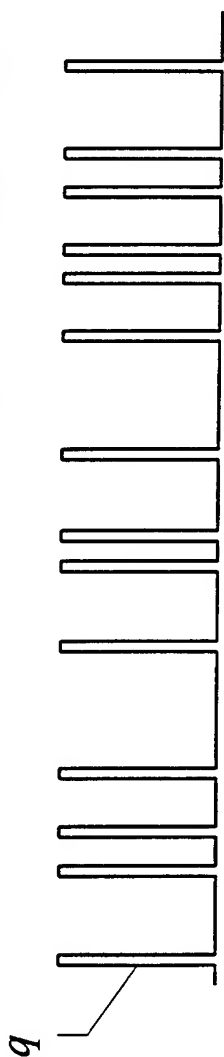
$$\text{For } q\Delta V < k_B T \quad i_n^2 \rightarrow 2 \frac{q\Delta V}{R} \left(\frac{2}{q\Delta V / k_B T} \right) df = 4 k_B T \frac{df}{R}$$

$$\text{For } q\Delta V \gg k_B T \quad i_n^2 \rightarrow 2 \frac{q\Delta V}{R} (1) df = 2 q I df$$



Photodetector Shot Noise:

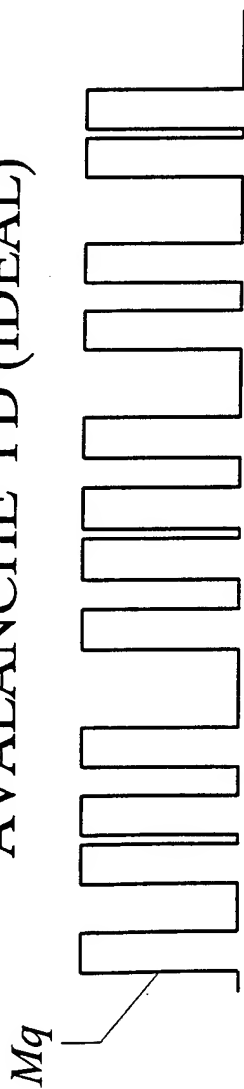
ORDINARY PHOTODETECTOR



$$\langle I \rangle = I_0$$

$$i_n^2 = 2 [q] I_0$$

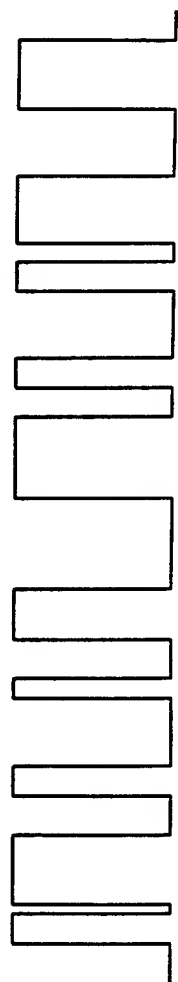
AVALANCHE PD (IDEAL)



$$\langle I \rangle = M I_0$$

$$i_n^2 = 2 [Mq] M I_0$$

AVALANCHE PD (REAL)



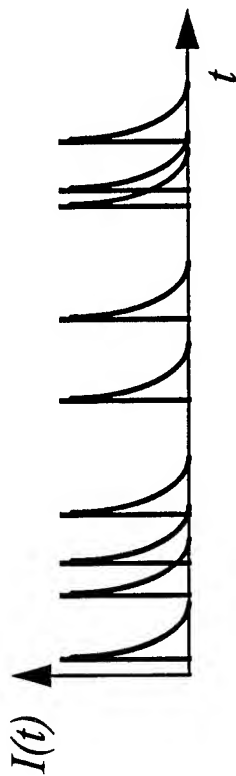
$$\langle I \rangle = M I_0$$

$$i_n^2 > 2 [Mq] M I_0$$

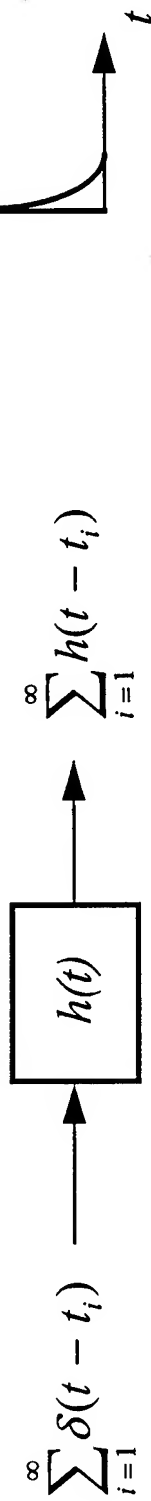
Shot Noise:

Suppose the current is a random sequence of non-impulsive responses:

$$I(t) = \sum_{i=1}^{\infty} h(t - t_i)$$



This current can be produced from a sequence of impulses:



If the power spectral density of the sequence of impulses is $s_n^2(\omega)$, then the power spectral density for the current is:

$$i_n^2(\omega) = s_n^2(\omega) |H(j\omega)|^2$$

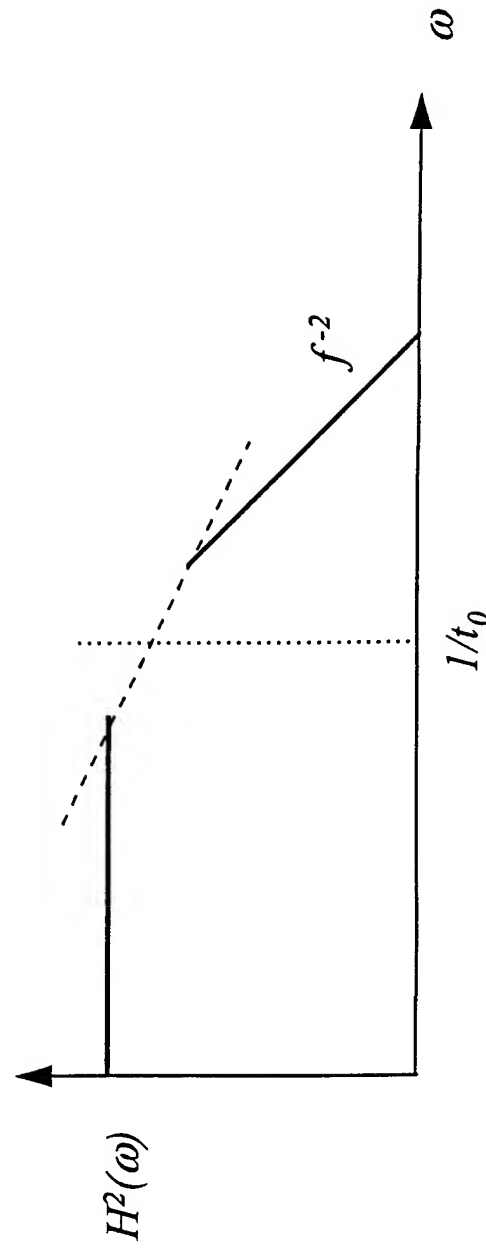
Shot Noise (Single Characteristic Process):

For example, if the current is produced by random events and each event has an exponential decay (with time constant, t_0):

$$I(t) = \sum_{i=1}^{\infty} h(t - t_i) \quad ; \quad h(t) = e^{-t/t_0} U(t)$$

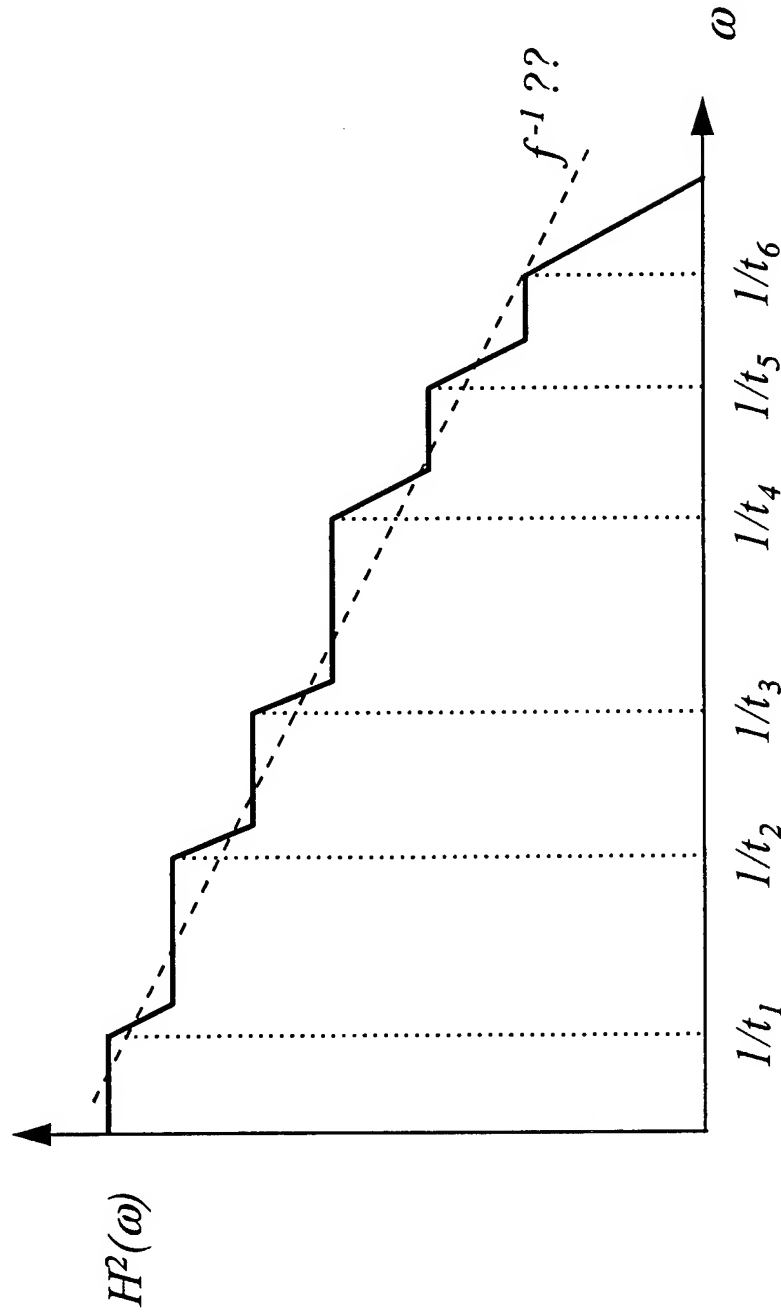
then the transfer function in the frequency domain, $H(j\omega)$, gives the spectral shape of the noise power:

$$|H(j\omega)|^2 = \frac{t_0^2}{1 + \omega^2 t_0^2}$$



Shot Noise (Multiple Characteristic Processes):

If there are many processes that can be triggered by the random impulses and each process is exponential with its own unique time constant, then the spectral distribution of the noise power can depart significantly from either white noise or a $1/f^2$ power distribution. This *may* be the way $1/f$ noise distributions are produced.



1/f Noise (a brief and inadequate introduction):

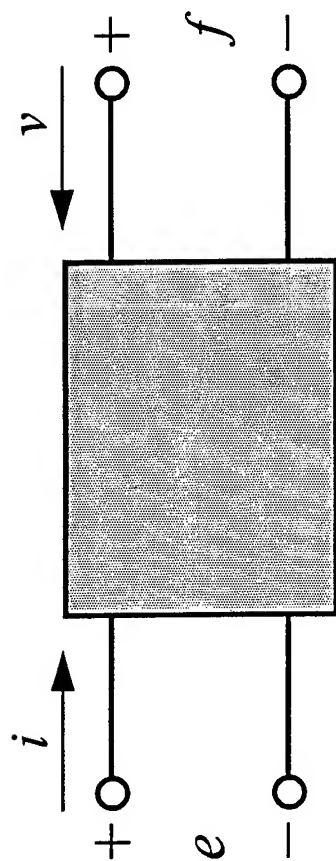
MANY physical processes produce fluctuations with a power spectrum that goes as $1/f$.

The noise power in excess of the equilibrium-thermal fluctuations is associated with power input to the system that drives the system away from equilibrium.

Observed 1/f noise can extend over many decades in frequency. If the multiple-exponential-process model is correct, then there must a correspondingly large spread in process time constants.

The integral over all frequency of a $1/f$ power distribution is infinite so *there must actually be a lower limit to the 1/f behavior.* This means that there are at least two free parameters: the total fluctuation power and the lower frequency limit.

Reciprocity:



$$e = A i + B v$$

$$f = C i + D v$$

If $B = C$ then the device is *reciprocal*:

$$\left(\frac{e}{v} \right)_{i=0} = \left(\frac{f}{i} \right)_{v=0}$$

Reciprocal transducers:

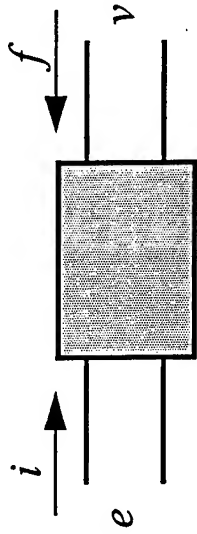
electrodynanic (moving-coil)
piezoelectric
capacitive (small-signal)

Nonreciprocal transducers:

piezoresistive
electron-tunneling

Reciprocity Calibration:

Given a transducer (not necessarily reciprocal):



What is its response?

Receiving response: $\alpha = \left(\frac{e}{v} \right)_{i=0}$

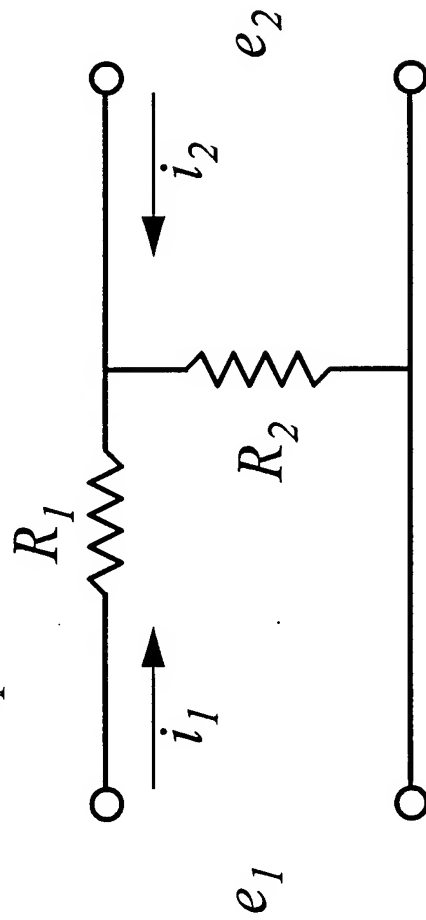
Transmitting response: $\beta = \left(\frac{f}{i} \right)_{v=0}$

It is often inconvenient and inaccurate to directly measure forces and velocities.

Reciprocity:

If a device is reciprocal, then the ratio of the output *potential* to the input *flow* is the same regardless of which port is taken to be the input.

For example:



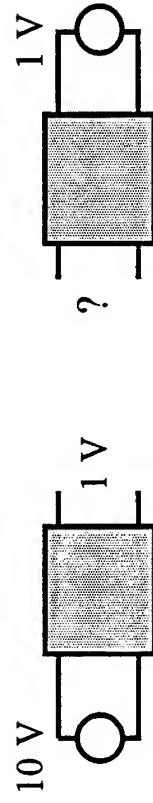
$$e_1 = (R_1 + R_2) i_1 + R_2 i_2$$

$$e_2 = R_2 i_1 + R_2 i_2$$

$$\left. \frac{e_2}{i_1} \right|_{i_2=0} = \left. \frac{e_1}{i_2} \right|_{i_1=0} = R_2 \quad (\text{A transfer impedance in general.})$$

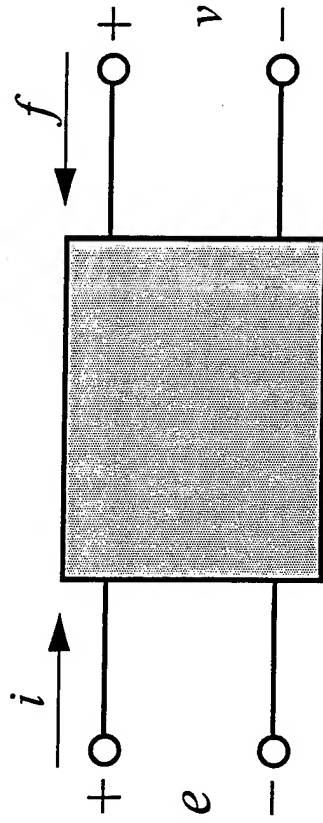
Reciprocity does *NOT* depend on the device being lossless.

Reciprocity does *NOT* mean that voltage ratios are identical.



Reciprocity:

If $B = -C$ then interchange the roles of the variables on one side of the device.



$$\begin{aligned} e &= A i + B f \\ v &= C i + D f \end{aligned}$$

$$\begin{aligned} A &= (AD - CB)/D \\ C &= -C/D \end{aligned}$$

$$\begin{aligned} B &= B/D \\ D &= 1/D \end{aligned}$$

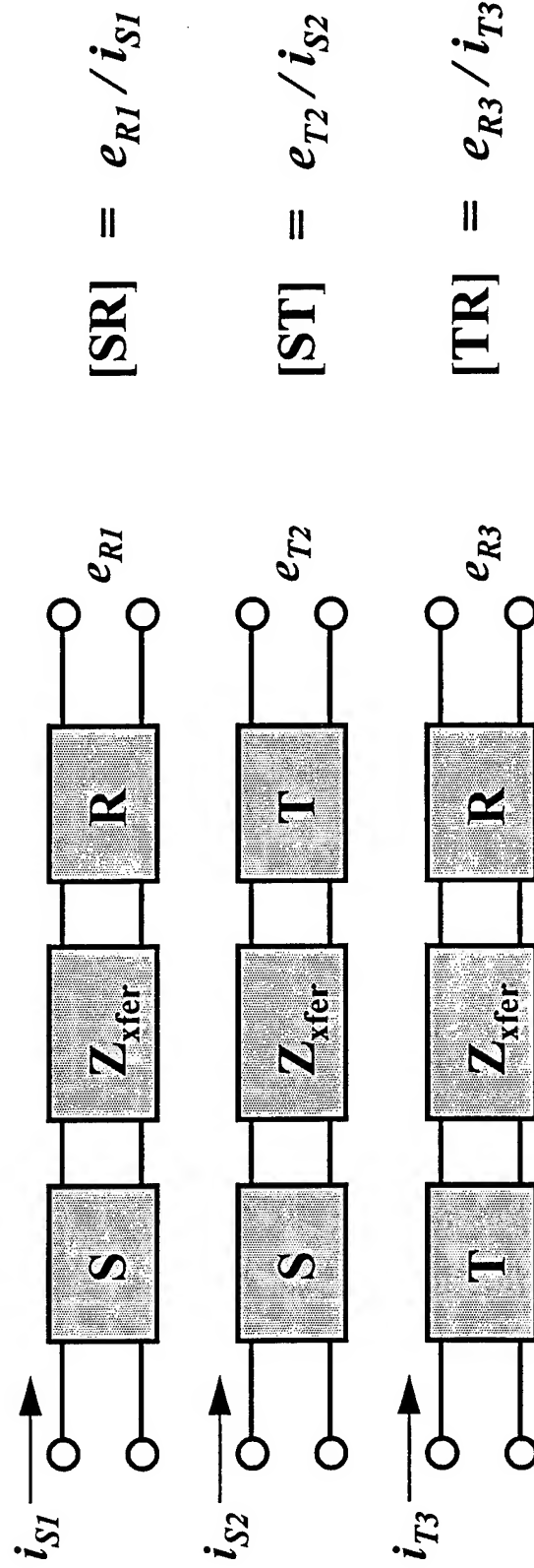
$$\text{Therefore } B = C$$

If B does not equal either C or $-C$, then the device is nonreciprocal.

Reciprocity Calibration:

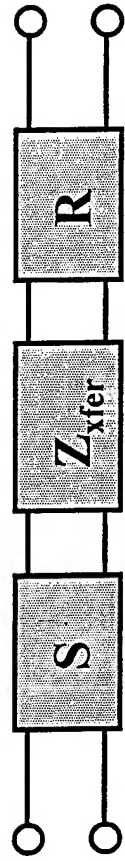
Use three transducers: a source (S), a receiver (R), and a reciprocal transducer (T). Altogether there are four unknowns: α_R , β_T , and β_S .

Connect the transducers *through a known transfer impedance* and make the following measurements:



This gives three equations for the four unknowns. Reciprocity provides the fourth equation and allows solving for all four responses.

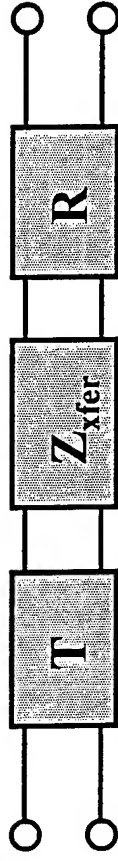
Reciprocity Calibration:



$$[SR] = \frac{1}{Z_{xfer}} \alpha_R \beta_S$$



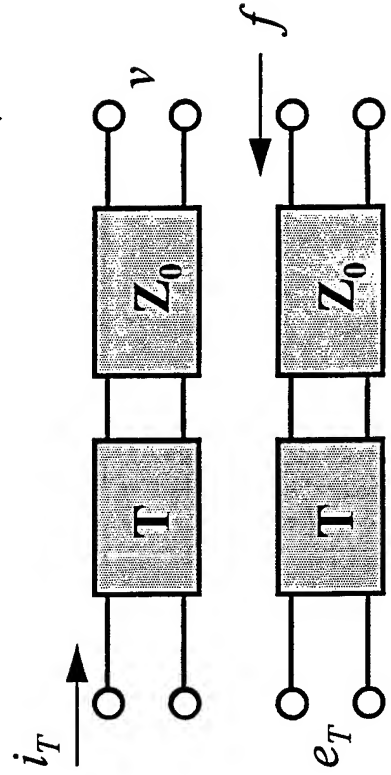
$$[ST] = \frac{1}{Z_{xfer}} \alpha_T \beta_S$$



$$[TR] = \frac{1}{Z_{xfer}} \alpha_R \beta_T$$

Reciprocity gives the relationship between α_T and β_T :

$$\frac{[SR][TR]}{[ST]} = \frac{1}{Z} \alpha_R^2 \frac{\beta_T}{\alpha_T}$$



$$\frac{v}{i_T} = \beta_T \frac{1}{Z_0} = \frac{e_T}{f} = \alpha_T \frac{1}{Z_0}$$

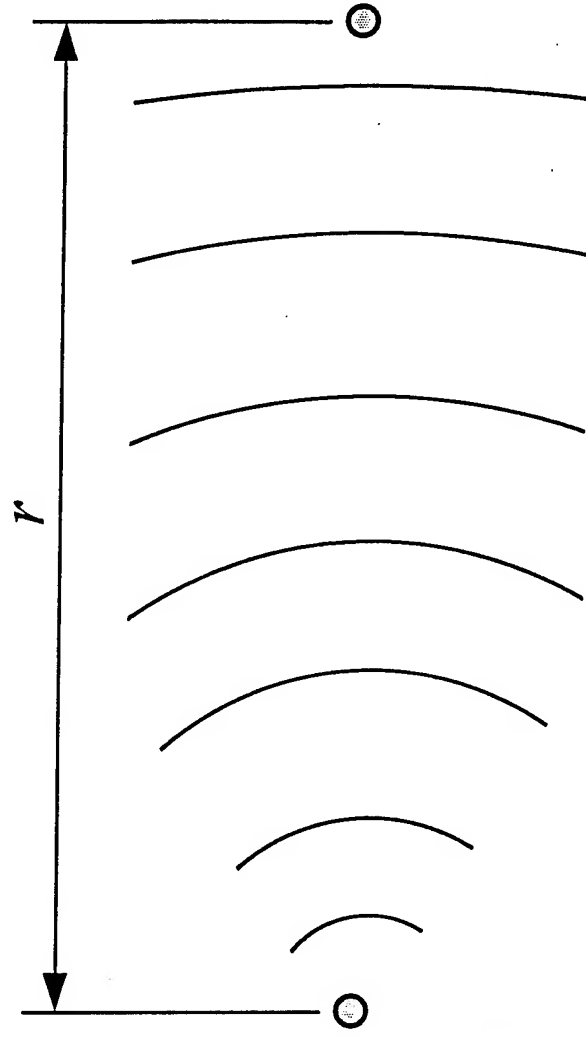
$$\alpha_T = \beta_T$$

Reciprocity Calibration (variations):

- a) Measure currents by measuring voltage across a resistor. Resistance and voltage ratios are easier to measure accurately than absolute voltages.
- b) Set $i_{S1} = i_{S2}$ and adjust i_{T3} so that $e_{R3} = e_{R1}$. This produces the same field at the receiver location for each measurement and also permits the use of source and receiver that are not linear.
- c) If two reciprocal transducers are available, measure the reciprocity explicitly to check the transducers and apparatus.
- d) If two "identical" reciprocal transducers are used, then only two measurements are required.
- e) In some circumstances, only one transducer is required: (1) excite a lightly damped system and measure response during decay, (2) transmit a pulse and measure a reflection.

Reciprocity Calibration (examples):

Free-Field



$$\alpha = \left(\frac{e}{p} \right)_{i=0}$$

$$Z_{xfer} = \frac{p_2}{U_1} = \frac{p_2}{4\pi a^2 u_1}$$

$$u_1 = \left(1 + \frac{i}{ka} \right) \frac{p_1}{\rho c} \approx \frac{i p_1}{ka \rho c} \quad (\text{for } ka \ll 1)$$

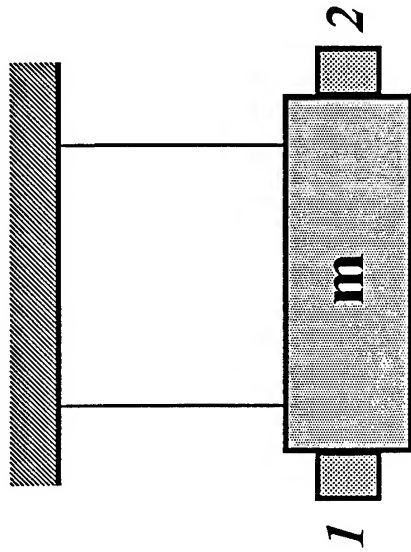
$$Z_{xfer} = \frac{\rho f}{2r}$$

Reciprocity Calibration (examples):

Pendulum

$$\alpha = \left(\frac{e}{u} \right)_{i=0}$$

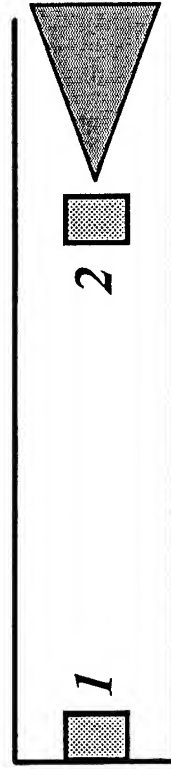
$$\boxed{Z_{xfer}} = \frac{F_2}{u_1} = \boxed{-i\omega m}$$



Traveling-Wave Tube

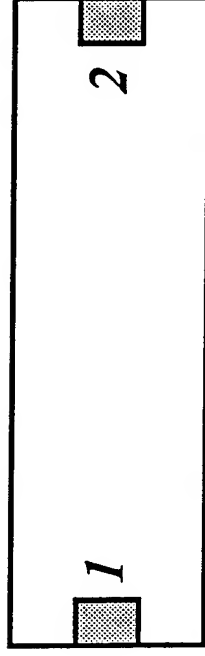
$$\alpha = \left(\frac{e}{p} \right)_{i=0}$$

$$\boxed{Z_{xfer}} = \frac{p_2}{U_1} = \boxed{\frac{\rho c}{A}}$$



Reciprocity Calibration (examples):

Rigid-Walled Resonator



Energy stored in tube, E:

$$E = PE + KE = \int_0^L \left\{ \frac{1}{2} \rho v^2 + \frac{1}{2} \frac{p^2}{\rho c^2} \right\} A dx = \frac{p_0^2 A L}{2 \rho c^2}$$

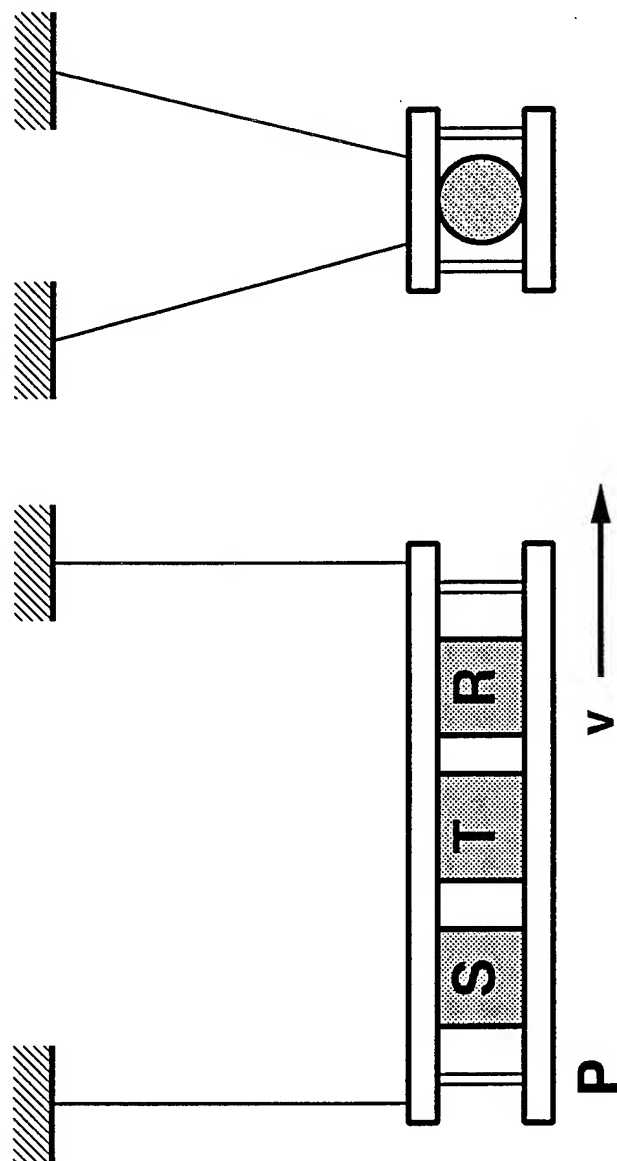
Energy lost *per cycle*, ΔE = Energy supplied by driver per cycle:

$$\Delta E = \frac{\text{power}}{\text{frequency}} = \frac{F_1 v_1}{f_n} = \frac{p_1 A v_1}{f_n} = \frac{p_0 U_1}{f_n}$$

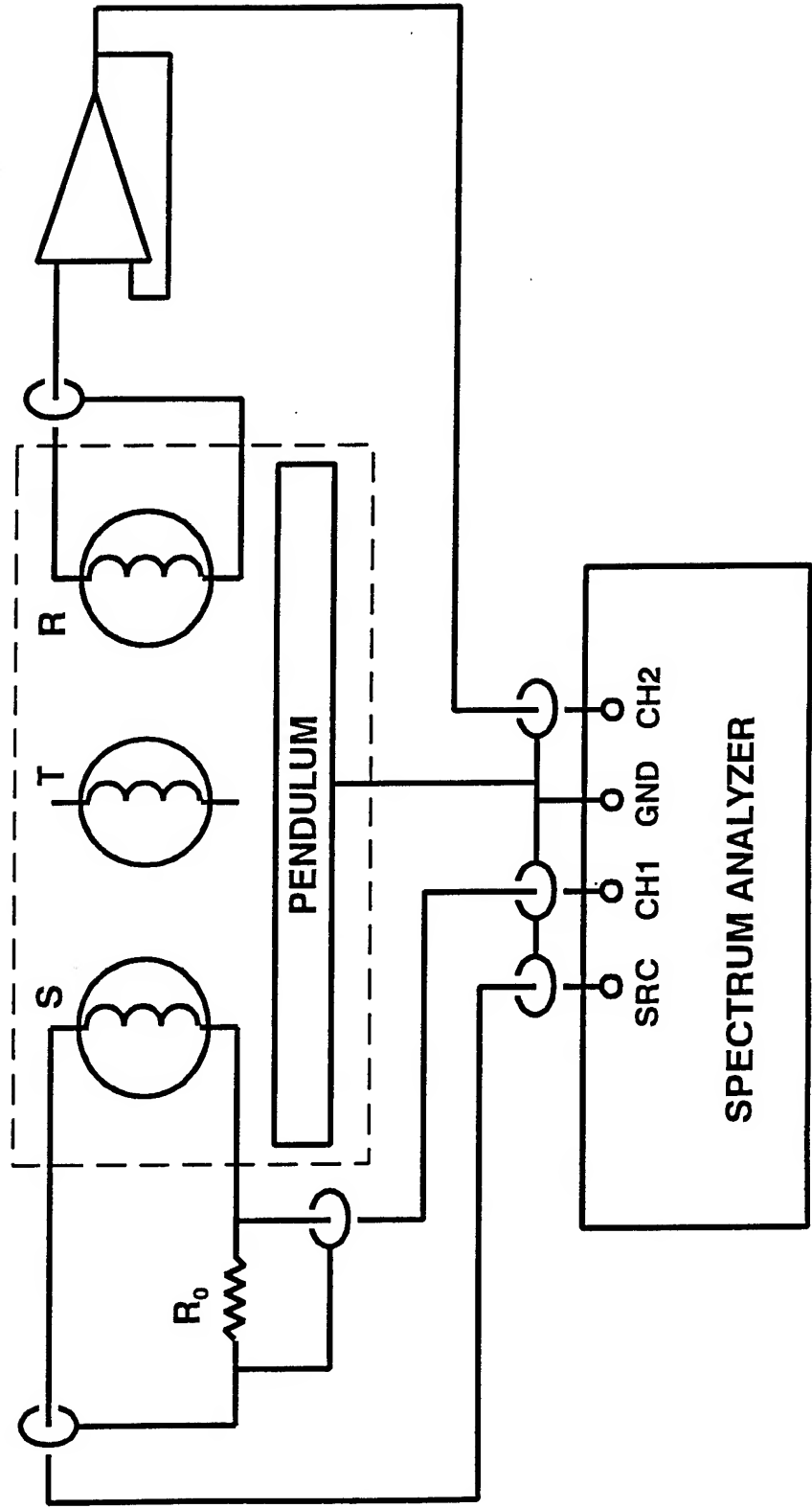
$$f_n = \frac{nc}{2L} ; Q_n = \frac{2\pi E}{\Delta E} = \frac{\pi n A p_0}{2 \rho c U_1}$$

$$Z_{xfer} = \frac{p_0}{U_1} = \frac{2 \rho c Q_n}{\pi n A}$$

Reciprocity Calibration (equipment):



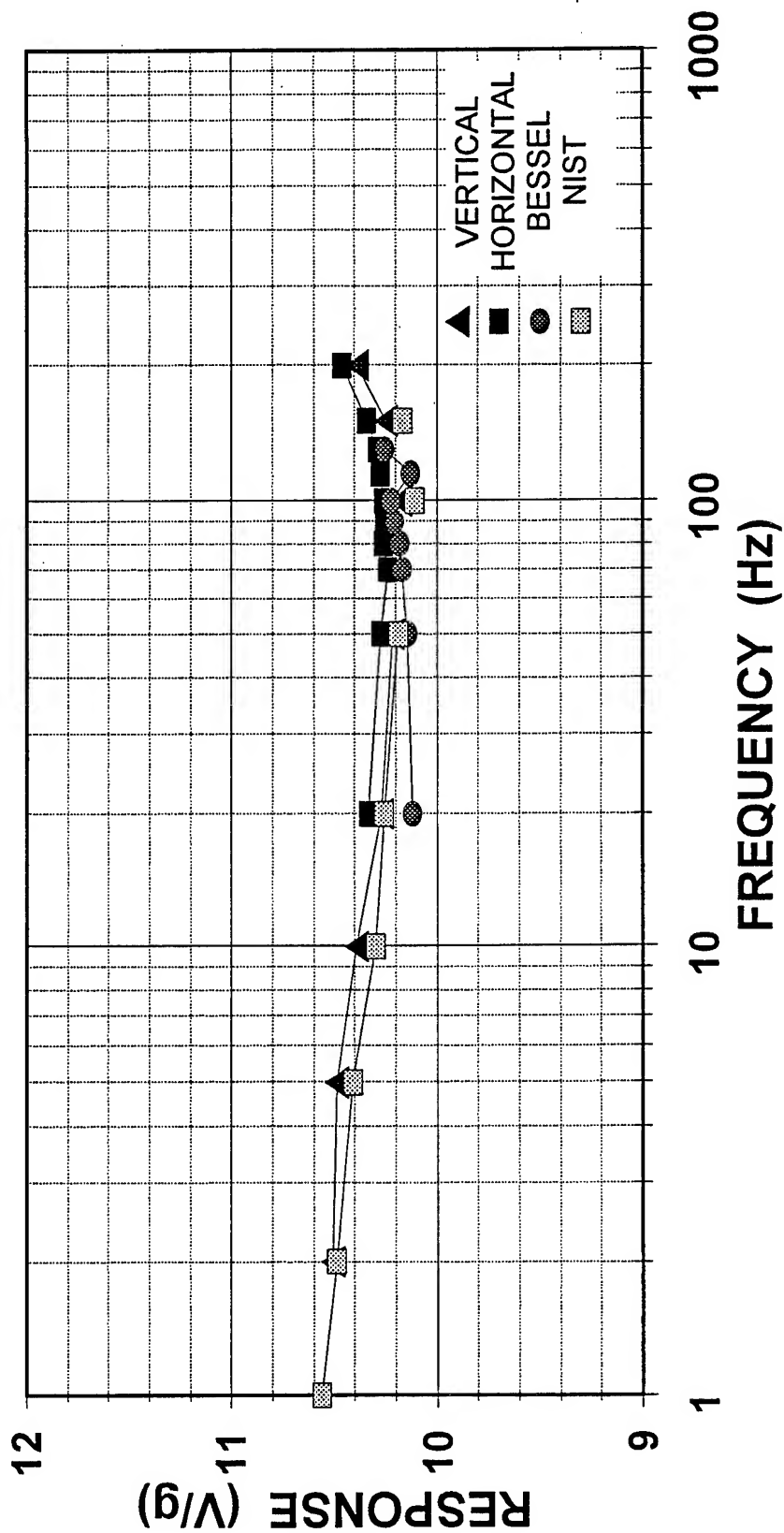
Reciprocity Calibration (equipment):



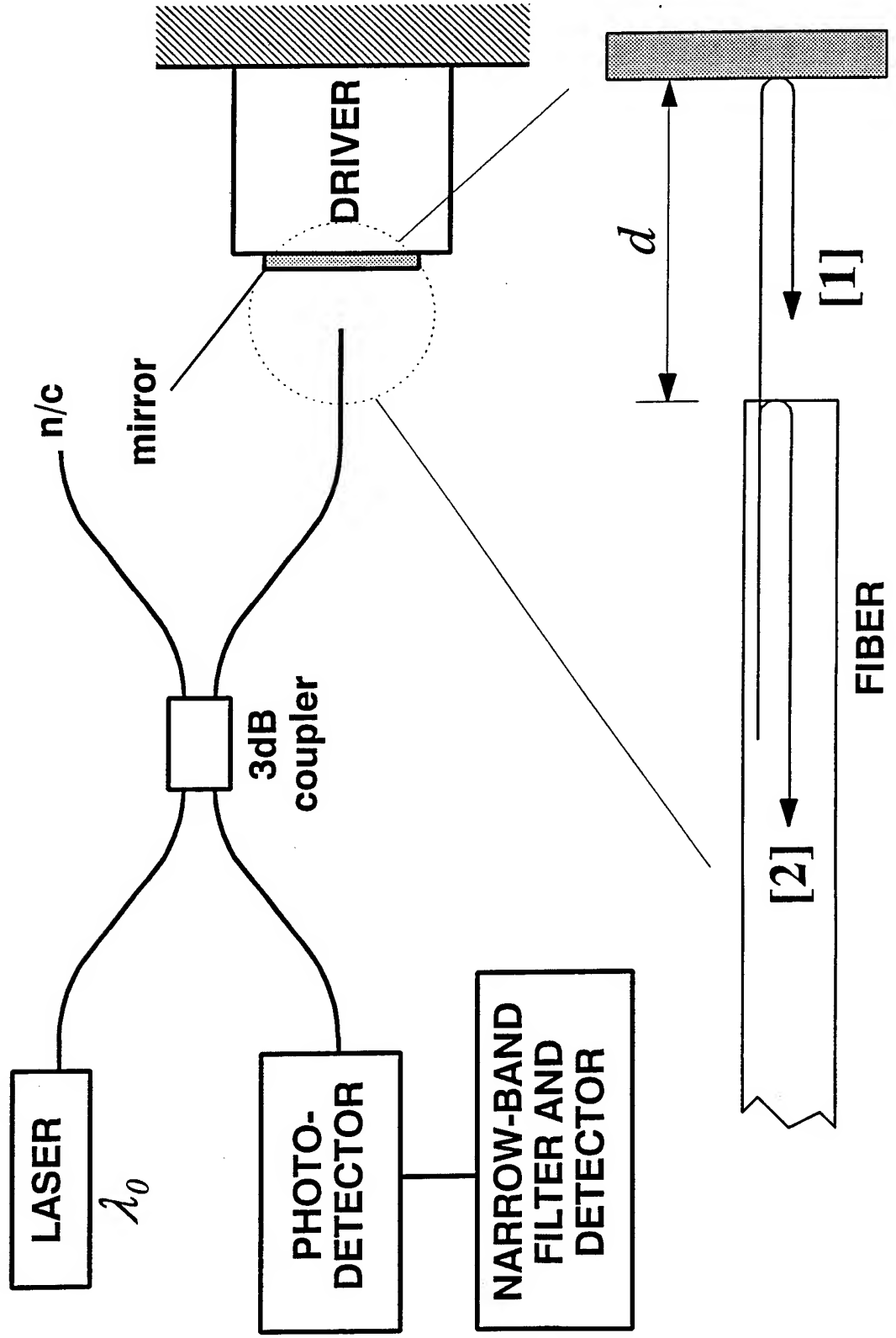
NAWC Aircraft Division
Code 4554 MS07
Warminster, PA 18974

Free-Mass Reciprocity Calibration

PCB 393A31 SN3001



Bessel-Null Calibration:



Bessel-Null Calibration:

Component that reflects from moving mirror:

$$[1] = A \cos(\omega_0 t + 2k_0 d)$$

Component that reflects from cleaved end of fiber:

$$[2] = B \cos(\omega_0 t)$$

Photodetector output (square-law detector):

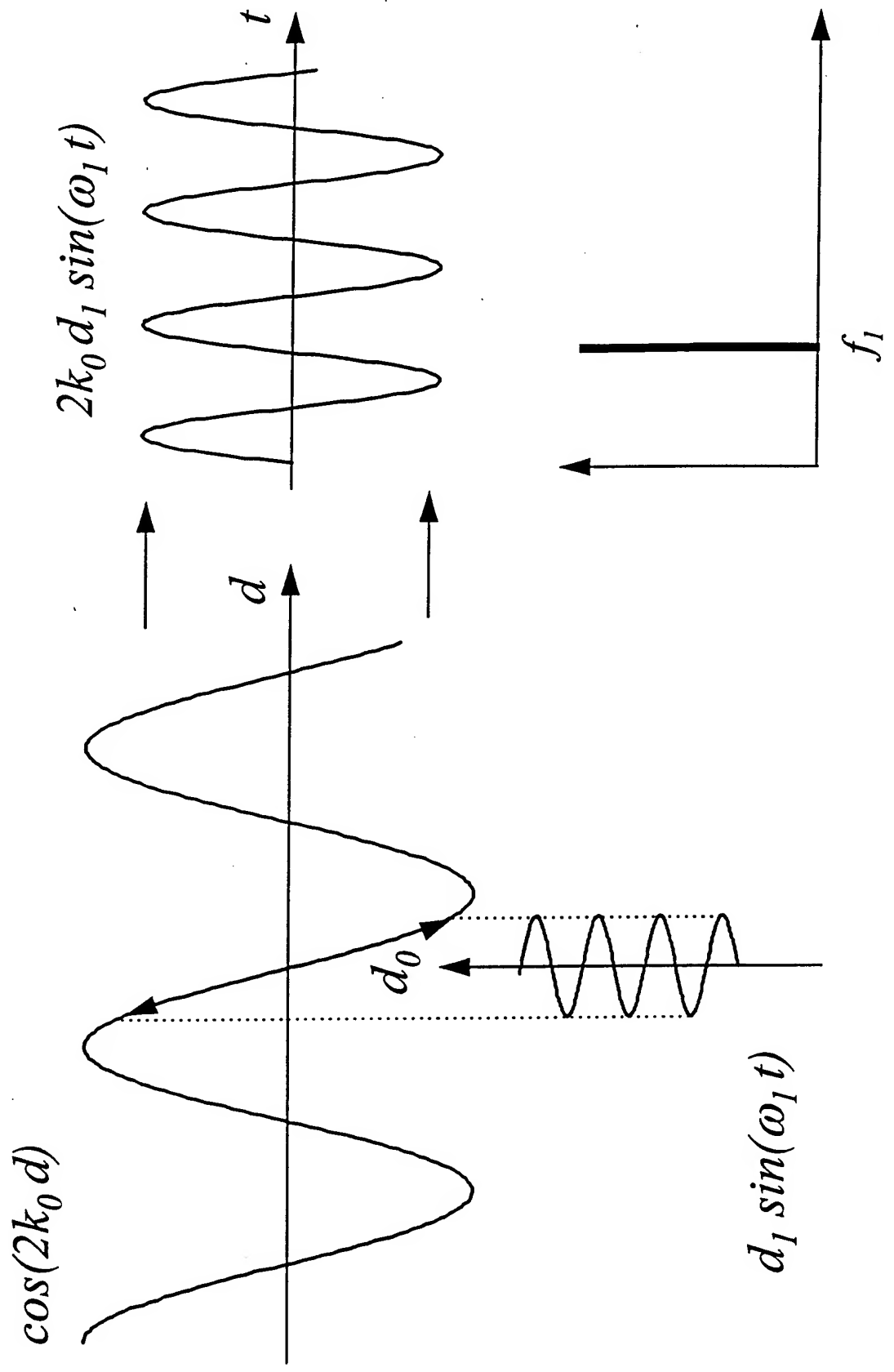
$$PD = \overline{([1] + [2])^2}$$

$$PD \rightarrow \cos(2k_0 d)$$

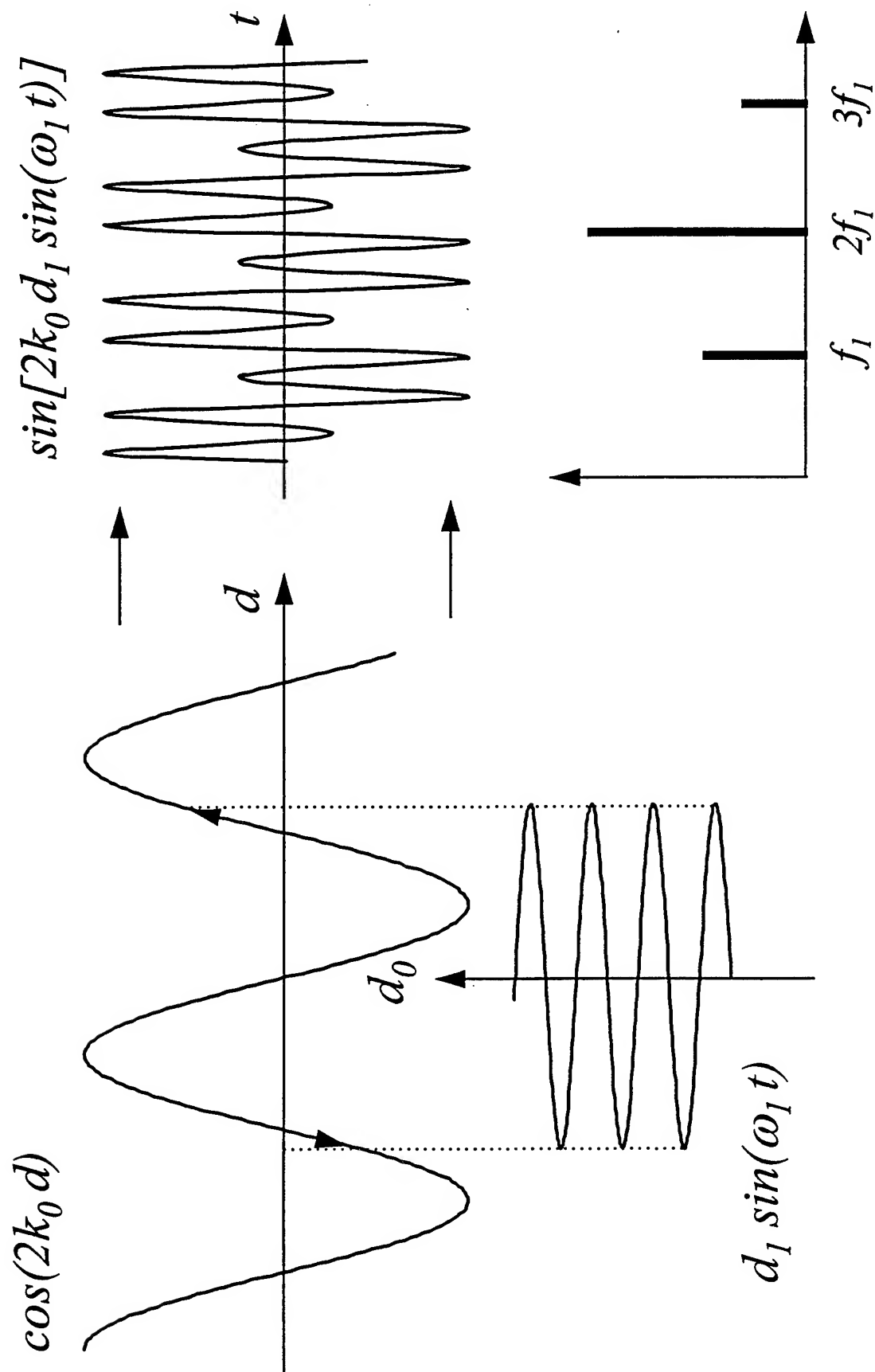
Sinusoidal motion of mirror:

$$d = d_0 + d_1 \sin(\omega_1 t)$$

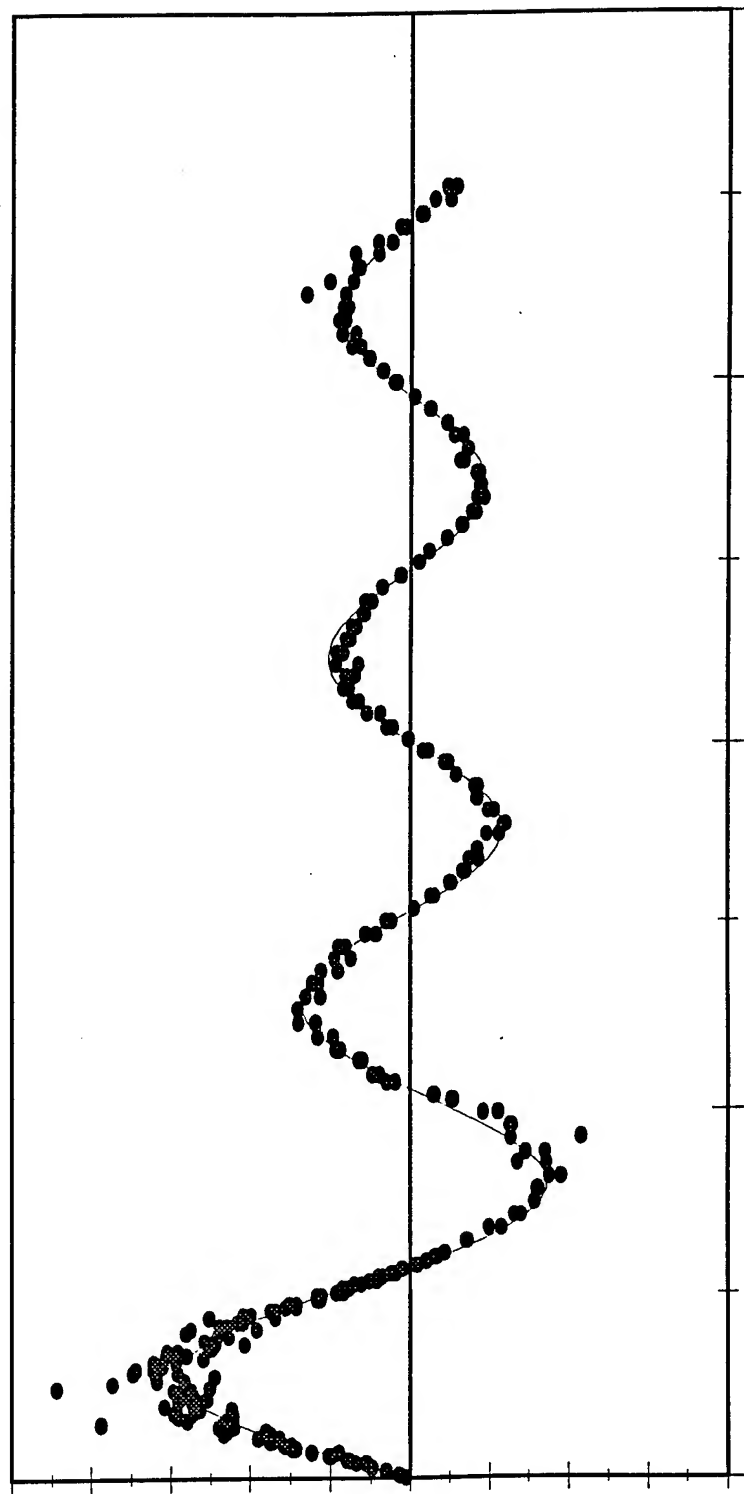
Interferometer Transfer Function (small signal):



Interferometer Transfer Function (large signal):



Large-Signal Photodetector Output:



Bessel-Null Calibration:

For “large” signals then, the photodetector output *at the drive frequency* is:

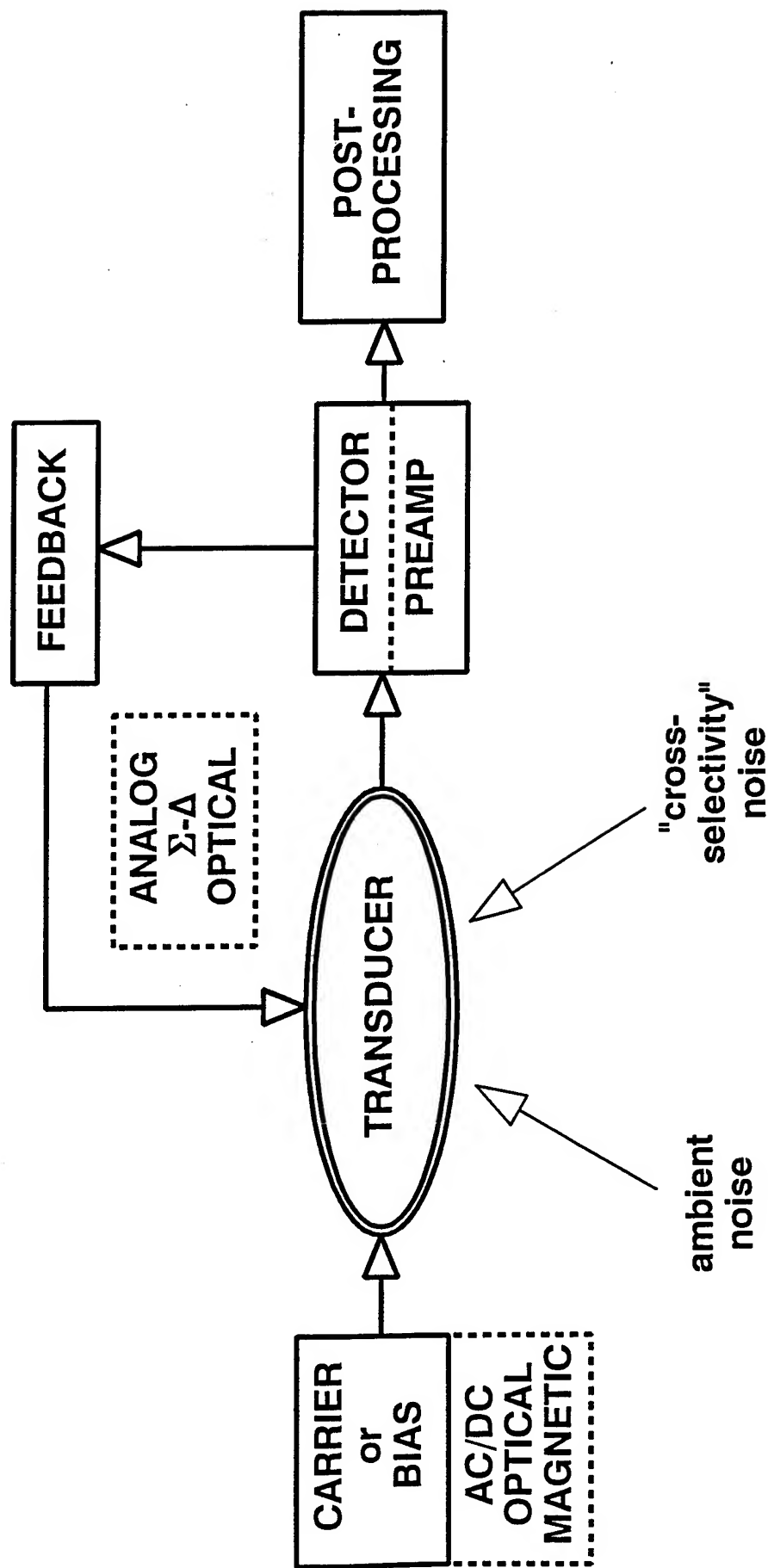
$$PD|_{\omega_1} \rightarrow \sin(2k_0 d_0) J_1(2k_0 d_1)$$

Adjust the drive level to null the output of the photodetector at the drive frequency. These nulls correspond to the zeros, z_i , of the Bessel function, J_1 . Consequently, the displacement amplitude, d_1 , is only a function of the laser wavelength, λ_0 :

$$d_1 = \frac{z_i}{2k_0} = \frac{\lambda_0 z_i}{4\pi}$$

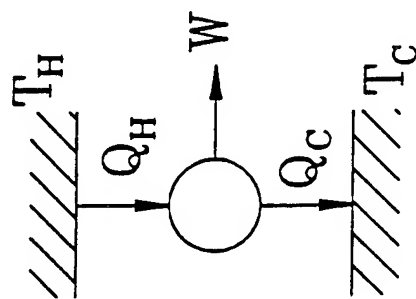
(where $z_i = 3.83171, 7.01559, 10.17347, 13.32369, \dots$)

Components of a Sensor System:



REVIEW: HEAT ENGINES AND REFRIGERATORS

Heat engine:

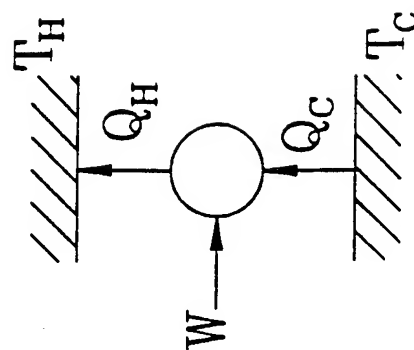


$$\text{1st law: } Q_H = W + Q_C$$

$$\text{2nd law: } \frac{Q_C}{T_C} \geq \frac{Q_H}{T_H}$$

$$\text{so efficiency} = \frac{W}{Q_H} \leq \frac{T_H - T_C}{T_H}$$

Refrigerator:



$$\text{1st law: } Q_H = W + Q_C$$

$$\text{2nd law: } \frac{Q_H}{T_H} \geq \frac{Q_C}{T_C}$$

$$\text{so COP} = \frac{Q_C}{W} \leq \frac{T_C}{T_H - T_C}$$

REVIEW: SOUND WAVES

Notation: pressure = $p_m + \text{Re}[p_1(x)e^{i\omega t}]$ etc

Momentum: $i\omega\rho_m u_1 = -\frac{dp_1}{dx}$

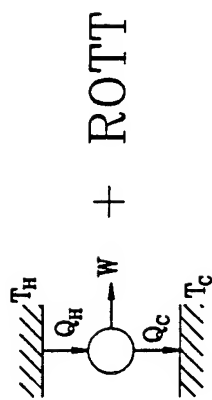
Continuity: $i\omega\rho_1 + \rho_m \frac{du_1}{dx} = 0$

Equation of state: $\frac{p_1}{\rho_1} = \left(\frac{\partial p}{\partial \rho}\right)_s = a^2$

Combine to get $p_1 + \frac{a^2}{\omega^2} \frac{d^2 p_1}{dx^2} = 0$

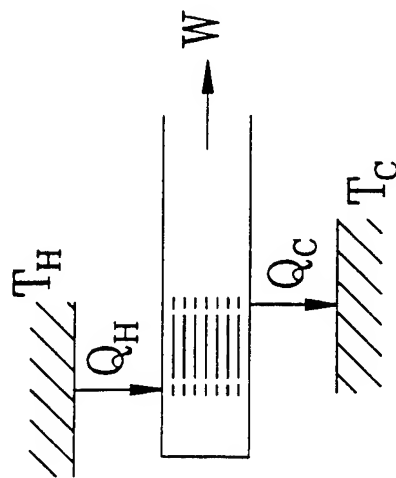
Rott's more elaborate result:

$$[1 + (\gamma - 1)f_\kappa]p_1 + \frac{a^2}{\omega^2} \rho_m \frac{d}{dx} \left(\frac{1 - f_\nu}{\rho_m} \frac{dp_1}{dx} \right) - \frac{a^2}{\omega^2} \frac{f_\kappa - f_\nu}{1 - \sigma} \frac{1}{T_m} \frac{dT_m}{dx} \frac{dp_1}{dx} = 0$$

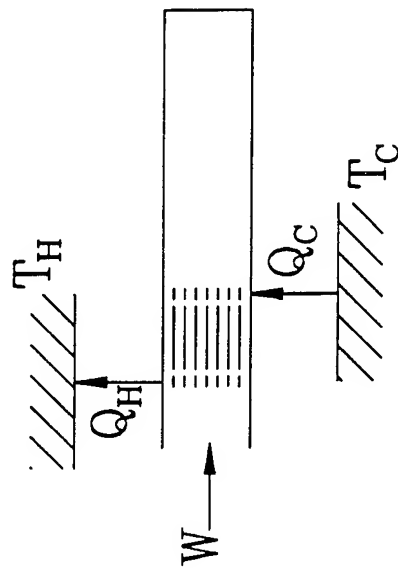


= THERMOACOUSTIC ENGINES & REFRIGERATORS

Engine:



Refrigerator:



Advantages: reliable, cheap
Shortcomings: big, inefficient

LENGTH SCALES

Along propagation direction x :

Wavelength $\lambda = a/f$

Gas displacement amplitude $|x_1| = |u_1|/\omega$

Perpendicular to x :

Thermal penetration depth $\delta_\kappa = \sqrt{2K/\omega\rho c_p}$

Viscous penetration depth $\delta_\nu = \sqrt{2\mu/\omega\rho}$

Relative sizes:

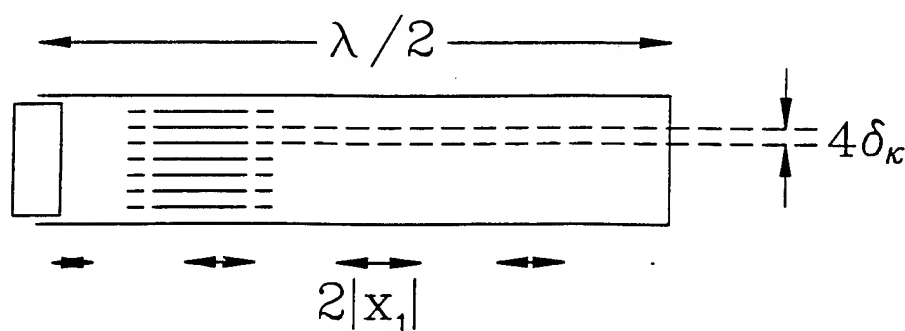
$$\frac{\delta_\nu}{\delta_\kappa} = \sqrt{\frac{\mu c_p}{K}} \lesssim 1$$

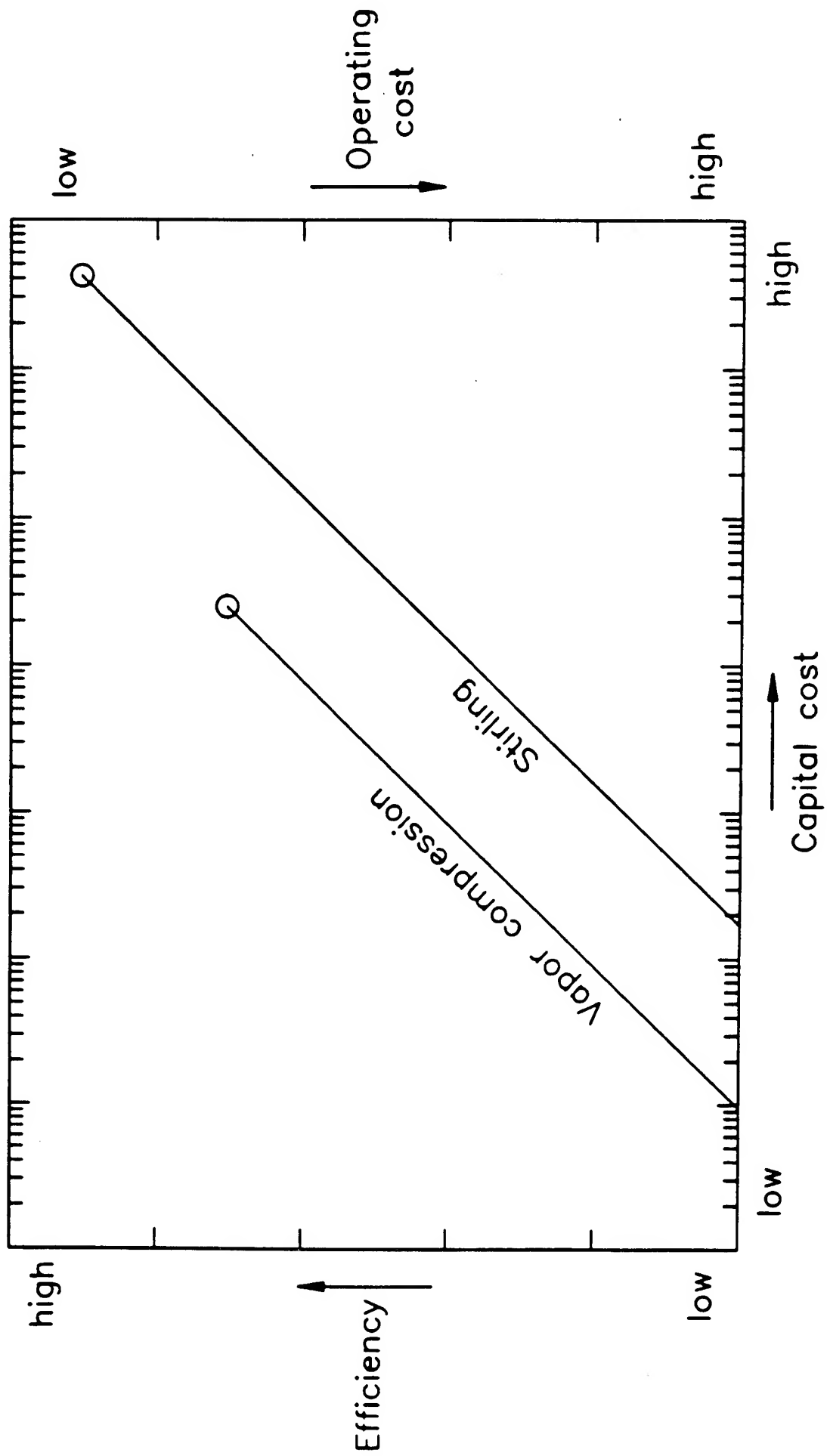
"Audio" acoustics:

$$|x_1| \ll \delta_\kappa \ll \lambda$$

Thermoacoustic engines and refrigerators:

$$\delta_\kappa \ll |x_1| \ll \lambda$$





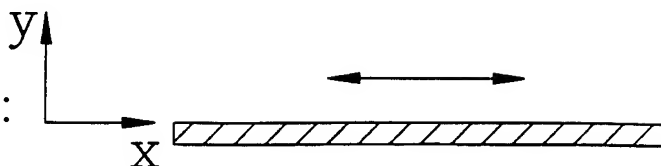
Outline of what will follow:

- Microscopic behavior
- Power and efficiency
- A detailed example
- Beyond the acoustic approximation

For a copy of computer animations and other software, <http://rott.esa.lanl.gov/>

VISCOSITY IN OSCILLATORY FLOW

Suppose acoustic
oscillation along a wall:



Momentum equation:

$$\rho \left(\frac{\partial \bar{\mathbf{v}}}{\partial t} + (\bar{\mathbf{v}} \cdot \bar{\nabla}) \bar{\mathbf{v}} \right) = -\bar{\nabla} p + \mu \nabla^2 \bar{\mathbf{v}} + \left(\mu + \frac{\xi}{3} \right) \bar{\nabla} (\bar{\nabla} \cdot \bar{\mathbf{v}}) + \bar{\nabla} \mu \bar{\nabla} \bar{\mathbf{v}} \text{ terms}$$

Boundary condition $\bar{\mathbf{v}}=0$ on surface.

Linearize by using

$$p = p_m + p_1(x) e^{i\omega t}$$

$$\rho = \rho_m(x) + \rho_1(x, y) e^{i\omega t}$$

$$\bar{\mathbf{v}} = \left(\hat{x} u_1(x, y) + \hat{y} v_1(x, y) \right) e^{i\omega t}$$

to get

$$i\omega \rho_m u_1 = -\frac{dp_1}{dx} + \mu \frac{\partial^2 u_1}{\partial y^2}$$

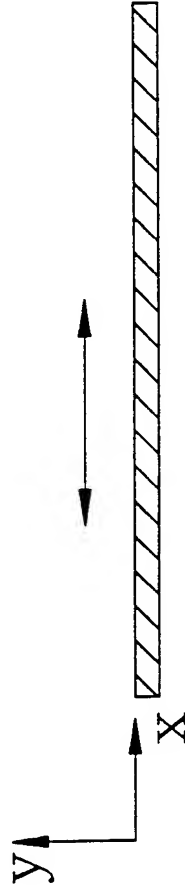
The solution is

$$u_1 = -\frac{1}{i\omega \rho_m} \frac{dp_1}{dx} \left(1 - e^{-(1+i)y/\delta_\nu} \right)$$

The characteristic dimension is

the viscous penetration depth $\delta_\nu = \sqrt{2\mu/\omega\rho}$

DISSIPATION BY VISCOSITY IN OSCILLATORY FLOW



Recall

$$u_1 = -\frac{1}{i\omega\rho_m} \frac{dp_1}{dx} \left(1 - e^{-(1+i)y/\delta_v} \right)$$

Viscosity and gradients in velocity
dissipate acoustic power.

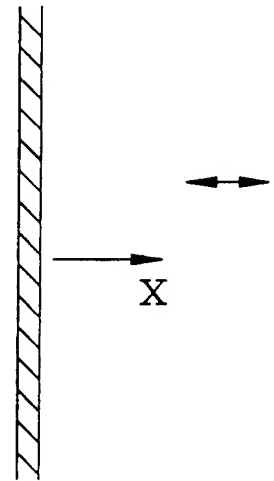
In this geometry, the instantaneous dissipation is

$$\mu \left(\frac{\partial \text{Re}[u_1 e^{i\omega t}]}{\partial y} \right)^2 dx dy dz \text{ in volume } dx dy dz.$$

The time average of this is largest on the surface,
and falls off as e^{-2y/δ_v}

TEMPERATURE DUE TO OSCILLATORY PRESSURE

Suppose acoustic
oscillation near a wall.



Equation of heat transfer:

$$\rho c_p \left(\frac{\partial T}{\partial t} + (\bar{\mathbf{v}} \cdot \bar{\nabla}) T \right) - \left(\frac{\partial p}{\partial t} + (\bar{\mathbf{v}} \cdot \bar{\nabla}) p \right) = -\bar{\nabla} \cdot (K \bar{\nabla} T) + \bar{\mathbf{v}}^2 \text{etc}$$

with boundary condition $T = T_m$ on surface.

Linearize by using

$$\begin{aligned} p &= p_m + \text{Re}[p_1 e^{i\omega t}] \\ T &= T_m + \text{Re}[T_1(x) e^{i\omega t}] \\ \rho &= \rho_m + \text{Re}[\rho_1(x) e^{i\omega t}] \\ \bar{\mathbf{v}} &= \text{Re}[\hat{x} u_1(x) e^{i\omega t}] \end{aligned}$$

and get

$$i\omega \rho_m c_p T_1 = i\omega p_1 + K \frac{\partial^2 T_1}{\partial x^2}$$

The solution is

$$T_1 = \frac{1}{\rho_m c_p} p_1 \left(1 - e^{-(1+i)x/\delta_\kappa} \right)$$

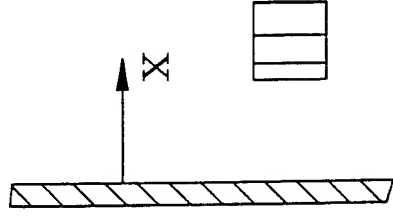
The characteristic dimension is the

thermal penetration depth $\delta_\kappa = \sqrt{2K/\omega \rho c_p}$

DISSIPATION BY OSCILLATORY THERMAL RELAXATION

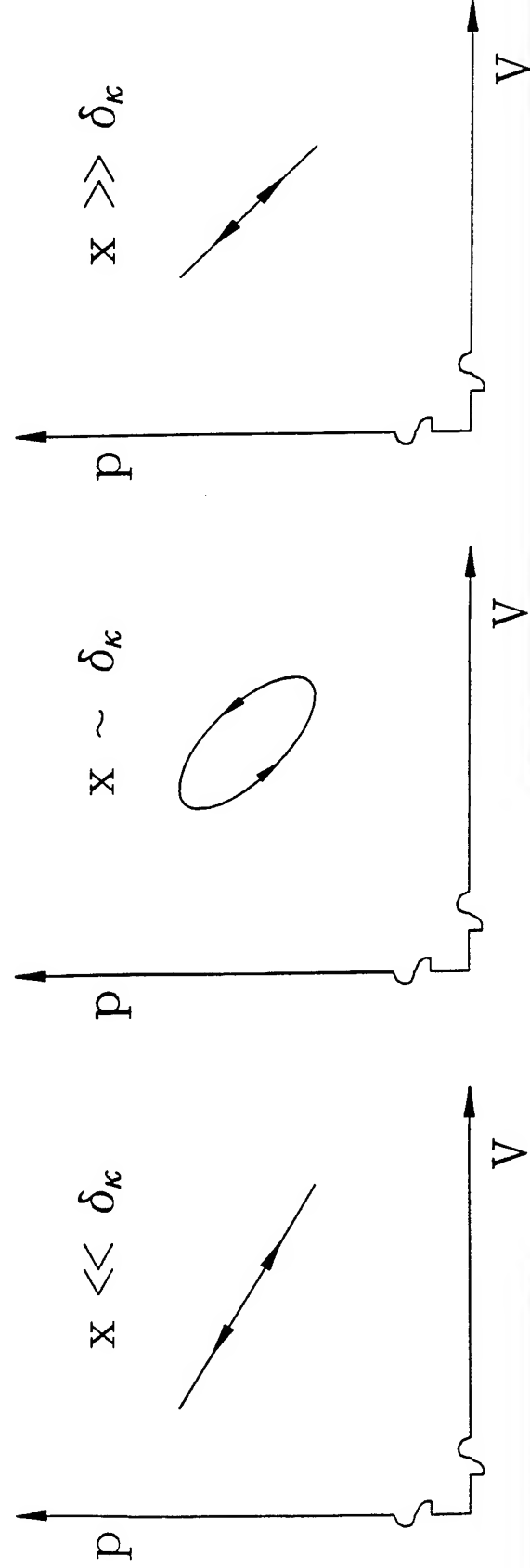
Recall

$$T_1 = \frac{P_1}{\rho_m c_p} \left(1 - e^{-(1+i)x/\delta_\kappa} \right)$$



$pV = nRT$ so V has complex x dependence.

Work absorbed by gas parcel is $\oint p dV$



CONNECTION TO THINGS SEEN ELSEWHERE: SOUND ATTENUATION

Bulk attenuation:

(Kinsler Frey Coppens Sanders eq 7.36)

$$\begin{aligned}\alpha &= \frac{\omega^2}{2\rho_m a^3} \left(\frac{4}{3}\mu + (\gamma-1)\frac{K}{C_p} \right) \\ &= \pi^2 \frac{\omega}{a} \left(\frac{4}{3} \frac{\delta_\nu^2}{\lambda^2} + (\gamma-1) \frac{\delta_\kappa^2}{\lambda^2} \right)\end{aligned}$$

Attenuation in pipes:

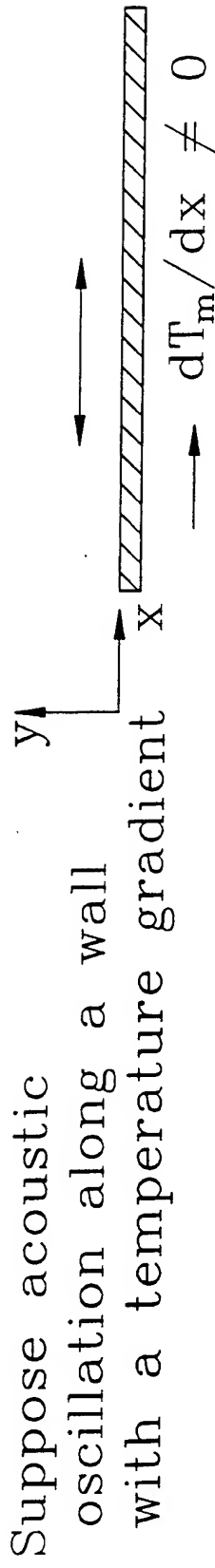
(Kinsler Frey Coppens Sanders eq 9.35)

$$\alpha = \frac{\omega}{2a} \left(\frac{\delta_\nu}{R} + (\gamma-1) \frac{\delta_\kappa}{R} \right)$$

Quality factor of a resonator:

$$\frac{1}{Q} = \frac{\delta_\nu}{R} + (\gamma-1) \frac{\delta_\kappa}{R} + \text{end corrections}$$

SIMPLEST THERMOACOUSTICS ($\mu=0$; gaps $\gg \delta_\kappa$)



The linearized equation of heat transfer is

$$i\omega\rho_m c_p T_1 = i\omega p_1 - \rho_m c_p \frac{dT_m}{dx} u_1 + K \frac{\partial^2 T_1}{\partial y^2}$$

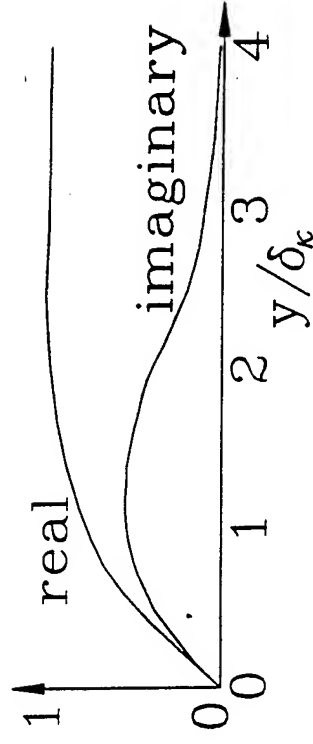
and its solution is

$$T_1 = \left(\frac{p_1}{\rho c_p} - \frac{i(dT_m/dx)u_1}{\omega} \right) \left(1 - e^{-(1+i)y/\delta_\kappa} \right)$$

Magnitude of T_1 :

y-dependence of T_1 :

adiabatic oscillations + motion along x



MOMENTUM EQUATION

$$\rho \left(\frac{\partial \bar{v}}{\partial t} + (\bar{v} \cdot \nabla) \bar{v} \right) = -\bar{\nabla} p + \mu \nabla^2 \bar{v} + \left(\xi + \frac{\mu}{3} \right) \bar{\nabla} (\bar{\nabla} \cdot \bar{v}) + \bar{\nabla} \mu \bar{\nabla} \bar{v} \text{ terms}$$

Acoustic approximation:

$$p = p_m + p_1(x) e^{i\omega t}$$

$$\bar{v} = \left(\hat{x} u_1(x, y, z) + \hat{y} v_1(x, y, z) + \hat{z} w_1(x, y, z) \right) e^{i\omega t}$$

$$\rho = \rho_m(x) + \rho_1(x, y, z) e^{i\omega t}$$

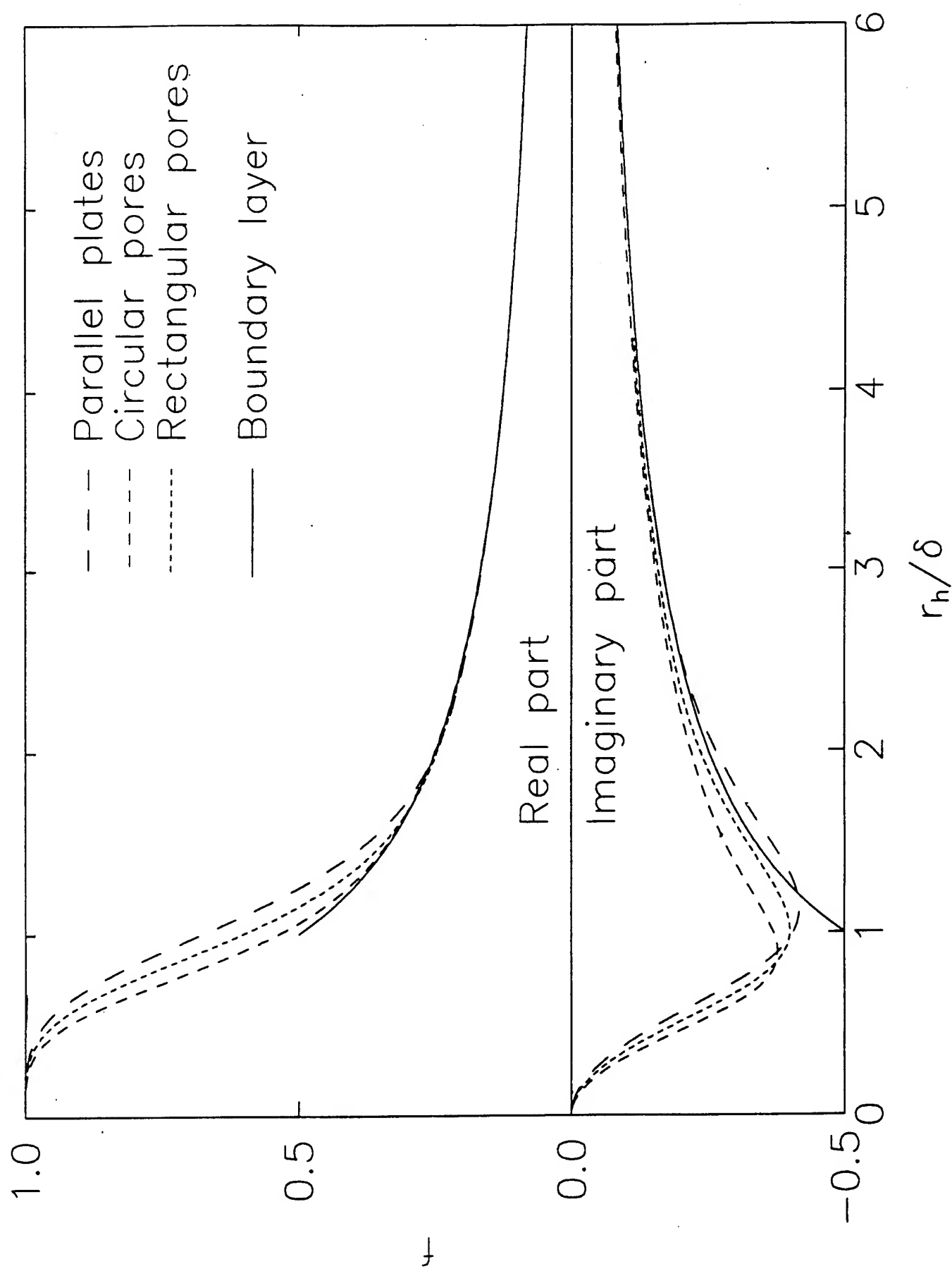
$$\mu = \text{similar to } \rho$$

$$i\omega \rho_m u_1 = -\frac{dp_1}{dx} + \mu \left(\frac{\partial^2 u_1}{\partial y^2} + \frac{\partial^2 u_1}{\partial z^2} \right)$$

Solve for $u_1(y, z)$

Integrate $dy \, dz$ to get $\langle u_1 \rangle$ and rearrange:

$$\frac{dp_1}{dx} = - \frac{i\omega \rho_m}{1 - f_\nu} \langle u_1 \rangle$$



CONTINUITY EQUATION

$$\frac{\partial \rho}{\partial t} + \bar{\nabla} \cdot (\rho \bar{\mathbf{v}}) = 0$$

$$i\omega \langle \rho_1 \rangle + \frac{d}{dx} (\rho_m \langle u_1 \rangle) = 0$$

with equation of state

$$\langle \rho_1 \rangle = \rho_m \left(\frac{p_1}{p_m} - \frac{\langle T_1 \rangle}{T_m} \right)$$

$$\frac{d \langle u_1 \rangle}{dx} = \frac{i\omega}{\rho_m a^2} [1 + (\gamma - 1) f_\kappa] p_1 + \frac{f_\kappa - f_\nu}{(1 - \sigma)(1 - f_\nu)} \frac{1}{T_m} \frac{dT_m}{dx} \langle u_1 \rangle$$

ROTT'S "WAVE" EQUATION

Combining the results of the momentum equation

$$\frac{dp_1}{dx} = - \frac{i\omega\rho_m}{1-f_\nu} \langle u_1 \rangle$$

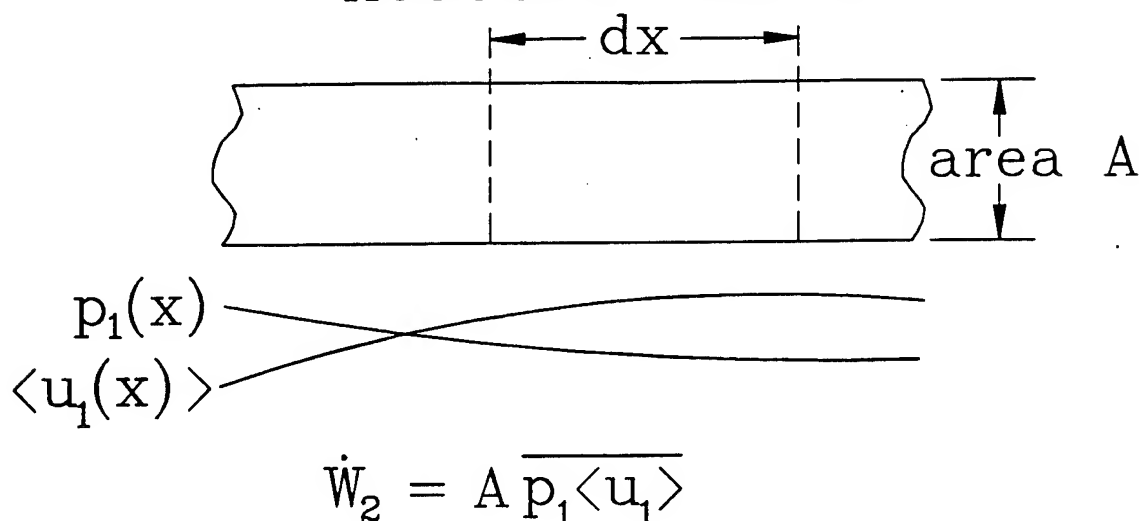
and the continuity equation

$$\frac{d\langle u_1 \rangle}{dx} = \frac{i\omega}{\rho_m a^2} [1 + (\gamma - 1)f_\kappa] p_1 + \frac{f_\kappa - f_\nu}{(1 - \sigma)(1 - f_\nu)} \frac{1}{T_m} \frac{dT_m}{dx} \langle u_1 \rangle$$

by eliminating $\langle u_1 \rangle$ yields Rott's 1969 equation:

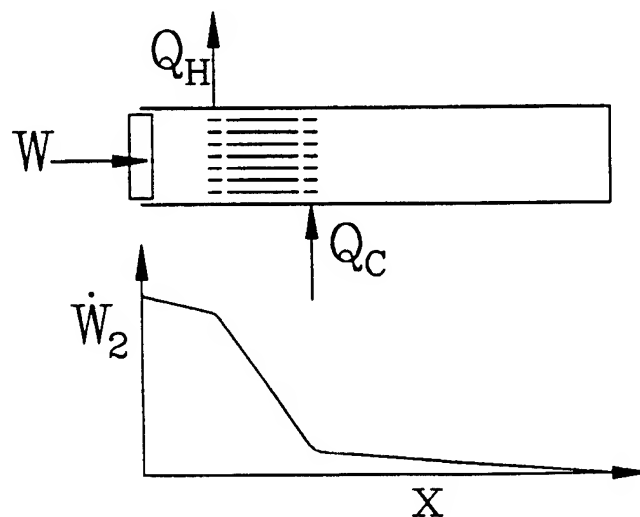
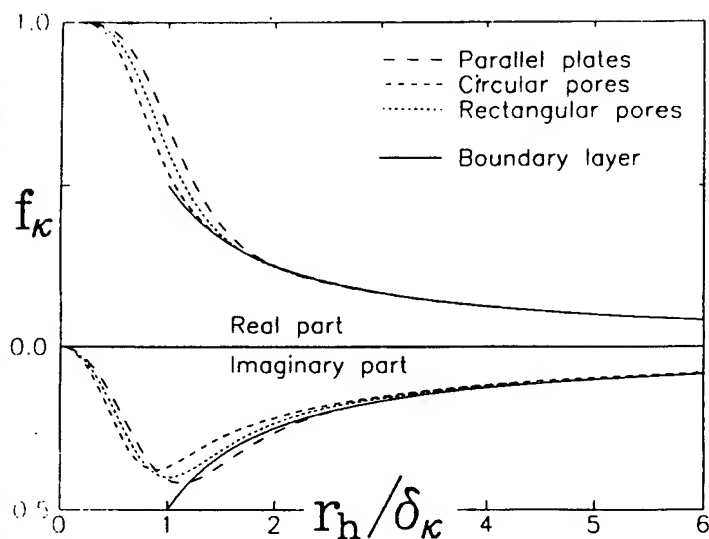
$$[1 + (\gamma - 1)f_\kappa] p_1 + \frac{a^2}{\omega^2} \rho_m \frac{d}{dx} \left(\frac{1 - f_\nu}{\rho_m} \frac{dp_1}{dx} \right) - \frac{a^2}{\omega^2} \frac{f_\kappa - f_\nu}{1 - \sigma} \frac{1}{T_m} \frac{dT_m}{dx} \frac{dp_1}{dx} = 0$$

ACOUSTIC POWER

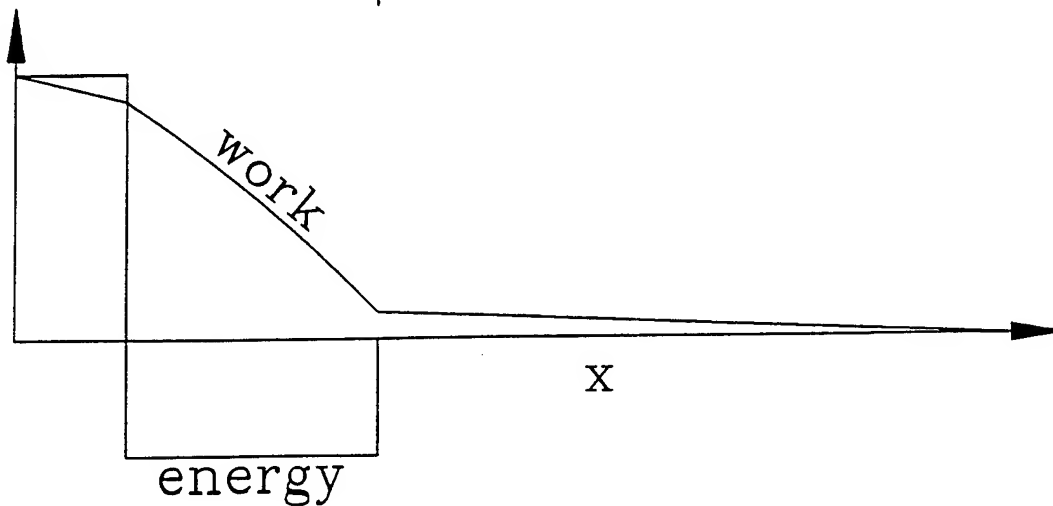
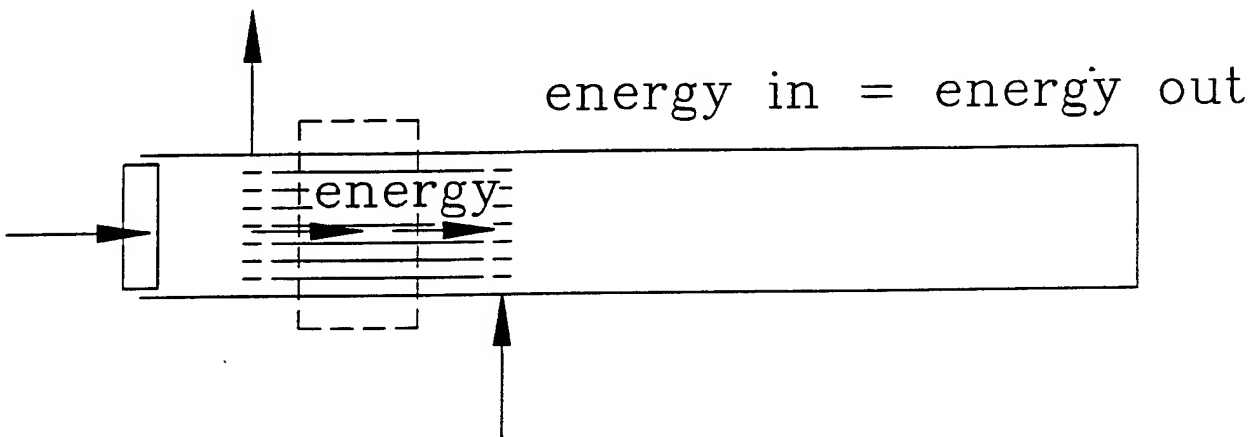
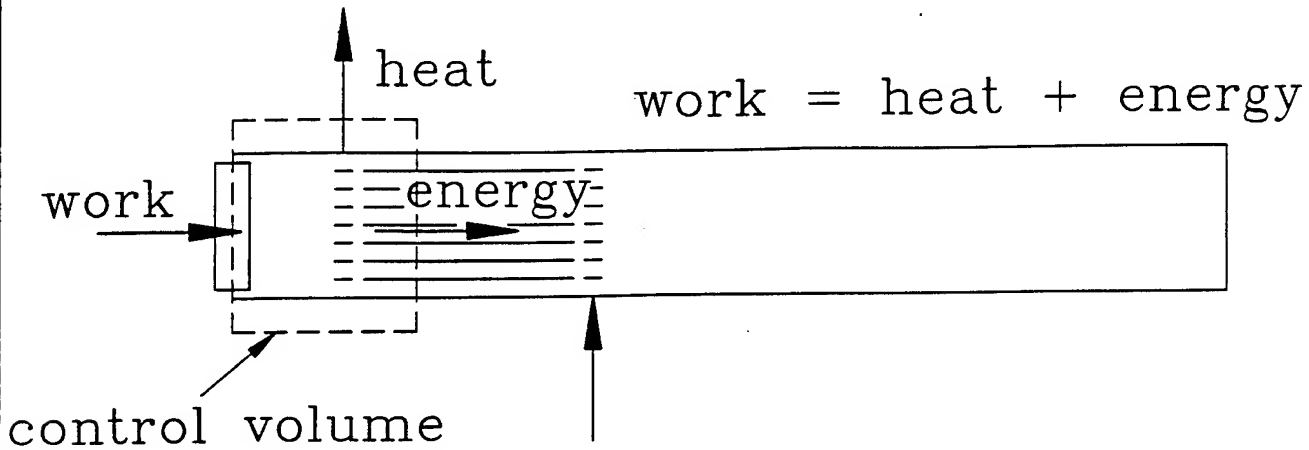


How much power is absorbed (or produced) in length dx ?

$$\begin{aligned} \frac{d\dot{W}_2}{dx} &= A \frac{d}{dx} \overline{p_1 \langle u_1 \rangle} = A \overline{\frac{dp_1}{dx} \langle u_1 \rangle} + A \overline{p_1 \frac{d\langle u_1 \rangle}{dx}} \\ &= \frac{A}{2} \left(\frac{\omega \rho_m |\langle u_1 \rangle|^2}{|1 - f_\nu|^2} \text{Im}[-f_\nu] + \frac{\omega(\gamma - 1) |p_1|^2}{\rho_m a^2} \text{Im}[-f_\kappa] + \right. \\ &\quad \left. + \frac{1}{T_m} \frac{dT_m}{dx} \text{Re} \left[\frac{(f_\kappa - f_\nu) \langle u_1 \rangle \tilde{p}_1}{(1 - \sigma)(1 - f_\nu)} \right] \right) \end{aligned}$$



TOTAL ENERGY



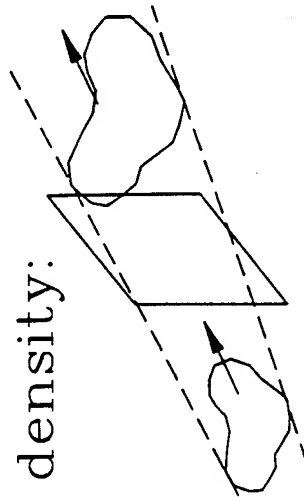
What do we mean here by "energy" ?

HEAT, WORK, AND ENERGY

Enthalpy $h = \varepsilon + p/\rho$.

Enthalpy is the "right" energy for fluid mechanics because $\bar{v}(\rho v^2/2 + \rho h)$ is the energy flux density:

kinetic + internal + pressure



Kinetic + internal are convected along.

Pressure is work done on fluid ahead of surface.

To 2nd order, the time-avg energy flux density is

$$\overline{\rho_m h_1 u_1}$$

$$dh = T ds + \frac{1}{\rho} dp$$

so energy flux density is

$$\overline{\rho_m T_m S_1 u_1} + \overline{p_1 u_1}$$

"heat" + "work"

$$dh = \rho_m c_p dT + \underbrace{\left[1 + \frac{T}{\rho} \left(\frac{\partial \rho}{\partial T} \right)_p \right]}_{=0 \text{ for ideal gas}} dp$$

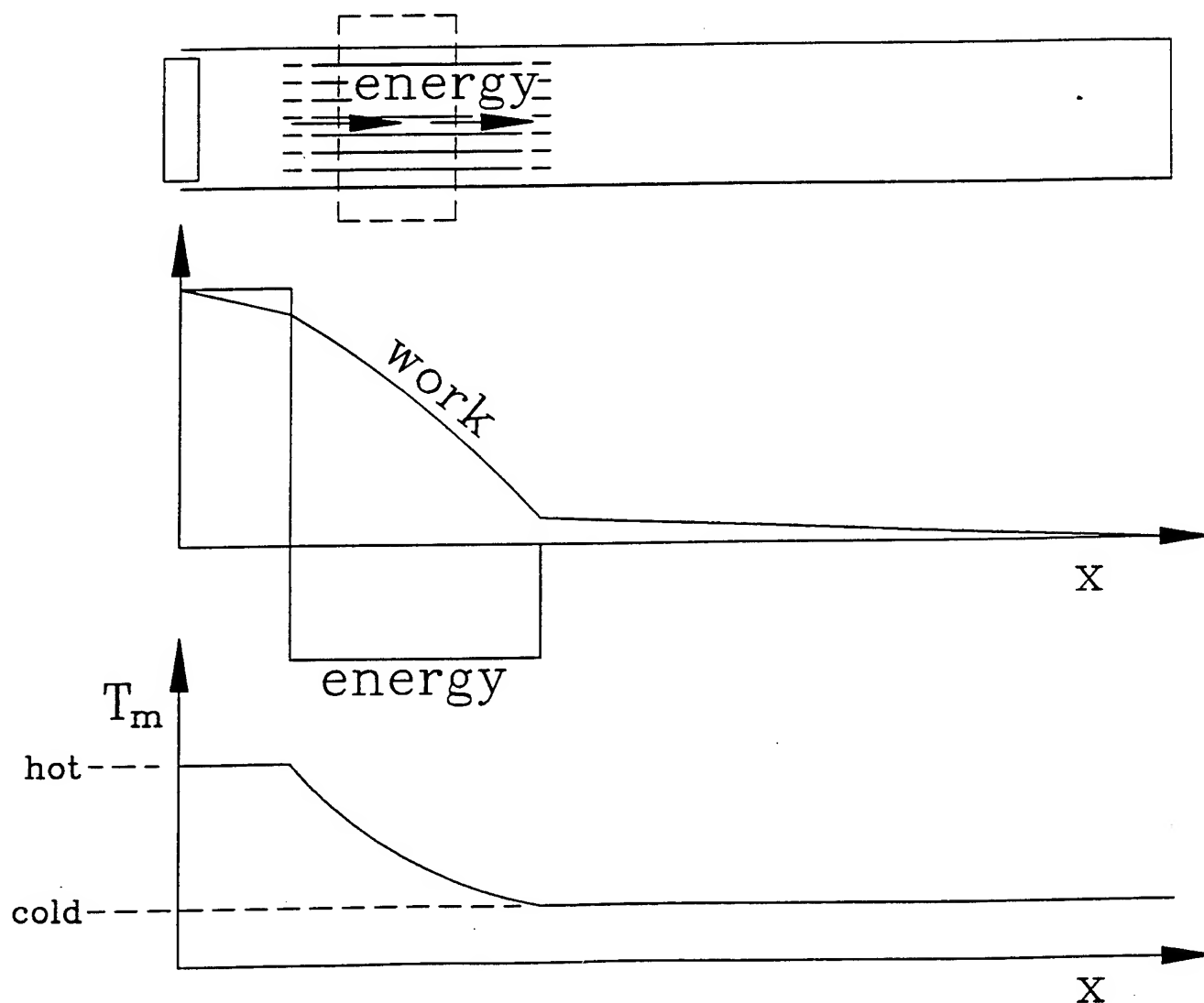
so energy flux density is

$$\overline{\rho_m c_p T_1 u_1}$$

ROTT'S ENERGY EQUATION

$$H_2 = \frac{A}{2} \operatorname{Re} \left[p_1 \langle \tilde{u}_1 \rangle \left(1 - \frac{f_\kappa - \tilde{f}_\nu}{(1+\sigma)(1-\tilde{f}_\nu)} \right) \right] \\ + \frac{A \rho_m c_p |\langle u_1 \rangle|^2}{2\omega(1-\sigma^2)|1-f_\nu|^2} \operatorname{Im} [f_\kappa - \sigma \tilde{f}_\nu] \frac{dT_m}{dx} \\ - AK \frac{dT_m}{dx}$$

can be regarded as a differential equation for $T_m(x)$ in the stack.



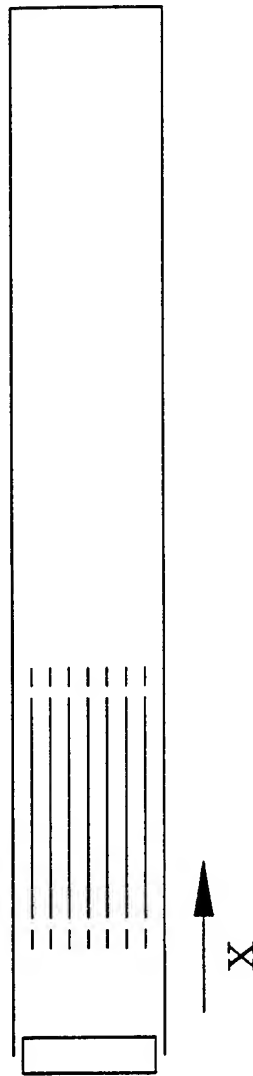
SUMMARY, BASIC THERMOACOUSTIC CALCULATION METHOD

Numerical integration of:

$$\text{Momentum equation} \quad \frac{dp_1}{dx} = g_1(p_1, \langle u_1 \rangle, T_m)$$

$$\text{Continuity equation} \quad \frac{d\langle u_1 \rangle}{dx} = g_2(p_1, \langle u_1 \rangle, T_m)$$

$$\text{Energy equation} \quad \frac{dT_m}{dx} = g_3(p_1, \langle u_1 \rangle, T_m)$$



Software to do this is documented and available; it is called DELTAE.

Many approximate methods exist. Typical approximations:

- f_κ and f_ν are given by boundary-layer limit
- $T_m(x)$ is linear
- gas properties are independent of temperature

AN EXAMPLE

Sponsor's specs:

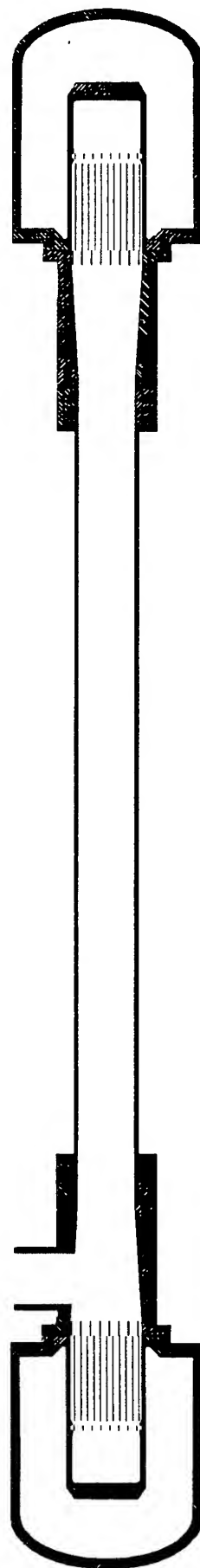
30 bar helium
400 Hz

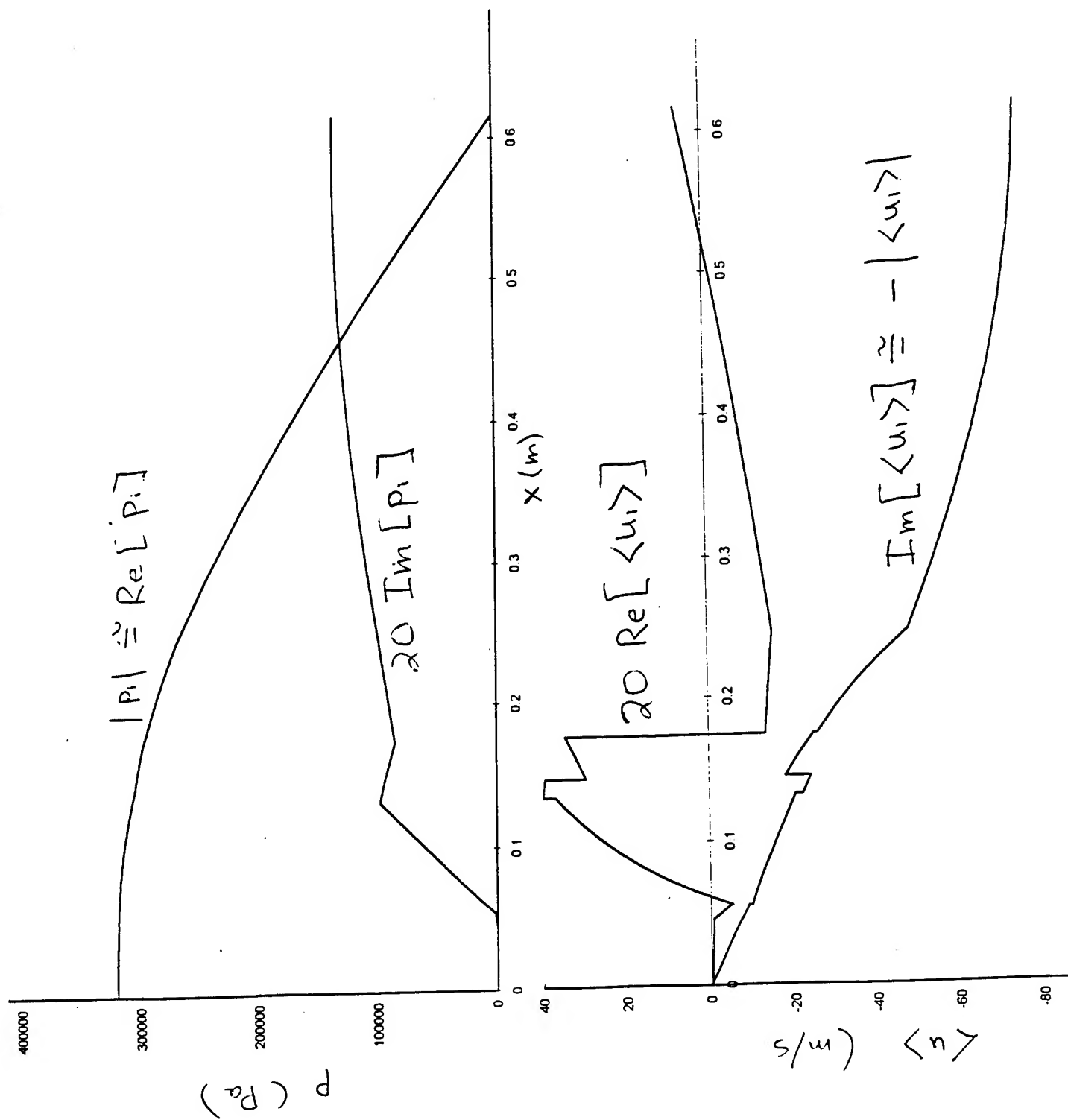
Deliver 1 kW to load

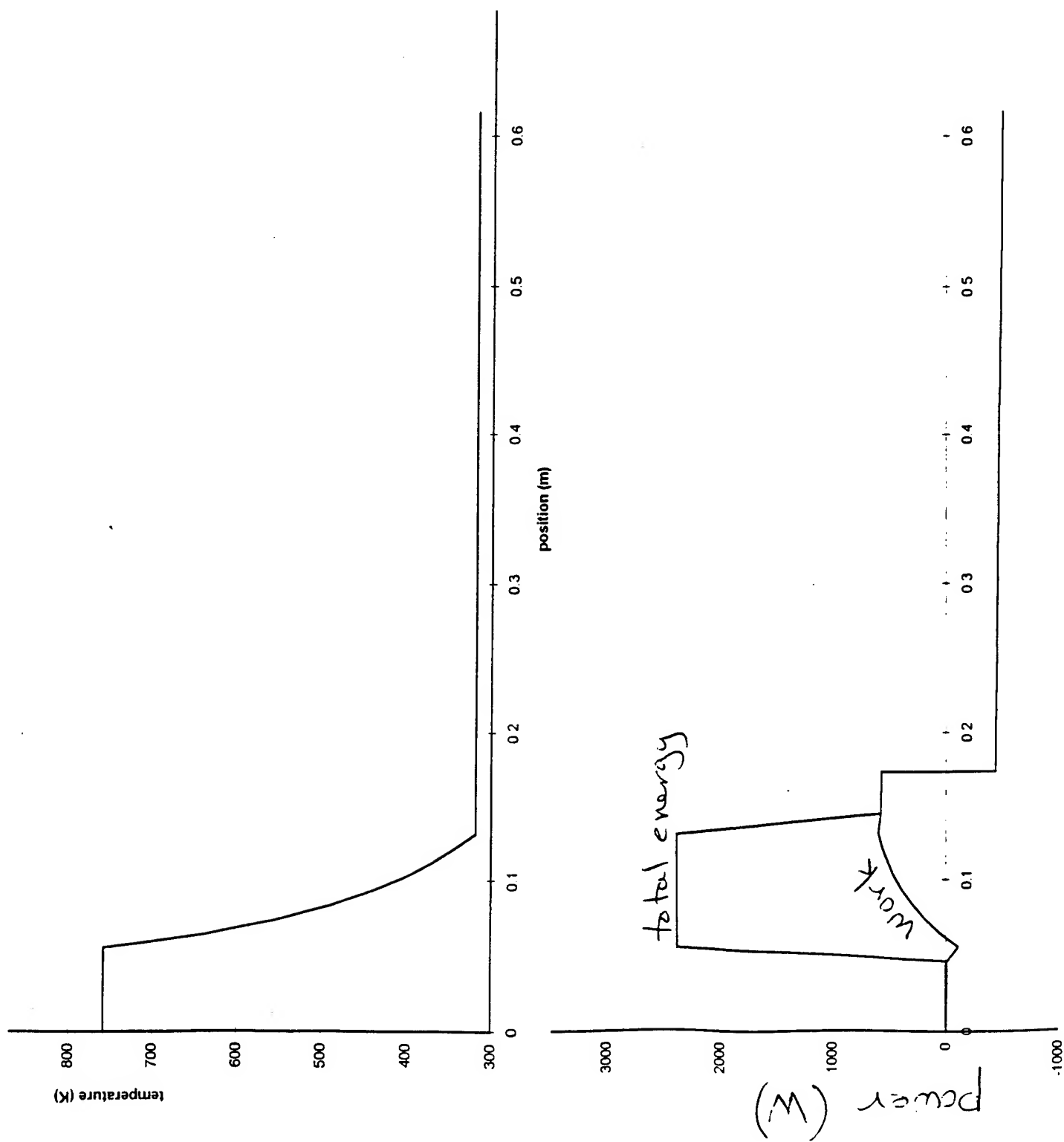
at pressure amplitude = 3 bar.

Load impedance has -30° phase
(mostly real, some compliance).

As small as possible,
as efficient as possible.







CALCULATED PERFORMANCE

1000 W work to load,
5380 W heater power.

Efficiency = $1000/5380 = 18\%$

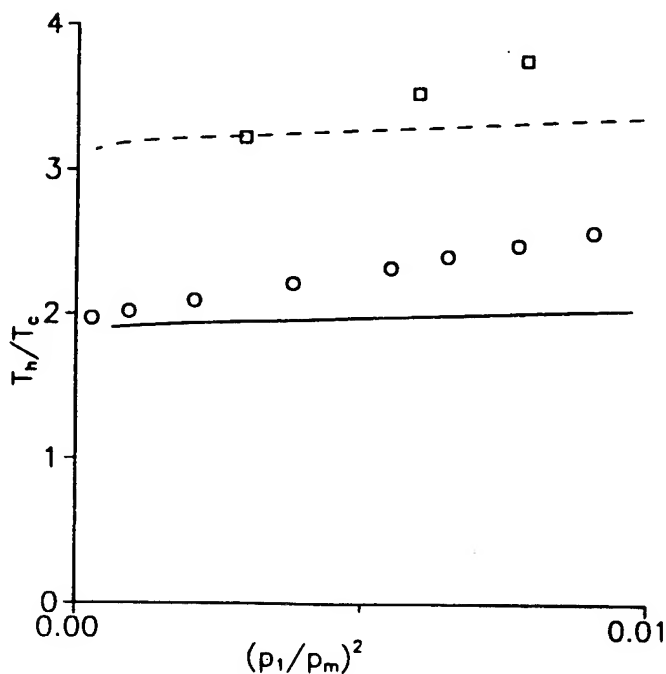
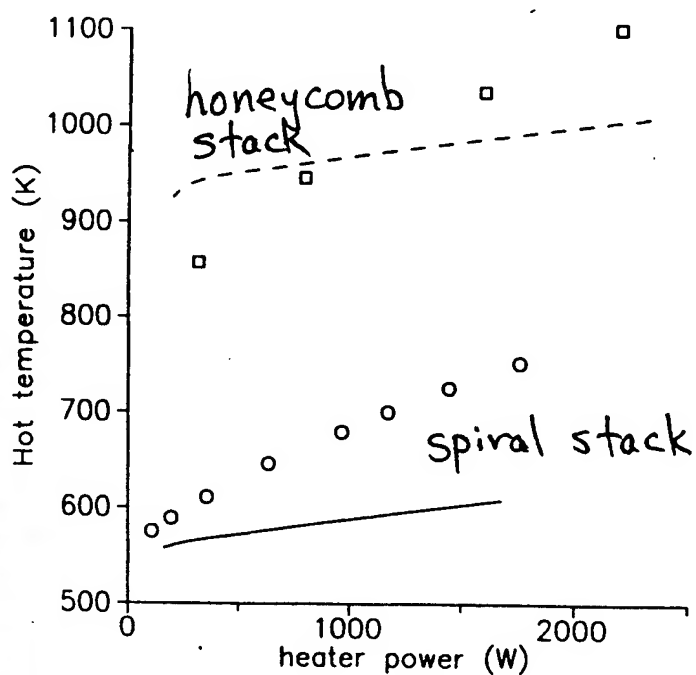
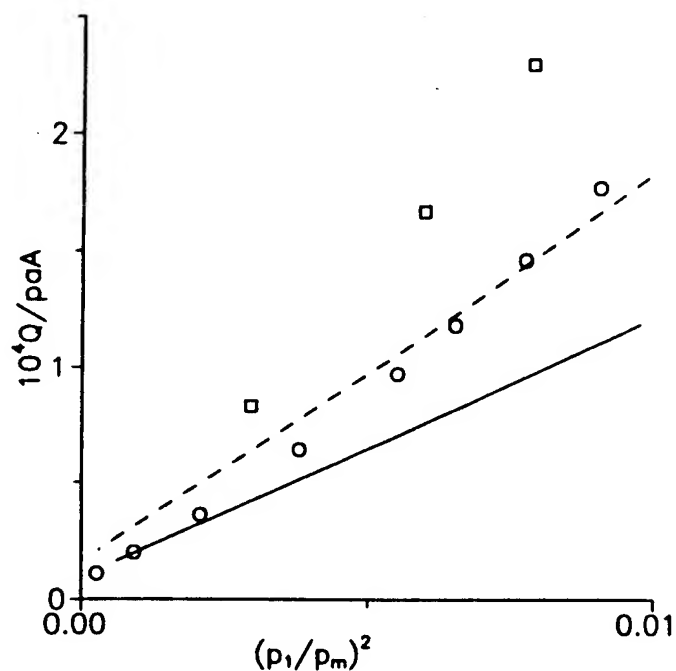
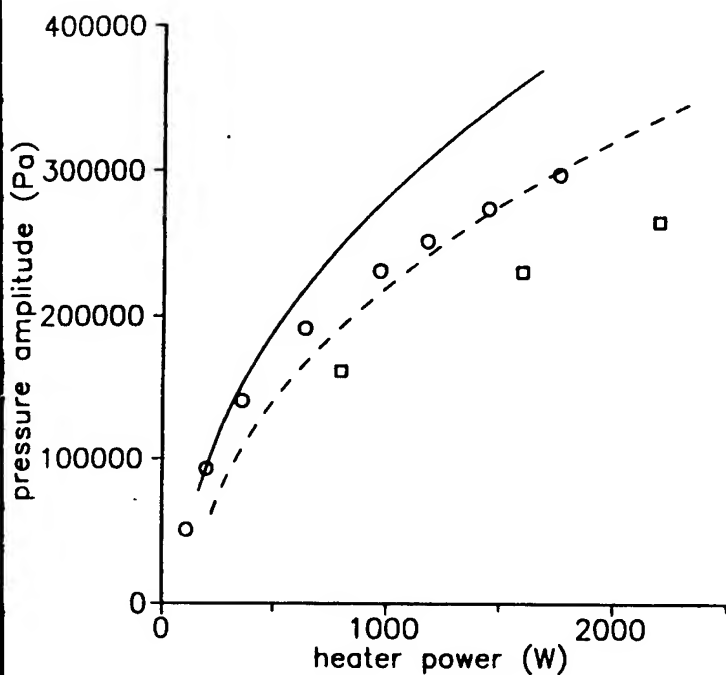
Carnot efficiency = 60%

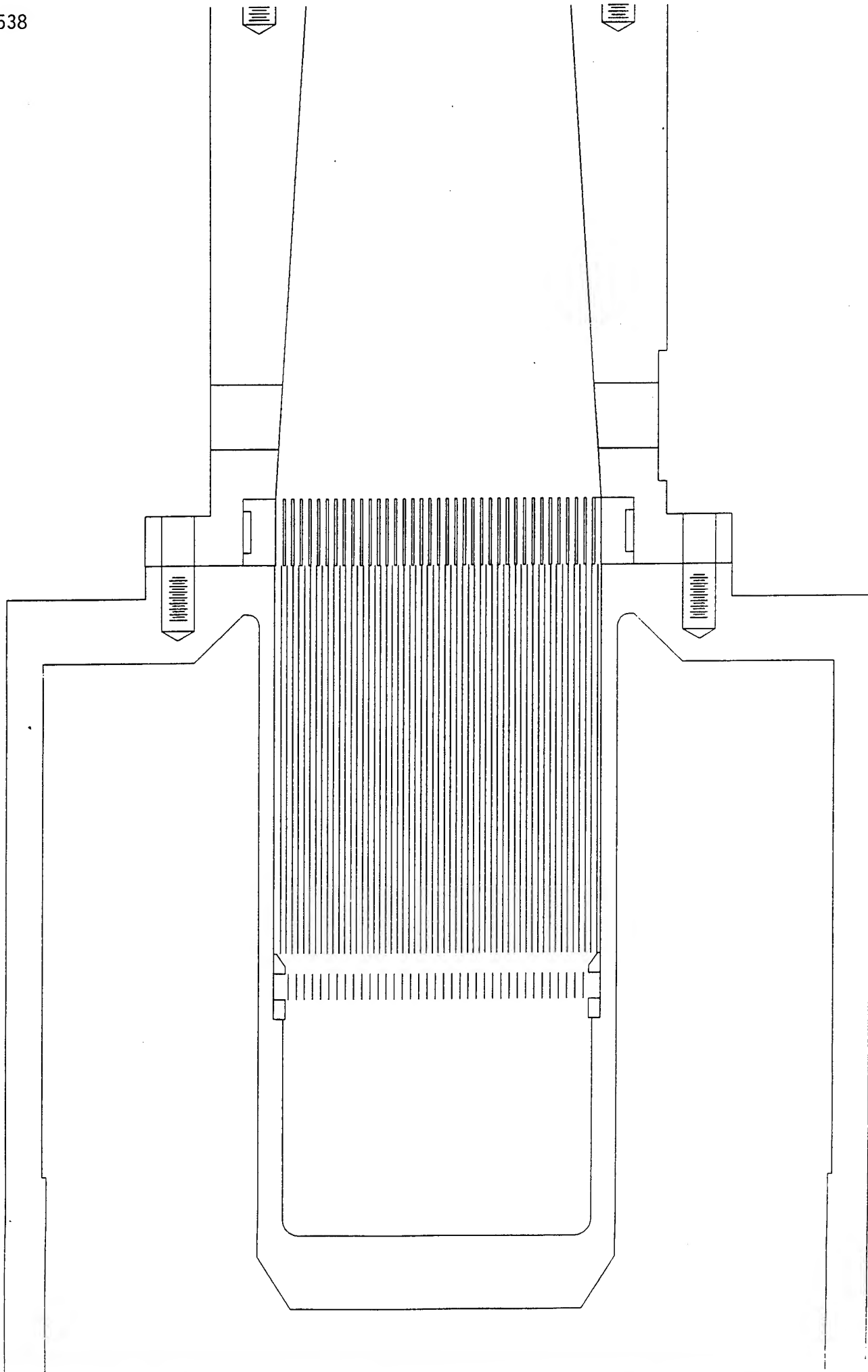
Percent of Carnot = $18/60 = 30\%$

Why so inefficient?

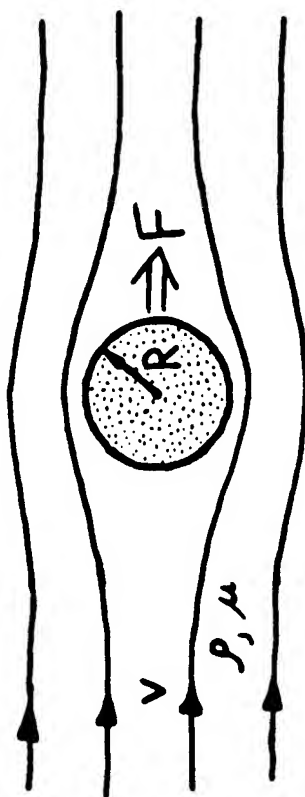
- 47% thermal relaxation loss in stack
- 13% viscous loss in stack
- 11% visc and therm in heat exchangers
- 9% heat leak to room
- 7% visc and thermal in resonator
- 5% conduction along stack case
- 4% conduction along stack
- 3% dT in heat exchangers

Only one hot heat exchanger and stack.
No load.





Consider the force exerted on a sphere by a moving, viscous fluid:



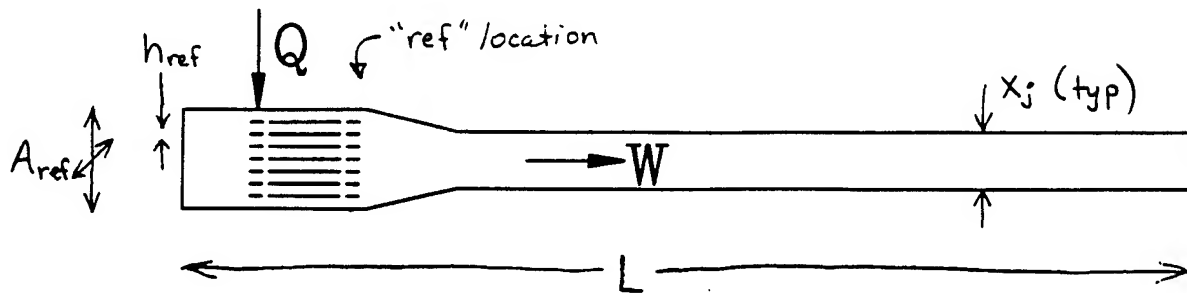
$$F = f(v, \rho, \mu, R)$$

By applying the principle of similitude, one can reduce the number of parameters necessary to describe the force :

$$\frac{F}{\rho v^2 R^2} = f' \left(\frac{\rho v R}{\mu} \right)$$

In general, the number of parameters can be reduced by m , where m is the number of independent units (m, L, t).

Similitude in thermoacoustics



Engine dimensions: $L, A_{\text{ref}}, h_{\text{ref}}, x_j,$

Gas properties: $\gamma, a_{\text{ref}}, K_{\text{ref}}, b_K, \mu_{\text{ref}}, b_\mu,$

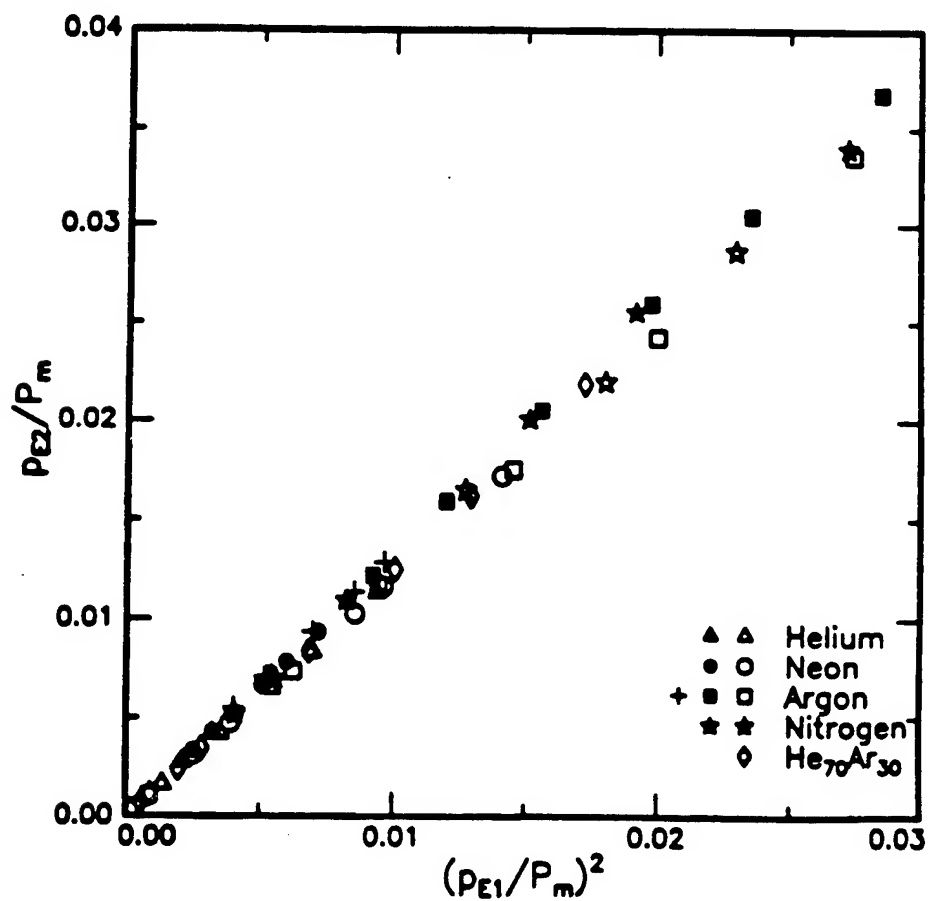
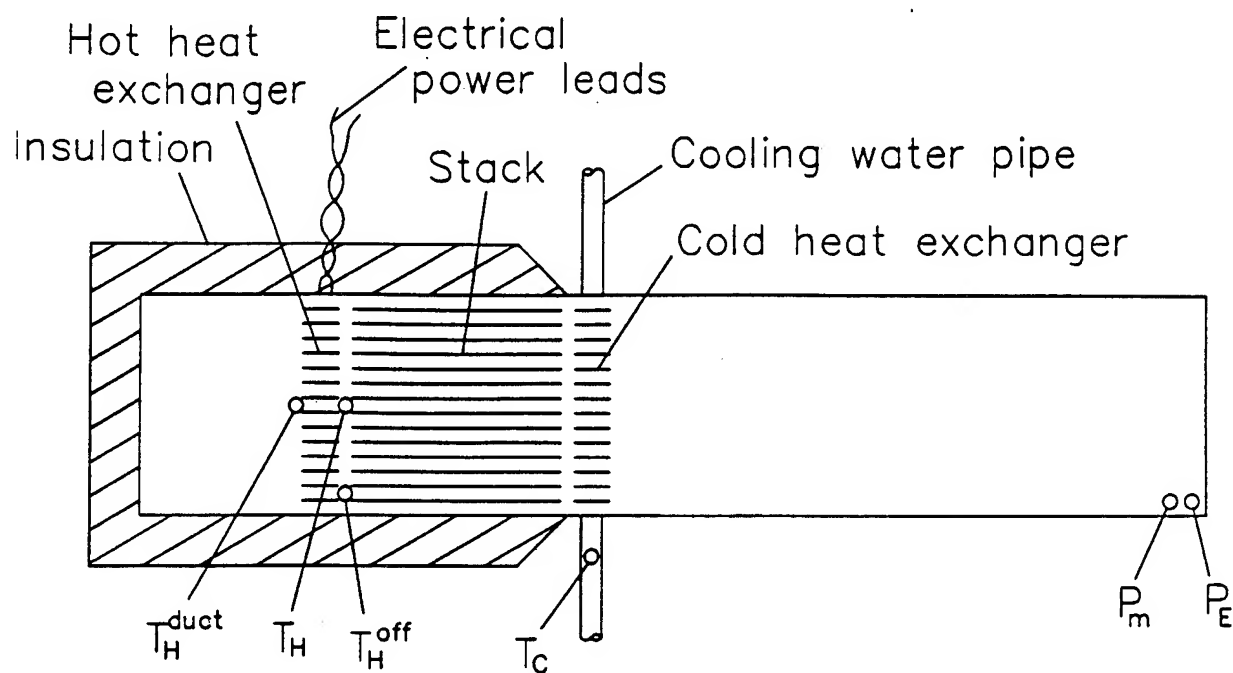
Solid properties: $K_{s,i}$

$\mu = \mu_{\text{ref}} \left(\frac{T}{T_{\text{ref}}} \right)^{b_\mu}$
similar for K

Miscellaneous: $Q, T_{\text{ref}}, P_m,$

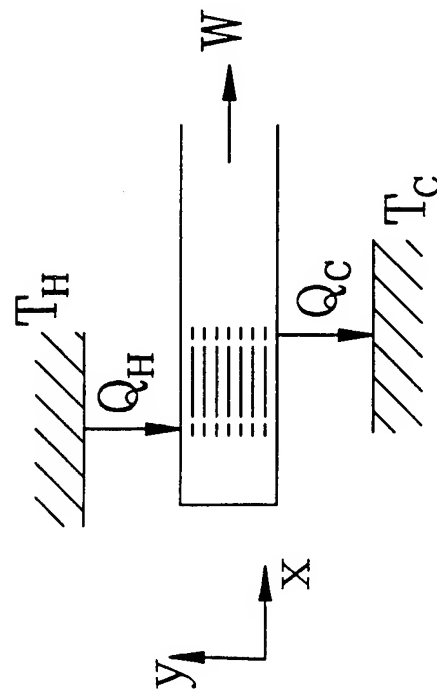
Dependent variables: $f, T(\mathbf{x}, t), \mathbf{v}(\mathbf{x}, t), p(\mathbf{x}, t), \dot{W}.$

$$\begin{pmatrix} fL/a_{\text{ref}} \\ T(\mathbf{x}, t)/T_{\text{ref}} \\ p(\mathbf{x}, t)/P_m \\ \mathbf{v}(\mathbf{x}, t)/a_{\text{ref}} \\ \dot{W}/P_m a_{\text{ref}} A_{\text{ref}} \end{pmatrix} = g \begin{pmatrix} A_{\text{ref}}/L^2, h_{\text{ref}}/L, x_j/L \\ \gamma, \sigma_{\text{ref}}, b_\mu, b_K \\ K_{s,i}/K_{\text{ref}} \\ Q/P_m a_{\text{ref}} A_{\text{ref}}, \delta_K/h_{\text{ref}} \end{pmatrix}$$



Pure similitude

Full size	Half size
helium	argon
450 psi	355 psi
temperatures	same
p_{osc}/p_{avg}	same
powers	$\div 16$



Equation of state
Momentum equation
Continuity equation
Heat transfer equation

Acoustic approximation

Integrate dy dz analytically

Rott's equations

Integrate along x

Obtain $p_1(x)$, $\langle u_1 \rangle(x)$, and $T_m(x)$ simultaneously

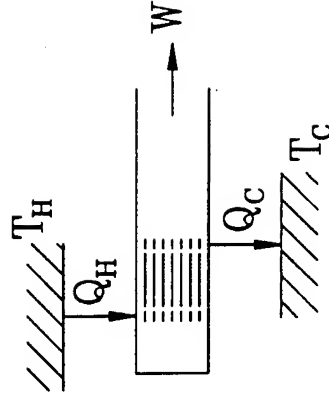
Status: Mostly understood in acoustic approximation

Future: Details at heat exchanger-stack interface

High amplitude effects: turbulence, streaming...
Real applications

SOURCES OF INEFFICIENCY

(Why can't thermoacoustic systems have Carnot's efficiency?)



1. Thermal relaxation losses in δ_κ
2. Viscous dissipation
3. Conduction of heat along x
4. Same, in heat exchangers and resonator
5. Solid/liquid bottlenecks in heat exchangers
6. Transducers
7. Things we don't yet understand

About 1/3 of Carnot is typical of current designs.

REPORT DOCUMENTATION PAGE

Form Approved
OMB No. 0704-0188

Public reporting burden for this collection of information is estimated to average 1 hour per response, including the time for reviewing instructions, searching existing data sources, gathering and maintaining the data needed, and completing and reviewing the collection of information. Send comments regarding this burden estimate or any other aspect of this collection of information, including suggestions for reducing this burden, to Washington Headquarters Services, Directorate for Information Operations and Reports, 1215 Jefferson Davis Highway, Suite 1204, Arlington, VA 22202-4302, and to the Office of Management and Budget, Paperwork Reduction Project (0704-0188), Washington, DC 20503.

1. AGENCY USE ONLY (Leave blank)		2. REPORT DATE	3. REPORT TYPE AND DATES COVERED Final 01 Feb 96 - 31 Jan 97	
4. TITLE AND SUBTITLE Proceedings of the 1997 Physical Acoustics Summer School: Volume II: Transparencies			5. FUNDING NUMBERS PE 61153N G N00014-96-1-0033	
6. AUTHOR(S) Henry E. Bass				
7. PERFORMING ORGANIZATION NAME(S) AND ADDRESS(ES) University of Mississippi NCPA University, MS 38677			8. PERFORMING ORGANIZATION REPORT NUMBER	
9. SPONSORING/MONITORING AGENCY NAME(S) AND ADDRESS(ES) Office of Naval Research ONR 331 800 North Quency Street Arlington, VA 22217-5660			10. SPONSORING/MONITORING AGENCY REPORT NUMBER	
11. SUPPLEMENTARY NOTES				
12a. DISTRIBUTION/AVAILABILITY STATEMENT Approved for public release; Distribution unlimited			12b. DISTRIBUTION CODE	
13. ABSTRACT (Maximum 200 words) Volume II of the Proceedings of the 1997 Physical Acoustic Summer School contains copies of the transparencies used during the lectures. Volume I contains verbatim transcriptions of the lectures and Volume III contains copies of the background materials sent to student participants prior to the summer school.				
14. SUBJECT TERMS Physical Acoustics, Molecular Acoustics, Acoustics Demonstrations, Resonant Ultrasound Spectroscopy, Sonoluminescence, Nonlinear and Atmospheric Acoustics, Sensor Physics, Thermoacoustics			15. NUMBER OF PAGES 544	
			16. PRICE CODE	
17. SECURITY CLASSIFICATION OF REPORT UNCLASSIFIED	18. SECURITY CLASSIFICATION OF THIS PAGE UNCLASSIFIED	19. SECURITY CLASSIFICATION OF ABSTRACT UNCLASSIFIED	20. LIMITATION OF ABSTRACT	